

# **Flexible and Rigid Non-glucose Cyclooligosaccharides: Synthesis, Structure, and Properties**

*Habilitationsschrift*

Dem Fachbereich Chemie der Technischen Universität Darmstadt  
für das Fachgebiet Organische Chemie vorgelegt von

**Stefan Immel**

Darmstadt, 2003



## **Annotations**

This thesis is divided into nine individual Chapters providing the original publications related to specific aspects of this work; all references are given within these publications. A short general introduction and a synopsis of the results have been added before the first Chapter.

## **Acknowledgments**

This work has been conducted at the Clemens-Schöpf-Institut für Organische Chemie und Biochemie, Technische Universität Darmstadt, and is the result of sharing of ideas addressed by a number individuals over the past several years. Acknowledging specific individuals by name carries the risk of overlooking key contributors: however, it would be a gross oversight not to recognize at least a few individuals for their support, unwavering encouragement, advocacy, and many lucid and critical discussions and suggestions. Above all, I would like to acknowledge my mentor Prof. Dr. F. W. Lichtenthaler, as well as Prof. Dr. J. Brickmann and Prof. Dr. H. J. Lindner for their valuable advice and support. Highly appreciated are also the contributions that have emerged from international cooperations with Prof. Dr. T. Nakagawa and Prof. Dr. K. Fujita. Not mentioned individually, but not less valuable, I would like to thank all my coauthors of my publications for having contributed to this work.



## Table of Contents

### Flexible and Rigid Non-glucose Cyclooligosaccharides: Synthesis, Structure, and Properties

Introduction	1
Synopsis	3
<b>Chapter 1 - From Cyclodextrins to Amylose: Structures and Lipophilicity Patterns</b>	<b>19</b>
Topography of the 1:1 $\alpha$ -Cyclodextrin - Nitromethane Inclusion Complex T. Nakagawa, S. Immel, F. W. Lichtenthaler, and H. J. Lindner, <i>Carbohydr. Res.</i> <b>2000</b> , 324, 141-146.	21
The Hydrophobic Topographies of Amylose and its Blue Iodine Complex S. Immel and F. W. Lichtenthaler, <i>Starch/Stärke</i> <b>2000</b> , 52, 1-8.	27
<b>Chapter 2 - Per-2,3-anhydro-<math>\alpha</math>-cyclomannin</b>	<b>35</b>
Structure and Lipophilicity Profile of 2,3-Anhydro- $\alpha$ -cyclomannin and its Ethanol Inclusion Complex S. Immel, K. Fujita, H. J. Lindner, Y. Nogami, and F. W. Lichtenthaler, <i>Chem. Eur. J.</i> <b>2000</b> , 6, 2327-2333.	37
The 2,3-Anhydro- $\alpha$ -cyclomannin - 1-Propanol Hexahydrate: Topography, Lipophilicity Pattern, and Solid-state Architecture S. Immel, F. W. Lichtenthaler, H. J. Lindner, K. Fujita, M. Fukudome, and Y. Nogami, <i>Tetrahedron: Asymmetry</i> <b>2000</b> , 11, 27-36.	45
<b>Chapter 3 - <math>\alpha</math>-Cycloaltrin</b>	<b>55</b>
Synthesis, Structure, and Conformational Features of $\alpha$ -Cycloaltrin: a Cyclooligosaccharide with alternating $^4C_1$ and $^1C_4$ Pyranose Chairs Y. Nogami, K. Nasu, T. Koga, K. Ohta, K. Fujita, S. Immel, H. J. Lindner, G. E. Schmitt, and F. W. Lichtenthaler, <i>Angew. Chem.</i> <b>1997</b> , 109, 1987-1991; <i>Angew. Chem. Int. Ed. Engl.</i> <b>1997</b> , 35, 1899-1902.	57
Solution Geometries and Lipophilicity Patterns of $\alpha$ -Cycloaltrin S. Immel, K. Fujita, and F. W. Lichtenthaler, <i>Chem. Eur. J.</i> <b>1999</b> , 5, 3185-3192.	61
Inclusion Complexes of Cycloaltrins S. Immel, K. L. Larsen, <i>unpublished results</i> .	69
<b>Chapter 4 - Mono-<i>altro</i>-<math>\beta</math>-cyclodextrin</b>	<b>73</b>
Guest-induced Conformational Change in a Flexible Host: Mono- <i>altro</i> - $\beta$ -cyclodextrin K. Fujita, W.-H. Chen, D.-Q. Yuan, Y. Nogami, T. Koga, T. Fujioka, K. Mihashi, S. Immel, and F. W. Lichtenthaler, <i>Tetrahedron: Asymmetry</i> <b>1999</b> , 10, 1689-1696.	75
<b>Chapter 5 - Cyclofructins and Cyclogalactofuranosides</b>	<b>83</b>
Cyclofructins with Six to Ten $\beta(1\rightarrow2)$ -linked Fructofuranose Units: Geometries, Electrostatic Profiles, Lipophilicity Patterns, and Potential for Inclusion Complexation S. Immel, G. E. Schmitt, and F. W. Lichtenthaler, <i>Carbohydr. Res.</i> <b>1998</b> , 313, 91-105.	85
Conformations and Lipophilicity Profiles of some Cyclic $\beta(1\rightarrow3)$ - and $\beta(1\rightarrow6)$ -linked Oligogalactofuranosides H. Gohlke, S. Immel, and F. W. Lichtenthaler, <i>Carbohydr. Res.</i> <b>1999</b> , 321, 96-104.	101
<b>Chapter 6 - Cyclodextrin-derived Crown Acetals</b>	<b>111</b>
Synthesis and Molecular Geometry of an Achiral 30-Crown-12 Polyacetal from $\alpha$ -Cyclodextrin S. Immel, T. Nakagawa, H. J. Lindner, and F. W. Lichtenthaler, <i>Chem. Eur. J.</i> <b>2000</b> , 6, 3366-3371.	113
Hydroxymethyl-substituted Crown Acetals with 35-C-14 and 40-C-16 Skeletal Backbones: Synthesis and Molecular Geometries S. Immel, F. W. Lichtenthaler, H. J. Lindner, and T. Nakagawa, <i>Tetrahedron: Asymmetry</i> <b>2001</b> , 12, 2767-2774.	119

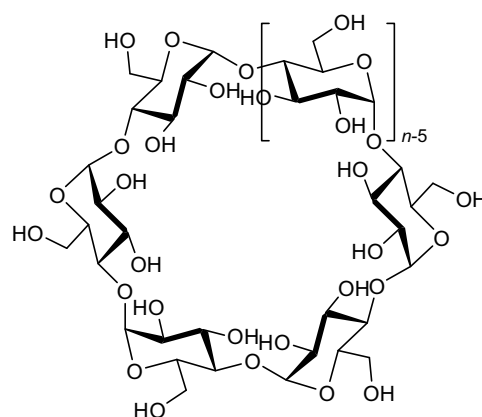
Large-ring Crown Acetals from Cyclodextrins	127
T. Nakagawa, S. Immel, H. J. Lindner, and F. W. Lichtenthaler, <i>Proc. 10<sup>th</sup> Int. Symp. Cyclodextrins</i> (Ed.: J. Szejtli), Mia Digital Publ., Ann Arbor, Michigan, <b>2000</b> , pp. 18-23.	
Flexible Non-glucose Cyclooligosaccharides	133
S. Immel, <i>Proc. 10<sup>th</sup> Int. Symp. Cyclodextrins</i> (Ed.: J. Szejtli), Mia Digital Publ., Ann Arbor, Michigan, <b>2000</b> , pp. 24-31.	
<b>Chapter 7 - Rigidified Bridged Cyclodextrins</b>	<b>141</b>
Two Stereoisomeric 3 <sup>l</sup> ,2 <sup>ll</sup> -Anhydro- $\alpha$ -cyclodextrins: A Molecular Dynamics and Crystallographic Study	143
S. Immel, K. Fujita, M. Fukudome, and M. Bolte, <i>Carbohydr. Res.</i> <b>2001</b> , 336, 297-308.	
The First Successful Crystallographic Characterization of a Cyclodextrin Dimer: Efficient Synthesis and Molecular Geometry of a Doubly Sulfur-bridged $\beta$ -Cyclodextrin	155
D.-Q. Yuan, S. Immel, K. Koga, M. Yamaguchi, and K. Fujita, <i>Chem. Eur. J.</i> <b>2003</b> , 9, 3501-3506.	
<b>Chapter 8 - Molecular Modelling of Saccharides</b>	<b>161</b>
Atropdiastereoisomers of Ellagitannin Model Compounds: Configuration, Conformation, and Relative Stability of D-Glucose Diphenoyl Derivatives	163
S. Immel, K. Khanbabaee, <i>Tetrahedron: Asymmetry</i> <b>2000</b> , 11, 2495-2507.	
Metabolism of Sucrose and Its Five Linkage-isomeric $\alpha$ -D-Glucosyl-D-fructoses by <i>Klebsiella pneumoniae</i>	177
J. Thompson, S. A. Robrish, S. Immel, F. W. Lichtenthaler, B. G. Hall, and A. Pikis, <i>J. Biol. Chem.</i> <b>2001</b> , 276, 37415-37425.	
Metabolism of Sucrose and Its Five $\alpha$ -D-Glucosyl-D-fructose Isomers by <i>Fusobacterium mortiferum</i>	189
A. Pikis, S. Immel, S. A. Robrish, and J. Thompson, <i>Microbiology</i> <b>2002</b> , 148, 843-852.	
<b>Chapter 9 - Molecular Graphics</b>	<b>199</b>
<i>MolArch</i> <sup>+</sup> - Molecular Architecture Modelling Program	201
S. Immel, <a href="http://caramel.oc.chemie.tu-darmstadt.de/immel/">http://caramel.oc.chemie.tu-darmstadt.de/immel/</a> .	
<b>Conclusion</b>	<b>211</b>
Concluding Remarks	213
<b>Appendix</b>	<b>215</b>
List of Publications	217
Poster Presentations and Conference Contributions	221
Oral Presentations	223
Curriculum Vitae	225

# Flexible and Rigid Non-glucose Cyclooligosaccharides: Synthesis, Structure, and Properties

## Introduction

At present, the evaluation of molecular recognition processes represents one of the most challenging fields of research. Molecular interactions are vital to almost every phenomenon in the field of chemistry, biochemistry, and biology, and many of the fundamental principles still remain to be fully understood. Amongst these processes, receptor-substrate and host-guest recognition are of particular importance. The amylose-derived natural cyclodextrins (CDs), small cyclooligosaccharides made up out of six or more  $\alpha(1\rightarrow4)$ -linked D-glucose residues, represent a prominent class of potential hosts to a wide range of small organic molecules. Their unique ability to include hydrophobic guest molecules into their hydrophobic central cavities in aqueous solution has been studied extensively and has led to numerous commercial applications in the field of e.g. pharmaceuticals, cosmetics, drug stabilization and delivery, biotechnology, and environmental applications. Among the driving forces for the formation of these inclusion complexes are dipole-dipole interactions and - most notably - hydrophobic interactions caused by the H-3 and H-5 protons of the glucose units pointing towards the center of the cyclodextrin cavities.

The molecular geometry of the cyclodextrins closely resembles truncated cone structures with the primary 6-CH<sub>2</sub>OH and the secondary 2- and 3-OH groups of the glucose moieties lined up on opposite sides of the macrocyclic torus. As evidenced by a large number of X-ray or neutron diffraction derived solid-state structures of  $\alpha$ -,  $\beta$ -, and  $\gamma$ -cyclodextrins and their inclusion complexes, these host molecules adopt rather rigid conformations with respect to the almost perpendicular alignment of the glucose residues in relation to the mean-planes of the macrocycles. In general, only little or no conformational changes are observed within the hosts upon inclusion of potential guest



### cyclodextrins

*cyclo*[D-Glcp  $\alpha(1\rightarrow4)$ ]<sub>n</sub>

$\alpha$ -cyclodextrin ( $n = 6$ )

$\beta$ -cyclodextrin ( $n = 7$ )

$\gamma$ -cyclodextrin ( $n = 8$ )

molecules. Further evidence for the greatly limited flexibility of the cyclodextrins stems from numerous NMR and theoretical (molecular mechanics and dynamics) studies on these assemblies. If at all, only slight elliptical distortions to accommodate elongated or disc-shaped (aromatic) guests are observed in the cyclodextrin complexes. With very few exceptions, the energetically favorable rigid  ${}^4C_1$  chair geometries of the glucose units are retained in all structures reported.

The molecular recognition abilities of the native cyclodextrins are greatly confined by their rigid  $C_n$  symmetrical structures, and, in general, the formation of inclusion complexes displays a significant degree of shape selectivity as the hosts are incapable of undergoing major conformational changes to adopt their shape towards guest molecules. This is of particular importance, as cyclodextrins have been treated as model structures for biomimetic recognition processes and enzyme models in the context of catalysis. However, when comparing the cyclodextrins with highly flexible structures such as enzymes a fundamental discrepancy becomes obvious: whereas enzymes recognize their substrates through conformational changes – which finally trigger the biological response – in an flexible *induced-fit*-type manner, the formation of inclusion complexes by cyclodextrins represents a rather rigid *lock-and-key*-type process. In general, cyclodextrins display little – if any – tendency to undergo significant conformational changes or to adapt their shape towards guest molecules. Therefore, in catalytic processes, cyclodextrins are rigid templates rather than flexible enzyme models, exerting their catalytic activity by bringing reactive groups and substrates in close proximity in the inclusion complexes. Chapter 1 of this work describes the molecular geometry of the yet unknown inclusion complex of  $\alpha$ -cyclodextrin with nitromethane. In addition, the structures and conformational properties of cyclodextrins with increasing ring size are compared to the geometry of amylose, pointing out significant differences and similarities.

In view of the obvious differences in molecular recognition by enzymes and cyclodextrins, it was of fundamental importance to develop flexible cyclodextrin hosts and study their inclusion complexes to obtain more realistic enzyme models. In this work, efforts directed towards the efficient synthesis of flexible cyclodextrin-derived molecular hosts are described along with their unequivocal structural and geometrical characterization in the solid-state, and in solution. In principle, the following approaches are appropriate to introduce conformational flexibility into the cyclodextrins:

- Per-O-alkylation or per-O-acylation introduces steric hindrance between the glucose residues, leading to more distorted structures of higher flexibility with increased ranges of accessible tilt angles between the constituent sugars. Simultaneously, the torus stabilization through intramolecular hydrogen bonds is reduced, or even totally eliminated.



- Deoxygenation of hydroxyl groups introduces flexibility through disruption of intramolecular hydrogen bonds ( $\rightarrow$  per-2,3-anhydro- $\alpha$ -cyclomannin, Chapter 2).
- Transformation of the rigid glucose moieties into more flexible sugar residues such as  $\alpha$ -D-altrose ( $\rightarrow$  cycloaltrins and mono-*altro*-cyclodextrins, Chapter 3 and 4); or replacement of the pyranose rings by more flexible furanoid structures ( $\rightarrow$  cyclofructins and cyclogalactofuranosides, Chapter 5).
- Cleavage of C-C-bonds in the constituent pyranoses generates highly flexible macrocycles ( $\rightarrow$  crown acetals, Chapter 6).

In all cases listed above, the flexibility of the new cyclodextrin-derived hosts is expected to drive the corresponding mechanism of inclusion complexation towards a more flexible *induced-fit*-type process of molecular recognition. However, it is also important to study the effects of the opposite approach, i.e. introducing enhanced rigidity into the hosts. Within this work, two routes towards rigidified cyclodextrin derivatives are pursued (Chapter 7):

- Intramolecular bridging between the constituent saccharide units leading to anhydro-cyclodextrins.
- Intermolecular bridging and generation of cyclodextrin dimers with the focus on short, single atom linkages between the macrocycles.

For both approaches, examples are detailed in Chapter 7, and the molecular structures of new intra- and intermolecularly bridged cyclodextrin derivatives are outlined.

## Synopsis

In the sequel, brief outlines are provided for each of the Chapters in this work. All details and the corresponding references are given in the original publications included after this summary in Chapter 1 - 9.

### 1. From Cyclodextrins to Amylose: Structures and Lipophilicity Patterns

Although cyclodextrins have been crystallized from a wide range of organic solvents (e.g. methanol, dimethylformamide, and dimethyl sulfoxide) and were characterized by the solid-state structures of the corresponding solvate hydrates, nitromethane, a standard organic solvent as well as a reagent, has not been reported to complex with  $\alpha$ -CD or any of the other cyclodextrins. In this context, suitable crystals for solid-state structural analysis were obtained by slow crystallization of  $\alpha$ -CD from a 9:1 water–nitromethane solution. In the crystal structure of the  $\alpha$ -CD – nitromethane pentahydrate complex, the comparatively unrestrained overall geometry of the  $\alpha$ -CD host is stabilized through an almost complete ring of O-2 $\cdots$ O-3

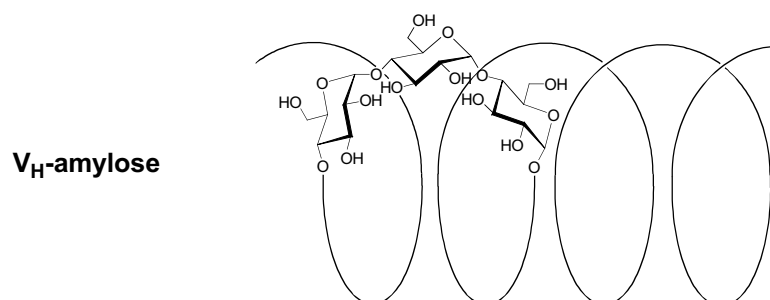
hydrogen bonds between five out of six adjacent glucose residues. The inclusion of nitromethane almost perpendicular to the molecular axis displays a counterbalance of hydrophobic effects and favorable antiparallel arrangement of dipoles, while the  $\alpha$ -CD cavity itself is large enough to allow for excessive thermal motions of the guest and rotation of the nitro group. The ready preparation of the complex, and the subtleties of its molecular structure clearly demonstrate the ease with which water is expelled from the  $\alpha$ -CD cavity by a co-solvent.

For details see Chapter 1, publication:

Topography of the 1:1  $\alpha$ -Cyclodextrin - Nitromethane Inclusion Complex.

T. Nakagawa, S. Immel, F. W. Lichtenthaler, and H. J. Lindner,  
*Carbohydr. Res.* **2000**, 324, 141-146.

A molecular modelling study on the A- and  $V_H$ -polymorphs of amylose based on fiber X-ray diffraction data was carried out, pointing out structural analogies to the cyclodextrins. Both amylose forms represent rod-shaped, left-handed helices of  $\alpha(1\rightarrow4)$ -linked D-glucose units. The A-form consists of parallel-stranded double helices with a pitch of approximately 21.4 Å; the structure of tightly twisted helices does not feature central cavities or channels that are accessible to the formation of inclusion complexes. On the other hand, the  $V_H$ -polymorph is made up of single helices with six glucose residues per turn and an average axial spacing of 8.05 Å per turn. In this respect, the structure of  $V_H$ -amylose strongly reminds that of  $\alpha$ -cyclodextrin with an average torus height of 8.1 Å, for both structures the inner cavity or channel displays a diameter of 5.0 – 5.5 Å.  $V_H$ -amylose does indeed form inclusion complexes with extended guest molecules such as fatty acids or long chain alcohols. In this study, the structure of the well-known, dark deep-blue colored iodine / iodide complex of amylose was compared to that of the corresponding complex formed by  $\alpha$ -cyclodextrin in the solid-state. Although both complexes are comparable in terms of cavity size and axial spacing, the alternating head-to-head and tail-to-tail arrangement of the  $\alpha$ -cyclodextrin units along a central axis results in distinctly different patterns in the distribution of the hydrophobicity regions on the surfaces of the molecular assemblies.



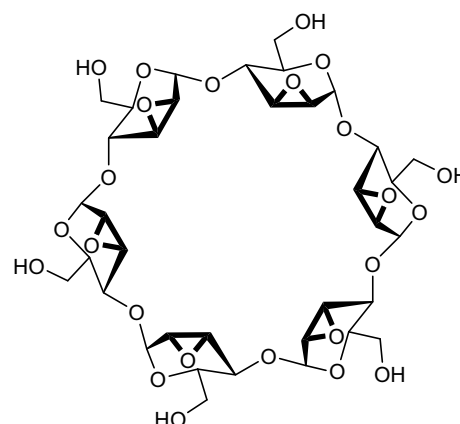
Based on molecular dynamics simulations in water, the structures of A-amylose are compared to structural motifs emerging in the solid-state structures of cyclodextrins with increasing ring size. Most notably, helical sub-structures with approximately six glucose units per turn seem to be the most predominant motif even in the geometries of the very large-ring cyclodextrins.

For details see Chapter 1, publication:

The Hydrophobic Topographies of Amylose and its Blue Iodine Complex.  
S. Immel and F. W. Lichtenthaler,  
*Starch/Stärke* **2000**, *52*, 1-8.

## 2. Per-2,3-anhydro- $\alpha$ -cyclomannin

The key-intermediate towards the synthesis of highly flexible cyclodextrin-derived artificial hosts turned out to be per-2,3-anhydro- $\alpha$ -cyclomannin. Chapter 2 details the straight forward synthesis of this compound starting from  $\alpha$ -cyclodextrin in three convenient steps: protection of the 6-CH<sub>2</sub>OH groups by *tert*-butyl-dimethylsilyl moieties is followed by one-step treatment with NaH / DMF and subsequent benzenesulfonation. This not only yields the selectively 2-O-sulfonated  $\alpha$ -cyclodextrin, but also concomitantly displaces the 2-sulfonyloxy groups by the vicinal 3-OH groups. Finally, deblocking of the primary hydroxyl groups yields the per-2,3-anhydro- $\alpha$ -cyclomannin in crystalline form and a total yield of about 48% over all steps. By precipitation from either aqueous ethanol or *n*-propanol, single crystals were obtained which allowed for an unequivocal structural characterization of this compound by X-ray crystal structure analysis. In each case, the corresponding ethanol or *n*-propanol complex was obtained in hydrated form. The macrocycles display an almost identical overall shape of approximate C<sub>6</sub> symmetry, resembling six-pointed stars with the epoxide rings being directed towards the outside of the cyclomannins, pointing away almost perpendicular from the central molecular axis. In both crystal structures, the arrangements of the macrocycles in an alternating head-to-head, tail-to-tail, and head-to-tail type fashion is almost identical. However, the mode with which the ethanol or *n*-propanol guest molecules are included differs significantly from each other: whereas two ethanol molecules form hydrogen-bonded dimers between two adjacent cavities of their hosts, the included *n*-propanol is hydrogen bonded to the 6-CH<sub>2</sub>OH of the cyclomannins, and its alkyl chain faces the hydrophobic chain of an adjacent *n*-propanol in the molecular stacks formed in the crystal lattice.



per-2,3-anhydro- $\alpha$ -cyclomannin

Most characteristically, by formation of the six anhydro (epoxide) rings from the altogether 12 secondary hydroxyl groups of  $\alpha$ -cyclodextrin, the distribution of hydrophilic and hydrophobic surface regions on the outside of both hosts is entirely reversed. Although the torus rim carrying the primary 6-OH groups of  $\alpha$ -cyclodextrin was less hydrophilic than the opposite rim made up by the secondary 2- and 3-OH groups, in the case of per-2,3-anhydro- $\alpha$ -cyclomannin this 6-CH<sub>2</sub>OH aperture is by far more hydrophilic; within this Chapter, consequences of this finding on the process of molecular recognition are discussed.

The synthesis of per-2,3-anhydro- $\alpha$ -cyclomannin not only provided the key-intermediate towards the efficient generation of highly flexible cyclodextrin-derived hosts – the cycloaltrins – but also for the first time the inclusion complexes of non-glucose cyclooligosaccharides have been obtained and unequivocally characterized by their solid-state structures.

For details see Chapter 2, publications:

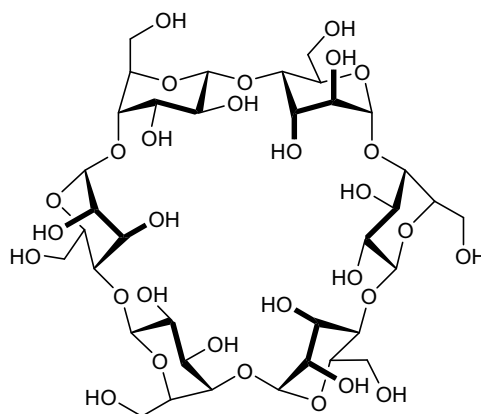
Structure and Lipophilicity Profile of 2,3-Anhydro- $\alpha$ -cyclomannin and its Ethanol Inclusion Complex.  
S. Immel, K. Fujita, H. J. Lindner, Y. Nogami, and F. W. Lichtenthaler,  
*Chem. Eur. J.* **2000**, 6, 2327-2333.

The 2,3-Anhydro- $\alpha$ -cyclomannin - 1-Propanol Hexahydrate: Topography, Lipophilicity Pattern, and Solid-state Architecture.

S. Immel, F. W. Lichtenthaler, H. J. Lindner, K. Fujita, M. Fukudome, and Y. Nogami,  
*Tetrahedron: Asymmetry* **2000**, 11, 27-36.

### 3. $\alpha$ -Cycloaltrin

With the synthesis of per-2,3-anhydro- $\alpha$ -cyclomannin, the first thoroughly flexible non-glucose cyclooligosaccharide  $\alpha$ -cycloaltrin became accessible through nucleophilic ring opening of all epoxide rings by water. The axial 2- and 3-OH groups of the constituent  $\alpha$ -D-altrose residues, as well as the axially disposed anomeric substituents leave these saccharide units highly flexible. Analysis of various solid-state structures of  $\alpha$ -D-altrose derivatives, as well as detailed molecular dynamics studies and free-energy calculations on this sugar unit in aqueous solution, provided evidence for both  ${}^4C_1$  and  ${}^1C_4$  conformations of  $\alpha$ -D-altrose having almost equal energies, and even intermediate  ${}^0S_2$  skew-boat geometries become energetically accessible. Based on NMR investigations on  $\alpha$ -cycloaltrin, neither of the above forms is realized exclusively, but surprisingly the chemically identical altrose residues adopt alternating arrangements of  ${}^4C_1$  and  ${}^1C_4$  structures in this macrocycle. Thus, the

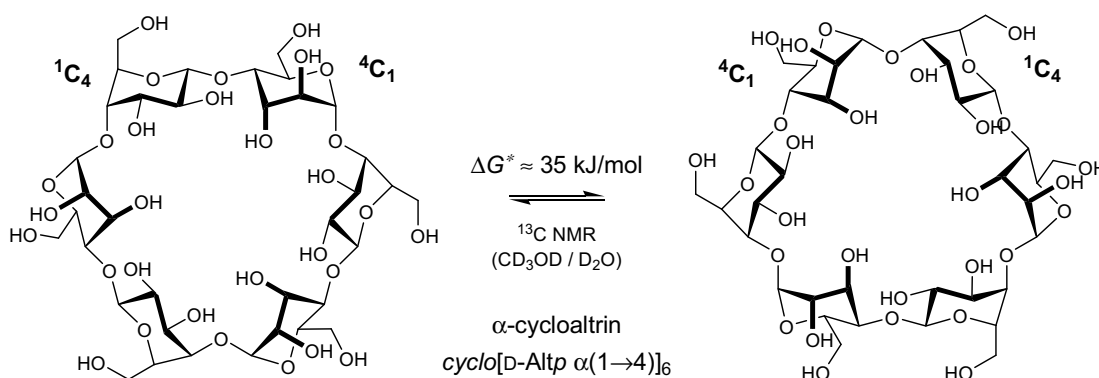


**$\alpha$ -cycloaltrin**

*cyclo*[D-Alt $\alpha$  (1 $\rightarrow$ 4)]<sub>6</sub>

shape of  $\alpha$ -cycloaltrin is reduced from  $C_6$  to  $C_3$  rotational symmetry only. The NMR data provided evidence for the intramolecular presence of multiple altrose conformers, but not for an equilibrium between structures of the all- ${}^4C_1$  and all- ${}^1C_4$  type.  $\alpha$ -Cycloaltrin displays dynamic exchange between  $[{}^4C_1 / {}^1C_4]_3$  and  $[{}^1C_4 / {}^4C_1]_3$  forms in (aqueous) solution with an activation barrier of approximately 35 kJ/mol at room temperature.

Molecular dynamics simulations on  $\alpha$ -cycloaltrin in solution, with additional constraints applied to certain torsion angles, shed some light on the mechanism of the process of conformational rearrangements: as one  $\alpha$ -D-altrose unit is forced to interconvert from a  ${}^4C_1$  into a  ${}^1C_4$  geometry via intermediate  ${}^0S_2 \leftrightarrow {}^3,0B$  forms, neighboring altrose residues engage in conformational transitions of the type  ${}^1C_4 \rightarrow {}^0S_2$ , too. Obviously, within the strait-jacket of the macrocyclic ring, the altrose can not be regarded separately, but conformational changes in any unit introduce rearrangements of the neighboring residues. In total, this process, once initiated, rolls around the macrocycle until finally all pyranose chair geometries are inverted. With this mechanism, the  $\alpha$ -cycloaltrin represents the first example of a highly flexible cyclooligosaccharide, for which conformational transitions result in a pseudorotational type behavior: conformational exchange results in structures which simply seem to have emerged from a rotation of the initial geometry around its central axis. In this work, further new and unique examples on pseudorotational phenomena in cyclooligosaccharides are described (see Chapter 5, the cyclofructins, and Chapter 6 on crown acetals and other flexible non-glucose cyclooligosaccharides).



The data on the solution conformation of  $\alpha$ -cycloaltrin is further substantiated by the unique crystal structure of this compound, which displays the alternating succession of the two different altrose conformations in the environment of water included in the crystal lattice. The molecular geometries of  $\alpha$ -cycloaltrin in the solid-state and in solution closely resemble each other, the heavily hydrated X-ray-derived geometry obviously represents a frozen snapshot geometry of the solution state. In both cases, the molecular surface of this host displays no central cavity, but it is fully closed at the 6- $\text{CH}_2\text{OH}$  side of the macrocycles.

On the basis of these findings,  $\alpha$ -cycloaltrin seemed not to be able to form inclusion complexes due to the lack of a central cavity. However, molecular dynamics simulations on  $\alpha$ -cycloaltrin indicate the flexibility of this compound, with conformations being accessible which have central cavities and torus like shapes resembling the cyclodextrins. Indeed, the  $K_{1:1}$  association constants of  $\alpha$ -cycloaltrin and its larger ring homologs  $\beta$ - and  $\gamma$ -cycloaltrin with various *para*-substituted sodium benzoates have been determined by capillary electrophoresis. The data shows the formation of weak inclusion complexes by the cycloaltrins, with lowered stability and less pronounced shape selectivity for the inclusion of guest molecules than is observed for the cyclodextrins. Obviously, the data reflects the entropic penalty to be paid for the formation of cycloaltrin conformers featuring a central cavity to include the guest molecules. The next Chapter provides additional data and first unequivocal evidence on the *induced-fit*-type inclusion complexation by a flexible cyclooligosaccharide.

For details see Chapter 3, publications:

Synthesis, Structure, and Conformational Features of  $\alpha$ -Cycloaltrin: a Cyclooligosaccharide with alternating  ${}^4C_1$  and  ${}^1C_4$  Pyranose Chairs.

Y. Nogami, K. Nasu, T. Koga, K. Ohta, K. Fujita, S. Immel, H. J. Lindner, G. E. Schmitt, and F. W. Lichtenthaler, *Angew. Chem.* **1997**, *109*, 1987-1991; *Angew. Chem. Int. Ed. Engl.* **1997**, *35*, 1899-1902.

Solution Geometries and Lipophilicity Patterns of  $\alpha$ -Cycloaltrin.

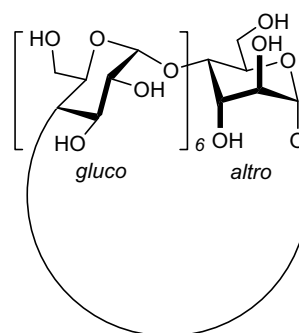
S. Immel, K. Fujita, and F. W. Lichtenthaler, *Chem. Eur. J.* **1999**, *5*, 3185-3192.

Inclusion Complexes of Cycloaltrins.

S. Immel, K. L. Larsen, *unpublished results*.

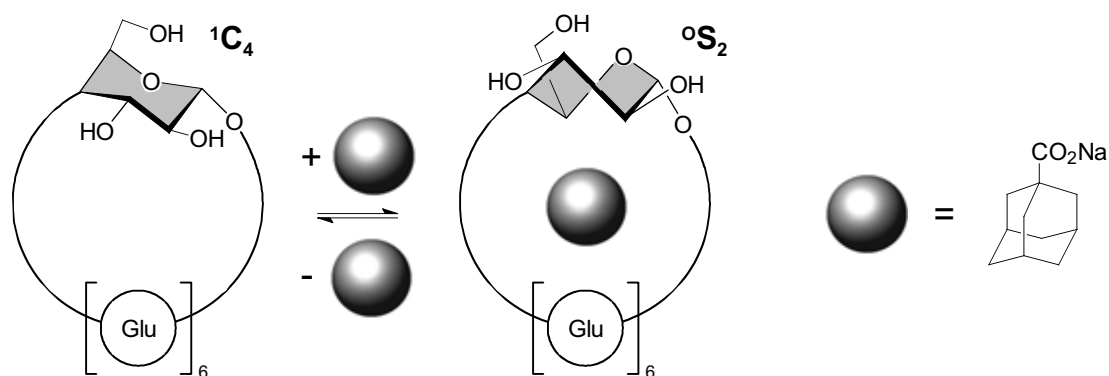
#### 4. Mono-*altro*- $\beta$ -cyclodextrin

Mono-*altro*- $\beta$ -cyclodextrin, accessible from  $\beta$ -cyclodextrin via configurational conversion of one of the glucose units into altrose, is shown to be a flexible host undergoing a distinct conformational change within its altropyranose geometry upon intracavity inclusion of adamantane-1-carboxylate. The detailed analysis of the  ${}^1H$  NMR spectra in  $D_2O$  at  $35^\circ C$ , and determination of all proton-proton coupling constants within the  $\alpha$ -D-altrose pyranoid ring upon titration of the host molecule with the adamantane guest reveals distinct changes in the coupling parameters. Correlation of the measured data with calculated coupling constants derived from molecular dynamics simulations on the host revealed evidence of a conformational transition of the altrose ring within the macrocycle upon inclusion complexation. In the free host, the altrose units preferably adopt a  ${}^1C_4$  chair geometry, whereas, in the complex, the conformational preferences are shifted towards the  ${}^0S_2$  skew-boat form.



**mono-*altro*- $\beta$ -cyclodextrin**

These results are further corroborated by a molecular dynamics and modelling study on the complex clearly revealing the cavity of the mono-*altro*- $\beta$ -cyclodextrin being most regularly round shaped in the case of the  ${}^{\circ}\text{S}_2$  altrose geometry in the macroring. Obviously, the conformational transition in this sugar unit is triggered by the incorporation of the ball-shaped adamantane guest upon entering the cavity to form the inclusion complex. However, the complex stability is significantly lower than the corresponding complex formed by  $\beta$ -cyclodextrin.



In this respect, mono-*altro*- $\beta$ -cyclodextrin represents the first example for the flexible *induced-fit*-type molecular recognition of guest molecules by a cyclooligosaccharide, rather than the rigid *lock-and-key*-type inclusion complexation common to the cyclodextrins.

For details see Chapter 4, publication:

Guest-induced Conformational Change in a Flexible Host: Mono-*altro*- $\beta$ -cyclodextrin.

K. Fujita, W.-H. Chen, D.-Q. Yuan, Y. Nogami, T. Koga, T. Fujioka, K. Mihashi, S. Immel, and F. W. Lichtenthaler, *Tetrahedron: Asymmetry* **1999**, *10*, 1689-1696.

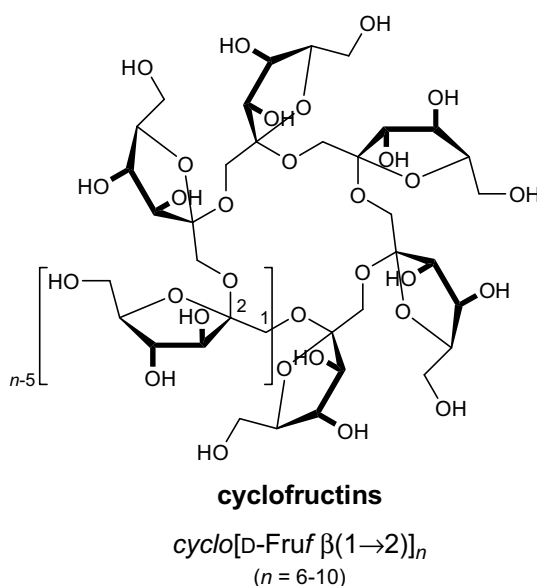
## 5. Cyclofructins and Cyclogalactofuranosides

The comparatively rigid pyranoid units of the amylose-derived cyclodextrins are contrasted by furanoid monosaccharides which contain a certain degree of an inherent flexibility, and cyclooligosaccharides composed thereof should portray this flexibility in their molecular recognition patterns. In this context, cyclofructins and some cyclogalactofuranosides (see below) have been subjected to a molecular modelling study to assess their structures, geometries, and potential for inclusion complexation.

Cyclofructins derived from inulin with six ( $\text{CF}_6$ ) to ten ( $\text{CF}_{10}$ )  $\beta(1\rightarrow2)$ -linked fructofuranose units were analyzed using molecular dynamics and *Monte-Carlo* simulations. It turned out, that the *spiro*-type anellation of fructofuranoses to a crown ether-type macrocyclic backbone renders these compounds highly flexible, although

some significant and unique conformational trends are retained for the entire series of ring size homologs: none of the cyclofructins retains full rotational symmetry, but in all cases the molecular symmetry is partially broken by an alternating inclination (“up” or “down”) of furanoid units in relation to the macroring.

The discontinuous arrangement of the sugar units substantially lowers the strain energy of the cyclofructins, the energy-minimum geometries of CF<sub>6</sub>, CF<sub>8</sub>, and CF<sub>10</sub> exhibit  $C_{n/2}$  rotational symmetry, while the odd-membered macrocycles, CF<sub>7</sub> and CF<sub>9</sub>, adopt  $C_1$  symmetry. Evidence for the relevance of the geometries obtained is derived from comparisons with the solid-state geometry of CF<sub>6</sub>. Most notably, the cyclofructins represent another example of a cyclooligosaccharide with flexible units (or flexible linkages between the individual residues) displaying the conformational



phenomenon of pseudorotation: structural rearrangements result in structures which appear to be rotated initial states only. Other examples along this vein are described in Chapter 3 (→ cycloaltrins) and Chapter 6 (→ crown acetals) of this work.

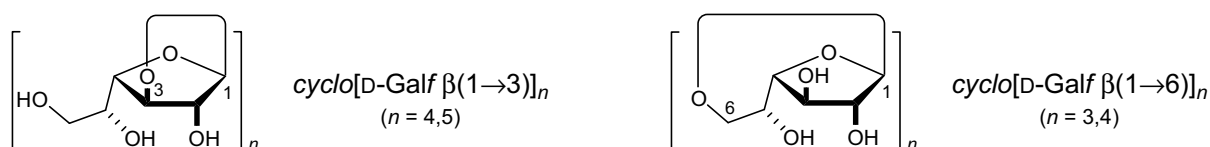
The molecular geometries and surfaces calculated for the energy-minimum structures establish a disk-type shape for CF<sub>6</sub>, CF<sub>7</sub>, and CF<sub>8</sub>, whereas further ring enlargement to CF<sub>9</sub> and CF<sub>10</sub> leads to torus-shaped molecules with through-going cavities. Surface mapping of molecular lipophilicity patterns (MLPs) and the electrostatic potential profiles (MEPs) revealed crown ether-like properties of the cyclofructins, and a high potential for the complexation of metal cations. Both CF<sub>9</sub> and CF<sub>10</sub> display significantly hydrophobic central cavities accessible for the formation of inclusion complexes; studies towards the molecular recognition and inclusion of amino acids are described along with hydrophobic as well as electrostatic interactions in the complexes.

For details see Chapter 5, publication:

Cyclofructins with Six to Ten β(1→2)-linked Fructofuranose Units: Geometries, Electrostatic Profiles, Lipophilicity Patterns, and Potential for Inclusion Complex Formation.  
S. Immel, G. E. Schmitt, and F. W. Lichtenthaler,  
*Carbohydr. Res.* **1998**, 313, 91-105.



As demonstrated for the cyclofructins, furanoid rings display a higher pseudorotational mobility than their pyranoid counterparts, and cyclooligosaccharides composed of furanoid sugar units are apt to be more flexible in their macrocycle. The same applies to the synthetically accessible cyclogalactins composed of  $\beta(1\rightarrow3)$ - and  $\beta(1\rightarrow6)$ -linked galactofuranose units which are likely to represent highly flexible host molecules for the *induced-fit*-type molecular recognition of potential guest molecules. Due to the rather modest yields in their preparation, the molecular geometries of the cyclogalactofuranosides composed of  $\beta(1\rightarrow3)$ - and  $\beta(1\rightarrow6)$ -linked galactofuranose units, i.e. *cyclo*[D-Galf  $\beta(1\rightarrow3)$ ]<sub>n</sub> with  $n = 4$  and  $5$ , and *cyclo*[D-Galf  $\beta(1\rightarrow6)$ ]<sub>n</sub> with  $n = 3$  and  $4$ , and their capabilities to form inclusion complexes were investigated by means of molecular dynamics and *Monte-Carlo* simulations. The latter compounds feature a significantly increased degree of flexibility, not the last due the larger number of atoms contained in the intersaccharidic linkages.



### cyclogalactofuranosides

The flexibility of the macrocyclic backbone strongly favors bent and asymmetrical conformations over round geometries. Generation of the molecular surfaces of the global energy-minimum structures reveal disk-type shapes for these hosts without through-going central cavities, yet distinct indentations close to the O-2/O-3-groups, respectively. The molecular lipophilicity patterns prove these surface dents to be hydrophobic for the  $\beta(1\rightarrow6)$ -linked cyclogalactins, whereas their  $\beta(1\rightarrow3)$ -linked counterparts display an inverse situation with a hydrophobic outer core structure.

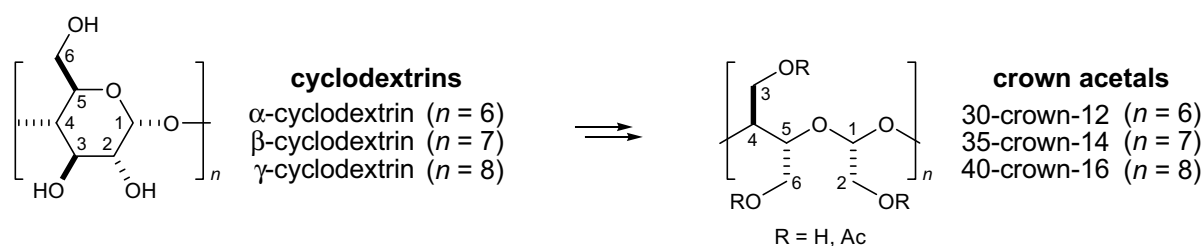
For details see Chapter 5, publication:

Conformations and Lipophilicity Profiles of some Cyclic  $\beta(1\rightarrow3)$ - and  $\beta(1\rightarrow6)$ -linked Oligogalactofuranosides.  
 H. Gohlke, S. Immel, and F. W. Lichtenthaler,  
*Carbohydr. Res.* **1999**, 321, 96-104.

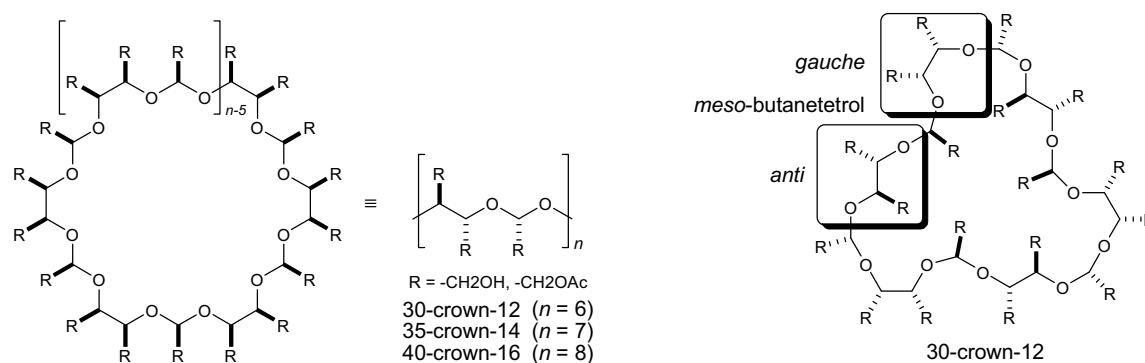
## 6. Cyclodextrin-derived Crown Acetals

An entirely different approach towards the generation of flexible macrocyclic hosts is demonstrated by the synthesis of cyclodextrin-derived crown acetals. Unlike crown ethers which have played a pivotal role in the development and understanding of supramolecular chemistry, cyclic compounds containing exclusively acetal oxygen atoms are rare and only a few examples have been reported so far; macrocycles of this type – as of now – are utter curiosities, and no attempts have been made previously to elucidate their structures and molecular geometries. A highly efficient

route towards the preparation of macrocyclic crown acetals derived from cyclodextrins is presented by the periodate oxidation and cleavage of the C-2 / C-3 bonds of the glucose residues: periodation, in situ reduction of the resulting polyaldehydes, and subsequent per-O-acetylation afforded macrocyclic polyhydroxymethylene and poly-acetoxymethylene substituted macrorings as crystalline compounds in over-all yields of about 90%. Starting from  $\alpha$ -,  $\beta$ -, and  $\gamma$ -cyclodextrins, the crown acetals of the 30-crown-12, 35-crown-14, and 40-crown-16 type were obtained. The macrorings are made up from six, seven, and eight alternating *meso*-butanetetrol and glycolaldehyde units, and thus represent achiral compounds.

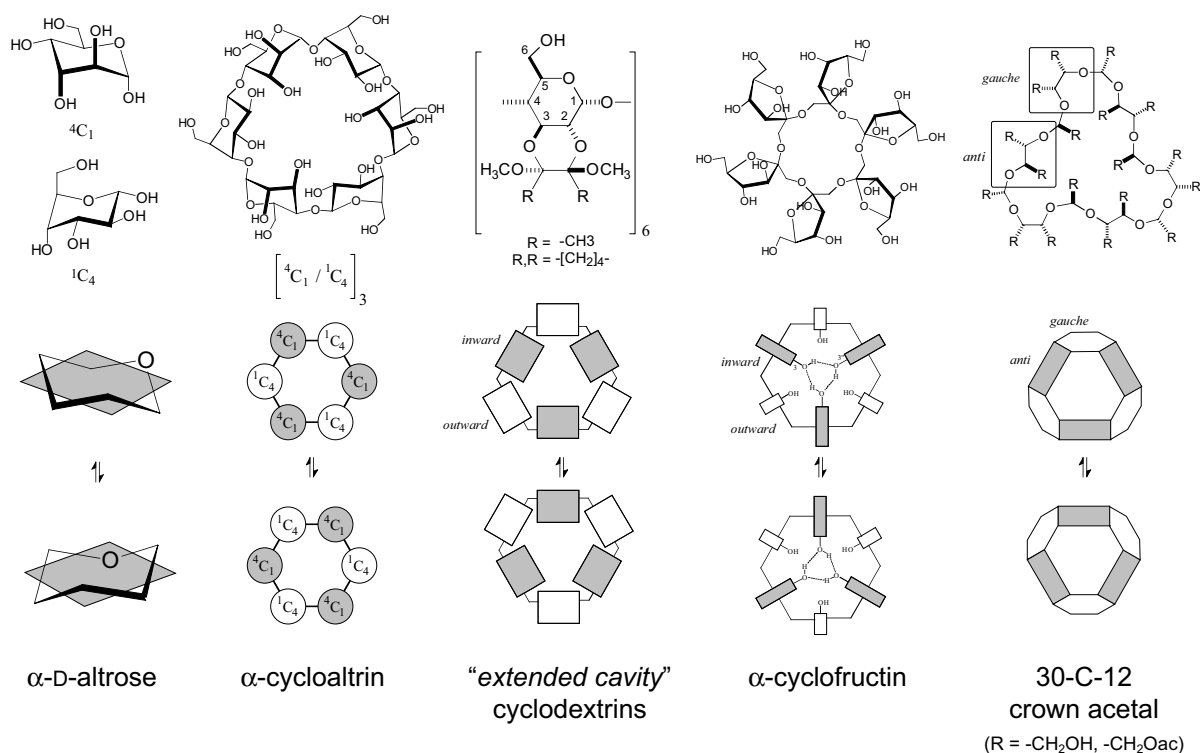


Although these large-ring crown acetals are anticipated to be highly flexible in solution, detailed temperature dependent NMR analysis revealed them to be less flexible than expected: at low temperatures, two signal sets are observed for the ring protons, revealing asymmetric conformations to be predominant in solution. These results are fully corroborated by the X-ray-derived solid-state structures of all polyacetoxymethylene 30-crown-12, 35-crown-14, and 40-crown-16 acetals. In the crystalline state as well as in solution these macrorings preferentially adopt less symmetric conformations through an alternating succession of *gauche* and *anti* geometries of the constituent *meso*-butanetetrol residues. Conformational exchange occurs with an activation barrier of about  $\Delta G^\ddagger \approx 60$  kJ/mol for the 30-crown-12 hexaacetal, the 40-crown-16 octaacetals appears to be even more flexible. However, the odd-membered  $\beta$ -cyclodextrin-derived 35-crown-14 heptaacetals represents the most flexible ring within this series of ring homologs.



With these results, not only is it the first time that the structures and molecular geometries of very large-ring crown acetals have been unraveled and reported in detail, but the crown acetals also provide another vivid example of the phenomenon

of pseudorotation in large-ring macrocycles and cyclooligosaccharides: breaking the symmetry of the rings reduces their strain energy, and conformational rearrangements of chemically equivalent, yet, geometrically distinctly different subunits results in dynamic exchange processes. In all cases – i.e. for the cycloaltrins (Chapter 3), cyclofructins (Chapter 5), and the crown acetals (this Chapter) – the symmetry of the ring structures is halved, and even-membered rings appear to be less flexible than their next lower and higher odd-membered homologs.



The last original publication provided in this Chapter lists the "extended cavity" cyclodextrins as an additional example of cyclooligosaccharides displaying the phenomenon of pseudorotation.

For details see Chapter 6, publications:

Synthesis and Molecular Geometry of an Achiral 30-Crown-12 Polyacetal from  $\alpha$ -Cyclodextrin.  
S. Immel, T. Nakagawa, H. J. Lindner, and F. W. Lichtenthaler,  
*Chem. Eur. J.* **2000**, *6*, 3366-3371.

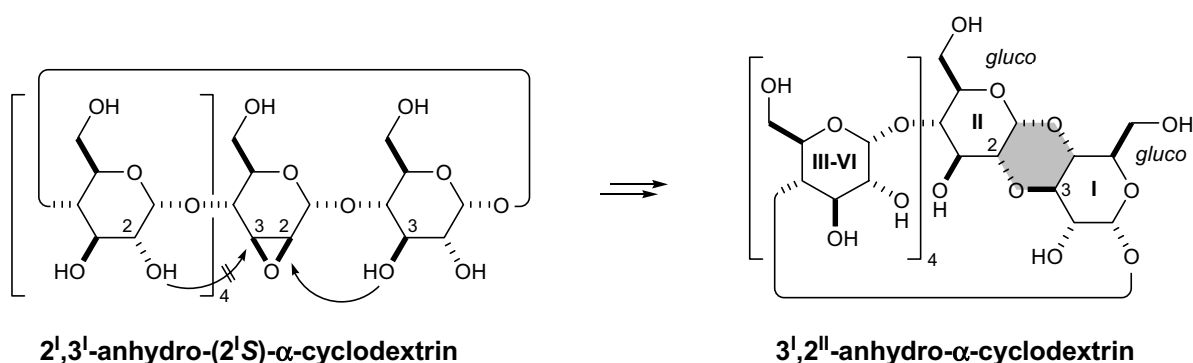
Hydroxymethyl-substituted Crown Acetals with 35-C-14 and 40-C-16 Skeletal Backbones:  
Synthesis and Molecular Geometries.  
S. Immel, F. W. Lichtenthaler, H. J. Lindner, and T. Nakagawa,  
*Tetrahedron: Asymmetry* **2001**, *12*, 2767-2774.

Large-ring Crown Acetals from Cyclodextrins.  
T. Nakagawa, S. Immel, H. J. Lindner, and F. W. Lichtenthaler,  
*Proc. 10<sup>th</sup> Int. Symp. Cyclodextrins* (Ed.: J. Szejtli), Mia Digital Publ., Ann Arbor, Michigan, **2000**, pp. 18-23.

Flexible Non-glucose Cyclooligosaccharides.  
S. Immel,  
*Proc. 10<sup>th</sup> Int. Symp. Cyclodextrins* (Ed.: J. Szejtli), Mia Digital Publ., Ann Arbor, Michigan, **2000**, pp. 24-31.

## 7. Rigidified Bridged Cyclodextrins

The introduction of flexibility into the cyclodextrins described so far, is opposed by the approach to increase the rigidity of the macrocycles through intramolecular bridging between the glucose residues. Although regioselective epoxide ring opening of 2<sup>1</sup>,3<sup>1</sup>-(2<sup>1</sup>S)-anhydro- $\alpha$ -cyclodextrin through intramolecular attack of neighboring hydroxyl groups is expected to occur in the usual diaxial fashion to yield the *altro*-configured product, the diequatorial ring opening is observed exclusively. This approach yields 3<sup>1</sup>,2<sup>11</sup>-anhydro- $\alpha$ -cyclodextrin with a rigid glucopyranose-dioxane-glucopyranose tricyclic ring system incorporated into the backbone of the macrocycle.



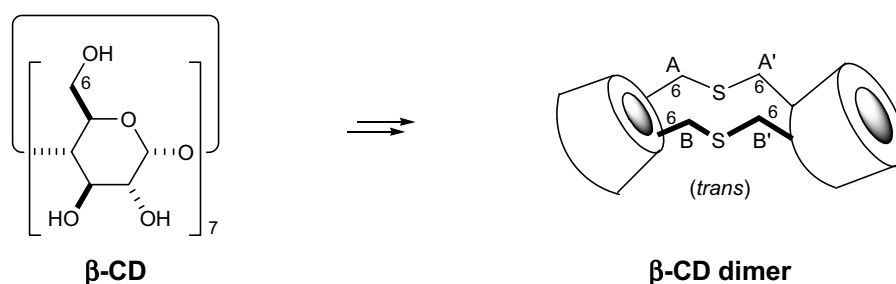
Molecular dynamics simulations in water were used to analyze the conformations of 2<sup>1</sup>,3<sup>1</sup>-(2<sup>1</sup>S)-anhydro- $\alpha$ -cyclodextrin and both stereoisomers of the epoxide ring opening reaction. From these simulations, the observed *gluco*-configured product not only emerged as being thermodynamically more stable than the alternate *altro*-configured stereoisomer, but also being the favored product on geometrical considerations. Within the strait jacket of the macrocycle of 2<sup>1</sup>,3<sup>1</sup>-(2<sup>1</sup>S)-anhydro- $\alpha$ -cyclodextrin, the intramolecular distances between the epoxide ring carbons and the hydroxyl groups of the adjacent glucose units, as well as their angle of attack obviously favors the unusual mode of ring opening.

The solid-state structure of the 3<sup>1</sup>,2<sup>11</sup>-anhydro- $\alpha$ -cyclodextrin · 3 *n*-PrOH nonahydrate complex displays an inverted concavity of the macroring compared to the parent  $\alpha$ -cyclodextrin, caused by contraction of the 2,3-OH side of the torus. In the environment of the crystal lattice, the three *n*-propanol molecules are distributed in the cavity of a dimeric unit of the host. Based on comparisons of the crystal structure with molecular dynamics simulations of this compound in water, the cyclodextrin derivative undergoes no significant conformational changes upon dissolution.

For details see Chapter 7, publication:

Two Stereoisomeric 3<sup>1</sup>,2<sup>11</sup>-Anhydro- $\alpha$ -cyclodextrins: A Molecular Dynamics and Crystallographic Study.  
S. Immel, K. Fujita, M. Fukudome, and M. Bolte,  
*Carbohydr. Res.* **2001**, 336, 297-308.

In addition to the intramolecular bridging of cyclodextrins described above, intermolecular bridging represents an appropriate approach towards rigidified cyclodextrin dimers with extended cavities. Although cyclodextrin dimers and oligomers have been studied in the past, this work focuses on the option to introduce the shortest possible single-atom linkages between individual cyclodextrin units. In this context,  $\beta$ -cyclodextrin is transannularly disulfonylated at the  $6^A$ - and  $6^B$ -positions, and then converted to the corresponding  $6^A,6^B$ -diiodide and  $6^A,6^B$ -dithiol. Cross-coupling of the latter two species yields a single head-to-head coupled  $\beta$ -cyclodextrin dimer with two sulfur-linkers at adjacent 6-methylene carbons. Although this approach is likely to yield two stereoisomeric *cis*- and *trans*-coupled cyclodextrin dimers differing in the orientation of the macro rings relative to each other, only the latter *trans*-type (“*aversive*”) linked product was observed and obtained in crystalline form.



NMR and X-ray analysis unequivocally revealed the type of linkage between both  $\beta$ -cyclodextrin rings in the new dimeric structure. For the first time, the solid-state structure of such a bridged cyclodextrin has been solved in the form of its hydrated methanol inclusion complex. The rather undistorted macrocycles feature almost parallel ring planes pointing away from each other, leaving the dimer with a “handcuff”-like appearance of approximate  $C_2$  symmetry, the rotational axis of symmetry passing through the hexagon described by the  $6^A$ -C-S- $6^{A'}$ -C and  $6^B$ -C-S- $6^{B'}$ -C atoms. This “dimeric” host opens up the possibility to specifically form inclusion complexes with potential guest molecules of 1 : 2 stoichiometry. Moreover, the rather rigid linkage of this host molecule with two separated cavities may allow to study included guest molecules and their long-range interactions at well-defined distances.

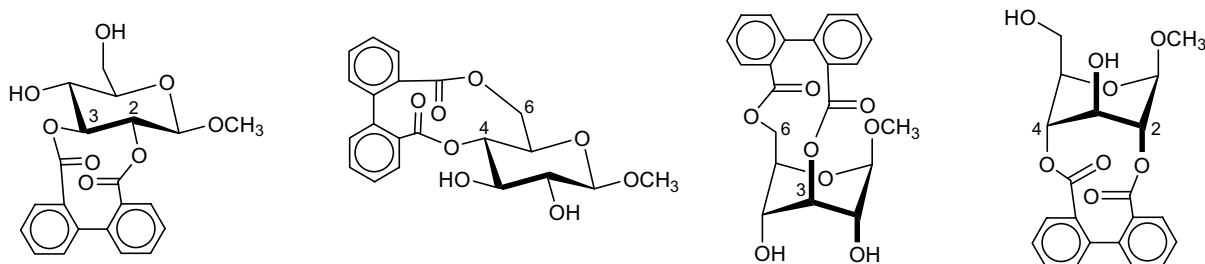
For details see Chapter 7, publication:

The First Successful Crystallographic Characterization of a Cyclodextrin Dimer: Efficient Synthesis and Molecular Geometry of a Doubly Sulfur-bridged  $\beta$ -Cyclodextrin.  
D.-Q. Yuan, S. Immel, K. Koga, M. Yamaguchi, and K. Fujita,  
*Chem. Eur. J.* **2003**, *9*, 3501-3506.

## 8. Molecular Modelling of Saccharides

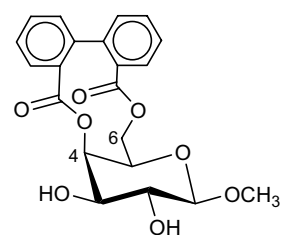
This Chapter describes molecular modelling studies on various saccharides not related to the concept of creating more flexible or rigidified molecular host-guest systems. However, the studies presented are of interest for evaluating the chemical, stereochemical, conformational as well as biological properties of low-molecular weight saccharides.

Ellagitannins represent a class of polyphenolic natural products contained in higher plants, their common structural element being hexahydroxydiphenoyl (HHDP) substituted  $\beta$ -D-glucopyranosides with varying substitution patterns, and these tannin-components exhibit a broad range of biological activities. The axially chiral diphenoyl units occur with specific configurations depending on the positions of attachment. In order to evaluate the effects determining the mode of chirality, a number of model compounds such as methyl 2,3-, 4,6-, 3,6-, and 2,4-*O*-diphenoyl  $\beta$ -D-glucopyranosides were subjected to a molecular modelling study; for comparison the corresponding non-natural 4,6-*O*-diphenoyl  $\beta$ -D-galactoside was included in this work.



**methyl *O*-diphenoyl- $\beta$ -D-glucosides**

On the basis of molecular mechanics and dynamics simulations, the 10- to 12-membered rings containing the diphenoyl residues are far less flexible than expected: the rather rigid ester linkages transfer the chiral information of the saccharide units specifically into the diphenoyl units, the chiral scaffold of the saccharides exerts a strong atropdiastereoselective effect onto the diphenoyl moieties. For the 2,3- and 4,6-*O*-diphenoyl bridged glucosides the (*S*)-diphenoyl configuration is energetically highly preferred, whereas for the 3,6- and 2,4-*O*-linked diphenoyl glucosides the opposite (*R*)-configuration is favored. All the results are in full accord with the absolute configurations found in the natural products, and thus provide explanations for the observed chirality on the basis of geometrical reasons. Notably, for the



**methyl 4,6-*O*-diphenoyl- $\beta$ -D-galactoside**

unknown 4,6-*O*-diphenoyl galactoside this effect is reversed, and the (*R*)-form is proposed to be more stable.

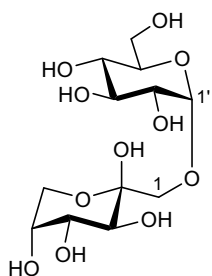
For details see Chapter 8, publication:

Atropidiastereoisomers of Ellagitannin Model Compounds: Configuration, Conformation, and Relative Stability of *D*-Glucose Diphenoyl Derivatives.

S. Immel, K. Khanbabaee,

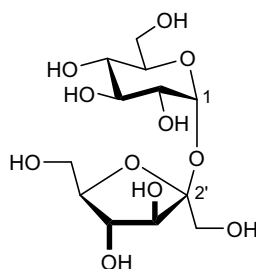
*Tetrahedron: Asymmetry* **2000**, *11*, 2495-2507.

*Klebsiella pneumoniae* – the first bacterial species identified in this respect – and *Fusobacterium mortiferum* utilize not only sucrose (*D*-fructofuranosyl- $\beta$ (2 $\leftrightarrow$ 1)  $\alpha$ -*D*-glucopyranoside), but also its five linkage-isomeric  $\alpha$ -*D*-glucosyl-*D*-fructoses trehalulose  $\alpha$ (1 $\rightarrow$ 1), turanose  $\alpha$ (1 $\rightarrow$ 3), maltulose  $\alpha$ (1 $\rightarrow$ 4), leucrose  $\alpha$ (1 $\rightarrow$ 5), and palatinose  $\alpha$ (1 $\rightarrow$ 6) as energy sources. Growth on the sucrose isomers induced the expression of proteins identified as an NAD<sup>+</sup> and metal ion-dependent 6-phospho- $\alpha$ -glucosidases not present in sucrose-grown cells; the corresponding genes have been identified, cloned, expressed, and characterized. The enzymes catalyzed the hydrolysis of a wide variety of 6-phospho- $\alpha$ -glucosides including the above sucrose isomers, but not sucrose 6-phosphate itself.



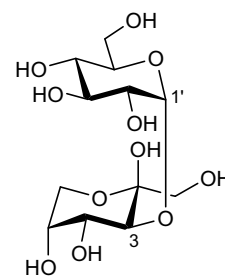
**$\beta$ -*p*-Trehalulose**

$\alpha$ -*D*-Glc $p$ -(1 $\rightarrow$ 1)-  
 $\beta$ -*D*-Fru $p$



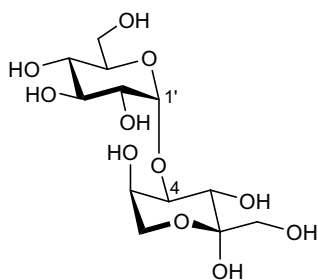
**Sucrose**

$\beta$ -*D*-Fru $f$ -(2 $\leftrightarrow$ 1)-  
 $\alpha$ -*D*-Glu $p$



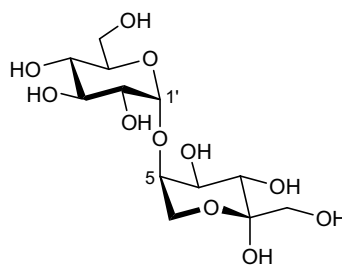
**$\beta$ -*p*-Turanose**

$\alpha$ -*D*-Glc $p$ -(1 $\rightarrow$ 3)-  
 $\beta$ -*D*-Fru $p$



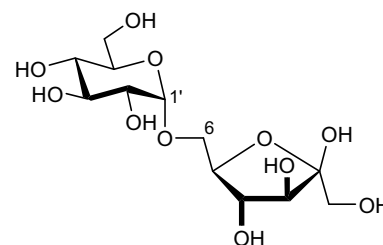
**$\beta$ -*p*-Maltulose**

$\alpha$ -*D*-Glc $p$ -(1 $\rightarrow$ 4)-  
 $\beta$ -*D*-Fru $p$



**$\beta$ -*p*-Leucrose**

$\alpha$ -*D*-Glc $p$ -(1 $\rightarrow$ 5)-  
 $\beta$ -*D*-Fru $p$



**$\beta$ -*f*-Palatinose**

$\alpha$ -*D*-Glc $p$ -(1 $\rightarrow$ 6)-  
 $\beta$ -*D*-Fru $f$

Based on conformational analysis and molecular dynamics simulations of the six disaccharides and their glucosyl 6-phosphates in aqueous solution, significant differences in molecular shape and lipophilicity potential between sucrose and its isomers have been identified. The results explain the enzymatic differences in selectivity on the basis of the substrate properties.

For details see Chapter 8, publications:

Metabolism of Sucrose and Its Five Linkage-isomeric  $\alpha$ -D-Glucosyl-D-fructoses by *Klebsiella pneumoniae*.  
J. Thompson, S. A. Robrish, S. Immel, F. W. Lichtenthaler, B. G. Hall, and A. Pikis,  
*J. Biol. Chem.* **2001**, 276, 37415-37425.

Metabolism of Sucrose and Its Five  $\alpha$ -D-Glucosyl-D-fructose Isomers by *Fusobacterium mortiferum*.  
A. Pikis, S. Immel, S. A. Robrish, and J. Thompson,  
*Microbiology* **2002**, 148, 843-852.

## 9. Molecular Graphics

All molecular graphics contained within this work have been generated using the self-written *Molecular Architecture Modelling Program MolArch<sup>+</sup>*. This program was developed for the purpose of simple automated analysis and 3D fitting of molecular structures, calculation of numerous geometry parameters, as well as providing the possibility to visualize organic and inorganic structures with different modes (wire models, capped-sticks, ball-and-stick models, CPK-type models). Solid-state crystal structures and packings (including thermal anisotropic ellipsoids and Hirshfeld surfaces), coordination polyhedra, molecular orbitals and surfaces with color-coded mapped properties, 3D grid and density data, and ribbon models of arbitrary (including non-protein) structures can be represented. Options are included to generate molecular animations for sets of molecular configurations along reaction coordinates or molecular dynamics simulations. *MolArch<sup>+</sup>* is fully interfaced to import and export a large variety of different file formats, and to produce high-quality color models with the *POVRAY* (“*Persistence of Vision*”) ray-tracing program or any *VRML* (“*Virtual Reality Modelling Language*”) viewing program. Chapter 9 gives an overview on the unique options provided by the *MolArch<sup>+</sup>* software.

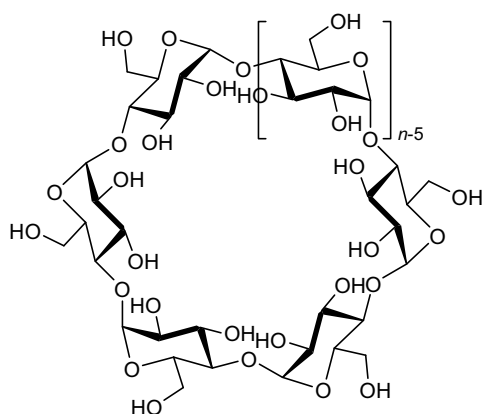
For details see Chapter 9:

*MolArch<sup>+</sup>* - *Molecular Architecture Modelling Program*.  
S. Immel,  
<http://caramel.oc.chemie.tu-darmstadt.de/immel/>.

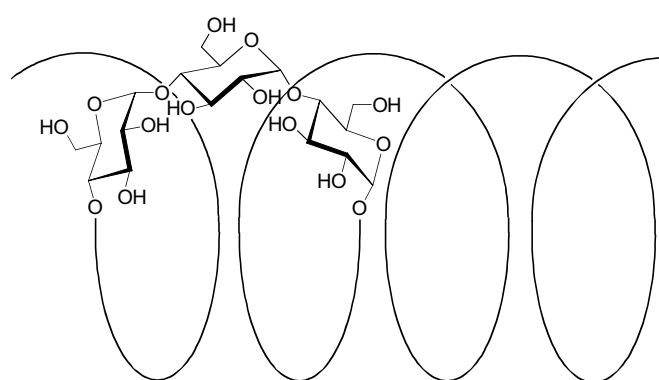


## Chapter 1

### From Cyclodextrins to Amylose: Structures and Lipophilicity Patterns



**cyclodextrins**



**V<sub>H</sub>-amylose**

#### Topography of the 1:1 $\alpha$ -Cyclodextrin - Nitromethane Inclusion Complex

T. Nakagawa, S. Immel, F. W. Lichtenthaler, and H. J. Lindner,  
*Carbohydr. Res.* **2000**, 324, 141-146.

#### The Hydrophobic Topographies of Amylose and its Blue Iodine Complex

S. Immel and F. W. Lichtenthaler,  
*Starch/Stärke* **2000**, 52, 1-8.





www.elsevier.nl/locate/carres

Carbohydrate Research 324 (2000) 141–146

CARBOHYDRATE  
RESEARCH

Note

# Topography of the 1:1 $\alpha$ -cyclodextrin–nitromethane inclusion complex<sup>☆</sup>

Toshio Nakagawa, Stefan Immel, Frieder W. Lichtenthaler\*, Hans J. Lindner

*Institut für Organische Chemie, Technische Universität Darmstadt, Petersenstraße 22, D-64287 Darmstadt, Germany*

Received 23 August 1999; accepted 12 October 1999

## Abstract

Dissolution of  $\alpha$ -cyclodextrin ( $\alpha$ -CD) in 9:1 water–nitromethane smoothly generates the title compound, which crystallizes as the pentahydrate in the orthorhombic space group  $P2_12_12_1$  with  $a = 9.452(4)$ ,  $b = 14.299(3)$ ,  $c = 37.380(10)$  Å, and  $Z = 4$ . Its crystal structure analysis revealed the  $\alpha$ -CD macrocycle in an unstrained conformation stabilized through a ring of O-2 $\cdots$ O-3' hydrogen bonds between five of the six adjacent glucose residues. The nitromethane is located in the  $\alpha$ -CD cavity in an orientation parallel to the plane of the macrocycle, and assumes two sites of equal population with the nitro group in excessive thermal motion; the guest is held by van der Waals contacts and C-H $\cdots$ O-type hydrogen bonds to the pyranose H-3 and H-5 protons. The packing of the macrocycles in the crystal lattice is of cage herringbone-type with an extensive intra- and intermolecular hydrogen bonding network. The ready formation of a nitromethane inclusion complex in aqueous nitromethane, and the subtleties of its molecular structure amply demonstrate the ease with which water is expelled from the  $\alpha$ -CD cavity by a more hydrophobic co-solvent. © 2000 Elsevier Science Ltd. All rights reserved.

*Keywords:*  $\alpha$ -Cyclodextrin; Nitromethane inclusion complex

## 1. Introduction

Various small organic molecules have been shown to be readily included into the apolar cavity of  $\alpha$ -cyclodextrin ( $\alpha$ -CD, Scheme 1), such as methanol [2], dimethylformamide [3], and dimethyl sulfoxide [4], and their topographies have been thoroughly characterized by solid-state structures. Surprisingly, nitromethane, a standard solvent as well as a

reagent, has not been reported to complex with  $\alpha$ -CD or any of the other cyclodextrins [5,6]. Here we report on the ready preparation of a 1:1  $\alpha$ -CD–CH<sub>3</sub>NO<sub>2</sub> inclusion complex (**1**) and its topography on its X-ray based structure.

## 2. Results and discussion

The atomic numbering scheme and the molecular structure of the  $\alpha$ -CD–nitromethane inclusion complex (**1**) are shown in Scheme 1 and Fig. 1; some averaged geometric parameters are listed in Table 1. The nitromethane is incorporated into the central cavity of the torus-shaped  $\alpha$ -CD, and five

<sup>☆</sup> Molecular modeling of saccharides, Part 23. For Part 22, see Ref. [1].

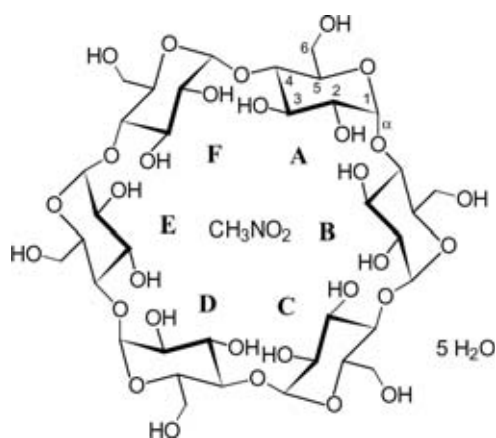
\* Corresponding author. Tel.: +49-61-5116-2376; fax: +49-61-5116-6674.

E-mail address: fwlicht@sugar.oc.chemie.tu-darmstadt.de (F.W. Lichtenthaler)

water molecules occupy interstitial positions between the CD macrocycles in the crystal lattice. The CD macrocycles are arranged in a typical herringbone-type pattern in the crystal environment (space group  $P2_12_12_1$ , views along the  $a$  and  $b$  axis are given in Fig. 2), as is, for example, also found in the three  $\alpha$ -CD hydrate solid-state structures [7–9].

**Conformation of the macrocycle.**—As indicated by the intersaccharidic  $\Phi/\Psi$  torsion angles (cf. Table 1) and their rather small fluctuations, the  $\alpha$ -CD macrocycle in **1** adopts its usual conical shape similar to the one realized in a large variety of related complexes [6,10,11]. The mean tilt angle  $\tau$  [11,12] of the glucose units in relation to the macroring displays a slight rotation of the pyranoses with their 6-OH sides towards the center of the molecule (i.e.,  $\tau > 90^\circ$ ), leaving the opposite 2-OH/3-OH face as the wider opening of the torus. All the 6-CH<sub>2</sub>OH groups point away from the central axis of **1** ( $gg$  arrangements,  $\omega \approx -70^\circ$ ). The glucose units are in the rather rigid  ${}^4C_1$  conformation with standard ring torsion angles  $\theta_1 - \theta_6$  around  $\pm 55^\circ$ , and with typical Cremer–Pople ring puckering parameters [13,14]. The intersaccharidic O-1 atoms are fairly coplanar (RMS deviation of only 0.06 Å from the common least-squares plane) and form a symmetrical hexagon with nearly identical diagonal distances of  $8.45 \pm 0.2$  Å.

**Hydrogen bonding.**—The comparatively unrestrained overall geometry of the  $\alpha$ -CD host



Scheme 1.  $\alpha$ -Cyclodextrin–nitromethane inclusion complex (**1**); the  $\alpha$ -(1  $\rightarrow$  4)-linked glucose units are labeled A–F.

is stabilized through an almost complete ring of O-2 $\cdots$ O-3' hydrogen bonds between five out of six adjacent glucose residues (cf. Fig. 3 and Table 2, hydrogen bonds labeled 1–5); and no other intramolecular hydrogen bonds are formed. However, the solid-state geometry displays an extensive three-dimensional hydrogen-bonding network between the  $\alpha$ -CD, the five water molecules of crystallization (Table 2, entries 6–11), and the symmetry-related molecules in the crystal lattice (entries 12–30) as is usually observed for carbohydrate crystal structures [15]. All hydroxyl groups satisfy their hydrogen-bonding requirements through formation of two to three H-bonds, and all water molecules are involved in three to four H-bonds.

**Geometry of the nitromethane inclusion.**—The nitromethane molecule is located in the void of the  $\alpha$ -CD macrocycle, with the methyl group being disordered over two sites with equal (50%) occupancy (Fig. 1), whereas the corresponding two nitrogen positions coincide in one fully occupied site. The oxygen atoms of the guest display excessive thermal motions (Fig. 1), indicating that the NO<sub>2</sub> group is statistically disordered; refinement of the structure was approximated by six positions over which the two oxygens are distributed (33% occupancy of each site). Only four 'reasonable' (in terms of bond angles) oxygen sites are retained in the ball-and-stick type representation of the complex, given in Fig. 4, with the superimposed molecular contact surfaces [16] visualizing the steric fit between the host and guest molecule. Side-view cross-sectional cuts through these surfaces (Fig. 4, bottom) show both nitromethane sites to be shifted away from the center of the  $\alpha$ -CD torus towards the wider opening (i.e., the 2-OH/3-OH face). In either geometry, the nitromethane C–N bond points almost perpendicular away from the central axis of the complex. Obviously, the guest is held in the cavity by van der Waals contacts to a circular array of the pyranose hydrogens at C-3 and C-5. Although the NO<sub>2</sub> group is not involved in hydrogen bonds with the hydroxyl groups of the host, it does form hydrogen bonds of the O $\cdots$ H–C type to the C-3 and C-5 protons, respectively;

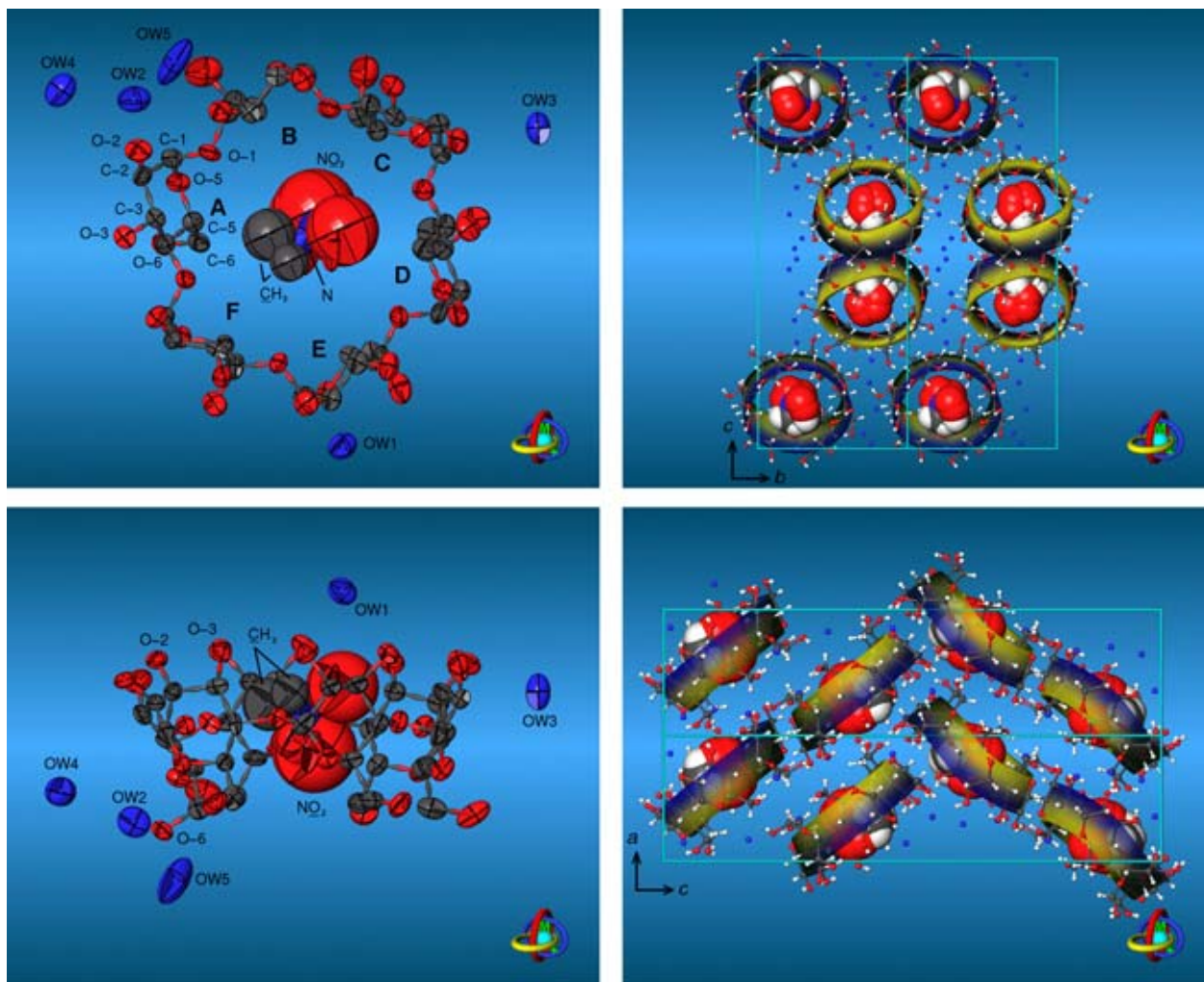


Fig. 1

Fig. 2

Fig. 1. Molecular structure of the asymmetric unit of the  $\alpha$ -CD–nitromethane inclusion complex (1) showing the heavy-atom 50% probability ellipsoids; hydrogens are omitted for clarity (gray, C; red, O; blue, nitrogen and water-oxygens). The glucose units of  $\alpha$ -CD are labeled A–F (cf. Scheme 1), and the water molecules located at interstitial positions outside the macrocycle are termed OW1–OW5. The nitromethane guest molecule shows excessive thermal motions and is disordered over two sites with equal occupancies; the statistical disordering of the  $\text{NO}_2$  oxygen atoms is approximated by six atomic positions.

Fig. 2. Ball-and-stick models of the herringbone-type molecular packing in the crystal structure of 1, as viewed down the  $a$  (top,  $1 \times 2 \times 1$  unit cells) and  $b$  axis (bottom,  $2 \times 1 \times 1$  cells). The  $\alpha$ -CD molecules are represented as solid colored ribbon models, whereby blue colors correspond to the 2-OH/3-OH side of the macrocycles, yellow colors to the 6-OH face. The disordered nitromethane molecules are visualized as CPK-models, and the unit cell boundaries are indicated by solid cyan lines.

for each  $\text{NO}_2$ -oxygen position the shortest  $\text{O} \cdots \text{H}-3$  and  $\text{O} \cdots \text{H}-5$  distances are in the range of 2.48–2.82 Å.

### 3. Conclusions

The solid-state structure of the  $\alpha$ -CD–nitromethane pentahydrate complex shows that the mode with which the guest molecule is incorporated into the cavity results from a balance of at least two effects contributing to

the stability of such assemblies; hydrophobic effects conceivably favor the hydrophobic methyl group pointing into the cavity, thereby leaving the nitro group to stick out of the  $\alpha$ -CD torus at the opposite, hydrophilic rim, whereas the antiparallel arrangement of dipoles of host and guest would lead to the opposite regioselectivity. The inclusion of nitromethane almost perpendicular to the molecular axis displays a counterbalance of these effects, while the  $\alpha$ -CD cavity itself is large enough to allow for excessive thermal

144

T. Nakagawa et al. / Carbohydrate Research 324 (2000) 141–146

Table 1

Selected geometric parameters (mean values averaged over all glucose units and root mean-square deviations) for the  $\alpha$ -CD macrocycle in **1**

<i>Intersaccharidic torsion angles</i> (°)	
$\Phi$ (O-5-C-1-O-1-C-4')	107.4 ± 4.8
$\Psi$ (C-1-O-1-C-4'-C-3')	129.4 ± 11.3
<i>Tilt angles</i>	
$\tau$ (°)	101.6 ± 9.3
<i>Pyranose torsion angles</i> (°)	
$\omega$ (O-5-C-5-C-6-O-6)	-68.8 ± 7.3
$\theta_1$ (O-5-C-1-C-2-C-3)	57.6 ± 2.3
$\theta_2$ (C-1-C-2-C-3-C-4)	-51.8 ± 2.7
$\theta_3$ (C-2-C-3-C-4-C-5)	49.7 ± 3.4
$\theta_4$ (C-3-C-4-C-5-O-5)	-50.8 ± 3.3
$\theta_5$ (C-4-C-5-O-5-C-1)	58.2 ± 1.6
$\theta_6$ (C-5-O-5-C-1-C-2)	-62.0 ± 2.2
<i>Cremer-Pople parameters</i>	
$Q$ (Å)	0.550 ± 0.023
$\theta$ (°)	5.5 ± 3.5
$\phi$ (°)	50.4 ± 29.7
<i>Distances</i> (Å)	
O-1(A)-O-1(D)	8.32
O-1(B)-O-1(E)	8.62
O-1(C)-O-1(F)	8.44

motions of the guest and rotation of the nitro group. The ready preparation of the complex, and the subtleties of its molecular structure presented here, amply demonstrate the ease with which water is expelled from the  $\alpha$ -CD cavity by a co-solvent.

## 4. Experimental

*Preparation of the  $\alpha$ -cyclodextrin – nitromethane complex.*—To a stirred solution of  $\alpha$ -CD (2.49 g, 2.56 mmol) in water (25 mL) was added dropwise nitromethane (3 mL), and the reaction mixture was kept overnight in a refrigerator. The colorless crystals formed were collected by filtration and dried in a desiccator over silica gel: 1.79 g (62%). A second crop (0.70 g, 24%) was obtained from the mother liquor on evaporation to about one third of its volume, followed by saturation with nitromethane. The crystals became opaque at 90–100 °C and started browning at ~265 °C.  $[\alpha]_D^{22} + 130^\circ$  (*c* 0.91, water);  $[\alpha]_D^{22} + 120^\circ$  (*c* 0.90, water saturated with CH<sub>3</sub>NO<sub>2</sub>); IR (KBr): NO<sub>2</sub> asymmetric stretching vibration band at 1561 cm<sup>-1</sup> and symmetric band at 1381 cm<sup>-1</sup>; <sup>1</sup>H and <sup>13</sup>C NMR spectra of the complex in [D<sub>6</sub>]Me<sub>2</sub>SO are of little significance, as they showed only minor chemical shift differences in comparison to those of pure  $\alpha$ -CD as well as nitromethane in [D<sub>6</sub>]Me<sub>2</sub>SO, conceivably due to formation — in part at least — of an  $\alpha$ -CD-[D<sub>6</sub>]Me<sub>2</sub>SO complex by displacement of the nitromethane from the cavity. Anal. Calcd for C<sub>36</sub>H<sub>60</sub>O<sub>30</sub>·CH<sub>3</sub>NO<sub>2</sub>·5 H<sub>2</sub>O (1123.96): C, 39.54; H, 6.55; N, 1.25. Found: C, 39.61; H, 6.41; N, 1.10.

The complex is stable at room temperature, yet loses nitromethane on heating to 110 °C in vacuum (90% after 12 h).

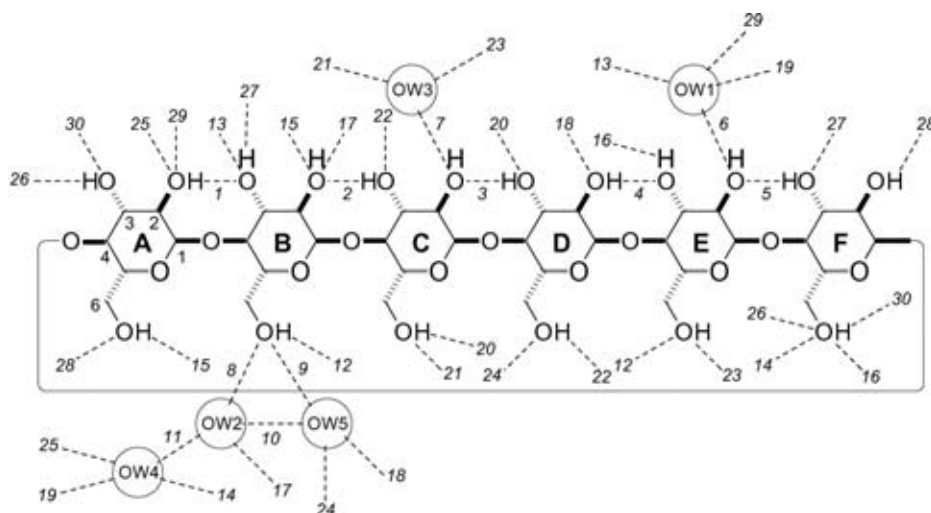


Fig. 3. Scheme of intra- and intermolecular hydrogen bonds in the solid-state structure of the  $\alpha$ -CD-nitromethane pentahydrate inclusion complex (**1**). The individual glucose residues are labeled A–F and the water molecules OW1–OW5, the numbers in italics correspond to the indices given in Table 2; ‘open-ended’ lines indicate H-bonds formed between symmetry related positions. The nitromethane guest molecule is not involved in the hydrogen-bonding pattern.

Table 2

Hydrogen bonds in the solid-state structure of  $\alpha$ -CD–nitromethane pentahydrate (**1**), listed for distances  $d(\text{H}\cdots\text{O}) < 2.5 \text{ \AA}$  and/or  $d(\text{O}\cdots\text{O}) < 3.2 \text{ \AA}$  only; the water molecules are labeled OW1–OW5, the glucose labeling A–F and the indices given in italics in the first column correspond to Fig. 3

No. (cf. Fig. 3)	Hydrogen bond	$d(\text{H}\cdots\text{O})$ (Å) <sup>a</sup>	$d(\text{O}\cdots\text{O})$ (Å)	$\phi(\text{O}–\text{H}\cdots\text{O})$ (°) <sup>a</sup>	Symmetry
<i>1</i>	O(2A)H $\cdots$ O(3B)	2.505	3.177	152.4	b
<i>2</i>	O(3C)H $\cdots$ O(2B)	2.295	3.030	172.5	b
<i>3</i>	O(3D)H $\cdots$ O(2C)	2.308	2.932	143.1	b
<i>4</i>	O(2D)H $\cdots$ O(3E)	2.192	2.899	159.9	b
<i>5</i>	O(3F)H $\cdots$ O(2E)	2.217	2.949	172.0	b
<i>6</i>	O(W1) $\cdots$ O(2E)		2.755		b
<i>7</i>	O(W3) $\cdots$ O(2C)		2.803		b
<i>8</i>	O(W2) $\cdots$ O(6B)		2.669		b
<i>9</i>	O(W5) $\cdots$ O(6B)		3.092		b
<i>10</i>	O(W5) $\cdots$ O(W2)		2.683		b
<i>11</i>	O(W4) $\cdots$ O(W2)		2.658		b
<i>12</i>	O(6B)H $\cdots$ O(6E)	2.136	2.864	168.8	c
<i>13</i>	O(3B) $\cdots$ O(W1)		2.834		c
<i>14</i>	O(W4) $\cdots$ O(6F)		2.978		c
<i>15</i>	O(6A)H $\cdots$ O(2B)	2.117	2.811	157.1	d
<i>16</i>	O(3E)H $\cdots$ O(6F)	2.056	2.788	172.1	e
<i>17</i>	O(2B) $\cdots$ O(W2)		2.628		e
<i>18</i>	O(2D) $\cdots$ O(W5)		2.657		f
<i>19</i>	O(W1) $\cdots$ O(W4)		3.008		f
<i>20</i>	O(6C)H $\cdots$ O(3D)	2.200	2.820	142.3	g
<i>21</i>	O(6C) $\cdots$ O(W3)		2.967		g
<i>22</i>	O(6D)H $\cdots$ O(3C)	2.341	2.927	137.4	h
<i>23</i>	O(6E) $\cdots$ O(W3)		2.780		h
<i>24</i>	O(6D) $\cdots$ O(W5)		2.646		i
<i>25</i>	O(2A) $\cdots$ O(W4)		2.852		j
<i>26</i>	O(3A)H $\cdots$ O(6F)	2.262	2.833	135.1	k
<i>27</i>	O(3B)H $\cdots$ O(3F)	2.366	2.817	120.9	k
<i>28</i>	O(2F)H $\cdots$ O(6A)	2.030	2.744	163.1	k
<i>29</i>	O(2A) $\cdots$ O(W1)		3.196		l
<i>30</i>	O(6F)H $\cdots$ O(3A)	2.200	2.833	144.3	l

<sup>a</sup> Hydrogen bond H $\cdots$ O distances and O–H $\cdots$ O angles omitted if hydrogen atoms were not located explicitly. Symmetry operations: <sup>b</sup> $x, y, z$ , <sup>c</sup> $x, y+1, z$ , <sup>d</sup> $x-1, y, z$ , <sup>e</sup> $x+1, y, z$ , <sup>f</sup> $x+1, y-1, z$ , <sup>g</sup> $-x+1, y+1/2, -z+3/2$ , <sup>h</sup> $-x+1, y-1/2, -z+3/2$ , <sup>i</sup> $-x, y-1/2, -z+3/2$ , <sup>j</sup> $x+1/2, -y+3/2, -z+2$ , <sup>k</sup> $x+1/2, -y+1/2, -z+2$ , <sup>l</sup> $x-1/2, -y+1/2, -z+2$ .

*Crystal structure determination.*—Suitable crystals for solid-state structural analysis were obtained by slow crystallization from a 9:1 water–nitromethane solution. A colorless single crystal, of dimensions  $0.25 \times 0.175 \times 0.15$  mm, was sealed in the presence of the mother liquor in a thin glass capillary, and then mounted on an Enraf–Nonius CAD-4 diffractometer with graphite-monochromated Mo K $\alpha$  ( $\lambda = 0.71093 \text{ \AA}$ ) radiation: prisms, orthorhombic, space group  $P2_12_12_1$  with  $a = 9.452(4)$ ,  $b = 14.299(3)$ , and  $c = 37.380(10) \text{ \AA}$ ,  $V = 5052.1(27) \text{ \AA}^3$ ,  $Z = 4$ ,  $T = 298(2) \text{ K}$ ,  $\mu(\text{Mo K}\alpha) = 0.126 \text{ mm}^{-1}$ , and  $D_x = 1.465 \text{ Mg m}^{-3}$ . A total of 5158 reflections were collected of

which 5004 were independent ( $R_{\text{int}} = 0.1236$ ). The structure was solved by direct methods using SHELXS-86 [17] and successive Fourier difference synthesis. Refinement (on  $F^2$ ) was performed by full-matrix least-squares method with SHELXL-93 [18].  $R(F) = 0.0812$  for 3270 reflections with  $I \geq 2\sigma I$ ,  $\omega R(F^2) = 0.2762$  for 5004 reflections with  $\omega = 1/(\sigma^2(F_o^2) + (0.1747P)^2 + 12.1519P)$ ; where  $P = (F_o^2 + 2F_c^2)/3$ . All non-hydrogen atoms were refined anisotropically. Hydrogen atoms were considered in calculated positions with the  $1.2 \times U_{\text{eq}}$  value of the corresponding atom; hydroxyl protons on the cyclodextrin were treated as idealized OH groups. Data reduction was

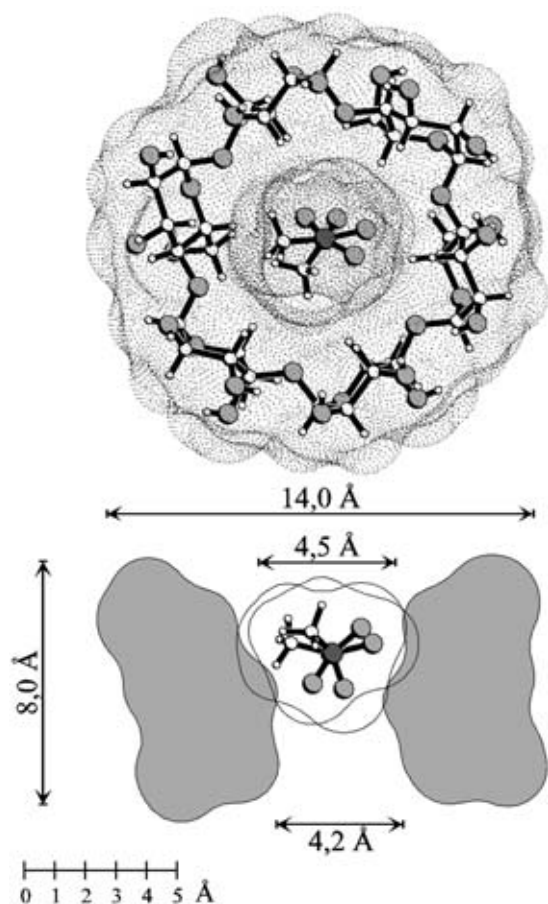


Fig. 4. Topology of the  $\alpha$ -CD–nitromethane inclusion complex (1) with the water molecules located at the CD outside left off for clarity. Top: Contact surfaces in dotted form with a ball-and-stick model insert, viewed from the wider opening (2-OH/3-OH side) of the truncated cone; oxygen and nitrogen atoms are shaded. — Bottom: Side-view surface cross sections through the complex (2-OH/3-OH face at top); approximate molecular dimensions are given in Å.

done by a Stoe-REDU4 program, for atomic coordinates any further details see Section 5. The molecular graphics of Figs. 1, 2 and 4 were generated by the MolArch<sup>+</sup> program [19].

## 5. Supplementary material

Table of atomic coordinates, bond lengths and bond angles have been deposited with the Cambridge Crystallographic Data Centre as supplementary publication no. CCDC 136109. Copies of the data can be obtained free of charge on application to CCDC, 12 Union

Road, Cambridge CB2 1EZ, UK (Fax: +44-1223-336033 or e-mail: deposit@ccdc.cam.ac.uk). Supporting information and additional molecular representations will be provided on the Internet in our graphics gallery at: <http://caramel.oc.chemie.tu-darmstadt.de/immelmolcad/gallery.html>.

## Acknowledgements

The authors thank the Fonds der Chemischen Industrie, Frankfurt, for support of this work, Mrs Sabine Foro for collecting the crystallographic data, and Dr. T. Wimmer, Wacker-Chemie, Burghausen, for a generous gift of  $\alpha$ -CD.

## References

- [1] H. Gohlke, S. Immel, F.W. Lichtenthaler, *Carbohydr. Res.*, 321 (1999) 96–104.
- [2] B. Hingerty, W. Saenger, *J. Am. Chem. Soc.*, 98 (1976) 3357–3365.
- [3] K. Harata, *Bull. Chem. Soc. Jpn.*, 52 (1979) 2451–2459.
- [4] K. Harata, *Bull. Chem. Soc. Jpn.*, 51 (1978) 1644–1648.
- [5] K. Harata, in J. Szejtli, T. Osa (Eds.), *Comprehensive Supramolecular Chemistry*, Vol. 3, Pergamon, Oxford, 1996, pp. 279–304.
- [6] M.V. Rekharsky, Y. Inoue, *Chem. Rev.*, 98 (1998) 1875–1917 particularly Table 1.
- [7] K.K. Chacko, W. Saenger, *J. Am. Chem. Soc.*, 103 (1981) 1708–1715.
- [8] B. Klar, B. Hingerty, W. Saenger, *Acta Crystallogr., Sect. B*, 36 (1980) 1154–1165.
- [9] K. Lindner, W. Saenger, *Acta Crystallogr., Sect. B*, 38 (1982) 203–210.
- [10] K. Lipkowitz, *Chirality*, 4 (1992) 205–215.
- [11] F.W. Lichtenthaler, S. Immel, *Liebigs Ann. Chem.*, (1996) 27–37.
- [12] S. Immel, J. Brickmann, F.W. Lichtenthaler, *Liebigs Ann. Chem.*, (1995) 929–942.
- [13] D. Cremer, J.A. Pople, *J. Am. Chem. Soc.*, 97 (1975) 1354–1358.
- [14] G.A. Jeffrey, J.H. Yates, *Carbohydr. Res.*, 74 (1979) 319–322.
- [15] G.A. Jeffrey, W. Saenger, *Hydrogen Bonding in Biological Structures*, Springer-Verlag, Berlin, 1991.
- [16] M.L. Connolly, *J. Appl. Cryst.*, 16 (1983) 548–558. (b) M.L. Connolly, *Science*, 221, 709–713.
- [17] G.M. Sheldrick, SHELXS-86, Program for the Solution of Crystal Structures, University of Göttingen, Germany, 1990.
- [18] G.M. Sheldrick, SHELXL-93, Program for the Refinement of Crystal Structures, University of Göttingen, Germany, 1993.
- [19] S. Immel, MolArch<sup>+</sup>–MOlecular ARCHitecture Modeling Program, Darmstadt University of Technology, Germany, 1999.



# The Hydrophobic Topographies of Amylose and its Blue Iodine Complex<sup>[1, 2]</sup>

Stefan Immel and Frieder W. Lichtenthaler,  
Darmstadt (Germany)

Two polymorphs of amylose, the native double-helical A-form and the single-stranded V<sub>H</sub> counterpart, as well as the amylose polyiodide complex were subjected to a molecular modeling study. Based on their X-ray diffraction-derived structures, the “solvent-accessible” contact surfaces were generated, onto which the computed molecular lipophilicity profiles (MLPs) were projected in color-coded form, easily allowing to locate hydrophobic and hydrophilic surface regions. Their detailed analysis revealed the double-stranded A-form to be a rather compact structure with an irregular distribution of hydrophilic and hydrophobic regions over the entire outer surface, with the interior of the double helix being inaccessible even for small molecules. By contrast, V<sub>H</sub>-amy-

lose, in accord with its water solubility, has a pronouncedly hydrophilic outside surface with an as distinctly hydrophobic channel. – In the dark-blue amylose-polyiodide complex, the hydrophobic channel of the single-helical V<sub>H</sub>-form serves as a well-ordered matrix for incorporation and alignment of the iodine-iodide species to elaborate a linear polyiodide chain in a nearly perfect steric fit and in full complementarity of hydrophobic regions of guest and host. Thus, the MLPs provide substantive credence to the view, that not only the amylose-iodine complex formation is mediated to an essential degree by hydrophobic attractions at the guest-host interface, but that the same factors determine the stability of this unique supramolecular assembly.

**Keywords:** Amylose; Starch-iodide complex;  $\alpha$ -Cyclodextrin-iodide, Inclusion compounds; Hydrophobicity patterns

## 1 Introduction

Amylose, the unbranched portion of starch, is the classical example of a linear polysaccharide composed of several thousand  $\alpha(1 \rightarrow 4)$ -linked D-glucose units, which adopts a helical structure. Fig. 1 provides a common textbook pictorial representation of this structure [3].

Besides leaving open whether the helix includes a central channel or not, this sketchy formulation of a single-stranded helix does not correctly depict the molecular organization of native amylose, since the two major amylose polymorphs A and B are double helical assemblies [4–7]. Single helices of the type depicted above, with six glucose units per turn, are only obtainable in the form of inclusion complexes with dimethyl sulfoxide [8], *n*-butanol [9, 10], *n*-pentanol [10], or in a dry (V<sub>A</sub>-amylose) or hydrated state (V<sub>H</sub>-form) [11–13] upon removing the organic solvents entrapped in these complexes.

As the solid-state structures may be considered as “frozen” molecular images of their solution conformations –

a presupposition that has yielded in the case of cyclodextrins [14] and their inclusion complexes [15] – we have entered the V<sub>H</sub>- [13] and A-type amylose [4, 5] as well as the amylose-iodine complex [16, 17] into a detailed molecular modeling study, comprising generation of their molecular geometries, their contact surfaces, and – most relevant in terms of understanding their inclusion capabilities – their lipophilicity patterns. The results [2] are subject of this paper.

## 2 Experimental

### 2.1 Molecular structures

The molecular models of the A- and V<sub>H</sub>-form of amylose were generated from atomic coordinates obtained from X-ray fiber diffraction [5, 13]. For A-amylose, two strands of 12 glucose units each were generated (two turns of the double helix,  $\equiv 2 \cdot C_{72}H_{122}O_{61}$ ), for V<sub>H</sub>-amylose and the amy-

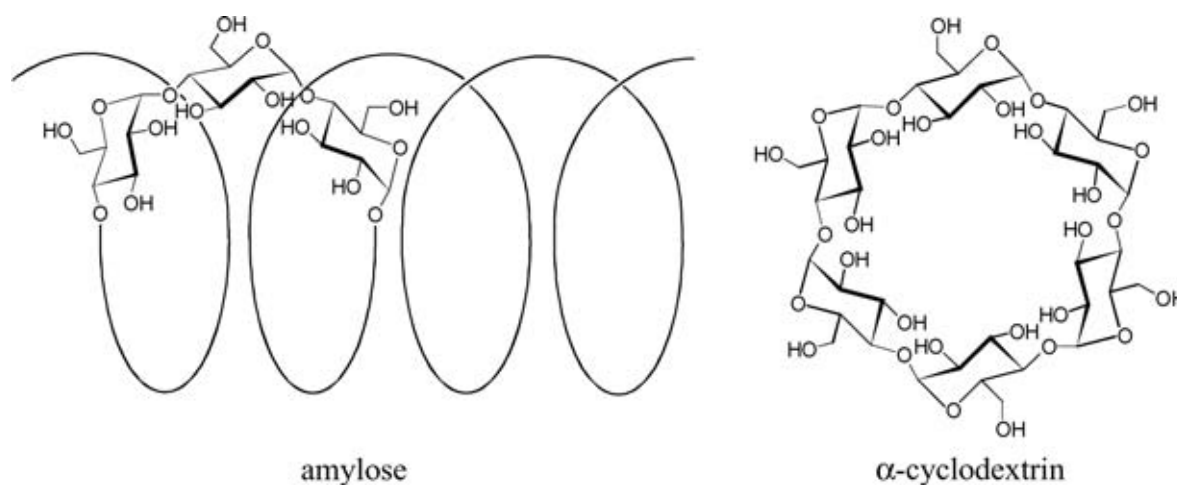


**Fig. 1.** Sketch representation of a left-handed, single-stranded helix of V<sub>H</sub>-amylose (*left*), adapted from [3], where incorrectly a right-handed helix is depicted, and of  $\alpha$ -cyclodextrin (*right*), which de facto represents a single turn of the amylose helix excised and re-connected by *Bacillus macerans*-derived enzymes (CGTases). The close analogy allows to consider V<sub>H</sub>-amylose as a tubular analog of the cyclodextrins.

lose-iodine complex five single-stranded turns of altogether 30 glucose residues were used ( $\equiv C_{180}H_{302}O_{151}$ ) resulting in molecular dimensions of approximately  $12 \times 12 \times 45 \text{ \AA}$  each. The solid-state structure of the *bis*- $\alpha$ -cyclodextrin/lithium triiodide-iodine octahydrate inclusion complex [29], i.e.  $[C_{36}H_{60}O_{30}]_2 \cdot LiI_3 \cdot I_2 \cdot 8 H_2O$  was obtained from the CCDF-Cambridge Crystallographic Data File (Refcode: CYDXLI10). Hydrogen atoms not included in the molecular structure determinations were positioned geometrically with standard bond lengths  $r_{C-H} = 1.08 \text{ \AA}$  and  $r_{O-H} = 0.90 \text{ \AA}$ , taking intramolecular hydrogen bonding interactions between spatially neighboring hydroxyl groups into account. All molecular parameters discussed within this study (cf. Tab. 1) were re-calculated from these data sets.

## 2.2 Molecular surfaces and molecular lipophilicity patterns (MLPs)

Calculation of the molecular contact surfaces [19] and the corresponding MLPs was carried out by using the MOLCAD [18, 24, 25] molecular modeling program, whereby the MLPs were computed after removal of all iodine species and for each molecule separately. Surfaces for the inclusion complexes were generated for the guest and host molecules separately, and were subsequently reassembled to the complex; surfaces of the amylose models were generated only for the center sections of approx.  $30 \text{ \AA}$  length each in order to exclude “end”-effects for the polysaccharides. Cyclodextrin cross-cut plots through the center of geometry were computed from the intersection of a plane with the molecular surfaces [19]; molecular plots were generated using the MolArch<sup>+</sup> program [49]. Visualization of the MLP surface qualities was done by color-coded projection of the computed values onto these surfaces by applying texture mapping [25], the surfaces of the iodine species were colored according to the atomic types (pink), and no surface qualities are mapped. Scaling of the molecular hydrophobicity patterns was performed in relative terms for each molecule separately, and no absolute values are displayed.

## 3 Results and Discussion

### 3.1 Molecular geometries and hydrogen bonding patterns of A- and $V_H$ -type amylose

The molecular models of A- [5] and  $V_H$ -amylose [13] were generated from their respective X-ray fiber diffraction data, using five single helix turns (= 30 glucose units) for  $V_H$ -amylose, and two turns of the double helix for its A-form (= two strands of 12 glucose units each). The resulting structures, each of approximately  $12 \times 12 \times 45 \text{ \AA}$  in size, are shown in Fig. 2 in ball-and-stick type representation, with their molecular contact surfaces [18, 19] – closely resembling the solvent (water) accessible surfaces [20] – molded around the rear half, clearly revealing the distinct differences of the two assemblies: a well-elaborated central channel in the single-stranded  $V_H$ -amylose, obviously capable of accommodating guests of appropriate dimensions, versus the double-helical A-form with its two strands so narrowly intertwined as to leave no interstitial space [21]. This basic dissimilarity of the two forms is even more lucidly illustrated in the projections along the helix axis (Fig. 3):  $V_H$ -amylose has an overall helix diameter of approximately  $13.5 \text{ \AA}$ , a channel of  $\approx 5.4 \text{ \AA}$  width, and an axial pitch of  $\approx 8.1 \text{ \AA}$  per turn, whilst the double-helical A-form reveals a substantial increase of the axial pitch (to  $21.4 \text{ \AA}$  per double turn), requiring the helix

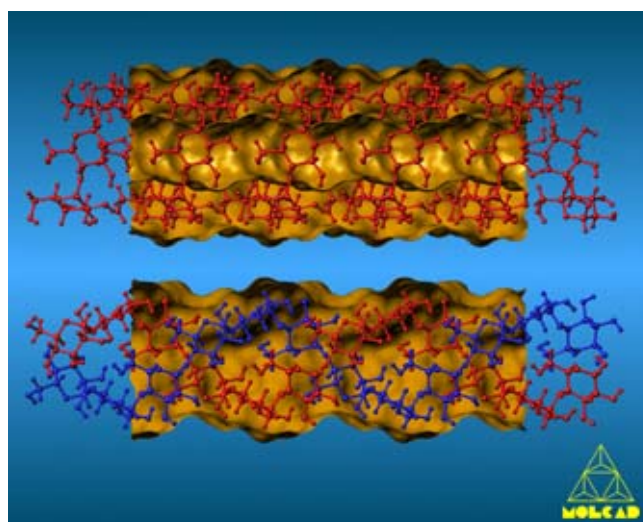


**Fig. 2.** Molecular geometries of  $V_H$ -type amylose (upper structure) and A-amylose (lower entry) [21]. Both forms consist of rod-shaped, left-handed helices of  $\alpha(1 \rightarrow 4)$ -linked glucose units with a uniform gauche-gauche arrangement of all hydroxymethyl groups in relation to their pyranoid rings. As  $V_H$ -amylose (*top*) represents a single helix of  $6_5$ -symmetry, i.e. six glucose residues per left-handed turn, the model comprises five such turns, corresponding to a molecular composition of  $C_{180}H_{302}O_{151}$  (axial spacing  $\approx 8.05 \text{ \AA}$  per turn). The two individual strands of the double-helical A-form (*bottom*) of  $2_1$  symmetry ( $\equiv 2 \cdot C_{72}H_{122}O_{61}$ , two turns with a pitch of  $\approx 21.4 \text{ \AA}$  per turn and 12 glucose units each) are colored blue and red, respectively, to facilitate identification. To exclude “end”-effects for the finite polymer segments of approximately  $45 \text{ \AA}$  length each, the yellow-colored and half-opened contact surfaces (roughly equivalent to the solvent-accessible surfaces [19, 20], i.e. how closely water molecules can approach) are shown only for the center sections of  $\approx 30 \text{ \AA}$  length.

diameter to decrease to  $10.3 \text{ \AA}$ , thereby eliminating any central channel. Thus, it is easily understood, that the water of crystallization in the solid-state A-form is only located on places outside the helices.

Apart from strong van der Waals attractive forces that must be an important factor for establishing the distinctly different folding patterns – for the two intertwined single strands of the A-form in particular – the elaboration of a specific hydrogen bonding network undoubtedly is another. A computational assessment of the possible hydrogen bonding contacts between the two strands in A-amylose and between adjacent coils in the single-stranded  $V_H$ -form gave the following picture: the A-form of amylose establishes various hydrogen bond-mediated  $2-O \cdots O-6$  contacts between glucose units of different strands (Fig. 4, left) with  $O \cdots H$  distances of  $1.9\text{--}2.1 \text{ \AA}$  and  $O-H \cdots O$  angles in the range of  $140\text{--}160^\circ$  (Tab. 1, entries A–D). In  $V_H$ -amylose, however, not only  $2-O \cdots O-6$  hydrogen bonds between spatially close glucose residues of the next spiral turn (Fig. 4, right entry and Tab. 1) are materialized, but these are also cooperatively strengthened by  $2-O \cdots O-3'$  hydrogen bonds between adjacent glucose units. The latter hydrogen bonds are – in agreement with Jeffrey’s and Saenger’s systematic analysis of H-bonding patterns in the crystal structures of carbohydrates [22] energetically highly favorable [23] and, by consequence, must be considered as an important factor in stabilizing the helical structures in amylose.

### 3.2 MLP profiles of A- and $V_H$ -amylose

Since the formation of inclusion complexes of V-amylose is closely related to hydrophobic interactions within the

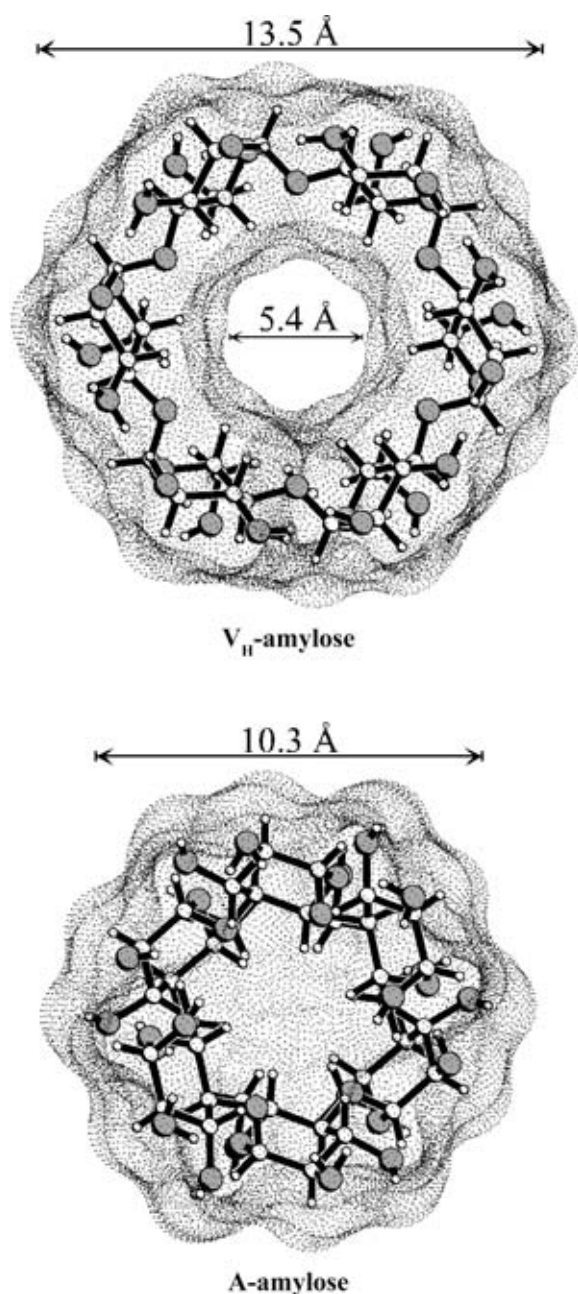


**Fig. 3.** Molecular surfaces (view along the helix axis) of V<sub>H</sub>-amylose (*top*) and A-amylose (*bottom*), illustrating the molecular geometries of Fig. 2 and their approximate molecular dimensions.

**Tab. 1.** Calculated hydrogen bond geometries (distances and angles) for the A- and V<sub>H</sub>-form of amylose. The letters denote the different types of H-bonds as marked in Fig. 4.

Compound	Type of hydrogen bond (cf. Fig. 4)	Distances [Å]		Angle [°]	
		<i>d</i> (O ... H)	<i>d</i> (O ... O)	φ (O-H ... O)	
A-amylose	<b>A</b>	2-OH ... O-6 <sup>a</sup>	2.08	2.93	158
	<b>B</b>	6-OH ... O-2 <sup>a</sup>	2.08	2.93	157
	<b>C</b>	2-OH ... O-6 <sup>a</sup>	1.90	2.75	156
	<b>D</b>	2-OH ... O-6 <sup>a</sup>	1.91	2.65	139
V <sub>H</sub> -amylose	<b>E</b>	3-OH ... O-2 <sup>b</sup>	1.94	2.84	177
	<b>F</b>	2-OH ... O-6 <sup>c</sup>	1.95	2.78	154

<sup>a</sup> Interstrand hydrogen bonds.

<sup>b</sup> H-bond between adjacent glucose units.

<sup>c</sup> H-bond between glucose units in adjacent turns.

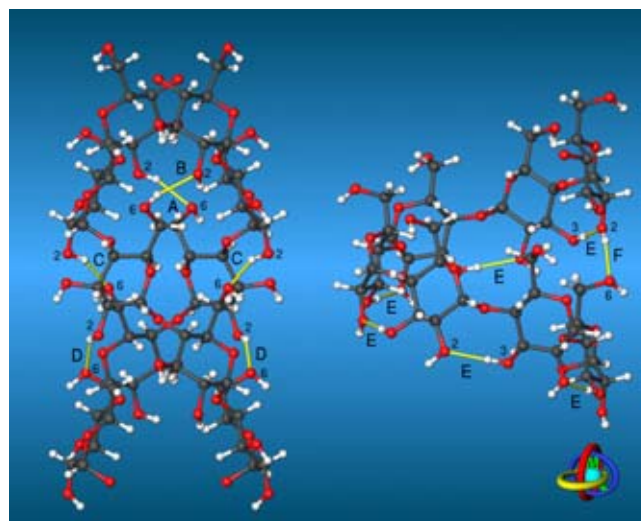


**Fig. 4.** Hydrogen bonding patterns (yellow lines) within the double helices of A-type starch (*left*) and the single helical V<sub>H</sub>-type amylose (*right*), calculated from the heavy atom positions of the crystal structures. The letters refer to different types of hydrogen bonds, of which the geometry parameters are listed in Tab. 1.

channel, it was deemed important to get an anticipation of the distribution of hydrophobic and hydrophilic regions on the surfaces of the A- and V<sub>H</sub>-polymorphs by generation of the respective molecular lipophilicity patterns (MLPs). These MLPs [24] were calculated and mapped onto the corresponding molecular contact surfaces of Fig. 2 by using the MOLCAD-program [18], and were visualized [24, 25] by applying a color-code graded into 32 shades, ranging from dark blue for the most hydrophilic surface regions to full yellow for the most hydrophobic areas.

As is apparent from the color-coded representations in Fig. 5 – the half opened surface models in the lower picture are particularly lucid in this respect – the hydrophobic characteristics of the V<sub>H</sub>-amylose and the A-form differ significantly. The latter exhibits an irregular distribution of hydrophobic and hydrophilic outer surface areas (Fig. 5, lower models each), as contrasted by the pronouncedly hydrophilic (blue) outside surface regions of V<sub>H</sub>-amylose (Fig. 5, top models): the outside surface regions are intensely hydrophilic (blue) – in accord with its comparatively high solubility in water – while its center channel is decisively hydrophobic (yellow). This distinctive inside-outside separation of hydrophobic and hydrophilic domains obviously preconditions the incorporation of iodide/iodine into the chan-

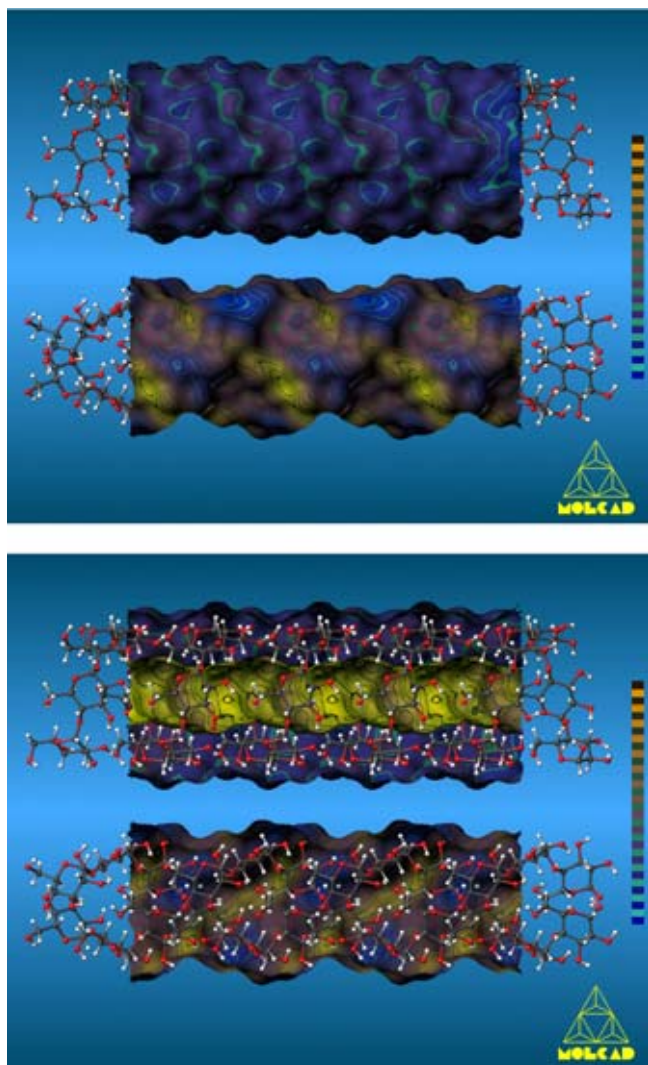


**Fig. 5.** Hydrophobic topographies for the amylose fraction of starch [21]: the MLP pattern (blue: hydrophilic surface regions, yellow: hydrophobic areas) on the contact surface of single-stranded  $V_H$ -amylose (upper structures each) is set against the parallel-stranded double-helical A-form (lower model, respectively). In both cases, fragments of approximately 45 Å length are shown, with the surfaces being depicted for the center sections of the rod-shaped polymers only ( $\approx 30$  Å, cf. Fig. 2). The outside surface area of  $V_H$ -type amylose is uniformly hydrophilic (in conformity with its solubility in water) whereas the center channel is as distinctly hydrophobic-predestined to incorporate equally hydrophobic guests such as iodine or fatty acids. By contrast, the double-helical A-form of amylose, devoid of a center channel, exhibits an irregular distribution of hydrophilic and hydrophobic regions over the entire surface [26].

nel as a successive linear chain of  $I_2/I_3^-$  molecules [16], or of fatty acids [27] and a variety of other guests [8–10].

### 3.3 $\alpha$ -Cyclodextrin-iodine inclusions: models for the blue amylose-iodine complex?

As  $\alpha$ -cyclodextrin represents an enzymatically excised and then re-connected single turn of the  $V_H$ -amylose helix (cf. Fig. 1) and, hence, may be considered a projection down its helix axis, its capability to form inclusion complexes with iodine [28] and polyiodide [29–31] may parallel that of amylose and serve as a conjectural model for the well-known deep-blue stained amylose-iodine-iodide complex. Accordingly, the generation of the molecular lipophilicity profiles and an assessment of the complementarity of the hydropho-

bic domains of guest (iodine) and host ( $\alpha$ -CD) were considered relevant in this context.

Co-crystallization of  $\alpha$ -CD with various polyiodides yields dark-brown to dark-blue stained complexes, which exhibit entirely different, infinite channel-type solid-state structures with approximately linear alignments of the polyiodide ions along the central axis [28–32]. Most notably, the *bis*- $\alpha$ -cyclodextrin lithium penta-iodide octahydrate complex  $(\alpha\text{-CD})_2 \cdot \text{LiI}_3 \cdot \text{I}_2 \cdot 8 \text{H}_2\text{O}$  [29] comprises two crystallographically independent cyclodextrin units which are “fused together” to a head-to-head dimer through an intense hydrogen bonding network between the secondary hydroxyl groups of the two  $\alpha$ -CD tori (Fig. 6). Into the resulting “double cavity” formed by this assembly, the iodine atoms (four ordered positions and one disordered) are embedded with unequal iodine-iodine distances (mean value  $\approx 3.1$  Å). The  $\text{Li}^+$  counter-ion is located outside this dimer assembly, hence out of range of strong electrostatic interactions with the anion [29].

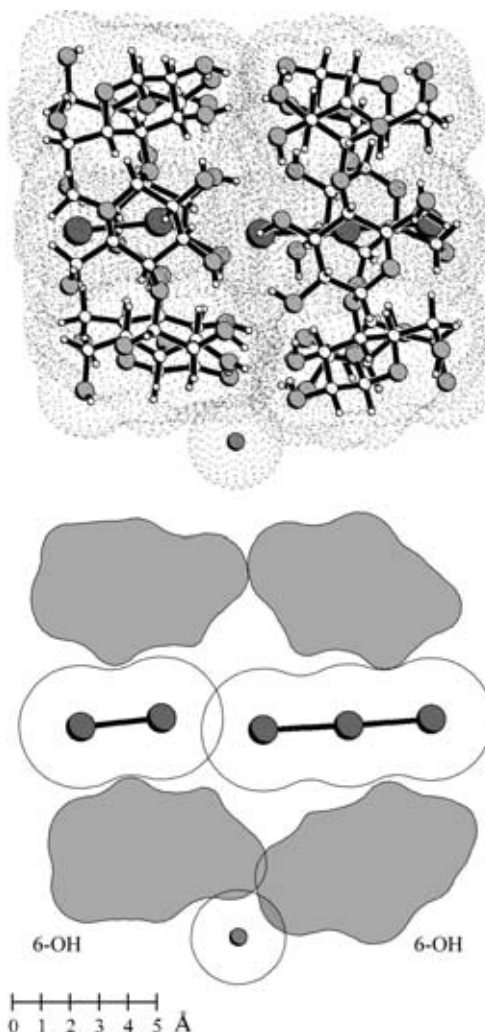


**Fig. 6.** *Top:* Ball-and-stick model and contact surface (in dotted form) of the complex  $(\alpha\text{-CD})_2 \cdot \text{LiI}_3 \cdot \text{I}_2 \cdot 8 \text{H}_2\text{O}$ , as it emerged from its X-ray structure [29], with the water of crystallization removed for clarity. The basic unit of this assembly consists of two  $\alpha$ -CD's forming a head-to-head-dimer through an intense hydrogen bonding network between the secondary 2- and 3-OH groups at their wider torus rims; the resulting “double cavity” is filled with an almost linear iodine-triiodide chain (represented by black balls in the center) with the counter-ion  $\text{Li}^+$  (small sphere) located at the interstice. *Bottom:* Surface cross-section cut through the center of the dimer assembly exposing the five iodine atoms included.

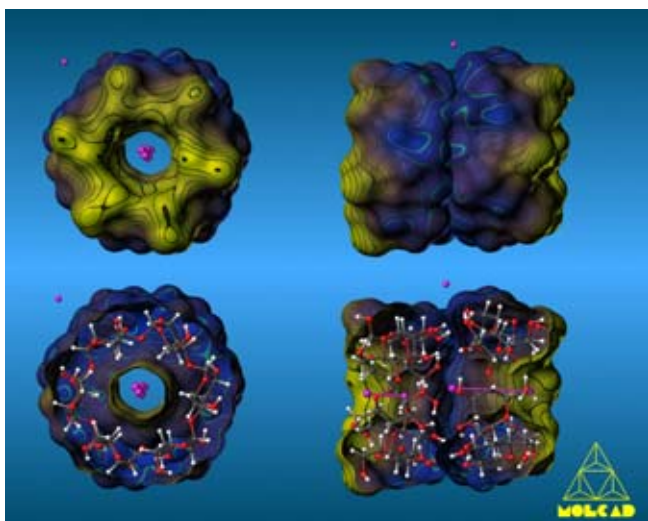


**Fig. 7.** Molecular lipophilicity patterns (MLPs) for the  $(\alpha\text{-CD})_2 \cdot \text{LiI}_3 \cdot \text{I}_2 \cdot 8 \text{H}_2\text{O}$  complex [29] of which the water of crystallization has been removed for clarity [21]. *Left:* View along the central channel axis, perpendicular to the  $\alpha\text{-CD}$  mean planes. *Right:* Side-view models representing the hydrophobic topographies of the dimeric units. The location of the lithium ion is indicated by the isolated pink ball at the lower, half-opened models.

Generation of the MLPs of this complex and their colored projection onto the contact surfaces given in Fig. 6 provides the picture in Fig. 7, illustrating the assembly of the two  $\alpha\text{-CD}$  macrocycles via their pronouncedly hydrophilic (blue) 2-OH/3-OH-sides which entails the two end sites, car-

rying the primary hydroxyl groups, to be as distinctly hydrophobic (yellow). Accordingly, the pentaiodide chain is packed into a channel-like “double cavity” with successive, alternating hydrophobic and hydrophilic surface regions.

Thus, the *bis*- $\alpha\text{-CD}$  – pentaiodide unit, due to its “finite” dimeric nature, provides only a limited analogy to the polymeric “infinite” amylose-iodine complex. However, when taking into account the packing of these dimeric units in the crystal lattice, a surprisingly close similarity emerges: infinite stacks with the elaboration of a somewhat uneven nanotube into which a nearly linear, continuous polyiodide chain is embedded as exemplified in Fig. 8. That this is materialized despite the alternating hydrophobic and hydrophilic zones along these nanotube channels is a strong indication for the pronounced proclivity of iodine or polyiodide species to associate with suitable hosts to polymeric supramolecular assemblies.

### 3.4 The amylose-iodine complex

The presence of iodine as well as iodide in aqueous solutions of amylose is a mandatory prerequisite for the formation of the blue complex [17], and binding occurs in a cooperative way by slow formation of stable  $\text{I}_{11}^{3-}$  nuclei inside the helices and rapid linear propagation [33]. With increasing iodide concentration the bluing species (polymeric unit of approx.  $(\text{C}_6\text{H}_{10}\text{O}_5)_{16.5} \cdot \text{I}_6$  [34]) seems to change from  $\text{I}_{10}^{2-}$  to  $\text{I}_8^{2-}$  and  $\text{I}_6^{2-}$  [35], simultaneously shifting the maximum absorption towards shorter wavelengths. The enthalpy of the amylose-iodine interaction is rather large with  $-50$  to  $-90$  kJ per mole molecular iodine bound [36]. All of these data give evidence that the solid-state structure of the amylose-iodine complex [16] (Fig. 9) is a useful model even for the solution

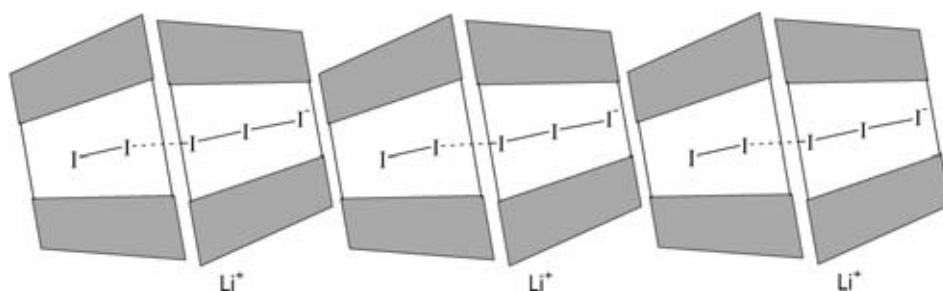


**Fig. 8.** Simplified illustration of the nearly nanotube-like stacking of the  $(\alpha\text{-CD})_2$ -pentaiodide units in the crystal lattice, thereby forming a continuous linear poly-iodine/iodide chain, an “endless” channel so to say.

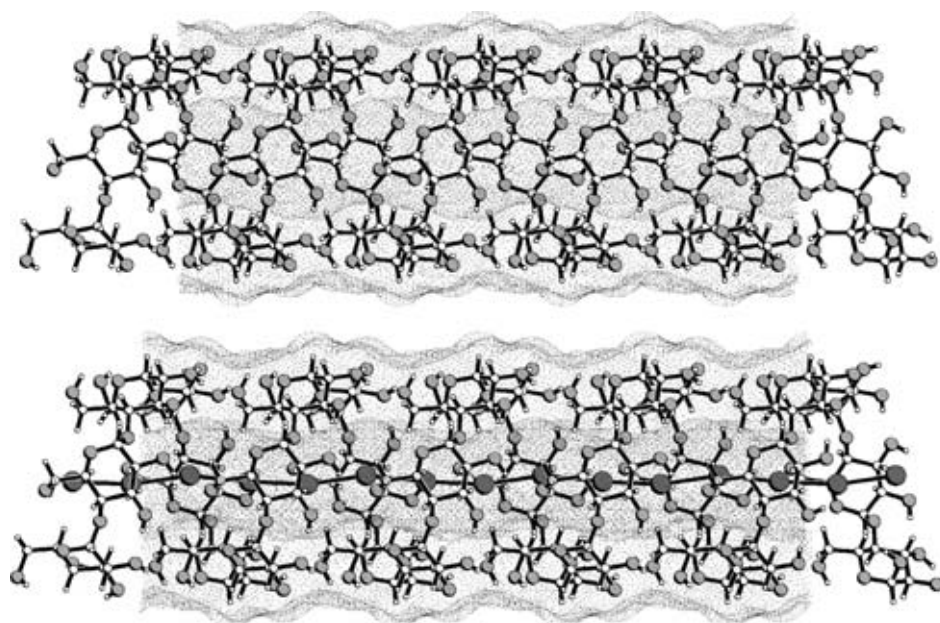


**Fig. 9.** Molecular geometry of the  $V_H$ -amylose with an “empty” channel (*top*, representation corresponding to Fig. 5) and with the essentially linear polyiodide chain (filled balls in the center) embedded (*bottom*), based on X-ray diffraction data [16] and calculation of the “solvent-accessible” contact surfaces [21].

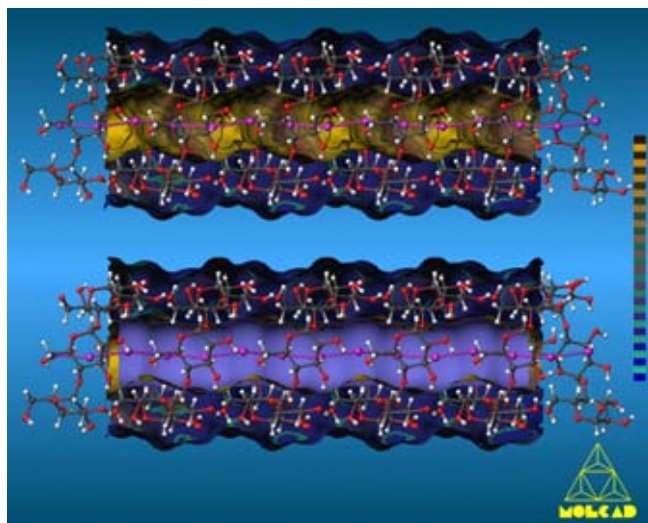


**Fig. 10.** Molecular lipophilicity profile (MLP) for the  $V_H$ -amylose-iodine-iodide complex [21]. *Top:* half-opened model based on its solid-state structure [16] with the linear polyiodide chain (pink balls) in the channel; the hydrophobicity distribution is essentially identical to that of the non-complexed  $V_H$ -structure (Fig. 5). *Bottom:* The linear polyiodide chain inserted into the central channel with its half-opened contact surface (violet area behind the pink balls) to illustrate the perfect steric fit.

state: a nearly linear polyiodide chain with  $I \cdots I$ -separations of  $\approx 2.91$ ,  $2.91$  and  $2.99$  Å, respectively, with the fiber repeat of the amylose helix ( $\approx 8.17$  Å) slightly increased over that of iodine-free  $V_H$ -amylose ( $\approx 8.05$  Å).

Generation of the contact surfaces of  $V_H$ -amylose and its polyiodine/iodide complex as depicted in Fig. 9, and the corresponding color-coded representation of the MLP profiles in Fig. 10, impressively illustrates the pronouncedly hydrophobic central channel which serves as a matrix for incorporation and alignment of the iodine species. Superimposition of the amylose helix with the iodine chain and its (pink-colored) contact surface (bottom structure of Fig. 10) documents the sterically perfect correspondence. The ideal guest-host complementarity not only manifests itself in a perfect fit of an almost linear iodine/iodide chain in an equally linear channel – not infinite in length, but long enough to include several consecutive polyiodide units but also in the matching of their hydrophobic domains.

Thus, the MLP profiles provide substantive credence to the view that amylose-iodine complex formation – to a very substantial degree – is mediated by the operation of attractive hydrophobic forces at the guest-host interface and provides a major element for engendering the stability of this unique supramolecular assembly.

## 4 Conclusion

The hydrophobic nature of the tubular channel in  $V_H$ -amylose and of the conical cavity in the cyclodextrins has been postulated and de facto taken for granted ever since their molecular structural features began to unravel about 60 years ago [37–39]. Yet still today, the “hydrophobic effect” – even if one has agreed on the exact definition of the term [40] – is an “elusive” entity; it can neither be quantified reliably, nor can it be separated from the various other factors involved in inclusion complex formation, such as guest-host correspondence of steric features, minimization of dipole-di-

pole interactions, and compensation of entropic and enthalpic parameters associated with changes in solvation.

The computation and visualization of hydrophobic and hydrophilic surface regions described here for amylose and its iodine inclusion complex not only permits – for the first time – a genuine and reproducible localization and differentiation of these regions. As significant is that the importance of complementary hydrophilic and hydrophobic surface domains at the guest-host interface is imposingly verified, their interplay thus being a decisive element in incorporation of the guest into the host.

Finally, the insights provided by these novel views at amylose – substantiated by similar results described elsewhere on the cyclodextrins [14, 15, 41], cyclomannins [41], cyclorhamnins [42], cycloaltrins [43–45], cyclogalactins [41, 46], cyclofructins [47], and on sucrose [48] – may not only provide a viable base for the preparation of new, useful inclusion complexes of amylose, but also for the design of new ensuing reactions towards a targeted exploitation of the chemistry of starch.

## Acknowledgements

The authors are grateful to Prof. J. Brickmann, Institut für Physikalische Chemie, Technische Universität Darmstadt, for generously providing us access to his MOLCAD modeling software package [18].

## Bibliography

- [1] This account is Part 24 of the series “Molecular Modeling of Saccharides”. Part 23: T. Nakagawa, S. Immel, and F. W. Lichtenthaler: Topography of a 1:1  $\alpha$ -cyclodextrin – nitromethane inclusion complex. *Carbohydr. Res.* **324** (2000), 141–146.
- [2] Portions of this work have been used by F.W.L. in his SPRI Science Award Lecture (Helsinki, 1995), of which an account has appeared: F. W. Lichtenthaler and S. Immel: Computersimulation of chemical and biological properties of sucrose, the cyclodextrins, and amylose. *Internat. Sugar J.* **97** (1995), 12–22.
- [3] P. M. Collins and R. J. Ferrier: *Monosaccharides, their chemistry and their roles in natural products*. Wiley, Chichester/New York 1995, p. 490.
- [4] H.-C. H. Wu and A. Sarko: The double-helical molecular structure of crystalline A-amylose. *Carbohydr. Res.* **61** (1978), 27–40.
- [5] A. Imberty, H. Chanzy, S. Pérez, A. Buléon, and V. Tran: The double-helical nature of the crystalline part of A-starch. *J. Mol. Biol.* **201** (1988), 365–378.
- [6] H.-C. H. Wu and A. Sarko: The double-helical molecular structure of crystalline B-amylose. *Carbohydr. Res.* **61** (1978), 7–25.
- [7] A. Imberty and S. Pérez: A revisit to the three-dimensional structure of B-type starch. *Biopolymers* **27** (1988), 1205–1221.
- [8] [8a] A. French and H. F. Zobel: X-Ray diffraction of oriented amylose fibers. The amylose-dimethyl sulfoxide complex. *Biopolymers* **5** (1967), 457–464.  
[8b] W. T. Winter and A. Sarko: Crystal and molecular structure of the amylose-DMSO complex *Biopolymers* **11** (1972), 849–852; **13** (1974), 1461–1468.
- [9] R. E. Rundle and F. C. Edwards: The configuration of the starch-iodine complex. An X-ray diffraction investigation of butanol-precipitated amylose. *J. Am. Chem. Soc.* **65** (1943), 2200–2203.
- [10] W. Hellert and H. Chanzy: Single crystals of V amylose complexed with *n*-butanol or *n*-pentanol: structural features and properties. *Int. J. Biol. Macromol.* **16** (1994), 207–213.
- [11] B. Zaslow, V. G. Murphy, and A. D. French: V-amylose-water system. Structural changes resulting from hydration. *Biopolymers* **13** (1974), 779–790.
- [12] P. Zugenmaier and A. Sarko: Packing analysis of carbohydrates and polysaccharides. B-Amylose. *Biopolymers* **15** (1976), 2121–2136.
- [13] G. Rappenecker and P. Zugenmaier: Detailed Refinement of the crystal structure of  $V_H$ -amylose. *Carbohydr. Res.* **89** (1981), 11–19.

- [14] *S. Immel and F. W. Lichtenthaler*: On the hydrophobic characteristics of cyclodextrins: computer-aided visualization of molecular lipophilicity patterns. *Liebigs Ann. Chem.* (1996), 27–37.
- [15] *F. W. Lichtenthaler and S. Immel*: Towards understanding formation and stability of cyclodextrin-inclusion complexes: computation and visualization of their lipophilicity patterns. *Starch/Stärke* **48** (1996), 145–154.
- [16] *T. L. Bluhm and P. Zugenmaier*: Detailed structure of the V<sub>H</sub>-amylose-iodine complex: A linear polyiodide chain. *Carbohydr. Res.* **89** (1981), 1–10.
- [17] *K. A. Murdoch*: The amylose-iodine complex. *Carbohydr. Res.* **233** (1992), 161–174.
- [18] [18a] *J. Brickmann*: MOLCAD – MOLEcular Computer Aided Design, Technische Hochschule Darmstadt, 1996. The major part of the MOLCAD-program is included in the SYBYL package of TRIPOS Associates, St. Louis, USA.  
[18b] *J. Brickmann*: Molecular graphics – how to see a molecular scenario with the eyes of a molecule. *J. Chim. Phys.* **89** (1992), 1709–1721.  
[18c] *J. Brickmann, T. Goetze, W. Heiden, G. Moeckel, S. Reiling, H. Vollhardt, and C.-D. Zachmann*: Interactive visualization of molecular scenarios with MOLCAD/SYBYL. In: *Data Visualization in Molecular Science – Tools for Insight and Innovation* (Ed.: J. E. Bowie), Addison-Wesley Publ., Reading, Mass. 1995, pp. 83–97.
- [19] *M. L. Connolly*: Solvent-accessible surfaces of proteins and nucleic acids. *Science* **221** (1983), 709–713.
- [20] *B. Leek and F. M. Richards*: Interpretation of protein structures: estimation of static accessibility. *J. Mol. Biol.* **55** (1971), 379–400.
- [21] All 3D-structures can be viewed on the WWW at: <http://caramel.oc.chemie.tu-darmstadt.de/immeld/3Dstructures.html>; MOLCAD graphics are available at: <http://caramel.oc.chemie.tu-darmstadt.de/immeld/molcad/gallery.html>.
- [22] *G. A. Jeffrey and W. Saenger*: Hydrogen bonding in biological structures. Springer Verlag, Berlin/New York 1991, chapter 13, pp. 169–219.
- [23] *I. Tvaroska and S. Pérez*: Conformational-energy calculations for oligosaccharides: a comparison of methods. *Carbohydr. Res.* **149** (1986), 389–410.
- [24] *W. Heiden, G. Moeckel, and J. Brickmann*: A new approach to analysis and display of local lipophilicity/hydrophilicity mapped on molecular surfaces (MLP). *J. Comput.-Aided Mol. Des.* **7** (1993), 503–514.
- [25] *M. Teschner, C. Henn, H. Vollhardt, S. Reiling, and J. Brickmann*: Texture mapping, a new tool for molecular graphics. *J. Mol. Graphics* **12** (1994), 98–105.
- [26] The V<sub>H</sub>-amylose part of this figure, first published in a lecture account [2], has been used as the frontispiece of a book: *Carbohydrates as Organic Raw Materials III*. Eds. *H. van Bekkum, H. Röper, and A. G. J. Voragen*: VCH Publ., Weinheim/New York 1996.
- [27] [27a] *T. L. G. Carlson, K. Larsson, N. Dinhuuyen, and N. Krog*: A study of the amylose-monoacylglyceride complex by Raman spectroscopy. *Starch/Stärke* **31** (1979), 222–224.  
[27b] *R. Stute and G. Konieczny-Janda*: DSC studies on starch-lipid complexes. *Starch/Stärke* **35** (1983), 340–347.  
[27c] *S. Raphaelides and J. Karkalas*: Thermal dissociation of amylose-fatty acid complexes. *Carbohydr. Res.* **172** (1988), 65–82.  
[27d] *G. Wulff and S. Kubik*: Helical amylose complexes with organic ligands. *Macromol. Chem.* **193** (1992), 1071–1080.  
[27e] *G. Wulff and S. Kubik*: Circular dichroism and UV spectroscopy of complexes of amylose. *Carbohydr. Res.* **237** (1992), 1–10.  
[27f] *S. Kubik and G. Wulff*: Characterization and chemical modification of amylose complexes. *Starch/Stärke* **45** (1993), 220–225.
- [28] *R. K. McMullan, W. Saenger, J. Fayos, and D. Mootz*: Topography of cyclodextrin inclusion complexes. Molecular geometry of the iodine-cyclohexaamylose complex. *Carbohydr. Res.* **31** (1973), 211–227.
- [29] *M. Noltemeyer and W. Saenger*: Structural chemistry of linear  $\alpha$ -cyclodextrin-polyiodide complexes. Models for the blue amylose-iodine complex. *J. Am. Chem. Soc.* **102** (1980), 2710–2722.
- [30] *F. Cramer, U. Bergmann, P. C. Manor, M. Noltemeyer, and W. Saenger*: Lineare Polyiodidketten in kanalförmiger Cyclodextrinmatrix. Kristallographische Daten und Vergleiche mit dem blauen Stärke-Polyiodid-Komplex. *Liebigs Ann. Chem.* (1976), 1169–1179.
- [31] *C. Betzel, B. Hingerty, M. Noltemeyer, G. Weber, W. Saenger, and J. A. Hamilton*:  $\beta$ -Cyclodextrin compound with potassium iodide. Spatial fitting of a polyiodide chain to a given matrix. *J. Inclusion Phenom. Mol. Recogn.* **1** (1983), 181–191.
- [32] *W. J. James, D. French, and R. E. Rundle*: Schardinger dextrins. Structure of the cyclohexaamylose-iodine complex. *Acta Crystallogr. Sect. B* **12** (1959), 385–389.
- [33] [33a] *J. C. Thompson and E. Hamori*: A kinetic investigation of the amylose-iodine reaction. *J. Phys. Chem.* **75** (1972), 272–280.  
[33b] *A. Cesàro, J. C. Benegas, and D. R. Ripoll*: Molecular model of the cooperative amylose-triiodide complex. *Phys. Chem.* **90** (1986), 2787–2791.
- [34] *M. Minick, K. Fotta, and A. Khan*: Polyiodine units in starch-iodine complex; INDO CI study of spectra. *Biopolymers* **31** (1991), 57–63.
- [35] [35a] *G. A. Gilbert and J. V. R. Marriot*: Starch-iodine complexes. *Trans. Faraday Soc.* **44** (1948), 84–93.  
[35b] *T. Handa, H. Yajima, and T. Kajiura*: On the blue color of triiodide ions in starch and starch fractions. Raman spectra of blue species in amylose. *Biopolymers* **19** (1980), 1723–1741.
- [36] [36a] *W. Banks, C. T. Greenwood, and K. M. Khan*: The interaction of linear amylose oligomers with iodine. *Carbohydr. Res.* **17** (1971), 25–33.  
[36b] *A. Cesàro, E. Jerian, and S. Saule*: Physicochemical studies of amylose in aqueous solution: thermodynamics of the iodine-triiodide complex. *Biopolymers* **19** (1980), 1491–1506.  
[36c] *T. Handa, H. Yajima, T. Yamamura, T. Ishii, and H. Aikawa*: Enthalpy change of amylose triiodide formation. *Starch/Stärke* **32** (1980), 194–197.
- [37] [37a] *K. Freudenberg, E. Schaaf, G. Dumpert, and Th. Ploetz*: Neue Ansichten über die Stärke. *Naturwiss.* **27** (1939), 850–853.  
[37b] *K. Freudenberg and H. Boppel*: Die Lage der Verzweigungsstelle in der Stärke. *Ber. Dtsch. Chem. Ges.* **73** (1940), 609–620.
- [38] [38a] *D. French and R. E. Rundle*: The molecular weights of the Schardinger  $\alpha$ - and  $\beta$ -dextrins. *J. Am. Chem. Soc.* **64** (1942), 1651–1653.  
[38b] *R. E. Rundle*: The configuration of starch in the starch-iodine complex. Fourier-projections from X-ray diagrams. *J. Am. Chem. Soc.* **69** (1947), 1769–1772.
- [39] *R. H. Marchessault and A. Sarko*: X-ray structure of polysaccharides. *Adv. Carbohydr. Chem.* **22** (1967), 421–481, particularly p. 468 ff.
- [40] *W. Blokzijl and J. B. F. N. Engebets*: Hydrophobic effects, opinion and facts. *Angew. Chem.* **105** (1993), 1610–1624; *Angew. Chem. Int. Ed. Engl.* **32** (1993), 1545–1559.
- [41] *F. W. Lichtenthaler and S. Immel*: Cyclodextrins, cyclomannins, and cyclogalactins with five and six (1→4)-linked sugar units: a comparative assessment of their conformations and hydrophobicity potential profiles. *Tetrahedron Asymmetry* **5** (1994), 2045–2060.
- [42] *F. W. Lichtenthaler and S. Immel*: The lipophilicity patterns of cyclodextrins and non-glucose cyclooligosaccharides. *J. Inclusion Phenom. Mol. Recogn. Chem.* **25** (1996), 3–16.
- [43] *Y. Nogami, K. Nasu, T. Koga, K. Ohta, K. Fujita, S. Immel, H. J. Lindner, G. E. Schmitt, and F. W. Lichtenthaler*: Synthesis, structure and conformational features of  $\alpha$ -cycloaltrin: a cyclooligosaccharide with alternating  $^4C_1/{}^1C_4$  pyranoid chairs. *Angew. Chem.* **109** (1997), 1987–1991; *Angew. Chem. Int. Ed. Engl.* **36** (1997), 1899–1902.
- [44] *S. Immel, K. Fujita, and F. W. Lichtenthaler*: Solution geometries and lipophilicity patterns of  $\alpha$ -cycloaltrin. *Chem. Eur. J.* **5** (1999), 3185–3192.
- [45] *K. Fujita, W. H. Chen, D.-Q. Yuan, Y. Nogami, T. Koga, T. Fujioka, M. Mihyshi, S. Immel, and F. W. Lichtenthaler*: Guest-induced conformational change in a flexible host: mono-*altro*- $\beta$ -cyclodextrin. *Tetrahedron Asymmetry* **10** (1999), 1689–1696.

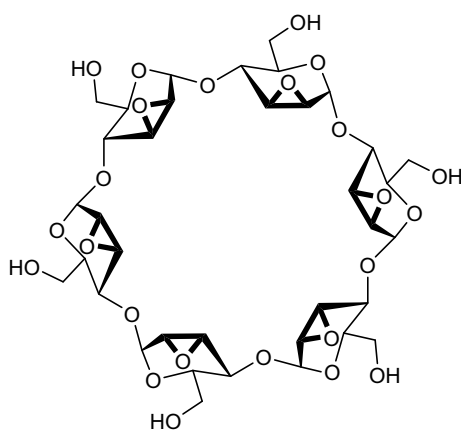
- [46] *H. Gohlke, S. Immel, and F. W. Lichtenthaler*: Conformations and lipophilicity profiles of some cyclic  $\beta(1 \rightarrow 3)$ - and  $\beta(1 \rightarrow 6)$ -linked oligogalactofuranosides. *Carbohydr. Res.* **321** (1999), 96–104.
- [47] *S. Immel, G. E. Schmitt, and F. W. Lichtenthaler*: Cyclofructins with six to ten  $\beta(1 \rightarrow 2)$ -linked fructofuranose units: geometries, lipophilicity patterns, and potential for inclusion complexation. *Carbohydr. Res.* **313** (1998), 91–105.
- [48] *F. W. Lichtenthaler and S. Immel*: Sucrose, sucralose, and fructose: Correlations between hydrophobicity potential profiles and AH-B-X assignments, in: *Sweet Taste Chemoreception*. Eds. *M. Mathiouthi, J. A. Kanters, and G. G. Birch*. Elsevier Applied Science, London/New York 1993, pp. 21–53.
- [49] *S. Immel*: MolArch<sup>+</sup>-MOLEcular ARCHitecture Modeling Program, Technische Universität Darmstadt, 1999.

**Address of authors:** Professor Dr. Dr.h.c. *Frieder W. Lichtenthaler* and Dr. *Stefan Immel*. Institut für Organische Chemie, Technische Universität Darmstadt. Petersenstraße 22, D-64287 Darmstadt (Germany). (Received: August 23, 1999).



## Chapter 2

### Per-2,3-anhydro- $\alpha$ -cyclomannin



#### Structure and Lipophilicity Profile of 2,3-Anhydro- $\alpha$ -cyclomannin and its Ethanol Inclusion Complex

S. Immel, K. Fujita, H. J. Lindner, Y. Nogami, and F. W. Lichtenthaler,  
*Chem. Eur. J.* **2000**, *6*, 2327-2333.

#### The 2,3-Anhydro- $\alpha$ -cyclomannin - 1-Propanol Hexahydrate: Topography, Lipophilicity Pattern, and Solid-state Architecture

S. Immel, F. W. Lichtenthaler, H. J. Lindner, K. Fujita, M. Fukudome, and Y. Nogami,  
*Tetrahedron: Asymmetry* **2000**, *11*, 27-36.



Molecular Modeling of Saccharides, Part 25<sup>†</sup>Structure and Lipophilicity Profile of 2,3-Anhydro- $\alpha$ -cyclomannin\*\* and Its Ethanol Inclusion ComplexStefan Immel,<sup>[a]</sup> Kahee Fujita,<sup>[b]</sup> Hans J. Lindner,<sup>[a]</sup> Yasuyoshi Nogami,<sup>[c]</sup> and Frieder W. Lichtenthaler\*<sup>[a]</sup>

**Abstract:** Readily available from  $\alpha$ -cyclodextrin in three steps, 2,3-anhydro- $\alpha$ -cyclomannin composed of six  $\alpha$ -(1  $\rightarrow$  4)-linked 2,3-anhydro-D-mannopyranose residues, crystallizes well when precipitated from aqueous ethanol. An X-ray structure reveals the macrocycle to contain ethanol in its cavity, thus representing the first inclusion complex of a non-glucose cyclooligosaccharide. The wider rim of the torus-shaped macrocycle holds the six epoxide rings whose oxygens point away from the cavity, thereby sculpturing the unique over-all shape of a six-pointed star.

**Keywords:**  $\alpha$ -2,3-anhydro- $\alpha$ -cyclomannin •  $\alpha$ -cyclodextrin • cyclooligosaccharides • inclusion complexes

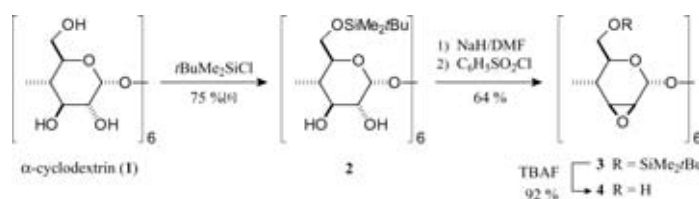
## Introduction

Cyclooligosaccharides composed of sugars other than glucose have gained considerable interest recently, as they are apt to provide host molecules with recognition features different from those of the rigid cyclodextrins.<sup>[1]</sup> However, despite of sufficiently hydrophobic CD-like cavities in the case of the cyclomannins,<sup>[2]</sup> 2,3-anhydro-cyclomannins,<sup>[3–5]</sup> cyclorhamnins,<sup>[1a]</sup> various analogues with alternating D-mannose/L-mannose and D-mannose/L-rhamnose residues,<sup>[6]</sup> and the conformationally flexible cycloaltrins,<sup>[7, 8]</sup> indications of their

interaction with suitable guests are exceedingly scarce: 2,3-anhydro- $\alpha$ -cyclomannin, based on sparse <sup>1</sup>H-NMR data, seems to be able to incorporate 4-nitrophenol,<sup>[3a, 9]</sup> and the cycloaltrins, on equally scant capillary electrophoretic evidence, appear capable of interacting with sodium 4-*tert*-butylbenzoate.<sup>[8]</sup> It is in this context, that here, with the X-ray-based unravelment of the unique molecular architecture of the title compound, we provide unequivocal proof for the first inclusion complex of a non-glucose cyclooligosaccharide.

## Results and Discussion

**Synthesis:** Our synthetic approach to 2,3-anhydro- $\alpha$ -cyclomannin,<sup>[4]</sup> as illustrated in Scheme 1, started from  $\alpha$ -cyclodextrin by protection of the six primary hydroxyl groups by



Scheme 1. Synthesis of 2,3-anhydro- $\alpha$ -cyclomannin (**4**) from  $\alpha$ -cyclodextrin (**1**).

the *tert*-butyl-dimethylsilyl moiety ( $\rightarrow$  **2**<sup>[6]</sup>). Ensuing deprotonation of the secondary hydroxyls in **2** by treatment with NaH in DMF was followed by the addition of benzenesulfonyl chloride, which not only effected selective 2-*O*-sulfonylation

[a] Prof. Dr. F. W. Lichtenthaler, Dr. S. Immel, Prof. Dr. H. J. Lindner  
Institut für Organische Chemie, Technische Universität Darmstadt  
Petersenstrasse 22, 64287 Darmstadt (Germany)  
Fax: (+49) 6151-166674  
E-mail: fwlicht@sugar.oc.chemie.tu-darmstadt.de

[b] Prof. Dr. K. Fujita  
Faculty of Pharmaceutical Sciences, Nagasaki University  
Nagasaki 852-8131 (Japan)

[c] Prof. Dr. Y. Nogami  
Daiichi College of Pharmaceutical Sciences  
Fukuoka 815 (Japan)

[†] Presented in part at the XVIIIth Japanese Cyclodextrin Symposium, Osaka, October 1999.—Part 24: S. Immel, F. W. Lichtenthaler, *Stärke Stärke* **2000**, *52*, 1–8.

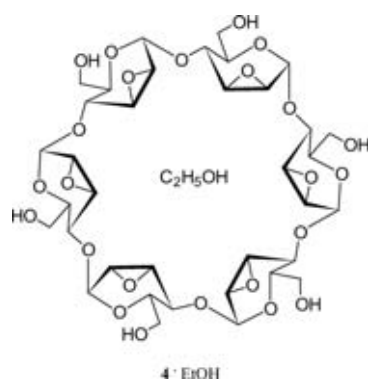
[\*\*] A cyclooligosaccharide composed of six  $\alpha$ -(1  $\rightarrow$  4)-linked 2,3-anhydro-D-mannopyranose units; for terminology used see ref. [5].

Supporting information for this article is available on the WWW under <http://caramel.oc.chemie.tu-darmstadt.de/immell/3Dstructures.html> (3D structures of Figure 1) and <http://caramel.oc.chemie.tu-darmstadt.de/immell/molcad/gallery.html> (MOLCAD graphics).

## FULL PAPER

F. W. Lichtenthaler et al.

but, concomitantly, displacement of the 2-sulfonyloxy group by the vicinal 3-OH to elaborate the 6-*O*-protected 2,3-anhydro- $\alpha$ -cyclomannin (**3**, 64%). Deblocking with TBAF/THF proceeded smoothly (4 h, 40°C) and led after crystallization from aqueous ethanol to a product in 84% yield, which, however, was not the free 2,3-anhydro- $\alpha$ -cyclomannin (**4**), but its ethanol inclusion complex **4**·C<sub>2</sub>H<sub>5</sub>OH with varying amounts of water. An intensively dried sample analyzed for the dihydrate, the crystal grown and used for the X-ray structural analysis revealed **4**·C<sub>2</sub>H<sub>5</sub>OH to be associated with 3.5H<sub>2</sub>O on the average (*vide infra*).



**X-ray Structure:** That the 2,3-anhydro- $\alpha$ -cyclomannin accumulated as the ethanol inclusion complex when crystallized from aqueous ethanol could neither be proved by mass spectral data—the complex does not survive the high vacuum MS conditions as only the  $[M]^+$  peak for the cyclooligosaccharide is detectable—nor by <sup>1</sup>H- or <sup>13</sup>C-NMR spectroscopy, since in [D<sub>5</sub>]pyridine solution it is unclear whether the ethanol-CH protons or its carbon atoms are inside or outside the cavity, in fact, the formation of a pyridine inclusion

complex being not unlikely. Only the X-ray structural analysis, invited by the high crystallinity of the product, revealed the ethanol to be located in the interior of the cavity (Figure 1). The geometry of the complex unfolds a high degree of regularity, with the backbone of the macrocycle best approximated by six-fold rotational symmetry (C<sub>6</sub>). All epoxide rings are lined up on one side of the torus-shaped molecule—the larger aperture in fact—and point away from the center molecular axis towards the outside of the macro-ring. These structural features result in the unique over-all shape of a six-pointed star (Figure 1).

The intersaccharidic torsion angles  $\Phi$  (O5-C1-O1-C4') and  $\psi$  (C1-O1-C4'-C3') show only small fluctuations ( $94.2 \pm 2.9$  and  $123.3 \pm 9.4^\circ$ , respectively), as do the atomic distances O1–O1 diagonally across the ring ( $8.74 \pm 0.26$  Å). The pyranose units are slightly tilted with their 6-OH towards the center axis, with tilt angles<sup>[11]</sup> of  $\approx 110.2 \pm 7.7^\circ$ . Table 1 records further characteristics such as the Cremer–Pople ring puckering parameters,<sup>[12]</sup> the pyranose conformation, and selected torsion angles, revealing nearly ideal <sup>0</sup>H<sub>5</sub> half-chair conformations, in which O-5 and C-5 are located above and below the mean-plane of the pyranoid rings, respectively. This implies an essentially planar arrangement of C-1 to C-4, as expressed in the very small value ( $0.5 \pm 3.4^\circ$ ) for the C1-C2-C3-C4 torsion angle. In Table 1, these geometry descriptors are compared with those found in the solid-state structure of methyl 2,3-anhydro-4,6-di-*O*-(*p*-bromobenzyl)- $\alpha$ -D-mannopyranoside (**5**),<sup>[13]</sup> whose <sup>0</sup>H<sub>5</sub> pyranoid ring conformation closely resembles that found in **4**. The primary 6-OH groups adopt *gauche*–*trans* (*gt*,  $\omega \approx +60^\circ$ ) and *gauche*–*gauche* (*gg*,  $\omega \approx -60^\circ$ ) relative to the pyranoid ring, that is either point towards the center of the cavity (*gt*) or away from it (*gg*).

As illustrated by the space-filling model in Figure 1 and, more lucidly, by the side-view plots therein, the ethanol guest

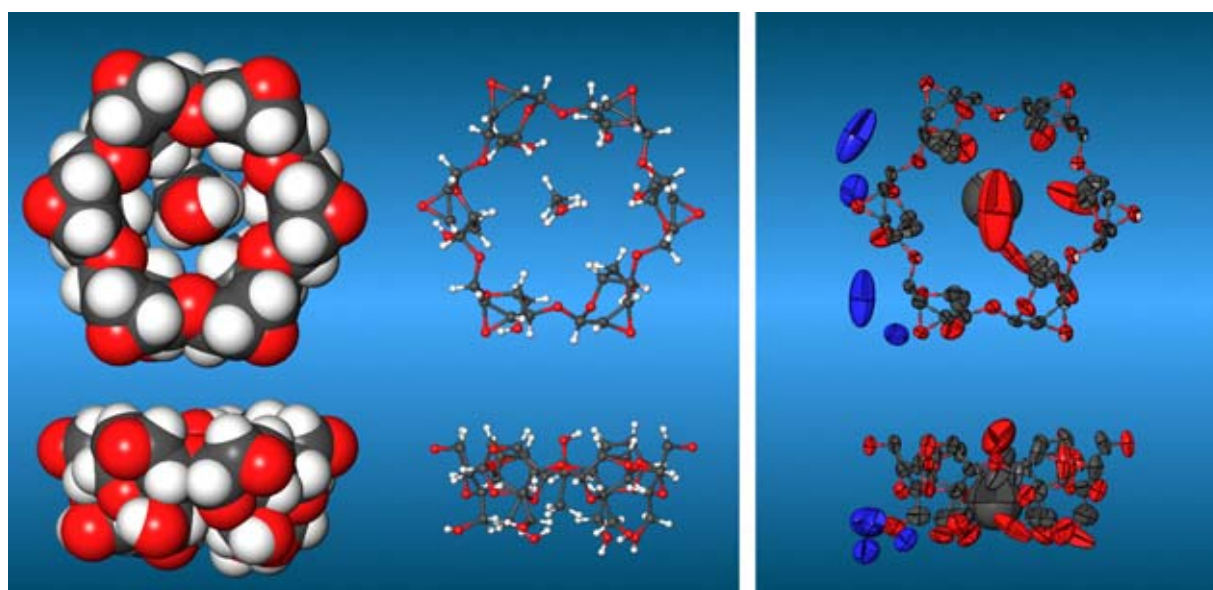


Figure 1. Molecular geometry of the 2,3-anhydro- $\alpha$ -cyclomannin–ethanol complex (**4**·EtOH) in the solid-state. Left and center: Space-filling and ball-and-stick models are shown perpendicular (top) and parallel (bottom) to the ring plane of the macrocycle; the water of crystallization and disorderings were omitted for clarity. Right: The anisotropic thermal 50% probability ellipsoids for all non-hydrogen atoms (blue: oxygen atoms of water molecules); two 6-CH<sub>2</sub>OH groups (2,3-anhydro-cyclomannoside units at top left and bottom right) are statistically disordered over two sites with equal weights.

2,3-Anhydro- $\alpha$ -cyclomannin

2327–2333

Table 1. Cremer–Pople ring puckering parameters,<sup>[12]</sup> pyranose conformations, and selected torsion angles in the solid-state structures of the 2,3-anhydro- $\alpha$ -cyclomannin–ethanol complex (**4**·EtOH) compared with those of methyl 4,6-di-*O*-(*p*-bromobenzyl)-2,3-anhydro- $\alpha$ -D-mannopyranoside (**5**).<sup>[13]</sup>

	<b>4</b> <sup>[a]</sup>	<b>5</b> <sup>[b]</sup>
Cremer–Pople parameters		
$Q$ [Å]	0.488 (0.02)	0.517
$\theta$ [°]	51.1 (2.6)	48.1
$\phi$ [°]	337.8 (4.9)	335.0
pyranose conformation		
ring torsion angles [°]	${}^oH_5$	${}^oH_5$
O5–C1–C2–C3	20.2 (4.0)	21.2
C1–C2–C3–C4	0.5 (3.4)	–3.2
C2–C3–C4–C5	10.7 (3.2)	15.8
C3–C4–C5–O5	–41.0 (2.5)	–47.3
C4–C5–O5–C1	67.2 (1.6)	71.5
C5–O5–C1–C2	–55.4 (3.2)	–56.5
other torsions		
O1–C1–C2–O2	–170.5 (2.5)	–170.2
O5–C1–C2–O2	–46.4 (3.4)	–49.5
O5–C5–C6–O6	69.5 (5.7) <sup>[c]</sup>	71.1
	–59.2 (3.7) <sup>[c]</sup>	

[a] Root-mean-square (RMS) deviations in parenthesis. [b] Single parameters without RMS values. [c] Independently averaged values for the *gauche*–*trans* ( $\omega \approx +60^\circ$ ) and *gauche*–*gauche* ( $\omega \approx -60^\circ$ ) arrangements of the 6-CH<sub>2</sub>OH groups.

is fully immersed into the host, with its OH-group located at the wider opening of the funnel-shaped cavity, that is the side carrying the six epoxide rings (Figure 2). As these point away from the cavity, there is no possibility of elaborating a guest–host hydrogen bond, engendering a pronounced mobility of the ethanol oxygen perpendicular to the central axis of the host (cf. thermal ellipsoids in Figure 1, right).

In the crystal lattice, the 2,3-anhydro- $\alpha$ -cyclomannin–ethanol complex forms layered structures that are complex yet architecturally appealing: Two units of the inclusion complex are “fused together” to head-to-head dimers with the wider, oxirane ring-bearing sides facing each other (Figure 3)—an arrangement obviously favored by the elaboration of an intense hydrogen bond between the entrapped ethanol OH-groups (O...O distance 3.03 Å). Each layer of these dimeric units is separated by a layer of water molecules (Figure 3), which are engaged in hydrogen bonding interactions with the primary 6-hydroxyls.

A detailed schematic plot of the hydrogen bonding patterns between the 6-OH groups and the water molecules is given in Figure 4; the corresponding geometry parameters are listed in Table 2. Although all hydroxyl groups and water molecules are engaged in at least two hydrogen bonds, neither the oxirane oxygens O-2 nor the pyranose ring oxygens O-5 are involved as acceptors in this network, and therefore these hydrogen-bonding patterns extend only along the layers without being interconnected in three dimensions. In addition, no hydrogen bond is observed between the ethanol guest molecule and the cyclomannin host.

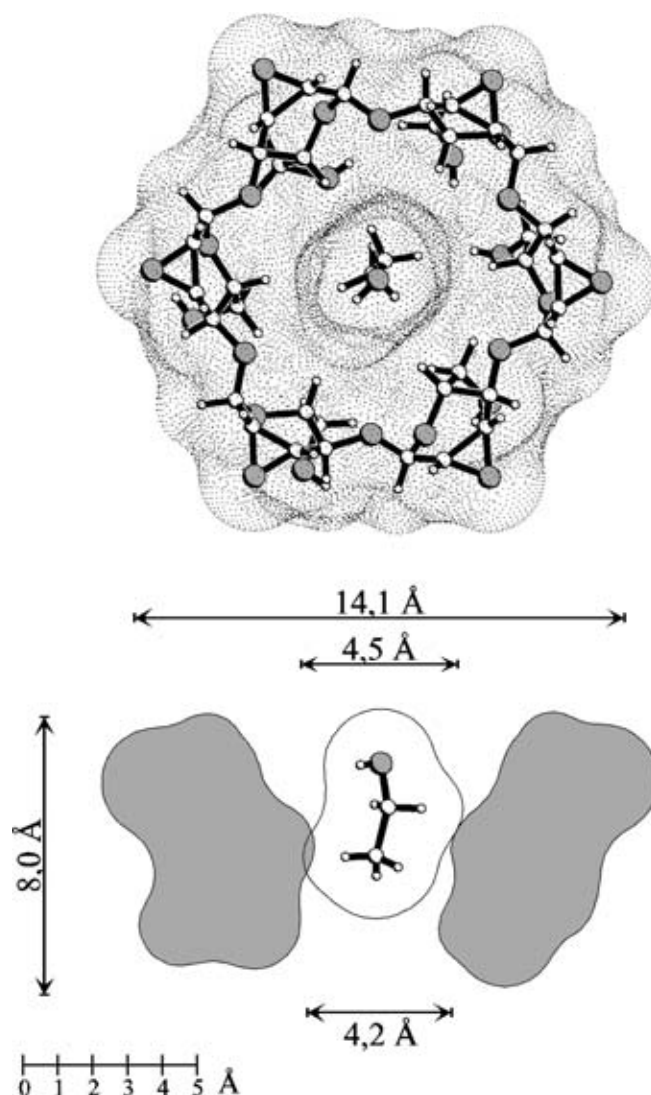


Figure 2. Top: Ball-and-stick representation of the 2,3-anhydro- $\alpha$ -cyclomannin–ethanol complex (**4**·EtOH) with the solvent accessible surface superimposed in dotted form; the wider opening carrying the oxirane rings is in front, the 6-CH<sub>2</sub>OH side at rear. Bottom: Side-view surface slice, illustrating the funnel-shaped cavity and the orientation of the guest ethanol (2-O atoms at top, 6-CH<sub>2</sub>OH face of the macrocycle at bottom); approx. molecular dimensions are included in Å.

Table 3 provides a list of some selected intermolecular atomic distances: The shortest cyclomannin host–host distances of around 3.2–3.3 Å indicate a tight packing between the molecules of each layer, as well as between the stacked macrocycles. The shortest distances between the ethanol molecules and their hosts are in the range of about 4.2–4.6 Å, thus leaving space for some thermal motions of the guests. The short O...O-distance of  $\approx 3.03$  Å between two symmetry related ethanol molecules is consistent with an hydrogen bond (vide supra), whereas the terminal methyl groups are separated by as much as 6.82 Å across two layers.

**Lipophilicity distribution:** Whilst the cavity dimensions of 2,3-anhydro- $\alpha$ -cyclomannin (**4**) are close to those of  $\alpha$ -cyclodextrin, the proportion of hydrophilic and hydrophobic surface regions is to be substantially different. Simple

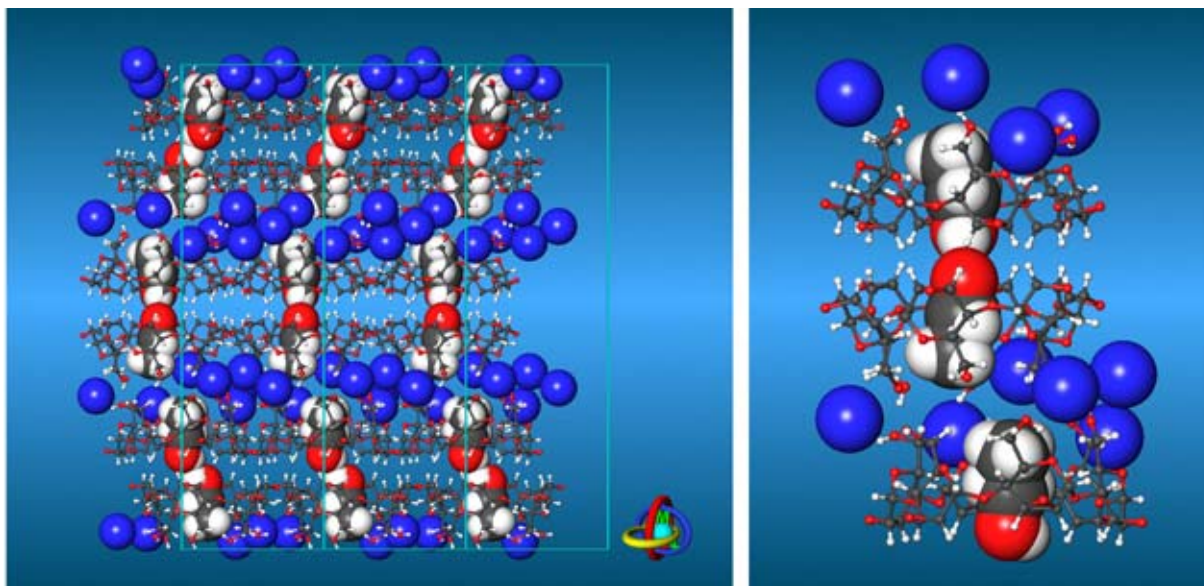


Figure 3. Assembly of the 2,3-anhydro- $\alpha$ -cyclomannin (**4**)–ethanol·3.5H<sub>2</sub>O complex in the crystal lattice: layers of head-to-head attached dimers of the macrocycle, held together by hydrogen bonding between the hydroxyl groups of two cavity-entrapped ethanol molecules, are separated by a layer of water molecules (blue spheres), which engage in hydrogen bonding with the primary 6-CH<sub>2</sub>OH groups at the narrow rim of the macrocycle.

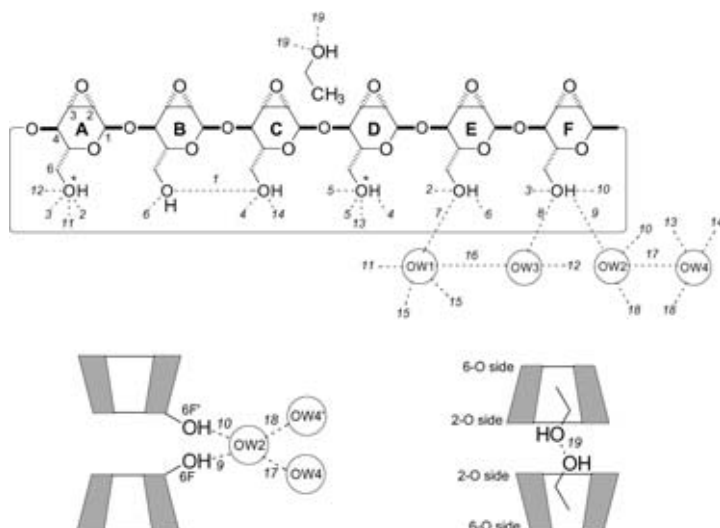


Figure 4. Scheme of intra- and intermolecular hydrogen bonds (top) in the solid-state structure of the 2,3-anhydro- $\alpha$ -cyclomannin–ethanol complex (**4**·EtOH). The individual 2,3-anhydro-mannose residues are labeled A–F and the disordered groups O(6A) and O(6D) are marked with “\*”; of the four water positions OW1–OW4 the molecule OW2 is located on a symmetry element. The numbers in italics correspond to the indices given in Table 2; “open-ended” lines indicate H-bonds formed between symmetry related positions: The ethanol guest forms a single hydrogen bond to its symmetry image. The bottom schemes visualize the H-bonding pattern between O(6F) of two stacked cyclomannins and the intercalated OW2 and OW4 molecules, as well as the hydrogen bond formed between two ethanol guest molecules.

plausibility considerations already indicate, that a “replacement” of the hydrophilic secondary hydroxyl face of  $\alpha$ -cyclodextrin<sup>[2, 16]</sup> by a torus carrying epoxide rings should lead to a distinct decrease in hydrophilicity, inasmuch as the oxirane hydrogens H-2 and H-3 are placed at the rim’s upper side. Hence, the hydrophobic nature of the cavity of **4** is expected to extend sizably towards the oxirane ring-bearing

aperture, which in turn should lead to an increase in its capacity—as compared with  $\alpha$ -CD—for inclusion complexation.

As lucidly borne out by the molecular lipophilicity pattern (MLP) of **4**, generated with the MOLCAD program<sup>[14]</sup> and visualized by projection onto the contact surface of Figure 2 in color-coded form<sup>[15]</sup> (cf. Figure 5), the macrocycle even has a lipophilicity distribution inverse to that of  $\alpha$ -CD: The most hydrophobic (yellow) are located at the wider, oxirane ring-carrying torus, obviously due to the 2-H and 3-H ring protons of the sugar units forming its rim, and inside the cavity, whereas the hydrophilic (blue) domains are centered on the opposite side around the 6-hydroxyl groups.

Surprising, at first sight, is the fact, that the hydrophilic and hydrophobic surface regions at the guest–host interface are non-complementary: The hydrophilic region of the included ethanol (i.e., its hydroxyl end) is located at the hydrophobic oxirane ring-carrying opening of the macrocycle, whereas the hydrophilic regions of the host surround the guest’s ethyl group. This impression, however, only holds for the “isolated” monomeric macrocycle with its guest. Inspection of the de facto head-to-head dimer realized in the crystal lattice, reveals a higher order of complementarity between hydrophilic and hydrophobic surface regions (Figure 6): not a guest–host matching of the respective domains, rather a host–host and guest–guest correspondence—an assembly obviously augmented by a distinct OH...O hydrogen bond between two entrapped ethanol molecules. This unique arrangement entails the outside of the dimeric complex to be largely hydrophilic, hence capable of being embedded, as horizontal stacks, into layers of water (Figure 3).

Nevertheless, the question remains why the ethanol guest in this supramolecular assembly does not place itself in the cavity in an inverse way, that it faces the hydrophilic torus rim with its hydroxyl group as this would have the advantage of allowing hydrogen bonding to one of the 6-CH<sub>2</sub>OH groups or

Table 2. Hydrogen-bond patterns in the solid-state structure of the 2,3-anhydro- $\alpha$ -cyclomannin–ethanol complex (**4**·EtOH), listed for distances  $d(\text{H}\cdots\text{O}) < 2.5 \text{ \AA}$  and/or  $d(\text{O}\cdots\text{O}) < 3.5 \text{ \AA}$  only; the water molecules are labeled OW1–OW4, the mannose labeling A–F and the indices given in the first column correspond to Figure 4.

No. (cf. Figure 4)	Hydrogen bond	$d(\text{H}\cdots\text{O}) [\text{\AA}]^{\text{[a]}}$	$d(\text{O}\cdots\text{O}) [\text{\AA}]$	$\varphi(\text{OH}\cdots\text{O}) [^\circ]^{\text{[a]}}$	Symmetry
<b>intramolecular host–host hydrogen bonds:</b>					
1	O(6B)⋯O(6C)	–	3.198	–	[b]
<b>intermolecular host–host hydrogen bonds:</b>					
2	O(6A1)⋯O(6E)	–	3.255	–	[c]
3	O(6A2)⋯O(6F)	–	2.838	–	[c]
4	O(6D1)H⋯O(6C)	1.845	2.586	149.5	[c]
5	O(6D2)⋯O(6D2)	–	2.662	–	[c]
6	O(6E)H⋯O(6B)	2.177	2.695	121.2	[c]
<b>host–water hydrogen bonds:</b>					
7	O(6E)⋯O(W1)	–	2.662	–	[b]
8	O(6F)⋯O(W3)	–	3.156	–	[b]
9	O(6F)H⋯O(W2)	2.145	2.871	147.4	[b]
10	O(6F)H⋯O(W2)	2.146	2.872	147.4	[c]
11	O(6A1)⋯O(W1)	–	2.917	–	[c]
12	O(6A2)⋯O(W1)	–	2.970	–	[c]
12	O(6A2)⋯O(W3)	–	2.894	–	[c]
13	O(6D1)⋯O(W4)	–	3.225	–	[d]
14	O(6C)⋯O(W4)	–	3.324	–	[e]
<b>water–water hydrogen bonds:</b>					
15	O(W1)⋯O(W1)	–	2.785	–	[f]
16	O(W1)⋯O(W3)	–	2.444	–	[b]
17	O(W2)⋯O(W4)	–	2.950	–	[b]
18	O(W2)⋯O(W4)	–	2.949	–	[c]
<b>guest–guest hydrogen bonds:</b>					
19	O(1)⋯O(1)	–	3.025	–	[g]

[a] Hydrogen-bond H⋯O distances and O–H⋯O angles omitted if hydrogen atoms were not located explicitly, labels O(6A1), O(6A2), O(6D1), and O(6D2) indicate disordered positions. Symmetry operations: [b]  $x,y,z$ ; [c]  $x,x-y,-z$ ; [d]  $x+1,y,z$ ; [e]  $x+1,x-y+1,-z$ ; [f]  $x,x-y-1,-z$ ; [g]  $-y,-x,-z+1/3$ .

Table 3. Selected intermolecular heavy atom distances in solid-state structure of the 2,3-anhydro- $\alpha$ -cyclomannin–ethanol complex (**4**·EtOH); labeling of the mannose units corresponds to Figure 4 and Table 2. For additional parameters on host–water distances see the list of hydrogen bonds given in Table 2.

Distances <sup>[a]</sup> ( $d < 3.3 \text{ \AA}$ )	$d [\text{\AA}]$	sym- metry	distances <sup>[a]</sup>	$d [\text{\AA}]$	sym- metry
<b>host–host (layered):</b>					
C(3D)⋯O(2A)	3.215	[d]	O(1)⋯O(1B)	4.188	[g]
C(4D)⋯O(2A)	3.270	[d]	O(1)⋯C(2C)	4.197	[g]
C(1C)⋯O(2A)	3.185	[d]	O(1)⋯C(3C)	3.979	[g]
O(2D)⋯C(3A)	3.173	[d]	O(1)⋯O(1)	4.68(15) <sup>[h]</sup>	[b]
O(2D)⋯C(4A)	3.236	[d]	O(1)⋯C(2)	5.54(20) <sup>[h]</sup>	[b]
O(2D)⋯C(1F)	3.234	[d]	O(1)⋯C(3)	5.40(15) <sup>[h]</sup>	[b]
C(3E)⋯O(2B)	3.152	[e]	C(1)⋯O(1)	4.39(40) <sup>[h]</sup>	[b]
C(4E)⋯O(2B)	3.201	[e]	C(1)⋯C(5)	4.46(39) <sup>[h]</sup>	[b]
O(2E)⋯C(3B)	3.156	[e]	C(2)⋯O(1)	4.57(16) <sup>[h]</sup>	[b]
O(2E)⋯C(4B)	3.175	[e]	C(2)⋯C(5)	4.19(27) <sup>[h]</sup>	[b]
<b>host–host (stacked):</b>					
C(6E)⋯O(6A1)	3.204	[c]	O(1)⋯O(1)	3.025	[g]
O(6C)⋯C(6D1)	3.229	[c]	C(2)⋯C(2)	6.821	[c]
O(2F)⋯C(2F)	3.290	[f]			
O(2F)⋯O(2F)	3.297	[f]			
<b>guest–guest:</b>					
			O(1)⋯O(1)	3.025	[g]
			C(2)⋯C(2)	6.821	[c]

[a] Disordered positions are indicated by the labels O(6A1), O(6A2), O(6D1), and O(6D2). Symmetry operations: [b]  $x,y,z$ ; [c]  $x,x-y,-z$ ; [d]  $x+1,y,z$ ; [e]  $x,y-1,z$ ; [f]  $-y+1,-x+1,-z+1/3$ ; [g]  $-y,-x,-z+1/3$ ; [h] Parameters averaged over all equivalent host–guest distances (e.g., distances EtOH⋯O1A–F) with root-mean-square deviations in parenthesis.

to a water molecule in the then adjoining water layer. On the other hand, though, this would conceivably create a “hydrophobic void” in the cavity as the ethyl portion of the guest is not long enough to fill it entirely. If this notion is correct,

higher alcohols are likely to form inclusion complexes with 2,3-anhydro- $\alpha$ -cyclomannin in which the orientation of the guests is inverse to that of ethanol.

## Conclusion

The solid-state structure of the 2,3-anhydro- $\alpha$ -cyclomannin–ethanol–water inclusion complex detailed herein provides a unique example of crystal engineering,<sup>[17]</sup> as three structurally diverse components assemble—with an amazing level of precision<sup>[18]</sup>—to a super-structure by mutual recognition of their steric, polar and non-polar features, the major directional force in its supramolecular construction undoubtedly being an optimal use of their hydrogen bonding capabilities.

Particularly intriguing is the finding that the 2,3-anhydro- $\alpha$ -cyclomannin host—lacking secondary hydroxyl groups at the wider torus, with which cyclodextrins form dimers via an intense hydrogen-bonding network—nevertheless finds a means to associate to dimers, that is via OH⋯OH hydrogen bonding between the ethanol guests, which is only possible though, when they are incorporated into the host in a “mismatch” of hydrophobic and hydrophilic surface regions at the guest–host interface. Thus, it is conceivable, that higher alcohols or phenols are being incorporated into the cavity of **4** in an inverse orientation with a more optimal complementarity of non-covalent guest–host interaction. As the 1-propanol inclusion complex of **4** has been obtained crystalline, the factors underlying the interplay of steric, polar, and non-

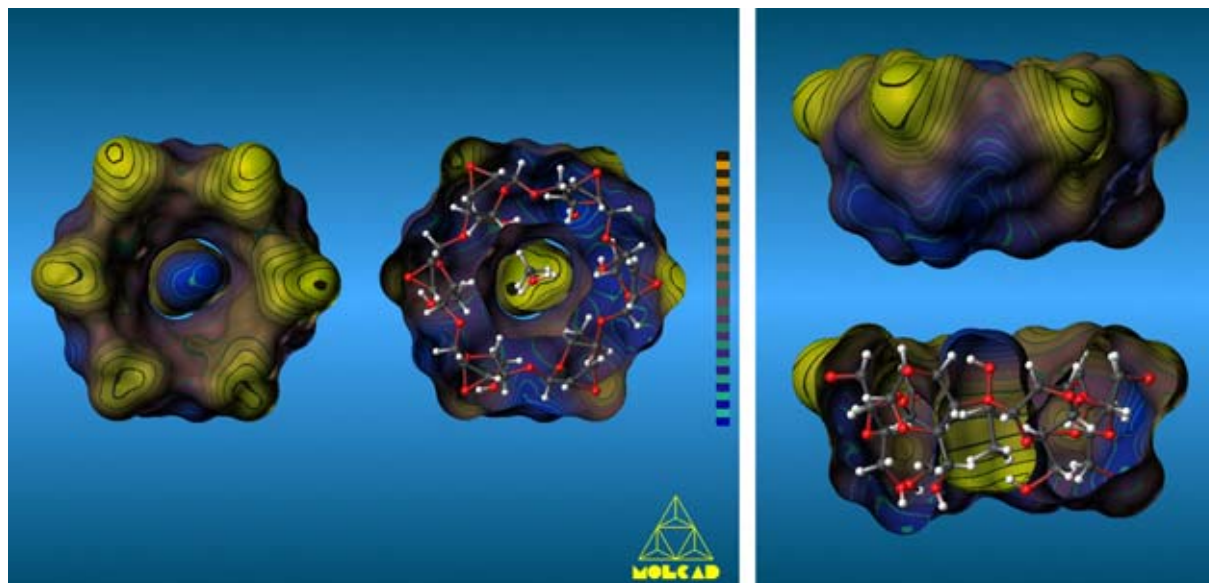


Figure 5. Molecular lipophilicity patterns (MLPs) of the 2,3-anhydro- $\alpha$ -cyclomannin ethanol complex ( $4 \cdot \text{EtOH}$ ): The relative hydrophobicity of guest and host were mapped in color-coded form onto their individual contact (i.e., solvent-accessible) surfaces, with the colors ranging from dark-blue (most hydrophilic areas) to yellow–brown (hydrophobic domains). Application and scaling of the MLPs was done for guest and host separately followed by reassembly of the complex. Left: View onto the wider opening of the macrocycle carrying the six oxirane rings, displaying the hydrophobic (yellow) side. The front-opened version (center) with ball-and-stick model insert exposes the distinctly hydrophilic (blue) rear side bearing the 6- $\text{CH}_2\text{OH}$  groups. Right: The side view representations clearly illustrate the apparent non-complementarity of hydrophobic and hydrophilic regions of guest–ethanol and host, the hydrophilic ethanol-OH group being located at the lipophilic side of the cavity.

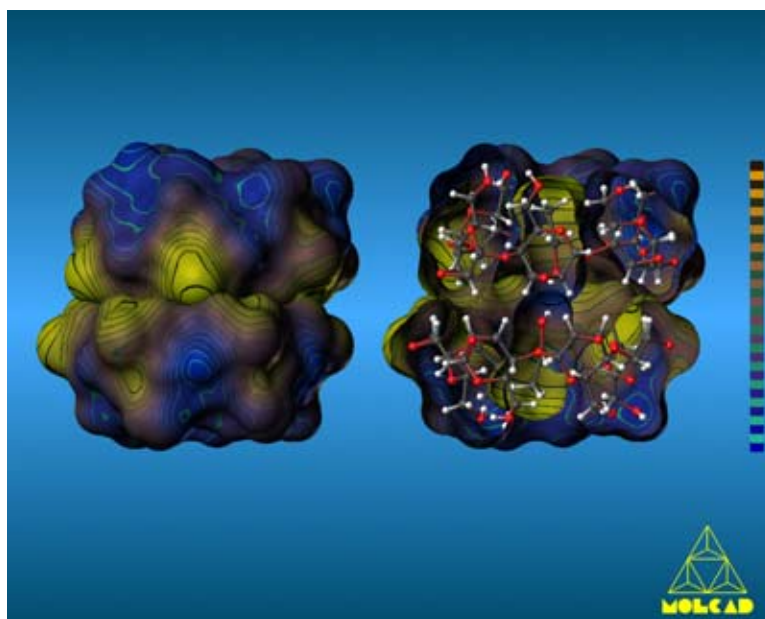


Figure 6. Molecular lipophilicity patterns (MLPs) of one dimeric unit of the 2,3-anhydro- $\alpha$ -cyclomannin–ethanol complex ( $4 \cdot \text{EtOH}$ ) as excised from the crystal lattice. Although a “mismatched” host–guest arrangement in terms of relative hydrophobicity is observed for the monomer (cf. Figure 5), the “matching” interactions become obvious in the “head-to-head” dimer: the cohesion of two macrocycles via their hydrophobic domains at the wider, oxirane-ring carrying torus is augmented by the distinct  $\text{OH} \cdots \text{O}$  hydrogen bond between the oxygens of the entrapped ethanol molecules, facing each other via their hydrophilic surface areas. This reciprocal complementarity of hydrophobic (host–host) and hydrophilic (guest–guest) surface regions entails the outside of the dimeric assembly to be largely hydrophilic; in the crystal lattice it packs into horizontal layers that are separated by water (cf. Figure 3).

covalent interactions between its structurally as diverse components as **4**, a suitable guest, and notably, water are being probed further.

## Experimental Section

**General:** All reactions were monitored by thin-layer chromatography on aluminum plates coated with silica gel 60  $F_{254}$ . Melting points are uncorrected.  $^1\text{H}$ - and  $^{13}\text{C}$ -NMR spectra were determined on a Varian Unity plus 500 spectrometer. FAB-MS were recorded on a JEOL JMS-DX 303 instrument.

**Per-6-*O*-*tert*-butyldimethylsilyl-2,3-anhydro- $\alpha$ -cyclomannin [cyclohexakis-6-*O*-*t*-butyldimethylsilyl-(1  $\rightarrow$  4)-2,3-anhydro- $\alpha$ -D-mannopyranosyl] (3):** Per-6-*O*-(*t*-butyldimethylsilyl)- $\alpha$ -cyclodextrin (**2**, 1.0 g, 0.6 mmol),<sup>[10]</sup> was added to a solution of NaH (0.40 g, 10.8 mmol) in anhydrous DMF (40 mL) and the mixture was kept under  $\text{N}_2$  at 60 °C for 2 h. After cooling, benzenesulfonyl chloride (568  $\mu\text{L}$ , 4.32 mmol) in anhydrous DMF (10 mL) was injected followed by stirring at room temperature for 30 min. Filtration and flash chromatography on a silica gel column (4  $\times$  15 cm) with benzene/EtOAc 4:1 (250 mL) afforded **3** (600 mg, 64%); m.p.: 203 °C (decomp.);  $[\alpha]_D^{25} = +70.1$  ( $c = 0.36$  in THF).  $^1\text{H}$  NMR (500 MHz,  $\text{CDCl}_3$ , relevant data):  $\delta = 3.11$  (d, 1H, 2-H), 3.32 (d, 1H, 3-H), 3.56 (d, 1H, 5-H), 3.64, 3.93 (2d, 1H), 6-H<sub>2</sub>), 4.24 (d, 1H, 4-H), 5.16 (s, 1H, 1-H),  $J_{1,2} = J_{3,4} = 0$ ,  $J_{2,3} = 3.7$ ,  $J_{4,5} = 11.5$  Hz;  $^{13}\text{C}$  NMR (125 MHz,  $\text{CDCl}_3$ ):  $\delta = -5.17$ ,  $-4.96$  ( $\text{Me}_2\text{Si}$ ), 18.31 ( $t\text{BuCSi}$ ), 25.91 ( $t\text{BuMe}_3$ ), 49.15 (C-2), 53.30 (C-3), 62.17 (C-6), 68.43 (C-4), 69.74 (C-5), 96.69 (C-1); MS [ $M$ ]<sup>+</sup> not detectable;  $\text{C}_{72}\text{H}_{132}\text{O}_{24}\text{Si}_6$  (1550.2): C 55.78, H 8.58; found: C 55.55, H 8.68.

**Per-2,3-anhydro- $\alpha$ -cyclomannin–ethanol inclusion complex [cyclohexakis-(1  $\rightarrow$  4)-2,3-anhydro- $\alpha$ -D-mannopyranosyl–ethanol] (4·EtOH):** A 1M solution of  $\text{Bu}_4\text{NF}$  in THF (4.6 mL) was added to a solution of silyl epoxide **3** (1.0 g, 0.65 mmol) in anhydrous THF (90 mL) under  $\text{N}_2$ , and the mixture was stirred at 40 °C for 4 h. Concentration in vacuo gave a syrupy residue, which was dissolved in commercially available 95% EtOH (10 mL).



Standing overnight in a refrigerator resulted in a precipitate which was collected and dried in vacuo over  $P_2O_5$  at ambient temperature for 24 h: **4**·EtOH (511 mg, 84%); m.p.: 267 °C (partial melting with browning, followed by gradual decomp.);<sup>[19]</sup>  $[\alpha]_D^{18} = +87$  ( $c = 0.3$  in DMSO).  $^1H$  NMR (500 MHz,  $[D_5]$ pyridine):  $\delta = 3.47$  (d, 1 H, 2-H), 3.73 (d, 1 H, 3-H), 4.18, 4.43 (2m, 1 H, 6-H<sub>2</sub>), 4.34 (m, 1 H, 5-H), 4.40 (d, 1 H, 4-H), 5.63 (s, 1 H, H-1),  $J_{1,2} = J_{3,4} = 0$ ,  $J_{2,3} = 3.5$ ,  $J_{4,5} = 9.0$  Hz, assignments were substantiated by  $^1H$ - $^1H$  and  $^1H$ - $^{13}C$  2D NMR;  $^{13}C$  NMR (125 MHz,  $[D_5]$ pyridine):  $\delta = 49.61$  (C-2), 54.03 (C-3), 62.81 (C-6), 70.10 (C-4), 71.27 (C-5), 96.37 (C-1); FAB-MS:  $m/z$ : 865  $[M]^+$ ;  $C_{36}H_{48}O_{24} \cdot C_2H_5OH \cdot 2H_2O$  (944.8): C 48.30, H 6.18; found: C 48.14, H 6.11.

Crystals suitable for X-ray analysis were grown by suspending **4**·EtOH (10 mg) in 95% ethanol (5 mL), followed by brief warming to 65 °C, filtration through a membrane filter, and standing of the filtrate at room temperature for about a week. Of the crystals obtained (3 mg) a colorless prism with dimensions of  $0.75 \times 0.4 \times 0.4$  mm was suited for X-ray exposure, its composition being  $C_{36}H_{48}O_{24} \cdot C_2H_5OH \cdot 3.5H_2O$  ( $M_r = 973.89$ ). It had space group  $P3_112$ , trigonal, with  $a = b = 14.076(6)$ ,  $c = 41.610(10)$  Å;  $V = 7139.8(46)$  Å<sup>3</sup>,  $Z = 6$ ,  $\rho = 1.349$  g cm<sup>-3</sup>,  $\mu(Mo_{K\alpha}) = 0.110$  mm<sup>-1</sup>,  $T = 293(2)$  K. A total of 8154 reflections were collected on an Enraf–Nonius CAD-4 diffractometer with graphite-monochromated  $Mo_{K\alpha}$  ( $\lambda = 0.71093$  Å) radiation, of which 5104 were independent ( $R_{int} = 0.1537$ ). The structure was solved by direct methods (SHELXS-86<sup>[20]</sup>) and successive Fourier difference synthesis. Refinement (on  $F^2$ ) was performed by full-matrix least squares method with SHELXL-93.<sup>[20]</sup>  $R(F) = 0.1069$  for 4036 reflections with  $I \geq 2\sigma I$ ,  $\omega R(F^2) = 0.2890$  for all 5104 reflections with  $\omega = 1/(\sigma^2(F_o^2) + (0.2025P)^2 + 3.4693P)$ ; where  $P = (F_o^2 + 2F_c^2)/3$ . The 6-CH<sub>2</sub>OH groups of two 2,3-anhydro-mannoside units diametrically across the macroring are disordered over two positions with occupancies of 50%, respectively (torsion angles  $\omega(O5-C5-C6-O6) \approx +70^\circ$  and  $-60^\circ$ ). All non-hydrogen atoms except the disordered carbon atoms were refined anisotropically; hydrogen atoms on the 2,3-anhydro- $\alpha$ -cyclomannin were considered in calculated positions with the  $1.2 \times U_{eq}$  value of the corresponding bound atom. The hydroxyl proton of the ethanol was subsequently positioned geometrically.

Crystallographic data (excluding structure factors) for the **4**·EtOH have been deposited with the Cambridge Crystallographic Data Centre as supplementary publication no. CCDC-143714. Copies of the data can be obtained free of charge on application to CCDC, 12 Union Road, Cambridge CB2 1EZ, UK (fax: (+44)1223-336-033; e-mail: deposit@ccdc.cam.ac.uk).

**Computational details:** Calculation of the molecular contact surfaces and the respective hydrophobicity potential profiles (MLP's) was performed using the MOLCAD molecular modeling program.<sup>[14, 15]</sup> Scaling of the MLP profiles was performed in relative terms (most hydrophilic to most hydrophobic surface regions); no absolute values are displayed. Molecular Graphics were generated using MolArch.<sup>[21]</sup>

## Acknowledgement

Financial support was provided by the Fonds der Chemischen Industrie. In addition, we thank Mrs. Sabine Foro for collecting the X-ray crystallographic data, Prof. Dr. J. Brickmann, Institut für Physikalische Chemie of this University, for access to the MOLCAD software package, and to the Japan Maize Products Co. Ltd. for providing  $\alpha$ -cyclodextrin.

- [1] For reviews, see: a) F. W. Lichtenthaler, S. Immel, *J. Inclusion Phenom. Mol. Recognit. Chem.* **1996**, *5*, 3–16; b) G. Gattuso, S. A. Nepogodiev, J. F. Stoddart, *Chem. Rev.* **1998**, *98*, 1930–1958.  
 [2] F. W. Lichtenthaler, S. Immel, *Tetrahedron: Asymmetry* **1994**, *5*, 2045–2060.  
 [3] a) A. W. Coleman, P. Zhang, C. C. Ling, J. Mahuteau, H. Parrot-Lopez, M. Miocque, *Supramol. Chem.* **1992**, *1*, 11–14; b) P. Zhang, A. W. Coleman, *Supramol. Chem.* **1993**, *2*, 255–263.  
 [4] Y. Nogami, K. Nasu, T. Koga, K. Ohta, K. Fujita, S. Immel, H. J. Lindner, G. E. Schmitt, F. W. Lichtenthaler, *Angew. Chem.* **1997**, *109*, 1987–1991; *Angew. Chem. Int. Ed. Engl.* **1997**, *36*, 1899–1902.  
 [5] Nomenclature: a) According to a recent proposal for a simplified designation of non-glucose cyclooligosaccharides<sup>[2, 3b]</sup> which has been

authoritatively endorsed,<sup>[5c]</sup> the mannose analogue of  $\alpha$ -cyclodextrin is termed  $\alpha$ -cyclomannin; as **4** is the 2,3-anhydro derivative thereof, we prefer, for practical reasons, the term 2,3-anhydro- $\alpha$ -cyclomannin<sup>[4]</sup> rather than cyclo- $\alpha$ -1,4-hexamanno-2,3-epoxide, also used previously.<sup>[3]</sup> The systematic name required by recent IUPAC recommendations (*Carbohydr. Res.* **1997**, *297*, 79, Rule 2-Carb-37.4.2) turns out to be *cyclohexakis-(1 → 4)-2,3-anhydro- $\alpha$ -D-mannopyranosyl*, which is not only less handy, but inconsistent, since **4** is not a series of “glycosyls”, but a glycoside, a hexasaccharide, in fact. To comply with the rules, the experimental section features both versions; b) S. Immel, J. Brickmann, F. W. Lichtenthaler, *Liebigs Ann. Chem.* **1995**, 929–942; c) J. Szejtli, in *Comprehensive Supramolecular Chemistry, Vol. 3 (Cyclodextrins)* (Eds.: J. Szejtli, T. Osa), Pergamon, Oxford, UK, **1996**, p. 7; J. Szejtli, *Chem. Rev.* **1998**, *98*, 1743–1754.

- [6] a) P. R. Ashton, C. L. Brown, S. Menzer, S. A. Nepogodiev, J. F. Stoddart, D. J. Williams, *Chem. Eur. J.* **1996**, *2*, 580–591; b) P. R. Ashton, S. J. Cantrill, G. Gattuso, S. Menzer, S. A. Nepogodiev, A. N. Shipway, J. F. Stoddart, D. J. Williams, *Chem. Eur. J.* **1997**, *3*, 1299–1314.  
 [7] a)  $\alpha$ -Cycloaltrin: [4]; b)  $\alpha$ -Cycloaltrin: K. Fujita, H. Shimada, K. Ohta, Y. Nogami, K. Nasu, *Angew. Chem.* **1995**, *107*, 1783–1784; *Angew. Chem. Int. Ed. Engl.* **1995**, *34*, 1621–1622; c)  $\alpha$ -Cycloaltrin: Y. Nogami, K. Fujita, K. Ohta, K. Nasu, H. Shimada, C. Shinohara, T. Koga, *J. Inclusion Phenom. Mol. Recognit. Chem.* **1996**, *25*, 53–56.  
 [8] S. Immel, K. Fujita, F. W. Lichtenthaler, *Chem. Eur. J.* **1999**, *5*, 3185–3192.  
 [9] It has been stated,<sup>[3a]</sup> albeit without any preparative or spectroscopic proof, that 2,3-anhydro- $\alpha$ -cyclomannin gives 1:1 complexes with anethole, vanillin, and *N*-acetylphenylalanine.  
 [10] K. Takeo, K. Uemura, H. Mitoh, *J. Carbohydr. Chem.* **1988**, *7*, 293–308.  
 [11] The tilt angle  $\tau^{[1b, 4]}$  is defined as the angle between the least-squares best-fit mean-plane of the macrocycle (all O-1 atoms) and each pyranose ring (atoms C-1 through C-5 and O-5).  
 [12] a) D. A. Cremer, J. A. Pople, *J. Am. Chem. Soc.* **1975**, *97*, 1354–1358; b) G. A. Jeffrey, R. Taylor, *Carbohydr. Res.* **1980**, *81*, 182–183.  
 [13] X. Wu, F. Kong, D. Lu, G. Li, *Carbohydr. Res.* **1992**, *235*, 163–178.  
 [14] a) J. Brickmann, *MOLCAD—MOLEcular Computer Aided Design*, Technical University of Darmstadt, **1996**; J. Brickmann, *J. Chim. Phys.* **1992**, *89*, 1709–1721. The major part of the MOLCAD program is included in the SYBYL package of TRIPOS Associates, St. Louis, USA; b) J. Brickmann, T. Goetze, W. Heiden, G. Moeckel, S. Reiling, H. Vollhardt, C.-D. Zachmann, *Interactive Visualization of Molecular Scenarios with the MOLCAD/SYBYL Package*, in *Data Visualization in Molecular Science: Tools for Insight and Innovation* (Ed.: J. E. Bowie), Addison-Wesley Publ., Reading, Mass., USA, **1995**, pp. 83–97; c) M. Teschner, C. Henn, H. Vollhardt, S. Reiling, J. Brickmann, *J. Mol. Graphics* **1994**, *12*, 98–105.  
 [15] a) W. Heiden, G. Moeckel, J. Brickmann, *J. Comput. Aided Mol. Des.* **1993**, *7*, 503–514; b) S. Reiling, M. Schlenkrich, J. Brickmann, *J. Comput. Chem.* **1996**, *17*, 450–468.  
 [16] S. Immel, F. W. Lichtenthaler, *Liebigs Ann.* **1996**, 27–36.  
 [17] G. R. Desiraju, *Angew. Chem.* **1995**, *107*, 2541–2558; *Angew. Chem. Int. Ed. Engl.* **1995**, *34*, 2311–2327.  
 [18] Diction borrowed from S. Dunitz, *Pure Appl. Chem.* **1991**, *63*, 177.  
 [19] The 2,3-anhydro- $\alpha$ -cyclomannin of m.p.: 166 °C—defacto a misprint; correct value 266 °C—and  $[\alpha]_D^{18} = +83.6$  ( $c = 0.34$  in DMSO) mentioned in [4] was precipitated from methanol, and, thus, conceivably was the methanol inclusion complex of **4**. The same is likely to apply to the “cyclo- $\alpha$ -1,4-hexamanno-2,3-epoxide” ( $\equiv$  **4**) of m.p.: 268–269.5 °C and  $[\alpha]_D^{20} = +128$  ( $c = 1.0$  in DMF), prepared by exposure of per-2-*O*-tosyl- $\alpha$ -CD to  $K_2CO_3/MeOH$  (6 h, 60 °C) and recrystallization of the product from water and then from methanol,<sup>[3b]</sup> despite of the fact that its microanalytical data were interpreted as to contain neither solvent.  
 [20] G. M. Sheldrick, *SHELXS-86 and SHELXL-93—Programs for Crystal Structure Solution and Refinement*, University of Göttingen, **1986** and **1993**.  
 [21] S. Immel, *MolArch+—MOLEcular ARCHitecture Modeling Program*, Technical University of Darmstadt, **1997**.

Received: August 18, 1999

Revised version: November 29, 1999 [F 1986]





Pergamon

Tetrahedron: Asymmetry 11 (2000) 27–36

---

---

**TETRAHEDRON:**  
**ASYMMETRY**

---

---

## The 2,3-anhydro- $\alpha$ -cyclomannin–1-propanol hexahydrate: topography, lipophilicity pattern and solid-state architecture<sup>†</sup>

Stefan Immel,<sup>a,\*</sup> Frieder W. Lichtenthaler,<sup>a</sup> Hans J. Lindner,<sup>a</sup> Kahee Fujita,<sup>b</sup>  
Makato Fukudome<sup>b</sup> and Yasuyoshi Nogami<sup>c</sup>

<sup>a</sup>*Institut für Organische Chemie, Technische Universität Darmstadt, D-64287 Darmstadt, Germany*

<sup>b</sup>*Faculty of Pharmaceutical Sciences, Nagasaki University, Nagasaki 852-8131, Japan*

<sup>c</sup>*Daiichi College of Pharmaceutical Sciences, Tamagawa-cho, Fukuoka 815, Japan*

Received 30 November 1999; accepted 13 December 1999

---

### Abstract

As evidenced by its X-ray structural analysis, 2,3-anhydro- $\alpha$ -cyclomannin **6**, a cyclooligosaccharide consisting of six  $\alpha$ -(1 $\rightarrow$ 4)-linked 2,3-anhydro-D-mannopyranose units, readily incorporates 1-propanol into its cavity such that hydrophobic and hydrophilic surface regions of guest and host match at their interfaces. Together with water, the macrocycle and its guest assemble into a unique solid-state architecture, featuring layers of head-to-head dimers of the macrocycle with its guest, separated by equally distinct layers of water molecules, which are engaged in an intense hydrogen bonding network with the 6-CH<sub>2</sub>OH and the propanol-OH groups. The overall guest–host topography is thus reverse to that of the respective ethanol inclusion complex.<sup>1</sup> © 2000 Elsevier Science Ltd. All rights reserved.

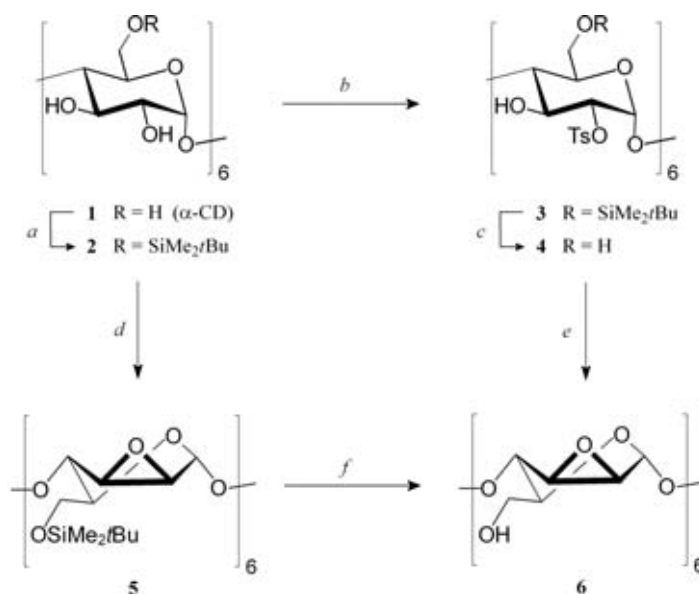
---

### 1. Introduction

2,3-Anhydro- $\alpha$ -cyclomannin **6**,<sup>2</sup> a cyclooligosaccharide composed of six  $\alpha$ -(1 $\rightarrow$ 4)-linked 2,3-anhydro-D-mannopyranose units, is readily accessible from  $\alpha$ -cyclodextrin via simple reaction sequences, the key steps being—in the 6-*t*-butyldimethylsilyl-blocked  $\alpha$ -CD **2**<sup>3</sup>—the selective sulfonation of the more acidic 2-OH and subsequent displacement of the 2-sulfonyloxy groups by the vicinal 3-OH to elaborate the oxirane rings. Of the two protocols that have been advanced for this conversion,<sup>4,5</sup> the one allowing sulfonation and epoxide formation to proceed in a one-pot operation, i.e. **2** $\rightarrow$ **5**, appears to be preparatively more propitious (44% overall yield for **1** $\rightarrow$ **6**<sup>5</sup>) than the other performing sulfonation (**2** $\rightarrow$ **3**) and generation of the oxirane ring (**4** $\rightarrow$ **5**) in separate operations (19% for **1** $\rightarrow$ **6**<sup>4</sup>) (Scheme 1).

\* Corresponding author. E-mail: lemmi@sugar.oc.chemie.tu-darmstadt.de

<sup>†</sup> Part 26 of the series Molecular Modelling of Saccharides. For Part 25, see Immel et al.<sup>1</sup>



Scheme 1. Key: (a) *t*BuMe<sub>2</sub>SiCl/imidazole, DMF, 75%;<sup>3</sup> (b) TsCl/DMAP, pyridine, 55%;<sup>4</sup> (c) BF<sub>3</sub>·Et<sub>2</sub>O, CHCl<sub>3</sub>, 51%;<sup>4</sup> (d) NaH/DMF, then C<sub>6</sub>H<sub>5</sub>SO<sub>2</sub>Cl, 64%;<sup>5</sup> (e) K<sub>2</sub>CO<sub>3</sub>, MeOH, 90%;<sup>4</sup> (f) Bu<sub>4</sub>NF, THF, 92%<sup>5</sup>

Thus, unlike other non-glucose cyclooligosaccharides with  $\alpha$ -(1 $\rightarrow$ 4)-linked hexose units,<sup>6–8</sup> 2,3-anhydro- $\alpha$ -cyclomannin is available in sufficient amounts to broadly study its molecular recognition properties, and in particular its capability to form inclusion complexes. Indeed, when recrystallized from aqueous ethanol, **6** was shown to accumulate as a hydrate with ethanol included in its cavity (Fig. 1, left entries).<sup>1</sup> The three crystal engineering entities—**6**, ethanol, and water—assemble to a unique superstructure in the solid-state, characterized by layers of head-to-head dimers of the macrocycle, stabilized by OH $\cdots$ OH hydrogen bonding between the cavity-included guest–ethanol molecules, followed by layers of water. The crystal engineering operative is unusual in that the hydrophilic and hydrophobic surface regions at the guest–host interface are non-complementary as the guest's OH group is placed at the hydrophobic, epoxide ring-carrying rim of the macrocycle.<sup>1</sup> This behavior is strongly contrasted by various inclusion complexes of the cyclodextrins of which the lipophilicity profiles have been determined,<sup>9,10</sup> as they reveal the guest–host matching of hydrophilic and hydrophobic surface regions to be a decisive factor for the orientation of the guest in the cavity.

We wish to report here the peculiar finding that simply by enlarging the guest molecule by a CH<sub>2</sub> group, i.e. by including 1-propanol instead of ethanol into the cavity of 2,3-anhydro- $\alpha$ -cyclomannin, the self-assembly of the three crystal engineering components—**6**, 1-propanol, and water—leads to a distinctly different solid-state architecture (Fig. 1, right entries), the guest now having the inverse orientation in the cavity, i.e. one in which hydrophobic and hydrophilic surface areas at the guest–host interface are complementary.

## 2. Results and discussion

2,3-Anhydro- $\alpha$ -cyclomannin **6**, when recrystallized from aqueous 1-propanol, accumulated as its 1-propanol inclusion complex of which the X-ray analysis, invited by the high crystallinity of the product, revealed it to be a hexahydrate. The geometry of the complex (Fig. 1, right entries) unfolds a high degree of regularity, with the backbone of the macrocycle best approximated by six-fold rotational symmetry

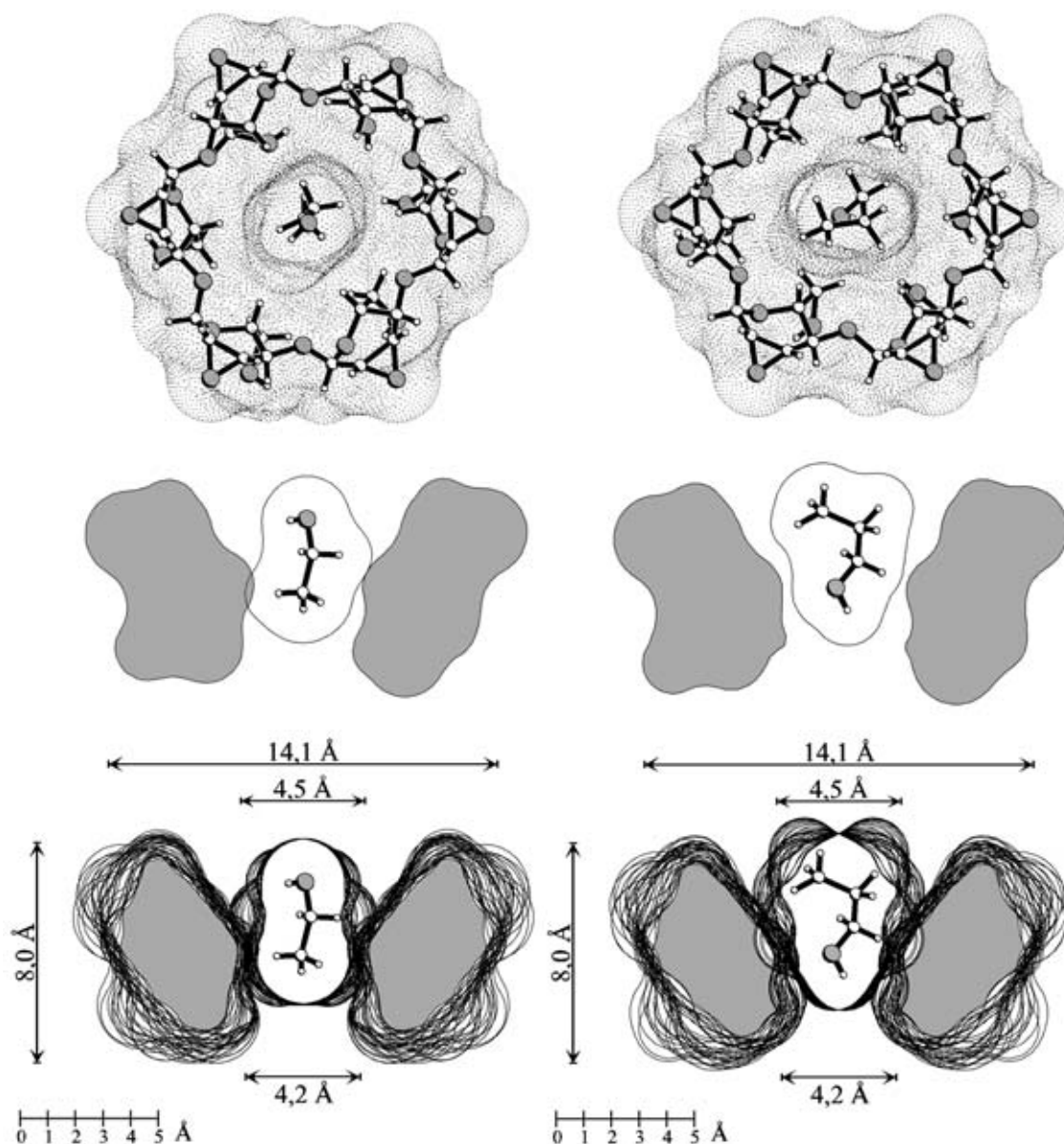


Fig. 1. Comparison of the inclusion complexes of 2,3-anhydro- $\alpha$ -cyclomannin **6** with ethanol<sup>1</sup> (left) and 1-propanol (right), clearly showing the inverse orientation of the guests in the macrocyclic cavity. Top: solvent-accessible surfaces in dotted form, with the oxirane rings pointing towards the front and the 6-CH<sub>2</sub>OH groups to the rear; disordered atomic positions and water molecules of crystallization have been left off for clarity. Center: single surface slice through the complexes to visualize the opposite mode of inclusion of ethanol and 1-propanol (approx. molecular dimensions in Å; the 6-CH<sub>2</sub>OH groups point downward). Bottom: superimposed surfaces cross-section cuts obtained from stepwise 10° rotation around the center of geometry (only one ball-and-stick model of the guest molecule is shown)

(C<sub>6</sub>). All epoxide rings are lined up on the larger aperture of the cone-shaped molecule with their oxygens directed towards the outside of the macro-ring. The overall shapes of the macrocycle and the hexose residues are almost identical to the geometry realized in the ethanol complex;<sup>1</sup> some geometry parameters are listed and compared for both inclusion complexes in Table 1. On the basis of the Cremer–Pople

ring puckering parameters,<sup>11</sup> the pyranose rings invariably adopt  ${}^0\text{H}_5$  half-chair conformations with very small fluctuations in the *endo*- and *exo*-cyclic torsion angles. In the propanol complex, the 6- $\text{CH}_2\text{OH}$  groups adopt *gauche-trans* and *gauche-gauche* conformations with statistical weights of 2:4. As illustrated by the solvent-accessible surface (Fig. 1) and, more lucidly, by the space-filling model (Fig. 2, left) and the side-view plots, the propanol guest is fully immersed into the host, with its OH group located next to the six  $\text{CH}_2\text{OH}$  groups at the narrow opening of the conically shaped cavity.

Table 1  
Cremer–Pople ring puckering parameters,<sup>11</sup> pyranose conformations, and some selected torsion angles in the crystal structure of the 2,3-anhydro- $\alpha$ -cyclomannin–1-propanol complex ( $6 \cdot \text{PrOH} \cdot 6\text{H}_2\text{O}$ ) as compared to those of the corresponding ethanol complex ( $6 \cdot \text{EtOH} \cdot 3.5\text{H}_2\text{O}$ )<sup>1</sup>

	$6 \cdot \text{PrOH} \cdot 6 \text{H}_2\text{O}^a$	$6 \cdot \text{EtOH} \cdot 3.5 \text{H}_2\text{O}^a$
Cremer-Pople parameters		
$Q$ [Å]	0.498 (0.02)	0.488 (0.02)
$\theta$ [°]	51.3 (3.0)	51.1 (2.6)
$\phi$ [°]	335.7 (6.4)	337.8 (4.9)
pyranose conformation	${}^0\text{H}_5$	${}^0\text{H}_5$
ring torsion angles [°]		
O5-C1-C2-C3	19.1 (4.3)	20.2 (4.0)
C1-C2-C3-C4	0.5 (3.9)	0.5 (3.4)
C2-C3-C4-C5	11.8 (3.2)	10.7 (3.2)
C3-C4-C5-O5	-43.1 (3.3)	-41.0 (2.5)
C4-C5-O5-C1	69.3 (2.1)	67.2 (1.6)
C5-O5-C1-C2	-55.6 (3.5)	-55.4 (3.2)
other torsions		
O1-C1-C2-O2	-170.9 (2.8)	-170.5 (2.5)
O5-C1-C2-O2	-48.9 (4.3)	-46.4 (3.4)
O5-C5-C6-O6	82 (14) <sup>b,c</sup>	69.5 (5.7) <sup>b,d</sup>
	-66.4 (6.7) <sup>b,c</sup>	-59.2 (3.7) <sup>b,d</sup>

<sup>a</sup> Parameters averaged over six pyranose units with root-mean-square (RMS) deviations in parenthesis; <sup>b</sup> independently averaged values for the *gauche-trans* (*gt*,  $\omega \approx +60^\circ$ ) and *gauche-gauche* (*gg*,  $\omega \approx -60^\circ$ ) arrangements of the 6- $\text{CH}_2\text{OH}$  groups; <sup>c</sup> statistical weights *gt* : *gg* = 2 : 4; <sup>d</sup> *gt* : *gg* = 3 : 3.

In the crystal lattice, the 2,3-anhydro- $\alpha$ -cyclomannin–propanol inclusion complex forms architecturally intricate layered structures: two guest–host macrocyclic units are ‘fused together’ to head-to-head dimers with the wider, oxirane ring-bearing sides facing each other, and each of these dimeric units is separated by a layer of water molecules (Fig. 3). Table 2 lists a selection of intermolecular non-hydrogen-bonding distances between heavy atoms of the crystal components, indicating the close contacts between the macrocycles in each layer, and particularly between the O-2 and C-2 atoms of stacked 2,3-anhydro- $\alpha$ -cyclomannins. The guest is held in the cavity by van der Waal’s contacts to the host’s O-1, 3-CH, and 5-CH groups, and the C-2 and C-3 atoms of two symmetry related 1-propanol molecules in the dimer approach each other to about 2.8–2.9 Å (cf. Table 2).

The crystal structure is characterized by an intense network of intermolecular hydrogen bonding interactions between the 6-hydroxyls of the macrocycle, 1-propanol, and water, with only one intramolecular H-bond of the 6-OH...O-6 type being realized; Table 3 gives a list of these hydrogen bonds and Fig. 4 provides a schematic drawing of the three-dimensional network of interactions which determine the crystal architecture. Most notably, the 1-propanol guest is not engaged in hydrogen bonding to the pyranose 6- $\text{CH}_2\text{OH}$  groups, but forms a distinct H-bond towards a water molecule (labeled OW4 in Fig. 4).

In this respect, the crystal structure of the  $6 \cdot \text{PrOH}$  complex is entirely different to the one observed

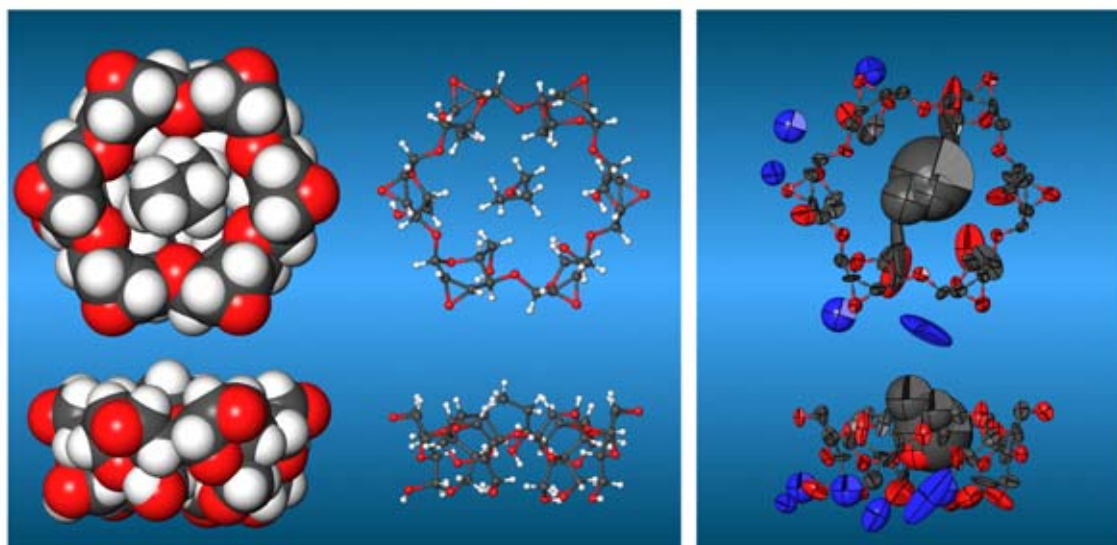


Fig. 2. Left: solid-state molecular geometry of the 2,3-anhydro- $\alpha$ -cyclomannin-1-propanol complex ( $6 \cdot \text{PrOH} \cdot 6\text{H}_2\text{O}$ ) in space-filling (CPK) form and as a ball-and-stick model. The inclusion complex is shown perpendicular (top) and parallel (bottom) to the ring plane of the macrocycle (water molecules of crystallization are omitted for clarity). Right: anisotropic thermal 50% probability ellipsoids for all non-hydrogen atoms (water oxygens in blue; the 1-propanol oxygen is hidden behind the disordered carbon atoms of the guest) in the asymmetric unit of the crystal structure

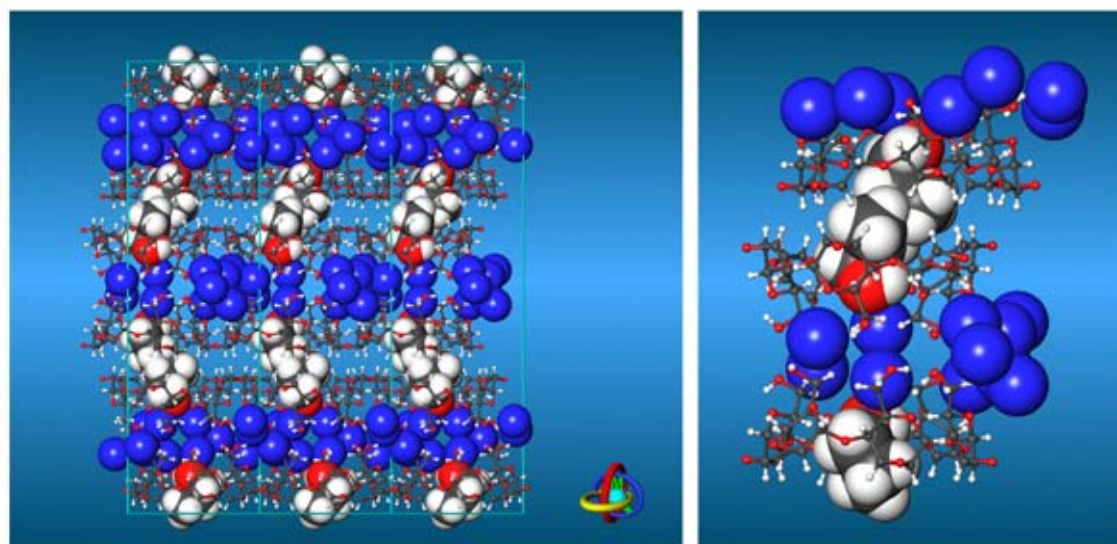


Fig. 3. Left: in the crystal lattice, the 2,3-anhydro- $\alpha$ -cyclomannin-1-propanol hexahydrate forms three layers of head-to-head arranged dimers, i.e. a total of six stacked macrocycles per unit-cell in the direction of the  $c$ -axis of the trigonal space group  $P3_212$  (view down the  $b$ -axis). The crystal water molecules (shown as blue spheres) likewise form distinct layers alternating with those of dimeric macrocycles, this unique crystal engineering obviously being effected by an intense hydrogen-bonding texture with the primary 6-OH groups of the macrocyclic host and the 1-propanol-OH. Right: section cut, illustrating in more detail the intricate assembly of the three crystal engineering components

Table 2

Selected intermolecular (non-hydrogen bonding) heavy atom distances in solid-state structure of the 2,3-anhydro- $\alpha$ -cyclomannin–1-propanol complex ( $6 \cdot \text{PrOH} \cdot 6\text{H}_2\text{O}$ ); labeling of the mannose units corresponds to Fig. 4, additional parameters on host–water distances are listed in Table 3

distances ( $d < 3.35 \text{ \AA}$ )	$d$ [ $\text{\AA}$ ]	symmetry	distances	$d$ [ $\text{\AA}$ ]	symmetry
<b>host–host (layered):<sup>a</sup></b>			<b>host–guest:</b>		
C(4D) – O(2A)	3.337	c	O(1G) – C(6E)	3.355	h
O(2E) – C(1A)	3.324	d	O(1G) – C(5E)	3.680	h
O(2B) – C(1D)	3.178	e	O(1G) – C(5A)	3.942	h
C(3B) – O(2E)	3.213	e	C(1G) – C(5B)	3.459	h
O(2B) – C(3E)	3.254	e	C(1G) – C(6B)	3.921	h
O(2B) – C(4E)	3.286	e	C(1G) – O(1A)	3.555	h
C(4B) – O(2E)	3.330	e	C(1G) – O(1B)	3.734	h
C(3C) – O(2F)	3.153	f	C(2G) – O(1C)	3.947	h
O(2C) – C(3F)	3.186	f	C(3G) – C(2D)	3.511	h
C(4C) – O(2F)	3.191	f	C(3G) – C(3D)	3.513	h
O(2C) – C(4F)	3.205	f	C(3G) – O(1D)	3.828	h
C(1B) – O(2F)	3.349	f			
<b>host–host (stacked):</b>			<b>guest–guest:</b>		
O(2A) – C(2A)	3.296	g	C(2G) – C(2G)	2.788	h
O(2A) – O(2A)	3.297	g	C(2G) – C(3G)	2.922	h
			C(3G) – C(3G)	2.991	h

<sup>a</sup> Atomic distances between 2,3-anhydro-cyclomannins contained in the same layer. Symmetry operations: <sup>b</sup>  $x, y, z$ ; <sup>c</sup>  $x, y-1, z$ ; <sup>d</sup>  $x+1, y, z$ ; <sup>e</sup>  $x-1, y, z$ ; <sup>f</sup>  $x-1, y-1, z$ ; <sup>g</sup>  $x, x-y, -z$ ; <sup>h</sup>  $x, x-y+1, -z$ .

for the respective ethanol inclusion compound (cf. Fig. 4, bottom left), which displays a hydrogen bond between the ethanol molecules trapped inside the dimeric cavity.

The unique packing features become more comprehensible on analyzing the molecular lipophilicity patterns (MLPs) of guest and host. Their generation with the MOLCAD program<sup>12</sup> and their visualization by projection onto the contact surface of Fig. 2 in color-coded form<sup>13</sup> results in Fig. 5, clearly showing the macrocycle to have its most hydrophobic (yellow) areas at the wider, oxirane ring-carrying opening of the torus, obviously due to the 2-H and 3-H ring protons of the sugar units forming its rim. The hydrophilic (blue) domains are centered on the opposite side around the 6-hydroxyl groups. Thus, the lipophilicity distribution in **6** is strikingly different from that manifested in the native cyclodextrins,<sup>9,14</sup> where the wider 2-OH/3-OH side of the respective macrocycles is distinctly hydrophilic versus the pronouncedly lipophilic domains at the opposite, narrower 6-CH<sub>2</sub>OH side and inside the cavity.

### 3. Conclusion

The solid-state structure of the 2,3-anhydro- $\alpha$ -cyclomannin–1-propanol hexahydrate detailed here, and the respective ethanol inclusion complex unraveled previously,<sup>1</sup> provide unique examples of the subtle intricacies operative in the crystal engineering. The three components involved—a cyclooligosaccharide, an alcohol, and water—self-assemble to substantially different superstructures by enlarging the alcohol component to be enclosed in the cavity by as little as one CH<sub>2</sub> group (cf. Fig. 4, bottom part). Obviously due to the fact that 1-propanol can fill out the hydrophobic, oxirane-carrying section of the macrocycle's cavity better than ethanol (cf. Fig. 1), it is included in such a way that hydrophobic and hydrophilic surface regions match at the guest–host interface (Fig. 5). The smaller ethanol occupies the cavity in an inverse way, whereby the non-complementarity in non-polar guest–host interactions is counterbalanced by the establishment of hydrogen-bonding between the cavity-inserted ethanol-OHs. The factors underlying this enthralling interplay of steric, polar, and non-covalent interactions between such



Table 3

Hydrogen bond patterns in the solid-state structure of the 2,3-anhydro- $\alpha$ -cyclomannin–1-propanol complex ( $6 \cdot \text{PrOH} \cdot 6\text{H}_2\text{O}$ ), listed for distances  $d(\text{H} \cdots \text{O}) < 2.5 \text{ \AA}$  and/or  $d(\text{O} \cdots \text{O}) < 3.5 \text{ \AA}$  only; the water molecules are labeled OW1–OW6, the mannose labeling A–F and the indices given in italics in the first column correspond to Fig. 4

no. (cf. Fig. 4)	hydrogen bond	$d(\text{H} \cdots \text{O})$ [ $\text{\AA}$ ] <sup>a</sup>	$d(\text{O} \cdots \text{O})$ [ $\text{\AA}$ ]	$\varphi(\text{O} \cdots \text{O})$ [ $^\circ$ ] <sup>a</sup>	symmetry
<b>intramolecular host-host hydrogen bonds:</b>					
<i>1</i>	O(6D) $\cdots$ O(6C)	-	3.093	-	<sup>b</sup>
<b>intermolecular host-host hydrogen bonds:</b>					
<i>2</i>	O(6A) $\cdots$ O(6B)	-	3.012	-	<sup>c</sup>
<i>3</i>	O(6F) $\cdots$ O(6C)	-	2.654	-	<sup>c</sup>
<i>4</i>	O(6E) $\cdots$ O(6E)	-	3.251	-	<sup>c</sup>
<i>5</i>	O(6E) $\cdots$ O(6D)	-	3.001	-	<sup>c</sup>
<b>host-water hydrogen bonds:</b>					
<i>6</i>	O(6A) $\cdots$ O(W5)	-	2.804	-	<sup>b</sup>
<i>7</i>	O(6A) $\cdots$ O(W3)	-	3.039	-	<sup>b</sup>
<i>8</i>	O(6C) $\cdots$ O(W4)	-	3.202	-	<sup>b</sup>
<i>9</i>	O(6D)H $\cdots$ O(W4)	2.252	2.890	134.9	<sup>b</sup>
<i>10</i>	O(6E) $\cdots$ O(W6)	-	3.372	-	<sup>b</sup>
<i>11</i>	O(6F)H $\cdots$ O(W1)	2.057	-	141.7	<sup>b</sup>
<i>12</i>	O(6B) $\cdots$ O(W2)	-	3.391	-	<sup>d</sup>
<i>13</i>	O(6B)H $\cdots$ O(W1)	2.475	3.093	132.6	<sup>c</sup>
<i>14</i>	O(6B)H $\cdots$ O(W3)	2.421	2.710	101.7	<sup>c</sup>
<i>15</i>	O(6A) $\cdots$ O(W5)	-	2.803	-	<sup>c</sup>
<i>16</i>	O(6D) $\cdots$ O(W2)	-	3.305	-	<sup>c</sup>
<b>guest-water hydrogen bonds:</b>					
<i>17</i>	O(1G)H $\cdots$ O(W4)	1.653	2.531	172.0	<sup>b</sup>
<b>water-water hydrogen bonds:</b>					
<i>18</i>	O(W1) $\cdots$ O(W3)	-	2.660	-	<sup>b</sup>
<i>19</i>	O(W1) $\cdots$ O(W6)	-	3.012	-	<sup>c</sup>
<i>20</i>	O(W3) $\cdots$ O(W6)	-	2.793	-	<sup>c</sup>
<i>21</i>	O(W2) $\cdots$ O(W5)	-	3.172	-	<sup>f</sup>
<i>22</i>	O(W2) $\cdots$ O(W5)	-	3.171	-	<sup>g</sup>
<i>23</i>	O(W1) $\cdots$ O(W6)	-	3.397	-	<sup>h</sup>

<sup>a</sup> Hydrogen bond H $\cdots$ O-distances and O-H $\cdots$ O-angles omitted if hydrogen atoms were not located explicitly. Symmetry operations: <sup>b</sup> x,y,z; <sup>c</sup> -y-1,-x-1,-z+1/3; <sup>d</sup> x-1,y,z; <sup>e</sup> x,y+1,z; <sup>f</sup> x+1,y,z; <sup>g</sup> -y,-x-1,-z+1/3; <sup>h</sup> y-1,-x,-z+1/3.

structurally incomparable crystal engineering components as water, a non-glucose cyclooligosaccharide, and a suitable guest are being further studied with the aim to eventually understand their intricacies.

#### 4. Experimental

2,3-Anhydro- $\alpha$ -cyclomannin **6**<sup>2</sup> was prepared in a three-step procedure from  $\alpha$ -cyclodextrin **1** involving protection of its six primary hydroxyl groups by the *t*-butyl-dimethylsilyl group (**1**  $\rightarrow$  **2**<sup>3</sup>), followed by per-sulfonation at *O*-2 with benzenesulfonyl chloride/NaH in DMF ( $\rightarrow$  **5**), and tetrabutylammonium fluoride-promoted desilylation.<sup>5</sup> A 30 mg sample of the resulting product—presumably the methanol inclusion compound due to its precipitation from methanol<sup>1</sup>—was suspended in 1 mL of 2:1 water:1-propanol, followed by brief warming to 60°C to effect dissolution, filtration through a membrane filter (TOSOH, H-13-2), and subsequent standing of the filtrate at ambient temperature for several days. This resulted in the generation of well-formed crystals having m.p. 267°C (decomp.) and  $[\alpha]_{\text{D}}^{20} = +83$

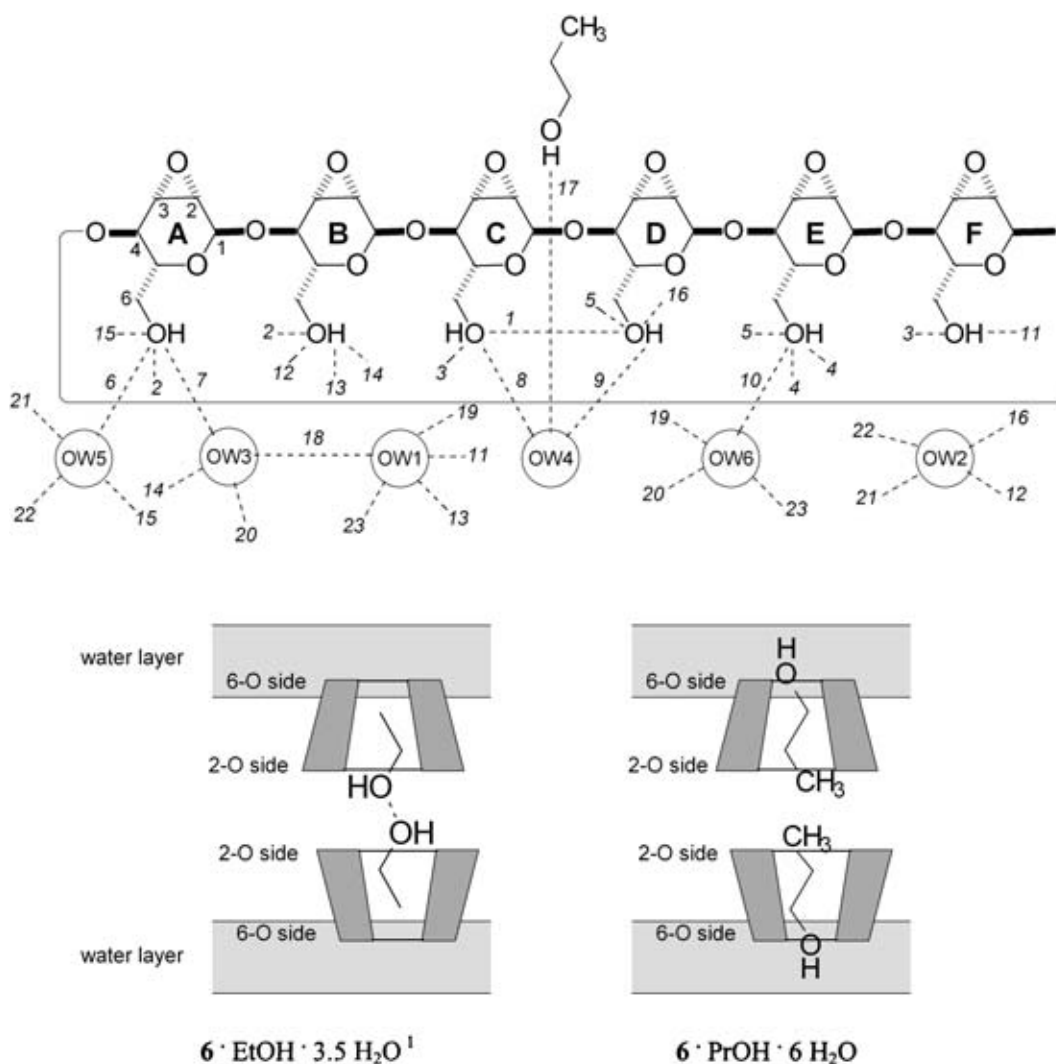


Fig. 4. Top: schematic drawing of the hydrogen-bonding pattern in the 2,3-anhydro- $\alpha$ -cyclomannin–1-propanol hexahydrate crystal structure. The pyranose residues are labeled A–F and the water positions OW1–OW6. The numbers in italics correspond to the indices given in Table 3; ‘open-ended’ dashed lines indicate H-bonds formed between symmetry-related positions. The cavity-inserted 1-propanol-OH forms a single hydrogen bond to a water molecule (OW4), yet none to the host’s 6-CH<sub>2</sub>OH groups. Bottom: comparative sketch of the opposite directional modes with which ethanol (left<sup>1</sup>) and 1-propanol (right) are embedded into the macrocyclic cavity, resulting in distinctly different interactions with the respective water layers

(*c* 0.3, DMSO). The analytical sample, vacuum dried over P<sub>2</sub>O<sub>5</sub> for 1 d, analyzed for the dihydrate C<sub>36</sub>H<sub>48</sub>O<sub>24</sub>·C<sub>3</sub>H<sub>7</sub>OH·2 H<sub>2</sub>O (960.86): calcd. C, 48.75; H, 6.29; found C, 48.55; H, 6.20.

The prismatic crystal used for the X-ray structure analysis, of the dimensions 0.25×0.25×0.1 mm, turned out to be a hexahydrate: C<sub>36</sub>H<sub>48</sub>O<sub>24</sub>·C<sub>3</sub>H<sub>7</sub>OH·6 H<sub>2</sub>O, *M*<sub>r</sub>=1032.95, trigonal, space group *P*3<sub>2</sub>12, *a*=*b*=14.105(2), *c*=41.787(6) Å, *V*=7199(18) Å<sup>3</sup>, *Z*=6,  $\rho$ =1.402 g cm<sup>-3</sup>,  $\mu(\text{MoK}\alpha)$ =0.080 mm<sup>-1</sup>, *T*=293(2) K. A total of 5018 reflections were collected on an Enraf–Nonius CAD-4 diffractometer using graphite-monochromated MoK $\alpha$  ( $\lambda$ =0.71093 Å) radiation, of which 4761 were independent (*R*<sub>int</sub>=0.1004). The structure was solved by direct methods (SHELXS-97<sup>15</sup>) and successive Fourier difference syntheses. Refinement (on *F*<sup>2</sup>) was performed by full-matrix least squares method with

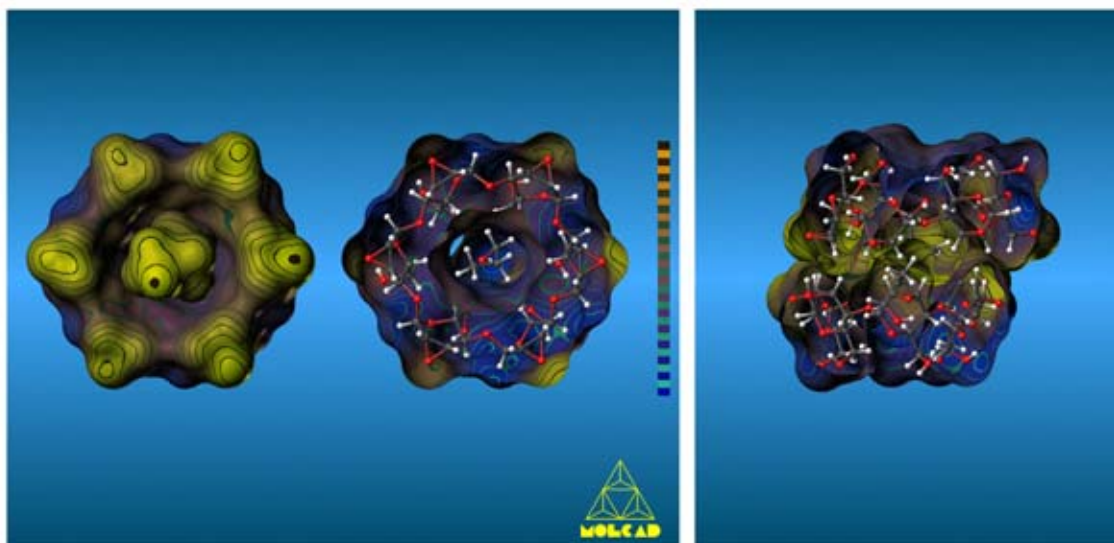


Fig. 5. Molecular lipophilicity patterns (MLPs) of the 2,3-anhydro- $\alpha$ -cyclomannin–1-propanol inclusion complex: the relative hydrophobicity of guest and host was mapped in color-coded form onto their individual contact surfaces, with the colors ranging from dark blue (most hydrophilic areas) to yellow–brown (hydrophobic domains). Computation and scaling of the MLPs was done separately for the guest and host, followed by reassembly of the complex. Left: view onto the wider opening of the macrocycle with the six oxirane rings, displaying the hydrophobic (yellow) side. The front-opened version (center) with the ball-and-stick model insert exposes the distinctly hydrophilic (blue) rear side bearing the 6-CH<sub>2</sub>OH groups. Right: MLP of one head-to-head dimeric unit, ‘fused together’ via their hydrophobic oxirane ring-carrying faces; in the crystal lattice these dimers assemble in horizontal layers that are enclosed on either of their hydrophilic ‘tails’ by layers of water

SHELXL-97.<sup>15</sup>  $R(F)=0.0817$  for reflections with  $I \geq 2\sigma I$ ,  $\omega R(F^2)=0.2822$  for all 4761 reflections with  $\omega=1/(\sigma^2(F_o^2)+(0.1584 P)^2+0.00 P)$ , where  $P=(F_o^2+2F_c^2)/3$ . All non-hydrogen atoms except for the 1-propanol carbon atoms were refined anisotropically, 1-propanol was refined as a rigid body molecule; hydrogen atoms on the 2,3-anhydro- $\alpha$ -cyclomannin were considered in calculated positions with the  $1.2 \times U_{eq}$  value of the corresponding bound atom. All hydroxyl groups were treated as idealized HO groups, the hydroxyl proton of 1-propanol was subsequently positioned geometrically.

Crystallographic data for the 6·1-propanol hexahydrate have been deposited with the Cambridge Crystallographic Data Centre as supplementary publication no. CCDC-138832. Copies of the data can be obtained free of charge on application to the Director, CCDC, 12 Union Road, Cambridge CB2 1EZ, UK (fax: (+44) 1223 336-033; e-mail: deposit@ccdc.cam.ac.uk).

## 5. Computational details

Calculation of the molecular contact surfaces and the respective hydrophobicity potential profiles (MLPs) was performed using the MOLCAD molecular modeling program.<sup>12,13</sup> Scaling of the MLP profiles was performed in relative terms (most hydrophilic to most hydrophobic surface regions) and no absolute values are displayed. Molecular Graphics were generated using MolArch<sup>+</sup>.<sup>16</sup>

## Acknowledgements

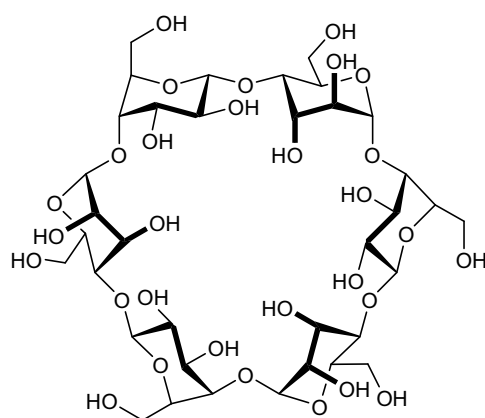
We are grateful to the Fonds der Chemischen Industrie and the Südzucker AG, Mannheim/Ochsenfurt, to Mrs. Sabine Foro for collecting the X-ray crystallographic data, and to Prof. Dr. J. Brickmann, Institut für Physikalische Chemie of this University, for access to his MOLCAD software package.

## References

1. Immel, S.; Fujita, K.; Lindner, H. J.; Nogami, Y.; Lichtenthaler, F. W. *Chem. Eur. J.* **2000**, *6*, in press.
2. As outlined previously,<sup>1</sup> we prefer the term 2,3-anhydro- $\alpha$ -cyclomannin<sup>1,5</sup> for **6** rather than *cyclo- $\alpha$ -1,4-hexamanno-2,3-epoxide*,<sup>4</sup> or cyclohexakis-(1 $\rightarrow$ 4)-2,3-anhydro- $\alpha$ -D-mannopyranosyl (systematic name required by IUPAC recommendations of *Carb. Res.* **1997**, *297*, 79, Rule 2-Carb-37.4.2), which is not only less handy, but inconsequential, since **6** is not a series of 'glycosyls', but a *glycoside* — a hexasaccharide in fact.
3. Takeo, K.; Uemura, K.; Mitoh, H. *J. Carbohydr. Chem.* **1988**, *7*, 293–308.
4. Zhang, P.; Coleman, A. W. *Supramol. Chem.* **1993**, *2*, 255–263.
5. Nogami, Y.; Nasu, K.; Koga, T.; Ohta, K.; Fujita, K.; Immel, S.; Lindner, H. J.; Schmitt, G. E.; Lichtenthaler, F. W. *Angew. Chem.* **1997**, *109*, 1987–1991; *Angew. Chem., Int. Ed. Engl.* **1997**, *36*, 1899–1902.
6. Cyclomannins: (a) Mori, M.; Ito, Y.; Ogawa, T. *Carbohydr. Res.* **1989**, *192*, 131–146; Mori, M.; Ito, Y.; Uzawa, J.; Ogawa, T. *Tetrahedron Lett.* **1990**, *31*, 3191–3194 (synthesis). (b) Lichtenthaler, F. W.; Immel, S. *Tetrahedron: Asymmetry* **1994**, *5*, 2045–2060 (molecular geometry and lipophilicity profile).
7. Cyclorhamnins: (a) Nishizawa, M.; Imagawa, H.; Kann, Y.; Yamada, H. *Tetrahedron Lett.* **1991**, *32*, 5551–5554; *Synlett* **1992**, 447–448; Nishizawa, M.; Imagawa, H.; Morikuni, E.; Hatakayama, S.; Yamada, H. *Chem. Pharm. Bull.* **1994**, *42*, 1356–1365 (preparation). (b) Lichtenthaler, F. W.; Immel, S. *J. Incl. Phenom. Mol. Recogn.* **1996**, *25*, 3–16 (geometry).
8. Cyclooligosaccharides composed of alternating D-mannose and L-rhamnose units: (a) Ashton, P. R.; Brown, C. L.; Menzer, S.; Nepogodiev, S. A.; Stoddart, J. F.; Williams, D. J. *Chem. Eur. J.* **1996**, *2*, 580–591. (b) Ashton, P. R.; Cantrill, S. J.; Gattuso, G.; Menzer, S.; Nepogodiev, A.; Shipway, A. N.; Stoddart, J. F.; Williams, D. J. *Chem. Eur. J.* **1997**, *3*, 1299–1314.
9. Lichtenthaler, F. W.; Immel, S. *Liebigs Ann. Chem.* **1996**, 39–44; *Starch/Stärke* **1996**, *48*, 145–154.
10. Immel, S.; Lichtenthaler, F. W. *Starch/Stärke* **2000**, *52*, in press.
11. (a) Cremer, D. A.; Pople, J. A. *J. Am. Chem. Soc.* **1975**, *97*, 1354–1358. (b) Jeffrey, G. A.; Taylor, R. *Carbohydr. Res.* **1980**, *81*, 182–183.
12. (a) Brickmann, J. *MOLCAD — MOLEcular Computer Aided Design*; Darmstadt University of Technology: Germany, 1996. The major part of the MOLCAD-program is included in the SYBYL package of TRIPOS Associates, St. Louis, USA. (b) Waldherr-Teschner, M.; Goetze, T.; Heiden, W.; Knoblauch, M.; Vollhardt, H.; Brickmann, J. In *Advances in Scientific Visualization*; Post, F. H.; Hin, A. J. S., Eds.; Springer: Heidelberg, Germany, 1992, pp. 58–67. (c) Brickmann, J.; Goetze, T.; Heiden, W.; Moeckel, G.; Reiling, S.; Vollhardt, H.; Zachmann, C.-D. In *Insights and Innovation in Data Visualization*; Bowie, J. E., Ed.; Manning: Greenwich, UK, 1994; pp. 83–97.
13. (a) Heiden, W.; Moeckel, G.; Brickmann, J. *J. Comp.-Aided Mol. Des.* **1993**, *7*, 503–514. (b) Teschner, M.; Henn, C.; Vollhardt, H.; Brickmann, J. *J. Mol. Graphics* **1994**, *12*, 98–105.
14. Immel, S.; Lichtenthaler, F. W. *Liebigs Ann. Chem.* **1996**, 27–36.
15. Sheldrick, G. M. SHELXS-97 and SHELXL-97 — Programs for Crystal Structure Solution and Refinement, University of Göttingen, 1997.
16. Immel, S. *MolArch<sup>+</sup> — MOLEcular ARCHitecture Modeling Program*; Darmstadt University of Technology, 1999.

## Chapter 3

### $\alpha$ -Cycloaltrin



#### Synthesis, Structure, and Conformational Features of $\alpha$ -Cycloaltrin: a Cyclooligosaccharide with alternating ${}^4C_1$ and ${}^1C_4$ Pyranose Chairs

Y. Nogami, K. Nasu, T. Koga, K. Ohta, K. Fujita, S. Immel, H. J. Lindner, G. E. Schmitt, and F. W. Lichtenthaler, *Angew. Chem.* **1997**, *109*, 1987-1991; *Angew. Chem. Int. Ed. Engl.* **1997**, *35*, 1899-1902.

#### Solution Geometries and Lipophilicity Patterns of $\alpha$ -Cycloaltrin

S. Immel, K. Fujita, and F. W. Lichtenthaler, *Chem. Eur. J.* **1999**, *5*, 3185-3192.

#### Inclusion Complexes of Cycloaltrins

S. Immel, K. L. Larsen, *unpublished results.*



### Synthesis, Structure, and Conformational Features of $\alpha$ -Cycloaltrin: A Cyclooligosaccharide with Alternating ${}^4C_1/{}^1C_4$ Pyranoid Chairs\*\*

Yasuyoshi Nogami, Kyoko Nasu, Toshitaka Koga, Kazuko Ohta, Kahee Fujita,\* Stefan Immel, Hans J. Lindner, Guido E. Schmitt, and Frieder W. Lichtenthaler\*

The wealth of knowledge that has accumulated on the starch-derived cyclodextrins and their unique ability to form inclusion complexes<sup>[1]</sup> is contrasted by a peculiar paucity of data on cyclooligosaccharides composed of sugars other than glucose.<sup>[2]</sup> Except for certain cyclofructins, obtainable by bacterial action on the polysaccharide inulin,<sup>[3]</sup> all of the non-glucose cyclooligosaccharides presently known have been acquired synthetically and require laborious multistep procedures to assemble the linear oligosaccharide from its monosaccharide units in a form suitable for cycloglycosylation. In this way,  $\alpha$ (1  $\rightarrow$  4)-linked cyclooligosaccharides composed of D-mannose<sup>[4]</sup> ( $\alpha$ -,  $\beta$ -, and  $\gamma$ -cyclomannin), of L-rhamnose<sup>[5]</sup> ( $\alpha$ -cyclorhamnin), and of alternating D-mannose/L-rhamnose units<sup>[6]</sup> have been prepared, yet in such minute amounts as to preclude investigations into their inclusion complex behavior. Molecular modeling studies on  $\alpha$ -cyclomannin<sup>[7]</sup> and its 6-deoxy L-analogue  $\alpha$ -cyclorhamnin<sup>[2]</sup> showed that their axially disposed 2-OH points away from the cavity; thus they fairly closely resemble  $\alpha$ -cyclodextrin in backbone structure, cavity dimensions, and lipophilicity patterns. The same, in fact, is to be expected for the cyclohexasaccharide with alternating D-mannose and L-rhamnose units. For a cyclogalactin composed of six  $\beta$ (1  $\rightarrow$  4)-linked galactopyranose residues, molecular modeling revealed an  $\alpha$ -CD-like geometry, yet a distinctly different lipophilicity distribution such that hydrophobic surface regions at the primary hydroxyl face are substantially enlarged.<sup>[7]</sup>

More profound changes in shape, cavity dimensions, and guest binding properties are to be anticipated for cyclooligosaccharides with axially disposed 3-OH groups in the pyranoid rings— $\alpha$ -cycloaltrin for example—as these would be directed towards the interior of the cavity, resulting in considerable steric congestion, which is likely to be released by deformation of the  ${}^4C_1$  chairs. Topologically even more interesting appears to be  $\alpha$ -cycloaltrin, as the  ${}^4C_1$  and  ${}^1C_4$  conformations of  $\alpha$ -altropyranoid chairs are very similar in stability<sup>[8]</sup> and, hence, in a macrocyclic array several conformations could be formed, such as the all- ${}^4C_1$  (**1a**) or all- ${}^1C_4$  forms (**1b**), or even more likely in solution, an equilibrium between the two, that passes through the skew  ${}^0S_2$  geometries (**1c**) of the pyranoid rings (Scheme 1).

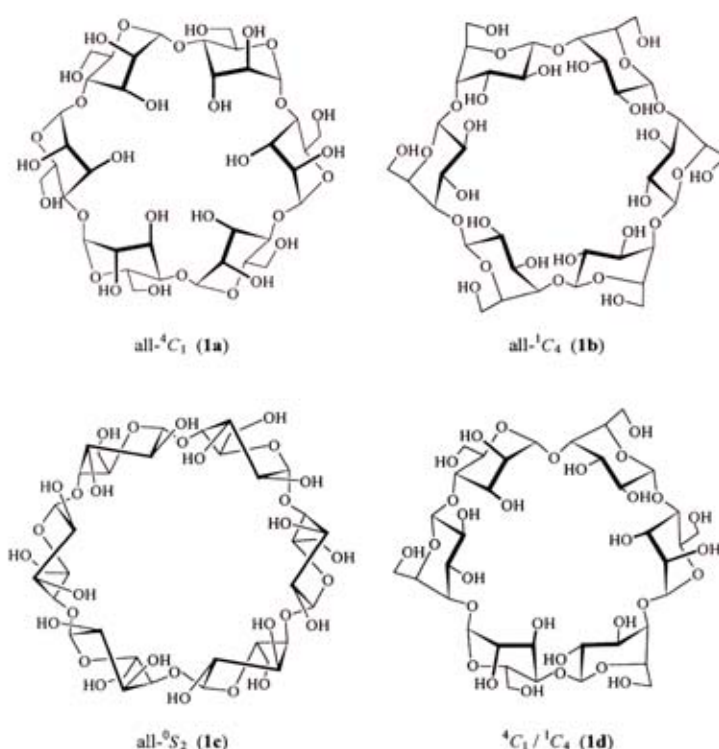
In context with our studies on non-glucose cyclooligosaccharides,<sup>[2]</sup> we report on a straightforward synthesis of  $\alpha$ -cycloaltrin

[\*] Prof. K. Fujita, K. Ohta  
Faculty of Pharmaceutical Sciences  
Nagasaki University  
Nagasaki 852 (Japan)  
Fax: Int. code + (958)46-5736

Prof. Dr. F. W. Lichtenthaler, Dr. S. Immel, Prof. Dr. H. J. Lindner, Dipl.-Ing. G. E. Schmitt  
Institut für Organische Chemie der Technischen Hochschule  
D-64287 Darmstadt (Germany)  
Fax: Int. code + (6151)16-6674

Prof. Y. Nogami, K. Nasu, Prof. T. Koga  
Daiichi College of Pharmaceutical Sciences, Fukuoka 815 (Japan)  
Fax: Int. code + (925)53-5698

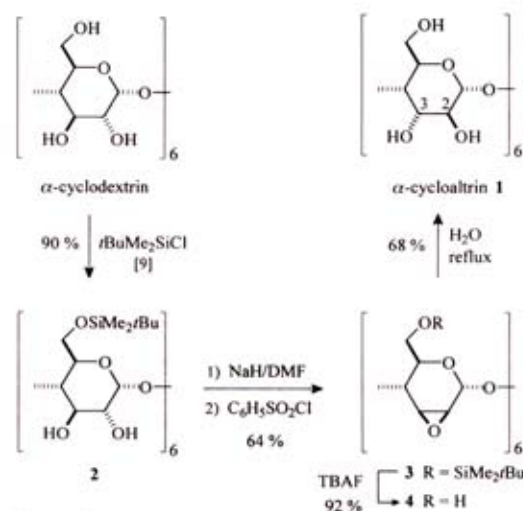
[\*\*] Molecular Modeling of Saccharides, Part 15. This work was supported by the Fonds der Chemischen Industrie and the Nihon Shokuhin Kako (Japan Maize Products Co.). Part 14: Ref. [2]



Scheme 1. Molecular geometries for  $\alpha$ -cycloaltrin (**I**), a cyclooligosaccharide composed of six  $\alpha$ (1  $\rightarrow$  4)-linked D-altropyranose residues. In aqueous solution, a dynamic equilibrium prevails between forms **1a–1c**, and various other intermediate conformations; in the solid state, the structure is that of **1d**, comprising a unique alternating sequence of  ${}^4C_1$  and  ${}^1C_4$  altropyranoid chair forms.

(**I**) from  $\alpha$ -cyclodextrin its molecular geometries in the solid state, revealing a unique alternating sequence of  ${}^4C_1$  and  ${}^1C_4$  chairs (**1d**), and in solution, in which a dynamic equilibrium of the type **1a**  $\rightleftharpoons$  **1c**  $\rightleftharpoons$  **1d** prevails.

The conversion of  $\alpha$ -cyclodextrin into **I** started with protection of the six primary hydroxyl groups by the *tert*-butyldimethylsilyl moiety ( $\rightarrow$  **2**<sup>[9]</sup>). Ensuing deprotonation of the secondary hydroxyls in **2** by treatment with NaH in DMF was followed by the addition of benzenesulfonyl chloride, which not only effected selective 2-*O*-sulfonylation but, concomitantly, displacement of the 2-sulfonyloxy group by the vicinal 3-OH to elaborate the key intermediate, the 6-*O*-protected 2,3-anhydro- $\alpha$ -cyclomannin (**3**, 64%). Deblocking with TBAF/THF yielded



Scheme 2. Synthesis of **I** from  $\alpha$ -cyclodextrin.

## COMMUNICATIONS

**4** (92%), which simply by refluxing in water was converted into **1** and isolated by reversed-phase chromatography (68%). The overall yield for the four-step sequence is a satisfactory 36%, but is lower than the conversion of  $\beta$ -cyclodextrin into its all-*altro* analogue (52%<sup>[10]</sup>), obviously reflecting the lesser steric strain, and hence cleaner reactions, in the cycloheptamer.

Cyclomaltrin **1** crystallized with 21 water molecules and is thus embedded in a water matrix in the solid state. Its X-ray structural analysis<sup>[11]</sup> not only gave evidence of the water molecules built into the crystal lattice (Figure 1), but revealed the unique

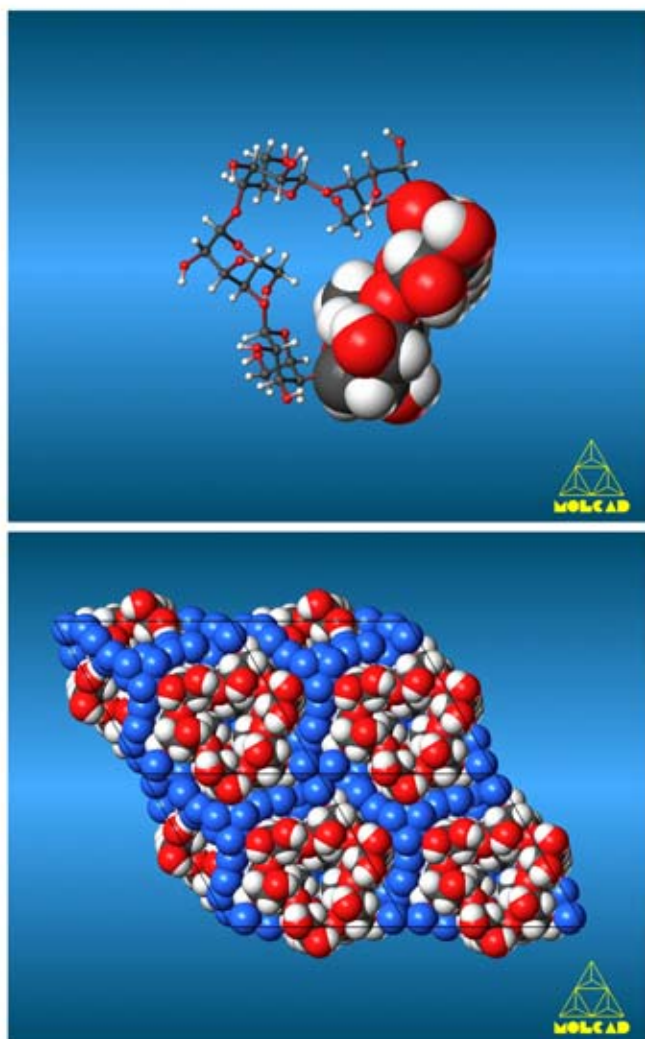


Figure 1. Structure of cyclomaltrin ( $\alpha$ -cycloaltrin, **1**) [12]. Top: Ball-and-stick model of the alternating sequence of  ${}^4C_1$  and  ${}^1C_4$  chair conformations of altropyranoid rings; in this way the macrocycle is constructed from three banana-shaped disaccharide units, one of which is depicted in a space-filling representation. Bottom: The macrocycle has a compact, disklike topology, devoid of a cavity and is embedded in a water matrix (**1** · 21  $H_2O$ ); the disks are stacked in offset layers.

conformational features of the altropyranoid rings: neither the all- ${}^4C_1$  form **1a** or the all- ${}^1C_4$  form **1b** is adopted, nor one of the various nonchair conformations conceivable (for instance, **1c**); instead, the altrose units display alternate  ${}^4C_1$  and  ${}^1C_4$  altropyranoid chair conformations (Figure 1, top), entailing the macrocycle to be made up of three banana-shaped disaccharide portions. The molecules are disk-shaped, devoid of a cavity, and stacked in transposed layers (Figure 1, bottom), the space in between being occupied by water molecules.

The closeness of the chair conformations to the ideal is remarkable: nearly perfect geometry in the  ${}^1C_4$ -portions with  $O_4$  and  $C_6$  in a fairly antiparallel disposition ( $167.5^\circ$ ) and with the six pyranoid ring torsion angles in the  $52$ – $58^\circ$  range. The  ${}^4C_1$  chairs, by contrast, are less ideal, as the  $C_1$ - $C_2$ - $C_3$ - $C_4$  torsion angle ( $-45.7^\circ$ ) reveals some flattening at C-2 and C-3, whilst  $O_1$ ,  $O_2$ , and  $O_3$  are still in a fairly antiparallel disposition ( $O_1$ - $C_1$ - $C_2$ - $O_2$   $166.2^\circ$ ,  $O_2$ - $C_2$ - $C_3$ - $O_3$   $166.5^\circ$ ). Another salient feature of the structure is the different orientations of the 6-OH groups relative to the pyranoid rings: *gauche*-*trans* disposition ( $\omega = 55.7^\circ$ <sup>[13]</sup>) in the three  ${}^1C_4$  forms in which the  $CH_2OH$  groups are directed towards the outside of the macrocycle versus a *gauche*-*gauche* arrangement ( $\omega = -66.8^\circ$ <sup>[13]</sup>) in the three  ${}^4C_1$  forms in which their equatorially disposed  $CH_2OH$  groups point towards the center of the macrocycle, thereby closing it (Figure 2). Accordingly, the disk-shaped molecule has a shallow

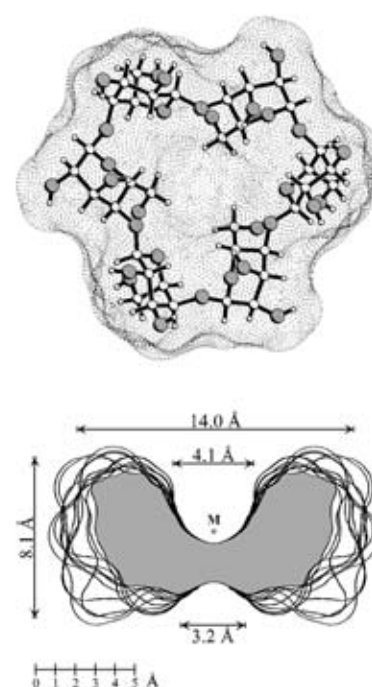


Figure 2. Top: Calculated [12] contact surface (in dotted form) of the solid-state structure of **1** with inserted ball-and-stick model. The three equatorial hydroxymethyl groups of the  ${}^4C_1$  altropyranoses are directed towards the macrocycle's interior, thereby closing it. Bottom: Cross-sections through the contact surface of **1** (2-OH/3-OH side up) and approximate molecular dimensions: surface contours were obtained for a plane perpendicular to the macrocycle's mean plane through successive  $10^\circ$  rotation steps around the geometrical center  $M$  and subsequently superimposed.

indentation on one side, and a pronounced hole-like depression on the other. Provided that this disk-shaped, solid-state structure of **1**, already embedded in a water matrix, is retained in aqueous solution, not only separate sets of NMR signals should be observed for the  ${}^4C_1$  and the  ${}^1C_4$  portions, but also distinctly different coupling patterns for the respective pyranoid ring protons as revealed by the calculated  $J$  values (Table 1).

The high resolution  ${}^1H$  and  ${}^{13}C$  NMR spectra of **1** in  $D_2O$ ,<sup>[14]</sup> however, unambiguously provide only one set of signals for both the altropyranoid hydrogen atoms and the carbon atoms, and the  ${}^1H$  coupling constants are an average of those calculated for the  ${}^4C_1$  and  ${}^1C_4$  conformations (Table 1); moreover, the observed  $J$ -values correlate surprisingly well with those calculated for the all-skew (twist-boat)  ${}^0S_2$  geometry of **1c**, which, in



Table 1. Dihedral angles as well as the  $^1\text{H}$ – $^1\text{H}$  coupling constants measured in  $\text{D}_2\text{O}$  (800 MHz [14], 30 °C) and those calculated for the altropyranoid ring in  $^4\text{C}_1$ ,  $^1\text{C}_4$ , and all- $^0\text{S}_2$ (skew) forms of **1**.

	$^4\text{C}_1$ [a]	$^1\text{C}_4$ [a]	$^0\text{S}_2$ [b]	found
Dihedral angle [°]				
H1-C1-C2-H3	–69.4	–178.0	–138.3	
H2-C2-C3-H3	70.4	–176.0	–176.2	
H3-C3-C4-H4	–61.5	51.8	–44.7	
H4-C4-C5-H5	–71.3	179.8	–141.9	
Coupling constant [Hz] [c]				
$J(1,2)$	2.2	8.0	4.0	4.73
$J(2,3)$	2.7	10.2	10.2	8.19
$J(3,4)$	3.4	2.4	4.5	3.71
$J(4,5)$	9.7	1.4	6.4	5.32

[a] Angles from the solid-state structure of **1**. [b] Data calculated for the global energy minimum (all-skew form) from HTA simulations. [c] Calculation based on the Karplus-type dependence of H-C-C-H torsion angles on coupling constants, including the electronegativity effect of the substitution pattern by use of the generalized Haasnoot equation [15].

fact, emerges from extensive HTA calculations<sup>[16]</sup> as the global energy minimum structure. Favored over the  $^4\text{C}_1$ / $^1\text{C}_4$  solid-state geometry by as much as  $36 \text{ kJ mol}^{-1}$ —a major portion of this energy gain undoubtedly stems from hydrogen bonding between the 2-OH of one altrose moiety to the O-3 of the next—this all-skew form features a cavity that pierces the disk (Figure 3) and a pyranose tilt inverse to that of the cyclodextrins.

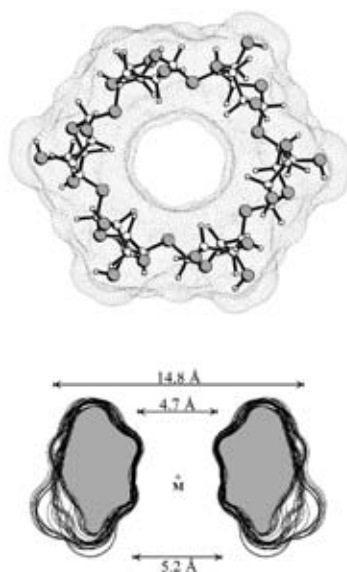


Figure 3. The all-skew (twist-boat)  $^0\text{S}_2$ -geometry of  $\alpha$ -cycloaltrin (**1**) emerging from HTA simulations [16] as the global energy minimum structure. Top: Contact surface. Bottom: The contour plots reveal a cavity whose conicity is inverse to that of the cyclodextrins.

Whether, however, the all-skew form **1e** is adopted in aqueous solution—in HTA simulations molecules are in vacuum rather than surrounded by a solvation shell—remains open. If prevalent in aqueous solution, its cavity is conceivably filled with water. Thus not only the six primary, but also the 12 secondary hydroxyl groups are likely to satisfy their hydrogen bonding requirements towards the solvent rather than intramolecularly. This results in a tightly associated first water shell around **1**, which will have to follow any geometry changes within the macrocycle. This hydration sphere could readily be character-

ized by molecular dynamics (MD) simulations in water, but contributed little to unraveling the nature of the  $^4\text{C}_1 \rightleftharpoons ^1\text{C}_4$  scrambling observed in the NMR spectra, since on subjection to a 600 ps MD simulation in a box of water,<sup>[17]</sup> not only the geometry of the hydrated all-skew  $^0\text{S}_2$  form (**1c**), but also that of the solid-state  $^4\text{C}_1$ / $^1\text{C}_4$  structure **1d**, remained in their respective geometries (Figure 4). Accordingly, no appreciable flexing

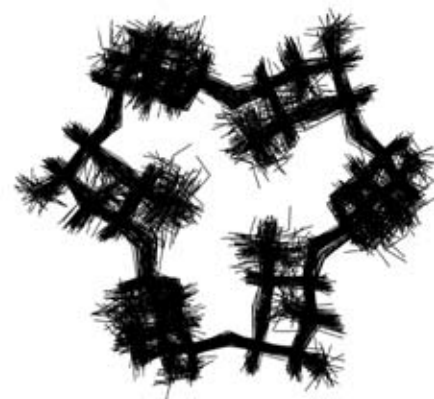


Figure 4. Superimposition of 60  $\alpha$ -cycloaltrin snapshot-geometries taken in 10 ps intervals from a 600 ps molecular dynamic simulation [17] on an assembly comprising  $\alpha$ -cycloaltrin in a box of 606 water molecules.

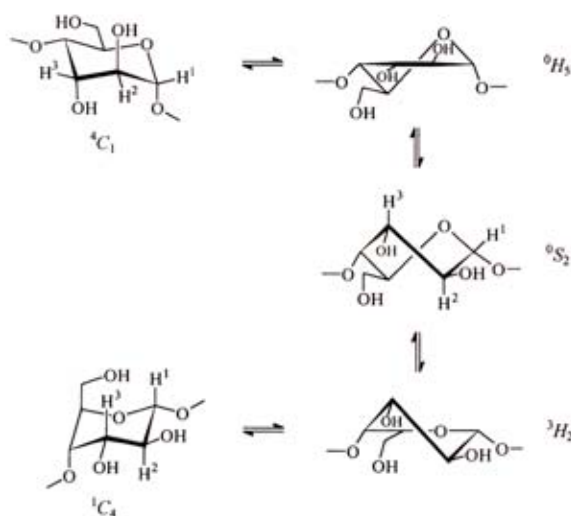
or flip over of the pyranoid chairs or skew forms to alternate topologies takes place within a 600 ps time frame; that is, profound conformational changes like the flipping from  $^4\text{C}_1$  to  $^1\text{C}_4$  within the macrocycle are comparatively slow, and require the  $10^6$  times longer, millisecond time frame of NMR spectroscopy to become observable.

The temperature-dependent  $^1\text{H}$  and  $^{13}\text{C}$  NMR studies proved to be more meaningful in determining the nature of the conformational changes occurring in aqueous solutions of **1**:<sup>[14]</sup> the coupling constant  $J_{2,3}$  of 8.2 Hz at 30 °C in  $\text{D}_2\text{O}$  decreases to 7.6 and 7.1 Hz at 20 and 4 °C, respectively, thereby narrowing the well-separated signal for 3-H; more profound effects are observed for the C-4 and C-5 signals, which, like all other carbon atoms, give rise to sharp singlets at 30 °C but show substantial broadening at 4 °C, which indicates the onset of “freezing out” certain conformations the  $^4\text{C}_1 \rightleftharpoons ^1\text{C}_4$  equilibrium. Consequently, in water,  $\alpha$ -cycloaltrin does not adopt a fixed geometry, such as the all- $^0\text{S}_2$ -form; rather, the D-altropyranoid rings, tied up in a macrocyclic “straitjacket”, adopt a variety of conformations within the  $^4\text{C}_1 \rightleftharpoons ^0\text{S}_2 \rightleftharpoons ^1\text{C}_4$  pseudorotational “turntable” (Scheme 3), and this necessarily in a coordinated way: flexure of one altropyranoid chair into the intermediate skew  $^0\text{S}_2$ -form via half-chair transition states forces the two adjoining altrose chairs to follow suit, thereby eliciting a consecutive “rolling around” in the probably elliptically distorted macrocycle. NMR data provide an averaged picture thereof and give evidence through the comparatively large  $J_{1,2}$  and, particularly,  $J_{2,3}$  couplings that the position of the equilibrium in water at 30 °C lies pronouncedly on the  $^1\text{C}_4 \rightleftharpoons ^0\text{S}_2$  side.

#### Experimental Section

**3:** To a solution of NaH (0.40 g, 10.8 mmol) in anhydrous DMF (40 mL) was added **2** (1.0 g, 0.6 mmol) [9], and the mixture was kept under  $\text{N}_2$  at 60 °C for 2 h. After cooling, benzenesulfonyl chloride (568  $\mu\text{L}$ , 4.32 mmol) in anhydrous DMF (10 mL) was injected followed by stirring at room temperature for 30 min. Filtration and flash chromatography on a silica gel column (4  $\times$  15 cm) with benzene/EtOAc (4/1, 250 mL) afforded 600 mg (64%) of **3**; m.p. 203 °C (decomp.);  $[\alpha]_D^{20} = +70.1$  ( $c = 0.36$  in THF).  $^1\text{H}$  NMR (500 MHz,  $\text{CDCl}_3$ , relevant data):  $\delta = 3.11$  (d, 1H, 2-H), 3.32 (d, 1H, 3-H), 3.56 and 4.24 (two d, 1H, 6-H<sub>2</sub>), 3.64 (d, 1H, 4-H), 3.93

## COMMUNICATIONS



Scheme 3. The chair/half-chair/skew pseudorotational "turntable" between  $\alpha$ -tropanoid rings in  ${}^4C_1$  and  ${}^1C_4$  conformation [18]. Due to the comparatively large  $J_{1,2}$  and  $J_{2,3}$  values found for **1** (4.7 and 8.2 Hz, respectively, in  $D_2O$ ), the conformational equilibrium in aqueous solution lies on the  ${}^1C_4 \rightleftharpoons {}^3H_2 \rightleftharpoons {}^0S_2$  side.

(m, 1H, 5-H), 5.16 (s, 1H, 1-H),  $J_{1,2}$  and  $J_{2,4} = 0$ ,  $J_{2,3} = 3.7$ ,  $J_{4,5} = 11.5$  Hz. MS:  $[M^+]$  not detectable. Elemental analysis calculated for  $C_{72}H_{132}O_{24}Si_6$ : C 55.78, H 8.58; found: C 55.55, H 8.68.

**4**: A 1 M solution of  $Bu_4NF$  in THF (4.6 mL) was added to a solution of silyl epoxide **3** (1.0 g, 0.65 mmol) in anhydrous THF (90 mL) under  $N_2$ , and the mixture was stirred at 40 °C for 4 h. Concentration in vacuo, addition of methanol (10 mL), and cooling in a refrigerator overnight resulted in a precipitate: 511 mg (92%) of **4**; m.p. 166 °C (decomp.);  $[\alpha]_D^{25} = +83.6$  ( $c = 0.34$  in DMSO).  ${}^1H$  NMR (500 MHz,  $D_2O$ , pyridine):  $\delta = 3.40$  (d, 1H, 2-H), 3.67 (d, 1H, 3-H), 4.10 (m, 1H, 5-H), 4.30 (m, 2H, 6-H<sub>2</sub>), 4.47 (d, 1H, 4-H), 5.57 (s, 1H, 1-H),  $J(1,2)$  and  $J(3,4) = 0$ ,  $J(2,3) = 3.5$ ,  $J(4,5) = 11.6$  Hz; FAB-MS:  $m/z$ : 865  $[M^+]$ .

**1**: A solution of epoxide **4** (1.0 g, 1.14 mmol) in distilled water (250 mL) was heated at reflux for 5 days. Concentration of the mixture in vacuo and chromatography on a reversed-phase column (Merck Lobar, size C) with water yielded **1** (765 mg (68%); m.p. 215 °C (decomp.);  $[\alpha]_D^{20} = +70.5$  ( $c = 0.3$  in  $H_2O$ )).  ${}^1H$  NMR (800 MHz [14],  $D_2O$ , 30 °C):  $\delta = 3.91$  (dd, 1H, 6-H<sub>2</sub>), 4.00 (m, 2H, 2-H, 6-H<sub>2</sub>), 4.03 (dd, 1H, 3-H), 4.14 (dd, 1H, 4-H), 4.44 (sext, 1H, 5-H), 4.95 (d, 1H, 1-H),  $J_{1,2} = 4.73$ ,  $J_{2,3} = 8.19$ ,  $J_{3,4} = 3.71$ ,  $J_{4,5} = 5.32$ ,  $J_{5,6a} = 3.60$ ,  $J_{5,6b} = 3.46$ ,  $J_{6,a} = 12.42$  Hz.  ${}^{13}C$  NMR (200 MHz [14],  $D_2O$ , 30 °C):  $\delta = 63.05$  (C-6), 71.98 (C-3), 73.26 (C-2), 76.07 (C-5), 79.65 (C-4), 105.53 (C-1). FAB-MS:  $m/z$ : = 973  $[M + H^+]$ , 995  $[M + Na^+]$ .

Received: February 19, 1997 [Z101391E]

German version: *Angew. Chem.* **1997**, *109*, 1987–1991

**Keywords:**  $\alpha$ -cyclomaltrin · cyclodextrins · macrocycles · molecular modeling

- [1] a) J. Szejtli, *Cyclodextrins and Their Inclusion Complexes*, Akadémiai Kiadó, Budapest, **1982**; b) *Trends in Cyclodextrins and Derivatives*, (Ed.: D. Duchêne), Edition de la Santé, Paris, **1991**; c) G. Wenz, *Angew. Chem.* **1994**, *106*, 851–870; *Angew. Chem. Int. Ed. Engl.* **1994**, *33*, 803–822; d) *Proceedings of the 8th International Symposium on Cyclodextrins*, (Eds.: J. Szejtli, L. Szenté), Kluwer, Dordrecht, **1996**, p. 600 ff.
- [2] Recent review: F. W. Lichtenthaler, S. Immel, *J. Inclusion Phenom. Mol. Recognit. Chem.* **1996**, *25*, 3–16.
- [3] a) M. Kawamura, T. Uchiyama, T. Kuramoto, Y. Tamura, K. Mizutani, *Carbohydr. Res.* **1989**, *192*, 83–90; b) M. Sawada, T. Tanaka, Y. Takai, T. Hanafusa, T. Taniguchi, M. Kawamura, T. Uchiyama, *ibid.* **1991**, *217*, 7–17; c) The inulin-derived cyclodextrins, composed of six to eight  $\beta(1 \rightarrow 2)$ -linked fructofuranose units, are disk-shaped molecules that are not pierced by the cavity [3d], and are hence unable to accommodate guests as the cyclodextrins can; due to their crown ether constitution, however, they exhibit cation binding properties [3b]; d) S. Immel, F. W. Lichtenthaler, *Liebigs Ann.* **1996**, 39–44.
- [4] M. Mori, Y. Ito, T. Ogawa, *Carbohydr. Res.* **1989**, *192*, 131–146; M. Mori, Y. Ito, J. Izawa, T. Ogawa, *Tetrahedron Lett.* **1990**, *31*, 3191–3194.
- [5] M. Nishizawa, H. Imagawa, Y. Kan, H. Yamada, *Tetrahedron Lett.* **1991**, *32*, 5551–5554; *Chem. Pharm. Bull.* **1994**, *42*, 1356–1365.
- [6] P. R. Ashton, C. L. Brown, S. Menzer, S. A. Nepogodiev, J. F. Stoddart, D. J. Williams, *Chem. Eur. J.* **1996**, *2*, 580–591.

- [7] F. W. Lichtenthaler, S. Immel, *Tetrahedron: Asymmetry* **1994**, *5*, 2045–2060.
- [8] a) S. J. Angyal, *Aust. J. Chem.* **1968**, *21*, 2737–2746; b) S. J. Angyal, V. A. Pickles, *ibid.* **1972**, *25*, 1695–1710.
- [9] K. Takeo, K. Uemura, H. Mitoh, *J. Carbohydr. Chem.* **1988**, *7*, 293–303.
- [10] K. Fujita, H. Shimada, K. Ohta, Y. Nogami, K. Nasu, T. Koga, *Angew. Chem.* **1995**, *107*, 1783–1784; *Angew. Chem. Int. Ed. Engl.* **1995**, *34*, 1621–1622.
- [11] Crystal structure analysis of **1**:  $C_{36}H_{60}O_{30} \cdot 21 H_2O$ ,  $M_r = 1351.18$ , hexagonal, space group  $P6_3$ ,  $a = b = 17.241(3)$ ,  $c = 13.323(2)$  Å,  $V = 3430(1)$  Å<sup>3</sup>,  $Z = 2$ ,  $\rho = 1.268$  g cm<sup>-3</sup>,  $\mu(MoK_{\alpha}) = 0.115$  mm<sup>-1</sup>, crystal dimensions  $0.5 \times 0.15 \times 0.125$  mm,  $T = 293$  K. Of 12711 reflections collected on a STOE IPDS diffractometer, graphite-monochromated  $MoK_{\alpha}$  ( $\lambda = 0.71069$  Å) radiation, 2253 are independent ( $R_{int} = 0.0284$ ). The structure was solved by direct methods (SHELXS-86) and successive Fourier difference synthesis. Refinement (on  $F^2$ ) performed by full-matrix least squares method with SHELXL-93.  $R(F) = 0.0568$  for 2036 reflections with  $I \geq 2\sigma(I)$ ,  $wR(F^2) = 0.1604$  for all 2253 reflections ( $w = 1/(\sigma^2(F_o^2) + (0.1189 P)^2 + 0.57 P)$ ;  $P = (F_o^2 + 2F_c^2)/3$ ). All non-hydrogen atoms (except one oxygen atom of the solvent water molecule) were refined anisotropically. Hydrogen atoms on the cyclomaltrin were considered in calculated positions with the  $1.2 U_{eq}$  value of the corresponding bound atom. Crystallographic data (excluding structure factors) for the structure reported in this paper have been deposited with the Cambridge Crystallographic Data Centre as supplementary publication no. CCDC-100196. Copies of the data can be obtained free of charge on application to The Director, CCDC, 12 Union Road, Cambridge CB2 1EZ, UK (fax: int. code + (1223) 336-033; e-mail: deposit@chemcris.cam.ac.uk).
- [12] a) The color graphics (Figure 1) and the molecular contact surfaces (Figures 2 and 3) were generated with the MOLCAD molecular modeling program and its texture mapping option: J. Brickmann, *MOLCAD—Molecular Computer Aided Design*, Technische Hochschule Darmstadt, **1992**. The major part of the MOLCAD program is included in the SYBYL package (TRIPOS Associates, St. Louis, USA); for details, see J. Brickmann, *J. Chim. Phys.* **1992**, *89*, 1709–1721; b) "Interactive Visualization of Molecular Scenarios with MOLCAD/SYBYL": J. Brickmann, T. Goetze, W. Heiden, G. Moeckel, S. Reiling, H. Vollhardt, C.-D. Zachmann, in *Insight and Innovation in Data Visualization* (Ed.: J. E. Bowie), Manning, Greenwich, **1994**, p. 83–97.
- [13] The orientation of the 6-OH groups relative to the pyranoid ring is defined by the exocyclic torsion angles  $O_5-C_5-C_6-O_6$  ( $\omega$ ) and  $C_4-C_5-C_6-O_6$ ; generally preferred are the *gg* and the *gr* forms where the first letter denotes the *gauche* orientation of  $O_6$  towards the pyranoid ring oxygen and the other that of  $O_4$  to  $C_4$ .
- [14] The  ${}^1H$  (800 MHz) and  ${}^{13}C$  (200 MHz) NMR spectra were recorded at the "Large Scale Facility for Biomolecular NMR" in Frankfurt. We are grateful to Prof. Dr. C. Griesinger and Dr. H. Schwalbe, Institut für Organische Chemie, Universität Frankfurt am Main, for support.
- [15] C. A. G. Haasnoot, F. A. A. M. De Leeuw, C. Altona, *Tetrahedron* **1980**, *36*, 2783–2792.
- [16] High-temperature annealing (HTA) calculations were performed with a force field program specially adapted to carbohydrates, comprising application of the verlet integrator in the MD simulation program CHARMM with a time step of 1 fs at constant temperature and dielectric constant  $\epsilon = 1$ . Every 1000 fs the respective conformation from the MD trajectories at 1200 K (4059 ps) was allowed to cool down to 300 K with a rate of 10 K fs<sup>-1</sup>, was held there for an additional 1100 fs, and was subsequently fully energy-minimized by an adapted Newton–Raphson algorithm of the CHARMM22 program package with a convergence criterion of  $10^{-7}$  kcal mol<sup>-1</sup>. For **1**, a total of 2736 (67%) different conformers (corresponding to 16416 altrose units) underwent geometry analysis.
- [17] The CHARMM force field with **1** in the center of a truncated octahedron ( $V \approx 16400$  Å<sup>3</sup>) was used for the MD simulations, and the remaining empty space was filled with water molecules.
- [18] For conformational notations see IUPAC–IUB Recommendations, *Pure Appl. Chem.* **1981**, *53*, 190–195; *Carbohydr. Res.* **1997**, *297*, 20–21.

Molecular Modeling of Saccharides, Part 21<sup>[‡]</sup>Solution Geometries and Lipophilicity Patterns of  $\alpha$ -Cycloaltrin\*\*Stefan Immel, Kahee Fujita, and Frieder W. Lichtenthaler\*<sup>[a]</sup>

**Abstract:** Detailed analysis of the conformational features of  $\alpha$ -cycloaltrin (**1**) in aqueous solution by temperature dependent <sup>1</sup>H and <sup>13</sup>C NMR studies, together with molecular dynamics simulations, reveal that the six altropyranose units are in a complex dynamic equilibrium within the <sup>4</sup>C<sub>1</sub> ⇌ <sup>0</sup>S<sub>2</sub> ⇌ <sup>1</sup>C<sub>4</sub> pseudorotational turntable. This gives rise to a large number of macrocyclic conformations, ranging from a disk-shaped molecule with a hydrophobic

central hole (alternating <sup>4</sup>C<sub>1</sub>/<sup>1</sup>C<sub>4</sub> form **1a**) to a torus form of the macrocycle with an equally hydrophobic through-going cavity (all skew-boat form **1b**). Constrained MD simulations throw light on the conformational transitions be-

tween these two extreme forms (**1a** ⇌ **1b**). Flexure of one altropyranoid chair into the skew-boat-<sup>0</sup>S<sub>2</sub> form forces adjoining altropyranoid units to follow suit, thereby eliciting a successive, synergistic “rolling around” within the, on average, elliptical macrocycle. Thus,  $\alpha$ -cycloaltrin is the first thoroughly flexible cyclooligosaccharide and can be used to probe the induced-fit mode of guest–host interactions.

**Keywords:**  $\alpha$ -cycloaltrin • cyclodextrins • lipophilicity patterns • molecular dynamics • molecular modeling • solution geometries

## Introduction

Research towards cyclooligosaccharides made from sugar units other than glucose<sup>[2–11]</sup> has been undertaken throughout the last decade. The foremost incentive in this pursuit is the generation of molecular receptors with recognition features different from those of the well-studied, overly rigid cyclodextrins (CDs). Unfortunately, only the inulin-derived<sup>[3a]</sup> cyclofructins with six and seven  $\beta(1 \rightarrow 2)$ -linked fructofuranose units became accessible in quantities sufficiently large to

demonstrate their ability to complex metal cations.<sup>[12]</sup> The guest-complexation behavior of all other non-glucose cyclooligosaccharides could only be assessed by molecular modeling studies. Those composed of D-mannose ( $\alpha$ - and  $\beta$ -cyclomannin<sup>[4]</sup>) and L-rhamnose ( $\alpha$ -cyclorhamnin<sup>[5]</sup>), or both,<sup>[9]</sup> have their axially oriented 2-OH group directed towards the outside of the macrocycle, as evident from the contact surface and cross section plot for  $\alpha$ -cyclomannin (Figure 1). A somewhat smaller torus height than in  $\alpha$ -cyclodextrin results, yet this has no principal effect on the backbone structure, the cavity dimensions, or the lipophilicity pattern.<sup>[6, 10]</sup> A similar  $\alpha$ -CD-like geometry was found for a cyclogalactin consisting of six  $\beta(1 \rightarrow 4)$ -linked galactopyranose residues (Figure 1, top right), yet its lipophilicity profile is different because hydrophobic surface regions at the primary hydroxyl face are substantially enlarged.<sup>[6]</sup>

More profound changes in shape, cavity dimensions, and guest-binding properties are to be anticipated for cyclooligosaccharides with axially disposed 3-OH groups in their pyranoid rings, since these 3-OH groups are directed towards the interior of the cavity. As illustrated in Figure 1 for the hexameric  $\alpha$ -cycloallin, steric congestion resulting therefrom induces the altropyranose units to adopt a wide range of tilt angles relative to the macrocycle and a substantial narrowing of the 2-OH/3-OH side of the torus, yet the pyranoid <sup>4</sup>C<sub>1</sub> geometries are retained without exception.<sup>[14]</sup>


For cyclic oligosaccharides composed of D-altropyranoses—those with six ( $\alpha$ -cycloaltrin **1**<sup>[11]</sup>), seven,<sup>[7]</sup> and eight  $\alpha(1 \rightarrow 4)$ -linked units<sup>[8]</sup> have recently become accessible from

[a] Prof. Dr. F. W. Lichtenthaler, Prof. K. Fujita,<sup>[‡]</sup> Dr. S. Immel  
Institut für Organische Chemie, Technische Universität Darmstadt  
Petersenstrasse 22, D-64287 Darmstadt (Germany)  
Fax: (+49) 6151-166674  
E-mail: fwlicht@sugar.oc.chemie.tu-darmstadt.de

[+] Permanent address:  
Faculty of Pharmaceutical Sciences, Nagasaki University  
Nagasaki 852-8131 (Japan)

[‡] Presented in part at the XIXth International Carbohydrate Symposium, San Diego (USA), August 1998; Abstract A 124. Part 20: K. Fujita, W.-H. Chen, D.-Q. Yuan, Y. Nogami, T. Koga, T. Fujioka, K. Mihashi, S. Immel, F. W. Lichtenthaler, *Tetrahedron: Asymmetry* **1999**, *10*, 1689–1696.

[\*\*] A cyclooligosaccharide composed of six  $\alpha(1 \rightarrow 4)$ -linked D-altropyranose residues; for derivation of the terminology used see ref. [1]

 Supporting information for this article in the form of 3D structures of Figure 1 and MOLCAD graphics is available on the WWW under <http://caramel.oc.chemie.tu-darmstadt.de/imm1/3Dstructures.html> and <http://caramel.oc.chemie.tu-darmstadt.de/imm1/molcad/gallery.html>, respectively.

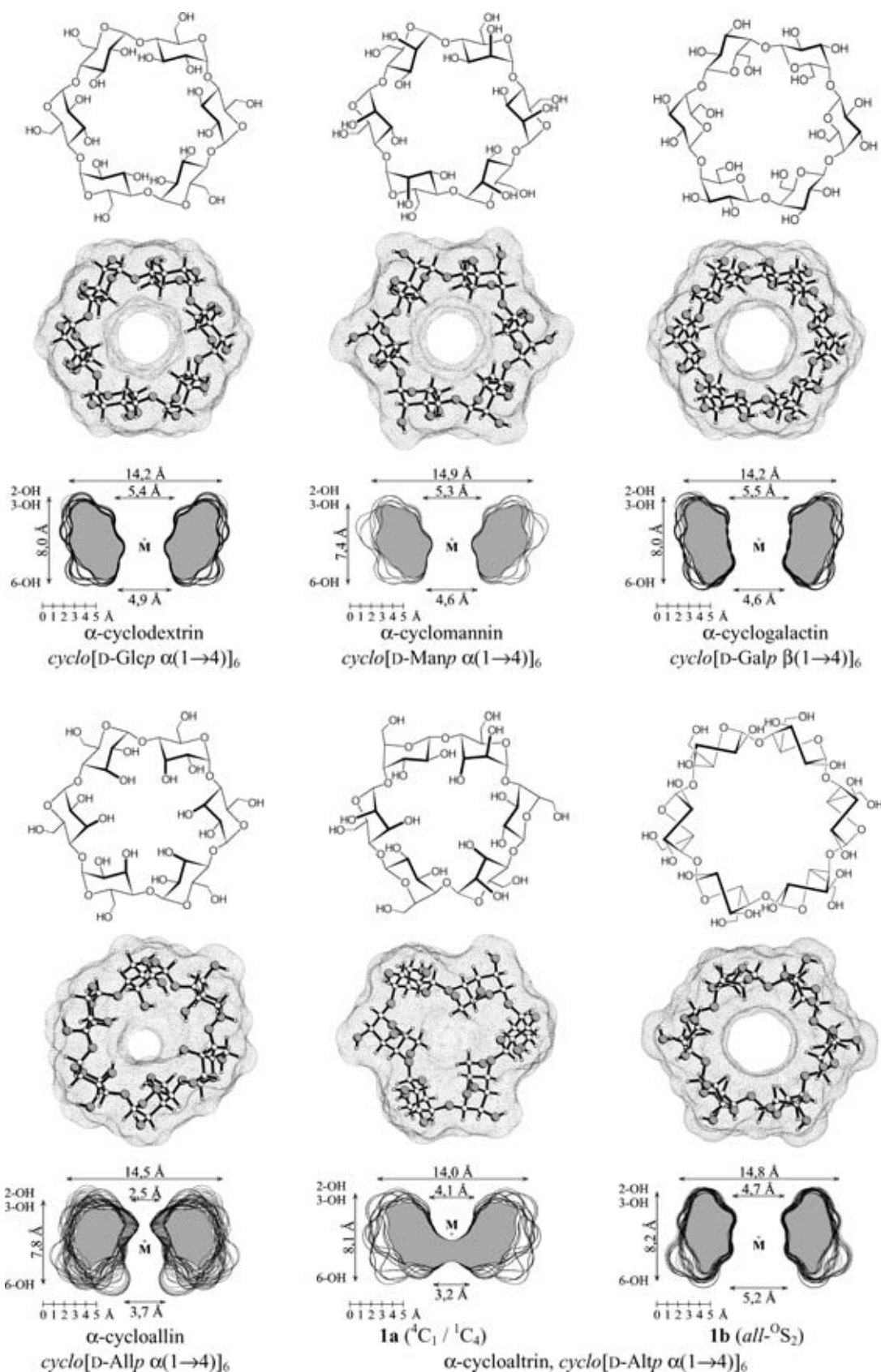


Figure 1. Molecular geometries of  $\alpha$ -cyclodextrin<sup>[13]</sup> compared to cyclooligosaccharide analogues composed of six identical hexopyranose residues in their macrocycle: D-mannose ( $\alpha$ -cyclomannin<sup>[6]</sup>), D-galactose ( $\alpha$ -cyclogalactin<sup>[6]</sup>), D-allose ( $\alpha$ -cycloallin<sup>[14]</sup>), and D-altrose ( $\alpha$ -cycloaltrin, in its solid-state form **1a** and the *all-skew- $\text{O}_2$*  geometry **1b** emerging from HTA simulations as the global minimum energy structure<sup>[10, 11]</sup>). Conventional chemical formulas (top entries), calculated contact surfaces (in dotted form with ball-and-stick-model insert, center), and cross-section plots with approximate molecular dimensions (2-OH and 3-OH sides up) are depicted.

the respective cyclodextrins in a high-yielding four-step procedure—retention of the  ${}^4C_1$  geometry for the altropyranoid rings (with axially disposed 2-OH and 3-OH groups) is highly unlikely, since there is ample calculatory<sup>[15]</sup> and  ${}^1H$  NMR evidence<sup>[16]</sup> that  $\alpha$ -D-altropyranose itself and a variety of its simple derivatives establish a dynamic equilibrium within the  ${}^4C_1 \rightleftharpoons {}^1C_4$  pseudorotational “turntable” (Figure 2). X-ray crystallography revealed that  $\alpha$ -cycloaltrin

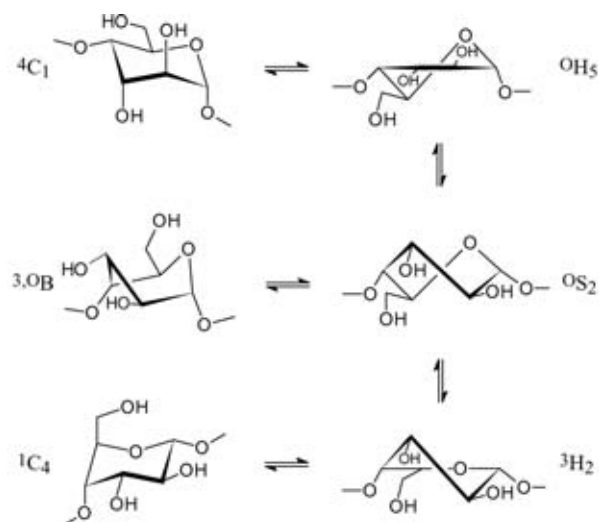


Figure 2. The chair/half-chair/skew (twist-boat) pseudorotational itinerary between  $\alpha$ -D-altropyranoid rings in  ${}^4C_1$  and  ${}^1C_4$  conformation. The  ${}^{3,0}B$  and  ${}^{1,0}S_2$  forms are closely related to each other, hence have similar coupling constants and are not differentiated in Table 1 and Figure 4; the two half-chair conformations  ${}^3H_5$  and  ${}^3H_2$  appear to be higher in energy and are transition states in the  ${}^4C_1 \rightleftharpoons {}^1C_4$  conformational itinerary.

adopts an architecturally unprecedented macrocyclic structure comprising an alternating sequence of  ${}^4C_1$  and  ${}^1C_4$  pyranoid chair conformations, resulting in a disk-shaped molecule with a central indentation rather than a through-going cavity (Figure 1, **1a**).<sup>[11]</sup> This unique topography in the solid state, in spite of being embedded into a matrix of 21 water molecules, does not survive on dissolution in water, for only one set of  ${}^1H$  NMR signals are observed.<sup>[11]</sup> This finding is compatible with either of the following two scenarios: operation of a dynamic equilibrium between the  ${}^4C_1$  and  ${}^1C_4$  chairs within the pseudorotational transitions illustrated in Figure 2, whereby NMR measurements average over the variety of macrocyclic conformations, or alternatively, adoption of a fixed conformation, an *all*-

skew (twist-boat) form conceivably, as this form emerges from high-temperature annealing (HTA) simulations as the global energy minimum structure (**1b** in Figure 1). Notably, this *all*- ${}^0S_2$  form **1b** contains a cavity that is larger and possesses the opposite concavity than that of  $\alpha$ -cyclodextrin, and **1b** should therefore be able to form inclusion complexes with sterically matching guests.

A detailed study towards a differentiation between these possibilities appeared warranted since—should a dynamic equilibrium prevail in solution—the cycloaltrins would be the first thoroughly flexible cyclooligosaccharides capable of adapting their overall geometries to binding of appropriate guests, a process that more closely corresponds to Koshland’s induced-fit mode of substrate-receptor interaction<sup>[17]</sup> than to the overly static lock-and-key model.<sup>[18]</sup> These issues are herein explored by temperature-dependent NMR analysis, standard and constrained MD simulations, and generation of the lipophilicity patterns of the closed and open forms **1a** and **1b**.

## Results and Discussion

**Temperature-dependent NMR analysis:** High-resolution  ${}^1H$  and  ${}^{13}C$  NMR spectra of  $\alpha$ -cycloaltrin (**1**) in  $D_2O$  (Figure 3) display only one set of signals for the six altropyranoses, indicating either fast averaging between different altropyranoid ring conformations, or alternatively adoption of a uniform geometry somewhere in between the  ${}^4C_1$  and  ${}^1C_4$  conformation for all six altrose units. Experimental  ${}^1H$  NMR coupling constants (Table 1) are consistent with either scenario.

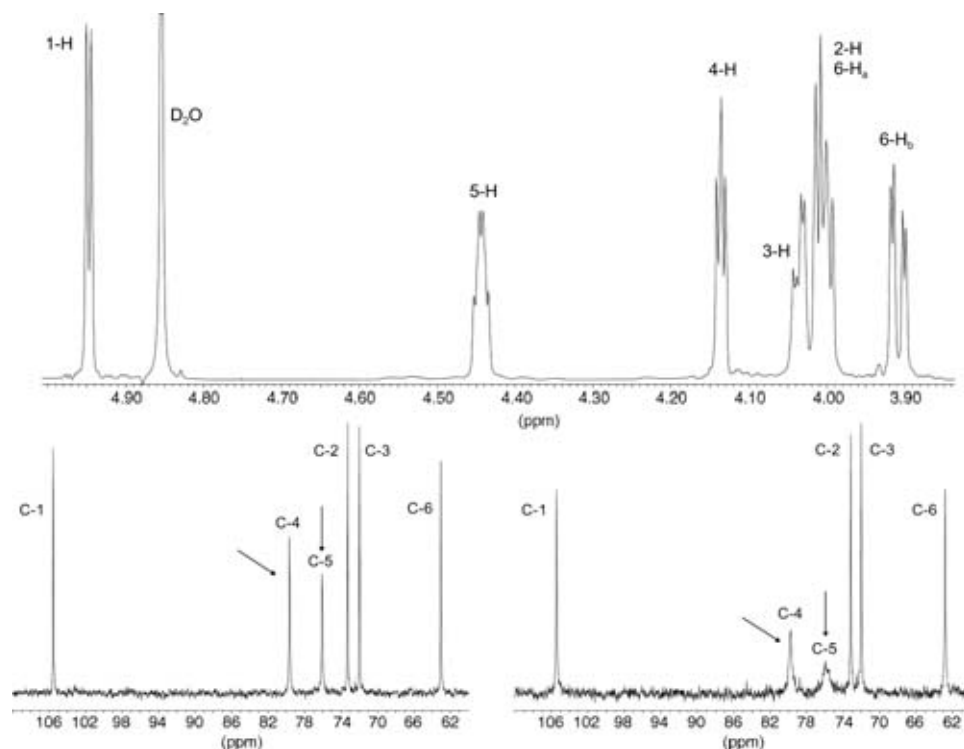


Figure 3. Top: 800 MHz  ${}^1H$  NMR spectrum of  $\alpha$ -cycloaltrin (**1**) in  $D_2O$  at 30 °C reveals one set of signals. Bottom: 200 MHz  ${}^{13}C$  NMR spectra of **1** in  $D_2O$  at 32 °C (left) and 4 °C (right). As indicated by the arrows, the signals of C-4 and C-5 are significantly broadened at lower temperatures.

## FULL PAPER

F. W. Lichtenthaler et al.

Table 1. Comparison of the altopyranoid ring  $^1\text{H}$ - $^1\text{H}$ -coupling constants for  $\alpha$ -cycloaltrin (800 MHz,  $\text{D}_2\text{O}$ ,  $30^\circ\text{C}$ ) with those calculated for its  $^4\text{C}_1$ ,  $^1\text{C}_4$ , and all- $^{\circ}\text{S}_2$  (skew) forms.

$J_{\text{HH}}$ [Hz]	Found	Calculated <sup>[a]</sup> for			
		$^4\text{C}_1$ <sup>[b]</sup>	$^1\text{C}_4$ <sup>[b]</sup>	$^{\circ}\text{S}_2$ <sup>[c]</sup>	$^4\text{C}_1/{}^1\text{C}_4/{}^{\circ}\text{S}_2$ <sup>[d]</sup>
$J_{1,2}$	4.73	2.2	8.0	4.0	4.9
$J_{2,3}$	8.19	2.7	10.2	10.2	8.3
$J_{3,4}$	3.71	3.4	2.4	4.5	3.5
$J_{4,5}$	5.32	9.7	1.4	6.4	5.5

[a] Calculation based on the Karplus-type H-C-C-H torsion angle dependency of coupling constants, including the electronegativity effect to the substitution pattern by use of the generalized Haasnoot equation.<sup>[19]</sup>

[b] Values obtained for the pyranose conformations realized in the crystal structure **1a**. [c] Data resulting from calculations on the HTA-derived global energy minimum all-skew form **1b**.<sup>[10, 11]</sup> [d] Least-squares fit for 26%  $^4\text{C}_1$ , 34%  $^1\text{C}_4$ , and 40%  $^{\circ}\text{S}_2$ , roughly corresponding to a 1:1:1 mixture of conformers.

The presence of a dynamic conformational equilibrium in aqueous solution is inferred from the temperature dependence of the  $^1\text{H}$  NMR data: the value for  $J_{2,3}$  decreases from 8.2 Hz at  $30^\circ\text{C}$  to 7.6 and 7.1 Hz at 20 and  $4^\circ\text{C}$ , respectively, thereby narrowing the well-separated signal for H-3. Although the smaller value of  $J_{2,3}$  at  $4^\circ\text{C}$  suggests a more intensely populated  $^4\text{C}_1$  altrose conformation in the  $^4\text{C}_1 \rightleftharpoons ^{\circ}\text{S}_2 \rightleftharpoons ^1\text{C}_4$  pseudorotational itinerary, the best fit of calculated<sup>[19]</sup> versus measured coupling constants emerging from the

triangle representation of Figure 4, revealed a composition of 26%  $^4\text{C}_1$ , 34%  $^1\text{C}_4$ , and 40%  $^{\circ}\text{S}_2$  (cf. center minimum of  $\sigma$ -contours at 0.18 Hz), indicating, within the margin of error, the presence of essentially equal proportions of the three forms.

More profound temperature effects are observed for the  $^{13}\text{C}$  signals of C-4 and C-5, which are substantially broadened on lowering the temperature from 30 to  $4^\circ\text{C}$  (cf. Figure 3). This is clearly indicative of a dynamic equilibrium of various altopyranoid geometries which starts to “freeze out” at  $4^\circ\text{C}$ . However, the NMR data neither reveal which of the many macrocyclic conformations within the sterically limiting “straitjacket” of **1** are preferred, nor answer the question of how the conformational transitions  $\mathbf{1a} \rightleftharpoons \mathbf{1b}$  occur.

**Molecular dynamics simulations:** MD simulations with explicit incorporation of the (aqueous) solvent were performed for both  $\alpha$ -cycloaltrin forms, **1a** and **1b**. Despite considerable flexibility in the macrocycles, no significant conformational transitions for the pyranose units were observed within a time frame of 600 ps (Figure 5). The solute hydration shells can be readily characterized from these calculations. An average of  $30.6 \pm 2.7$  and  $39.6 \pm 3.4$  water molecules are hydrogen-bonded to **1a** and **1b**, respectively. Any change of the altopyranose conformations entails substantial rearrangements in this tightly bound first hydration shell, rendering these processes too slow to be observable during standard MD simulations. The crucial role of water in the rearrangement process becomes particularly evident when comparing the MDs in solution with HTA simulations on  $\alpha$ -cycloaltrin in vacuum: at high (1200 K) as well as at low temperatures (300 K) frequent and unhindered conformational transitions are observed for the altrose units in the isolated macrocycle.

The effects on the macrocycle of changing a  $^4\text{C}_1$  altrose unit in the  $^4\text{C}_1/{}^1\text{C}_4$  form **1a** along the  $^4\text{C}_1 \rightarrow ^{\circ}\text{S}_2 \rightarrow ^1\text{C}_4$  pathway can be monitored within a reasonable nanosecond time frame by means of constrained MD techniques: two pyranose ring torsion angles  $\text{O}_5\text{-C}_1\text{-C}_2\text{-C}_3$  and  $\text{C}_3\text{-C}_4\text{-C}_5\text{-O}_5$  of one altrose unit are restrained in such a way that the  $^4\text{C}_1$  conformation is forced to vary in the desired direction (Figure 6, gray shaded altrose residue **B**). As this ring flip is artificially induced, the neighboring unconstrained monosaccharide units—each in the  $^1\text{C}_4$  form—are subject to considera-

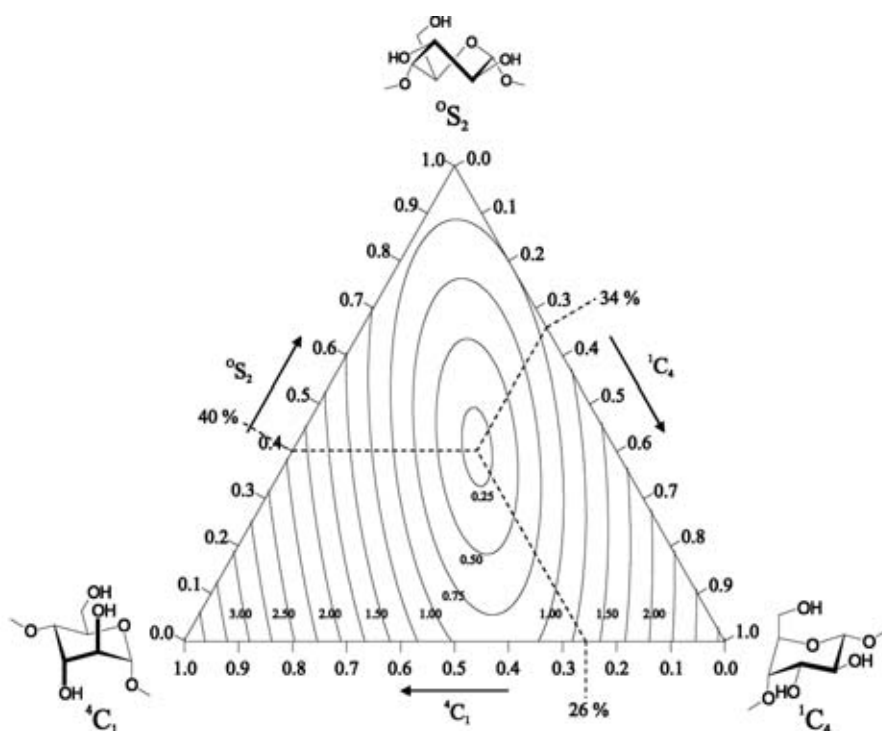


Figure 4. Triangular contour plot of the root-mean-square deviation (i.e. the error  $\sigma$ ) of the calculated pyranose ring coupling constants ( $J_{1,2}$ ,  $J_{2,3}$ ,  $J_{3,4}$ , and  $J_{4,5}$ ) versus those found experimentally. Contours are given as a function of the altrose conformational equilibrium between  $^4\text{C}_1$  (left corner of the triangle),  $^1\text{C}_4$  (right), and  $^{\circ}\text{S}_2$  forms (top corner), and are plotted at levels of  $\sigma = 0.25$  to 4.00 Hz in 0.25 Hz steps; the triangle axes are in units of molecular fractions  $\chi_i = 0.0$ –1.0. The  $^3J_{\text{HH}}$  coupling constants for the pure  $^4\text{C}_1$ ,  $^1\text{C}_4$ , and  $^{\circ}\text{S}_2$  pyranose forms (triangle corners) were obtained from the solid-state structure and the minimum-energy geometry of **1**. The values are listed in Table 1. The best-fit of calculated versus experimental data (center minimum of the  $\sigma$ -contours at  $\sigma_{\text{min}} = 0.18$  Hz) emerged for 26%  $^4\text{C}_1$ , 34%  $^1\text{C}_4$ , and 40%  $^{\circ}\text{S}_2$  (equilibrium composition marked by hatched lines); all other mixtures yielded larger errors.

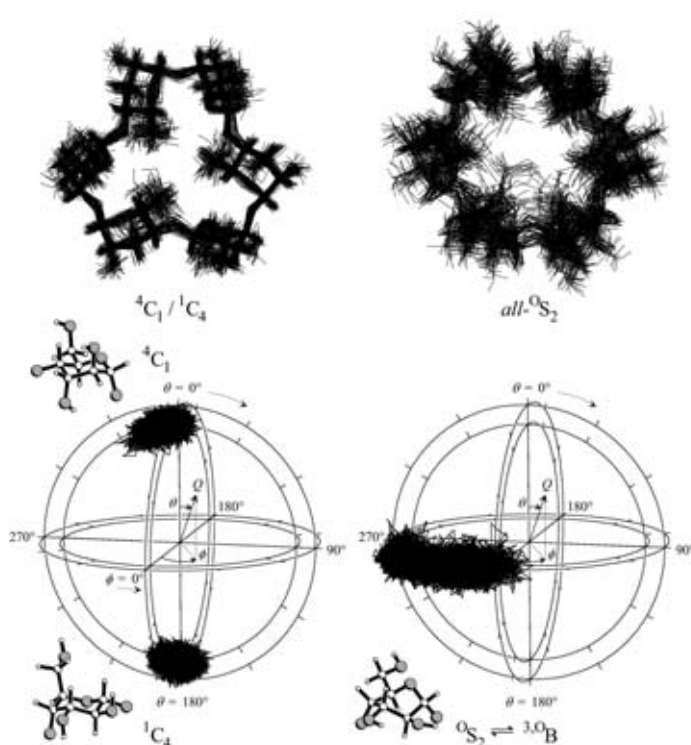


Figure 5. Top: Superimpositions of 60  $\alpha$ -cycloaltrin snapshot geometries taken in 10 ps intervals from MD simulations of **1a** (left) and **1b** (right) in water illustrate the flexibility of the macrocycles, despite relative conformational rigidity of the pyranose rings. Bottom: Polar-coordinate plots of the pyranose Cremer–Pople ring-puckering parameters<sup>[28]</sup> derived from MD simulations of **1a** (left plot, solid-state structure) and **1b** (right, HTA-derived start geometry) in water. In both cases a time series (trajectory) of the pyranose pucker parameters  $Q$ ,  $\phi$  and  $\theta$  is plotted in 3D-polar coordinates (height, longitude, and latitude): On the left, the well-separated trajectories for the  ${}^4C_1$  and  ${}^1C_4$  altrose units lack any conformational transitions between the different chair geometries within the MD time frame of approximately 600 ps; similarly, **1b** displays no significant deviations from the  ${}^0S_2 \rightleftharpoons {}^3,0B$  geometries during the entire MD simulation.

ble intrinsic strain in the macro-ring: one is only slightly distorted towards the half-chair form ( ${}^1C_4 \rightarrow {}^3H_2$ , unit **A** in Figure 6), whereas the residue on the other side (**C**) displays a full transition along  ${}^1C_4 \rightarrow {}^0S_2 \rightleftharpoons {}^3,0B$ . As this ring-flip was not induced by additionally applied MD potentials, it reveals the way conformational changes occur within the macrocycle: flexure of one altropyranoid chair into the intermediate skew- ${}^0S_2$  form via half-chair transition states forces the two adjoining altrose chairs, tied up in a macrocyclic “straitjacket” type clamp, to follow suit, and so on, thereby eliciting a consecutive “rolling around” in the probably elliptically distorted macrocycle.

As the above mechanism for interconversion involves energy concentration on one altrose unit (the restrained residue) with consecutive geometry changes in the macrocycle, there might be an alternative transition pathway: structural changes through excitation of low-energy macromolecular vibrational modes by thermal collisions with the solvent. Although such a mode of interconversion is difficult to induce through constrained MDs and was not observed during the standard MD simulations, it cannot be ruled out

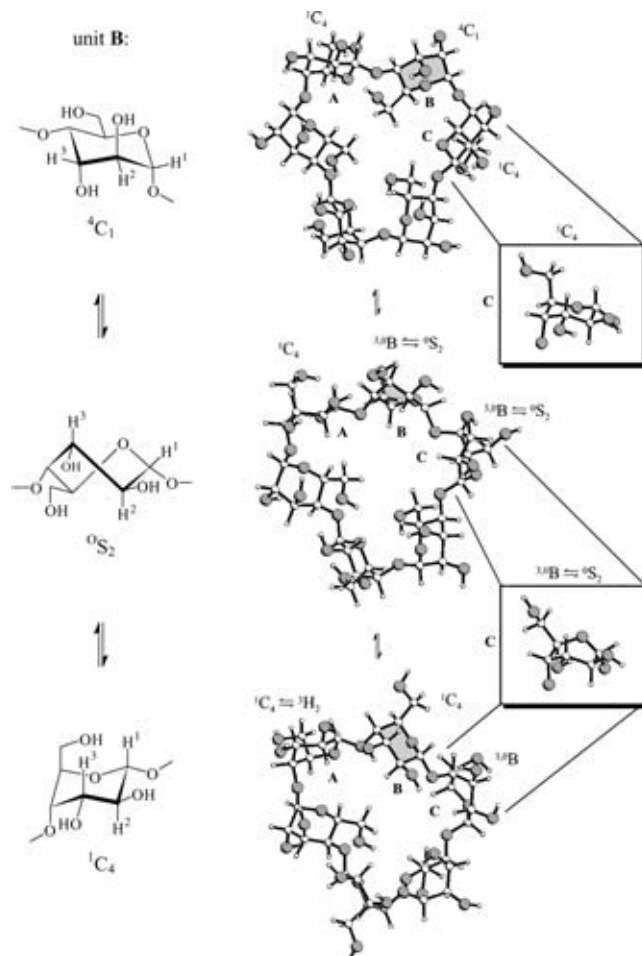


Figure 6. Constrained MD simulations of  $\alpha$ -cycloaltrin exhibit a conformational transition of the central  ${}^4C_1$  altropyranose (gray-shaded unit **B**) of a  ${}^1C_4$ - ${}^4C_1$ - ${}^1C_4$ -fragment (units **A**-**B**-**C**) in the macrocycle: as **B** is driven along the  ${}^4C_1 \rightarrow {}^3,0B/{}^0S_2 \rightarrow {}^1C_4$  reaction coordinate (formulas, left column), the conformation of the neighboring residue **A** varies very little with slight distortions  ${}^1C_4 \rightarrow {}^3H_2$  only, but the altrose unit **C** cooperatively flips into a  ${}^3,0B \rightleftharpoons {}^0S_2$  geometry (zoomed structures on the right). The unperturbed and cooperative conformational transitions of adjacent pyranose units point towards complex dynamic processes, in the course of which altrose residues cannot be considered independent; each conformational change induces new strains in neighboring units (all  $\alpha$ -cycloaltrin snapshot structures were taken from a 130 ps MD perturbation, and constraints were applied to unit **B** only).

entirely. However, the question of whether structural changes in the macrocycle induce transitions in the monomers or vice-versa is bound to remain open as both conformational motions seem to be so intricately interwoven to the extent of being inseparable.

In either case, the overall result is a statistical scrambling over the  ${}^4C_1$ ,  ${}^0S_2$ , and  ${}^1C_4$  forms for the six altropyranose residues, of which the NMR data (Figure 3 and Table 1) provide an averaged picture. Although the distinct forms **1a** and **1b** cannot be identified directly from the NMR data presented in Figures 3 and 4, they should be taken into account as limiting structures in this complex conformational equilibrium.

**Molecular lipophilicity patterns:** Generation of molecular lipophilicity patterns (MLP)<sup>[20]</sup> of the solid-state conformation

## FULL PAPER

F. W. Lichtenthaler et al.

**1a**<sup>[11]</sup> and of the HTA-derived energy-minimum *all*-<sup>0</sup>S<sub>2</sub> form **1b**<sup>[10, 11]</sup> was achieved by the MOLCAD program,<sup>[21]</sup> and was projected<sup>[22]</sup> in color-coded form onto their contact surfaces<sup>[23]</sup> depicted in Figure 1. The results displayed in Figure 7 allow a first assessment of the inclusion-complexation capabilities of  $\alpha$ -cycloaltrin. Both the disk- (**1a**) and torus-shaped form (**1b**) reveal a distinct front–rear differentiation of hydrophobic and hydrophilic surface regions. The 2-OH, 3-OH side—in analogy to the cyclodextrins<sup>[6, 10]</sup>—turns out to be the most hydrophilic part of the molecule, in contrast to a significantly more hydrophobic reverse side owing to the primary 6-CH<sub>2</sub>OH groups. Although **1a** lacks a central “through-going” cavity, this conformer has a hydrophilic surface indentation and an outer core made up of irregularly distributed hydrophilic and hydrophobic regions (Figure 7,

top right). In contrast, the cyclodextrin-like, torus-shaped form **1b** displays a more uniform pattern of the corresponding surface qualities (Figure 7, bottom): the most hydrophobic surface areas extend from the 6-CH<sub>2</sub>OH side well into the cavity, yet the tilt of the pyranose units in the macrocycle is the inverse of that present in  $\alpha$ -cyclodextrin (Figure 1, top left).

## Conclusion

These results provide unambiguous insight into the solution geometries of  $\alpha$ -cycloaltrin (**1**) and into the comparable stabilities of the <sup>4</sup>C<sub>1</sub>- and <sup>1</sup>C<sub>4</sub>-chair forms of its altropyranose residues. A large variety of macrocyclic shapes are possible within the constraints of its cyclohexasaccharide “straitjack-

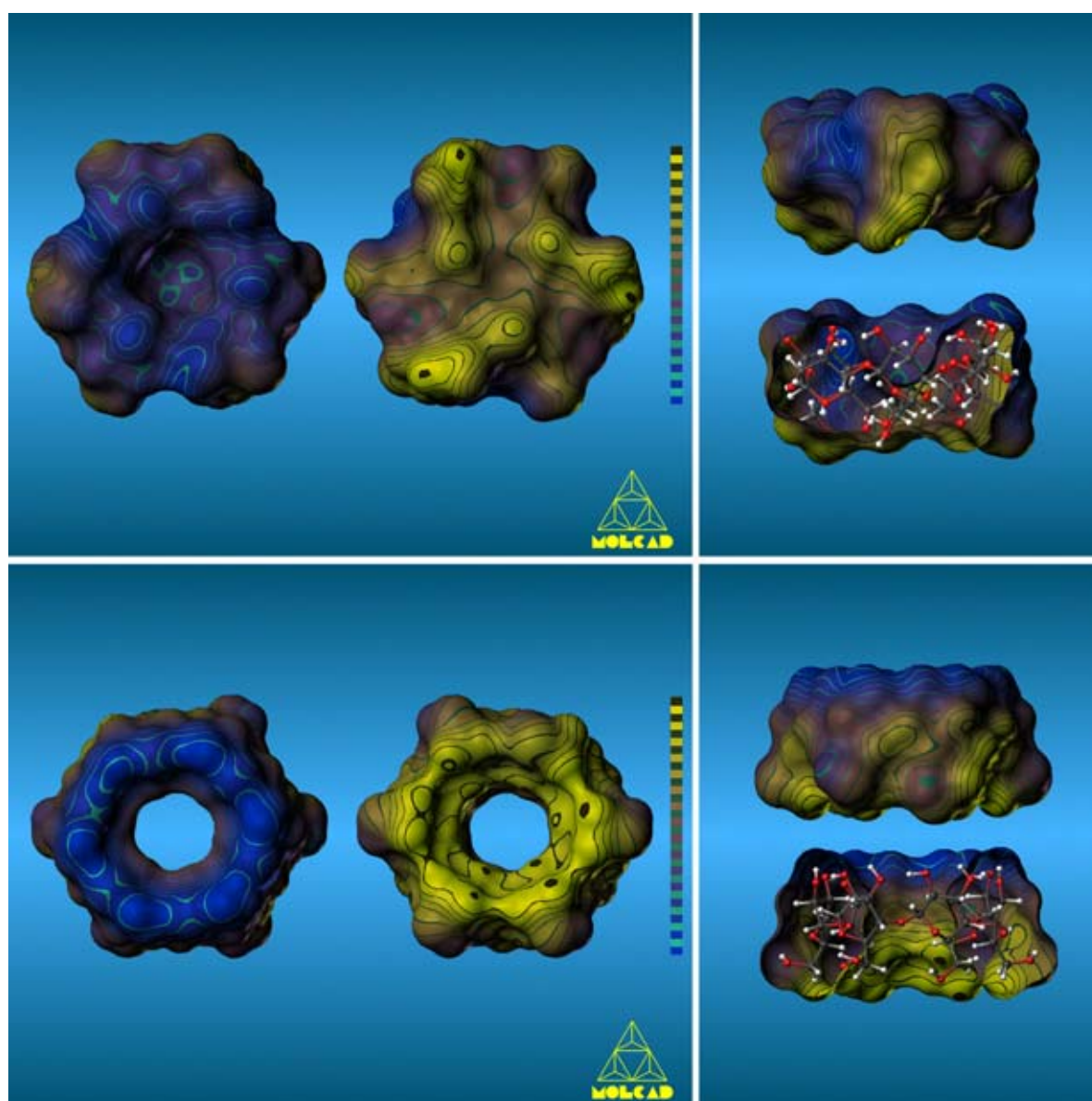


Figure 7. Molecular lipophilicity patterns of  $\alpha$ -cycloaltrin (**1**) projected onto the contact surfaces of the solid-state conformation (**1a**, top) and the *all*-<sup>0</sup>S<sub>2</sub> form (**1b**, bottom). The color code applied ranges from dark blue for the most hydrophilic surface areas to full yellow corresponding to the most hydrophobic regions. On the left, the macrocycles are viewed from both sides perpendicular to the mean ring plane, exposing either the pronouncedly hydrophilic (blue) 2-OH/3-OH side of the torus or the opposite, hydrophobic rim made up from the primary 6-CH<sub>2</sub>OH hydroxyl groups. The graphics on the right display the corresponding side views in closed and bisected form each, with the 2-OH and 3-OH groups directed upwards and the CH<sub>2</sub>OH moieties at the lower rim.



et”. The shapes range from a disk-shaped macrocycle with a distinctly hydrophobic central hole, which is realized when the pyranose units adopt an alternating sequence of  ${}^4C_1$  and  ${}^1C_4$  conformations (**1a**), to a torus shape with an equally hydrophobic through-going cavity, realized when all pyranoid rings are in the skew-boat- ${}^0S_2$  form (**1b**). Both forms are limiting structures of a complex dynamic equilibrium. Accordingly,  $\alpha$ -cycloaltrin (**1**) constitutes the first thoroughly flexible cycloligosaccharide with which to realistically probe the induced-fit mode<sup>[17]</sup> of guest–host interactions. All previous utilizations of the overly rigid cyclodextrins as artificial enzymes<sup>[24]</sup> have only served as models for the stationary lock-and-key type<sup>[18]</sup> of enzyme action.

First evidence from capillary electrophoresis studies indicates that  $\alpha$ -cycloaltrin and 4-*tert*-butylbenzoate form inclusion complexes. We hope that a sufficiently large number of guests interacting with  $\alpha$ -cycloaltrin will justify broad exploration of this system.

### Experimental Section

Temperature-dependent  ${}^1H$  (800 MHz) and  ${}^{13}C$  (200 MHz) spectra were recorded at the “Large Scale Facility for Biomolecular NMR” of the University of Frankfurt.

HTA<sup>[10, 11]</sup> and MD calculations were carried out using the CHARMM<sup>[25]</sup> force field for carbohydrates<sup>[26]</sup> and application of periodic boundaries (MDs, truncated octahedron filled with 606 (**1a**) and 611 (**1b**) water molecules, box size approximately 32 Å), isothermal ( $T=300$  K), and isobaric conditions ( $p=1$  bar) during a simulation time of 600 ps (equilibration time 25 ps, time step 1 fs); analysis of the MD trajectories was accomplished with external computer programs.<sup>[27]</sup>

Constrained MD computations of  $\alpha$ -cycloaltrin (cf. Figure 6) were carried out using the isothermal and isobaric simulation system as described above. Starting from the solid-state conformation **1a**, the ring torsion angles  $O_5-C_1-C_2-C_3$  ( $\theta_1$ ) and  $C_3-C_4-C_5-O_5$  ( $\theta_4$ ) of one altropyranose unit were constrained and driven during 39 independent MD runs with steps of  $3^\circ$  each, forcing one  ${}^4C_1$  altrose geometry to vary slowly into the inverted  ${}^1C_4$  conformation (“reaction parameters”  $\theta_1: +57^\circ \rightarrow -57^\circ$ ,  $\theta_4: -57^\circ \rightarrow +57^\circ$ ). Each MD trajectory was carried out for a 10 ps equilibration and a 25 ps data acquisition period, the final structures were used as a starting point for the next MD run after re-setting the torsion angles to the new values along the reaction coordinate. The conformational transitions of the remaining five unconstrained altrose residues were monitored by use of Cremer–Pople parameters.<sup>[28]</sup>

Calculation of the molecular contact surfaces and the respective hydrophobicity potential profiles<sup>[29]</sup> was performed by using the MOLCAD<sup>[21]</sup> molecular modeling program and its texture mapping option.<sup>[22]</sup> The MLP profiles were scaled in relative terms (most hydrophilic to most hydrophobic surface regions) for each molecule separately; no absolute values are displayed.

The minimum-energy structure of  $\alpha$ -cycloaltrin was derived from a 675 ps MD study in water (CHARMM force field,<sup>[25, 26]</sup>  $T=300$  K,  $p=1$  bar, 609 water molecules, parameters as above), with subsequent full energy minimization of a total of 13248 isolated solute structures by application of the PIMM91 force field,<sup>[29]</sup> which is particularly suitable for carbohydrate structures without solvent.

Least-squares fitting of the  $J$  values for three conformations  ${}^4C_1$ ,  ${}^1C_4$ , and  ${}^0S_2$  was achieved with root-mean-square deviations of  $\sigma_J=0.18$  Hz, whereas a two-state model  ${}^4C_1 \rightleftharpoons {}^1C_4$  yielded  $\sigma_J=0.80$  Hz.

### Acknowledgements

We are grateful for financial support from Fonds der Chemischen Industrie, Frankfurt, and for a fellowship (to K.F.) from the Deutscher Akademischer Austauschdienst, Bonn. In addition, we thank Prof. Dr. C. Griesinger and Dr. H. Schwalbe, Goethe Universität Frankfurt, for recording the  ${}^1H$

(800 MHz) and  ${}^{13}C$  (200 MHz) NMR spectra, and Prof. Dr. J. Brickmann, Institut für Physikalische Chemie, Technische Universität Darmstadt, for providing access to his MOLCAD software package.

- [1] a) The naming of non-glucose cycloligosaccharides, in particular of those composed of different sugar units, can be exasperating. According to recent IUPAC Recommendations (*Carbohydr. Res.* **1997**, 297, 78 ff.), the systematic name for **1** turns out to be *cyclohexakis-(1 $\rightarrow$ 4)- $\alpha$ -D-altropyranosyl*, implying that **1** represents an assembly of “glycosyls” rather than being a “glycoside”. In fact it is a hexasaccharide. Alternatively the semi-systematic name *cyclo- $\alpha$ -(1 $\rightarrow$ 4)-D-altro-hexaoside*, abbreviated as “*cyclo[D-Alt $\alpha$ -(1 $\rightarrow$ 4)]<sub>6</sub>”, may be used, based on a recent proposal for a simplified nomenclature,<sup>[1b, 6]</sup> which has been authoritatively endorsed.<sup>[1c]</sup> The most simple and practical designation, however—at least for cycloligosaccharides with a single type of sugar unit—is inferred from traditional CD terminology (dextrose being an old name for glucose), syllogistically leading to “cycloaltrin” and the Greek letters  $\alpha$ ,  $\beta$ , and  $\gamma$  designating the respective species with six, seven, and eight hexose units. Accordingly, **1** is appropriately termed  *$\alpha$ -cycloaltrin*,<sup>[11]</sup> and the next higher homologues,  $\beta$ -<sup>[7]</sup> and  $\gamma$ -*cycloaltrin*.<sup>[8]</sup> Correspondingly, other known non-glucose cycloligosaccharides with one type of monosaccharide unit are reasonably named  $\alpha$ -,  $\beta$ -, and  $\gamma$ -*cyclomannin*,<sup>[4, 6]</sup>  *$\alpha$ -cyclorhamnin*,<sup>[5]</sup> and  $\alpha$ - and  $\beta$ -*cyclofructin*.<sup>[3]</sup> b) S. Immel, J. Brickmann, F. W. Lichtenthaler, *Liebigs Ann. Chem.* **1995**, 929–942; c) J. Szejtli, in *Comprehensive Supramolecular Chemistry, Vol. 3 (Cyclodextrins)*, (Eds.: J. Szejtli, T. Osa), Pergamon, Oxford, UK, **1996**, pp. 7 ff.; J. Szejtli, *Chem. Rev.* **1998**, 98, 1743–1753.*
- [2] L. V. Backinowsky, S. A. Nepogodiev, N. K. Kochetkov, *Carbohydr. Res.* **1989**, 185, C1–C3; L. V. Backinowsky, S. A. Nepogodiev, N. K. Kochetkov, *Tetrahedron* **1990**, 46, 139–150.
- [3] a) M. Kawamura, T. Uchiyama, T. Kuramoto, Y. Tamura, K. Mizutani, *Carbohydr. Res.* **1989**, 192, 83–90; b) M. Sawada, T. Tanaka, Y. Takai, T. Hanafusa, T. Taniguchi, M. Kawamura, T. Uchiyama, *Carbohydr. Res.* **1991**, 217, 7–17; c) S. Immel, F. W. Lichtenthaler, *Liebigs Ann. Chem.* **1996**, 39–44; d) S. Immel, G. E. Schmitt, F. W. Lichtenthaler, *Carbohydr. Res.* **1998**, 313, 91–105.
- [4] M. Mori, Y. Ito, T. Ogawa, *Carbohydr. Res.* **1989**, 192, 131–146; M. Mori, Y. Ito, J. Uzawa, T. Ogawa, *Tetrahedron Lett.* **1990**, 31, 3191–3194.
- [5] a) M. Nishizawa, H. Imagawa, Y. Kan, H. Yamada, *Tetrahedron Lett.* **1991**, 32, 5551–5554; *Synlett* **1992**, 447–448; b) M. Nishizawa, H. Imagawa, E. Morikuni, S. Hatekayama, H. Yamada, *Chem. Pharm. Bull.* **1994**, 42, 1356–1365.
- [6] F. W. Lichtenthaler, S. Immel, *Tetrahedron: Asymmetry* **1994**, 5, 2045–2060.
- [7] K. Fujita, H. Shimada, K. Ohta, Y. Nogami, K. Nasu, *Angew. Chem.* **1995**, 107, 1783–1784; *Angew. Chem. Int. Ed. Engl.* **1995**, 34, 1621–1622.
- [8] Y. Nogami, K. Fujita, K. Ohta, K. Nasu, H. Shimada, C. Shinohara, T. Koga, *J. Inclusion Phenom. Mol. Recognit. Chem.* **1996**, 25, 53–56.
- [9] P. R. Ashton, C. L. Brown, S. Menzer, S. A. Nepogodiev, J. F. Stoddart, D. J. Williams, *Chem. Eur. J.* **1996**, 2, 580–591.
- [10] F. W. Lichtenthaler, S. Immel, *J. Inclusion Phenom. Mol. Recognit. Chem.* **1996**, 5, 3–16.
- [11] Y. Nogami, K. Nasu, T. Koga, K. Ohta, K. Fujita, S. Immel, H. J. Lindner, G. E. Schmitt, F. W. Lichtenthaler, *Angew. Chem.* **1997**, 109, 1987–1991; *Angew. Chem. Int. Ed. Engl.* **1997**, 36, 1899–1902.
- [12] a) N. Yoshie, H. Hamada, S. Takada, Y. Inoue, *Chem. Lett.* **1993**, 353–356; b) T. Uchiyama, M. Kawamura, T. Urugami, H. Okuno, *Carbohydr. Res.* **1993**, 241, 245–248.
- [13] F. W. Lichtenthaler, S. Immel, *Liebigs Ann. Chem.* **1996**, 27–37.
- [14] S. Immel, G. E. Schmitt, unpublished results.
- [15] a) S. J. Angyal, *Aust. J. Chem.* **1968**, 21, 2737–2746; b) M. K. Dowd, A. D. French, P. J. Reilly, *Carbohydr. Res.* **1994**, 264, 1–19.
- [16] F. W. Lichtenthaler, S. Mondel, *Carbohydr. Res.* **1997**, 303, 293–302.
- [17] D. E. Koshland, Jr., *Angew. Chem.* **1994**, 106, 2368–2372; *Angew. Chem. Int. Ed. Engl.* **1994**, 33, 2375–2378.
- [18] a) E. Fischer, *Ber. Dtsch. Chem. Ges.* **1894**, 27, 2985–2993; b) F. W. Lichtenthaler, *Angew. Chem.* **1994**, 106, 2456–2467; *Angew. Chem. Int. Ed. Engl.* **1994**, 33, 2364–2374.

## FULL PAPER

F. W. Lichtenthaler et al.

- [19] C. A. G. Haasnoot, F. A. A. M. DeLeeuw, C. Altona, *Tetrahedron* **1980**, *36*, 2783–2792.
- [20] W. Heiden, G. Moeckel, J. Brickmann, *J. Comput.-Aided Mol. Des.* **1993**, *7*, 503–514.
- [21] a) J. Brickmann, *MOLCAD - MOLEcular Computer Aided Design*, Darmstadt University of Technology, **1996**; *J. Chem. Phys.* **1992**, *89*, 1709–1721; b) J. Brickmann, T. Goetze, W. Heiden, G. Moeckel, S. Reiling, H. Vollhardt, C.-D. Zachmann, *Interactive Visualization of Molecular Scenarios with the MOLCAD/SYBYL Package*, in *Data Visualization in Molecular Science: Tools for Insight and Innovation* (Ed.: J. E. Bowie), Addison–Wesley, Reading, MA **1995**, pp. 83–97.
- [22] M. Teschner, C. Henn, H. Vollhardt, S. Reiling, J. Brickmann, *J. Mol. Graphics* **1994**, *12*, 98–105.
- [23] M. L. Connolly, *J. Appl. Crystallogr.* **1983**, *16*, 548–558.
- [24] a) R. Breslow in *Inclusion Compounds, Vol. 3* (Eds.: J. L. Atwood, J. E. D. Davies, D. D. MacNicol), Academic Press, London, **1984**, pp. 473–508; M. Komiyama, H. Shikigawa in *Comprehensive Supramolecular Chemistry, Vol. 3* (Eds.: J. Szejtli, T. Osa), Pergamon, Oxford, **1996**, pp. 401–422; b) R. Breslow, S. D. Dong, *Chem. Rev.* **1998**, *98*, 1997–2011.
- [25] B. R. Brooks, R. E. Bruccoleri, B. D. Olafson, D. J. States, S. Swaminathan, M. Karplus, “CHARMM: A program for macromolecular energy, minimization, and dynamics calculations” in *J. Comp. Chem.* **1983**, *4*, 187–217.
- [26] S. Reiling, M. Schlenkrich, J. Brickmann, *J. Comput. Chem.* **1996**, *17*, 450–468.
- [27] S. Immel, *MolArch<sup>+</sup> – MOLEcular ARCHitecture Modeling Program*, Darmstadt University of Technology, **1997**.
- [28] a) D. Cremer, J. A. Pople, *J. Am. Chem. Soc.* **1975**, *97*, 1354–1358; b) G. A. Jeffrey, R. Taylor, *Carbohydr. Res.* **1980**, *81*, 182–183.
- [29] a) H. J. Lindner, M. Kroeker, *PIMM91-Closed Shell PI-SCF-LCAO-MO-Molecular Mechanics Program*, Darmstadt University of Technology, **1996**; b) A. E. Smith, H. J. Lindner, *J. Comput.-Aided Mol. Des.* **1991**, *5*, 235–262.

Received: March 30, 1999 [F 1709]

## Inclusion Complexes of Cycloaltrins

S. Immel and K. L. Larsen, *unpublished results*.

The formation of inclusion complexes by the  $\alpha$ -<sup>[1]</sup>  $\beta$ -<sup>[2]</sup> and  $\gamma$ -cycloaltrins<sup>[3]</sup> with various *para*-substituted sodium benzoates and the corresponding 1:1 association constants were determined by capillary electrophoresis<sup>[4]</sup> according to the protocol previously described for the measurement of stability constants for complexes formed by cyclodextrins of varying ring size.<sup>[5]</sup> The electrophoresis capillary was filled with the sodium benzoates and the cycloaltrins were injected as the analyte; the mobility of the macrocycles was monitored as a function of benzoate concentration and the formation of the complexes was detected by UV absorbance (Table 1, *method 1*). Table 1 lists the corresponding  $K_{1:1}$  complex formation constants obtained by non-linear regression along with their standard deviations, respectively. For comparison, the association constants between  $\alpha$ - and  $\gamma$ -cyclodextrin and the benzoate guest molecules were determined by the same method. In addition, Table 1 lists stability constants for  $\alpha$ -,  $\beta$ -, and  $\gamma$ -CD complexes determined by an inverse protocol of the capillary electrophoresis (*method 2*).

For the stabilities of the inclusion complexes formed by the native cyclodextrins – despite some minor discrepancies emerging from the two different methods listed in Table 1 – these data show a clear correlation between the size of the *para*-substituent of the guest benzoate and the association constant of the complex formed. With increasing size of the substituent  $F < Cl < Br < I$  the stability of the complexes of the cyclodextrins increases, irrespective of the ring size of the host macrocycle. For  $\beta$ - and  $\gamma$ -cyclodextrin, this also applies to *para-tert*-butyl benzoate, which forms complexes that are more stable than with any of the *para*-halogenated benzoates. In this context, the central cavity of  $\alpha$ -cyclodextrin seems to be too small to fully accommodate the *tert*-butyl group, which results in a decreased stability of the complex formed between the smallest of the native cyclodextrins with the sterically most demanding host molecule. The complexes formed by  $\alpha$ - and  $\beta$ -cyclodextrin exhibit complex formation constants of similar order of magnitude, whereas the complexes of  $\gamma$ -cyclodextrin are generally significantly weaker than those formed by  $\beta$ -cyclodextrin. The most stable complex, obviously, is formed between  $\beta$ -cyclodextrin and *para-tert*-butyl benzoate.

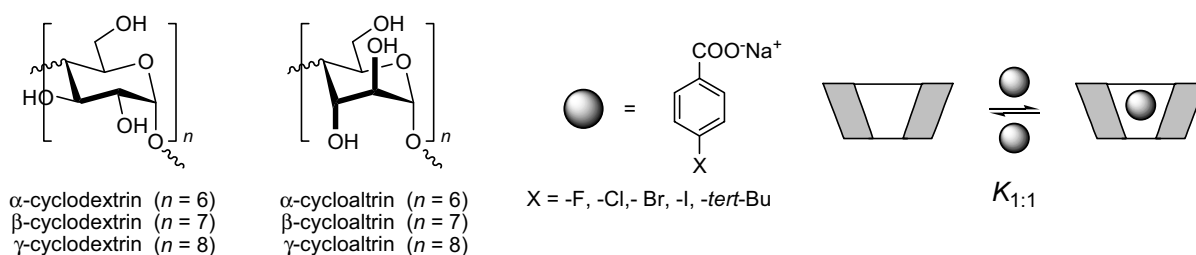


Table 1: Association constants  $K_{1:1}$  [ $\text{l mol}^{-1}$ ] between  $\alpha$ -,  $\beta$ -, and  $\gamma$ -cycloaltrins or cyclodextrins and various *para*-substituted benzoates (X = -F, -Cl, -Br, -I, and -*tert*-Bu) determined by capillary electrophoresis using different procedures. – *Method 1*: The capillary was filled with buffers containing various concentrations of benzoate derivatives and the various macrocycles was injected as analyte. The mobility of the macrocycles was monitored as a function of benzoate concentration. – *Method 2*: The capillary was filled with buffers containing various concentrations of cyclodextrin and the benzoate derivatives were injected as analyte. The mobility of the benzoate derivatives was monitored as a function of cyclodextrin concentration. – All association constants were obtained by non-linear regression with standard deviations given in parenthesis; “*large*” and “*small*” indicates association constants that are, respectively, too large or too small to be assessed by this method.

host ( <i>method 1</i> )	X = -F	X = -Cl	X = -Br	X = -I	X = - <i>tert</i> -Bu
$\alpha$ -cycloaltrin	14.9(0.9)	“ <i>small</i> ”	7.9(1.1)	12.0(0.6)	20.6(1.7)
$\beta$ -cycloaltrin	14.4(1.3)	11.1(3.4)	10.3(0.6)	9.5(0.8)	16.5(1.6)
$\gamma$ -cycloaltrin	14.8(2.6)	8.1(0.9)	9.1(1.0)	“ <i>small</i> ”	16.6(1.9)
$\alpha$ -cyclodextrin	21.4(0.8)	“ <i>large</i> ”	“ <i>large</i> ”	“ <i>large</i> ”	102.6(4.5)
$\gamma$ -cyclodextrin	6.1(0.8)	8.9(1.5)	16.4(2.0)	46.6(7.6)	80.4(4.3)
host ( <i>method 2</i> )	X = -F	X = -Cl	X = -Br	X = -I	X = - <i>tert</i> -Bu
$\alpha$ -cyclodextrin	11.9(0.9)	129.3(1.9)	370.2(10.7)	780.4(86.8)	71.7(13.1)
$\beta$ -cyclodextrin	36.8(3.6)	139.5(9.6)	236.2(7.6)	608.8(20.6)	7304.8(103.9)
$\gamma$ -cyclodextrin	0.6(2.0)	6.9(1.4)	12.6(1.3)	30.2(1.3)	93.4(1.6)

In contrast to the cyclodextrins, the cycloaltrins display, in all cases, quite low stability constants  $K_{1:1}$  ranging only from 8 to 20  $\text{l mol}^{-1}$ . There also seems to be no obvious effect of ring size of the cycloaltrin host. From the data presented in Table 1, it can be concluded that the most stable complexes are formed with *para-tert*-butyl benzoate, the same guest molecule that forms the most stable complexes with the cyclodextrins. However, curiously the weakest complex former of the *para*-halogenated benzoates (*para*-fluoro benzoate) with the native CD seems to be the best for the cycloaltrins, and again no effect of cycloaltrin macrocycle size can be detected. Yet, it is noteworthy, that with the *para*-fluoro, *para*-chloro, and *para*-bromo benzoates, the cycloaltrin complexes are more stable or comparable to the complexes formed by  $\gamma$ -cyclodextrin.

In total, the data presented seems to suggest that the inclusion complexes formed by the cycloaltrins are based on weak unspecific interactions. The selectivity of the cycloaltrins with respect to the size and shape of the guest molecules is less pronounced than for the cyclodextrins of the same ring size. This may be interpreted in terms of the increased conformational flexibility of the cycloaltrins, which seem to

be able to accommodate their shape towards a greater range of guest molecules than the cyclodextrins are. On the other hand, the rather low absolute association constants also reflect a significant entropy penalty to be paid upon the formation of inclusion complexes by the cycloaltrins.

All the data presented suggests two entirely different mechanisms for the formation of inclusion complexes: whereas the cyclodextrins follow the rather rigid *lock-and-key*-type mechanism of complex formation, the cycloaltrins are of significantly higher flexibility. The formation of complexes by cycloaltrins is best described by the flexible *induced-fit* mechanism which implies considerable geometrical flexibility of the host, along with its conformational adaptation towards potential guest molecules. Further evidence for this hypothesis is derived from the formation of inclusion complexes by mono-altro- $\beta$ -cycloaltrin<sup>[6]</sup> described in the next Chapter of this work.

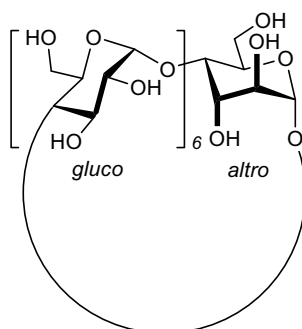
## References

- [1] Y. Nogami, K. Nasu, T. Koga, K. Ohta, K. Fujita, S. Immel, H. J. Lindner, G. E. Schmitt, and F. W. Lichtenthaler, *Angew. Chem., Int. Ed. Engl.* **1997**, *36*, 1899-1902; S. Immel, K. Fujita, and F. W. Lichtenthaler, *Chem. Eur. J.* **1999**, *5*, 3185-3192.
- [2] K. Fujita, H. Shimada, K. Ohta, Y. Nogami, K. Nasu, and T. Koga, *Angew. Chem., Int. Ed. Engl.* **1995**, *34*, 1621-1622.
- [3] Y. Nogami, K. Fujita, K. Ohta, K. Nasu, H. Shimada, C. Shinohara, and T. Koga, *J. Inclusion Phenom. Mol. Recognit. Chem.* **1996**, *25*, 57-60.
- [4] K. L. Larsen, F. Mathiesen, and W. Zimmermann, *Carbohydr. Res.* **1997**, *298*, 59-63.
- [5] K. L. Larsen, T. Endo, H. Ueda, and W. Zimmermann, *Carbohydr. Res.* **1998**, *309*, 153-159.
- [6] K. Fujita, W.-H. Chen, D.-Q. Yuan, Y. Nogami, T. Koga, T. Fujioka, K. Mihashi, S. Immel, and F. W. Lichtenthaler, *Tetrahedron: Asymmetry* **1999**, *10*, 1689-1696.



## Chapter 4

### Mono-*altro*- $\beta$ -cyclodextrin



#### Guest-induced Conformational Change in a Flexible Host: Mono-*altro*- $\beta$ -cyclodextrin

K. Fujita, W.-H. Chen, D.-Q. Yuan, Y. Nogami, T. Koga, T. Fujioka, K. Mihashi, S. Immel, and F. W. Lichtenthaler, *Tetrahedron: Asymmetry* **1999**, *10*, 1689-1696.







Pergamon

Tetrahedron: *Asymmetry* 10 (1999) 1689–1696

---

---

**TETRAHEDRON:  
ASYMMETRY**

---

---

## Guest-induced conformational change in a flexible host: mono-*altro*- $\beta$ -cyclodextrin<sup>†</sup>

Kahee Fujita,<sup>a,\*</sup> Wen-Hua Chen,<sup>a</sup> De-Qi Yuan,<sup>a</sup> Yasuyoshi Nogami,<sup>b</sup> Toshitaka Koga,<sup>b</sup>  
Toshihiro Fujioka,<sup>c</sup> Kunihide Mihashi,<sup>c</sup> Stefan Immel<sup>d</sup> and Frieder W. Lichtenthaler<sup>d,\*</sup>

<sup>a</sup>*Faculty of Pharmaceutical Sciences, Nagasaki University, Bunkyo-machi, Nagasaki 852-8131, Japan*

<sup>b</sup>*Daiichi College of Pharmaceutical Sciences, Tamagawa-cho, Minami-ku, Fukuoka 815, Japan*

<sup>c</sup>*Faculty of Pharmaceutical Sciences, Fukuoka University, Nanakuma, Fukuoka 814-0180, Japan*

<sup>d</sup>*Institut für Organische Chemie, Technische Universität Darmstadt, Petersenstrasse 22, D-64287 Darmstadt, Germany*

Received 10 March 1999; accepted 1 April 1999

---

### Abstract

Mono-*altro*- $\beta$ -cyclodextrin **1**, a  $\beta$ -cyclodextrin with one of the seven glucose units being configurationally changed to an altrose, is shown to be a flexible host undergoing a distinct conformational change within its altropyranose geometry upon intracavity inclusion of adamantanecarboxylate, thus representing an induced-fit model of binding rather than one following the rigid lock-and-key type pattern. © 1999 Elsevier Science Ltd. All rights reserved.

---

### 1. Introduction

In the common cyclodextrins, the six ( $\alpha$ -CD), seven ( $\beta$ -CD), and eight  $\alpha(1\rightarrow4)$ -linked glucose units ( $\gamma$ -CD)<sup>2</sup> are ‘locked up’ in a strait-jacket type belt,<sup>3–5</sup> so that their macrocycles exhibit remarkable structural rigidity: the glucopyranose rings inevitably adopt the energetically favorable <sup>4</sup>C<sub>1</sub> chair form, and the very limited rotational movements about the interglucosidic links, at best, allow one glucose unit to rotate out of the tilt of the others.<sup>5,6</sup> This pronounced rigidity even persists on inclusion-complex formation with a large structural variety of guests, since no significant guest-induced conformational changes have ever been observed.<sup>7</sup> Accordingly, the formation of inclusion complexes by  $\alpha$ -,  $\beta$ - and  $\gamma$ -CD closely corresponds to Emil Fischer’s classic lock-and-key concept for enzyme specificity,<sup>8</sup> i.e. to the insertion of a lipophilic key into an equally lipophilic cyclodextrin molecular lock. Although this process is overly static, it has nevertheless been extensively exploited towards ‘artificial enzymes’ or enzyme

---

\* Corresponding authors. E-mail: fujita@net.nagasaki-u.ac.jp and fwlicht@sugar.oc.chemie.tu-darmstadt.de

<sup>†</sup> Part 20 of the series *Molecular Modeling of Saccharides*. Part 19.<sup>1</sup>

1690

K. Fujita et al. / *Tetrahedron: Asymmetry* 10 (1999) 1689–1696

models.<sup>9</sup> On the other hand, however, there is overwhelming evidence that the majority of enzymes act in an ‘induced fit’ fashion,<sup>10,11</sup> implying the induction of significant conformational changes in the enzyme upon ‘docking’ of the substrate — a dynamic process essential for the catalytic groups to assume the required transition state geometry. Hence, if low molecular weight cyclodextrins are to be *realistic* enzyme models, flexibility has to be introduced into their macrocycles so that they can mimic the dynamic induced-fit mode of action rather than the stationary lock-and-key approach.

With these considerations in mind, we have undertaken a study of the inclusion complexation properties of cyclodextrins in which one,<sup>12,13</sup> two,<sup>14</sup> or essentially all glucose units<sup>15–17</sup> — by inversion of their configuration at C-2 and C-3 — have been converted into altropyranose residues, which have been shown by calculation<sup>18</sup> and NMR evidence<sup>19</sup> to be conformationally flexible within the  ${}^4C_1 \rightleftharpoons {}^0S_2 \rightleftharpoons {}^1C_4$  pseudorotational itinerary (Fig. 1). As a result we report here on the inclusion of adamantane-1-carboxylate into mono-*altro*- $\beta$ -cyclodextrin **1**, representing — to the best of our knowledge — the first example of a guest-induced fit into a cyclooligosaccharide host.

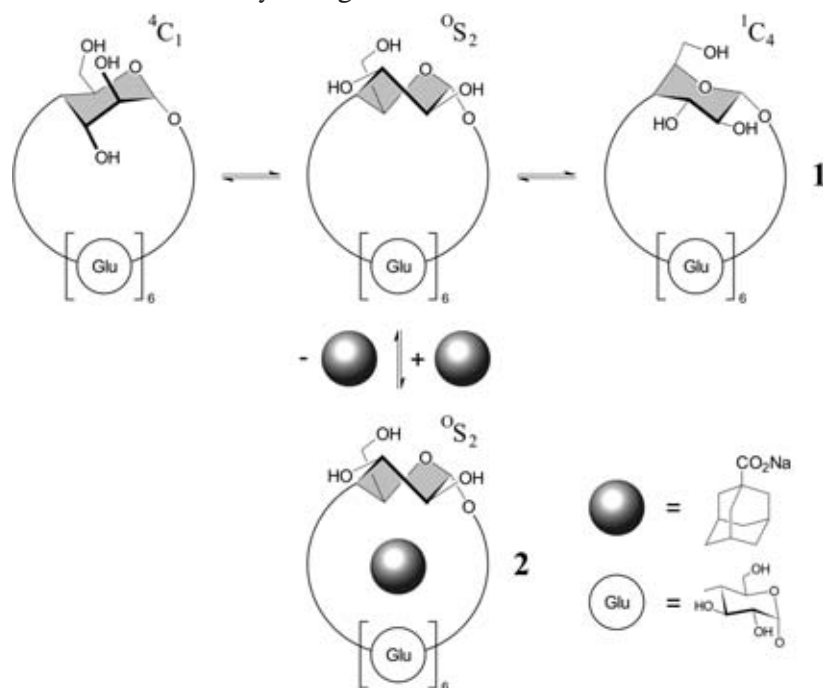


Figure 1. Schematic representation of mono-*altro*- $\beta$ -cyclodextrin **1** with its altropyranoid unit in  ${}^4C_1$ ,  ${}^0S_2$ , and  ${}^1C_4$  conformation, respectively, and its adamantanecarboxylate inclusion complex **2** in which the altrose residue is induced to preferentially adopt the  ${}^0S_2$  form

## 2. Results and discussion

Mono-*altro*- $\beta$ -CD **1**,<sup>2</sup> readily accessible from  $\beta$ -CD in a 3-step sequence,<sup>13,20</sup> shows distinct NMR signals for all of its protons (Fig. 2) from which the altrose hydrogens and their couplings could be identified either directly (H-1, H-5,  $J_{1,2}$ ), or by use of H–H COSY, homo-decoupling and 1D–HOHANA techniques (H-2–H-4,  $J_{2,3}$ – $J_{4,5}$ ). Comparison of the coupling constants thus determined with those calculated for  $\alpha$ -D-altropyranoid rings in idealized  ${}^4C_1$ ,  ${}^0S_2$ , and  ${}^1C_4$  conformations clearly reveals the altrose portion in **1** to essentially be in an  ${}^0S_2 \rightleftharpoons {}^1C_4$  equilibrium with an approximate 2:1 preponderance

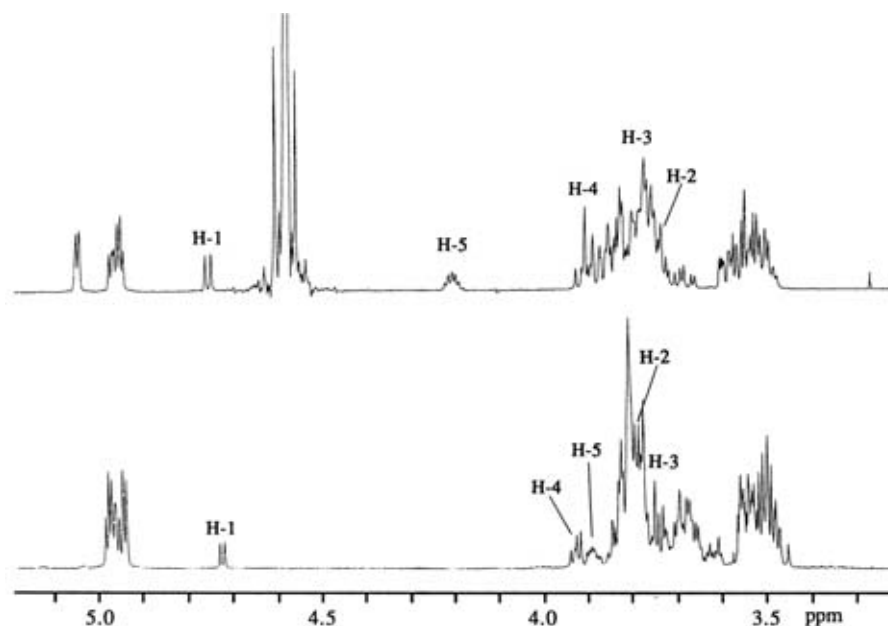


Figure 2. 500 MHz  $^1\text{H}$  NMR spectra of mono-*altro*- $\beta$ -cyclodextrin **1** (top), and of its adamantanecarboxylate inclusion complex **2** (bottom, 90% binding) in  $\text{D}_2\text{O}$  at  $35^\circ\text{C}$ . The altopyranose ring hydrogens are marked

of the  $^1\text{C}_4$  form. The exact positioning of the equilibrium between the three forms can most readily be inferred from the triangle representation in Fig. 3 (top entry), where the experimental coupling constants exhibit a best fit at a composition of 61%  $^1\text{C}_4$ , 31%  $^0\text{S}_2$ , and 8%  $^4\text{C}_1$  form — not surprising as the coupling constants found for **1** and those calculated for the  $^4\text{C}_1$  form (cf. Table 1) are indeed drastically different. That the  $^4\text{C}_1$  conformation is substantially under-represented in this equilibrium may be rationalized on the fact that it extends its axially oriented 3-OH into the interior of the mono-*altro*- $\beta$ -CD cavity, thereby causing steric hindrance as well as an interruption of the prevailing intra- and intermolecular hydrogen bond patterns.

For an assessment of the overall molecular shape of **1**, its cavity dimensions, and its potential for the formation of inclusion compounds, the molecular contact surface was generated (Fig. 4) as well as its molecular lipophilicity profile (Fig. 5), based on MD simulations in water. Accordingly, the altrose residue of **1** in water invariably adopts the  $^0\text{S}_2$  geometry (top pyranose unit in Fig. 4), entailing a solvent-accessible surface in slight elliptical distortion with a distinct cavity. In that, the overall shape of **1** closely resembles that of  $\beta$ -CD,<sup>21</sup> hence, should be capable of serving as host for guests featuring the adamantane moiety, as these represent perfect fits for  $\beta$ -CD.<sup>22</sup> This prediction can also be made on the basis of the close similarity of the molecular lipophilicity patterns of  $\beta$ -CD<sup>21</sup> and **1** (Fig. 5), as both exhibit a distinctly hydrophilic (blue) 2-OH/3-OH face vs. a hydrophobic (yellow) 6- $\text{CH}_2\text{OH}$  side.

Indeed, adamantane-1-carboxylate, which forms a 1:1 inclusion complex with  $\beta$ -CD with the guest fully inserted into its cavity,<sup>22</sup> is capable of intracavity complexation by **1**: upon addition to a  $\text{D}_2\text{O}$  solution of **1**, the NMR signals of the altroside portion of **1** gradually change with respect to both chemical shifts and coupling constants. H-5 is shifted upfield by as much as 0.3 ppm (cf. Fig. 2), a substantial shielding by the guest, indicating this ring hydrogen is now being directed towards the interior of the cavity (rather than to the outside as in the preferred  $^1\text{C}_4$  form of the ‘empty’ host **1**). Following this shift by NMR titration provided an association constant for **2** of  $839 \text{ M}^{-1}$ .

As distinct as the guest-induced chemical shifts are the changes in the  $J_{\text{HCCH}}$  coupling constants of the

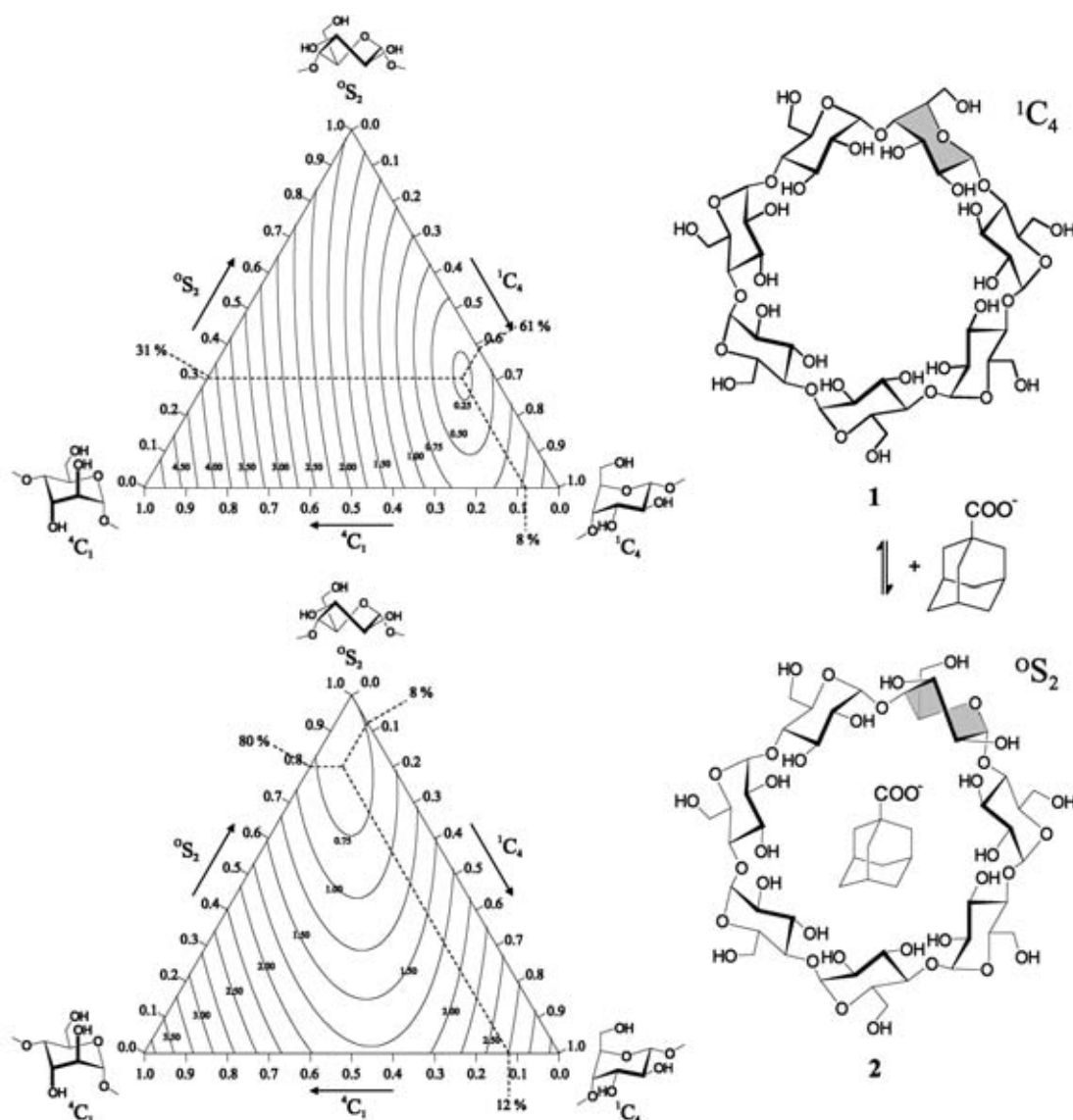


Figure 3. Triangular comparison of experimentally determined altopyranose ring couplings  $J_{1,2}$ ,  $J_{2,3}$ ,  $J_{3,4}$  and  $J_{4,5}$  (cf. Table 1) with those calculated for three-component equilibrium mixtures of the  ${}^4C_1$ ,  ${}^0S_2$ , and  ${}^1C_4$  forms. Contours signify the root mean-square deviation (i.e. the error  $\sigma$ ) between experimental data and those calculated for the three forms as a function of equilibrium composition, the contour minimum corresponding to the best fit attainable for the distribution of the individual conformers; contour levels are given in hertz within the range 0.25–4.5 Hz. The ‘empty’ mono-*altro*- $\beta$ -CD (**1**, top triangle) has its best fit at  $\sigma_{\min}=0.21$  Hz, corresponding to an equilibrium composition of the altopyranose conformations of 61%  ${}^1C_4$ , 31%  ${}^0S_2$ , and 8%  ${}^4C_1$ , i.e., in practical terms, to the presence of  ${}^0S_2$  and  ${}^1C_4$  forms in a 1:2 proportion. In the inclusion complex **2** (bottom triangle), the equilibrium is substantially shifted towards the  ${}^0S_2$  form (top triangle corner),  $\sigma_{\min}=0.61$  Hz implying an equilibrium composition of 12%  ${}^4C_1$ , 80%  ${}^0S_2$ , and 8%  ${}^1C_4$  form (i.e., the  ${}^0S_2$  form outweighs the others by 4:1)

altrose residue, most notably the doubling of  $J_{4,5}$  (from 3.5 to 7.0 Hz, cf. Table 1), while the others are influenced less extensively ( $J_{3,4}$  from 3.5 to 4.6 Hz) or not at all ( $J_{2,3}$ ). Comparison of the couplings found for **2** with those of the individual idealized altopyranose conformers (Table 1) clearly points towards the  ${}^0S_2$  form as the predominant geometry, or in terms of the triangle representation of the equilibrium

Table 1  
Vicinal  $^1\text{H}$ – $^1\text{H}$  coupling constants calculated for an  $\alpha$ -D-altropyranoid ring in idealized  $^4\text{C}_1$ ,  $^0\text{S}_2$ , and  $^1\text{C}_4$  conformations as compared to those found for mono-*altro*- $\beta$ -CD **1** and its adamantanecarboxylate inclusion complex **2**

$J$ (Hz)	Calcd <sup>a</sup> for ideal altropyranose geometries			Found for		Calcd <sup>b</sup> for 100 % <b>2</b>
	$^4\text{C}_1$	$^0\text{S}_2$	$^1\text{C}_4$	<b>1</b>	90 % <b>2</b> + 10 % <b>1</b>	
$J_{1,2}$	2.2	4.0	8.0	6.4	5.2	5.1
$J_{2,3}$	2.7	10.2	10.2	9.5	9.3	9.3
$J_{3,4}$	3.4	4.5	2.4	3.5	4.5	4.6
$J_{4,5}$	9.7	6.4	1.4	3.5	6.7	7.0

<sup>a</sup> Calculated according to the generalized Haasnoot-equation<sup>23</sup>

<sup>b</sup> Calculated for the fully developed inclusion complex with the experimental data for **1** and the inclusion equilibrium of 90 % **2** and 10 % **1**

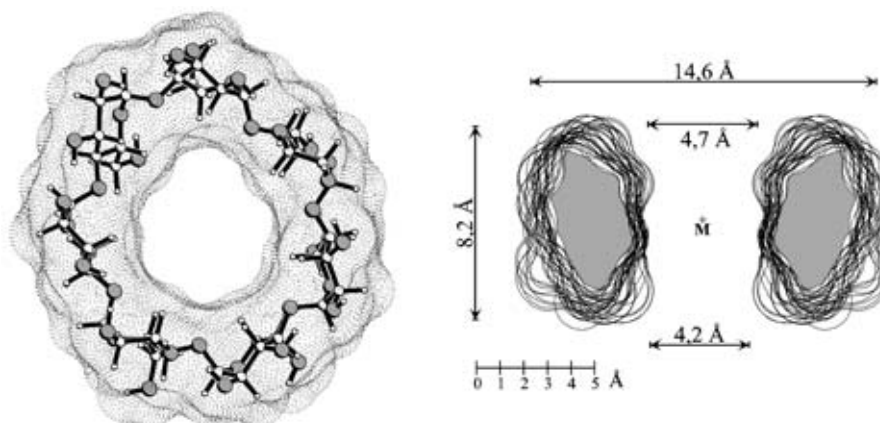


Figure 4. Ball-and-stick model of mono-*altro*- $\beta$ -CD (**1**) with the solvent-accessible surface superimposed in dotted form (left); the structure represents the mean geometry obtained from molecular dynamics simulations on **1** in water and subsequent energy minimization. In contrast to the glucose units (all  $^4\text{C}_1$ ), the altropyranose ring (top unit) adopts a  $^0\text{S}_2$  conformation; all pyranose rings are aligned almost perpendicular to the macrocycle mean-plane. The central cavity of **1** is only slightly elliptically distorted, and thus able to accommodate round shaped guest molecules like the adamantane carboxylate. On the right, the side-view cross-section cuts through the surface display the effective extension of the macrocycle and its cavity, with approximate molecular dimensions in Å

mixture to a composition of 12%  $^4\text{C}_1$ , 80%  $^0\text{S}_2$ , and 8%  $^1\text{C}_4$  (cf. Fig. 3). Hence, in essence, intracavity inclusion of adamantanecarboxylate into mono-*altro*- $\beta$ -CD results in a significant conformational change within the altrose portion, such that the  $^1\text{C}_4$  form predominating the equilibrium mixture in the ‘empty’ host is induced in the inclusion complex to shift to the  $^0\text{S}_2$  conformation which outweighs others by a factor of 4:1.

In summary, recourse to flexibility-modified cyclodextrins offers highly attractive lipophilic hosts for mimicking the dynamic induced-fit mode of enzyme action and thus has high potential for the design of realistic artificial enzymes. To this end, further inclusion complexation studies with the various di-*altro*-cyclodextrins<sup>14</sup> and the highly flexible cycloaltrins with six,<sup>15</sup> seven,<sup>16</sup> and eight<sup>17</sup>  $\alpha$ (1 $\rightarrow$ 4)-linked altrose units are presently being pursued and shall be reported on in due course.

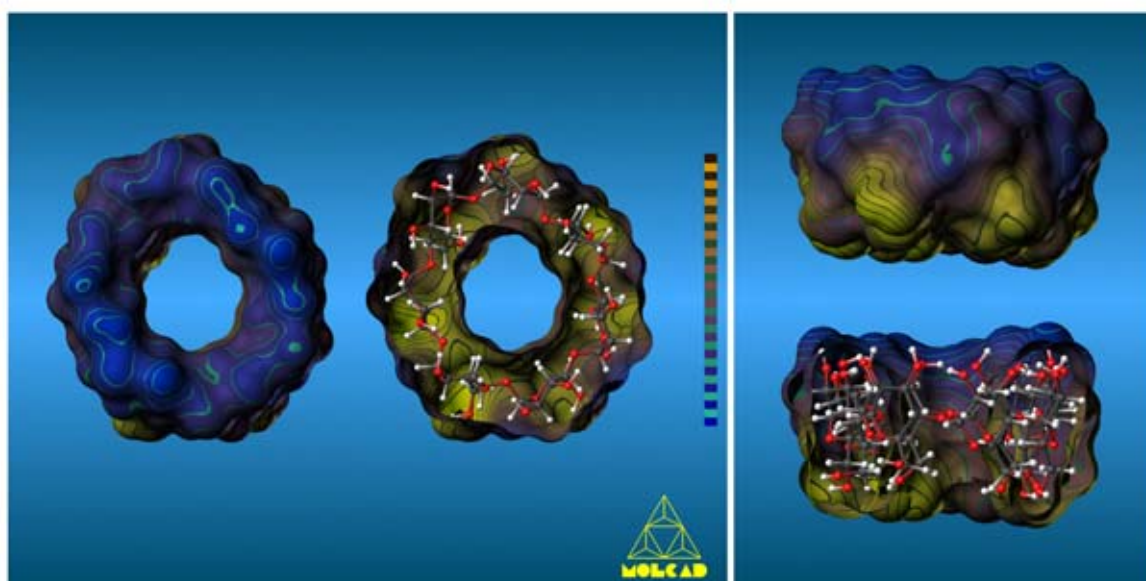


Figure 5. MOLCAD program-generated molecular lipophilicity patterns (MLPs) of **1**: the relative hydrophobicity on the molecular surface of **1** is visualized using a color-code ranging from dark blue (most hydrophilic areas) to yellow-brown (most hydrophobic regions). On the left, the intensively hydrophilic (blue) side of the macrocycle carries the 2-OH/3-OH groups; the half-opened surface with the ball-and-stick model insert displays the hydrophobic (yellow) surface regions around the 6-CH<sub>2</sub>OH groups. The right picture provides the side-view MLP of **1**, with closed and bisected surface representations exposing the shape and lipophilic characteristics of the central cavity as well as the most hydrophobic molecular regions around the primary 6-OH groups

### 3. Experimental

The NMR measurements were performed on a JEOL JNM A-500 spectrometer equipped with standard additions for H–H COSY homo-decoupling and HOHAHA techniques, whose application was necessary for determining in **1** the chemical shifts for the altrose ring protons H-2, H-3, H-4, and one of the H-6, as well as  $J_{2,3}$ ,  $J_{3,4}$  and  $J_{4,5}$ . For the inclusion complex **2**, only the chemical shift and  $J_{1,2}$  of the anomeric altrose proton can directly be extracted from the <sup>1</sup>H NMR spectrum; all other data (cf. Fig. 2 and Table 1) required recourse to H–H COSY and HOHAHA techniques as well as NOE experiments (irradiation with H-1).

The measurements of chemical shift changes as a function of concentrations (so-called NMR titrations) for determination of the association constant  $K$  followed standard methodology.<sup>24</sup>

Calculation of the molecular contact surfaces and the respective hydrophobicity potential profiles (MLPs) was performed using the MOLCAD<sup>25,26</sup> molecular modeling program and its texture mapping option.<sup>27</sup> Scaling of the MLP profiles was performed in relative terms (most hydrophilic to most hydrophobic surface regions); no absolute values are displayed.

### Acknowledgements

Support of this work by the Nihon Shokukin Kako (Japan Maize Products Co.) and the Fonds der Chemischen Industrie is gratefully acknowledged. Our thanks are also due to M.Sc. Yoshihiro Ikegami

for experimental assistance, and to Prof. Dr. J. Brickmann, Institut für Physikalische Chemie of the TUD, for providing us with his MOLCAD modeling software package.<sup>25</sup>

## References

1. Immel, S.; Schmitt, G. E.; Lichtenthaler, F. W. *Carbohydr. Res.* **1998**, *313*, 91–105.
2. The systematic name for **1** emerges from the most recent 'IUPAC Recommendations for the Nomenclature of Carbohydrates' (*Carbohydr. Res.* **1997**, *297*, 79, Rule 2-Carb-37.4.2) as *cyclo*[(1→4)- $\alpha$ -D-altropyranosyl-hexakis-(1→4)- $\alpha$ -D-glucopyranosyl], which, aside of being clumsy, implies it to be an assembly of 'glycosyls' rather than a 'glycoside', a heptasaccharide in fact. As semisystematic names, e.g. *cyclo*[mono- $\alpha$ (1→4)-D-*altro*-hexa- $\alpha$ (1→4)-D-gluco]-heptaoside for **1**, are equally impractical, we prefer the designation mono-*altro*- $\beta$ -CD as a reasonably descriptive, convenient acronym.
3. Szejtli, J. In *Comprehensive Supramolecular Chemistry*; Szejtli, J.; Osa, T., Eds. Chemistry, physical and biological properties of cyclodextrins; Elsevier: Oxford, 1996; Vol. 3, pp. 6–40. *Chem. Rev.* **1998**, *98*, 1743–1753.
4. Harata, K. In *Comprehensive Supramolecular Chemistry*; Szejtli, J.; Osa, T., Eds. Crystallographic studies of cyclodextrins; Elsevier: Oxford, 1996; Vol. 3, pp. 279–304. *Chem. Rev.* **1998**, *98*, 1803–1827.
5. Saenger, W.; Jacob, J.; Gessler, K.; Steiner, T.; Hoffmann, D.; Sanbe, H.; Koizumi, K.; Smith, S. M.; Takaha, T. *Chem. Rev.* **1998**, *98*, 1787–1802.
6. Szejtli, J. In *Comprehensive Supramolecular Chemistry*; Szejtli, J.; Osa, T., Eds. Inclusion of guest molecules, selectivity and molecular recognition by cyclodextrins; Elsevier: Oxford, 1996; Vol. 3, pp. 189–203. Fenyvesi, E.; Szente, L.; Russel, N. R.; McNamara, M. Specific guest types. *Ibid.*; Vol. 3, pp. 305–366.
7. Appreciable distortions of the glucopyranose <sup>4</sup>C<sub>1</sub> chair conformation have only been observed for the *m*-iodophenol inclusion complex of permethylated  $\beta$ -CD, in which one 2,3,6-tri-*O*-methyl-glucose residue adopts the <sup>0</sup>S<sub>2</sub> skew-boat form, see: Harata, K. *J. Chem. Soc., Chem. Commun.* **1988**, 928–929; and for permethyl  $\beta$ -CD monohydrate, in which one glucopyranoid ring—in the absence of a hydrophobic guest—is inverted to the <sup>1</sup>C<sub>4</sub> chair, see: Caira, M. R.; Griffith, V. J.; Nassimbeni, L. R.; van Oudtshoorn, B. *J. Chem. Soc., Perkin Trans. 2*, **1994**, 2071–2072.
8. Fischer, E. *Ber. Dtsch. Chem. Ges.* **1894**, *27*, 2985–2993. Lichtenthaler, F. W. *Angew. Chem.* **1994**, *106*, 2456–2467; *Angew. Chem., Int. Ed. Engl.* **1994**, *33*, 2364–2374.
9. Breslow, R. In *Inclusion Compounds*; Atwood, J. L.; Davies, J. E. D.; MacNicol, D. D., Eds. Enzyme models related to inclusion compounds; Academic Press: London, 1984; Vol. 3, pp. 473–508. Komiyama, M.; Shikegawa, H. In *Comprehensive Supramolecular Chemistry*; Szejtli, J.; Osa, T., Eds. Cyclodextrins as enzyme models; Elsevier: Oxford, 1996; Vol. 3, pp. 401–422. Breslow, R.; Dong, S. D. *Chem. Rev.* **1998**, *98*, 1997–2011.
10. Koshland Jr., D. E. *Angew. Chem.* **1994**, *106*, 2368–2372; *Angew. Chem., Int. Ed. Engl.* **1994**, *33*, 2375–2378.
11. Gerstein, M.; Lesk, A. M.; Clothia, C. *Biochemistry* **1994**, *33*, 6739–6749.
12. Fujita, K.; Nagamura, S.; Imoto, T. *Tetrahedron Lett.* **1984**, *24*, 5673–5676.
13. Fujita, K.; Ohta, K.; Ikegami, Y.; Shimada, H.; Tahara, T.; Nogami, Y.; Koga, T.; Saito, K.; Nakajima, T. *Tetrahedron Lett.* **1994**, *35*, 9577–9580.
14. Ohta, K.; Fujita, K.; Shimada, H.; Ikegami, Y.; Nogami, Y.; Koga, T. *Chem. Pharm. Bull.* **1997**, *45*, 631–635.
15. Nogami, Y.; Nasu, K.; Koga, T.; Ohta, K.; Fujita, K.; Immel, S.; Lindner, H. J.; Schmitt, G. E.; Lichtenthaler, F. W. *Angew. Chem.* **1997**, *109*, 1987–1991; *Angew. Chem., Int. Ed. Engl.* **1997**, *36*, 1899–1902.
16. Fujita, K.; Shimada, H.; Ohta, K.; Nogami, Y.; Nasu, K.; Koga, T. *Angew. Chem.* **1995**, *107*, 1783–1784; *Angew. Chem., Int. Ed. Engl.* **1995**, *34*, 1621–1622.
17. Nogami, Y.; Fujita, K.; Ohta, K.; Nasu, K.; Shimada, H.; Shinohara, C.; Koga, T. *J. Inclusion Phenom. Mol. Recogn. Chem.* **1996**, *25*, 53–56.
18. Angyal, S. J. *Aust. J. Chem.* **1968**, *21*, 2737–2746. Dowd, M. K.; French, A. D.; Reilly, P. J. *Carbohydr. Res.* **1994**, *264*, 1–19.
19. Lichtenthaler, F. W.; Mondel, S. *Carbohydr. Res.* **1997**, *303*, 293–302.
20. Ref. 12, footnote 8.
21. Lichtenthaler, F. W.; Immel, S. *Liebigs Ann. Chem.* **1996**, 27–37.
22. Hamilton, J. A.; Sabesan, M. N. *Acta Crystallogr., Sect. B* **1982**, *38*, 3063–3069. Lichtenthaler, F. W.; Immel, S. *Starch/Stärke* **1996**, *48*, 145–154.
23. Haasnoot, C. A. G.; De Leeuw, F. A. A. M.; Altona, C. *Tetrahedron* **1980**, *36*, 2783–2792.
24. Schneider, H.-J.; Hacket, F.; Rüdiger, Y. *Chem. Rev.* **1998**, *98*, 1768 ff., and literature cited therein.

1696

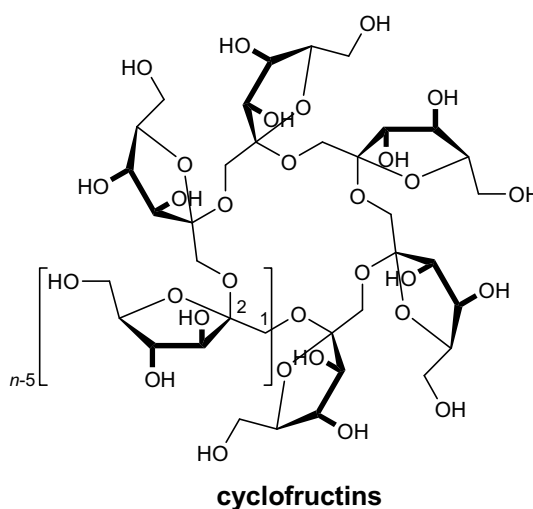
*K. Fujita et al. / Tetrahedron: Asymmetry 10 (1999) 1689–1696*

25. (a) Brickmann, J. *MOLCAD—MOLEcular Computer Aided Design*, Darmstadt University of Technology: Germany, 1996; *J. Chim. Phys.* **1992**, *89*, 1709–1721. (b) Waldherr-Teschner, M.; Goetze, T.; Heiden, W.; Knoblauch, M.; Vollhardt, H.; Brickmann, J. In *Advances in Scientific Visualization*; Post, F. H.; Hin, A. J. S., Eds. Springer: Heidelberg, Germany, 1992, pp. 58–67. (c) Brickmann, J.; Goetze, T.; Heiden, W.; Moeckel, G.; Reiling, S.; Vollhardt, H.; Zachmann, C.-D. In *Insight and Innovation in Data Visualization*; Bowie, J. E., Ed. Manning: Greenwich, UK, 1994; pp. 83–97.
26. Heiden, W.; Moeckel, G.; Brickmann, J. *J. Comp.-Aided Mol. Des.* **1993**, *7*, 503–514.
27. Teschner, M.; Henn, C.; Vollhardt, H.; Brickmann, J. *J. Mol. Graphics* **1994**, *12*, 98–105.



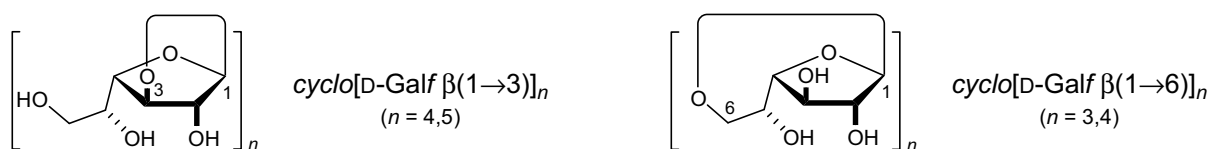
## Chapter 5

### Cyclofructins and Cyclogalactofuranosides



Cyclofructins with Six to Ten  $\beta(1\rightarrow2)$ -linked Fructofuranose Units: Geometries, Electrostatic Profiles, Lipophilicity Patterns, and Potential for Inclusion Complexation

S. Immel, G. E. Schmitt, and F. W. Lichtenthaler,  
*Carbohydr. Res.* **1998**, 313, 91-105.



#### cyclogalactofuranosides

Conformations and Lipophilicity Profiles of some Cyclic  $\beta(1\rightarrow3)$ - and  $\beta(1\rightarrow6)$ -linked Oligogalactofuranosides

H. Gohlke, S. Immel, and F. W. Lichtenthaler,  
*Carbohydr. Res.* **1999**, 321, 96-104.





ELSEVIER

Carbohydrate Research 313 (1998) 91–105

CARBOHYDRATE  
RESEARCH

# Cyclofructins with six to ten $\beta$ -(1 $\rightarrow$ 2)-linked fructofuranose units: Geometries, electrostatic profiles, lipophilicity patterns, and potential for inclusion complexation<sup>1</sup>

Stefan Immel, Guido E. Schmitt, Frieder W. Lichtenthaler\*

*Institut für Organische Chemie, Technische Universität Darmstadt, Petersenstraße 22,  
D-64287 Darmstadt, Germany*

Received 7 June 1998; accepted 24 July 1998

## Abstract

Cyclofructins composed of six (**1**, “CF<sub>6</sub>”) to ten (**5**, “CF<sub>10</sub>”)  $\beta$ -(1 $\rightarrow$ 2)-linked fructofuranose units were subjected to conformational analysis using Monte Carlo simulations based on the PIMM91 force-field. Breaking the molecular symmetry partially by alternating inclination of the *spiro*-type anellated fructofuranoses relative to the crown ether ring core, i.e. the 3-OH groups pointing either towards or away from the molecular center, substantially lowers the strain energy of the cyclofructins. The global energy-minimum geometries of CF<sub>6</sub>, CF<sub>8</sub>, and CF<sub>10</sub> exhibit  $C_{n/2}$  rotational symmetry, whilst the odd-membered macrocycles in CF<sub>7</sub> and CF<sub>9</sub> adopt  $C_1$  symmetry. Identical conformations of the solid-state geometry of CF<sub>6</sub> (**1**) and its computer-generated form manifest the reliability of the computational analysis. The molecular surfaces calculated for the energy-minimum structures establish a disk-type shape for CF<sub>6</sub> (**1**), CF<sub>7</sub> (**2**), and CF<sub>8</sub> (**3**), whereas further ring enlargement to CF<sub>9</sub> (**4**) and CF<sub>10</sub> (**5**) leads to torus-shaped molecules with through-going cavities. Color-coded projection of the molecular lipophilicity patterns (MLPs) and the electrostatic potential profiles (MEPs) onto these surfaces cogently displays the crown ether-like properties, favoring the complexation of metal cations via strong electrostatic interactions through the 3-OH groups located on the hydrophilic molecular side. The central cavities of CF<sub>9</sub> and CF<sub>10</sub> are characterized not only by significantly enhanced hydrophobicity, but also by highly negative electrostatic potentials around the narrow aperture of the tori made up by the 3-OH/4-OH groups, and positive potentials on the opposite rim. Accordingly, CF<sub>9</sub> and CF<sub>10</sub> are capable to form inclusion complexes, the cavity of the latter being approximately as large as the one of  $\alpha$ -cyclodextrin. Calculation of the inclusion complex geometries of CF<sub>9</sub> with  $\beta$ -alanine and of CF<sub>10</sub> with *p*-aminobenzoic acid revealed the guest to be deeply incorporated into the respective cavities, masking the guest’s hydrophobic parts. Analysis of the electrostatic interactions at the interface of the zwitter-ionic guests with the oppositely polarized hosts predicts a high degree of regiospecificity for complex formation. © 1998 Elsevier Science Ltd. All rights reserved

\* Corresponding author. Fax: +49-6151-166674; e-mail: fwlicht@sugar.oc.chemie.tu-darmstadt.de

<sup>1</sup> Molecular modeling of saccharides, Part 19. For Part 18, see ref. [1].

**Keywords:** Cyclofructins, molecular geometries of; Molecular modeling; Lipophilicity patterns; Electrostatic potential profiles; Inclusion complexation, capability for

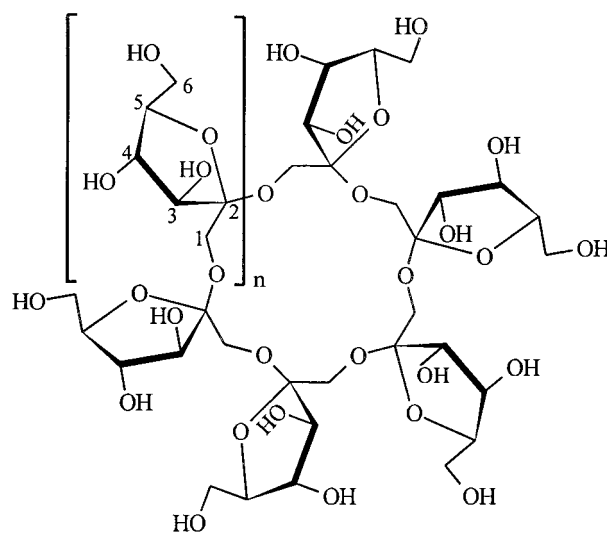
## 1. Introduction

Exposure of inulin, a polysaccharide made up of  $\beta$ -(1 $\rightarrow$ 2)-linked fructofuranose residues, to digestion with a *Bacillus circulans*-derived [2] fructosyltransferase not only leads to the generation of linear oligosaccharides, but to a number of cyclic ones, namely those containing six (**1**), seven (**2**), and eight (**3**) fructofuranose units [3,4]. In line with the simplified nomenclature recently proposed [5] for cyclooligosaccharides composed of sugar units other than glucose, **1** is designated a cyclo- $\beta$ -(1 $\rightarrow$ 2)-fructohexaoside or  $\alpha$ -cyclofructin [5,6], thereby alluding to its analogy to  $\alpha$ -cyclodextrin which is similarly composed of six sugar (glucose) units. Correspondingly, the higher homologs could be termed  $\beta$ - and  $\gamma$ -cyclofructin<sup>2</sup> which becomes impractical, however, when further increasing the number of fructose units in the macrocycle. Thus, we here propose and use the abbreviated designation CF<sub>6</sub> for **1**, and CF<sub>7</sub> to CF<sub>10</sub> for the next larger ones, i.e., **2–5**, respectively (Scheme 1).

In the solid state [21], the cyclohexamer **1** (CF<sub>6</sub>) possesses a unique 18-crown-6 skeleton as the central core, onto which the furanoid rings are *spiro*-anellated in a propeller-like fashion, pointing alternatively in opposite directions with respect to the plane of the macrocycle. Computation of the

contact surface of **1** [6] revealed a disk-shaped molecular geometry with shallow central indentations on either side, thus precluding the formation of cyclodextrin-analog inclusion complexes which would require a “through-going” cavity. As the lipophilicity pattern of **1** shows a distinct “front/back”-differentiation of hydrophilic and hydrophobic surface regions [6], sandwich-type guest–host interactions appear conceivable, i.e., encapsulation of a neutral molecule by two cyclofructin disks. Whilst these have as of now not been detected, the cyclofructins **1–3** are capable of complexing metal cations in decreasing affinity CF<sub>6</sub> > CF<sub>7</sub> > CF<sub>8</sub> [22]. Therefrom, Ba<sup>2+</sup> evolved as a favorably predisposed match for the CF<sub>6</sub>, obviously due its propitious nestling in or rather above the central indentation of **1** [23]—a behavior that can be rationalized on the basis of the Molecular Electrostatic Potential (MEP) profile on the contact surface, which reveals one side of **1** to have distinctly electropositive central surface regions, whilst the other is as pronouncedly electronegative [6]. Interestingly, the preference for Ba<sup>2+</sup> binding

<sup>2</sup> For designating higher homologs of cyclooligosaccharides, e.g., the various cyclodextrins available today ranging from five [7] to several hundred [8] glucose residues in the macrocycle, it becomes inopportune to differentiate them by letters of the Greek alphabet. It is inconvenient, for example, to assign an appropriate letter to the cyclo- $\alpha$ -(1 $\rightarrow$ 4)-glucopentaoside, which has not only been shown by molecular modeling to be viable [9], but has yielded to synthesis [7]; the abbreviated designation “CD<sub>5</sub>” appears not only simpler but practical. In a similar fashion, it would be advisable to abandon Greek letters for designating large-ring CDs, as the last to be named this way ( $\omega$ -CD) would be the one having 29 glucose units; by contrast, the acronym “CD<sub>29</sub>” is considerably more lucid and comprehensible. Accordingly, the already known  $\delta$ - [10],  $\epsilon$ - [11–13],  $\zeta$ - [11],  $\eta$ - [14],  $\theta$ - [11],  $\iota$ - [13,15],  $\lambda$ - [15], and  $\mu$ -cyclodextrins [15] are more comprehensively referred to as CD<sub>9</sub> through CD<sub>17</sub>, respectively; similarly a “cyclomaltooctadecaose” [16], “cyclomaltonadecaose” [16], and the “cyclomaltooligosaccharide of dp 21” [17] are preferably abbreviated as CD<sub>18</sub>, CD<sub>19</sub>, and CD<sub>21</sub>. The recent use of the cycloamylose-derived abbreviation “CA” for higher cyclodextrin homologs [13,17] appears unfortunate, as this acronym should be reserved for the cycloaltrins that have recently become accessible, i.e., CA<sub>6</sub> [18], CA<sub>7</sub> [19], and CA<sub>8</sub> [20].



- |          |   |                     |
|----------|---|---------------------|
| <b>1</b> | <i>cyclo</i> [D-Fruf- $\beta$ -(1 $\rightarrow$ 2)] <sub>6</sub>  | (CF <sub>6</sub> )  |
| <b>2</b> | <i>cyclo</i> [D-Fruf- $\beta$ -(1 $\rightarrow$ 2)] <sub>7</sub>  | (CF <sub>7</sub> )  |
| <b>3</b> | <i>cyclo</i> [D-Fruf- $\beta$ -(1 $\rightarrow$ 2)] <sub>8</sub>  | (CF <sub>8</sub> )  |
| <b>4</b> | <i>cyclo</i> [D-Fruf- $\beta$ -(1 $\rightarrow$ 2)] <sub>9</sub>  | (CF <sub>9</sub> )  |
| <b>5</b> | <i>cyclo</i> [D-Fruf- $\beta$ -(1 $\rightarrow$ 2)] <sub>10</sub> | (CF <sub>10</sub> ) |

Scheme 1.

is even more pronounced in the per-*O*-methylated  $\alpha$ -cyclofructin [23].

Thus, in a rather unique way, cyclofructins of type **1–3** combine crown ether-type metal complexation with the capability for lipophilicity-mediated guest–host interactions, which are expected to become more dominant on increasing the ring size, i.e., on enlarging the central dents to pockets and eventually to through-going cavities. As these potentialities could open up new molecular recognition patterns in the cyclooligosaccharide field, we have deemed it of interest to extend our molecular modeling—confined to the hexamer **1** as of now [6]—to the higher homologs with seven to ten fructofuranose units. The results presented here provide a clear description of their molecular geometries, their MEP and MLP profiles, and, for CF<sub>9</sub> (**4**) and the decamer CF<sub>10</sub> (**5**) a first assessment of their capabilities to form inclusion compounds.

## 2. Results and discussion

As the global geometries, molecular shapes, and the total molecular conformational energies of the

cyclofructins mainly depend on the backbone torsion angles  $\Phi$ ,  $\Psi$ , and  $\Theta$ , as well as on the propeller angles  $\zeta$  of the fructose units that directly denote their inclinations towards the mean plane of the macrocycle (cf. Fig. 1), these parameters were determined by PIMM91 force-field mediated [24] Monte Carlo (MC) calculations and unrestricted “random-walk” simulations [25] using adapted corner-flipping procedures [26]. Thereby, the respective starting geometries for **1–5** were derived from the solid-state structure of CF<sub>6</sub>-trihydrate (**1**·3 H<sub>2</sub>O) [21] by assembling two different fructofuranosyl geometries of the asymmetric unit to symmetrical and asymmetrical macrocycles. Out of a total of approximately 130000 structures optimized for each of the cyclofructins, the global energy-minimum geometries were determined [27]; their individual parameters are listed in Table 1. The corresponding molecular conformations are displayed in Fig. 2 in the form of ball-and-stick models, onto which their MOLCAD program-generated [28] contact surfaces [29,30] were superimposed. All cyclofructins emerge as essentially unstrained macrocycles of disk- (**1**, **2**, and **3**) or torus-type shape (**4** and **5**), with the primary 6-CH<sub>2</sub>OH

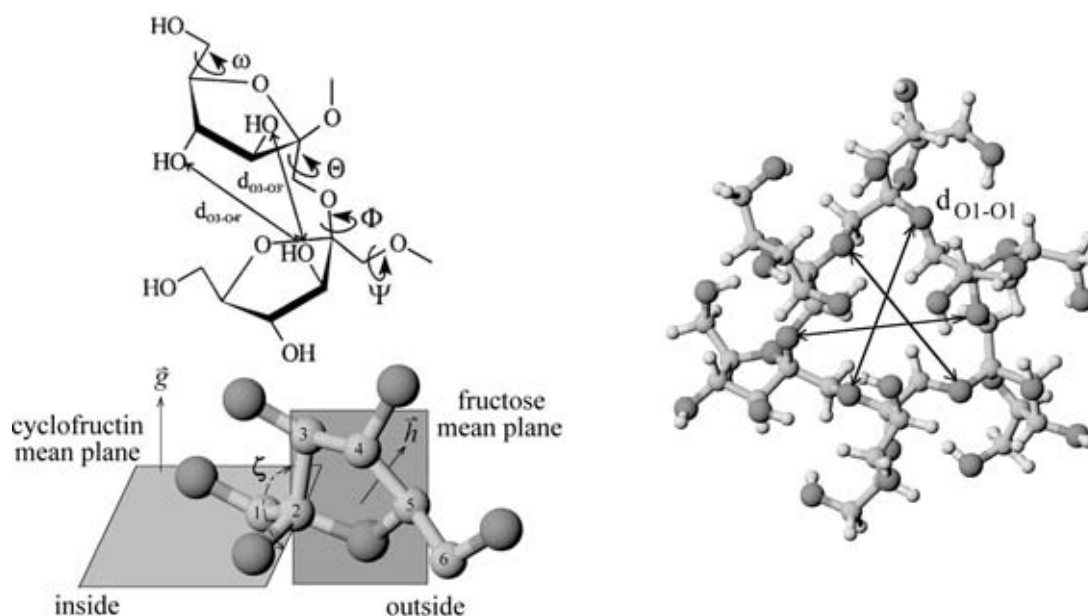


Fig. 1. Cyclofructin geometry descriptors: the torsion angles describing the conformations of the crown ether backbone are denoted as  $\Phi$  (C-1–C-2–O-1'–C-1'),  $\Psi$  (C-2–O-1'–C-1'–C-2'), and  $\Theta$  (O-1–C-1–C-2–O-1'); the exocyclic torsion angle  $\omega$  (O-5–C-5–C-6–O-6) describes the orientation of the primary 6-OH group relative to the furanoid ring. The 3-O $\cdots$ O-3'– and 3-O $\cdots$ O-4'– interresidue distances are displayed as  $d_{O3-O3'}$  and  $d_{O3-O4'}$  (top left). The propeller angle  $\zeta$  denotes the inclination of the furanose rings towards the macrocycle of the crown ether backbone. It is defined as the angle of the least-squares best-fit mean plane through the five furanoid ring atoms (C-2–C-3–C-4–C-5–O-5, bottom left; hydrogen atoms omitted for clarity) versus the mean plane through all backbone oxygen (O-1) atoms, i.e., the angle between the normal vectors  $\mathbf{g}$  (pointing towards the 3-OH/4-OH side of the furanoid rings) and  $\mathbf{h}$  (pointing in direction of a clockwise view on C-2–C-5 and O-5). Values of  $\zeta \approx 90^\circ$  indicate a perpendicular orientation of both planes. The atomic distances between the crown ether backbone oxygens (O-1) diagonally across the macrocyclic ring are denoted as  $d_{O1-O1'}$  (right).

Table 1

Mean molecular geometry parameters as defined in Fig. 1 of the calculated cyclofructin structures (PIMM91) with six (**1**, CF<sub>6</sub>), seven (**2**, CF<sub>7</sub>), eight (**3**, CF<sub>8</sub>), nine (**4**, CF<sub>9</sub>), and ten (**5**, CF<sub>10</sub>) fructose units in β(1→2)-linkages; root-mean-square (RMS) deviations in parentheses. The data derived from the crystal structure of **1** are included for comparison.

Cyclofructins		CF <sub>6</sub> ( <b>1</b> , <i>crystal</i> )	CF <sub>6</sub> ( <b>1</b> )	CF <sub>7</sub> ( <b>2</b> )	CF <sub>8</sub> ( <b>3</b> )	CF <sub>9</sub> ( <b>4</b> )	CF <sub>10</sub> ( <b>5</b> )
<i>n</i> -Fold Rotational symmetry		C <sub>3</sub>	C <sub>3</sub>	C <sub>1</sub>	C <sub>4</sub>	C <sub>1</sub>	C <sub>5</sub>
Furanoid ring conformation <sup>a</sup>		E <sub>3</sub> (→ <sup>4</sup> T <sub>3</sub> )	E <sub>3</sub> (→ <sup>4</sup> T <sub>3</sub> )	E <sub>3</sub> (→ <sup>4</sup> T)	<sup>4</sup> T <sub>3</sub> (→E <sub>3</sub> )	<sup>4</sup> T <sub>3</sub> (→E <sub>3</sub> )	<sup>4</sup> T <sub>3</sub> (→E <sub>3</sub> )
Cremer–Pople parameters <sup>b</sup>	$\langle q \rangle$	0.40(0.02)	0.41(0.01)	0.43(0.02)	0.43(0.02)	0.43(0.03)	0.43(0.03)
	$\langle \phi \rangle$	260.5(1.2)	257.9(1.5)	255.0(16.0)	261.4(19.0)	266.0(6.7)	265.0(6.1)
Intersaccharidic torsion angles <sup>c</sup> [°]	$\langle \Phi_1 \rangle$	57.1 <sup>d</sup>	64.3(0.1) <sup>e</sup>	70.1(9.6) <sup>e</sup>	63.0(1.6) <sup>e</sup>	64.0(5.3) <sup>e</sup>	62.1(0.1) <sup>e</sup>
	$\langle \Phi_2 \rangle$	48.2 <sup>d</sup>	56.9(0.1)	60.9(2.2)	65.4(2.6)	64.2(0.3)	61.2(0.1)
	$\langle \Phi_3 \rangle$	— <sup>f</sup>	— <sup>f</sup>	−47.3 <sup>g</sup>	— <sup>f</sup>	−47.8 <sup>g</sup>	— <sup>f</sup>
	$\langle \Psi_1 \rangle$	177.6 <sup>d</sup>	173.6(0.1)	176.1(3.4)	174.0(5.3)	168.2(1.9)	169.1(0.1)
	$\langle \Psi_2 \rangle$	178.3 <sup>d</sup>	−177.2(0.1)	173.8(4.2)	168.1(2.6)	158.0(4.2)	150.5(0.1)
	$\langle \Psi_3 \rangle$	— <sup>f</sup>	— <sup>f</sup>	−157.7 <sup>g</sup>	— <sup>f</sup>	−146.0 <sup>g</sup>	— <sup>f</sup>
	$\langle \Theta_1 \rangle$	163.4 <sup>d</sup>	163.1(0.1)	173.6(7.5)	176.3(5.5)	179.6(2.5)	178.5(0.1)
	$\langle \Theta_2 \rangle$	52.3 <sup>d</sup>	40.9(0.1)	39.1(10.7)	33.2(4.7)	42.4(2.3)	56.7(0.1)
	$\langle \Theta_3 \rangle$	— <sup>f</sup>	— <sup>f</sup>	179.8 <sup>g</sup>	— <sup>f</sup>	−173.6 <sup>g</sup>	— <sup>f</sup>
Propeller angle <sup>c</sup>	$\langle \zeta_1 \rangle$	85.7 <sup>d</sup>	85.5(0.1)	81.2(1.8)	86.7(8.9)	83.1(1.4)	84.5(0.1)
	$\langle \zeta_2 \rangle$	113.5 <sup>d</sup>	115.5(0.1)	117.7(2.8)	118.1(2.7)	117.5(1.1)	117.4(0.1)
O-5–C-5–C-6–O-6	$\langle \omega \rangle$	−62.1(0.5)	−62.5(0.5)	−176.3(91.9)	−33.6(94.2)	119.0(61.2)	117.6(60.9)
Atomic distances [Å]	$\langle O_1-O_{1'} \rangle^h$	6.2 <sup>d</sup>	6.4(0.2)	7.3(0.5)	8.2(0.8)	9.1(0.7)	10.2(0.1)
	$\langle O_3-O_{3'} \rangle^i$	4.7(0.1)	4.8(0.1)	4.6(0.7)	5.2(0.4)	4.8(0.7)	5.1(0.2)
	$\langle O_3-O_{4'} \rangle^i$	6.3(1.0)	6.3(1.1)	6.2(1.2)	6.5(1.3)	6.1(1.4)	6.1(1.5)
	$\langle O_4-O_{4'} \rangle^i$	7.8(0.3)	7.9(0.3)	7.4(0.7)	7.9(0.7)	7.3(0.8)	7.6(0.2)
	$\langle O_6-O_{6'} \rangle^i$	6.8(0.9)	6.9(0.9)	7.3(1.8)	7.8(1.8)	8.6(1.3)	8.9(1.0)
	$\langle O_3-O_{3''} \rangle^k$	3.1 <sup>d</sup>	3.2(0.1)	3.0(0.1)	3.4(0.4)	4.1(0.2)	4.3(0.1)
	$\langle O_3-O_{3'''} \rangle^l$	8.9 <sup>d</sup>	9.1(0.1)	9.0(0.3)	9.0(0.2)	9.7(0.2)	8.6(0.2)

<sup>a</sup> Mean conformation as derived from the mean Cremer–Pople ring puckering parameters.

<sup>b</sup> Cremer–Pople ring puckering amplitude  $q$  (in Å) and puckering angle  $\phi$  (in °).

<sup>c</sup>  $\Phi$ : C-1–C-2–O-1'–C-1';  $\Psi$ : C-2–O-1'–C-1'–C-2';  $\Theta$ : O-1–C-1–C-2–O-1';  $\omega$ : O-5–C-5–C-6–O-6;  $\zeta$ : angle between the best-fit mean plane of the macrocycle (defined by all O-1 atoms) and each fructose-mean plane (atoms C-2 to C-5, and O-5). The index “1” corresponds to parameters for “inward” inclined fructose units with the 3-OH group pointing towards the molecular center; index “2” designates “outward” inclined residues (3-OH directed perpendicular to the macrocycle or away from the center axis). For the odd-membered CF<sub>7</sub> (**2**) and CF<sub>9</sub> (**4**), the index “3” denotes the single torsion between the two vicinal, abnormally parallel, “inward” inclined fructosyl residues; e.g.,  $\Theta_1$ ,  $\Theta_2$ , and  $\Theta_3$  occur with a ratio of 3:3:1 in **2** versus 4:4:1 in **4**.

<sup>d</sup> Due to C<sub>3</sub> symmetry of **1** in the solid-state, no root-mean-square (RMS) fluctuations are given.

<sup>e</sup> For the calculated structures only approximate symmetries are given, i.e., RMS values indicate the “degree of symmetry”.

<sup>f</sup> Not defined for even-membered cyclofructins **1**, **3**, and **5**.

<sup>g</sup> Single value for which no RMS fluctuation could be given.

<sup>h</sup> O-1/O-1' atomic distances diagonally across the cyclofructin ring.

<sup>i</sup> Atomic distances between corresponding atoms contained in adjacent fructofuranosyl residues.

<sup>k</sup> O-3/O-3'' distances between two adjacent, “inward” inclined fructose moieties in a 1,3-like relationship.

<sup>l</sup> Analogous to k, but for two adjacent, “outward” inclined units.

groups and the furanoid ring oxygens O-5 located on one side of the molecule, and the secondary 3-OH and 4-OH groups on the other.

**Molecular geometries of cyclofructins 1–5.**—Despite the imposing pictorial representation of the gross molecular features of cyclofructins **1–5** in Fig. 2, the abundance of data obtained and collected in Table 1 requires a brief discussion of the various individual parameters, such as conformations of the furanoid rings, of the crown ether

backbone, of the hydroxymethyl groups, the inter-residue distances, and the over-all dimensions.

**Fructofuranose conformation.** Although two different fructofuranosyl units can be distinguished on the basis of the macrocyclic crown ether backbone torsion angles, the fructofuranose ring conformations do not differ significantly in terms of the Cremer–Pople ring puckering parameters  $\langle q \rangle$  and  $\langle \phi \rangle$  [31]. All furanoid rings exhibit medium distortions of  $q \approx 0.40$ – $0.45$  Å (root-mean-square

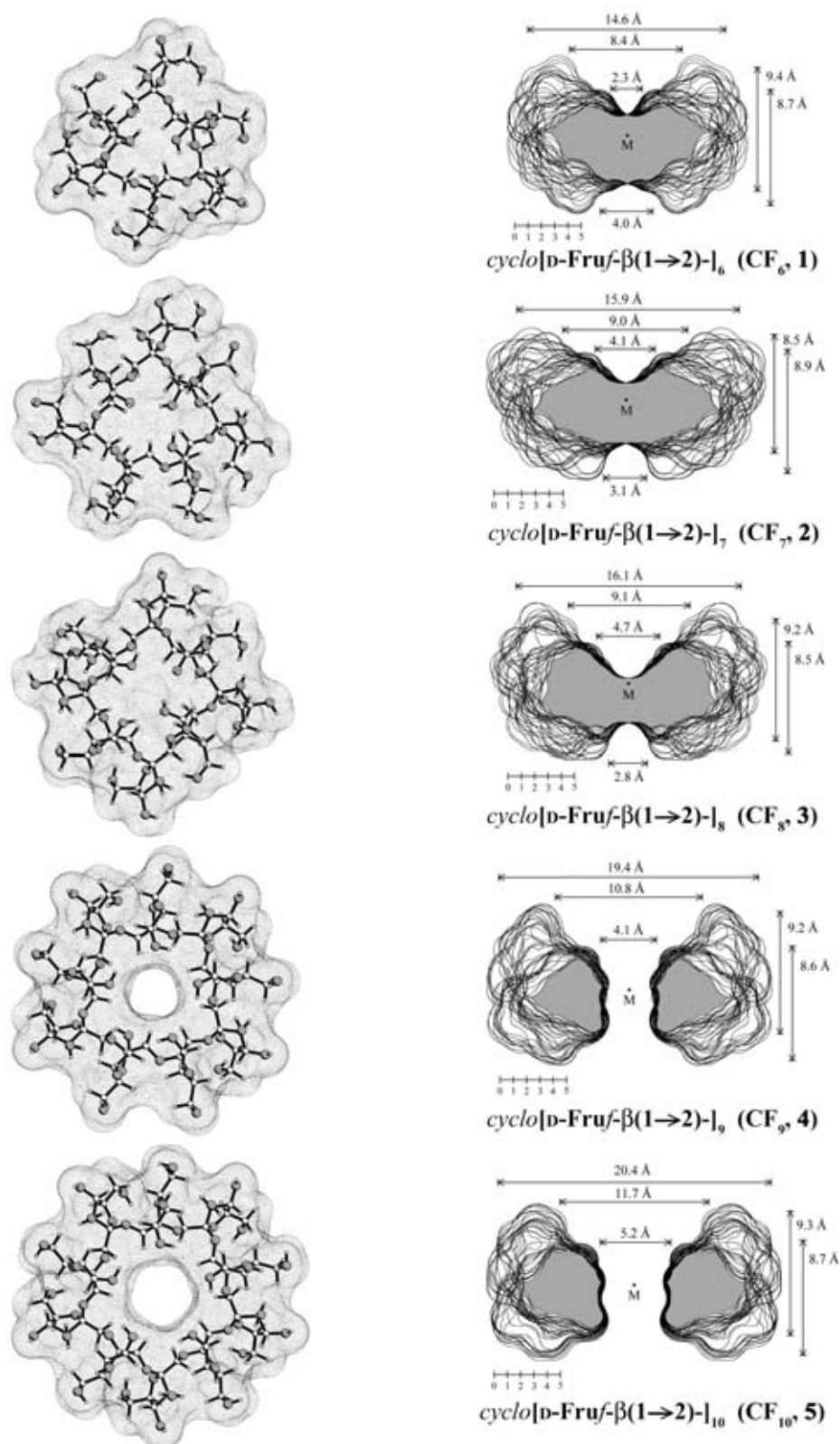


Fig. 2. Ball-and-stick model representations of the global energy-minimum geometries of the cyclofructins 1–5 with the contact surfaces superimposed in dotted form, and the corresponding cross-section plots. Structures on the left are shown perpendicular to the mean ring plane of the macrocycles; the 3-OH/4-OH side of the furanoid rings points towards the viewer, and the 6-CH<sub>2</sub>OH groups and the 5-O atoms away from him; oxygens are shaded. Surface contours (right) were obtained for successive 10° rotation steps around the geometrical center M and superimposed. In each case the 6-CH<sub>2</sub>OH groups are located on the top, and the 3-OH/4-OH groups on the bottom side of the models; approximate molecular dimensions are included in Å.

deviations from planarity), with the conformations uniformly being settled in the  ${}^4T_3 \leftrightarrow E_3$  sector ( $\phi \approx 255\text{--}265^\circ$ ) of the pseudorotational itinerary for five-membered rings [32] (Fig. 3).

The orientation of the primary 6-OH groups relative to the furanoid ring, as defined by the O-5–C-5–C-6–O-6 torsion angle  $\omega$ , is uniformly (–)-*gauche* in either the solid-state geometry or the PIMM91-generated form of the cyclohexamer CF<sub>6</sub>. For the larger cyclofructins CF<sub>7</sub> to CF<sub>10</sub>, however, no characteristic conformational preferences prevail. The very large RMS fluctuations of  $\omega$  (cf. Table 1), indicate this torsion to adopt almost any value in the  $-180^\circ$  to  $+180^\circ$  range. Since the 6-CH<sub>2</sub>OH groups are not involved in any intramolecular hydrogen bonding interactions (vide infra), they are expected to be almost freely rotatable in all compounds 1–5.

**Symmetries.** Invariably, the global energy-minimum geometries of the five cyclofructins feature  $n$ -polygons of the O-1 atoms with average deviations from the least-squares best-fit mean plane of less than 0.20(5) Å. In fact, all Monte-Carlo simulations starting from different symmetrical structures (i.e.  $C_n$  rotational symmetry with  $n=6\text{--}10$  for 1–5) unequivocally demonstrate one trend: “breaking” the high symmetry substantially lowers the molecular energy, i.e., the fructofuranosyl residues avoid the comparatively close spatial arrangements in the  $C_n$  symmetrical structures by diminishing steric repulsions through contra-rotatory movement of two adjacent monosaccharide units. This effect leads to an alternating “inward” (down) and “outward” (up) arrangement of the fructofuranoses relative to the mean plane of the macrocyclic backbone. As a consequence, half of the 3-OH groups (cf. Fig. 4) point towards the center of the macrocycle (“inward” rotation), whereas the others are situated nearly perpendicular on the ring perimeter (“outward” tilting).

In the even-membered cyclofructins, these conformational preferences reduce the symmetry from  $C_n$  to  $C_{n/2}$ , i.e., an  $n/2$ -fold rotational axis for CF<sub>6</sub> (1), CF<sub>8</sub> (3), and CF<sub>10</sub> (5). Their odd-membered counterparts CF<sub>7</sub> (2) and CF<sub>9</sub> (4) cannot adopt  $C_{n/2}$  symmetries a priori; however, the alternating arrangement is retained as largely as possible, with the “last” residue being “inward” inclined, parallel to one adjacent fructosyl unit. This arrangement reduces the backbone symmetry to  $C_1$ .

**Backbone conformations.** With respect to the conformations of the crown ether core of the cyclofructin macrocycles, consideration of the C-1–C-2–O-1′–C-1′ torsion angles  $\Phi_1$  (for inward inclined fructose units) and  $\Phi_2$  (for those directed towards the outside) provides the following picture: in CF<sub>6</sub>, uniformly, an all-(+)-*gauche*-arrangement with alternating values of  $\Phi_1 \approx 64.3^\circ$  and  $\Phi_2 \approx 56.9^\circ$  is adopted (cf. Table 1), in direct relation to the alternating “inward” and “outward” inclination of the fructosyl moieties ( $C_3$  symmetry,  $\Phi_1$  as well as  $\Phi_2$  being realized thrice each). This alternating sequence is retained throughout the entire series 1–5, with the differences between  $\Phi_1$  and  $\Phi_2$  becoming smaller with increasing ring size. However, the  $\Phi_3$  torsion angle for the “unusual” intersaccharidic linkage between the two parallel “inward” inclined fructofuranoses in the odd-membered cyclofructins 2 and 4, exhibits a (–)-*gauche*-arrangement of  $\approx -47^\circ$ . Analogous trends are observed for the  $\Psi$  (C-2–O-1′–C-1′–C-2′) torsion: an approximate *trans*-relationship is retained in all cases, with  $\Psi_1$  and  $\Psi_2$  slightly decreasing on increasing ring size of the macrocycles ( $\Psi_{1/2} \approx 173.6^\circ/-177.2^\circ$  for CF<sub>6</sub>, versus  $\Psi_{1/2} \approx 169.1^\circ/150.5^\circ$  for CF<sub>10</sub>). The *trans*-arrangement is also retained in  $\Psi_3$  for CF<sub>7</sub> and CF<sub>9</sub>.

The largest variations are found in the  $\Theta$  (O-1–C-1–C-2–O-1′) torsion angles, which invariably adopt an alternating *trans*- ( $\Theta_1 \approx 165^\circ\text{--}180^\circ$ )

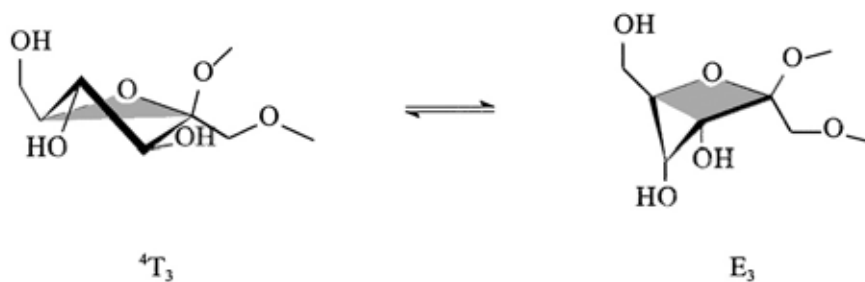


Fig. 3. Ring conformations of fructofuranose units in cyclofructins 1–5. The orientation of the primary 6-OH relative to O-5, graphically implied here, is (–)-*gauche*, as found for the solid-state and force-field-generated geometries of CF<sub>6</sub> (1). For the larger cyclofructins no characteristic preferences prevail.



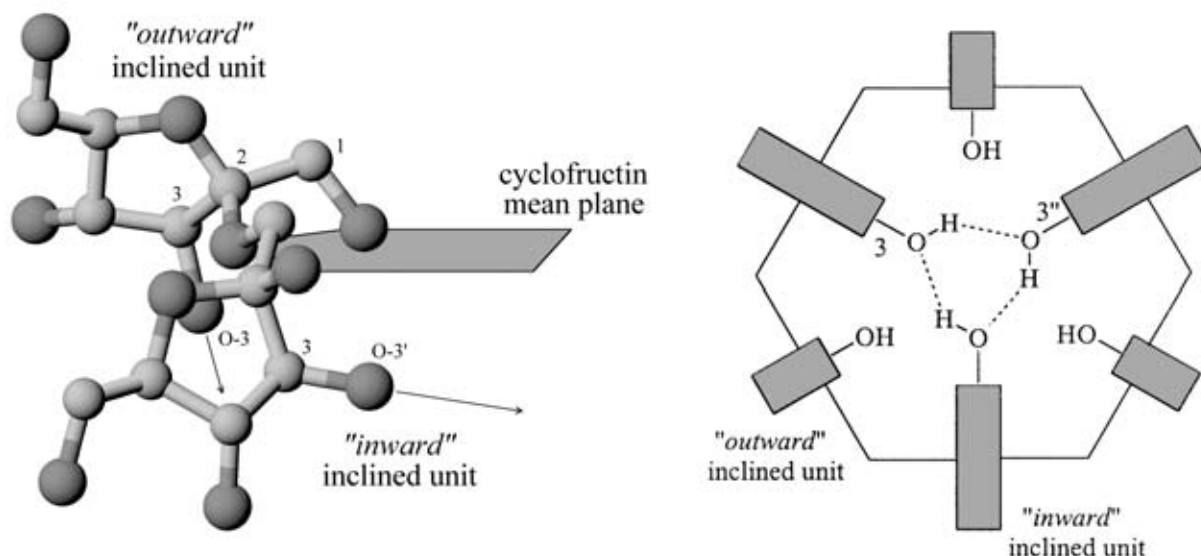


Fig. 4. Typical molecular fragment of a fructofuranosyl- $\beta$ -(1 $\rightarrow$ 2)fructofuranose disaccharide unit. Left: Display of the alternating “inward” and “outward” inclination of the two furanoses, within the O-3 atoms pointing either towards or away from the molecular center (hydrogen atoms omitted for clarity). Right (schematic drawing): In the solid-state structure as well as in the computer-generated form of CF<sub>6</sub>, homodromic cycles of cooperatively strengthened intramolecular hydrogen bonds of the  $[\cdots 3\text{-HO}\cdots\text{HO-}3''\cdots]_n$ -type are observed between the “inward” inclined fructofuranose residues.

and (+)-*gauche*-sequence ( $\Theta_2 \approx 35^\circ\text{--}55^\circ$ ) of settings. The “unusual” intersaccharidic linkages in CF<sub>7</sub> and CF<sub>9</sub> are characterized by a *trans*-relation with  $\Theta_3 \approx 179.8^\circ$  and  $-173.6^\circ$ , respectively. The unique *tgtgtg*-succession of torsion angles  $\Theta_1$  and  $\Theta_2$  is not only realized in the computer-generated global energy-minimum conformation of CF<sub>6</sub> (**1**), but is also observed in its solid-state geometry (cf. Table 1); it must be attributed to the sterically demanding *spiro*-type anellation of furanoid rings onto the crown ether backbone as, by contrast, the unsubstituted 18-crown-6 ether crystallizes in the *gtgggt*-form [33], and its metal complexes favor *all-gauche*-arrangements [34]. The essentially identical molecular shapes and the excellent conformity of the backbone of CF<sub>6</sub> with its “frozen” solid-state structure also validate a previous molecular modeling study, in which only the solid-state geometry of **1** was used [6].

The propeller angle  $\zeta$  indicates the inclination of the mean planes of the “inward” ( $\zeta_1$ ) and “outward” ( $\zeta_2$ ) oriented fructofuranose units towards the mean plane of the macrocycle (cf. Fig. 5 for a schematic plot of a typical molecular fragment). The observed alternating order of  $\zeta_1 \approx 80\text{--}85^\circ$  and  $\zeta_2 \approx 113\text{--}118^\circ$  establishes a “V”-type relationship between vicinal monosaccharide units of the cyclofructins **1–5**.

*Interresidue atomic distances and hydrogen bonding.* Monitoring O $\cdots$ O-distances on opposite faces

of the macrocycles (cf. Table 1) provides a general picture of the possible types of intramolecular hydrogen-bond interactions, even if these do not actually prevail in the low-energy conformers. Whilst the distances between all combinations of O-3 and O-4 atoms are nearly constant and independent from the ring size of the cyclofructins, the O-6/O-6' distances gradually become larger ( $6.9 \pm 0.9 \text{ \AA}$  in CF<sub>6</sub> $\rightarrow$  $8.9 \pm 1.0 \text{ \AA}$  in CF<sub>10</sub>). Provided the O $\cdots$ H-length of standard hydrogen bonds to be in the range of 1.8  $\text{\AA}$  up to 2.5  $\text{\AA}$ , the limiting criterion for the corresponding O $\cdots$ O-distances

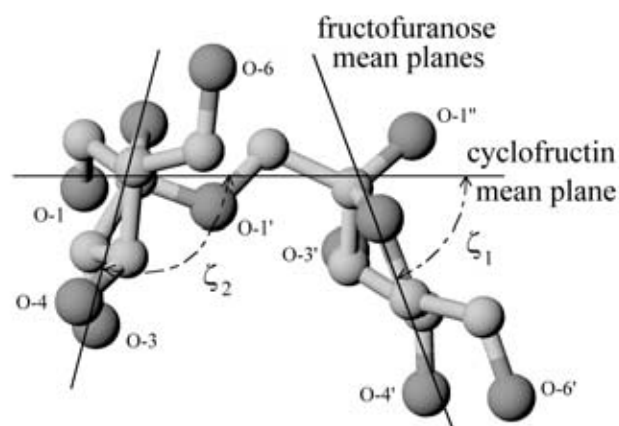


Fig. 5. Propeller angles between two fructofuranose residues as viewed from the outside of the macrocycle in the direction of its mean plane (hydrogen atoms omitted for clarity).

is a maximum of 3.5 Å. The data listed in Table 1 indicate all oxygen-oxygen distances between vicinal fructoses to be larger than 4.6 Å (up to 8.9 Å), thus prohibiting the formation of any stable intramolecular hydrogen bonds of this type. The only exception is found for the O-3/O-3' distances between the adjacent, abnormally parallel "inward" inclined fructose residues in CF<sub>7</sub> (**2**) and CF<sub>9</sub> (**4**) of  $\approx 3.4$  Å and 3.1 Å, respectively. Yet, both allow for direct hydrogen bonding, albeit the 3-O...HO-3'-type bridge is realized in the computed structure of **4** only (length of H-bond  $\approx 2.23$  Å).

By contrast, the corresponding O-3/O-3'' distances for 1,3-related fructose moieties display different trends for "inward" or "outward" tilted furanoses. In the latter case, distances of  $>9.0$  Å indicate the absence of any hydrogen bonding interaction. If both 1,3-related units are inclined "inwards", i.e., having their 3-OH groups directed towards the central axis of the molecule, the O-3/O-3'' distances are in the range of 3.1 Å for CF<sub>6</sub> and CF<sub>7</sub>, 3.4 Å for CF<sub>8</sub>, and  $\approx 4.2$  Å for CF<sub>9</sub> and CF<sub>10</sub>, respectively. Thus, in CF<sub>6</sub> through CF<sub>8</sub> at least, intramolecular H-bonding networks made up by cooperatively strengthened, homodromic cycles of the type [ $\cdots 3\text{-HO}\cdots\text{HO-3}''\cdots$ ]<sub>n</sub> are formed, as exemplified by the schematic drawing of CF<sub>6</sub> (Fig. 4, right). In fact, such an intramolecular hydrogen bond cycle is realized in the solid-state structure of CF<sub>6</sub>.

*Contact surfaces and cavity dimensions.* In contrast to the almost perfectly round-shaped cyclodextrins, in which the  $\alpha$ -(1 $\rightarrow$ 4)-linked glucose units are regularly and uniformly tilted towards the macrocycle [9,35], the alternating "inward/outward" inclination of the fructofuranosyl residues in **1–5** leaves the cyclofructins with a deeply fissured, irregular over-all shape. Cross-cut plots obtained from the intersection of a rotating plane with the cyclofructin contact surfaces (Fig. 2) clearly display

a disk-type shape of **1**, **2**, and **3**, versus the torus-like (doughnut) appearance of **4** and **5**; the approximate molecular dimensions displayed by these plots are listed in Fig. 2 and Table 2.

With increasing ring size, the mean macrocyclic diameters increase from approximately 14.6 Å for CF<sub>6</sub> (**1**), to  $\approx 20.4$  Å in CF<sub>10</sub> (**5**), whilst the mean molecular height is almost constant in the range of  $\approx 8.5$ – $9.2$  Å. The "top" and "bottom" sides of **1**, **2**, and **3** are slightly indented (to an increasing extent in that order), whereas CF<sub>9</sub> (**4**) and CF<sub>10</sub> (**5**) possess a central cavity passing through the entire molecule. In contrast to the outer shape of these macrocycles, the cavities have a nearly perfect cylinder-type appearance. The cavity radius of approx. 5.2 Å for CF<sub>10</sub> (**5**) is similar to that of  $\alpha$ -cyclodextrin (CD<sub>6</sub>:  $\approx 4.5$ – $5.0$  Å [5,9]), whilst the cavity of CF<sub>9</sub> (**4**) is substantially narrowed ( $d \approx 4.1$  Å).

The wide-opened rim of the tori is made up by the 6-CH<sub>2</sub>OH groups, the narrow rim is formed by the 3-OH and 4-OH groups, respectively.

Of the total cyclofructin surface area (cf. Table 2;  $\approx 115$ – $120$  Å<sup>2</sup> per fructose unit), the cavity interior of **4** and **5** comprises  $\approx 5$ – $10\%$ . The spatial volume included by the contact surfaces of **1–5** is computed to approx. 165– $170$  Å<sup>3</sup> per fructose unit. As the estimated cavity volumes of CF<sub>9</sub> (90 Å<sup>3</sup>) and CF<sub>10</sub> (150 Å<sup>3</sup>) turn out to be only slightly smaller than those for the  $\alpha$ - and  $\beta$ -cyclodextrins (100 Å<sup>3</sup> for CD<sub>6</sub>, 160 for CD<sub>7</sub> [9]), similar inclusion complexations—with respect to their geometric fit—are to be expected.

*Molecular electrostatic potentials (MEPs).*—In view of the well-established capability of crown ethers to complex metal cations by chelate coordination and electrostatic interactions [33], we have calculated the MEP profiles of the cyclofructins **1–5** by using the MOLCAD molecular modeling program [28], whereby the relative potential values in the range of approximately  $-100$  to  $+100$  kJ/mol were projected in color-coded form onto the mole-

Table 2  
Approximate molecular dimensions, surface extensions, and cavity characteristics of cyclofructins **1–5**

Cyclofructin	Torus diameter (Å)		Height (Å)	Surface area (Å <sup>2</sup> )		Surface volume (Å <sup>3</sup> )	
	Outer	Inner		Total	Cavity	Total	Cavity
CF <sub>6</sub> ( <b>1</b> )	14.6	—	8.7–9.4	690	—	1000	—
CF <sub>7</sub> ( <b>2</b> )	15.9	—	8.5–8.9	810	—	1180	—
CF <sub>8</sub> ( <b>3</b> )	16.1	—	8.5–9.2	910	—	1370	—
CF <sub>9</sub> ( <b>4</b> )	19.4	4.1	8.6–9.2	1090	90 <sup>a</sup>	1520	90 <sup>a</sup>
CF <sub>10</sub> ( <b>5</b> )	20.4	5.2	8.7–9.3	1200	115 <sup>a</sup>	1710	150 <sup>a</sup>

<sup>a</sup> Height of cavity approximately 7.0 Å.

cular contact surfaces. As imposingly set forth by the resulting color graphics (Fig. 6, left half), the 6- and 1-CH<sub>2</sub>-groups are characterized by positive electrostatic potentials (red colors, Fig. 6 top left), with the cavity surfaces of CF<sub>9</sub> (**4**) and CF<sub>10</sub> (**5**) being highly polarized along the molecular axis (cf. Fig. 6 bottom entries). By contrast, the opposite side made up by the negatively charged O-1, O-3, and O-4 atoms of the fructofuranoses, contributes to high negative electrostatic potentials (blue to violet colors in center entries of Fig. 6).

On the basis of the MEPs presented here, and the overwhelming NMR evidence for the complexation of the metal cations Pb<sup>2+</sup>, Ba<sup>2+</sup>, K<sup>+</sup>, Rb<sup>+</sup>, and Cs<sup>+</sup> by CF<sub>6</sub> (**1**) and CF<sub>7</sub> (**2**) [22,23] in aqueous solution as well as in organic solvents, it becomes obvious that the oxygen atoms O-1 and, in particular, O-3 are involved in capturing cations. The highly negative electrostatic potentials around the O-1, O-3, and O-4 atoms act as a long-range trap for cations, with repulsive positive potentials on the opposite molecular side [6]. Thus, the mechanism of complex formation must involve simultaneous or successive rotation of the *spiro*-annellated furanosyl residues to open a center pocket, whereby the resulting symmetry of the adduct depends on the strength of the Coulomb interactions (i.e., the charge of the cations) [22,23] and the preferred type of coordination.

*Molecular lipophilicity patterns (MLPs).*—Of the various effects that have been brought forward as the actual driving forces for host–guest complexation [36], hydrophobic interactions undoubtedly play a major role although it is exceedingly difficult to quantitatively separate hydrophobic effects [37] from the variety of binding interactions. Recently, however, we have been able to demonstrate that the molecular lipophilicity patterns (MLPs)—generated by the MOLCAD program [28] and mapped onto the respective contact surfaces [29] in color-coded form [38,39]—are a proper means to portray the hydrophobic topographies of inherently hydrophilic sugars—an approach that has provided for the first time a lucid picture of the hitherto elusive distribution of the hydrophilic and hydrophobic areas on the surface of sucrose [40,41], non-carbohydrate sweeteners [40], cyclodextrins [5,9,35] and their inclusion complexes [42], non-glucose oligosaccharides [5,18,43,44], and of the amylose portion of starch [41]. Accordingly, it was obvious to extend these studies to the cyclofructins **1–5**.

As intelligibly set forth by the color representations in Fig. 6 (right entries), the cyclofructins **1–5** exhibit a distinct differentiation of hydrophilic and hydrophobic surface regions with respect to the front and reverse sides of the disk-shaped molecules. The proximity of the 3-OH and 4-OH groups and O-1 of each fructofuranosyl moiety on the one molecular side leads to a pronouncedly hydrophilic surface area (blue areas in the half-opened models, Fig. 6, center). The molecular regions on the opposite side, however, reveal the distinctly hydrophobic character (yellow areas) around the center indentation (Fig. 6, top right), obviously originating from the 1- and 6-methylene groupings and the O-5–C-5–H-5 fragments. Clearly separated hydrophilic and hydrophobic surface areas are maintained throughout the entire series of the cyclofructins with only little changes on increasing the ring size from six to 10 fructose residues. The side view representations of the MLPs (Fig. 6, bottom) reveal the central cavities of CF<sub>9</sub> (**4**) and CF<sub>10</sub> (**5**) to have enhanced hydrophobic character.

*Inclusion complexation potential.*—In the case of the disk-shaped cyclofructins CF<sub>6</sub>, CF<sub>7</sub>, and CF<sub>8</sub>, the concentration of lipophilic regions on one side may—at least in the solid-state—give rise to sandwich-type guest–host interactions, i.e., a neutral guest molecule being enclosed by the hydrophobic sides of two head-to-head oriented cyclofructins. The larger ring homologs CF<sub>9</sub> (**4**) and CF<sub>10</sub> (**5**), however, on account of their sizable cavities, are surmised to engage in cyclodextrin-like inclusion complexations. In order to gain a first notion on their capabilities to incorporate suitable guests into their cavities, the electrostatic iso-energy contour surfaces were generated. In the case of CF<sub>10</sub>, for example, the dipolar character of the cavity is well embodied by the graphical presentation in Fig. 7, in which the iso-energy contours cap both ends of the cavity in a lid-like fashion, displaying an “electrostatic energy lock” that is apt to favor inclusion complex formation if oppositely polarized or even charged head groups of a guest can penetrate the low-energy regions.

Accordingly, on the basis of a mixed molecular dynamics and molecular mechanics approach (cf. Experimental) we have calculated the most stable forms of conceivable zwitterionic inclusion complexes of CF<sub>9</sub> with  $\beta$ -alanine and of CF<sub>10</sub> with *p*-aminobenzoic acid. Of the two possible guest–host alignments, the ones shown in Fig. 8 are highly favored due to an opposite alignment of the

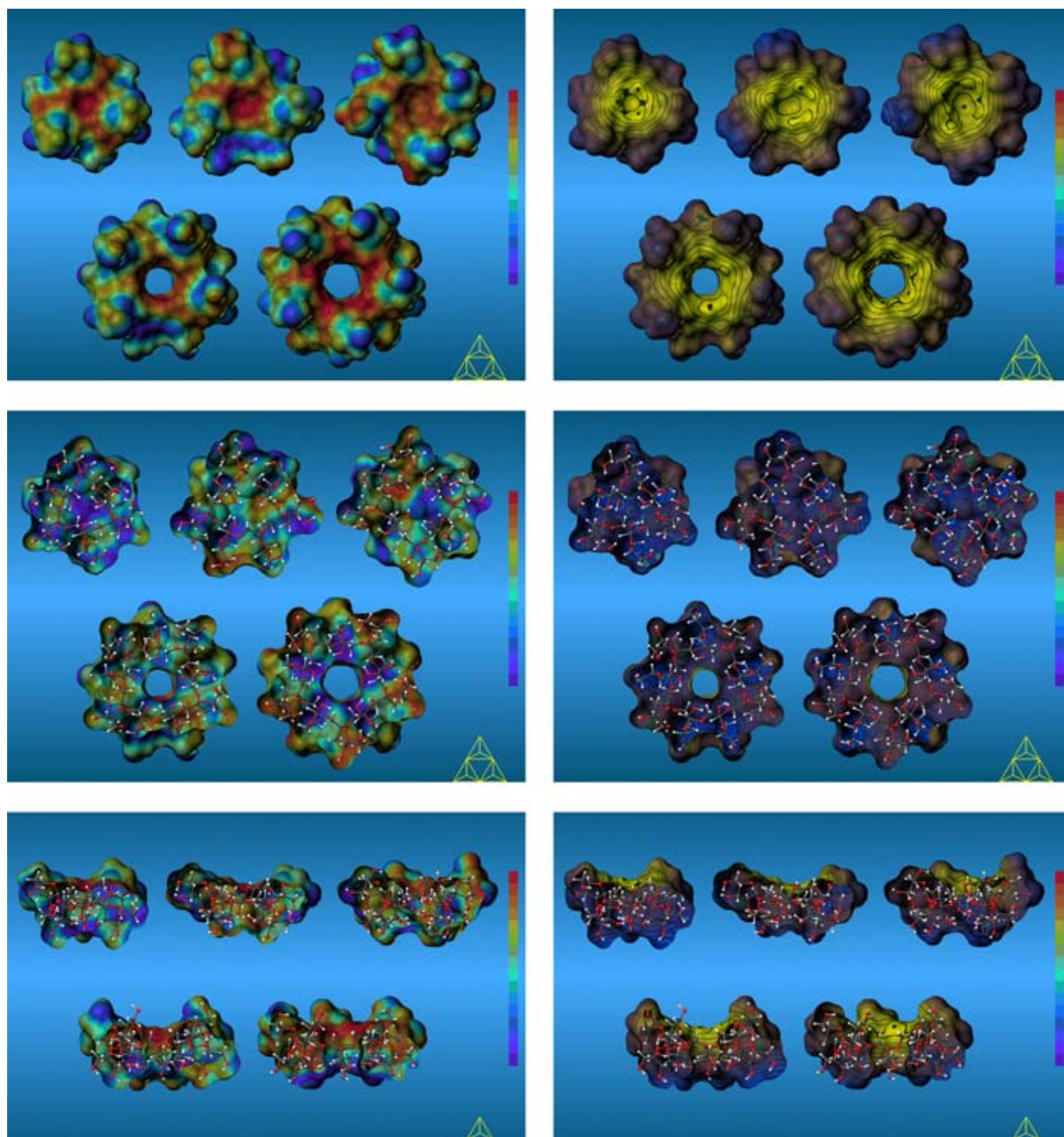


Fig. 6. MOLCAD program-generated molecular electrostatic potential profiles (MEPs, left half) and molecular lipophilicity patterns (MLPs, right half), projected onto the contact surfaces of CF<sub>6</sub> (1, upper left), CF<sub>7</sub> (2, center), CF<sub>8</sub> (3, upper right), CF<sub>9</sub> (4, lower left) and CF<sub>10</sub> (5, lower right); molecular orientations and modes of viewing of the top and center plots are opposite to those in Fig. 2. For visualization of the MEPs (left half), a 16-color code ranging from violet (most negative potential) to red (most positive potential) is applied in relative terms for each molecule separately. The MLPs (right half) are visualized by applying a two-color code graded into 32 shades, adapted to the range of relative hydrophobicity calculated for each molecule; the 16 colors ranging from dark blue (most hydrophilic areas) to full yellow (most hydrophobic regions) are used for mapping the computed values onto the surface, whereas the remaining 16 color shades (light blue to brown) indicate iso-contour lines in between former color scale, allowing a more quantitative assessment of the relative hydrophobicity on different surface regions. The top right picture exposes the intensively hydrophobic (yellow) 1- and 6-methylene groups and the O-5-C-5-H-5-fragments of the molecules; in the center, the front half of the surfaces has been removed, providing an inside view on the hydrophilic (blue) reverse side formed by the 3-OH/4-OH side; the bisected side-view MLPs (bottom right) disclose the hydrophobic central cavities of CF<sub>9</sub> (4) and CF<sub>10</sub> (5).

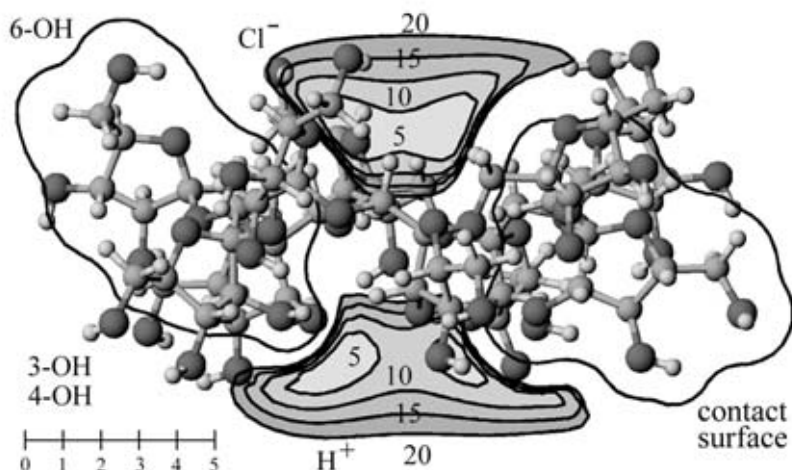


Fig. 7. Iso-energy contour surfaces for the interaction of  $\text{CF}_{10}$  (**5**) with positively ( $\text{H}^+$ ) and negatively ( $\text{Cl}^-$ ) charged probe spheres; energy contours are given at levels of +5.0, +10.0, +15.0, and +20.0 kJ/mol relative to the global energy minimum. On low-energy levels, these volumes designate favorable interactions with cations and anions, or partially positively and negatively charged groups of guest molecules, respectively. The side-view orientation of **5** corresponds to Figs. 2 and 6, with the 3-OH and 4-OH pointing down versus an upward direction of the 5-O and 6- $\text{CH}_2\text{OH}$  groups. The contact surface is superimposed onto the contours and sliced through the center of geometry.

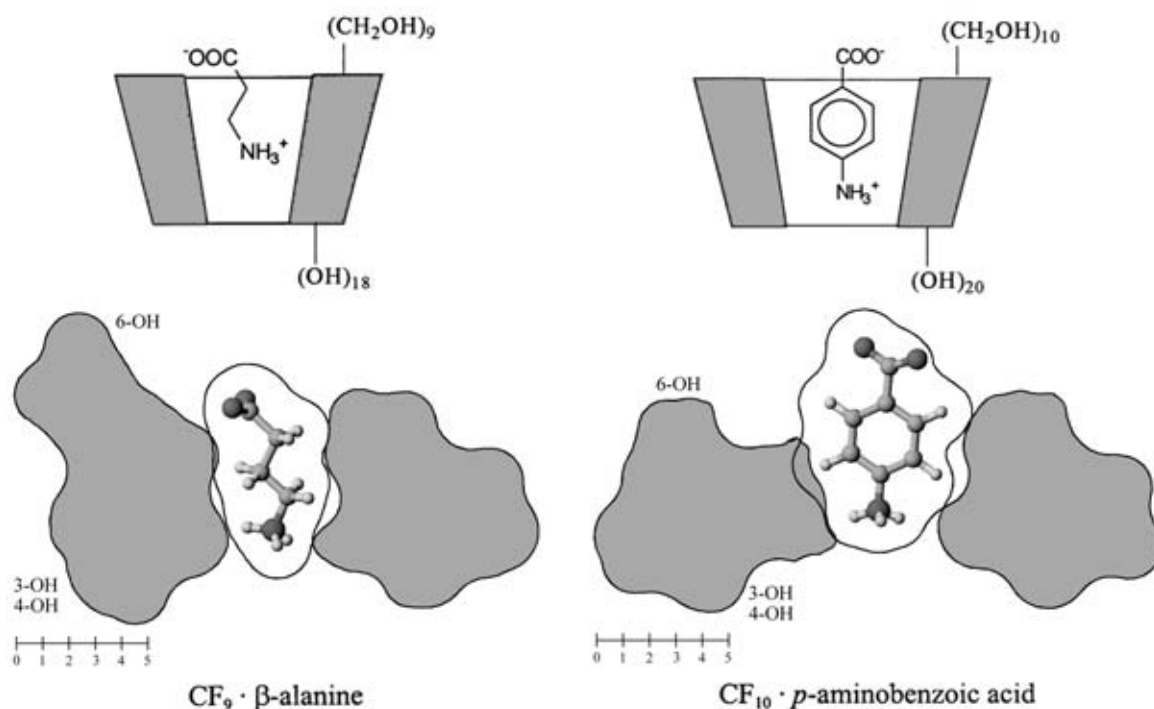


Fig. 8. Surface cross section cuts through the global energy-minimum structures of the inclusion complex of  $\text{CF}_9$  with 3-aminopropionic acid ( $\beta$ -alanine, left) and of the  $\text{CF}_{10}$ -*p*-aminobenzoic acid adduct (right). The geometries depicted correspond to the “matched” host–guest orientations with antiparallel alignment of the dipoles and inclusion of the hydrophobic parts of the guest molecule in the respective cavities. The irregular shape of the cyclodextrin surface cross-section cuts is related to the alternating “inward/outward” inclination of the fructofuranose residues. Whilst the  $\text{CF}_9$  cavity and the zigzag-chain of  $\beta$ -alanine result in a nearly perfect steric fit,  $\text{CF}_{10}$  requires elliptical distortion to accommodate the disk-shaped aromatic guest.

host and guest dipoles. Indeed,  $\beta$ -alanine proves to be an essentially perfect steric fit for  $\text{CF}_9$ , the hydrophobic parts of the *all-trans*, zigzag arranged aliphatic spacer fully penetrate the cylindrical

cavity and fixing the charged hydrophilic head groups at both ends, i.e., the guest’s carboxylate group close to the 6- $\text{CH}_2\text{OH}$  side of the macrocycle, and the amino function at the other, close to

the 3-OH/4-OH groups. Correspondingly, *p*-aminobenzoic acid “matches” the steric as well as electrostatic features of CF<sub>10</sub>, whereby an “*induced-fit*” type mechanism [45] describes the formation of the complex in a more realistic way than the static “*lock-and-key*” concept [46]: the benzene ring is deeply incorporated into the cavity, and the host displays a pronounced elliptical distortion in order to accommodate the disk-shape of the guest.

### 3. Conclusion

Both the MLP and the MEP patterns clearly illustrate the crown ether-type properties of the cyclofructins **1–3** with six to eight fructose residues, with respect to capturing and complexing metal ions; the results obtained agree with experimental data, and the functional groups involved in cation complexation are identified. In relation to the inclusion complex formation of cyclodextrins that is mainly governed by hydrophobic interactions, the cyclofructins **1–3** are devoid of a central cavity, yet represent an interesting complementary example to study electrostatic interactions of carbohydrates with metal cations. The larger ring homologs, CF<sub>9</sub> (**4**) and CF<sub>10</sub> (**5**) exhibit torus-like shape with “through-going” cavities, providing both, electrostatic complexation and hydrophobic inclusion. The computer-assisted evaluation of possible inclusion phenomena by **4** and **5** revealed both—depending on the steric complementarity of host and guest—“*lock-and-key*” as well as “*induced-fit*” type complex formation, during which the host adapts its shape in a more or less pronounced fashion to the steric requirements of the guest. Further insights into the metal cation and inclusion complexation capabilities of the cyclofructins are expected to emerge from molecular dynamics simulations in water, which are to be reported in due course. In the case of CF<sub>6</sub>, a 750 ps MD simulation in a box of 606 water molecules has already been performed [47], showing its solute conformation to be very similar to the calculated in vacuo energy-minimum geometry of Fig. 2.

### 4. Experimental

*Solid-state structure of α-cyclofructin CF<sub>6</sub>, (1).*—The atomic coordinates of the CF<sub>6</sub>-trihydrate

solid-state geometry [21] (C<sub>36</sub>H<sub>60</sub>O<sub>30</sub>·3 H<sub>2</sub>O) were retrieved from the Cambridge Crystallographic Data File [48] (CCDF-Refcode VIPRAN10, space group R3, Z=3), missing hydrogen atoms in the structure determination were geometrically repositioned, the water of crystallization was removed; all molecular parameters listed in Table 1 were recalculated from this data set.

*Force-field calculations.*—All molecular geometry calculations are based on the PIMM91 force-field program [24]; structures were fully energy-optimized without any geometry restraints for in vacuo conditions (ε = 1.0), with a convergence criterion of root-mean-square deviations of the gradients of less than 5.0 × 10<sup>-4</sup> eV/Å.

*Mode of generation of cyclofructin start structures.*—For **1–5**, in each case, two C<sub>n</sub> symmetrical starting structures were generated by *n*-fold assembly of each of the two crystallographically independent fructofuranose geometries contained in the asymmetric unit of the crystal structure of CF<sub>6</sub> (**1**), both in <sup>4</sup>T<sub>3</sub> conformations with Θ (O-1-C-1-C-2-O-1') torsion angles of Θ<sub>1</sub> = 163.4° and Θ<sub>2</sub> = 52.3°, respectively. Fitting of the O-1 atoms to form regular propeller-type anellated *n*-polygons was performed via a rigid body rotation and fitting procedure [49,50]. Analogous fitting of the asymmetric disaccharide unit Fru<sub>f</sub>-β-(1→2)-Fru<sub>f</sub> yielded C<sub>n/2</sub> symmetrical starting structures for the even-membered cyclofructins **1**, **3**, and **5**, with *n/2*-polygons formed by the O-1/O-1'' atoms; for the odd-membered CF<sub>7</sub> (**2**) and CF<sub>9</sub> (**4**), a fructofuranose of either type was added as the remaining last unit. After geometrically repositioning all CH and OH hydrogens, all structures were fully energy-optimized and entered into Monte Carlo (MC), and “*random-walk*” conformational analysis procedures.

*Monte Carlo (MC) and “random-walk” simulations.*—All structure manipulations were performed through external computer programs [50], by which PIMM91 was controlled and used for the energy-optimizations only. Geometry variations of the cyclofructins **1–5** involved re-setting all freely rotatable 4*n* *exocyclic* torsion angles (H-3-C-3-O-3-H, H-4-C-4-O-4-H, C-5-C-6-O-6-H, and ω, i.e., O-5-C-5-C-6-O-6) to random values in each simulation step. To simultaneously vary the furanose ring conformations as well as the cyclofructin backbones, one or two “*corner-flap angles*” [26] out of a total of 8*n* parameters (five furanose ring torsions and three intersaccharidic dihedrals

per monosaccharide residue) were randomly altered; the adjacent *endocyclic* ring torsion angles and the positions of the substituents were adjusted accordingly to diminish steric overlaps. All newly generated conformations were fully energy-minimized (PIMM91); during the “*random-walk*” simulations the resulting conformations were accepted in any case as the starting structures for the next computational cycle; in the Monte-Carlo runs, structures were accepted according to the standard energy-weighted scheme [25]. In all cases, MC calculations and the “*random-walks*” yielded converging molecular conformations and energies (total number of optimized structures for CF<sub>6</sub> (**1**): 135 890, CF<sub>7</sub> (**2**): 136 961, CF<sub>8</sub> (**3**): 109 237, CF<sub>9</sub> (**4**): 86 281, and CF<sub>10</sub> (**5**): 84 654).

*Molecular surfaces, molecular lipophilicity patterns (MLPs), and electrostatic potential profiles (MEPs).*—Calculation of the molecular contact surfaces, MLPs, and MEPs (using the PIMM91 atomic charges) was carried out by using the MOLCAD [28,38,39] molecular modeling program (Fig. 6). Surfaces for the inclusion complexes were generated for the guest and host molecules separately, and subsequently reassembled to the complex. Cross-cut plots were computed from the intersection of a plane with the molecular surfaces [50]; all black-and-white molecular plots were generated using the MolArch<sup>+</sup> program [50]. Visualization of the MEP and MLP surface qualities was done with MOLCAD [28] by color-coded projection of the computed values onto these surfaces applying texture mapping [39]. Scaling of the molecular hydrophobicity patterns and electrostatic potential profiles was performed in relative terms for each molecule separately, and no absolute values are displayed.

*Iso-energy contour surfaces.*—The iso-energy contour surfaces for the interaction of the cyclofructins **1–5** with charged probe spheres were generated by superimposing a three-dimensional grid of 0.25 Å step size to each cyclofructin [50]. For each grid point, the interaction energy of the cyclofructin with a proton (H<sup>+</sup>), or alternatively for a chloride ion (Cl<sup>−</sup>), was calculated by considering the sum of electrostatic and van der Waals energy terms [50]; energy terms were used as implemented in the PIMM91 force-field program [24]: electrostatics are computed using the PIMM91 partial atomic charges of the fully energy-optimized structures and Ohno-Klopman-type distance dependencies. All atomic interaction

parameters, as well as the van der Waals energy terms (mixed exponential and 12-6-terms) were extracted from the PIMM91 force-field [24].

*Cyclofructin inclusion complexes.*—Start structures of the inclusion complexes of CF<sub>9</sub> (**4**) with 3-aminopropionic acid (C<sub>54</sub>H<sub>90</sub>O<sub>45</sub>·C<sub>3</sub>H<sub>7</sub>O<sub>2</sub>N) and of CF<sub>10</sub> (**5**) with *p*-aminobenzoic acid (C<sub>60</sub>H<sub>100</sub>O<sub>50</sub>·C<sub>7</sub>H<sub>7</sub>O<sub>2</sub>N) were generated with either host-guest alignment and geometry optimized (PIMM91). MD simulations (timestep 1 fs, *T* = 300 K) of 25 ps length were performed for each complex, structures were saved every 25 fs. Subsequently, all complex geometries obtained (1000 configurations each) were fully energy-minimized; the global energy-minimum conformations are depicted in Fig. 8.

### Acknowledgements

We thank Professor Dr. J. Brickmann, Institut für Physikalische Chemie, Technische Universität Darmstadt, for providing us with the MOLCAD molecular modeling software package, and Professor Dr. H.J. Lindner for access to the PIMM91 source code.

### References

- [1] S. Immel, G.E. Schmitt, and F.W. Lichtenthaler, in J.J. Torres Labandeira (Ed.), *Proceedings 9th Internat. Cyclodextrin Symp.*, Kluwer Academic, Dordrecht, The Netherlands, in press.
- [2] M. Kawamura and T. Uchiyama, *Carbohydr. Res.*, 260 (1994) 297–304.
- [3] M. Kawamura, T. Uchiyama, T. Kuramoto, Y. Tamura, and K. Mizutani, *Carbohydr. Res.*, 192 (1989) 83–90.
- [4] T. Uchiyama, *Inulin and Inulin-Containing Crops*, Elsevier Science, Amsterdam, The Netherlands, 1993, pp. 143–148.
- [5] F.W. Lichtenthaler and S. Immel, *Tetrahedron: Asymmetry*, 5 (1994) 2045–2060.
- [6] S. Immel and F.W. Lichtenthaler, *Liebigs Ann. Chem.*, (1996) 39–44.
- [7] T. Nakagawa, K. Ueno, M. Kashiwa, and J. Watanabe, *Tetrahedron Lett.*, 35 (1994) 1921–1924.
- [8] (a) T. Takaha, M. Yanase, H. Takata, S. Okada, and S.M. Smith, *J. Biol. Chem.*, 271 (1996) 2902–2908; (b) Y. Tesada, M. Yanase, H. Takata, T. Takaha, and S. Okada, *J. Biol. Chem.*, 272 (1997) 15729–15733.
- [9] S. Immel, J. Brickmann, and F.W. Lichtenthaler, *Liebigs Ann. Chem.*, (1995) 929–942.
- [10] (a) T. Fujiwara, N. Tanaka, and S. Kobayashi, *Chem. Lett.*, (1990) 739–742; (b) I. Miyazawa,

- T. Endo, H. Ueda, S. Kobayashi, and T. Nagai, *Eur. J. Pharm. Sci.*, 3 (1995) 153–162; (c) R. Uchida, A. Nasu, K. Tobe, T. Oguma, and N. Yamaji, *Carbohydr. Res.*, 287 (1996) 271–274.
- [11] T. Endo, H. Nagase, H. Ueda, S. Kobayashi, and T. Nagai, *Chem. Pharm. Bull.*, 45 (1997) 532–536.
- [12] H. Ueda, T. Endo, H. Nagase, S. Kobayashi, and T. Nagai, *J. Inclusion Phenom. Mol. Recogn. Chem.*, 25 (1996) 17–20.
- [13] J. Jacob, K. Geßler, D. Hoffmann, H. Sanbe, K. Koizumi, S.M. Smith, T. Takaha, and W. Saenger, *Angew. Chem.*, 110 (1998) 626–629; *Angew. Chem. Int. Ed.*, 37 (1998) 605–609.
- [14] T. Endo, H. Ueda, S. Kobayashi, and T. Nagai, *Carbohydr. Res.*, 269 (1995) 369–373.
- [15] T. Endo, H. Nagase, H. Ueda, A. Shigihara, S. Kobayashi, and T. Nagai, *Chem. Pharm. Bull.*, 45 (1997) 1856–1859.
- [16] H. Ueda, T. Endo, H. Nagase, S. Kobayashi, and T. Nagai, in J.J. Torres Labandeira (Ed.), *Proceedings 9th Internat. Cyclodextrin Symp.*, Kluwer Academic, Dordrecht, The Netherlands, in press.
- [17] S. Kitamura, H. Isuda, J. Shimada, T. Takada, T. Takaha, S. Okada, M. Mimura, and K. Kajiwara, *Carbohydr. Res.*, 304 (1997) 303–314.
- [18] Y. Nogami, K. Nasu, T. Koga, K. Ohta, K. Fujita, S. Immel, H.J. Lindner, G.E. Schmitt, and F.W. Lichtenthaler, *Angew. Chem.*, 109 (1997) 1987–1991; *Angew. Chem. Int. Ed. Engl.*, 36 (1997) 1899–1902.
- [19] K. Fujita, H. Shimada, K. Ohta, Y. Nogami, K. Nasu, and T. Koga, *Angew. Chem.*, 107 (1995) 1783–1784; *Angew. Chem. Int. Ed. Engl.*, 34 (1995) 1621–1622.
- [20] Y. Nogami, K. Fujita, K. Ohta, K. Nasu, H. Shimada, C. Shinohara, and T. Koga, *J. Inclusion Phenom. Mol. Recogn. Chem.*, 25 (1996) 53–56.
- [21] M. Sawada, T. Tanaka, Y. Takai, T. Hanafusa, T. Taniguchi, M. Kawamura, and T. Uchiyama, *Carbohydr. Res.*, 217 (1991) 7–17.
- [22] (a) N. Yoshie, H. Hamada, S. Takada, and Y. Inoue, *Chem. Lett.*, (1993) 353–356; (b) T. Uchiyama, M. Kawamura, T. Urugami, and H. Okuno, *Carbohydr. Res.*, 241 (1993) 245–248.
- [23] Y. Takai, Y. Okumura, T. Tanaka, M. Sawada, S. Takahashi, M. Shiro, M. Kawamura, and T. Uchiyama, *J. Org. Chem.*, 59 (1994) 2967–2975.
- [24] (a) H.J. Lindner and M. Kroeker, PIMM91—Closed Shell PI-SCF-LCAO—MO-Molecular Mechanics Program, Darmstadt University of Technology, Germany, 1996; (b) A.E. Smith and H.J. Lindner, *J. Comput.-Aided Mol. Des.*, 5 (1991) 235–262.
- [25] (a) N. Metropolis, A.W. Rosenbluth, M.N. Rosenbluth, A. Teller, and E. Teller, *J. Chem. Phys.*, 21 (1953) 1087–1092; (b) W. F. van Gunsteren and H.J.C. Berendsen, *Angew. Chem.*, 102 (1990) 1020–1050; *Angew. Chem. Int. Ed. Engl.*, 29 (1990) 992–1023.
- [26] H. Goto and E. Osawa, *J. Am. Chem. Soc.*, 111 (1989) 8950–8951.
- [27] The 3D-structures can be viewed at: <http://caramel.oc.chemie.tu-darmstadt.de/imm/3Dstructures.html>; MOLCAD graphics are available at: <http://caramel.oc.chemie.tu-darmstadt.de/imm/molcad/gallery.html>.
- [28] (a) J. Brickmann, *MOLCAD—MOLEcular Computer Aided Design*, Darmstadt University of Technology, Germany, 1996; *J. Chim. Phys.*, 89 (1992) 1709–1721; (b) M. Waldherr-Teschner, T. Goetze, W. Heiden, M. Knoblauch, H. Vollhardt, and J. Brickmann, in F.H. Post and A.J.S. Hin (Eds.), *Advances in Scientific Visualization*, Springer, Heidelberg, Germany, 1992, pp. 58–67; (c) J. Brickmann, T. Goetze, W. Heiden, G. Moeckel, S. Reiling, H. Vollhardt, and C.-D. Zachmann, in J.E. Bowie (Ed.), *Insight and Innovation in Data Visualization*, Manning, Greenwich, U.K., 1994, pp. 83–97.
- [29] (a) F.M. Richards, *Ann. Rev. Biophys. Bioeng.*, 6 (1977) 151–176; *Carlsberg. Res. Commun.*, 44 (1979) 47–63; (b) M.L. Connolly, *J. Appl. Cryst.*, 16 (1983) 548–558; *Science*, 221 (1983) 709–713.
- [30] B. Lee and F.M. Richards, *J. Mol. Biol.*, 55 (1971) 379–400.
- [31] (a) D. Cremer and J.A. Pople, *J. Am. Chem. Soc.*, 97 (1975) 1354–1358; (b) G.A. Jeffrey and R. Taylor, *Carbohydr. Res.*, 81 (1980) 182–183.
- [32] J.E. Kilpatrick, K.E. Pitzer, and R. Spitzer, *J. Am. Chem. Soc.*, 69 (1947) 2483–2488.
- [33] (a) J.D. Dunitz and P. Seiler, *Acta Crystallogr., Sect. B*, 30 (1974) 2339–2341; (b) E. Maverick, P. Seiler, B. Schweizer, and J.D. Dunitz, *Acta Crystallogr., Sect. B*, 36 (1980) 615–620.
- [34] (a) C.J. Pedersen, *J. Am. Chem. Soc.*, 89 (1967) 2495–2496; 7017–7036; (b) J.W.H.M. Uiterwijk, S. Harkema, and D. Feil, *J. Chem. Soc., Perkin Trans. 2*, (1987) 721–731.
- [35] F.W. Lichtenthaler and S. Immel, *Liebigs Ann. Chem.*, (1996) 27–37.
- [36] R.J. Clarke, J.H. Coates, and S.F. Lincoln, *Adv. Carbohydr. Chem. Biochem.*, 46 (1988) 205–249.
- [37] W. Blokzijl and J.B.F.N. Engberts, *Angew. Chem.*, 105 (1993) 1610–1648; *Angew. Chem. Int. Ed. Engl.*, 32 (1993) 1545–1579.
- [38] W. Heiden, G. Moeckel, and J. Brickmann, *J. Comput.-Aided Mol. Des.*, 7 (1993) 503–514.
- [39] M. Teschner, C. Henn, H. Vollhardt, S. Reiling, and J. Brickmann, *J. Mol. Graphics*, 7 (1994) 98–105.
- [40] F.W. Lichtenthaler and S. Immel, in M. Mathlouthi, J.A. Kanters, and G.G. Birch (Eds.), *Sweet Taste Chemoreception*, Elsevier Applied Science, London/New York, 1993, pp. 21–53.



- [41] F.W. Lichtenthaler and S. Immel, *Internat. Sugar J.*, 97 (1995) 12–22.
- [42] F.W. Lichtenthaler and S. Immel, *Starch/Stärke*, 48 (1996) 145–154.
- [43] F.W. Lichtenthaler and S. Immel, in J. Szejtli and L. Sente (Eds.), *Proc. 8th Internat. Symp. on Cyclodextrins*, Kluwer Academic, Dordrecht, The Netherlands, 1996, pp. 3–16; *J. Inclusion Phenom. Mol. Recognit. Chem.*, 25 (1996) 3–16.
- [44] H. Gohlke, S. Immel, F.W. Lichtenthaler, and G.E. Schmitt in J.J. Torres Labandeira (Ed.), *Proc. 9th Internat. Symp. on Cyclodextrins*, Kluwer Academic, Dordrecht, The Netherlands, in press.
- [45] D.E. Koshland, Jr., *Angew. Chem.* 106 (1994) 2468–2471; *Angew. Chem. Int. Ed.*, 33 (1994) 2408–2412.
- [46] (a) E. Fischer, *Ber. Dtsch. Chem. Ges.*, 27 (1894) 2985–2993; (b) F.W. Lichtenthaler, *Angew. Chem.*, 106 (1994) 2456–2467; *Angew. Chem. Int. Ed. Engl.*, 33 (1994) 2364–2374.
- [47] S. Immel, G.E. Schmitt, and F.W. Lichtenthaler, in J.J. Torres Labandeira (Ed.), *Proceedings 9th Internat. Cyclodextrin Symp.*, Kluwer Academic, Dordrecht, The Netherlands, in press.
- [48] (a) *Cambridge Crystallographic Data File*, Version 5.09, 1995; (b) F.H. Allen, S.A. Bellard, M.D. Brice, B.A. Cartwright, A. Doubleday, H. Higgs, T. Hummelink, B.G. Hummelink-Peters, O. Kennard, W.D.S. Motherwell, J.R. Rodgers, and D.G. Watson, *Acta Crystallogr., Sect. B*, 35 (1979) 2331–2339; (c) F.H. Allen, O. Kennard, and R. Taylor, *Acc. Chem. Res.*, 16 (1983) 146–153.
- [49] D.J. Heisterberg, *QTRFIT—Rigid Body Rotation and Fitting Program*, The Ohio Supercomputer Center, Columbus, Ohio 43212, 1991.
- [50] S. Immel, *MolArch<sup>+</sup>—MOLEcular ARCHitecture Modeling Program*, Darmstadt University of Technology, Germany, 1997.





# Conformations and lipophilicity profiles of some cyclic $\beta$ -(1 $\rightarrow$ 3)- and $\beta$ -(1 $\rightarrow$ 6)-linked oligogalactofuranosides<sup>☆</sup>

Holger Gohlke, Stefan Immel, Frieder W. Lichtenthaler \*

*Institut für Organische Chemie, Technische Universität Darmstadt, Petersenstraße 22, D-64287 Darmstadt, Germany*

Received 26 April 1999; accepted 2 July 1999

## Abstract

The conformational features of cyclooligosaccharides composed of  $\beta$ -(1  $\rightarrow$  3)- and  $\beta$ -(1  $\rightarrow$  6)-linked galactofuranose units, i.e., *cyclo*[D-Galf $\beta$ -(1  $\rightarrow$  3)]<sub>n</sub> with *n* = 4 (**1**) and 5 (**2**), and *cyclo*[D-Galf  $\beta$ -(1  $\rightarrow$  6)]<sub>n</sub> with *n* = 3 (**3**) and 4 (**4**), were investigated by means of Monte Carlo simulations. The flexibility of the macrocyclic backbone strongly favors bent and asymmetrical conformations over round geometries. Generation of the molecular surfaces of the global minimum-energy structures reveals disk-type shapes for **1–4** without through-going central cavities, yet distinct indentations close to the O-2/O-3 groups, respectively. The molecular lipophilicity patterns prove these surface dents to be hydrophobic for the  $\beta$ -(1  $\rightarrow$  6)-linked cyclogalactans **3** and **4**, whereas their  $\beta$ -(1  $\rightarrow$  3)-linked counterparts display an inverse situation with a hydrophobic outer core structure. © 1999 Elsevier Science Ltd. All rights reserved.

*Keywords:* Oligogalactosides, cyclic; Cyclodextrin analogs; Cyclogalactofuranosides

## 1. Introduction

The starch-derived cyclodextrins with six, seven, and eight  $\alpha$ -(1  $\rightarrow$  4)-linked glucopyranose units have enjoyed a preeminent position in supramolecular chemistry as their capability to form inclusion complexes and, hence, to function as enzyme models has contributed substantially to our understanding of molecular recognition processes in general, and enzyme reactions in particular [2]. Their macrocycles are characterized by a remarkable structural rigidity, such that they are capable

of mimicking the classic lock-and-key concept of enzyme specificity [3] rather than the more realistic induced-fit mode [4], which entails guest-induced conformational changes toward a transition state geometry.

Several options have been realized — by synthetic means invariably — to introduce flexibility into the common, overly rigid cyclodextrins. Thus, the  $\alpha$ -(1  $\rightarrow$  4) linkup of the glucopyranose residues has been changed to  $\alpha$ -(1  $\rightarrow$  6) [5] and  $\beta$ -(1  $\rightarrow$  6) [6] connections, thereby ‘elongating’ the intersaccharidic link from a singular oxygen to an O–CH<sub>2</sub> joint; unfortunately, the respective cyclooligosaccharides have only been characterized as their benzyl ethers [5] or peracetates [6] and, except for a dimer [7], hardly any information is available on the conformation of their macrocycles [5b]. Configurational inversion of the glucose-2-OH in the cyclodextrins, resulting (formally) in the cyclomannins [8], had little

<sup>☆</sup> Molecular modeling of saccharides, Part 22. For Part 21, see Ref. [1]. — Presented in part at the 9th International Symposium on Cyclodextrins, Santiago de Compostela, Spain, May 1998, Abstract 2-P-4.

\* Corresponding author. Tel.: +49-6151-162-376; fax: +49-6151-166-674.

E-mail address: fwlicht@sugar.oc.chemie.tu-darmstadt.de (F.W. Lichtenthaler)

effect on the flexibility of the macrocycles, as the  ${}^4C_1$  geometry of the pyranoid rings is rigid enough to be retained [9] — a state that also holds for the cyclorhamnins [10,11] and for cyclooligosaccharides with alternating L-rhamnose and D-mannose units [12].

The first non-glucose cyclooligosaccharides with substantial macrocyclic flexibility proved to be those containing altrose residues, i.e., cyclodextrins in which the configuration at C-2 and C-3 has been inverted: mono-*altro*- $\beta$ -cyclodextrin undergoes conformational changes in its altrose moiety upon inclusion of adamantane-carboxylate [13], and the cycloaltrins composed of six [14], seven [15], and eight [16]  $\alpha$ -(1 $\rightarrow$ 4)-linked D-altropyranose units are thoroughly flexible, adopting a variety of macrocyclic conformations in solution [1].

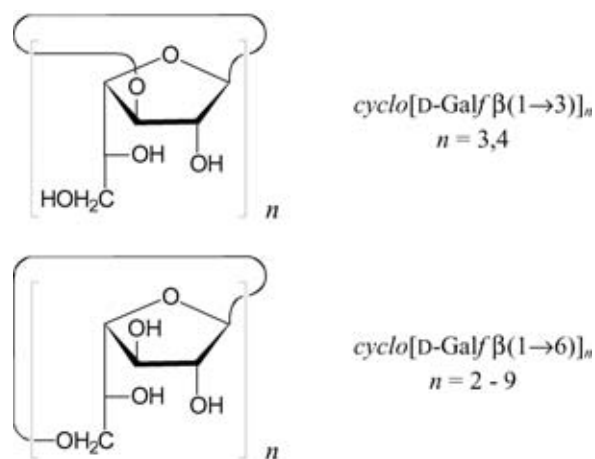
As furanoid rings display a higher pseudorotational mobility than their pyranoid counterparts, cyclooligosaccharides composed of furanoid sugar units are apt to be more flexible in their macrocycle. This expectation, however, has not materialized in the inulin-derived [17] cyclofructins; their six, seven, or eight  $\beta$ -(1 $\rightarrow$ 2)-linked fructofuranose units are spiro-anellated onto a crown-ether backbone thereby conferring rigidity on their macrocycles [18]. By contrast, the cyclogalactans composed of  $\beta$ -(1 $\rightarrow$ 3)-,  $\beta$ -(1 $\rightarrow$ 5)-, and  $\beta$ -(1 $\rightarrow$ 6)-linked galactofuranose units (Scheme 1) — in fact the first non-glucose cyclooligosaccharides prepared synthetically [19] — are likely to provide larger macro-

cyclic flexibility, not only due to the higher pseudorotational mobility of the furanoid rings, but as a consequence of, in the  $\beta$ -(1 $\rightarrow$ 6)-linked species in particular, the larger number of atoms bridging the furanose residues and the steric strain imposed by the respective macrocyclic assemblies.

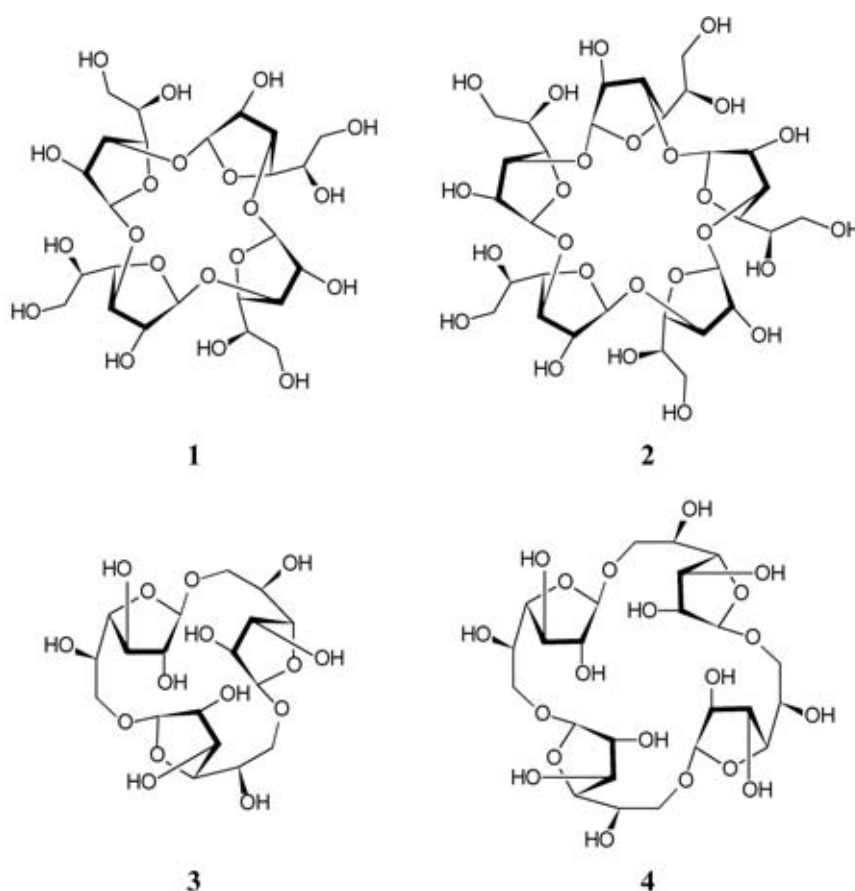
Due to the rather modest yields in their preparation by cycloglycosylation of tritylated 1,2-*O*-(1-cyano)ethylidene derivatives of D-galactofuranose [19], neither the molecular geometries of these cyclogalactans nor their capabilities to form inclusion complexes were investigated. In view of their potential to function as flexible hosts in molecular recognition processes, we have initiated a molecular modeling study, for which we selected, as examples, the tetra- and pentamer of the  $\beta$ -(1 $\rightarrow$ 3)-cyclogalactofuranosides **1** and **2**, and, due to their higher flexibility, the trimer (**3**) and tetramer (**4**) of the  $\beta$ -(1 $\rightarrow$ 6)-type analogs (Scheme 2).

## 2. Results and discussion

*Conformational analysis of  $\beta$ -D-galactofuranose.*—Since comparatively few furanoid ring systems of pentoses and hexoses have been analyzed in detail — D-ribose, 2-deoxy-D-ribose [20], D-arabinose [21], D-fructofuranose [22], and D-psicose [23] are notable examples — a pre-condition for elaborating the molecular geometries of furanoid cyclogalactans was a detailed conformational assessment of their building unit, i.e.,  $\beta$ -D-galactofuranose itself. The adiabatic energy potential surface of the ring conformations of  $\beta$ -D-galactofuranose, determined using the PIMM91 force field [24], reveals a single, broad energy minimum in the western part of the pseudorotational turntable within the  ${}^4T_3 \rightleftharpoons {}^4E \rightleftharpoons {}^4T_0 \rightleftharpoons E_0$  region for the furanose rings (cf. Fig. 1). This distinct preference for the western part of the Cremer–Pople parameter [25] plot ( $q/\phi$  plane) is obviously due to the opposite tendency of the bulky exocyclic substituent at C-4 and the anomeric OH to occupy pseudoequatorial and pseudoaxial orientations towards the ring, respectively.



Scheme 1.



Scheme 2.

The three  $\beta$ -D-galactofuranose structures in the CCDF data file [26], i.e., compounds **5** [27], **6**<sup>1</sup> [28], and **7**<sup>1</sup> [29] (Scheme 3), have  ${}^1T_0 \rightleftharpoons {}^1E \rightleftharpoons {}^1T_2$  geometries. Thus, the conformational preference of the furanoid ring in the highly O- and C-substituted galactose derivatives **5–7** with different anomeric substituents is only slightly shifted from the  ${}^4E$  global minimum for the unsubstituted  $\beta$ -D-galactofuranose (Fig. 1) — a reasonable agreement between in vacuo force-field calculations and crystal structure results.

Further supportive evidence for the relevance of the in vacuo geometries calculated can be derived [30] from the  ${}^1\text{H}$  NMR  ${}^3J_{\text{H-H}}$  coupling constants of 31  $\beta$ -D-galactofuranose derivatives<sup>2</sup> described in the literature

<sup>1</sup> The furanoid ring conformation for **6** is incorrectly given as  ${}^4E$  in Ref. [28]; the ring geometry of **7** was reconstructed from Ref. [29] due to missing 3D-coordinates in the database.

<sup>2</sup> A detailed discussion and conformational evaluation of these  $\beta$ -D-galactofuranose derivatives on the basis of the coupling patterns (mainly in  $\text{CDCl}_3$ , yet some in  $\text{D}_2\text{O}$ , acetone- $d_6$  and pyridine- $d_5$ ) is contained in Ref. 31.

[27–31], as the majority (22) of their furanoid solution geometries fall into the  ${}^4E \rightleftharpoons {}^4T_0 \rightleftharpoons E_0 \rightleftharpoons {}^1T_0$  range, i.e., into the western part of the pseudorotational itinerary within 10 kJ/mol above the force-field-derived global energy minimum depicted in Fig. 1. This congruence of computational and  ${}^1\text{H}$  NMR-derived data attests to the relevance of the furanoid geometries obtained by either of the two methods.

*Molecular geometries of the cyclooligogalactosides 1–4.*—For generation of the macrocyclic geometries of **1–4**, a pre-optimized galactofuranose unit was used to construct various symmetrical and asymmetrical starting structures, which were then subjected to conformational analysis using Monte Carlo and Random Walk techniques [32] to search for the global energy minimum of each compound. An adapted corner-flipping procedure [33] was used to effectively vary the ring geometries of the furanose units as well as of the macrocyclic backbone without breaking bonds

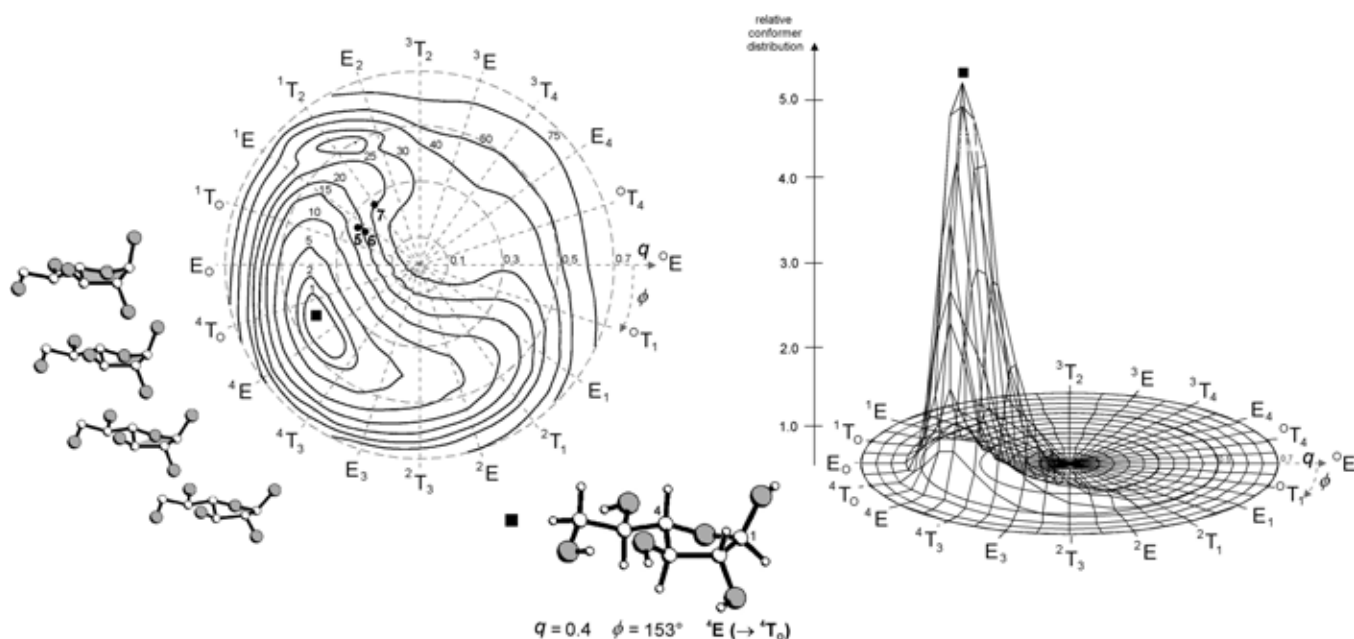


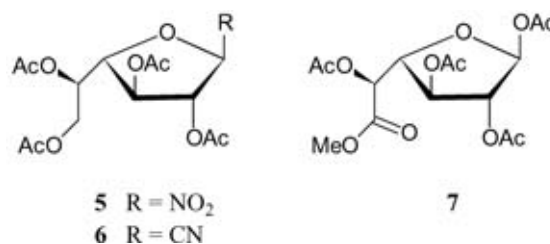
Fig. 1. Left: Adiabatic energy map of  $\beta$ -D-galactofuranose as a function of the Cremer–Pople parameters [25] — i.e., the puckering amplitude  $q$  and the phase angle  $\phi$  — calculated by molecular mechanics using the PIMM91 [24] force field. The bold-faced square marks the global energy minimum corresponding to the conformation displayed underneath ( ${}^4E$  form slightly distorted towards the  ${}^4T_0$  geometry), the structures to the left represent the furanose conformations within the  ${}^4T_3 \rightleftharpoons E_0$  range of the pseudorotational turntable. The solid-state conformations of 5–7 are indicated by the solid points on the energy potential surface. Right: a 3D plot of the relative Boltzmann distribution of conformers calculated for  $T=300$  K, indicating finite conformer probabilities within the 10 kJ/mol level.

in the different rings. From these extensive procedures, the global minimum-energy structures for the cyclogalactans emerged as  ${}^1E$  for the preferred furanose geometry of the  $\beta$ -(1  $\rightarrow$  3)-linked species **1** and **2**, versus the  ${}^4T_3$  envelope form for the  $\beta$ -(1  $\rightarrow$  6) analogs **3** and **4**<sup>3</sup>. Although the furanose ring shapes in **1–4** appear to be high in energy as they are located approximately +15 kJ/mol above the global minimum of the  $\beta$ -D-galactofuranose energy potential surface (Fig. 1), these structures reflect the different types of substitution of the five-membered rings [free furanose versus  $\beta$ -(1  $\rightarrow$  3)- and  $\beta$ -(1  $\rightarrow$  6)-linkages] (Fig. 2). In toto, the experimental (solid-state structures and NMR) and computational data both point towards preferred furanose geometries in the western part of Fig. 1.

The high flexibility of the furanoid rings, most notably in the  $\beta$ -(1  $\rightarrow$  6)-linked species in

**3** and **4** with four torsion angles involved, leads to structures of low symmetry being favored with increasing ring size of the macrocycles. The energy-minimum geometries of **1–4** displayed in Fig. 3 show that the small ring homologs **1** and **3** retain symmetry as much as possible ( $C_4$  and  $C_3$ , respectively), but **2** and **4** prefer  $C_1$  (asymmetric) and  $C_2$ -type structures.

In the case of **3**, and to a lesser extent in **4**, the conformational symmetry is only retained through favorable intramolecular hydrogen bonding interactions of the 3-OH $\cdots$ O-6 and 5-OH $\cdots$ O-4' type. As in aqueous solutions, these effects are expected to become less important, conceivable conformational equilibria are likely to be shifted towards asymmetric forms.



Scheme 3.

<sup>3</sup>The 3D structures can be viewed at <http://caramel.oc.chemie.tu-darmstadt.de/immell/3Dstructures.html>; MOLCAD graphics are available at <http://caramel.oc.chemie.tu-darmstadt.de/immell/molcad/gallery.html>.

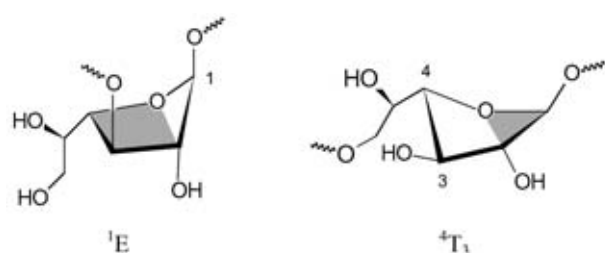


Fig. 2. Schematic representation of the furanose geometries calculated for cyclogalactofuranosides 1–4:  ${}^1E$  conformation for the  $\beta$ -(1  $\rightarrow$  3)-linked cyclooligosaccharides 1 and 2 vs.  ${}^4T_3$  form for the  $\beta$ -(1  $\rightarrow$  6) analogs 3 and 4.

The molecular contact surfaces computed for 1–4 as well as the corresponding surface cross-section cuts (cf. Fig. 3), provide evidence for the disk-type shapes of these macrocycles with small puckering amplitudes (i.e., out-of-plane deviations of ring atoms between the furanose units) of less than 0.5 Å along their backbones. The surface models not only display the effective steric extensions of these molecules and their lack of central cavities to form inclusion complexes, but also allow the mapping of their lipophilicity patterns in color-coded form, as has already proved useful in earlier studies to assess the properties of cyclodextrins [34] and related compounds [11].

**Molecular lipophilicity patterns (MLPs).**— Besides the steric demands in 1–4, their hydrophobic characteristics are of major interest to evaluate their properties. In Fig. 4, the corresponding MLPs were computed and mapped in color-coded form onto the contact surfaces of Fig. 3. Most remarkably, these graphics reveal a fundamental difference in the distribution of hydrophilic and hydrophobic surface areas for both classes of the  $\beta$ -(1  $\rightarrow$  3)- and  $\beta$ -(1  $\rightarrow$  6)-linked cyclogalactans. In the former case, i.e., 1 and 2 (Fig. 4, top), the surface is significantly indented in the center without elaborating ‘through-going’ central cavities. Due to their association with the O<sup>1</sup>–C<sup>2</sup>H–C<sup>3</sup>H fragments of the galactofuranose moieties, these surface dents are remarkably hydrophobic, whereas O-4 and the side chain 5-OH and 6-OH groups render the opposite molecular sides much more hydrophilic. Most notably, the outer rim of the disk-shaped molecules carrying the 2-OH hydroxyls is predominantly hydrophilic.

A different situation prevails for the  $\beta$ -(1  $\rightarrow$  6)-cyclogalactosides 3 and 4 (Fig. 4, bottom): the type of intersaccharidic linkage, their increased flexibility, and the altered orientation of the furanoid rings in relation to the macrocycle cause an inverse alignment of hydrophilic and hydrophobic surface regions. As the 5-OH groups are directed towards the central surface dents, they provide a hydrophilic environment that is augmented by the 3-OH groups, whereas on the back the close alignment of the O-4 ring atoms contributes to the slightly less hydrophilic regions. The most hydrophobic surface areas of 3 and 4 are situated on the outer edge of the macrocycles, and are made up by the C<sup>1</sup>H, C<sup>3</sup>H, and C<sup>5</sup>H–C<sup>6</sup>H<sub>2</sub> fragments.

In sum, this molecular modeling study of the furanoid cyclogalactans 1–4 provides reliable insights into their molecular architecture, such that they not only lack round geometries — the circular shapes depicted in the chemical formulae for 1–4 are grossly misleading — but also central cavities with which to form inclusion complexes similar to those given by the cyclodextrins. At most, the formation of loose sandwich-type adducts is conceivable. The larger homologs of the  $\beta$ -(1  $\rightarrow$  6)-cyclogalactosides, however — from the hexamer on, presumably — should be capable of adopting a plethora of macrocyclic conformations in solution, including some with a through-going cavity, from which a guest may select the one most suited for its inclusion. Thus, these galactofurano-cyclooligosaccharides are apt to evolve into attractive flexible models for mimicking the dynamic induced-fit mode of molecular recognition, once they become accessible on a scale to study their supramolecular properties.

### 3. Experimental

All calculations were carried out using the PIMM91 force-field [24] program with external conformational search algorithms [35], which has been shown [36] to accurately reproduce anomeric and exoanomeric effects. A dielectric constant of  $\epsilon = 1.0$  was used for all calculations without the implicit incorporation

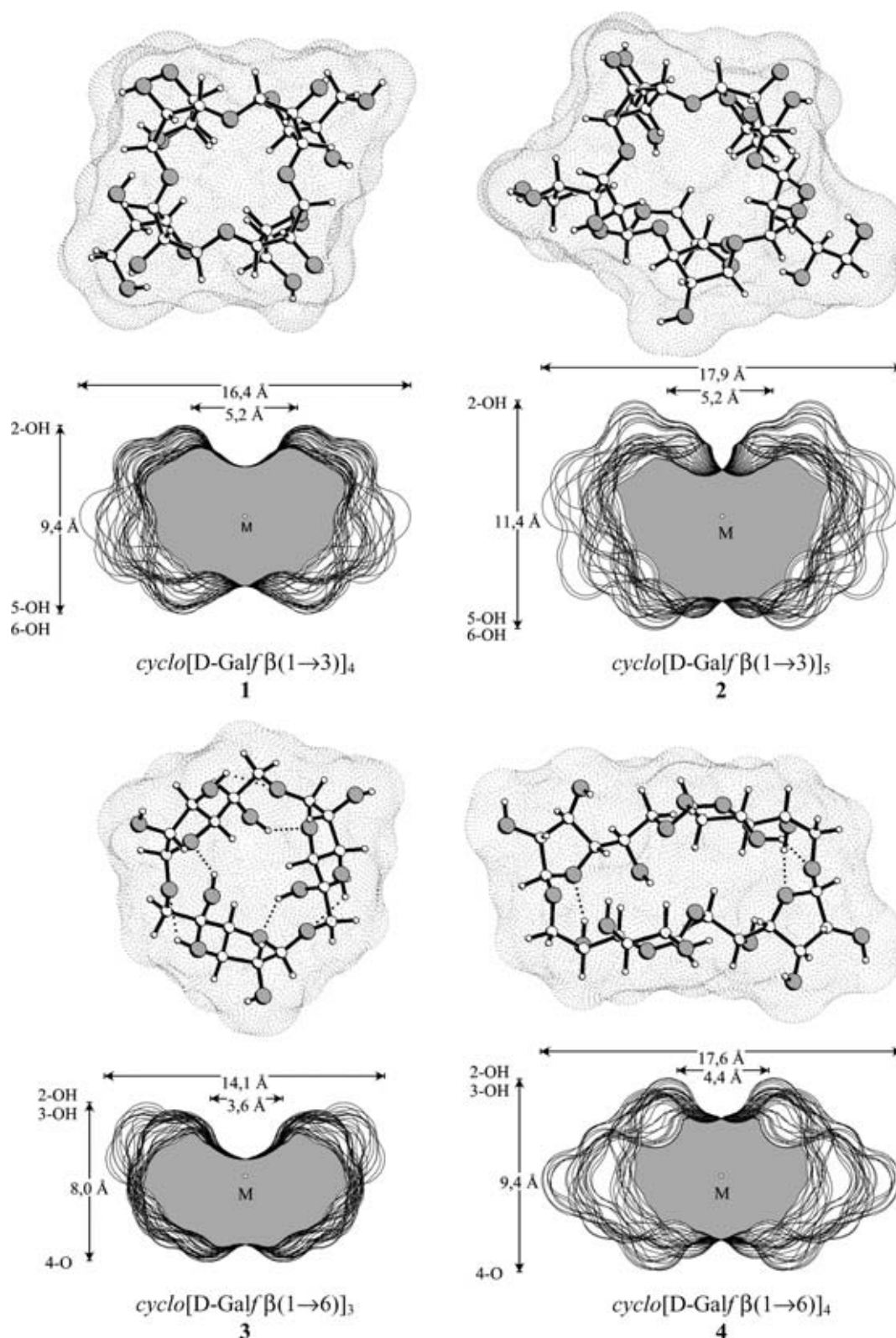


Fig. 3. Global minimum-energy structures of the cyclogalactofuranosides 1–4 with their contact surfaces in dotted form; intramolecular hydrogen bonding interactions are indicated by bold dots. All structures are displayed perpendicular to the macrocycles with the O-2/O-3 sides facing the viewer. In addition, surface cross-section plots are shown with approximate molecular dimensions in Å; cross-cuts were obtained from the intersection of molecular surfaces with a rotating plane (360° in steps of 10°) perpendicular to the mean macro-ring planes, and superimposed.



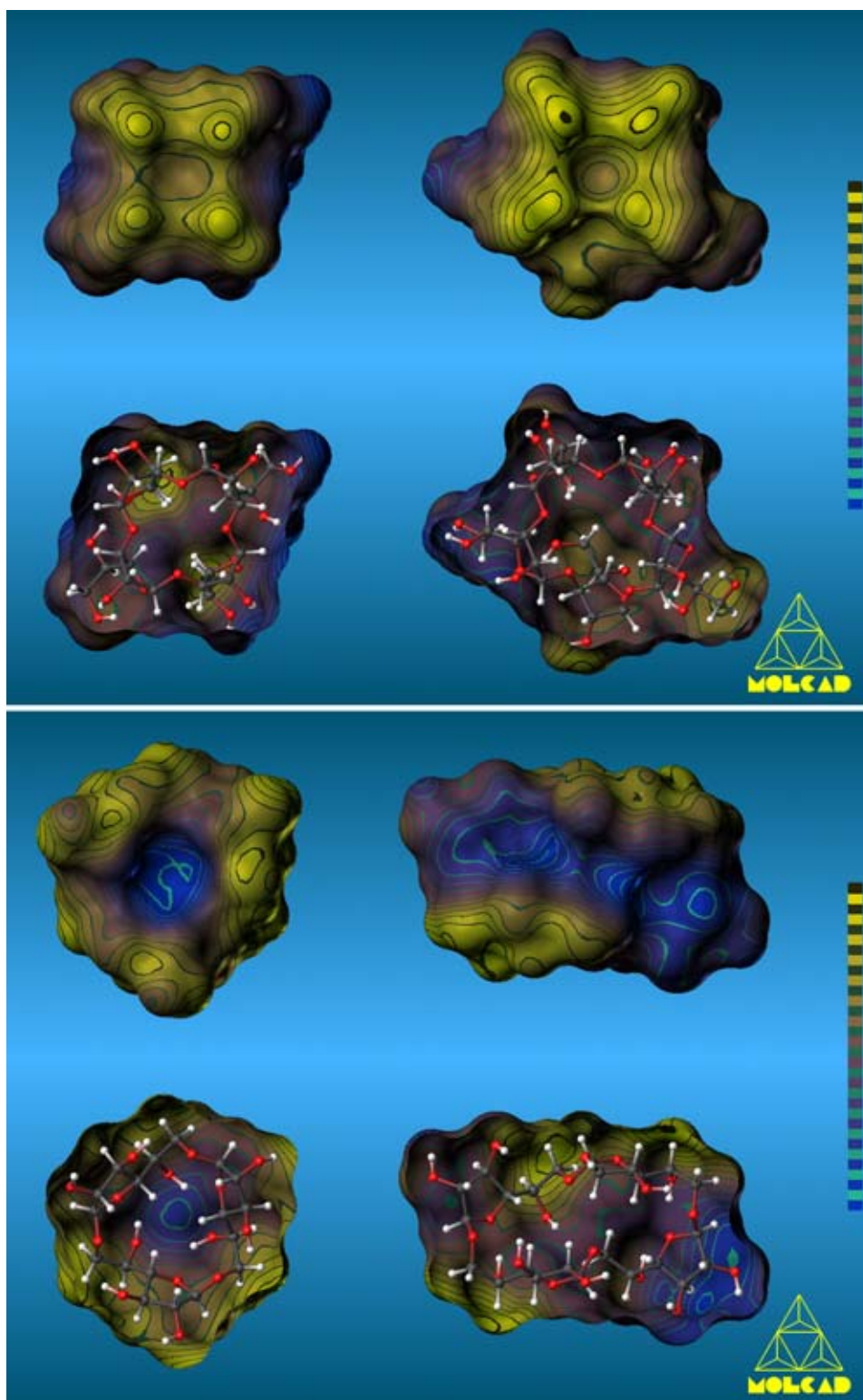


Fig. 4. MOLCAD program-generated molecular lipophilicity patterns (MLPs) projected onto the contact surfaces of the  $\beta$ -(1  $\rightarrow$  3)- (top: **1** and **2**) and  $\beta$ -(1  $\rightarrow$  6)-linked cyclolactofuranosides (bottom: **3** and **4**). The color code was adapted to the range of relative hydrophobicity calculated for each molecule, ranging from dark-blue for the most hydrophilic areas to full yellow corresponding to the most hydrophobic surface regions. The orientation of all models is such that the O-2/O-3 atoms face the viewer (cf. Fig. 3), whereas the furanoid ring oxygens (O-4) are directed toward the rear; the half-opened models on the bottom each visualize the molecular orientation as well as the surface properties of the rear side.

of solvent models. A pre-optimized galactofuranose unit was assembled to various symmetrical and asymmetrical starting structures of the cyclogalactofuranosides **1–4**, which were then subjected to conformational analysis using Monte Carlo and Random Walk simulations [32]. An adapted corner-flipping procedure [33] was used to effectively vary the ring geometries of the furanose units as well as the macrocyclic backbone without breaking bonds in the different rings; all exocyclic torsion angles ( $-\text{OH}$  and  $-\text{CHOH}-\text{CH}_2\text{OH}$  groups) were treated as flexible. Proper sampling of the conformational space was ensured by converging global minimum-energy structures and molecular parameters. For the global minimum-energy structures obtained, the molecular contact surfaces [37], cross-section cuts (Fig. 3) [35], and lipophilicity patterns (MLPs, Fig. 4) [38] were computed; color-coded representations were generated using the MOLCAD [38] modeling program. Color-coded projection of the MLPs onto the corresponding contact surfaces was done by applying texture mapping strategies [39], using a two-color code graded into 32 shades, ranging from dark-blue for the most hydrophilic to yellow for the most hydrophobic areas. Scaling of the MLP profiles was performed in arbitrary units and in relative terms for each molecule separately (from most hydrophilic to most hydrophobic surface regions); no absolute values are displayed. Color graphics were photographed from the computer screen of a Silicon-Graphics workstation.

### Acknowledgements

We thank the Fonds der Chemischen Industrie for support of this investigation and Professor Dr J. Brickmann, Institut für Physikalische Chemie, Technische Universität Darmstadt, for providing us with the MOLCAD molecular modeling software package.

### References

[1] S. Immel, K. Fujita, F.W. Lichtenthaler, *Chem. Eur. J.*, 5 (1999) in press.

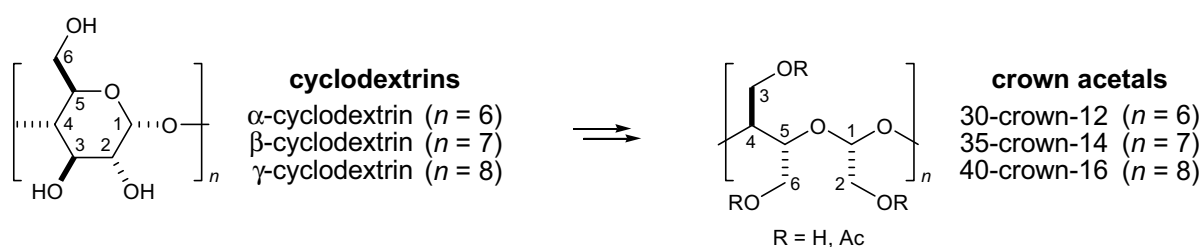
- [2] J. Szejtli, T. Osa (Eds.), *The Cyclodextrins, Comprehensive Supramolecular Chemistry*, Vol. 3, Pergamon, Oxford, UK, 1996, 626 pp.
- [3] (a) E. Fischer, *Ber. Dtsch. Chem. Ges.*, 27 (1894) 2985–2993. (b) F.W. Lichtenthaler, *Angew. Chem.*, 106 (1994) 2456–2467; *Angew. Chem., Int. Ed. Engl.*, 33 (1994) 2364–2374.
- [4] D.E. Koshland, Jr., *Angew. Chem.*, 106 (1994) 2368–2372; *Angew. Chem., Int. Ed. Engl.*, 33 (1994) 2375–2378.
- [5] (a) S. Houdier, P.J.A. Vottéro, *Carbohydr. Res.*, 248 (1993) 377–384; *Angew. Chem., Int. Ed. Engl.*, 33 (1994) 354–356. (b) S. Houdier, P.J.A. Vottéro, *Carbohydr. Lett.*, 1 (1994) 13–18.
- [6] (a) D. Gagnaire, M. Vignon, *Carbohydr. Res.*, 51 (1976) 140–144. (b) D. Bassieux, D. Gagnaire, M. Vignon, *Carbohydr. Res.*, 56 (1977) 19–33. (c) G. Bonas, G. Excoffier, M. Paillet, M. Vignon, *Recl. Trav. Chim. Pays-Bas*, 108 (1989) 259–261.
- [7] (a) D. Gagnaire, S. Pérez, V. Tran, *Carbohydr. Res.*, 82 (1980) 185–194. (b) E. Duée, A. Grand, V. Tran, *Acta Crystallogr., Sect. B*, 37 (1981) 850–857.
- [8] (a) M. Mori, Y. Ito, T. Ogawa, *Carbohydr. Res.*, 192 (1989) 131–146. (b) M. Mori, Y. Ito, J. Izawa, T. Ogawa, *Tetrahedron Lett.*, 31 (1990) 3191–3194.
- [9] F.W. Lichtenthaler, S. Immel, *Tetrahedron: Asymmetry*, 5 (1994) 2045–2060.
- [10] (a) M. Nishizawa, H. Imagawa, Y. Kan, H. Yamada, *Tetrahedron Lett.*, 32 (1991) 5551–5554. (b) M. Nishizawa, H. Imagawa, K. Kubo, Y. Kan, H. Yamada, *Synlett*, (1992) 447–448. (c) M. Nishizawa, H. Imagawa, E. Morikuni, S. Hatekayama, H. Yamada, *Chem. Pharm. Bull.*, 42 (1994) 1356–1365.
- [11] For a review, see: F.W. Lichtenthaler, S. Immel, *J. Incl. Phenom. Mol. Recognit. Chem.*, 25 (1996) 3–16.
- [12] (a) P.R. Ashton, C.L. Brown, S. Menzer, S.A. Nepogodiev, J.F. Stoddart, D.J. Williams, *Chem. Eur. J.*, 2 (1996) 580–591. (b) P.R. Ashton, S.J. Cantrill, G. Gattuso, S. Menzer, S.A. Nepogodiev, A.N. Shipway, J.F. Stoddart, D.J. Williams, *Chem. Eur. J.*, 3 (1997) 1299–1314.
- [13] K. Fujita, W.-H. Chen, D.-Q. Yuan, Y. Nogami, T. Koga, T. Fujioka, K. Mihashi, S. Immel, F.W. Lichtenthaler, *Tetrahedron: Asymmetry*, 10 (1999) 1689–1696.
- [14] Y. Nogami, K. Nasu, T. Koga, K. Ohta, K. Fujita, S. Immel, H.J. Lindner, G.E. Schmitt, F.W. Lichtenthaler, *Angew. Chem.*, 109 (1997) 1987–1991; *Angew. Chem., Int. Ed. Engl.*, 36 (1997) 1899–1902.
- [15] K. Fujita, H. Shimada, K. Ohta, Y. Nogami, K. Nasu, *Angew. Chem.*, 107 (1995) 1783–1784; *Angew. Chem., Int. Ed. Engl.*, 34 (1995) 1621–1622.
- [16] Y. Nogami, K. Fujita, K. Ohta, K. Nasu, H. Shimada, C. Shinohara, T. Koga, *J. Incl. Phenom. Mol. Recognit. Chem.*, 25 (1996) 53–56.
- [17] (a) M. Kawamura, T. Uchiyama, T. Kuramoto, Y. Tamura, K. Mizutani, *Carbohydr. Res.*, 192 (1989) 83–90. (b) M. Sawada, T. Tanaka, Y. Takai, T. Hanafusa, T. Taniguchi, M. Kawamura, T. Uchiyama, *Carbohydr. Res.*, 217 (1991) 7–17.
- [18] (a) S. Immel, F.W. Lichtenthaler, *Liebigs Ann. Chem.*, (1996) 39–44. (b) S. Immel, G.E. Schmitt, F.W. Lichtenthaler, *Carbohydr. Res.*, 313 (1998) 91–105.
- [19] L.V. Backinowsky, S.A. Nepogodiev, N.K. Kochetkov, *Carbohydr. Res.*, 185 (1989) C1–C3; *Tetrahedron*, 46 (1990) 139–150; *Russ. Chem. Bull.*, 42 (1993) 1418–1422.
- [20] W. Saenger, in C.R. Cantor (Ed.), *Principles of Nucleic Acid Structure*, Springer, Heidelberg, 1984, pp. 61–65.

- [21] S. Cros, C. Herve du Penhoat, S. Pérez, A. Imberty, *Carbohydr. Res.*, 248 (1993) 81–93.
- [22] (a) A.D. French, V. Tran, *Biopolymers*, 29 (1990) 1599–1611. (b) S. Immel, *Dissertation*, Technische Hochschule Darmstadt, 1995.
- [23] A.D. French, M.K. Dowd, *J. Comput. Chem.*, 15 (1994) 561–570.
- [24] (a) H.J. Lindner, M. Kroeker, *PIMM91 — Closed Shell PI-SCF-LCAO-MO-Molecular Mechanics Program*, Darmstadt University of Technology, 1997. (b) A.E. Smith, H.J. Lindner, *J. Comput.-Aided Mol. Des.*, 5 (1991) 235–262.
- [25] (a) D. Cremer, J.A. Pople, *J. Am. Chem. Soc.*, 97 (1975) 1354–1358. (b) G.A. Jeffrey, R. Taylor, *Carbohydr. Res.*, 81 (1980) 182–183.
- [26] F.H. Allen, O. Kennard, *Chem. Des. Automat. News*, 8 (1993) 1,31–37; *Cambridge Crystallographic Data File* (April 1999), Version 5.17. Refcodes: FACRAC [27], VAJGIW [28], and MACGAL [29].
- [27] D. Beer, J.H. Bieri, I. Macher, R. Prewo, A. Vasella, *Helv. Chim. Acta*, 69 (1986) 1172–1190.
- [28] P. Köll, J. Kopf, D. Wess, H. Brandenburg, *Liebigs Ann. Chem.*, (1988) 685–693.
- [29] P. Beale, N.C. Stephenson, J.D. Stevens, *J. Chem. Soc., Chem. Commun.*, (1971) 25.
- [30] (a) H.M. Zuurmond, P.A.M. van der Klein, G.H. Veeneman, J.H. van Boom, *Recl. Trav. Chim. Pays-Bas*, 109 (1990) 437–441. (b) G.H. Veeneman, S. Notermans, P. Hoogerhout, J.H. van Boom, *Recl. Trav. Chim. Pays-Bas*, 108 (1989) 344–350. (c) J. Thiem, H.-P. Wessel, *Liebigs Ann. Chem.*, (1983) 2173–2184. (d) J.E. Nam Shin, A.S. Perlin, *Carbohydr. Res.*, 76 (1979) 165–176. (e) O. Varela, C. Marino, R.M. De Lederkremer, *Carbohydr. Res.*, 155 (1986) 247–251. (f) T. Ziegler, E. Eckhardt, G. Herold, *Liebigs Ann. Chem.*, (1992) 441–451.
- [31] H. Gohlke, *Diploma Thesis*, Darmstadt University of Technology, 1997, 69 pp.
- [32] (a) N. Metropolis, A.W. Rosenbluth, M.N. Rosenbluth, A. Teller, E. Teller, *J. Chem. Phys.*, 21 (1953) 1087–1092. (b) W.F. van Gunsteren, H.J.C. Berendsen, *Angew. Chem.*, 102 (1990) 1020–1055; *Angew. Chem., Int. Ed. Engl.*, 29 (1990) 992–1023.
- [33] H. Goto, E. Osawa, *J. Am. Chem. Soc.*, 111 (1989) 8950–8951.
- [34] F.W. Lichtenthaler, S. Immel, *Liebigs Ann. Chem.*, (1996) 27–37; *Starch/Stärke*, 48 (1996) 145–154.
- [35] S. Immel, *MolArch<sup>+</sup> — MOlecular ARCHitecture Modeling Program*, Darmstadt University of Technology, 1999.
- [36] (a) I. Tvaroska, T. Bleha, *Adv. Carbohydr. Chem. Biochem.*, 47 (1989) 45–123. (b) G.E. Schmitt, *Diploma Thesis*, Darmstadt University of Technology, 1995.
- [37] M.L. Connolly, *J. Appl. Cryst.*, 16 (1983) 548–558.
- [38] J. Brickmann, *MOLCAD — MOlecular Computer Aided Design*, Darmstadt University of Technology, 1997. The major part of the MOLCAD program is included in the SYBYL package of TRIPOS associates, St. Louis, MI, USA. (b) J. Brickmann, *J. Chim. Phys.*, 89 (1992) 1709–1721. (c) W. Heiden, G. Moeckel, J. Brickmann, *J. Comput.-Aided Mol. Des.*, 7 (1993) 503–514.
- [39] M. Teschner, C. Henn, H. Vollhardt, S. Reiling, J. Brickmann, *J. Mol. Graphics*, 12 (1994) 98–105.



## Chapter 6

### Cyclodextrin-derived Crown Acetals



#### Synthesis and Molecular Geometry of an Achiral 30-Crown-12 Polyacetal from $\alpha$ -Cyclodextrin

S. Immel, T. Nakagawa, H. J. Lindner, and F. W. Lichtenthaler,  
*Chem. Eur. J.* **2000**, *6*, 3366-3371.

#### Hydroxymethyl-substituted Crown Acetals with 35-C-14 and 40-C-16 Skeletal Backbones: Synthesis and Molecular Geometries

S. Immel, F. W. Lichtenthaler, H. J. Lindner, and T. Nakagawa,  
*Tetrahedron: Asymmetry* **2001**, *12*, 2767-2774.

#### Large-ring Crown Acetals from Cyclodextrins

T. Nakagawa, S. Immel, H. J. Lindner, and F. W. Lichtenthaler,  
*Proc. 10<sup>th</sup> Int. Symp. Cyclodextrins* (Ed.: J. Szejtli), Mia Digital Publ., Ann Arbor, Michigan, **2000**, pp. 18-23.

#### Flexible Non-glucose Cyclooligosaccharides

S. Immel,  
*Proc. 10<sup>th</sup> Int. Symp. Cyclodextrins* (Ed.: J. Szejtli), Mia Digital Publ., Ann Arbor, Michigan, **2000**, pp. 24-31.



Molecular Modeling of Saccharides, Part 27<sup>#</sup>Synthesis and Molecular Geometry of an Achiral 30-Crown-12 Polyacetal from  $\alpha$ -CyclodextrinStefan Immel, Toshio Nakagawa, Hans J. Lindner, and Frieder W. Lichtenthaler\*<sup>[a]</sup>

**Abstract:** Periodate oxidation of  $\alpha$ -cyclodextrin followed by borohydride reduction readily provided an octadecahydroxymethyl-substituted 30-crown-12 polyacetal **1**, its 30-membered macrocycle being composed of six *meso*-butanetetrol/glycolaldehyde acetal units, which is, consequently, optically inactive. Its solid-state molecular geometry emerged from the X-ray structural analysis of the well-crystallizing octadeca-

acetate **2**, which revealed the undulated macrocycle to be molded into three loops with a unique order of succession of the -CHR-CHR-O-CHR-O- units: alternating *gauche*- and *anti*-conformations of the *meso*-butanetetrol portions

and consecutive disposition of the glycolaldehyde-acetoxymethyl groups above and below the mean-plane of the macrocycle. In solution, however, as evidenced by <sup>1</sup>H- and <sup>13</sup>C-NMR spectra, the macrocycle is highly flexible at ambient and higher temperatures, its mobility becoming distinctly restricted only below -20 °C.

**Keywords:** cyclodextrins • crown acetals • macrocyclic polyacetals • oligosaccharides

## Introduction

Unlike crown ethers that have played a pivotal role in the development of supramolecular chemistry,<sup>[1]</sup> macrocycles with acetalic oxygen atoms have received comparatively little attention, conceivably because their cation complexation properties—as compared to the more basic ether oxygens—are less propitious. Thus, Pedersen<sup>[2]</sup> noted already thirty years ago “that -O-CH<sub>2</sub>-O- is a less favorable linkage than -O-CH<sub>2</sub>CH<sub>2</sub>-O- for complexation”, based on crown ether acetals of the type 18-C-6, 20-C-7, and 22-C-8, namely cyclic polyethers with one or two acetal groupings in their skeletal backbone. Various other investigators have since amply corroborated the drastic decrease in cation binding ability

by introducing acetal groupings into crown ethers even when bearing the same number of oxygen atoms.<sup>[3–6]</sup>

Macrocycles exclusively containing acetal-oxygen atoms, and, hence, deserving the designation *crown acetal*,<sup>[7, 8]</sup> are rare, the presently known examples being limited to systems with two formaldehyde/alkanediol acetal units, that is containing only four oxygens in the ring (Figure 1).

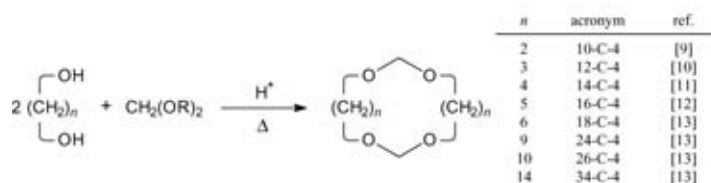


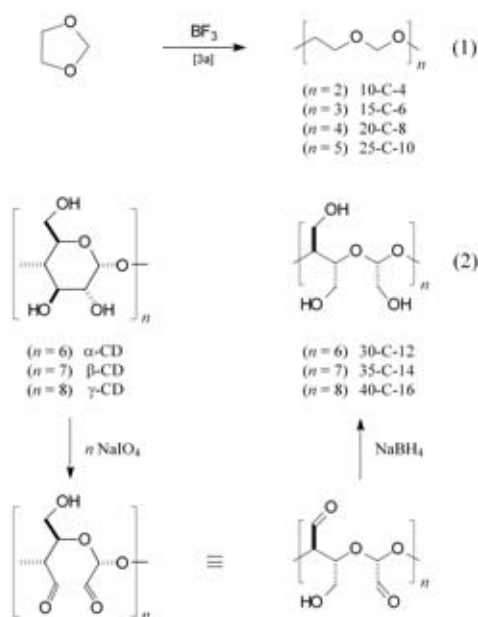
Figure 1. Crown acetals<sup>[7]</sup> composed of two alkanediol/formaldehyde units. Of these, only the geometries of 10-C-4<sup>[9]</sup> and 14-C-4<sup>[11]</sup> have been verified by X-ray structural analysis.

[a] Prof. Dr. F. W. Lichtenthaler, Dr. S. Immel, Prof. Dr. T. Nakagawa, Prof. Dr. H. J. Lindner  
Institut für Organische Chemie, Technische Universität Darmstadt  
Petersenstrasse 22, 64287 Darmstadt (Germany)  
Fax: (+49) 6151-166674  
E-mail: fwlicht@sugar.oc.chemie.tu-darmstadt.de

<sup>#</sup> Presented in part at the 10th International Cyclodextrin Symposium Ann Arbor, Michigan (USA), May 2000; Abstract 1-04.  
Part 26: S. Immel, F. W. Lichtenthaler, H. J. Lindner, K. Fujita, M. Fukudome, Y. Nogami, *Tetrahedron: Asymmetry* **2000**, *11*, 27–36.

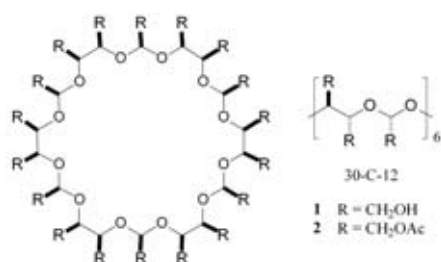
Supporting information for this article is available on the WWW under <http://caramel.oc.chemie.tu-darmstadt.de/imm/3Dstructures.html> (3D structures of Figure 2) and <http://caramel.oc.chemie.tu-darmstadt.de/imm/molcad/gallery.html> (MOLCAD graphics).

unequivocal structural characterization—not surprising in view of the manifold possibilities of elaborating cyclic acetal and hemiacetal structures. Of the products ensuing from these “CD-polyaldehydes” upon chlorite oxidation<sup>[15]</sup> and borohydride reduction,<sup>[16]</sup> only the per-hydroxymethylated 30-crown-12 and 35-crown-14 polyacetals—prepared from  $\alpha$ - and  $\beta$ -CD in modest yields—have been unequivocally characterized as such and as their per-*O*-acetates,<sup>[16a]</sup> yet the sparse NMR data provided gave no clues as to their molecular geometries.



Scheme 1. Synthetic access to large ring crown acetals with repetitive C-C-O-C-O-fragments in their skeletal backbones. *Top*: Systems with two to five ethyleneglycol/formaldehyde units<sup>[3a]</sup> [Eq. (1)]. *Lower part*: cyclodextrin-derived substituted analogues composed of six, seven, and eight consecutive D-erythrose/glyoxal<sup>[14]</sup> or—upon hydride reduction—*meso*-butanetetrol/glycolaldehyde segments [Eq. (2)].

Our past interest in the generation of flexible cyclooligosaccharide hosts<sup>[17]</sup> to mimic the induced-fit mode<sup>[18]</sup> rather than the rigid lock-and-key principle<sup>[19]</sup> has led presently to the preparatively satisfactory, high-yield preparation of the  $\alpha$ -cyclodextrin-derived 30-crown-12 polyacetal **1** composed of six consecutive *meso*-butanetetrol/glycolaldehyde acetal units, and to the unravelment of its molecular geometry through an X-ray structural analysis of its octadeca-acetate **2**.



## Results and Discussion

Of the three native cyclodextrins readily accessible,  $\alpha$ -cyclodextrin ( $\alpha$ -CD), with six  $\alpha$ -(1  $\rightarrow$  4)-linked glucose units the smallest, undergoes periodate oxidation of its diol functionalities slowest,<sup>[14]</sup> yet when reacted with a 3.0 molar excess of oxidant for 11 d at  $\approx 0^\circ\text{C}$ , the conversion was complete. The resulting polyaldehyde, due to its manifold possibilities of forming hemiacetals and/or hemialdal hydrates, was only characterized as a chromatographically uniform powder, and then subjected to reduction with sodium borohydride in methanol to provide the octadeca-hydroxymethyl 30-crown-12 polyacetal **1**. Its characterization in pure form is best accomplished by in situ acetylation to yield its well-crystallizing, octadeca-acetate **2** (92% based on  $\alpha$ -CD) and subsequent Zemplén deacetylation. Neither **1** nor **2** showed any rotational value—expectedly, since the six butanetetrol units generated from  $\alpha$ -CD by the periodation–reduction sequence have *erythro*-configuration and erythritol is a *meso*-compound.

Invited by the high crystallinity of the 30-crown-12 polyacetal **2**, an X-ray structural analysis could be performed (Figure 2), which revealed the unique conformational intricacies of the 30-membered macrocycle: The ring adopts a three-loop shape, which is not planar but assumes a distinct undulating form. The ring symmetry is reduced from  $C_{6v}$  to approximately  $C_3$ , with the six acetoxyethyl groups of the glycolaldehyde acetal units pointing alternately above and below the mean-plane of the macrocyclic backbone. In addition, each of the six pairs of vicinal acetoxyethyl groups of the *meso*-butanetetrol units features one OAc group pointing towards the front, and the next directed to the rear relative to the ring periphery. As is lucidly borne out by the color representations of Figure 2 and particularly by the side-view ribbon model therein, a total of nine acetoxyethyl groups point away from either side of the macrocyclic backbone in an alternating fashion. This entails for the crown acetal **2** a compact, nearly cylindrical overall shape. Albeit **2** was crystallized from EtOH, the crystals do not contain any residual solvent since the molecular packing is very tight and the center of the molecule seems to be inaccessible for any guest. As detailed in Figure 2 (bottom plots), the three-looped structure is caused by a characteristic alternating *gauche*- and *anti*-arrangement for the O-C-C-O-torsion angles of the six *meso*-butanetetrol units, a conformational feature that was translated into a conventional formula drawing in Figure 3.

As **2** itself is an achiral compound with an achiral space group (monoclinic,  $Pn$ ), each unit cell contains two symmetry related formula units of **2**, one being the exact mirror geometry of the other. Thus, the *meso*-butanetetrol units in the solid-state geometry of **2** adopt either successive (+)-*gauche/anti*- or (–)-*gauche/anti*-conformations, of which only the former are shown in Figure 2. The ring torsion angles  $\theta_1 - \theta_5$  for each *meso*-butanetetrol/glycolaldehyde unit *A–F* of the 30-membered macroring are listed in Table 1: Of these values,  $\theta_3$  reflects directly the alternating *gauche/anti*-arrangements described above, whilst the other torsion angles display less pronounced fluctuations only.

Although the 30-crown-12 macrocycle is anticipated to be quite flexible in solution, both temperature dependent <sup>1</sup>H-



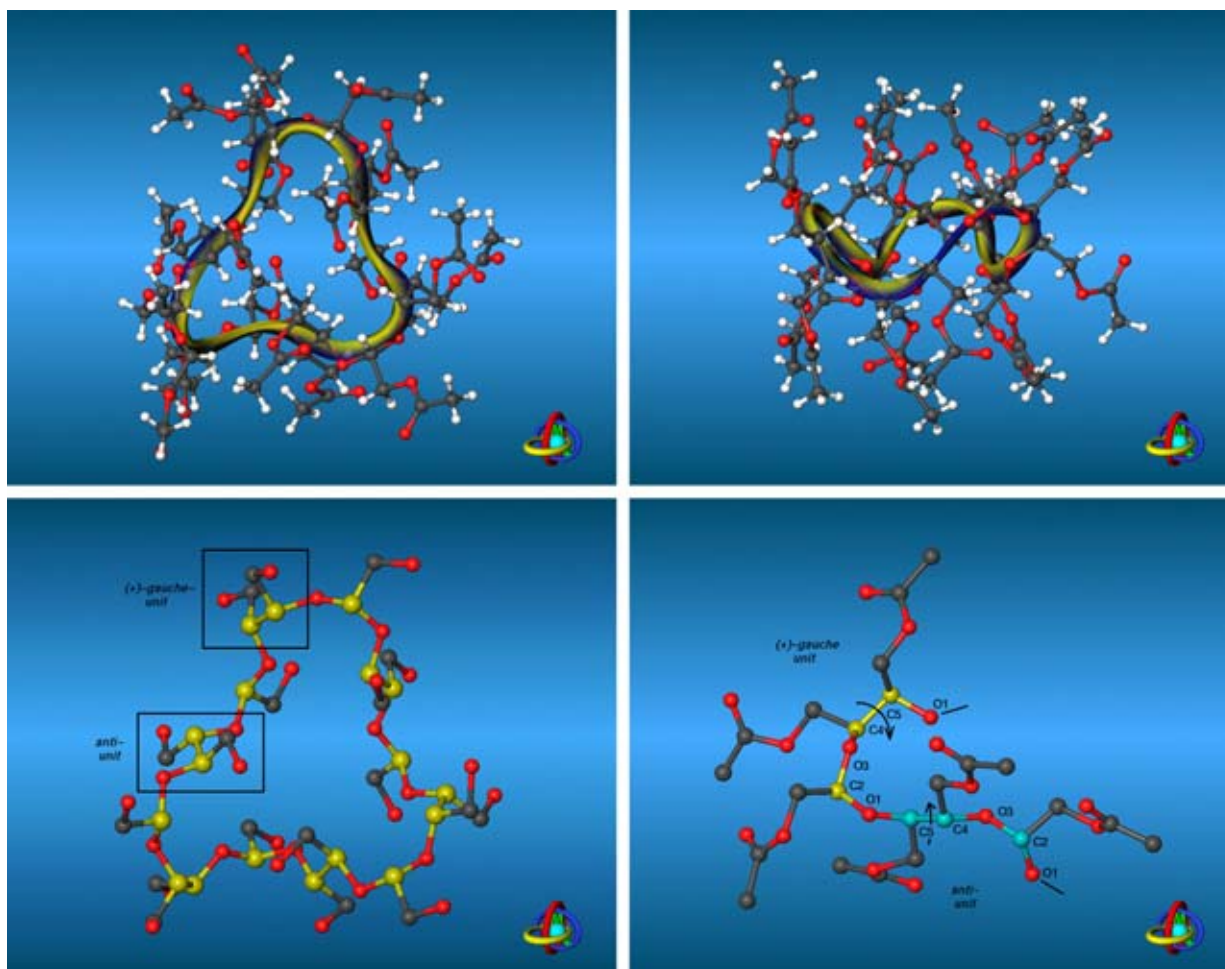


Figure 2. Solid-state topography for the asymmetric unit of the octadeca-(acetoxymethyl)-30-crown-12 polyacetal **2** in ball-and-stick type representations. *Top*: Ribbon models of the macrocyclic core, amply illustrating its three-looped shape, which, as shown in the side view (left), is not planar but adopts an undulatory form with the yellow-blue coloring of the braid; this indicates the twist of the backbone. In the crystal lattice, two formula units of achiral **2**—the geometry shown here and its symmetry related mirror image—occupy each unit cell. *Bottom*: Accentuation of the skeletal backbone of the 30-membered macrocycle (left) with acetyl groups and hydrogens omitted for clarity and all ring carbon atoms marked yellow; the molecular orientation corresponds to the top left plot. The *meso*-butanetetrol units are successively in *gauche*- and *anti*-arrangements (as labeled), whereas the acetoxymethyl groups of the six glycolaldehyde units are alternatingly directed towards both sides of the macrocycle. On the right, a single-loop segment of the macrocycle is enlarged, with one (+)-*gauche meso*-butanetetrol/glycolaldehyde unit colored yellow and atoms labeled; in the following -OCCOCO- repeating unit, of which the carbon atoms are in green color, the butanetetrol unit is in *anti*-arrangement.

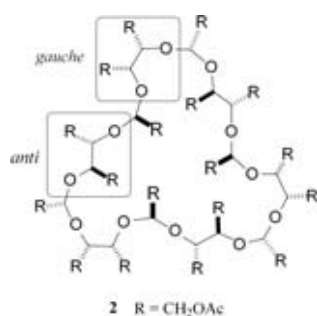


Figure 3. Conventional formula drawing of the crown acetal **2** in the same orientation as given in the left plots of Figure 2 to visualize the successive *gauche/anti*-arrangements of the *meso*-butanetetrol units.

and  $^{13}\text{C}$ -NMR patterns in  $\text{CD}_2\text{Cl}_2$  and  $\text{C}_2\text{D}_2\text{Cl}_4$ , point towards the overall shape of the solid-state conformation being largely retained in these solvents. At ambient temperature ( $24^\circ\text{C}$ ) the individual ring protons, that is the acetalic hydrogen H-2, the

secondary hydrogens of the butanetetrol units (cf.  $^1\text{H}$  NMR in Figure 4), and the ring carbons C-2, C-4, and C-5 ( $^{13}\text{C}$  NMR) are largely unresolved and display unusually broad signals. At elevated temperatures (up to  $+100^\circ\text{C}$ ), the NMR spectra (in  $\text{C}_2\text{D}_2\text{Cl}_4$ ) exhibit one set of signals consistent with a time-averaged  $C_{6v}$  symmetrical structure of **2**: a single low-field triplet for H-2, chemically equivalent resonances for H-4, H-5, and 4,5- $\text{CH}_2$ , and the 2- $\text{CH}_2$  signals (although 4,5- $\text{H}^{\text{A}}$  and 4,5- $\text{H}^{\text{B}}$  are magnetically nonequivalent and thus, largely separated). The acetyl resonances are resolved into two peaks with an integral ratio of 12:6 for the *meso*-butanetetrol and glycolaldehyde units ( $^1\text{H}$  NMR in Figure 4, the  $^{13}\text{C}$ -NMR spectra display analogous characteristics). At lower temperatures ( $-90$  to  $0^\circ\text{C}$  in  $\text{CD}_2\text{Cl}_2$ ), all signals are significantly broadened or split; most notably the H-2 protons are clearly split at  $-60^\circ\text{C}$  into two triplets (cf. Figure 4), and the acetyl groups split into four peaks with a ratio of 6:6:3:3. Below  $-60^\circ\text{C}$  the C-4 and C-5 signals are separated into a total of four peaks. All of these data are consistent with the

Table 1. Succession of 30 ring torsion angles in the solid-state geometry of the 30-crown-12 acetal **2** with estimated standard deviations in parenthesis.<sup>[a]</sup>

Torsion angles [°]	$\Theta_1$ O1-C2-O3-C4	$\Theta_2$ C2-O3-C4-C5	$\Theta_3$ O3-C4-C5-O1'	$\Theta_4$ C4-C5-O1'-C2'	$\Theta_5$ C5-O1'-C2'-O3'
A	119.3(7)	-148.7(6)	71.6(8)	161.8(7)	-115.7(7)
B	98.9(7)	-147.3(6)	-170.0(5)	135.6(6)	-80.7(7)
C	136.3(6)	-136.8(6)	65.9(7)	148.6(6)	-127.4(7)
D	82.2(7)	-145.1(6)	-173.0(6)	160.5(6)	-64.7(8)
E	116.2(7)	-142.9(7)	70.1(7)	150.7(7)	-99.0(8)
F	109.5(7)	-144.4(7)	-171.6(6)	146.9(7)	-65.4(9)

[a] Torsions are listed in row-column order, equivalent torsions for **2** are listed in columns; the atom numbering Scheme corresponds to Figure 4 (i.e., [-O1-C2-O3-C4-C5]<sub>6</sub> with units labeled A–F for the 30-membered macroring), primed atom designators refer to the neighboring unit. The torsion angles  $\Theta_1$  and  $\Theta_5$ , as well as  $\Theta_2$  and  $\Theta_4$  are chemically equivalent (clockwise and anti-clockwise ring numbering, symmetry  $C_{6v}$ ); the alternating *gauche*–*trans* sequence of units in **2** is manifested through the O–C–C–O-torsion angle of the *meso*-butanetetrol units ( $\Theta_3$ ). All torsion angles are listed for one molecule of **2** contained in the unit cell only, the second molecule being the exact mirror image of the former with all torsion angles of opposite sign, respectively.

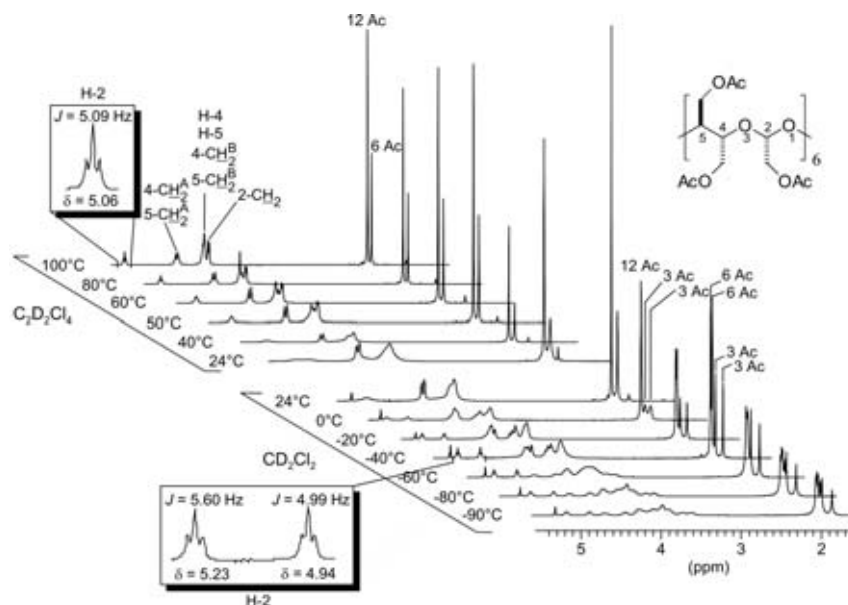


Figure 4. <sup>1</sup>H NMR (300 MHz) spectral patterns of **2** at different temperatures recorded in CD<sub>2</sub>Cl<sub>2</sub> ( $T = -90$ – $+24$  °C) and C<sub>2</sub>D<sub>2</sub>Cl<sub>4</sub> ( $T = +24$ – $+100$  °C). At  $-60$  °C the H-2 resonances of the glycolaldehyde acetal protons are separated into two triplets with equal populations, whereas at  $100$  °C both signals collapse into a single triplet (see box insertions and enlarged spectra); coalescence is observed at about room temperature. The very broad low-temperature ( $-90$  °C) signals between  $\delta = 3.5$ – $4.7$  evolve into sharply resolved single peaks at above  $50$  °C, as the acetyl group resonances start to form separate singlets with an integral ratio of 12:6 (i.e., twelve equivalent OAc groups at C-4 and C-5 versus six glycolaldehyde OAc residues).

notion that the solid-state geometry of **2** is largely retained in solution as the succession of *anti*- and ( $\pm$ )-*gauche*-*meso*-butanetetrol units reduces the ring symmetry and accounts for the NMR patterns observed.

At higher temperatures the *gauche*  $\leftrightarrow$  *anti* transitions are sufficiently fast and display the time-averaged patterns, whereas at lower temperatures **2** starts to freeze into its solid-state geometry. The coalescence temperature  $T_C$  for the H-2 and C-2 resonances is observed at about room temperature, although the solvent had to be changed at around  $24$  °C. From the low-temperature separation of the signals, and dynamic NMR line shape analysis,<sup>[20]</sup> the rough estimate  $T_C \approx 290 \pm 25$  K yields an activation barrier of approximately  $\Delta G^\ddagger \approx 60 \pm 5$  kJ mol<sup>-1</sup> for the *gauche*  $\leftrightarrow$  *anti* transitions of the

butanetetrol segments within the macroring. The strait-jacket of the macrocycle obviously favors low-symmetry conformations energetically over all-*gauche* or all-*anti* arrangements, with the conformational transitions occurring in a cooperative fashion. Hence, the solid-state geometry of **2** can be considered a realistic snapshot over the state in solution.

## Conclusion

The solid-state structure of the per-acetoxymethyl-substituted 30-C-12 crown acetal **2** detailed herein provides the second X-ray diffraction study of a 30-membered crown compound, the first being the simple aliphatic 30-C-10 crown ether.<sup>[21]</sup> A comparison of their molecular geometries is interesting in such as they are distinctly different—not unexpected as -OCH<sub>2</sub>CH<sub>2</sub>O- units in crown ethers and the respective -OCH<sub>2</sub>CH<sub>2</sub>OCH<sub>2</sub>O- units in the crown acetal are apt to follow different crystal engineering patterns. Thus, whilst the 30-membered ring in crown acetal **2** adopts an undulating three-loop shape (Figure 2), the 30-C-10 crown ether macrocycle organizes itself in a planar, rectangular form, characterized by the bridging of two parallel sets of three -OCH<sub>2</sub>CH<sub>2</sub>- units in *anti*-arrangement with two *gauche*-oriented ethylenedioxy units on either end in a handle-

like fashion (Figure 5).<sup>[21]</sup> In solution, however, both macrocycles are highly flexible and thus capable of elaborating variously sized cavities, which in their size can adapt to the size of the potential guest molecules or cations to be incorporated. In the case of 30-C-10 this has been already evidenced by the X-ray structure of its tetrahydrate, which has the four water molecules located inside the substantially widened macrocycle.

Attempts to induce the 30-C-12 crown acetals **1** and **2** to form inclusion compounds, as of now, have not been successful. More favorable in this respect are the  $\beta$ -CD- and  $\gamma$ -CD-derived 35-C-14 and 40-C-16 crown acetal analogues of **1** and **2**. The prospects for their acquisition in a form suitable for X-ray structural investigations appear to be favorable, as

## FULL PAPER

F. W. Lichtenhaler et al.

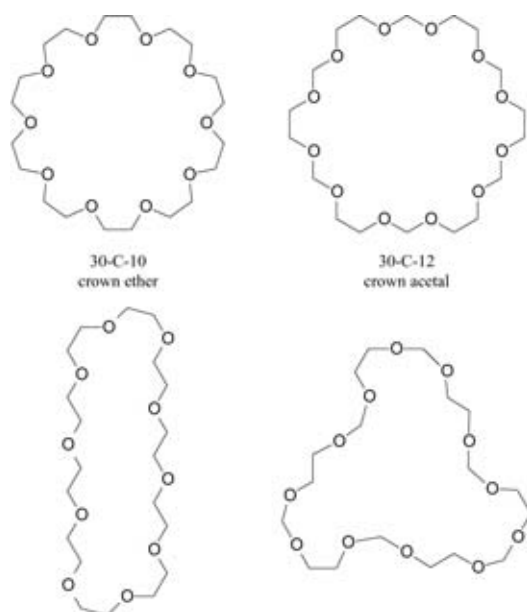


Figure 5. Solid-state molecular geometries of the 30-membered macrocycles in a 30-C-10 crown ether<sup>[21]</sup> and in the 30-C-12 crown acetal detailed herein, that is a planar rectangular shape versus an undulated three-looped structure.

the  $\beta$ -CD- and  $\gamma$ -CD derived analogue of **2**, that is the peracetoxymethyl-substituted 35-crown-14 and 40-crown-16 polyacetals with seven and eight CCOCO-units in the macrocyclic core, have already been crystallized (m.p. 109–111 and 143.5–145 °C). The solid-state molecular geometry of the crown acetal with the “uneven” (seven) *meso*-butanetetrol/glycolaldehyde acetal units may be predicted to resemble that of **2**, with the “uneven” unit inserted in *gauche*-orientation into the alternating *gauche/anti*-arrangements, inasmuch as two successive *anti*-disposed glycol fragments would inflict considerable strain into the macrocycle. For the  $\gamma$ -CD-derived 40-C-16 crown acetal analogues of **1** and **2**, however, we envisage an undulated four-loop structure, not unlike the shape of a four-leaf clover. We hope to be in a position to report on these issues in the near future.

## Experimental Section

**Octadeca-(acetoxymethyl)-30-crown-12 polyacetal (2)**:<sup>[22]</sup>  $\alpha$ -Cyclodextrin (1.95 g, 2.00 mmol) was added to a stirred and cooled (0–5 °C) aqueous solution of NaIO<sub>4</sub> (3.85 g, 18.0 mmol, in 90 mL) and the clear solution was kept at 0 °C in a dark ice-box for 11 d, whereafter TLC revealed a single spot ( $R_f = 0.64$ , 2:2:1 *n*BuOH/MeOH/water) of the dodeca-aldehyde (in one of the various hemiacetal and/or hemialdal hydrate forms possible). Then, 1,2-ethanediol (0.34 mL, 6.1 mmol) was added while stirring to decompose excess NaIO<sub>4</sub>, the mixture was kept in a dark ice-box overnight, and an aqueous BaCl<sub>2</sub> solution (1.90 g, 9.12 mmol, in 10 mL) was added to the mixture. The solution as allowed to stand for a few hours at ambient temperature, and the resulting precipitate was filtered off, followed by evaporation of the filtrate to dryness in vacuo. The residue was suspended in dry MeOH (20 mL), kept in a refrigerator overnight, the solids were filtered off upon addition of charcoal, and the filtrate was evaporated to dryness in vacuo at  $\approx 35$  °C. This procedure was repeated twice to give a white powder (2.33 g), which was dissolved in MeOH/water (40 mL, 3:1). Upon cooling (0 °C) NaBH<sub>4</sub> (600 mg) was added while stirring and the mixture was kept at room temperature overnight. Addition of acetone

(3 mL) to remove excess reagent, neutralization with cation-exchange resin (IR 120, H<sup>+</sup> form), evaporation to dryness, and several co-evaporations of the residue from dry MeOH left the polyol **1** as a colorless solid. Polyol **1** was dissolved in a mixture of Ac<sub>2</sub>O (15 mL) and pyridine (30 mL), and stirred overnight at room temperature. Subsequent evaporation to dryness in vacuo at 40 °C, followed by co-evaporation with toluene (3  $\times$  25 mL) afforded a syrup which was dissolved in hot EtOAc, treated with charcoal, filtered, and evaporated to dryness. The residue was crystallized by trituration with EtOAc/EtOH, affording **2** (3.20 g, 92 %) as colorless plates of m.p. 171–173 °C. Lit.:<sup>[16a]</sup> m.p. 162–164 °C; yield 0.6%.  $[\alpha]_D^{25} = 0.00$  ( $c = 2$ , CHCl<sub>3</sub>); <sup>1</sup>H NMR (300 MHz, C<sub>2</sub>D<sub>2</sub>Cl<sub>4</sub>, 100 °C):  $\delta = 5.06$  (t, 6H,  $J = 5.1$  Hz, 2-H), 4.40 (dd, 12H,  $J = 8.6, 4.0$  Hz, 4-CH<sub>2</sub><sup>A</sup>, 5-CH<sub>2</sub><sup>A</sup>), 4.15–4.03 (brm, 24H, 4-H, 4-CH<sub>2</sub><sup>B</sup>, 5-H, 5-CH<sub>2</sub><sup>B</sup>), 4.01 (d,  $J = 5.1$  Hz, 12H, 2-CH<sub>2</sub>), 2.03 (s, 36H, 12AcCH<sub>3</sub>), 1.98 (s, 18H, six 2-AcCH<sub>3</sub>); <sup>13</sup>C NMR (75 MHz, C<sub>2</sub>D<sub>2</sub>Cl<sub>4</sub>, 100 °C):  $\delta = 170.4, 170.3$  (AcCO), 101.4 (C-2), 77.1 (4-CH<sub>2</sub>, 5-CH<sub>2</sub>), 65.0 (2-CH<sub>2</sub>), 64.2 (C-4, C-5); for other temperatures, see Figure 4; ESI-MS:  $m/z$ : 1763.5 [ $M + Na$ ]<sup>+</sup>; C<sub>72</sub>H<sub>108</sub>O<sub>48</sub> (1741.6): calcd C 49.65, H 6.25; found C 49.29, H 6.18.

Crystals suitable for X-ray analysis were obtained by slow crystallization of **2** from EtOH containing a small amount of EtOAc. A colorless crystal of dimensions 0.55  $\times$  0.20  $\times$  0.18 mm was analyzed on a Enraf-Nonius CAD-4 diffractometer using graphite-monochromated MoK $\alpha$  ( $\lambda = 0.71093$  Å) radiation. Crystal data of **2**: C<sub>72</sub>H<sub>108</sub>O<sub>48</sub>,  $M_r = 1741.59$  g mol<sup>-1</sup>, monoclinic, space group  $Pn$ ,  $a = 15.729(2)$ ,  $b = 12.757(1)$ ,  $c = 22.333(5)$  Å,  $\beta = 96.04(2)$ ,  $V = 4456.3(12)$  Å<sup>3</sup>,  $Z = 2$ ,  $\rho = 1.298$  g cm<sup>-3</sup>,  $\mu(\text{MoK}\alpha) = 0.103$  mm<sup>-1</sup>,  $T = 298(2)$  K. Of 7333 reflections collected, 7333 are independent ( $R_{\text{int}} = 0.0000$ ). The structure was solved by direct methods (SHELXS-86)<sup>[23]</sup> and successive synthesis. Refinement (on  $F^2$ ) was performed by full-matrix least squares method with SHELXL-97.<sup>[23]</sup>  $R(F) = 0.0608$  for reflections with  $I \geq 2\sigma I$ ,  $\omega R(F^2) = 0.2022$  for all 7333 reflections ( $\omega = 1/[\sigma^2(F_o^2) + (0.1293P)^2 + 2.3009P]$ ; where  $P = (F_o^2 + 2F_c^2)/3$ ); goodness-of-fit on  $F^2$ :  $S = 1.045$ . All non-hydrogen atoms were refined anisotropically; hydrogen atoms were considered in calculated positions with the 1.2  $U_{\text{eq}}$  value of the corresponding bound atom. Graphics of Figure 2 were generated using the MolArch<sup>+</sup> program.<sup>[24]</sup>

Crystallographic data (excluding structure factors) for the structure **2** reported in this paper have been deposited with the Cambridge Crystallographic Data Centre as supplementary publication no. CCDC-143715. Copies of the data can be obtained free of charge on application to CCDC, 12 Union Road, Cambridge CB21 1EZ, UK (fax: (+44) 1223-336-033; e-mail: deposit@ccdc.cam.ac.uk).

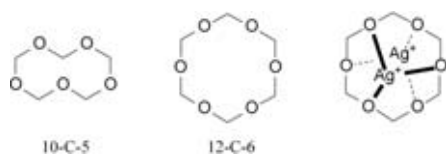
**Octadeca-(hydroxymethyl)-30-crown-12 polyacetal (1)**:<sup>[22]</sup> A few drops of 2*N* methanolic sodium methoxide were added to a solution of octadeca-acetate **2** (2.75 g, 1.58 mmol) in dry MeOH (50 mL) and the mixture was stirred at room temperature overnight. After neutralization with IR-120 (H<sup>+</sup> form) the solution was evaporated to dryness in vacuo, and the residue was crystallized from 1-propanol as colorless plates (1.30 g, 84 %); m.p. 200–203 °C; <sup>1</sup>H NMR (300 MHz, [D<sub>6</sub>]DMSO):  $\delta = 4.92$  (t, 6H,  $J = 5.6$  Hz, 2-OH), 4.88 (t, 6H,  $J = 4.9$  Hz, 2-H), 4.65 (t, 12H,  $J = 5.4$  Hz, 4-OH, 5-OH), 3.84 (brs, 12H, 4-H, 5-H), 3.65–3.45 (m, 24H, 4-CH<sub>2</sub>, 5-CH<sub>2</sub>), 3.45–3.37 (br t,  $J = 5.0$  Hz, 2-CH<sub>2</sub>); <sup>13</sup>C NMR (75 MHz, [D<sub>6</sub>]DMSO):  $\delta = 103.2$  (C-2), 78.3 (4-CH<sub>2</sub>, 5-CH<sub>2</sub>), 63.1 (2-CH<sub>2</sub>), 60.9 (C-4, C-5); ESI-MS:  $m/z$ : 1007.6 [ $M + Na$ ]<sup>+</sup>; C<sub>36</sub>H<sub>72</sub>O<sub>30</sub> · 1.5H<sub>2</sub>O (1012.0): calcd C 42.73, H 7.47; found: C 42.69; H 7.52.

## Acknowledgement

Appreciation is expressed to the Fonds der Chemischen Industrie, Frankfurt, and the Südzucker AG, Mannheim/Ochsenfurt, for financial support. Our thanks are also due to Wacker-Chemie, Burghausen, for a gift of  $\alpha$ -cyclodextrin, and to Mrs. Sabine Foro for collecting the crystallographic data.

- [1] *Comprehensive Supramolecular Chemistry, Vol. 1* (Ed.: G. W. Gokel), Pergamon/Elsevier, 1996, p. 850.
- [2] C. J. Pedersen, *J. Am. Chem. Soc.* **1970**, *92*, 391–394.
- [3] a) Y. Kawakami, Y. Yamashita, *Macromolecules* **1977**, *10*, 837–839; b) Y. Kawakami, J. Suzuki, Y. Yamashita, *Polym. J.* **1977**, *9*, 519–524;

- c) Y. Kawakami, T. Sugiura, Y. Yamashita, *Bull. Chem. Soc. Jpn.* **1978**, *51*, 3053–3056.
- [4] V. Gold, C. M. Sghibartz, *J. Chem. Soc. Perkin Trans. 1* **1983**, 453–457; D. S. Baker, V. Gold, C. M. Sghibartz, *J. Chem. Soc. Perkin Trans. 2* **1983**, 1121–1128.
- [5] T. Oshima, R. Nishioka, S. Ueno, T. Nagai, *J. Org. Chem.* **1982**, *47*, 2114–2117; T. Oshima, T. Nagai, *Bull. Chem. Soc. Jpn.* **1986**, *59*, 3979–3980; T. Oshimura, F. Matsuda, K. Fukushima, H. Tamura, G. Matsubayashi, R. Arakawa, *J. Chem. Soc. Perkin Trans. 2* **1998**, 145–148.
- [6] M. Ouchi, Y. Inoue, T. Kanzaki, T. Hakushi, *Bull. Chem. Soc. Jpn.* **1984**, *57*, 887–888; Y. Inoue, M. Ouchi, T. Hakushi, *Bull. Chem. Soc. Jpn.* **1985**, *58*, 525–530.
- [7] *Nomenclature*: Although macrocyclic polyacetals, such as **1** or its peracetate **2**, do not adopt a crown-like molecular geometry—the terminology for macrocyclic ethers was derived from their crown-like shape—it appears not only logical but practical to extend this well-introduced notational mode to the acetal analogues of crown ethers, resulting in the term *crown acetals* for macrocycles with acetal oxygens only; similarly adapting the description established for ring size and number of oxygens, **2** is the octadeca-(hydroxymethyl) derivative of a 30-crown-12 polyacetal, the  $\beta$ -CD- and  $\gamma$ -CD-derived analogues are macrocycles with a 35-crown-14 and 40-crown-16 skeletal backbone.
- [8] a) The cyclic pentamer and hexamer of formaldehyde—abbreviated in correspondence to crown ether terminology as 10-C-5 and 12-C-6, respectively—are neither crown ethers nor crown acetals, but de facto *crown aldals*,<sup>[8b]</sup> as they originate from the reaction between two aldehydes rather than between two diols or between an aldehyde and a diol.



Whilst the X-ray-confirmed molecular geometries of 10-C-5<sup>[8c]</sup> and 12-C-6<sup>[8d]</sup> show close analogies to those of the crown acetals of the same ring size, their cation binding capabilities are apt to be different, as evidenced, for example, by the unique di-silver ion complex of 12-C-6.<sup>[8e]</sup> b) The terms aldal, hemialdal, and hemialdal hydrate are commonly used in carbohydrate chemistry to denote the various forms adopted by sugar-derived dialdehydes: R. D. Guthrie, *Adv. Carbohydr. Chem.* **1970**, *16*, 118–140; c) Y. Chatani, K. Kitahama, *Bull. Chem. Soc. Jpn.* **1973**, *46*, 2300–2305; d) Y. Chatani, T. Ohno, T. Yamauchi, Y. Miyake, *J. Polym. Sci. Polym. Phys.* **1973**, *11*, 369–373; e) H. W. Roesky, E. Peymann, J. Schimkowiak, M. Noltemeyer, W. Pinkert, G. M. Sheldrick, *J. Chem. Soc. Chem. Commun.* **1983**, 981–982.

[9] I. W. Bassi, R. Scordamaglia, L. Fiori, *J. Chem. Soc. Perkin Trans. 2* **1975**, 1129–1132. For the dicyclohexano-10-C-4 analogue see: A. Terzis, T. B. Grindley, J. B. Faught, *Can. J. Chem.* **1976**, *55*, 2692–2699;

- A. Terzis, T. B. Grindley, *Can. J. Chem.* **1979**, *57*, 2154–2157. Some hydroxymethyl- and/or methyl-substituted 10-C-4 crown acetals have been prepared from dianhydrides of ribose (J. F. Stoddart, W. A. Szarek, *Can. J. Chem.* **1968**, *46*, 3061–3069) and allose (R. G. S. Grindley, J. F. Stoddart, D. M. Vyas, W. A. Szarek, *Carbohydr. Res.* **1974**, *32*, 279–285).
- [10] G. Borgen, J. Dale, *J. Chem. Soc. Chem. Commun.* **1974**, 484–485; J. Dale, *Tetrahedron* **1974**, *30*, 1683–1694.
- [11] I. W. Bassi, R. Scordamaglia, L. Fiori, *J. Chem. Soc. Perkin Trans. 2* **1972**, 1726–1729.
- [12] J. Dale, T. Ekeland, *Acta Chem. Scand. Ser. A* **1973**, *27*, 1519–1525; P. Groth, *Acta Chem. Scand. Ser. A* **1975**, *29*, 642–643.
- [13] J. W. Hill, W. H. Carothers, *J. Am. Chem. Soc.* **1935**, *57*, 925–928.
- [14] a) D. French, R. J. McIntyre, *J. Am. Chem. Soc.* **1950**, *72*, 5148–5150; b) M. Hisamatsu, Y. Yamada, K. Nakashima, K. Tobata, *Starch/Stärke* **1992**, *44*, 188–191.
- [15] M. S. Nieuwenhuizen, A. P. G. Kieboom, H. van Bekkum, *Starch/Stärke* **1985**, *37*, 192–197.
- [16] a) J. F. Stoddart, W. A. Szarek, J. K. N. Jones, *Can. J. Chem.* **1969**, *47*, 3213–3215; b) L. Kandra, A. Lipták, I. Jodál, P. Nánási, J. Szejtli, *J. Inclusion Phenom.* **1984**, *2*, 869–875.
- [17] a) Y. Nogami, K. Nasu, T. Koga, K. Ohta, K. Fujita, S. Immel, H. J. Lindner, G. E. Schmitt, F. W. Lichtenthaler, *Angew. Chem.* **1997**, *109*, 1987–1991; *Angew. Chem. Int. Ed. Engl.* **1997**, *36*, 1899–1902; b) K. Fujita, W.-H. Chen, D.-Q. Yuan, Y. Nogami, T. Koga, T. Fujioka, K. Mihashi, S. Immel, F. W. Lichtenthaler, *Tetrahedron: Asymmetry* **1999**, *10*, 1689–1696; c) S. Immel, K. Fujita, F. W. Lichtenthaler, *Chem. Eur. J.* **1999**, *5*, 3185–3192; d) H. Gohlke, S. Immel, F. W. Lichtenthaler, *Carbohydr. Res.* **1999**, *321*, 96–104.
- [18] D. E. Koshland, Jr., *Angew. Chem.* **1994**, *106*, 2368–2372; *Angew. Chem. Int. Ed. Engl.* **1994**, *33*, 2375–2378.
- [19] a) E. Fischer, *Ber. Dtsch. Chem. Ges.* **1894**, *27*, 2985–2993; b) F. W. Lichtenthaler, *Angew. Chem.* **1994**, *106*, 2456–2467; *Angew. Chem. Int. Ed. Engl.* **1994**, *33*, 2364–2374.
- [20] a) K. Marat, *Xsim—NMR Spectral Simulation and Analysis Package*, The University of Manitoba, Winnipeg, Manitoba, Canada, **1997**; b) G. Binsch, D. Kleier, *DNMR3—Dynamic NMR Simulation of Exchange Broadened Lineshapes*, University of Notre Dame, Notre Dame, Indiana, USA, **1997**.
- [21] M. C. Bheda, J. S. Merola, W. A. Woodward, V. J. Vesudevan, H. W. Gibson, *J. Org. Chem.* **1994**, *59*, 1694–1702.
- [22] Systematic name for **1**: 2,4,5,7,9,10,12,14,15,17,19,20,22,24,25,27,29,30-octadeca-(hydroxymethyl)-1,3,6,8,11,13,16,18,21,23,26,28-dodecaoxacyclotriacontane; the polyacetal **2**, correspondingly, is the octadeca-acetate thereof.
- [23] G. M. Sheldrick, *SHELXS-86 and SHELXL-97—Programs for Crystal Structure Solution and Refinement*, University of Göttingen, Germany, **1990** and **1997**.
- [24] S. Immel, *MolArch+—MOLEcular ARCHitecture Modeling Program*, Darmstadt University of Technology, Germany, **1999**.

Received: May 8, 2000 [F2359]



Pergamon

Tetrahedron: Asymmetry 12 (2001) 2767–2774

TETRAHEDRON:  
ASYMMETRY

# Hydroxymethyl-substituted crown acetals with 35-C-14 and 40-C-16 skeletal backbones: synthesis and molecular geometries<sup>†</sup>

Stefan Immel,\* Frieder W. Lichtenthaler, Hans J. Lindner and Toshio Nakagawa

Institut für Organische Chemie, Technische Universität Darmstadt, D-64287 Darmstadt, Germany

Received 18 October 2001; accepted 19 October 2001

**Abstract**—An oxidation/reduction sequence readily converts  $\beta$ - and  $\gamma$ -cyclodextrin into hydroxymethyl-substituted crown acetals with 35-C-14 and 40-C-16 skeletal cores. X-Ray analysis of their well crystallizing peracetates reveals the 40-membered ring of the  $\gamma$ -CD derived octaacetal to mould into an undulated four-loop structure with alternating *gauche* and *anti*-conformations of the eight *meso*-butanetetrol units, the overall shape resembling a four-leaf clover. In the  $\beta$ -CD derived, 35-membered crown heptaacetal, six of the seven glycolaldehyde/butanetetrol segments are lined up in alternating *gauche/anti* arrangements with the seventh, uneven unit inserted in *gauche* orientation. In solution, however, the macrocycles are highly flexible as evidenced by their  $^1\text{H}$  and  $^{13}\text{C}$  NMR spectra, which at 300 K show only one set of signals for the respective -CHR-CHR-O-CHR-O- units ( $\text{R} = \text{CH}_2\text{OH}$  or  $\text{CH}_2\text{OAc}$ ). © 2001 Elsevier Science Ltd. All rights reserved.

## 1. Introduction

Macrocycles exclusively containing acetal oxygens, and hence, deserving the designation *crown acetal*,<sup>2</sup> are rare, the presently known examples being limited to systems with one<sup>3</sup> or two<sup>4</sup> formaldehyde/alkanediol acetal units, i.e. containing only two or four oxygens in the ring.<sup>5</sup> Cycloacetals with a higher number of ring oxygen atoms, albeit never considered as such, happen to be the products generated by periodate oxidation of cyclic oligosaccharides. The polyaldehydes derived from  $\alpha$ -,  $\beta$ -, and  $\gamma$ -cyclodextrin<sup>6</sup> de facto constitute macrocycles with 30-crown-12, 35-crown-14, and 40-crown-16 skeletal backbones, yet have eluded unequivocal structural characterization due to their manifold possibilities of elaborating cyclic acetals, hemiacetals and hemialdals. Of the products ensuing from borohydride reduction, the  $\alpha$ - and  $\beta$ -cyclodextrin-derived polyhydroxymethyl-30-C-12 and 35-C-14 crown acetals **1** and **3** have been prepared,<sup>7,8</sup> yet only the 30-membered ring of the well-crystallizing peracetate of **1**, i.e. **2**, has yielded to an X-ray analysis, unveiling the macrocycle to be molded into an undulated three-loop core with a unique order

of succession of the -CHR-CHR-O-CHR-O- units: alternating *gauche* and *anti*-conformations of the *meso*-butanetetrol portions and consecutive disposition of the glycolaldehyde-acetoxymethyl groups above and below the mean-plane of the backbone.<sup>8</sup> In solution, however, the macrocycle is highly flexible,<sup>8</sup> providing a suitable host for mimicking the induced-fit mode of molecular recognition<sup>9</sup>—rather than the rigid lock-and-key-type mechanism<sup>10</sup>—as the host can sterically adapt to a guest to be bound and incorporated. In continuation of our studies towards the generation of flexible hosts<sup>11</sup> to probe the induced-fit mode of guest inclusion, we here wish to report on the equally unique molecular geometries for the  $\beta$ - and  $\gamma$ -CD-derived crown acetals **4** and **6**.

## 2. Results and discussion

Periodate oxidation of  $\beta$ - and  $\gamma$ -CD was performed on a preparative scale (5–10 g) by keeping their aqueous solutions with a three molar excess of oxidant at 0–4°C for 5–7 days. The resulting CD-polyaldehydes obtained as chromatographically uniform powders, were subjected directly to reduction with  $\text{NaBH}_4$  in methanol, yet the polyhydroxymethyl-substituted crown acetals **3** and **5** are preferably isolated the well-crystallizing peracetates **4** and **6**, respectively, obtainable with yields in the 80–90% range based on  $\beta$ - and  $\gamma$ -CD. Subsequent

\* Corresponding author. Tel.: +49-6151-16 5277; fax: +49-6151-16 6674; e-mail: lemmit@sugar.oc.chemie.tu-darmstadt.de

<sup>†</sup> Part 29 of the series Molecular Modeling of Saccharides. For Part 28, see Ref. 1.

Zemplén deacetylation (NaOMe/MeOH) then smoothly afforded the respective polyols, i.e. the heneicosa-(hydroxymethyl)-35-crown-14 heptaacetal **3**, and its homolog, the tetraicosa-(hydroxymethyl)-40-crown-16 octaacetal **5**, both in crystalline form. None of the crown acetals prepared showed any rotational value, which was to be expected, as the butanetetrol units generated from the CDs by the periodation–reduction sequence have *erythro* configuration and erythritol is a *meso* compound (Scheme 1).

Unlike the hydroxymethyl-substituted crown acetals **3** and **5**, which as of now, only gave crystals unsuitable for X-ray analysis, their peracetates **4** and **6** did, straightforwardly unravelling their molecular geometries (cf. Fig. 1).

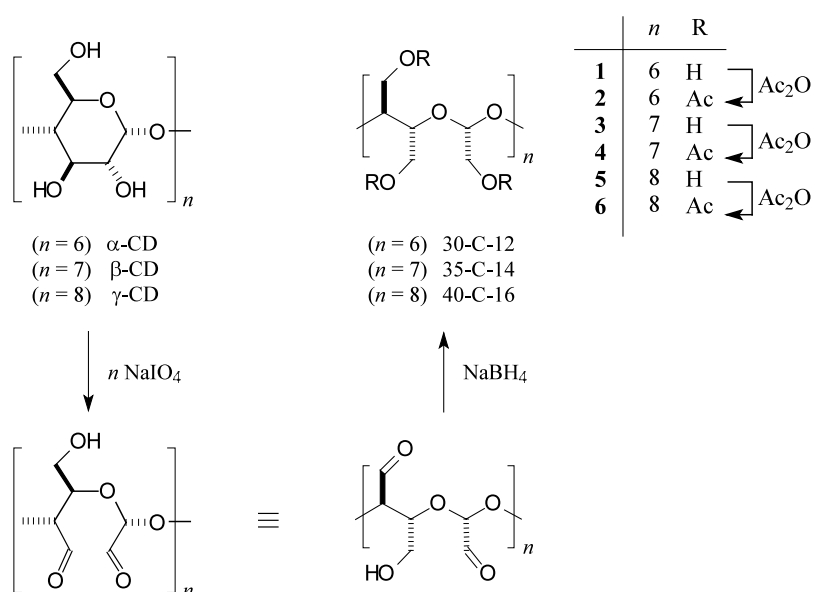
In the  $\gamma$ -CD-derived 40-C-16 octaacetal **6**, the 40-membered macrocycle is molded into four loops with the eight acetoxymethyl groups of the glycolaldehyde acetal units pointing alternately above and below the undulated mean-plane of the macrocyclic backbone. Similarly, the eight *meso*-butanetetrol units adopt alternating *gauche*- and *anti*-arrangements of their two acetoxymethyl groups (Fig. 1, top right). In this, the molecular arrangement is reminiscent of the folding of the  $\alpha$ -CD-derived 30-C-12 analog **2**, in which the 30-membered ring is organized into three loops (Fig. 1, top left). Insertion of two further -CHR-CHR-O-CHR-O- groupings (with R=CH<sub>2</sub>OAc) into the three looped 30-membered ring of **2** simply results in the elaboration of a fourth loop.

In the case of the  $\beta$ -CD-derived crown heptaacetal **4**, having seven, i.e. an uneven number of butanetetrol/glycolaldehyde segments, six of these units are lined up in alternating *gauche/anti* arrangements with the seventh residue being inserted into the macrocycle in

*gauche* conformation (Fig. 1, top center); obviously incorporation of the ‘uneven’ butanetetrol unit in an *anti*-geometry would result in two successive *anti*-disposed glycol fragments inflicting considerable strain into the macrocycle.

The center row of Fig. 1 displays a single unit cell for the solid-state structures of **2**, **4**, and **6** with a colored representation of the Hirshfeld surfaces<sup>12</sup> of each molecule. These surfaces are roughly equivalent to the solvent accessible surfaces<sup>13</sup> for each molecule, yet for crystal lattices they are obtained as non-overlapping molecular surfaces arising from partitioning of the crystal space according to the volume occupied by each molecule. The front opened forms with ball-and-stick models inserted display the unit cell of **2** (Fig. 1, center left) to contain two molecules of the 30-C-12 hexaacetal, both molecules being symmetry-related with each other ( $Z=2$ , space group  $P_n$ ) through a sliding mirror plane. Obviously, the achiral compound **2** adopts two mirror image conformations with alternating (+)-*gauche/anti* (yellow Hirshfeld surface) and (–)-*gauche/anti* (orange) arrangements, respectively. Similar conditions are observed in the structures of **4** and **6** (space groups  $\bar{P}$  and  $C2/c$ ) in which four molecules per unit cell were established: in the case of **4**, two symmetry independent molecules are correlated with their mirror image conformers through symmetry operations (Fig. 1, center), whilst for **6** (Fig. 1, center right) all four molecules are symmetry related in the crystal lattice (pair wise mirror image conformers). In particular, the ribbon models of Fig. 1 (bottom row) display the mode of stacking of the individual macrorings in the solid-state structures.

Unlike the 30-C-12 crown acetal **2**, which crystallized from 95% ethanol as such, both the 35-C-14 and 40-C-16 homolog obtained in crystalline form from the same



**Scheme 1.** Synthetic access to large ring crown acetals with repetitive C-C-O-C-O- fragments in their skeletal backbones:  $\alpha$ -,  $\beta$ -, and  $\gamma$ -cyclodextrin-derived hydroxymethyl substituted analogs composed of six, seven, and eight consecutive D-erythrose/glyoxal or—upon hydride reduction—*meso*-butanetetrol/glycolaldehyde segments.

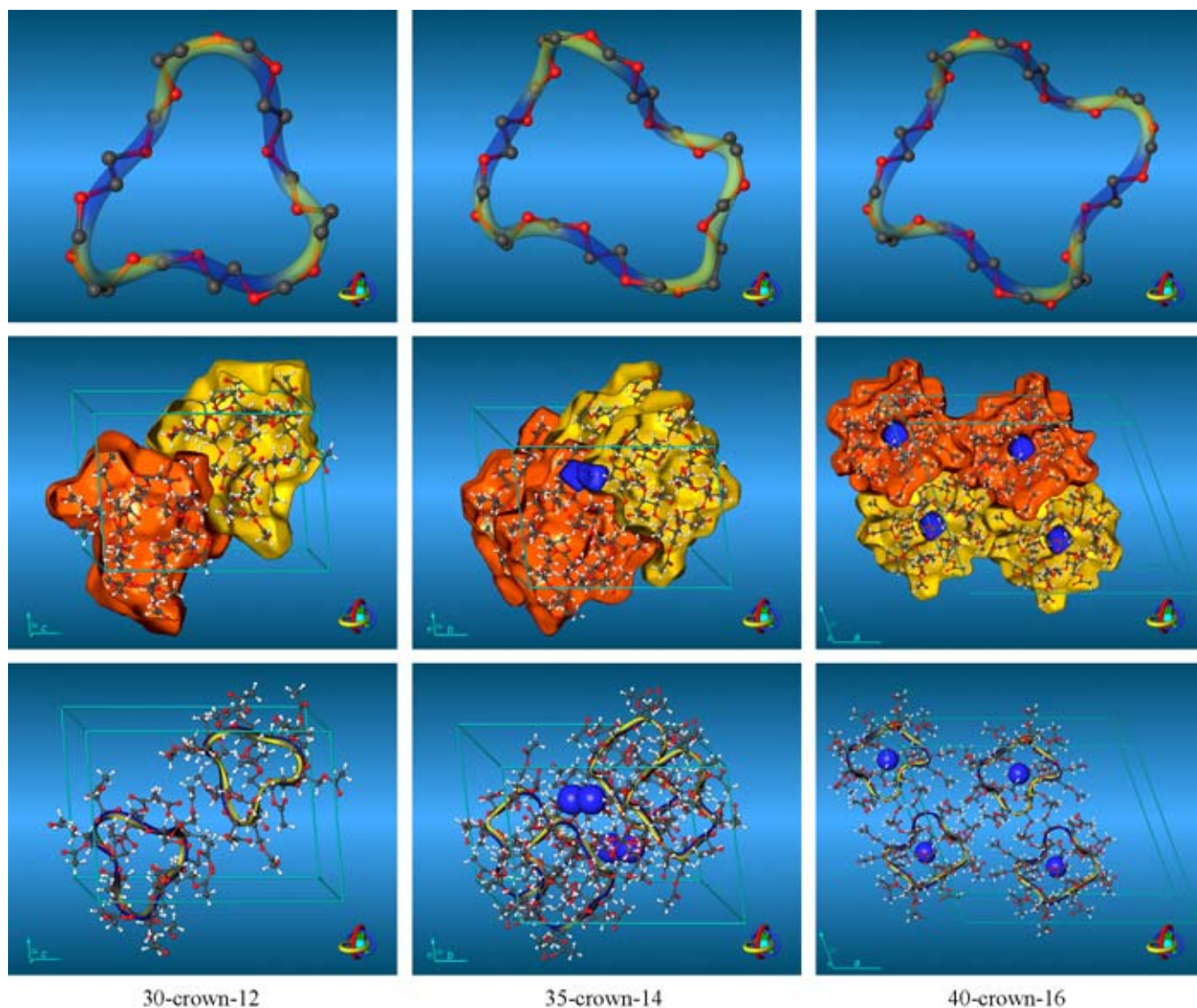


**Figure 1.** Solid-state structures of the 30-C-12 (**2**, left), 35-C-14 (**4**·H<sub>2</sub>O, center), and 40-C-16 (**6**·H<sub>2</sub>O, right) polyacetal peracetates. In the top row, all -CH<sub>2</sub>OAc ring substituents and hydrogen atoms have been removed for visualization, the semi-transparent ribbon models are colored according to the alternating (+)-*gauche* (yellow) and *anti* (blue) conformations of the constituting *meso*-butanetetrol residues. The center entries display a single unit cell for each structure with the non-overlapping Hirshfeld surfaces indicating the crystal volumes occupied by each molecule. Symmetry related mirror image conformations of the achiral compounds with alternating (+)-*gauche/anti* and (–)-*gauche/anti* *meso*-butanetetrol units are labelled by yellow and red surface colors, respectively. The bottom row ribbon models show the mode with which water molecules (blue spheres) are incorporated into the crystal lattice of **4** and **6**: whilst in **4** the water occupies interstitial positions between the macrocycles (center row), in **6** each water molecule is fully included into a 40-C-16 octaacetal host (right row).

solvent, incorporated one water molecule per macrocycle (rather than ethanol) into the crystal lattice. Whilst in **4** the four water molecules per unit cell (blue surfaces and blue spheres in Fig. 1) occupy interstitial places between the macrocycles (in Fig. 1, center, only two of the four water molecules are visible, the others being covered by the surfaces of front crown-acetals), the water of crystallization is fully immersed into the macrocyclic hosts of **6**, occupying almost the center of geometry of the 40-C-16 octaacetals in an inclusion complex type fashion, de facto filling their entire inner space.

A detailed plot of the ring geometries of **4** and **6** is provided by Fig. 2, in which selected *meso*-butanetetrol residues

have been labelled according to their conformation about the central C–C bond. Whilst the ‘even’ membered 40-C-16 octaacetal **6** allows for an fully alternating *gauche/anti* succession of the repeating unit within the ring, the ‘uneven’ 35-C-14 heptaacetal features two neighboring *gauche* residues in the macrocycle.

## 2.1. Solution geometries

The quite elaborate, well-organized structures found for the solid-state do not survive on dissolution in water in the case of the hydroxymethyl substituted crown acetals **3** and **5**, or in organic solvents such as chloroform for the peracetates **4** and **6**. As clearly evidenced by their <sup>1</sup>H

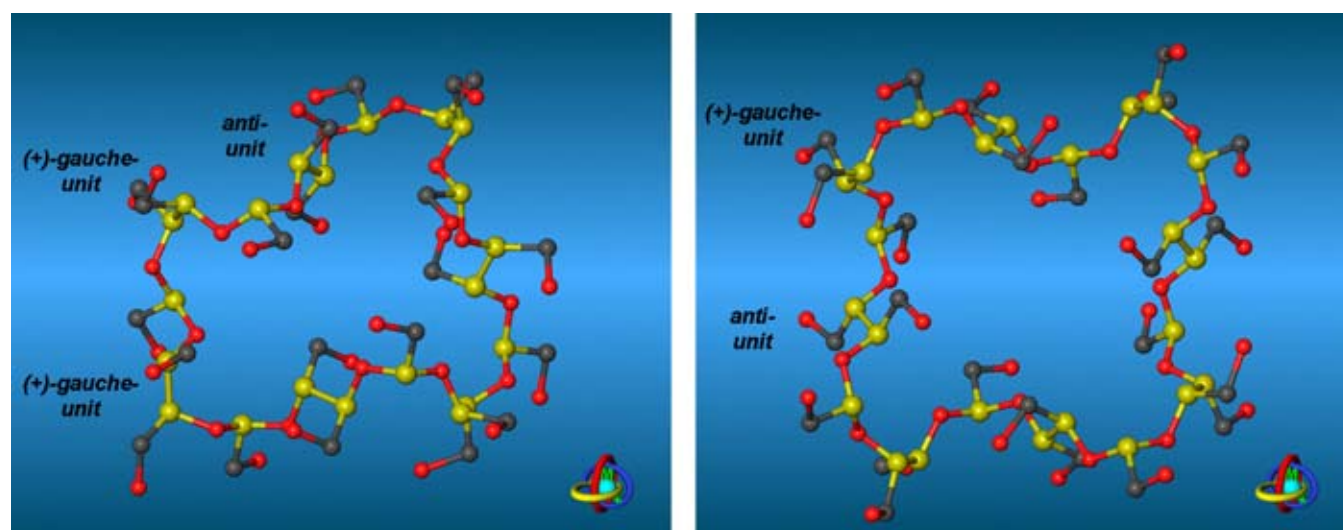


**Figure 2.** Comparison and ball-and-stick models of the solid-state ring conformations of the 35-C-14 heptaacetal and 40-C-16 octaacetal peracetates **4** and **6**. For visualization of the macrorings all ring carbon atoms are colored yellow, all hydrogen atoms and the acetyl groups of the substituents were left off for clarity. Representative *meso*-butanetetrol units are labeled according to their conformation (+)-*gauche* and *anti*; note the two consecutive (+)-*gauche*-oriented residues in the structure of the ‘uneven’ 35-membered ring of **2** on the left.

and  $^{13}\text{C}$  NMR spectra, as of now measured only at 27°C (300 K), the macrocyclic crown acetals are highly flexible. Thus, for each, i.e. **3** and **5** in  $\text{D}_2\text{O}$ , **4** and **6** in  $\text{CDCl}_3$ , only one averaged set of signals is observed for the seven resp. eight  $-\text{CHR}-\text{CHR}-\text{O}-\text{CHR}-\text{O}-$  units: 5 Hz triplets for H-2 and doublets for the  $\text{CH}_2$ -protons of the glycolaldehyde acetal groups, 9–9.5 Hz triplets for H-4/H-5, and, invariably, the butanetetrol-4- and 5- $\text{CH}_2\text{OH}$  protons as the AB part of an ABX system, with X being H-4 and H-5; the same holds for the  $^{13}\text{C}$  NMR signals, showing three distinct resonances for the core carbons of the macrocycles, which could be unequivocally assigned on the basis of CH-decouplings. By consequence, in solution the 35-C-14 and 40-C-16 crown acetals are highly flexible macrocycles in which the seven resp. eight monomeric  $-\text{CHR}-\text{CHR}-\text{O}-\text{CHR}-\text{O}-$  units (with  $\text{R}=\text{CH}_2\text{OAc}$ ), strung together to 35- and 40-membered cycles, are fully equilibrated and, hence, identical when observed in NMR time scale.

In turn, this high flexibility predisposes the crown acetals to adapt their conformation to guests for incorporation in a guest–host relationship and thus meet our aims for acquiring flexible hosts to study the induced-fit mode of molecular recognition. The peracetylated crown acetals **4** and **6**, as evidenced by Fig. 1 (mid-center and center right), display a distinct affinity to water, incorporating one molecule per macrocycle even when crystallized from 95% ethanol. The inclusion behavior of the crown acetals **3** and **5**, featuring 21 resp. 24 highly hydrophilic hydroxymethyl groups around the macrocycle, is different. The 35-C-14 heptaacetal **3** exhibits a distinct predilection for alcohols forming, on the basis of  $^1\text{H}$  and  $^{13}\text{C}$  NMR evidence, 1:1 complexes with ethanol or *n*-propanol when crystallized from

these solvents. Fig. 3, depicting the surprisingly simple  $^1\text{H}$  NMR spectrum of 3-*n*-PrOH in  $\text{D}_2\text{O}$  gives ample proof of 1:1 complex. The type of binding though, i.e. whether the guest sits inside or outside the cavity—in  $\text{D}_2\text{O}$  it may be even in solution—must await X-ray analysis of the crystals, which as of now have not been obtained in a suitable form.

By contrast, the 40-crown-16 octaacetal **6** has no tendency at all to incorporate low molecular weight alcohols when crystallized therefrom, conceivably because its cavity can entertain only larger, possibly more hydrophobic guests. Investigations along this vein are presently being performed.

### 3. Experimental

#### 3.1. General methods

Melting points were determined on a Bock Monoskop apparatus and are uncorrected. High-resolution mass spectra (ESI-MS) were recorded on Varian MAT 311 and MAT 212 spectrometers.  $^1\text{H}$  and  $^{13}\text{C}$  NMR spectra were recorded on a Bruker Avance 500 instrument at 500 and 125 MHz at 300 K, respectively;  $^{13}\text{C}$  NMR were proton decoupled. Chemical shifts are given in ppm relative to tetramethylsilane ( $\text{CDCl}_3$ ) and sodium 2,2,3,3-tetradeutera-3-trimethylsilylpropionate ( $\text{D}_2\text{O}$ ) as internal standards. Elemental analysis were determined on a Perkin–Elmer 240 elemental analyzer. Analytical thin-layer chromatography (TLC) was performed on precoated Merck plastic sheets (0.2 mm silica gel 60  $\text{F}_{254}$ ) with detection by UV (254 nm) and/or spraying with  $\text{H}_2\text{SO}_4$  (50%) and heating.



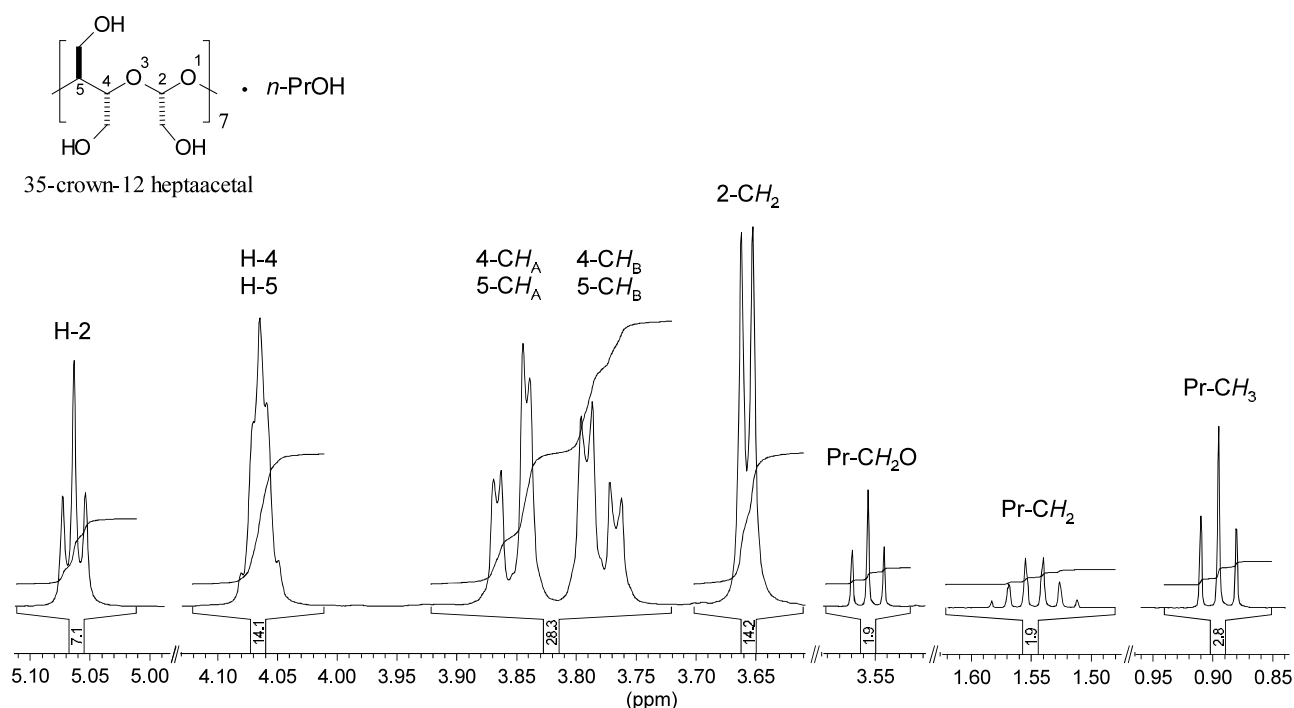


**Figure 3.**  $^1\text{H}$  NMR spectrum (500 MHz in  $\text{D}_2\text{O}$ ) of the 35-C-14 heptaacetal **3** obtained after dissolution of a sample of **3** previously crystallized from *n*-propanol. Besides a single time-averaged set of signals observed for the seven repeating units of **3**, the *n*-propanol resonances show the formation of a 1:1 inclusion complex.

**3.1.1. X-Ray structures.** Suitable crystals of cycloacetals **4** and **6** were analyzed on a Siemens CCD three-circle diffractometer with graphite-monochromated Mo  $\text{K}\alpha$  ( $\lambda = 0.71073 \text{ \AA}$ ) radiation. The structures were solved by direct methods (SHELXL-97) and successive Fourier synthesis. Refinement (on  $F^2$ ) was performed by the full-matrix least-squares method with SHELXL-97.<sup>14</sup> All non-hydrogen atoms were refined anisotropically; hydrogen atoms were considered in calculated positions with the 1.2  $U_{\text{eq}}$  value of the corresponding bound atom. Experimental details of the structure determinations are summarized in Table 1.

Crystallographic data (excluding structure factors) for **4** and **6** have been deposited with the Cambridge Crystallographic Data Centre as supplementary publication no. CCDC-143712 and CCDC-143713. Copies of the data can be obtained free of charge on application to CCDC, 12 Union Road, Cambridge CB2 1EZ, UK, fax: (+44) 1223 336-033, or e-mail: [deposit@ccdc.cam.ac.uk](mailto:deposit@ccdc.cam.ac.uk).

**3.1.2. Computational details.** Calculation of the molecular Hirshfeld surfaces<sup>12</sup> and generation of molecular graphics was performed using the MolArch<sup>+</sup> program.<sup>15</sup>

### 3.2. Heneicosa-(acetoxymethyl)-35-crown-14 heptaacetal **4**<sup>16,17</sup>

$\beta$ -Cyclodextrin (7.39 g, 6.5 mmol) was added with stirring to a cooled ( $0$ – $5^\circ\text{C}$ ), aqueous solution of  $\text{NaIO}_4$  (13.9 g, 65 mmol, in 400 mL) and the clear solution was kept at  $0^\circ\text{C}$  in a dark ice-box for 7 days, whereafter TLC revealed a single spot ( $R_f = 0.75$  in 2:2:1 *n*BuOH/

MeOH/ $\text{H}_2\text{O}$ ) of the respective tetradeca-aldehyde in one of the various hemiacetal and/or hemialdal hydrate forms possible. Then 1,2-ethanediol (1.09 mL, 19.5 mmol) was added with stirring to decompose excess  $\text{NaIO}_4$  and the mixture was kept at  $0^\circ\text{C}$  overnight. An aqueous  $\text{BaCl}_2$  solution (6.86 g, 32.9 mmol, in 30 mL) was then stirred into the mixture resulting in a precipitate, followed by evaporation of the filtrate to dryness in vacuo. The residue was suspended in dry MeOH (60 mL), kept in a refrigerator overnight, the solids were filtered off upon addition of charcoal, and the filtrate was evaporated to dryness in vacuo at  $\approx 35^\circ\text{C}$ . This procedure was repeated twice to give a white powder (8.4 g), which was dissolved in MeOH/water (100 mL, 3:1). Upon cooling ( $\sim 0^\circ\text{C}$ ),  $\text{NaBH}_4$  (2.0 g) was added with stirring and the mixture was kept at rt overnight. Addition of acetone (20 mL) to destroy the excess reagent, neutralization with cation exchange resin (IR-120,  $\text{H}^+$  form), evaporation to dryness, and several co-evaporations of the residue with absolute MeOH left polyol **4** as a colorless solid which was dissolved in a mixture of pyridine (100 mL) and  $\text{Ac}_2\text{O}$  (50 mL), and kept overnight at rt. Subsequent evaporation to dryness in vacuo at  $40^\circ\text{C}$ , followed by co-evaporation with toluene ( $3 \times 50 \text{ mL}$ ) afforded a syrup which was dissolved in hot EtOAc, treated with charcoal, filtered, and evaporated to dryness. The residue crystallized on dissolution in 95% EtOH and addition of small amounts of EtOAc to afford 11.62 g (88%) of **4** as colorless plates of mp  $109$ – $111^\circ\text{C}$ ;  $[\alpha]_D^{25}$  0.0 (*c* 2,  $\text{CHCl}_3$ ); lit.:<sup>7a</sup> mp  $106$ – $107^\circ\text{C}$ , 11% yield. ESI-MS:  $m/z$  2053.2 ( $\text{M} + \text{Na}^+$ ).  $^1\text{H}$  NMR ( $\text{CDCl}_3$ ):  $\delta$  5.14 (t, 7H,  $J = 5.1 \text{ Hz}$ , 2-H), 4.47 (d, 14H,  $J = 9.5 \text{ Hz}$ , 4-H, 5-H), 4.12 (broad 28H-m, AB part of an ABX system, 4- $\text{CH}_2$ , 5- $\text{CH}_2$ ),

4.03 (d, 14H,  $J=5.1$  Hz, 2-CH<sub>2</sub>), 2.09 (s, 42H, 14AcCH<sub>3</sub>), 2.05 (s, 21H, 7AcCH<sub>3</sub>). <sup>13</sup>C NMR (CDCl<sub>3</sub>):  $\delta$  169.5 (AcCO), 99.5 (C-2), 74.7 (C-4, C-5), 63.5 (2-CH<sub>2</sub>), 62.7 (4-CH<sub>2</sub>, 5-CH<sub>2</sub>), 19.6 and 19.7 (AcCH<sub>3</sub>). Anal. calcd for C<sub>84</sub>H<sub>126</sub>O<sub>56</sub>·H<sub>2</sub>O<sup>17</sup> (2049.9): C, 49.22; H, 6.29. Found: C, 49.34; H, 6.21.

Crystals suitable for X-ray analysis were obtained by slow crystallization of **4** from 95% EtOH containing a small amount of EtOAc; crystal data are summarized in Table 1.

**Table 1.** Crystal data and structure refinement for the crown acetal per-*O*-acetates **4** and **6**

Compound	<b>4</b> ·H <sub>2</sub> O	<b>6</b> ·H <sub>2</sub> O
Empirical formula	C <sub>84</sub> H <sub>126</sub> O <sub>56</sub> ·H <sub>2</sub> O	C <sub>96</sub> H <sub>144</sub> O <sub>64</sub> ·H <sub>2</sub> O
Formula weight	2049.87	2340.13
Temperature (K)	173(2)	293(2)
Wavelength (Å)	0.71073	0.71073
Crystal system	Triclinic	Monoclinic
Space group	$\bar{P}$	<i>C</i> 2/ <i>c</i>
Unit cell dimensions		
<i>a</i> (Å)	17.140(2)	36.654(3)
<i>b</i> (Å)	23.284(3)	12.219(1)
<i>c</i> (Å)	26.374(3)	30.577(3)
$\alpha$ (°)	97.50(1)	90
$\beta$ (°)	97.28(1)	116.41(2)
$\gamma$ (°)	97.41(1)	90
Volume (Å <sup>3</sup> )	10237(2)	12265.4(19)
<i>Z</i>	4	4
<i>D</i> <sub>calcd</sub> (g cm <sup>-3</sup> )	1.330	1.267
Absorption coefficient (mm <sup>-1</sup> )	0.106	0.101
<i>F</i> (000)	4344	4959
Crystal size (mm)	0.33 × 0.22 × 0.10	0.55 × 0.40 × 0.35
$\theta$ Range (°)	0.79–27.53	1.24–27.30
Limiting indices	–21 ≤ <i>h</i> ≤ 21; –29 ≤ <i>k</i> ≤ 30; –33 ≤ <i>l</i> ≤ 32	–46 ≤ <i>h</i> ≤ 46; –15 ≤ <i>k</i> ≤ 15; –39 ≤ <i>l</i> ≤ 39
Reflections collected	92760	77665
Independent reflections	39750 ( <i>R</i> <sub>int</sub> = 0.0942)	12680 ( <i>R</i> <sub>int</sub> = 0.0493)
Absorption correction	Empirical	Empirical
Max. and min. transmission	0.9927 and 0.9767	0.9761 and 0.9628
Refinement method	Full-matrix least-squares on <i>F</i> <sup>2</sup>	Full-matrix least-squares on <i>F</i> <sup>2</sup>
Data/restraints/parameters	39750/66/2671	12680/14/756
Goodness-of-fit on <i>F</i> <sup>2</sup>	1.071	1.384
Final <i>R</i> indices	<i>R</i> <sub>1</sub> = 0.1305; <i>wR</i> <sub>2</sub> = 0.2569	<i>R</i> <sub>1</sub> = 0.1463; <i>wR</i> <sub>2</sub> = 0.4019
<i>R</i> indices (all data)	<i>R</i> <sub>1</sub> = 0.2578; <i>wR</i> <sub>2</sub> = 0.3170	<i>R</i> <sub>1</sub> = 0.2436; <i>wR</i> <sub>2</sub> = 0.4648
Largest difference peak and hole (e Å <sup>-3</sup> )	0.916 and –0.392	0.859 and –0.281

<sup>a</sup> For **4**:  $w = 1/[\sigma^2(F_o^2) + (0.1165P)^2 + 15.8740P]$ ; for **6**:  $w = 1/[\sigma^2(F_o^2) + 0.2000P^2 + 0.0000P]$ , where  $P = (F_o^2 + 2F_c^2)/3$ .

### 3.3. Heneicosa-(hydroxymethyl)-35-crown-14 hepta-acetal **3**<sup>16</sup>

**3.3.1. 1:1 Complex with 1-propanol (3·*n*-C<sub>3</sub>H<sub>7</sub>OH).** To a solution of **4** (5.00 g, 2.46 mmol) in absolute MeOH (125 mL) were added a few drops of 2N methanolic NaOMe and the mixture was stirred at rt overnight. After neutralization with IR-120 (H<sup>+</sup> form) the solution was evaporated to dryness in vacuo, and the residue was crystallized from 1-PrOH: 2.54 g (86%) of colorless plates of mp 145–157°C. ESI-MS: *m/z* 1172.1 (M+Na<sup>+</sup>). <sup>1</sup>H NMR (D<sub>2</sub>O):  $\delta$  5.06 (t, 7H,  $J=4.9$  Hz, 2-H), 4.06 (m, 14H, X-part of an ABX-system, 4-H, 5-H), 3.86 (dd, 14H,  $J=3.0$  and 12.2 Hz, 4-CH<sub>2</sub><sup>A</sup>, 5-CH<sub>2</sub><sup>A</sup>), 3.78 (dd, 14H,  $J=4.8$  and 12.2 Hz, 4-CH<sub>2</sub><sup>B</sup>, 5-CH<sub>2</sub><sup>B</sup>), 3.66 (d, 14H,  $J=4.9$  Hz, 2-CH<sub>2</sub>), 3.56 (t, 2H,  $J=7.4$  Hz, EtCH<sub>2</sub>O), 1.55 (sext., 2H,  $J=7.4$  Hz, MeCH<sub>2</sub>CH<sub>2</sub>O), 0.89 (t, 3H,  $J=7.4$  Hz, PrCH<sub>3</sub>). <sup>13</sup>C NMR (D<sub>2</sub>O):  $\delta$  101.6 (C-2), 77.4 (C-4, C-5), 62.7 (EtCH<sub>2</sub>O), 62.2 (2-CH<sub>2</sub>), 59.7 (4-CH<sub>2</sub>, 5-CH<sub>2</sub>), 23.7 (MeCH<sub>2</sub>CH<sub>2</sub>O), 8.7 (PrCH<sub>3</sub>). Anal. calcd for C<sub>42</sub>H<sub>84</sub>O<sub>35</sub>·C<sub>3</sub>H<sub>7</sub>OH (1209.2): C, 44.70; H 7.67. Found: C, 44.65; H, 7.78.

**3.3.2. 1:1 Complex with ethanol (3·EtOH).** An aqueous solution of **3**·PrOH (0.85 g in 20 mL) was evaporated to dryness at 50°C in vacuo and the residue was subjected to another two evaporations from water. The resulting powder was crystallized from ethanol to yield 0.74 g (87%) of colorless plates exhibiting an unusually wide melting range of 125–157°C without decomposition, undoubtedly due to release of ethanol on melting; lit.<sup>7b</sup> mp 125–132°C for a sample believed to be **3**, but obtained by crystallization from ethanol. <sup>1</sup>H NMR (D<sub>2</sub>O):  $\delta$  5.07 (t, 7H,  $J=4.8$  Hz, 2-H), 4.6 (m, 14H, X-part of an ABX system, 4-H, 5-H), 3.86 and 3.77 (two dd for the AB part of an ABX system, 14H each, 4-CH<sub>2</sub> and 5-CH<sub>2</sub>), 3.67 (d, 14H, 2-CH<sub>2</sub>), 3.64 (q, 2H, EtCH<sub>2</sub>), 1.19 (t, 3H, EtCH<sub>3</sub>). <sup>13</sup>C NMR (D<sub>2</sub>O):  $\delta$  105.4 (C-2), 80.8 (C-4, C-5), 65.9 (2-CH<sub>2</sub>), 63.4 (4-CH<sub>2</sub>, 5-CH<sub>2</sub>). Anal. calcd for C<sub>42</sub>H<sub>84</sub>O<sub>35</sub>·C<sub>2</sub>H<sub>5</sub>OH (1195.2): C, 44.22; H, 7.59. Found: C, 44.98; H, 7.50.

### 3.4. Tetraicosa-(acetoxymethyl)-40-crown-16 octaacetal **6**<sup>16</sup>

To a stirred and cooled (0–5°C) aqueous solution of NaIO<sub>4</sub> (12.95 g, 60.5 mmol, in 400 mL)  $\gamma$ -cyclodextrin (7.14 g, 5.5 mmol) was added and the clear solution was kept at 0°C in a dark ice-box for 5 days whereafter TLC revealed a single spot (*R*<sub>f</sub> = 0.75 in 2:2:1 *n*BuOH/MeOH/H<sub>2</sub>O). Then, 1,2-ethanediol (0.92 mL, 16.5 mmol) was added with stirring to decompose excess NaIO<sub>4</sub> and the reaction was worked up in a manner analogous to that described above for the periodation of  $\beta$ -CD. The respective polyaldehyde was obtained as white powder (8.32 g). Subsequent reduction with NaBH<sub>4</sub> (2.0 g) and acetylation with pyridine/Ac<sub>2</sub>O (2:1, 150 mL) as described for the acquisition of **4** from  $\beta$ -CD gave a syrup that gradually crystallized on titration with EtOH/EtOAc and was isolated on standing overnight at ambient temperature: 10.6 g (82%) as colorless plates of mp 143.5–145°C;  $[\alpha]_D^{25}$  0.0 (*c* 2, CHCl<sub>3</sub>). ESI-MS: *m/z* 2345.1 (M+Na<sup>+</sup>). <sup>1</sup>H NMR (CDCl<sub>3</sub>):  $\delta$  5.16 (t, 8H,  $J=4.9$  Hz, 2-H), 4.49 (dd, 16H,

$J=9.4$  and  $1.3$  Hz, 4-H, 5-H, X-part), 4.13 and 4.09 (16H, dd and 16H-m, 4-CH<sub>2</sub> and 5-CH<sub>2</sub> as an ABX system), 4.00 (d, 16H,  $J=5.0$ , 2-CH<sub>2</sub>), 2.08 (s, 48H, 4-AcCH<sub>3</sub>, 5-AcCH<sub>3</sub>), 2.05 (s, 24H, 2-AcCH<sub>3</sub>). <sup>13</sup>C NMR (CDCl<sub>3</sub>):  $\delta$  170.4 and 170.3 (AcCO), 101.0 (C-2), 76.3 (C-4, C-5), 64.7 (2-CH<sub>2</sub>), 63.9 (4-CH<sub>2</sub>, 5-CH<sub>2</sub>), 20.7 and 20.6 (AcCH<sub>3</sub>). Anal. calcd for C<sub>96</sub>H<sub>144</sub>O<sub>64</sub>·H<sub>2</sub>O<sup>17</sup> (2340.1): C, 49.27; H, 6.29. Found: C, 49.29; H, 6.26.

Crystals for X-ray analysis were obtained by slow crystallization of **6** from 95% EtOH containing a small amount of EtOAc; crystal data are summarized in Table 1.

### 3.5. Tetraicosa-(hydroxymethyl)-40-crown-16 octaacetal **5**<sup>16</sup>

Zemplén deacetylation of **6** (2.00 g, 0.85 mmol) was carried out in a similar manner described above for (**4**→**3**). Crystallization from 1-PrOH afforded colorless needles (1.00 g, 89%) of mp 163–165°C. ESI-MS:  $m/z$  1335.3 (M+Na<sup>+</sup>). <sup>1</sup>H NMR (D<sub>2</sub>O):  $\delta$  5.07 (t, 8H,  $J=4.5$  Hz, 2-H), 4.07 (broad m, 16H, X-part of an ABX-system, 4-H and 5-H), 3.83 and 3.78 (two dd of an AB system, 16H each, 4-CH<sub>2</sub> and 5-CH<sub>2</sub>), 3.67 (d, 16H, 2-CH<sub>2</sub>). <sup>13</sup>C NMR (D<sub>2</sub>O):  $\delta$  105.7 (C-2), 81.1 (C-4, C-5), 65.7 (2-CH<sub>2</sub>), 63.1 (4-CH<sub>2</sub>, 5-CH<sub>2</sub>). Anal. calcd for C<sub>48</sub>H<sub>96</sub>O<sub>40</sub> (1313.3): C, 43.90; H, 7.36. Found: C, 43.65; H, 7.44.

### Acknowledgements

Appreciation is expressed to the Fonds der Chemischen Industrie, Frankfurt, and the Südzucker AG, Mannheim/Ochsenfurt, for financial support. Our thanks are also due to Wacker-Chemie, Burghausen, for a gift of  $\beta$ - and  $\gamma$ -cyclodextrin.

### References

1. Immel, S.; Khanbabae, L. *Tetrahedron: Asymmetry* **2000**, *11*, 2495–2507.
2. *Nomenclature*: Although polyacetals such as **1–6** are unlikely to adopt crown-like molecular geometries—the terminology for macrocyclic ethers was derived from their crown-like shape—it appears logical and practical as well to extend this generally accepted notational mode for crown ethers to their acetal analogs, resulting in the term *crown acetals* for macrocycles with acetal oxygens only. Likewise, it appears most appropriate to adopt the crown ether-type description for ring size and number of oxygens; accordingly, **1** is the octadeca-(hydroxymethyl)-derivative of a 30-crown-12 hexaacetal, whereas the respective  $\beta$ -CD and  $\gamma$ -CD-derived analogs **3** and **5** are cyclic hepta- and octaacetals with a 35-crown-14 and 40-crown-16 backbone, respectively.
3. (a) Pedersen, C. J. *J. Am. Chem. Soc.* **1970**, *92*, 391–394; (b) Kawakami, Y.; Suzuki, J.; Yamashita, Y. *Polym. J.* **1977**, *9*, 519–524; Kawakami, Y.; Sugiura, T.; Yamashita, Y. *Bull. Chem. Soc. Jpn.* **1978**, *51*, 3053–3056; (c) Gold, V.; Sghibartz, C. M. *J. Chem. Soc., Perkin Trans. 1* **1983**, 453–457; (d) Oshima, T.; Nishioka, R.; Ueno, S.; Nagai, T. *J. Org. Chem.* **1982**, *47*, 2114–2117; Oshima, T.; Nagai, T. *Bull. Chem. Soc. Jpn.* **1986**, *59*, 3979–3980; (e) Oshima, T.; Matsuda, F.; Fukushima, K.; Tamura, H.; Matsubayashi, G.; Arakawa, R. *J. Chem. Soc., Perkin Trans. 2* **1998**, 145–148; (f) Ouchi, M.; Inoue, Y.; Kanzaki, T.; Hakushi, K. *Bull. Chem. Soc. Jpn.* **1984**, *57*, 887–888; Inoue, Y.; Ouchi, M.; Hakushi, K. *Bull. Chem. Soc. Jpn.* **1985**, *58*, 525–530.
4. Known tetraoxacycloalkanes with two acetal units in their *n*-crown-4 skeletal backbone: (a) 10-C-4: Bassi, I. W.; Scordamaglia, T.; Fiori, L. *J. Chem. Soc., Perkin Trans. 2* **1975**, 1129–1132; (b) Substituted 10-C-4-systems: Terzis, A.; Grindley, T. B. *Can. J. Chem.* **1979**, *57*, 2154–2158; Stoddart, J. F.; Szarek, W. A. *Can. J. Chem.* **1968**, *46*, 3061–3069; (c) 12-C-4; Borgen, G.; Dale, J. J. *J. Chem. Soc., Chem. Commun.* **1974**, 484–485; Dale, J. *Tetrahedron* **1974**, *30*, 1683–1694; (d) 14-C-4: Bassi, I. W.; Scordamaglia, R.; Fiori, L. *J. Chem. Soc. Perkin Trans. 2* **1972**, 1726–1729; (e) 16-C-4: Dale, J.; Ekeland, T. *Acta Chem. Scand., Ser. A* **1973**, *27*, 1519–1525; Groth, P. *Acta Chem. Scand., Ser. A* **1975**, *29*, 642–643; (f) 18-C-4, 24-C-4, 26-C-4, and 34-C-4: Hill, J. W.; Carothers, W. H. *J. Am. Chem. Soc.* **1935**, *57*, 925–928.
5. The *cyclo*-polyacetals generated by acid promoted oligomerization of 1,3-dioxolane are presumed to have 15-C-6, 20-C-8, and 25-C-10 structural backbones (Kawakami, Y.; Yamashita, Y. *Macromolecules* **1977**, *10*, 837–839), yet their ring size has not been established unambiguously.
6. (a) French, D.; McIntyre, R. J. *J. Am. Chem. Soc.* **1950**, *72*, 5148–5150; (b) Hisa-matsu, M.; Yamada, Y.; Nakashima, K.; Tobata, K. *Starch/Stärke* **1992**, *44*, 188–191.
7. (a) Stoddart, J. F.; Szarek, W. A.; Jones, J. K. N. *Can. J. Chem.* **1969**, *47*, 3213–3215; (b) Kandra, L.; Lipták, A.; Jodál, I.; Nánási, P.; Szejtli, J. *J. Inclusion Phenom.* **1984**, *2*, 869–875.
8. Immel, S.; Nakagawa, T.; Lindner, H.-J.; Lichtenthaler, F. W. *Chem. Eur. J.* **2000**, *6*, 3366–3371.
9. Koshland, D. E. *Angew. Chem.* **1994**, *106*, 2468–2472; *Angew. Chem., Int. Ed. Engl.* **1994**, *33*, 2375–2378.
10. (a) Fischer, E. *Ber. Dtsch. Chem. Ges.* **1884**, *27*, 2985–2993; (b) Lichtenthaler, F. W. *Angew. Chem.* **1994**, *106*, 2456–2467; *Angew. Chem., Int. Ed. Engl.* **1994**, *33*, 2364–2374.
11. (a) Nogami, A.; Nasu, K.; Koga, T.; Ohta, K.; Fujita, K.; Immel, S.; Lindner, H.-J.; Schmitt, G. E.; Lichtenthaler, F. W. *Angew. Chem.* **1997**, *109*, 1987–1991; *Angew. Chem., Int. Ed. Engl.* **1997**, *36*, 1899–1902; (b) Fujita, K.; Chen, W.-H.; Yuan, D.-Y.; Nogami, Y.; Koga, T.; Fujioka, T.; Mihashi, K.; Immel, S.; Lichtenthaler, F. W. *Tetrahedron: Asymmetry* **1999**, *10*, 1689–1696; (c) Immel, S.; Fujita, K.; Lichtenthaler, F. W. *Chem. Eur. J.* **1999**, *5*, 3185–3192; (d) Gohlke, H.; Immel, S.; Lichtenthaler, F. W. *Carbohydr. Res.* **1999**, *321*, 96–104.
12. McKinnon, J. J.; Mitchell, A. S.; Spackman, M. A. *Chem. Eur. J.* **1998**, *4*, 2136–2141.
13. (a) Connolly, M. L. *J. Appl. Crystallogr.* **1983**, *16*, 548–558; (b) Connolly, M. L. *Science* **1983**, *221*, 709–713.

2774

*S. Immel et al. / Tetrahedron: Asymmetry 12 (2001) 2767–2774*

14. Sheldrick, G. M. *SHELXS-97 and SHELXL-97—Programs for Crystal Structure Solution and Refinement*; University of Göttingen: Germany, 1997.
15. Immel, S. *MolArch+—MOlecular ARCHitecture Modeling Program*; Darmstadt University of Technology: Germany, 2001.
16. Systematic name for 35-crown-14 heptaacetal: 2,4,5,7,9,10,12,14,15,17,19,20,22,24,25,27,29,30,32,34,35-heneicosahydroxymethyl-1,3,6,8,11,13,16,18,21,23,26,28,31,33-tetradeca-oxa-cyclopentatriacontane, **4** is the per-*O*-acetyl derivative thereof. Correspondingly, the 40-crown-16 octaacetals **5** and **6** are the tetracosahydroxymethyl and tetracosacetoxymethyl derivatives of a hexadeca-oxa-cyclotetracontane.
17. That the crown acetal peracetates **4** and **6** crystallize with one molecule of water each—crystallization was effected from 95% EtOH/EtOAc—emerged from the X-ray data (cf. Fig. 1) and not from their microanalysis, as differentiation on that basis between anhydrous compound and monohydrate is not possible.

*Proc. 10<sup>th</sup> Int. Symp. Cyclodextrins* (Ed.: J. Szejtli), Mia Digital Publ., Ann Arbor, Michigan, **2000**, pp. 18-23.

## LARGE-RING CROWN ACETALS FROM CYCLODEXTRINS

T. NAKAGAWA, S. IMMEL, H. J. LINDNER, F. W. LICHTENTHALER

*Institute of Organic Chemistry, Darmstadt University of Technology,  
D-64287 Darmstadt, Germany*

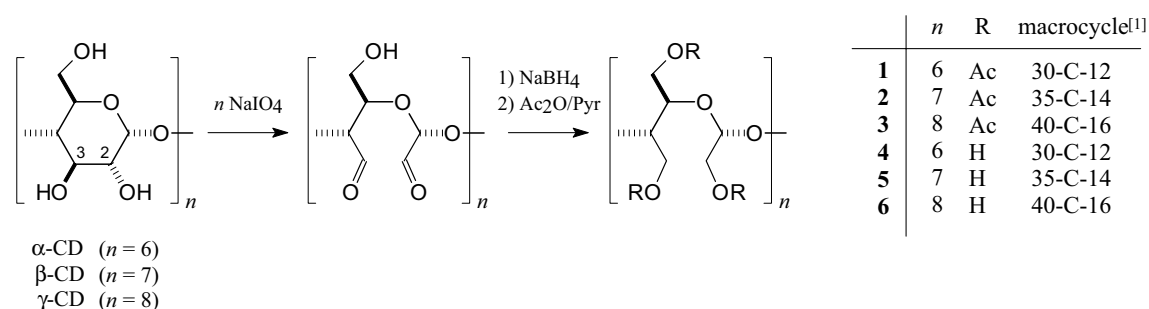
### ABSTRACT

Periodate oxidation followed by borohydride reduction readily converts  $\alpha$ -,  $\beta$ -, and  $\gamma$ -cyclodextrin into crown acetals with 30-C-12, 35-C-14, and 40-C-14 skeletal backbones and a hydroxymethyl group at each of the carbon atoms. Isolated as their crystalline peracetate (**1-3**) or as such (**4-6**) in yields of 82-92 %, X-ray structures revealed their unique molecular geometries: the 30-membered ring in  $\alpha$ -CD-derived **1** adopts a three-looped, undulated shape with alternating *gauche* and *anti* conformations of the six *meso*-butanetetrol units, and above / below positioning of the six glycolaldehyde acetoxymethyl groups. Key structural features of the  $\gamma$ -CD-derived 40-membered macrocycle with 16 ring oxygens are a four-looped, clover-leaf type shape in similarly undulated form. In solution though, the macrocycle **1** is highly flexible showing one set of NMR signals ( $^1\text{H}$  and  $^{13}\text{C}$ ) at high temperature ( $\sim 80^\circ\text{C}$ ), and distinct broadening at ambient temperature, whilst the signals fall into two sets at  $-60^\circ\text{C}$ , indicating a "freezing out" of the solid state molecular geometry.

### 1. INTRODUCTION

Macrocycles exclusively containing acetal oxygens, and, hence, deserving the designation crown acetal,<sup>[1]</sup> are rare, the presently known examples being limited to systems with two formaldehyde/alkanediol acetal units, i. e. containing four oxygens in the ring.<sup>[2]</sup> Cycloacetals with a higher number of ring oxygen atoms, albeit never considered as such, happen to be the products generated by periodate oxidation of cyclic oligosaccharides. The polyaldehydes derived from  $\alpha$ -,  $\beta$ -, and  $\gamma$ -cyclodextrin<sup>[3]</sup> constitute macrocycles with 30-crown-12, 35-crown-14, and 40-crown-16 skeletal backbones, yet have eluded unequivocal structural characterization, conceivably due to the manifold possibilities of elaborating cyclic acetals, hemiacetals and hemialdals. Of the products ensuing from borohydride reduction and subsequent acetylation,<sup>[4]</sup> only the per-acetoxy methyl 30-C-12 crown acetal **1** and its 35-C-4 analog **2** have been prepared – in yields of 0.6 and 11 %<sup>[4a]</sup> for the three steps from  $\alpha$ - and  $\beta$ -CD, respectively – and fairly well characterized, yet the sparse NMR data given provided no indications as to their molecular geometries.

Our past interest in the generation of flexible cyclooligosaccharide hosts<sup>[5]</sup> to mimic the induced-fit mode of enzyme action<sup>[6]</sup> rather than Emil Fischer's classical static lock-and-key concept<sup>[7]</sup> has now led us to preparatively satisfactory syntheses for the  $\alpha$ -,  $\beta$ - and  $\gamma$ -CD-derived crown acetals **1-6** in crystalline form each, their unequivocal characterization and an exploitation of their conformational features via X-ray and NMR.



## 2. MATERIALS AND METHODS

**Preparation.** Periodate oxidation of  $\alpha$ -,  $\beta$ -, and  $\gamma$ -CD was performed on a preparative scale (5-10 g) by keeping their aqueous solutions with a 3 molar excess of oxidant at 0-4 °C for 5-11 d. The resulting CD-polyaldehydes obtained as chromatographically uniform powders, were directly subjected to reduction with NaBH<sub>4</sub> in aqueous methanol, yet the polyhydroxymethyl-substituted crown acetals **4**, **5** and **6** are preferably not isolated at this stage, because peracetylation with acetic anhydride/pyridine provides the well-crystallizing peracetates **1-3**, isolable in yields in the 80-90 % range based on the CDs. Subsequent Zemplén deacetylation (NaOMe/MeOH) then smoothly affords the respective polyols, i. e. the octadecakis(hydroxymethyl)-30-crown-12 hexaacetal **4**,<sup>[8]</sup> and its 35-crown-14 and 40-crown-16 analogs **5** and **6**.<sup>[8]</sup> Selected data for **1 - 6**:

- 1:** mp 171-173 °C, 92 % yield over 3 steps from  $\alpha$ -CD (lit.<sup>[4a]</sup> mp 162-164 °C, 0.6 %), ESI-MS 1763.5 (M + Na<sup>+</sup>).
- 2:** mp 109-111 °C, 88 % from  $\beta$ -CD, ESI-MS 2053.6 (M + Na<sup>+</sup>).
- 3:** mp 143.5-145.5 °C, 82 % from  $\gamma$ -CD, ESI-MS 2343.2 (M + Na<sup>+</sup>).
- 4:** mp 200-203 °C, 84 % from **1**, ESI-MS 1007.6 (M + Na<sup>+</sup>).
- 5:** mp 145-157 °C (cryst. from n-PrOH), 80 % from **2**, ESI-MS 1171.4 (M + Na<sup>+</sup>).
- 6:** mp 163-165 °C, 85 % from **3**, ESI-MS 1335.6 (M + Na<sup>+</sup>).

**X-Ray Structures.** Details on the X-ray analysis of the  $\alpha$ -CD-derived **1** are published elsewhere<sup>[9]</sup>; see also CCDC 143 715. – Crystallographic data for **3**: C<sub>96</sub>H<sub>144</sub>O<sub>64</sub> • H<sub>2</sub>O,  $M_r = 2340.18$  g mol<sup>-1</sup>, monoclinic, space group *C2/c*,  $a = 36.654(3)$ ,  $b = 12.219(1)$ ,  $c = 30.577(3)$  Å,  $\beta = 116.41(2)$ ,  $V = 12265.4(19)$  Å<sup>3</sup>,  $Z = 4$ ,  $\rho = 1.266$  g cm<sup>-3</sup>,  $\mu(\text{MoK}\alpha) = 0.101$  mm<sup>-1</sup>, crystal dimensions 0.55 x 0.40 x 0.35 mm,  $T = 293(2)$ . Of

77665 reflections collected on a Siemens CCD diffractometer, graphite-monochromated  $\text{MoK}\alpha$  ( $\lambda = 0.71073 \text{ \AA}$ ) radiation, 12680 are independent ( $R_{\text{int}} = 0.0493$ ). The structure was solved by direct methods (SHELXS-97<sup>[10]</sup>) and successive Fourier synthesis. Refinement (on  $F^2$ ) was performed by full-matrix least squares method with SHELXL-97.<sup>[10]</sup>  $R(F) = 0.1463$  for reflections with  $I \geq 2\sigma I$ ,  $\omega R(F^2) = 0.4648$  for all 12680 reflections ( $\omega = 1/[\sigma^2(F_o^2) + (0.2000P)^2 + 0.0000P]$ ; where  $P = (F_o^2 + 2F_c^2)/3$ ). All non-hydrogen atoms were refined anisotropically; hydrogen atoms were considered in calculated positions with the  $1.2 U_{\text{eq}}$  value of the corresponding bound atom. Crystallographic data (excluding structure factors) for **3** have been deposited with the Cambridge Crystallographic Data Centre as supplementary publication no. CCDC-143 713.

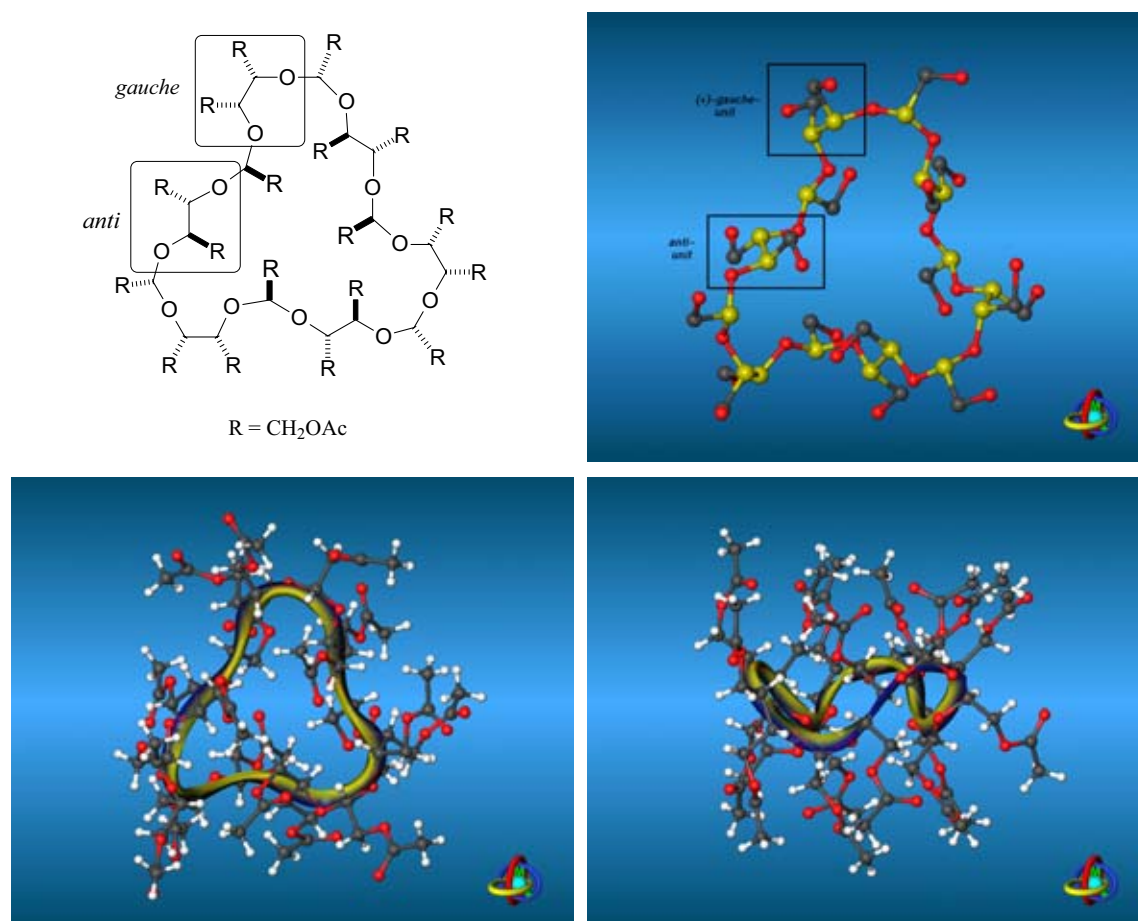


*Figure 1.* Solid-state topography of the octadecakis(acetoxymethyl)-30-crown-12 hexaacetal **1** in conventional formula drawing (upper left) and in ball-and-stick representation with the hydrogen atoms and 18 acetyl residues omitted for clarity (upper right): The *meso*-butanetetrol units alternating in *gauche* and *anti*-conformation versus above / below succession of glycolaldehyde acetal groups. The ribbon models (bottom entries) amply illustrate the three-looped shape (bottom left) and its undulatory form (bottom right) with the yellow/blue-coloring of the braid signifying the twist of the backbone.<sup>[11]</sup>

21

### 3. RESULTS AND DISCUSSION

None of the crown acetals prepared showed any rotational value, which was to be expected, as the butanetetrol units generated from the CDs by the periodation-reduction sequence have *erythro*-configuration and erythritol is a *meso*-compound. An X-ray analysis of the  $\alpha$ -CD-derived 30-crown-12 hexaacetal **1**<sup>[9]</sup> revealed the 30-membered macrocycle to be molded into three loops with six acetoxymethyl groups of the glycolaldehyde acetal units pointing alternately above and below the mean-plane of the macrocyclic backbone; the six *meso*-butanetetrol units are similarly alternating between *gauche*- and *anti*-arrangements for the two acetoxymethyl groups and, hence, O–C–C–O–torsion angles (Figure 1). Although the 30-crown-12 macrocycle of **1** is anticipated to be quite flexible in solution, both temperature dependent <sup>1</sup>H<sup>[9]</sup> and <sup>13</sup>C NMR patterns in CD<sub>2</sub>Cl<sub>2</sub> and C<sub>2</sub>D<sub>2</sub>Cl<sub>4</sub>, respectively (cf. Figure 2), point towards the over-all shape of the solid-state conformation being largely retained in these solvents.

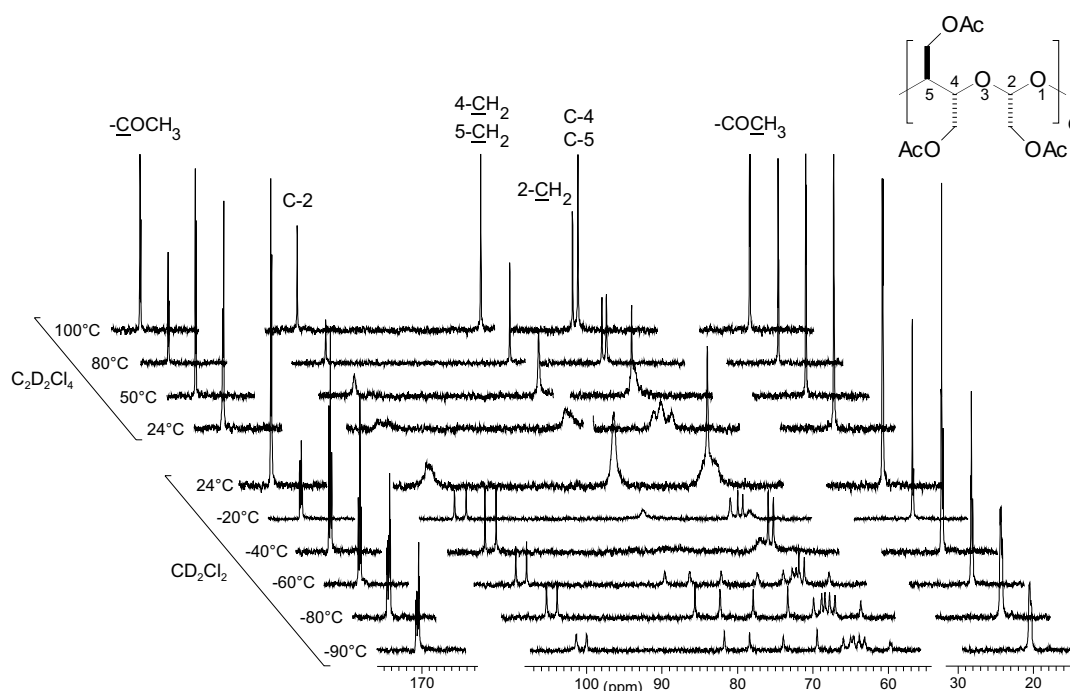


**Figure 2.** <sup>13</sup>C NMR spectral patterns of **1** in dependence of temperature, recorded in CD<sub>2</sub>Cl<sub>2</sub> ( $T = +24$  to  $-90$  °C) and C<sub>2</sub>D<sub>2</sub>Cl<sub>4</sub> (24 - 100 °C). At 100 °C there is only one set of carbon atoms indicating full flexibility of the macrocyclic core with fast interconversions of any individual conformations; coalescence is observed at about room temperature whilst at  $-90$  °C each of the signals is doubled, consistent with the notion that the solid-state geometry of **1** with its alternating *gauche* / *anti* arrangements of the six butanetetrol units and the above / below positioning of the glycolaldehyde acetoxymethyl groups has been "frozen out".



Preliminary X-ray structural data on the  $\gamma$ -CD-derived tetracosakis(acetoxymethyl)-40-crown-12 octaacetal **3** showed the 40-membered ring to have an undulated four-loop structure (cf. Figure 3), not unlike the shape of a four-leaf clover. For the 35-C-14 analog **2**, comprising seven *meso*-butanetetrol/glycolaldehyde acetal units, we envisage its conformational features to resemble that of **1** with the "uneven" unit inserted in *gauche*-orientation into the alternating *gauche* / *anti*-arrangements, because two successive *anti*-disposed glycol fragments would enter considerable strain into the macrocycle.

Unequivocal evidence for inclusion compounds of the crown acetals **1** - **6**, as of now, is not available, yet the unusually broad melting range of the  $\beta$ -CD-derived **5**, when crystallized from *n*-propanol (145-157 °C), and the  $^1\text{H}$  NMR in  $\text{D}_6$ -DMSO, which reveals the presence of one equivalent of *n*-propanol, is strongly indicative of the product being a 1:1 complex  $\mathbf{5} \cdot n\text{-PrOH}$ . Whether the guest though sits inside the 35-C-14-macrocycles cavity or is only associated to hydroxymethyl substituents remains to be established.

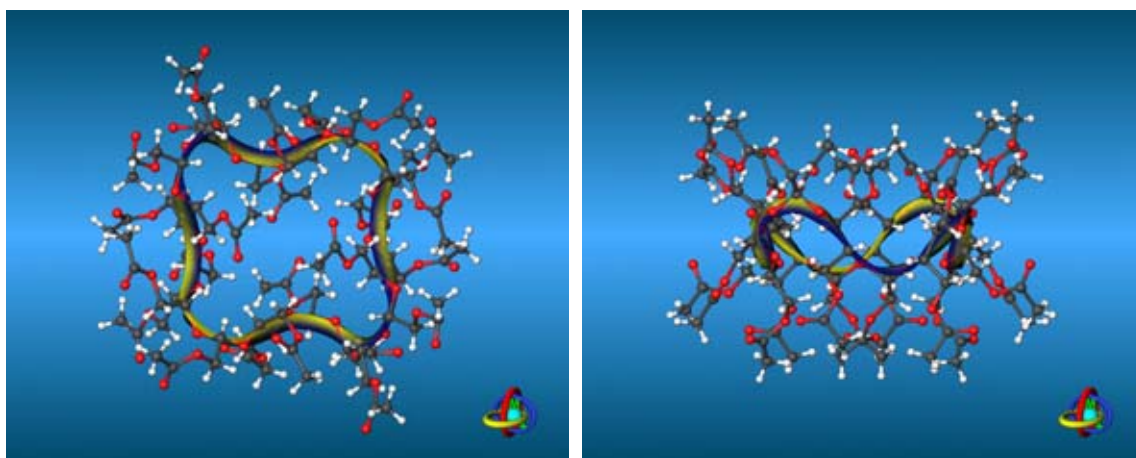


Figure 3. X-ray-derived molecular geometry of the  $\gamma$ -CD-derived tetracosakis(acetoxymethyl)-40-crown-16 octaacetal **3** in ball-and-stick representation, illustrating the four-looped clover-leaf type structure and its distinctly waved form.<sup>[11]</sup>

## ACKNOWLEDGMENTS

Appreciation is expressed to the Fonds der Chemischen Industrie, Frankfurt, and the Südzucker AG, Mannheim / Ochsenfurt, for financial support, to Mrs. S. Foro for collecting the X-ray data of **1** and **3**, and to Wacker-Chemie, Burghausen, for generous gifts of the cyclodextrins.

## NOTES AND REFERENCES

- [1] *Nomenclature*: Although macrocyclic polyacetals such as **1** - **6** are improbable to adopt a crown-like molecular geometry – the terminology for macrocyclic ethers was derived from their crown-like shape – it appears logical as well as practical to extend this well-introduced notational mode to the acetal analogs of crown ethers, resulting in the term *crown acetals* for macrocycles with acetal oxygens only. Likewise, it appears most appropriate to adopt for crown acetals the crown ether-type description for ring size and number of oxygens; accordingly, **4** is the octadecakis(hydroxymethyl) derivative of a 30-crown-12 hexaacetal, whereas the respective  $\beta$ -CD- and  $\gamma$ -CD-derived analogs **5** and **6** are macrocycles with a 35-crown-14 and 40-crown-16 backbone.
- [2] *Crown acetal skeletal backbones*: (a) 10-C-4: Bassi, I. W., Scordamaglia, R., Fiori, L., *J. Chem. Soc., Perkin Trans. 2* **1975**, 1129-1132. – (b) Substituted 10-C-4-systems: Terzis, A., Grindley, T. B., *Can. J. Chem.* **1979**, *57*, 2154-2157. – Stoddart, J. F., Szarek, W. A., *Can. J. Chem.* **1968**, *46*, 3061-3069. – (c) 12-C-4: Borgen, G., Dale, J., *J. Chem. Soc., Chem. Commun.* **1974**, 484-485; Dale, J., *Tetrahedron* **1974**, *30*, 1683-1694. – (d) 14-C-4: Bassi, I. W., Scordamaglia, R., Fiori, L., *J. Chem. Soc., Perkin Trans. 2* **1972**, 1726-1729. – (e) 16-C-4: Dale, J., Ekeland, T., *Acta Chem. Scand., Ser. A* **1973**, *27*, 1519-1525. – Groth, P., *ibid.* **1975**, *29*, 642-643. – (f) 18-C-4, 24-C-4, 26-C-4, and 34-C-4: Hill, J. W., Carothers, W. H., *J. Am. Chem. Soc.* **1935**, *57*, 925-928.
- [3] (a) French, D., McIntyre, R. J., *J. Am. Chem. Soc.* **1950**, *72*, 5148-5150. – (b) Hisamatsu, M., Yamada, Y., Nakashima, K., Tobata, K., *Starch/Stärke* **1992**, *44*, 188-191.
- [4] (a) Stoddart, J. F., Szarek, W. A., Jones, J. K. N., *Can. J. Chem.* **1969**, *47*, 3213-3215. – (b) Kandra, L., Lipták, A., Jodál, I., Nánási, P., Szejtli, J., *J. Inclusion Phenom.* **1984**, *2*, 869-875.
- [5] (a) Nogami, A., Nasu, K., Koga, T., Ohta, K., Fujita, K., Immel, S., Lindner, H. J., Schmitt, G. E., Lichtenthaler, F. W., *Angew. Chem.* **1997**, *109*, 1987-1991; *Angew. Chem. Int. Ed. Engl.* **1997**, *36*, 1899-1902. – (b) Fujita, K., Chen, W.-H., Yuan, D.-Y., Nogami, Y., Koga, T., Fujioka, T., Mihashi, K., Immel, S., Lichtenthaler, F. W., *Tetrahedron: Asymmetry* **1999**, *10*, 1689-1696. – (c) Immel, S., Fujita, K., Lichtenthaler, F. W., *Chem. Eur. J.* **1999**, *5*, 3185-3192. – (d) Gohlke, H., Immel, S., Lichtenthaler, F. W., *Carbohydr. Res.* **1999**, *321*, 96-104.
- [6] Koshland, D. E., *Angew. Chem.* **1994**, *106*, 2368-2372; *Angew. Chem. Int. Ed. Engl.* **1994**, *33*, 2375-2378.
- [7] Fischer, E., *Ber. Dtsch. Chem. Ges.* **1884**, *27*, 2985-2993. – Lichtenthaler, F. W., *Angew. Chem.* **1994**, *106*, 2456-2467; *Angew. Chem. Int. Ed. Engl.* **1994**, *33*, 2364-2374.
- [8] Systematic name for **4**: 2,4,5,7,9,10,12,14,15,17,19,20,22,24,25,27,29,30-octadecakis(hydroxymethyl)-1,3,6,8,11,13,16, 18,21,23,26,28-dodecaoxacyclotriacontane; the hexaacetal **1** is the octadeca-acetate thereof. Correspondingly, **5** is a derivative of tetradecaoxacyclopentatriacontane; **6** one of a hexadecaoxacyclopentetracontane.
- [9] Immel, S., Nakagawa, T., Lindner, H. J., Lichtenthaler, F. W., *Chem. Eur. J.* **2000**, *6*, in press (October issue).
- [10] Sheldrick, G. M., *SHELXS-97* and *SHELXL-97* – *Programs for Crystal Structure Solution and Refinement*, University of Göttingen, Germany, **1990** and **1997**.
- [11] Graphics of Figures 1 and 3 were generated using the MolArch<sup>+</sup> program: Immel, S. *MolArch<sup>+</sup> MOLEcular ARCHitecture Modeling Program*. Darmstadt University of Technology, Germany, **1999**.

*Proc. 10<sup>th</sup> Int. Symp. Cyclodextrins* (Ed.: J. Szejtli), Mia Digital Publ., Ann Arbor, Michigan, **2000**, pp. 24-31.

## FLEXIBLE NON-GLUCOSE CYCLOOLIGOSACCHARIDES

S. IMMEL

*Institute of Organic Chemistry, Darmstadt University of Technology,  
D-64287 Darmstadt, Germany*

### ABSTRACT

Despite lack of torus stabilization through interresidue hydrogen bonds, per-2,3-anhydro- $\alpha$ -cyclomannin adopts almost  $C_6$  symmetrical conformations in the solid-state structures of its ethanol and 1-propanol inclusion complexes. Thoroughly flexible cyclooligosaccharides are obtained from incorporation of  $\alpha$ -D-altropyranose residues into the macroring: mono-*altro*  $\beta$ -cyclodextrin displays an "induced-fit" type complexation of adamantane 1-carboxylate, and  $\alpha$ -cycloaltrin ( $\alpha$ -CA) is characterized by an alternating sequence  ${}^4C_1 / {}^1C_4$  altrose geometries. Analysis of the conformational properties of  $\alpha$ -CA reveals a mechanism of global pseudorotational motions in the macrocycle. Similar effects are observed in highly substituted cyclodextrin derivatives, as well as in cyclofructins, and CD-derived large ring crown acetals.

### 1. INTRODUCTION

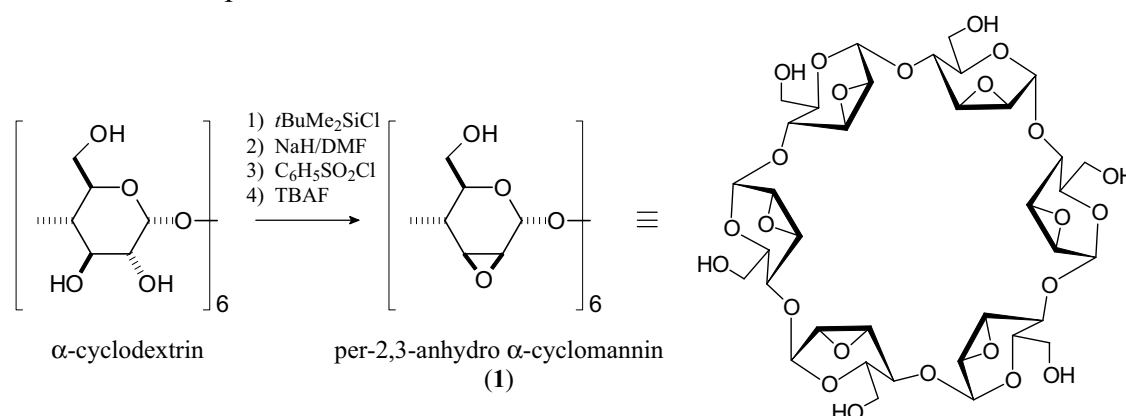
The rather static "lock-and-key"<sup>[1]</sup> type formation of inclusion complexes by cyclodextrins (CDs) is caused by their rigid, truncated-cone type structures, which — at least for  $\alpha$ -,  $\beta$ -, and  $\gamma$ -CD — generally undergo only minor structural changes upon incorporation of guest molecules.<sup>[2]</sup> To mimic biological "induced-fit"<sup>[3]</sup> type mechanisms of inclusion, the strait-jacket of the macrocycles has to be released, and some flexibility needs to be introduced into the host molecules. Of the various possibilities to affect such modifications, substitution of OH-groups on both the secondary and/or primary face of the CDs increases their flexibility through steric hindrance and repulsion between neighboring substituents, often also implying a lowered torus stabilization through disruption of the ring of interresidue 2-O ... O-3' hydrogen bonds.<sup>[4]</sup> Thoroughly flexible cyclooligosaccharides are also generated from exchange of the rather stiff  $\alpha$ -D-glucose residues against more flexible pyranose units such as  $\alpha$ -D-altrose,<sup>[5,6]</sup> or by per-iodate oxidation of the C-2 - C-3 bonds as demonstrated by the CD-derived large ring crown acetals.<sup>[7,8]</sup> This account describes some conformational properties of various flexible non-glucose cyclooligosaccharides.

25

## 2. RESULTS AND DISCUSSION

### 2.1 Per-2,3-anhydro- $\alpha$ -cyclomannin (**1**)

Per-2,3-anhydro- $\alpha$ -cyclomannin **1**<sup>[5,9]</sup> is readily available from  $\alpha$ -CD in a straightforward four-step sequence of reactions, implying protection of the primary 6-OH groups and base-induced activation of the 2-OH groups, followed by epoxide ring formation and deprotection.<sup>[5]</sup>



When crystallized from aqueous ethanol or 1-propanol, **1** accumulates as the ethanol<sup>[10]</sup> or 1-propanol<sup>[11]</sup> 1 : 1 inclusion complex, respectively, with varying amounts of co-crystallized water. X-Ray solid-state structural analysis reveals both crystal structures to be isomorphic (both trigonal, space group  $P3_212$ ,  $Z = 6$ ); Figure 1 displays segments of the structures. In both complexes, the cyclomannin hosts are stacked in an alternating head-to-head and tail-to-tail like fashion along the  $c$ -axis, forming layers of complex dimers through the epoxide ring carrying faces of the macrocycles. These dimeric units are embedded between layers of water molecules, which in turn form a hydrogen bonding network with the primary 6-OH groups.<sup>[10,11]</sup>

Ethanol and 1-propanol are included with opposite regioselectivities: the two ethanol molecules entrapped in the cavity of a dimeric unit of the complex form a hydrogen bond between their hydroxyl groups.<sup>[10]</sup> In the 1-propanol complex, the hydroxyl groups of the guest molecules form hydrogen bonds towards water molecule in the layer around the 6-OH groups, and the two propyl side chains face each other.<sup>[11]</sup> Obviously, ethanol is not large enough to fully occupy the cavity of **1** while forming ethanol - water hydrogen bonds, thus leading to the elaboration of a guest-guest hydrogen bond rather than leaving a hydrophobic void in the cavity. The 1-propanol guest fills the cavity more effectively, and allows for hydrophobic contacts between the alkyl chains in the cavity.

Without introducing steric hindrance, the six epoxide rings in **1** block the formation of 2-O  $\cdots$  O-3' interresidue hydrogen bonds, leaving the torus less stabilized than in the CDs. However, the two inclusion complexes of **1** display very little variations in the almost  $C_6$  symmetrical macrocyclic ring conformations of the host molecules. This may be — at least in part — attributed to the still rather rigid conformations of the 2,3-anhydro mannoside residues, which invariably adopt  ${}^0\text{H}_5$  pyranose ring geometries.

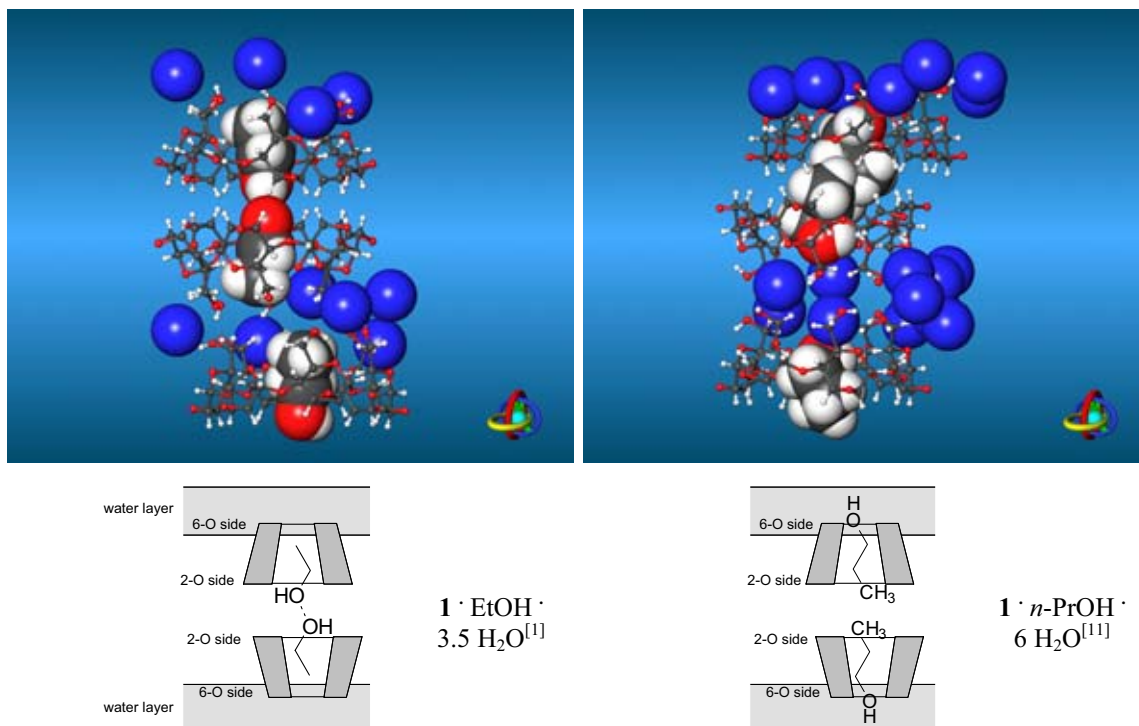


Figure 1. Segments of the crystal structures of the per-2,3-anhydro- $\alpha$ -cyclomannin (**1**) ethanol<sup>[10]</sup> (left) and 1-propanol<sup>[11]</sup> inclusion complex (right). Both isomorphous structures feature stacks of head-to-head oriented hosts, separated through layers of water molecules (blue spheres). The two guest molecules entrapped in the cavity of a complex dimer are displayed as CPK-type models; the opposite mode of inclusion of ethanol and 1-propanol is indicated by the schematic plots.

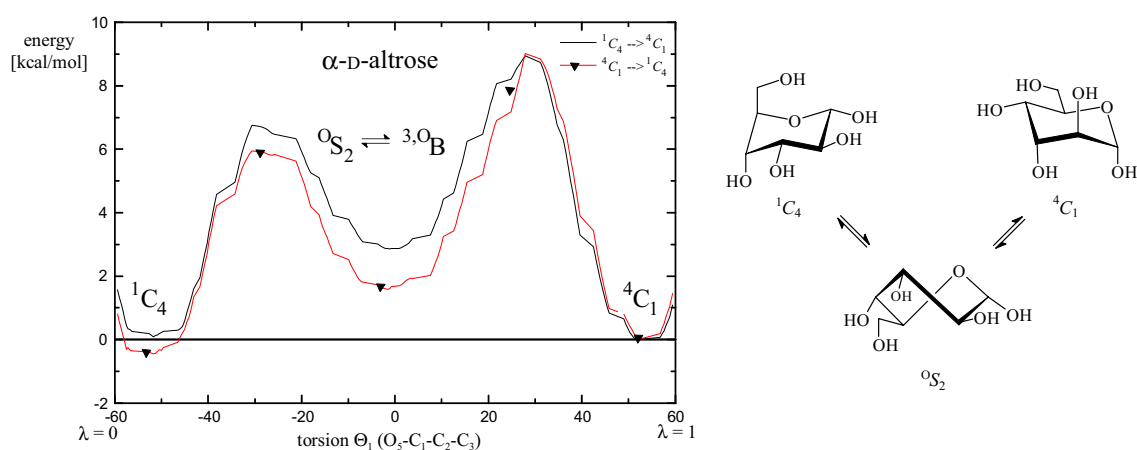
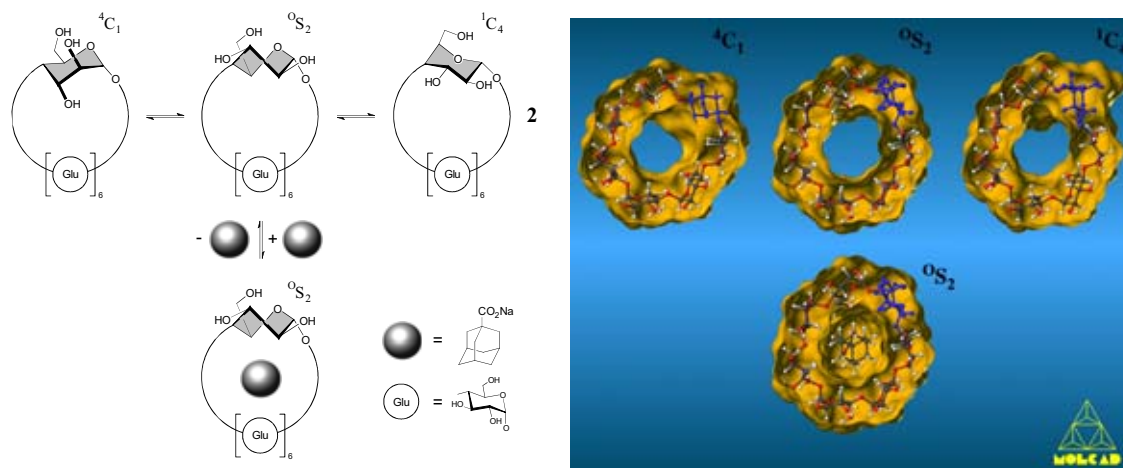


Figure 2. Calculated free energy profile ("potential of mean force", CHARMM) of  $\alpha$ -D-altrose in aqueous solution (explicit incorporation of solvent water molecules) as a function of the pyranose ring conformation; energies are given in kcal/mol. Conformations were driven along the reaction coordinate  $\lambda=0.0 \rightarrow 1.0$  through two constrained pyranose ring torsion angles  $\theta_1$  ( $O_5-C_1-C_2-C_3$ ) and  $\theta_4$  ( $C_3-C_4-C_5-O_5$ ); the hysteresis in the forward and backward direction of  $\lambda$  indicates the error in energy.

27



**Figure 3.** *Left:* Schematic representation of the "induced-fit" type formation of the inclusion complex between mono-*altro*- $\beta$ -cyclodextrin (**2**) and adamantane-1-carboxylate. The altropyranoid unit is conformational flexible in the free host, although the  ${}^1C_4$  form is slightly preferred over the  ${}^4C_1$  and  ${}^0S_2$  forms. This equilibrium is significantly shifted towards the  ${}^0S_2$  form upon inclusion of the guest. *Right:* Molecular models of **2** (top row: free host) and its adamantane-1-carboxylate complex (bottom), with the corresponding molecular surfaces superimposed; the altrose units in the macrorings are colored blue, respectively. Of the  ${}^4C_1$ ,  ${}^0S_2$ , and  ${}^1C_4$  forms, only the  ${}^0S_2$  geometry features an almost symmetrical round cavity which is able to include the ball-shaped adamantane guest without major steric hindrance.

## 2.2 Mono-*altro*- $\beta$ -cyclodextrin (**2**)

More flexible than glucopyranose rings or the above 2,3-anhydro mannopyranose are altrose residues, which are synthetically accessible via diaxial-opening of the epoxide precursors. It is well established that the  ${}^4C_1$  and  ${}^1C_4$   $\alpha$ -D-altropyranose chair and anti-chair conformations are highly flexible.<sup>[12]</sup> Figure 2 gives the calculated free-energy profile for the  ${}^4C_1 \rightleftharpoons {}^0S_2 / {}^3,0B \rightleftharpoons {}^1C_4$  pathway of  $\alpha$ -D-altrose: both chair and anti-chair geometries are almost equal in energy, whilst the intermediate  ${}^0S_2 / {}^3,0B$  forms are slightly less stable.<sup>[13]</sup>

In the case of mono-*altro*  $\beta$ -CD (**2**), NMR titrations yielded all proton-proton coupling constants of the altropyranose rings in the free host, as well as in its adamantane 1-carboxylate inclusion complex.<sup>[14]</sup> Analysis of these values as a function of the altrose conformations displays a highly characteristic "induced-fit" type inclusion complex formation: the slightly preferred  ${}^1C_4$  altrose ring geometry in free **2** is shifted towards a  ${}^0S_2$  skew-boat form in the complex.<sup>[14]</sup> As indicated in Figure 3, only the intermediate skew-boat form features a round-shaped cavity, which is able to accommodate the ball-shaped guest molecule without steric hindrance.

## 2.3 $\alpha$ -Cycloaltrin (**3**)

In the solid-state,  $\alpha$ -Cycloaltrin ( $\alpha$ -CA, **3**)<sup>[5]</sup> surprisingly adopts a structure comprising an alternating sequence of  ${}^4C_1$  and  ${}^1C_4$  pyranoid chair conformations (Figure 4), leaving the molecule of disk-type shape with a central indentation only rather than a through-

going cavity.<sup>[5]</sup> At ambient temperatures, the  $^1\text{H}$  (800 MHz) and  $^{13}\text{C}$  (200 MHz) NMR spectra in  $\text{D}_2\text{O}$  show one set of signals for the time-averaged,  $C_6$  symmetrical structure of **3** only, yet at 4 °C broadened  $^{13}\text{C}$  signals C-4 and C-5 are indicative for dynamic conformational equilibria in  $\alpha$ -CA in aqueous solution.<sup>[6,15]</sup>

$^1\text{H}$  NMR (500 MHz) data in  $\text{CD}_3\text{OD} / \text{D}_2\text{O}$  (9 : 1) at -80 °C display a split set of signals, which is consistent with the solid-state structure of **3** as the major form prevailing also in solution.<sup>[16]</sup> Although standard molecular dynamics (MD) simulations of  $\alpha$ -CA (**3**) in aqueous solution proved to be too slow to monitor conformational transitions in the altrose units of the macrocycle, we have used constrained MD techniques to simulate the dynamics of **3** in water.<sup>[6]</sup> From these calculations, it can be derived that any single conformational transition in the altrose residues induces subsequent conformational changes in neighboring units in the macrocyclic ring. The geometry variations in the pyranose units induce adjacent residues to follow suit within the strait-jacket of the macrocycle, inducing a "rolling-around" of conformational transitions along the macrocycle.<sup>[6]</sup>

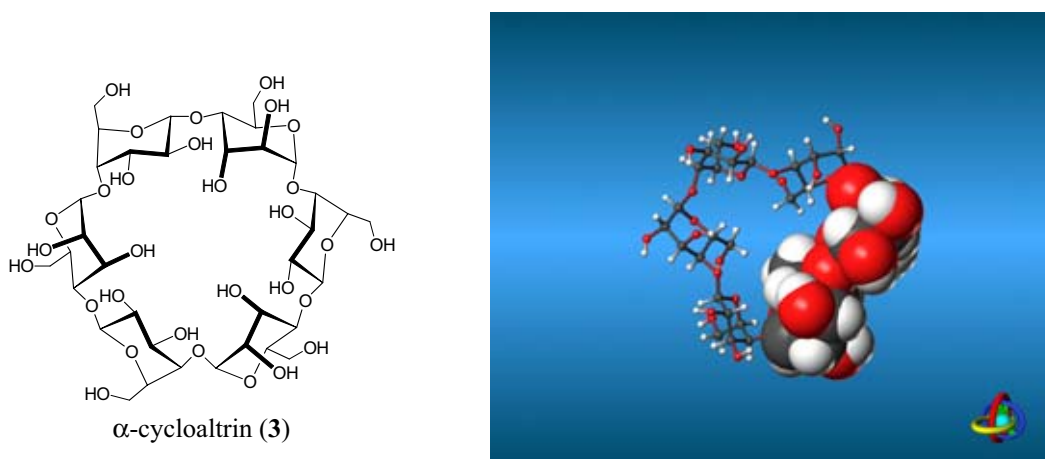


Figure 4. Molecular geometry of  $\alpha$ -CA (**3**) in the solid-state:<sup>[5]</sup> the altropyranose rings adopt  ${}^4\text{C}_1$  and  ${}^1\text{C}_4$  conformations in an alternating sequence, rendering the molecule with three-fold rotational symmetry ( $C_3$ ). On the right, the asymmetric  ${}^4\text{C}_1 / {}^1\text{C}_4$  disaccharide unit of **3** is rendered as a CPK-type model.

#### 2.4 Local versus Global Pseudorotation in Cyclooligosaccharides

In solution, the alternating  $[{}^4\text{C}_1 / {}^1\text{C}_4]_3$  structure of  $\alpha$ -CA (**3**) with its symmetry reduced to  $C_3$  represents only a limiting structure in a complex conformational equilibrium.<sup>[6]</sup> Thermal motions lead to an exchange between  $[{}^4\text{C}_1 / {}^1\text{C}_4]_3$  and  $[{}^1\text{C}_4 / {}^4\text{C}_1]_3$  forms in a "jelly-fish"-like fashion with an activation barrier of about 8.5 kcal/mol (Figure 5).<sup>[16]</sup> The transition between both forms cannot occur instantaneously, but must necessarily involve multiple intermediate altropyranose conformations such as  ${}^0\text{S}_2$  forms, as well as different macrocyclic shapes, such as the *all*- ${}^0\text{S}_2$  form of **3**, conceivably. The over-all process is a stereoisomerization of  $\alpha$ -CA (**3**) resulting in a structure that appears to have been produced by simple rotation of the entire initial molecule by 60° around its central axis. This mechanism of "global pseudorotation" of the entire macrocycle of  $\alpha$ -CA is

inseparably correlated with local motions in the altrose residues and their chair / anti-chair transitions ("*local pseudorotation*"). In total, the symmetry of  $\alpha$ -CA is lowered from  $C_6$  to  $C_3$ , and only time-averaged data accounts for the  $^1\text{H}$  and  $^{13}\text{C}$  NMR spectra of **3** at room temperatures.

The concept of global pseudorotation is not only applicable to  $\alpha$ -CA, but is also manifested in a number of structurally diverse flexible cyclooligosaccharides (cf. Figure 5). A force-field based molecular modeling study of the "*extended cavity*"  $\alpha$ -CD derivatives of Wenz et al.<sup>[17]</sup> indicates that these compounds cannot adopt  $C_6$  symmetrical structures due to steric hindrance between neighboring glucose units. Instead, the substituted glucopyranoses are alternatingly tilted "*inward*" and "*outward*" in relation to the central molecular axis (Figure 5), and any exchange must involve successive contra-rotatory movements of neighboring units in the over-all process of "*global pseudorotation*". Similar effects are observed for the corresponding  $\beta$ - and  $\gamma$ -CD derivatives, too.

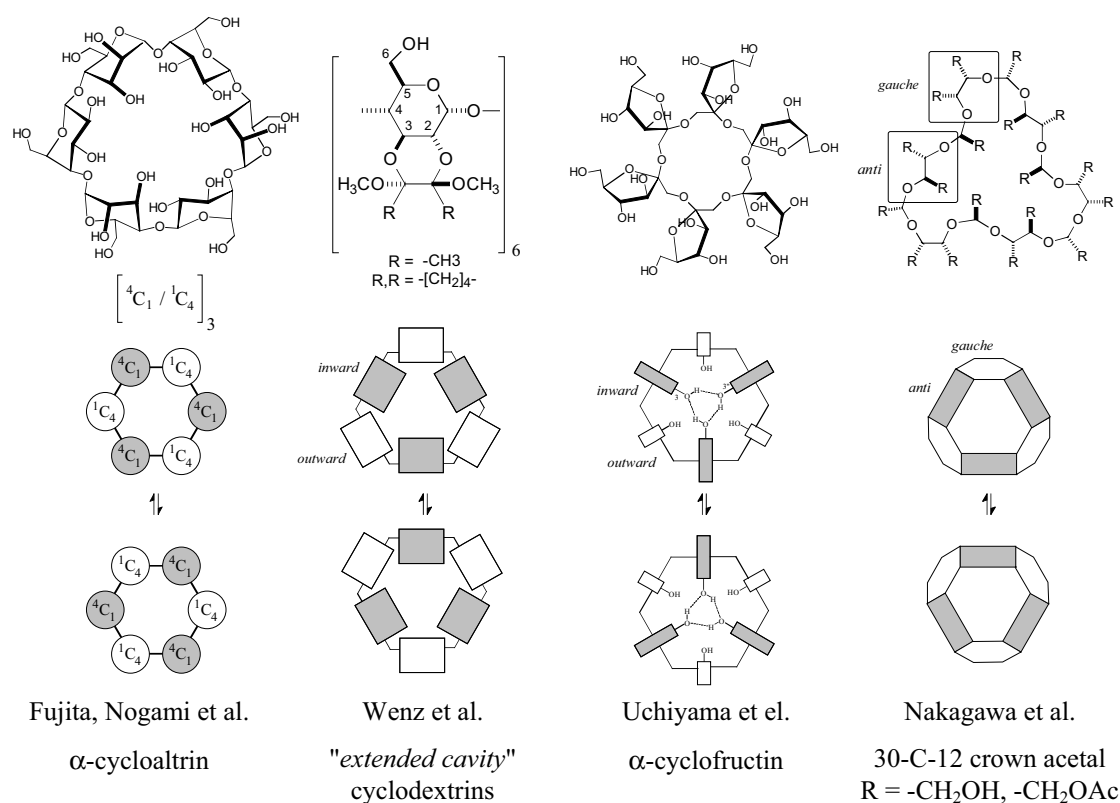


Figure 5. Schematic representation of the "*global pseudorotation*" observed for various flexible cyclooligosaccharides: none of the compounds listed above adopts fully  $C_6$  symmetrical structures, yet in all cases symmetry is lowered to  $C_3$  by either alternating pyranose ring geometries, alternating "*inward*" and "*outward*" tilting of individual monosaccharide units, or alternating "*anti*" and "*gauche*" disposition of ring torsion angles. Although initiated through different "*local*" molecular motions, in any case above, structures of the  $[\text{AB}]_3$ -type undergo interconversion to  $[\text{BA}]_3$ - geometries through a process of "*global pseudorotation*".



The solid-state structure of  $\alpha$ -cyclofructin<sup>[18]</sup> also displays  $C_3$  symmetry, the  $\beta(1\rightarrow2)$  *spiro*-type anellation of the fructofuranose residues to the 18-crown-6 backbone is characterized by an alternating "*inward/outward*" inclination of the furanose rings relative to the macrocycle. In each case the 3-OH groups of the three "*inward*" directed units form an homodromic cycle of hydrogen bonds in the center of the molecule (Figure 5). Indeed, a detailed molecular modeling study on cyclofructins composed of six to ten fructofuranose units displayed analogous conformational properties to be maintained throughout the entire series.<sup>[19]</sup>

The large-ring crown acetals<sup>[8]</sup> derived from the CDs via periodate oxidation, fit into the same scheme of "*global pseudorotational*" effects: conformational transitions involve interconversions of the alternatingly "*anti*" and "*gauche*" disposed *meso*-butanetetrol units in the macroring.<sup>[8]</sup>

### 3. CONCLUSION

Introducing flexibility into macrocyclic compounds seems to simultaneously lower the symmetry of preferred low-energy conformations in the solid-state as well as in solution. For the four compounds listed in Figure 5, symmetry is invariably reduced from  $C_6$  to  $C_3$  through alternating local geometry parameters such as pyranose ring conformations, tilting of monosaccharide residues, and ring torsion angles. The mechanism of "*global pseudorotation*" accounts for the dynamic conformational exchange phenomena observed for these compounds, and their time-averaged symmetrical structures in solution. Presently we are looking forward to study the dynamics of these exchange processes in greater detail.

### ACKNOWLEDGMENTS

Appreciation is expressed to the Fonds der Chemischen Industrie, Frankfurt, and the Südzucker AG, Mannheim / Ochsenfurt, for financial support.

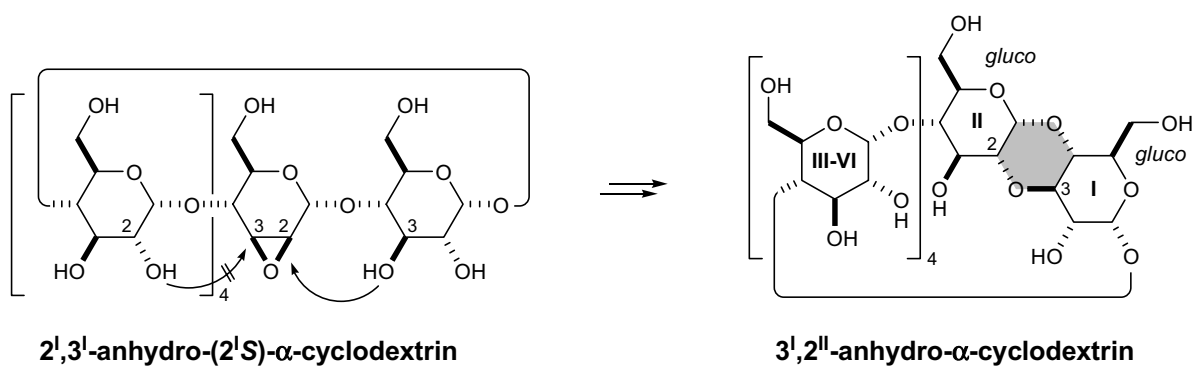
### NOTES AND REFERENCES

- [1] Fischer, E., *Ber. Dtsch. Chem. Ges.* **1884**, 27, 2985-2993. – Lichtenthaler, F. W., *Angew. Chem.* **1994**, 106, 2456-2467; *Angew. Chem. Int. Ed. Engl.* **1994**, 33, 2364-2374.
- [2] Lichtenthaler, F. W., Immel, S., *Liebigs Ann. Chem.* **1996**, 27-37.
- [3] Koshland, D. E., *Angew. Chem.* **1994**, 106, 2368-2372; *Angew. Chem. Int. Ed. Engl.* **1994**, 33, 2375-2378.
- [4] Saenger, W., Jacob, J., Gessler, K., Steiner, T., Hoffmann, D., Sanbe, H., Koizumi, K., Smith, S. M., Takaha, T., *Chem. Rev.* **1998**, 98, 1787-1802.
- [5] Nogami, A., Nasu, K., Koga, T., Ohta, K., Fujita, K., Immel, S., Lindner, H. J., Schmitt, G. E., Lichtenthaler, F. W., *Angew. Chem.* **1997**, 109, 1987-1991; *Angew. Chem. Int. Ed. Engl.* **1997**, 36, 1899-1902.
- [6] Immel, S., Fujita, K., Lichtenthaler, F. W., *Chem. Eur. J.* **1999**, 5, 3185-3192.

- [7] (a) Stoddart, J. F., Szarek, W. A., Jones, J. K. N., *Can. J. Chem.* **1969**, *47*, 3213-3215. – (b) Kandra, L., Lipták, A., Jodál, I., Nánási, P., Szejtli, J., *J. Inclusion Phenom.* **1984**, *2*, 869-875.
- [8] Nakagawa, T., Immel, S., Lindner, H. J., Lichtenthaler, F. W., *Proceedings of the 10<sup>th</sup> Internat. Symp. on Cyclodextrins* (Ed.: Szejtli, J.), see this volume. – Immel, S., Nakagawa, T., Lindner, H. J., Lichtenthaler, F. W., *Chem. Eur. J.* **2000**, *6*, in press.
- [9] Coleman, A. W., Zhang, P., Ling, C. C., Mahuteau, J., Parrot-Lopez, H., Miocque, M., *Supramol. Chem.* **1992**, *1*, 11-14; – Zhang, P., Coleman, A. W., *Supramol. Chem.* **1993**, *2*, 255-263.
- [10] Immel, S., Fujita, K., Lindner, H. J., Nogami, Y., Lichtenthaler, F. W., *Chem. Eur. J.* **2000**, *6*, 2327-2333.
- [11] Immel, S., Lichtenthaler, F. W., Lindner, H. J., Fujita, K., Fukudome, M., Nogami, Y., *Tetrahedron: Asymmetry* **2000**, *11*, 27-36.
- [12] Lichtenthaler, F. W., Mondel, S., *Carbohydr. Res.* **1997**, *303*, 293-302.
- [13] Schmitt, G., *Dissertation*, Darmstadt University of Technology, **1999**.
- [14] Fujita, K., Chen, W.-H., Yuan, D.-Y., Nogami, Y., Koga, T., Fujioka, T., Mihashi, K., Immel, S., Lichtenthaler, F. W., *Tetrahedron: Asymmetry* **1999**, *10*, 1689-1696.
- [15] Immel, S., Schmitt, G. E., Lichtenthaler, F. W., *Proceedings of the 9<sup>th</sup> Internat. Symp. on Cyclodextrins* (Eds.: Torres-Labandeira, J. J., Vila Jato, J. L.), Kluwer Acad. Publ., Dordrecht, NL, **1998**, 41-48.
- [16] Fujita, K., Ohta, K., Nogami, Y., Nasu, K., Shiratani, T., Sudo, M., Koga, T., *Proceedings of the 9<sup>th</sup> Internat. Symp. on Cyclodextrins* (Eds.: Torres-Labandeira, J. J., Vila Jato, J. L.), Kluwer Acad. Publ., Dordrecht, NL, **1998**, 113-115.
- [17] Dörr, S., *Diploma Thesis*, Universität Karlsruhe, **1999**. – Immel, S., Wenz, G., unpublished results.
- [18] Sawada, M., Tanaka, T., Takai, Y., Hanafusa, T., Hirotsu, K., Higuchi, T., Kawamura, M., Uchiyama, T., *Chem. Lett.* **1990**, 2011-2014. – Sawada, M., Tanaka, T., Takai, Y., Hanafusa, T., Taniguchi, T., Kawamura, M., Uchiyama, T., *Carbohydr. Res.* **1991**, *217*, 7-17.
- [19] Immel, S., Schmitt, G. E., Lichtenthaler, F. W., *Carbohydr. Res.* **1998**, *313*, 91-105. – Immel, S., Schmitt, G. E., Lichtenthaler, F. W., *Proceedings of the 9<sup>th</sup> Internat. Symp. on Cyclodextrins* (Eds.: Torres-Labandeira, J. J., Vila Jato, J. L.), Kluwer Acad. Publ., Dordrecht, NL, **1998**, 57-62.

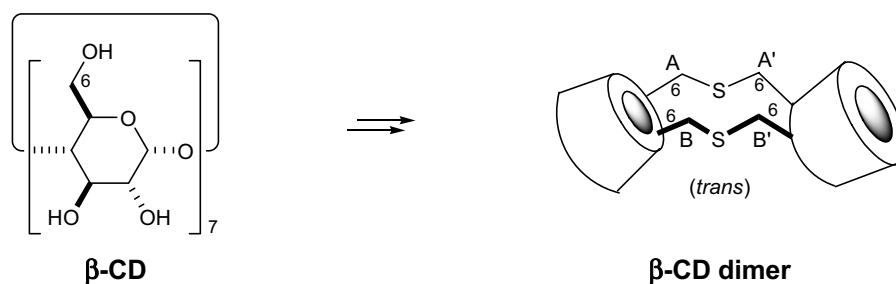
## Chapter 7

### Rigidified Bridged Cyclodextrins



Two Stereoisomeric 3',2''-Anhydro- $\alpha$ -cyclodextrins: A Molecular Dynamics and Crystallographic Study

S. Immel, K. Fujita, M. Fukudome, and M. Bolte,  
*Carbohydr. Res.* **2001**, 336, 297-308.



The First Successful Crystallographic Characterization of a Cyclodextrin Dimer:  
 Efficient Synthesis and Molecular Geometry of a Doubly Sulfur-bridged  $\beta$ -Cyclodextrin

D.-Q. Yuan, S. Immel, K. Koga, M. Yamaguchi, and K. Fujita,  
*Chem. Eur. J.* **2003**, 9, 3501-3506.





# Two stereoisomeric 3<sup>I</sup>,2<sup>II</sup>-anhydro- $\alpha$ -cyclodextrins: a molecular dynamics and crystallographic study<sup>☆</sup>

Stefan Immel,<sup>a,\*</sup> Kahee Fujita,<sup>b</sup> Makoto Fukudome,<sup>b</sup> Michael Bolte<sup>c,†</sup>

<sup>a</sup>*Institut für Organische Chemie, Technische Universität Darmstadt, Petersenstraße 22,  
D-64287 Darmstadt, Germany*

<sup>b</sup>*Faculty of Pharmaceutical Sciences, Nagasaki University, 1-14 Bunkyo-machi Nagasaki 852-8521, Japan*

<sup>c</sup>*Institut für Organische Chemie, J.W. Goethe-Universität Frankfurt, Marie-Curie-Straße 11,  
D-60439 Frankfurt (Main), Germany*

Received 10 August 2001; accepted 8 October 2001

## Abstract

Regioselective epoxide ring opening of 2<sup>I</sup>,3<sup>I</sup>-(2<sup>I</sup>*S*)-anhydro- $\alpha$ -cyclodextrin (**1**) through intramolecular attack of hydroxyl groups of neighboring glucose rings occurs in diequatorial fashion to yield 3<sup>I</sup>,2<sup>II</sup>-anhydro- $\alpha$ -cyclodextrin (**3**) with a rigid glucopyranose–dioxane–glucopyranose tricyclic ring system, the usual diaxial opening and the gluco/altro-configured stereoisomer **2** cannot be detected. Molecular dynamic simulations in water were used to analyze the conformations of **1–3** and the stereochemical implications of this reaction. Due to the contracted 2,3-OH side of the torus, **3** features an inverted conicity compared to the parent  $\alpha$ -cyclodextrin. A crystallographic study on the bis-3:3 *n*-PrOH nonahydrate not only displays little variations between the solid-state and solution geometries of **3**, but also provides a molecular picture of a unique inclusion complex in which three *n*-propanol molecules are distributed in the cavity of a dimeric unit of **3** (monoclinic, space group *P*2<sub>1</sub>, *a* = 14.257(1), *b* = 22.623(2), *c* = 16.644(1) Å,  $\beta$  = 104.82(1)°, all 19278 reflections with *I* > 2 $\sigma$ (*I*) yield *R*(*F*) = 0.1017). © 2001 Elsevier Science Ltd. All rights reserved.

**Keywords:** 2<sup>I</sup>,3<sup>I</sup>-(2<sup>I</sup>*S*)-Anhydro- $\alpha$ -cyclodextrin; 3<sup>I</sup>,2<sup>II</sup>-Anhydro- $\alpha$ -cyclodextrin; Molecular dynamics; Crystal structure; *n*-Propanol inclusion complex

## 1. Introduction

Cyclodextrin (CD) 2,3-*manno*-epoxides<sup>2–10</sup> are highly useful intermediates in the course of chemical transformations of the backbone structure of these macrocycles.<sup>11,12</sup> In general,

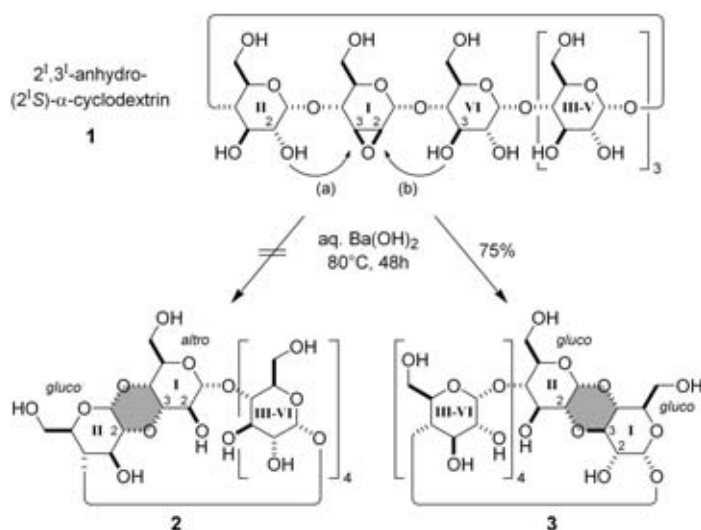
epoxide ring opening occurs highly selectively through nucleophilic attack in a trans-diaxial type fashion at C-3, offering versatile synthetic routes towards, e.g., per-3-deoxy-cyclomannans,<sup>13</sup> mono-*altro*-CDs,<sup>14–16</sup> di-*altro*-CDs,<sup>17</sup> and cycloaltrans ( $\alpha$ -,  $\beta$ -, and  $\gamma$ -‘cycloaltrin’),<sup>18–22</sup> although the alternative diequatorial ring opening at C-2 has also been observed to occur to a lesser extent for various sulfur- and nitrogen-containing nucleophiles.<sup>23</sup> It therefore may be surmised, that intramolecular variations of this reaction proceed with similar stereo- and regioselectivity. In the case of 2<sup>I</sup>,3<sup>I</sup>-(2<sup>I</sup>*S*)-anhydro- $\alpha$ -CD (**1**), the in-

<sup>☆</sup> Molecular modeling of saccharides, Part 30. For Part 29, see Ref. 1.

\* Corresponding author. Tel.: +49-6151-165277; fax: +49-6151-166674.

E-mail address: lemmi@sugar.oc.chemie.tu-darmstadt.de (S. Immel).

<sup>†</sup> X-ray analysis, solution, and refinement.



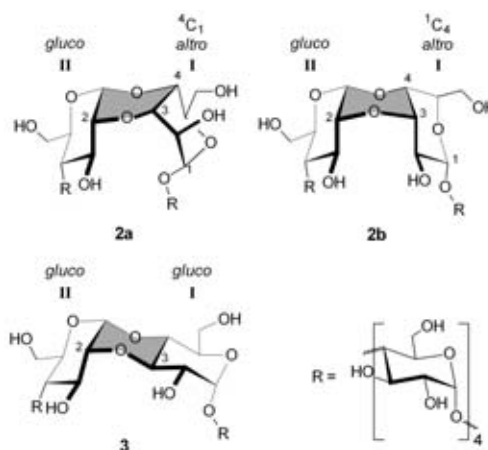
Scheme 1. Competing pathways (a) and (b) for the intramolecular ring opening of the mono-epoxide of  $\alpha$ -cyclodextrin **1** through attack of neighboring hydroxyl groups (along pathway (b) the labeling of the sugar units changes).

tramolecular attack on the epoxide can involve either the 2<sup>II</sup>-OH or 3<sup>VI</sup>-OH group of the adjacent glucose residues (cf. Scheme 1). Along pathway (a), the trans-diaxial type opening leaves the pyranoid ring I with alto-configuration, whereas the alternative reaction path (b) generates a glucopyranoid ring I (diequatorial epoxide opening). Unexpectedly, the base-induced formation of the 1,4-dioxane ring exclusively proceeds via pathway (b), i.e. **1**  $\rightarrow$  **3**, the formation of **2** was not observed.<sup>24</sup>

As an interpretation of this finding, it was brought forth that the trans-diaxial opening of the epoxide is sterically hindered by the macrocyclic structure of the CD derivative.<sup>24</sup> Although flexible CD derivatives or non-glucose cyclooligosaccharides<sup>25</sup> receive interest in mimicking the induced-fit type molecular recognition<sup>16</sup> by enzymes,<sup>26</sup> a study on the binding ability of methyl orange towards a number of CDs with deformed cavities indicated that the higher homolog of **3**, i.e. 3<sup>I</sup>,2<sup>II</sup>-anhydro- $\beta$ -CD (**4**) is the only candidate amongst the compounds studied to exhibit stronger binding (by about a factor of 2.8 at 10 °C) than  $\beta$ -CD itself.<sup>27</sup> In this context of rigidified, lock-and-key type<sup>28</sup> hosts with increased affinity towards guest molecules, we here report on the molecular structures and conformations of the compounds involved in the formation of 3<sup>I</sup>,2<sup>II</sup>-anhydro-CDs, based on a molecular modeling study in conjunction with a crystallographic analysis of **3**.

## 2. Results and discussion

Although compounds **2** and **3** result from different regioselectivities in the course of epoxide ring opening, both are in fact stereoisomers rather than regioisomers due to the symmetry of the macrocycle. In **2**, a cis-cis type junction of a glucopyranoid ring and an altropyranose is realized via a central 1,4-dioxane ring (cf. Scheme 2). As altrose itself exhibits considerable intrinsic flexibility in which the ring adopts either a <sup>4</sup>C<sub>1</sub> chair or an



Scheme 2. Molecular configurations and possible conformations of 3<sup>I</sup>,2<sup>II</sup>-anhydro- $\alpha$ -cyclodextrin: trans-diaxial epoxide ring opening (**1**  $\rightarrow$  **2**, pathway (a) in Scheme 1) conceivably results in two conformers with the altropyranose residue I adopting either the <sup>4</sup>C<sub>1</sub> (**2a**) or <sup>1</sup>C<sub>4</sub> (**2b**) geometry. Through the alternative pathway (b) both pyranose rings retain gluco-configuration (**1**  $\rightarrow$  **3**). The central dioxane ring of each compound is highlighted by shading.

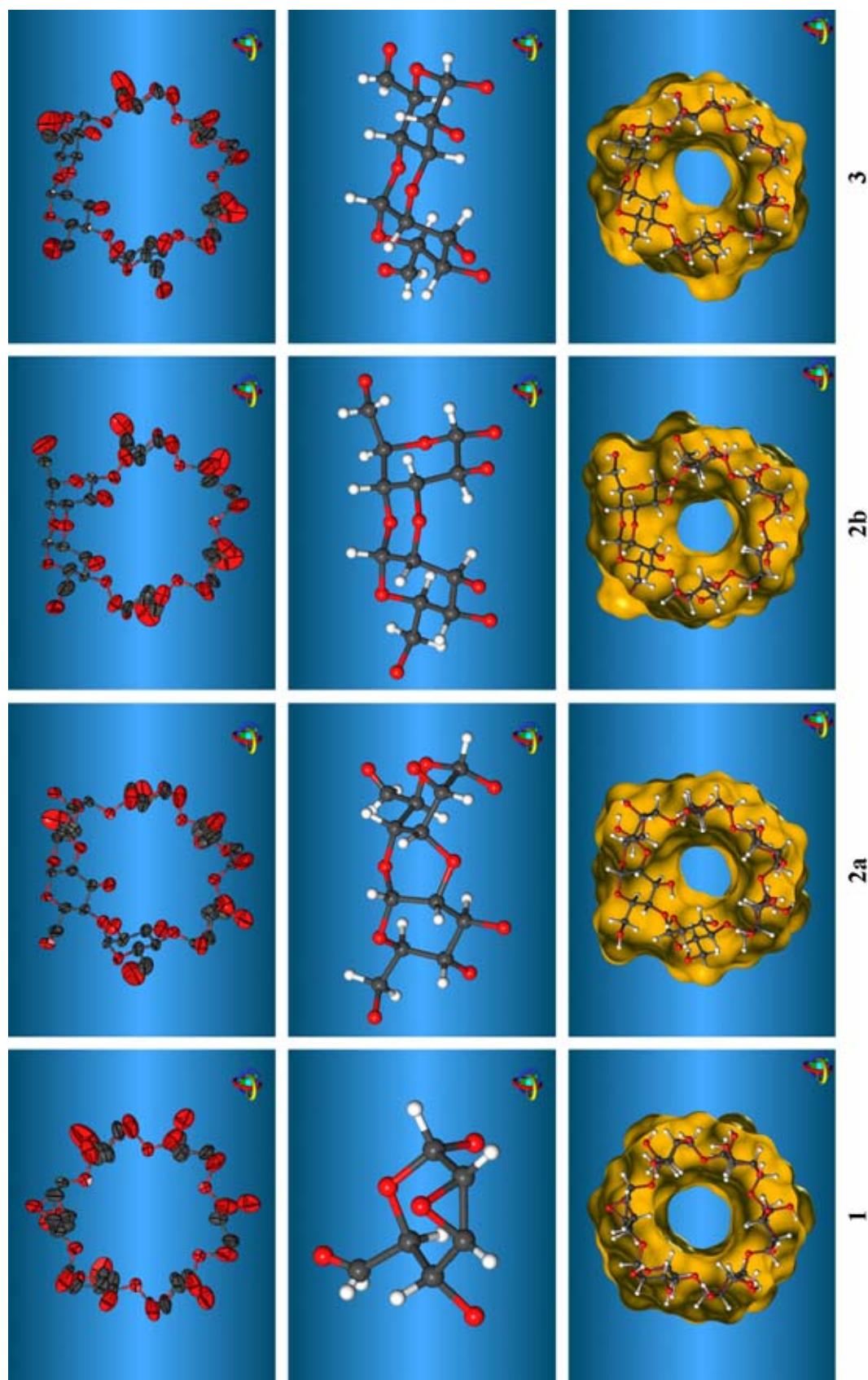


Fig. 1. Mean molecular geometries (heavy atom positions only) and anisotropic thermal ellipsoids (top row) of 2',3'-anhydro-(2'S)- $\alpha$ -CD (**1**) and the isomeric 3',2''-anhydro- $\alpha$ -CDs (**2a**, **2b**, and **3**) as derived from MD simulations in water. Center row: Enlarged ball-and-stick-type model of the sugar 2,3-epoxide unit in **1** (left) and the 3',2''-anhydro units in **2a** and **2b** (gluco/altro-configuration) as well as of **3** (gluco/glucos-steroisomer); hydroxyl-hydrogen atoms are omitted due to their flexibility. Bottom: Solvent-accessible surface models (yellow) of typical snapshot geometries extracted from the MD trajectories displaying the distorted ring conformations of the macrocycles. All molecular orientations correspond to each other, the center row models represent the topmost sugar units in the macrocycles, respectively.

Table 1

Cremer–Pople puckering parameters ( $Q$ ,  $\theta$ , and  $\phi$ ),<sup>37,38</sup> ring conformations, and tilt angles  $\tau$ <sup>39</sup> for the pyran and dioxane rings of **1–3** (MD-derived averages with root-mean-square deviations in parentheses)

Compound	Ring	Configuration	$Q$ (Å) <sup>a</sup>	$\theta$ (°) <sup>a</sup>	$\phi$ (°) <sup>a,b</sup>	Conformation	Tilt $\tau$ (°) <sup>c</sup>
<b>1</b>	I	manno	0.557(33)	50.9(5.4)	353(10.0)	<sup>o</sup> H <sub>5</sub> ( $\rightarrow$ <sup>o</sup> E)	100(12)
	II–VI <sup>d</sup>	gluco	0.620(29)	14.9(5.4)	38(24.3)	<sup>4</sup> C <sub>1</sub>	94(12)
<b>2a</b>	I	altro	0.588(29)	19.2(4.9)	356(18.1)	<sup>4</sup> C <sub>1</sub>	97.4(6.7)
	dioxane		0.759(37)	87.4(2.9)	136.3(5.5)	<sup>o4</sup> , <sup>c4</sup> B	56.7(5.3)
	II	gluco	0.613(30)	14.0(5.2)	316(26.2)	<sup>4</sup> C <sub>1</sub>	30.4(4.8)
<b>2b</b>	III–VI <sup>d</sup>	gluco	0.625(29)	15.1(5.9)	36(26.0)	<sup>4</sup> C <sub>1</sub>	86(15)
	I	altro	0.575(33)	171.5(4.8)	190(74.0)	<sup>1</sup> C <sub>4</sub>	56.0(6.2)
	dioxane		0.547(30)	156.2(5.1)	187(16.5)	<sup>o3</sup> C <sub>O4'</sub> $\leftrightarrow$ <sup>c4</sup> H <sub>O4</sub>	67.7(6.0)
<b>3</b>	II	gluco	0.597(31)	16.2(5.8)	331(25.5)	<sup>4</sup> C <sub>1</sub>	59.2(6.1)
	III–VI <sup>d</sup>	gluco	0.624(29)	16.5(5.9)	43(21.4)	<sup>4</sup> C <sub>1</sub>	88.0(9.2)
	I	gluco	0.647(28)	6.4(3.2)	37(65.9)	<sup>4</sup> C <sub>1</sub>	68.3(5.7)
	dioxane		0.589(29)	171.7(3.8)	242(51.4)	<sup>o3</sup> C <sub>O4'</sub> <sup>e</sup>	70.9(5.3)
	II	gluco	0.618(30)	10.8(4.6)	342(36.3)	<sup>4</sup> C <sub>1</sub>	50.2(5.1)
	III–VI <sup>d</sup>	gluco	0.623(29)	15.4(5.0)	40(21.2)	<sup>4</sup> C <sub>1</sub>	89(12)

<sup>a</sup> Ring numbering scheme for pyranoses: O-5-C-1-C-2-C-3-C-4-C-5; dioxane rings: O-4-C-4-C-3-O-3-C-2'-C-1'.

<sup>b</sup> For  $\theta \rightarrow 0^\circ$  (<sup>4</sup>C<sub>1</sub>) and  $\theta \rightarrow 180^\circ$  (<sup>1</sup>C<sub>4</sub>), the parameter  $\phi$  becomes insignificant.

<sup>c</sup> Angle between the least-squares best-fit mean plane of the macrocycle (defined by all intersaccharidic O-4 atoms) and the mean plane of the pyranose or dioxane rings; values of  $\tau < 90^\circ$  indicate inward tilting of the C-2 and C-3 side of the pyranoses.

<sup>d</sup> Combined averages for all unmodified glucopyranose rings in the macrocycle.

<sup>e</sup> <sup>o3</sup>C<sub>O4'</sub>  $\equiv$  <sup>o3</sup>C<sub>O4</sub>  $\equiv$  <sup>c1</sup>C<sub>C3</sub>.

inverted <sup>1</sup>C<sub>4</sub> chair geometry with almost equal energies,<sup>20–22,25,29</sup> two different conformers **2a** and **2b** need to be considered. In contrast, the tricyclic pyran–dioxane–pyran system in **3** features a rigid cis–trans type linkage, allowing for standard chair conformations of all six-membered rings. Similar arrangements are observed in the class of spectinomycin antibiotics and related compounds.<sup>30</sup>

**Molecular dynamic simulations.**—A detailed conformational analysis of the structures of **2a**, **2b**, and **3** was carried out using independent molecular dynamic (MD) simulations with the explicit incorporation of water as the solvent (cf. Section 4); for comparison, their common precursor **1** was also included in this study. In each case, constant temperature ( $T \approx 300$  K) and constant pressure ( $P \approx 1$  bar) MD trajectories of 1 ns length were generated on periodic boxes (truncated octahedron) filled with the solute and a total of 609 TIP3-type water molecules, using CHARMM<sup>31,32</sup> and a force-field adapted to properly treat carbohydrate structures.<sup>33,34</sup> The MD-derived mean-solute structures, their thermal-displacement ellipsoids, as well as solvent-accessible surface<sup>35,36</sup> models of typical solution snap-

shot geometries are displayed by Fig. 1. Not unexpectedly, all macrocyclic structures are characterized by rather limited flexibility of their backbones, with only the 2-OH, 3-OH, and 6-CH<sub>2</sub>OH groups undergoing significant torsional transitions. In particular, neither MD run on conformers **2a** and **2b** displays any interconversion between these forms, both apparently being too rigid to equilibrate on the MD time scale.

Particular emphasis was put on the analysis of the pyranose and dioxane ring portions of **1–3** in terms of their geometries and their relative alignments. Table 1 gives a detailed listing of their Cremer–Pople puckering parameters<sup>37,38</sup> for all six-membered rings. The combined averages over all glucopyranoses (rings II–VI in **1**, and III–VI in **2a**, **2b**, and **3**) correlate with their generally favored <sup>4</sup>C<sub>1</sub> conformations ( $\theta$  less equal approx. 16°), significant deviations are only observed for the anhydro-residues. Due to the epoxide, the ring I in **1** (Fig. 1, center row, left) adopts a typical <sup>o</sup>H<sub>5</sub> half-chair geometry (slightly distorted towards an <sup>o</sup>E envelope), which agrees well with previous crystallographic studies on inclusion complexes of 2,3-*per*-anhydro- $\alpha$ -cycloman-



nan<sup>6,7</sup> and other related sugar epoxides<sup>40</sup> contained in the Cambridge Crystallographic Database.<sup>41,42</sup>

As was already deduced from the formula drawing of Scheme 2, the cis–trans linked tricyclic system in **3** consists of rigidly anelated, almost relaxed chair-type rings even for the center dioxane portion. Significant distortions of the dioxane ring are observed for **2a** and **2b** with the ring I of the altropyranose residue adopting either the <sup>4</sup>C<sub>1</sub> (ideal values of  $\theta \approx 0^\circ$ ) or <sup>1</sup>C<sub>4</sub> ( $\theta \approx 180^\circ$ ) form. In **2a**, the cis–cis-type junction forces the center ring into a strained boat form, simultaneously transferring some energy into distortions of the altrose ring I as evidenced by the rather large value of  $\langle \theta \rangle = 19.2^\circ$ . Most notably, a similar boat conformation was found for the center dioxane ring in the X-ray structure of cyclobis-(1 → 2)- $\alpha$ -D-glucopyranosyl peracetate.<sup>43</sup> For **2b**, the close spatial proximity of both axially disposed H-2<sup>I</sup> (altrose) and H-3<sup>II</sup> (glucose) protons (Fig. 1) pointing towards each other excerpts considerable strain on the center dioxane ring, which is therefore flattened (lowest puckering amplitude  $Q$  of all rings) and distorted towards a half-chair.

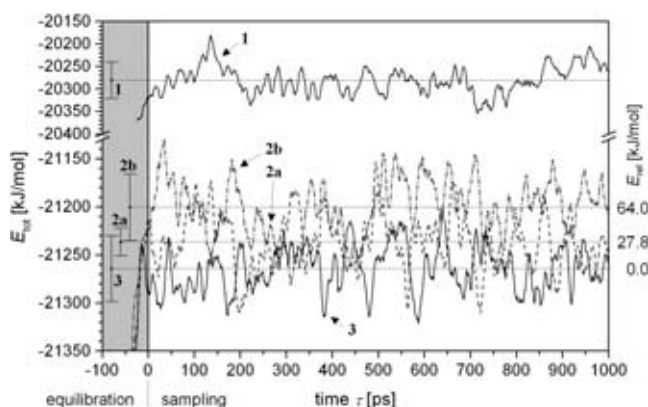


Fig. 2. Time series of total energies during the MD simulations of **1**, **2a**, **2b**, and **3** in periodic boxes (truncated octahedron) filled with 609 H<sub>2</sub>O molecules (all box sizes approx.  $33.5 \pm 0.1$  Å,  $\langle T \rangle = 295.3$  K,  $\langle P \rangle = 1$  bar), respectively, plotted as running averages smoothed over 100 configurations (5 ps) each. Negative times ( $\tau = -100 - 0$  ps) indicate the equilibration phase, followed by a total data acquisition period of 1 ns. The average energies and the corresponding root-mean-square fluctuations of the energies during the sampling simulation are indicated by the dotted lines and the error bars on the left. Besides indicating the completed equilibration of all MD systems, the two conformers **2a** and **2b** appear to be 27.8 and 64.0 kJ/mol less stable than their stereoisomer **3**.

The overall molecular shape of cyclodextrins is characterized by the tilt angle  $\tau$  formed between both the plane of the macrocycle and the ring plane of each sugar unit.<sup>39</sup> In general, the glucose units of unmodified CDs and their inclusion complexes are slightly tilted with their 6-CH<sub>2</sub>OH groups pointing towards the central molecular axis, and thus the 2- and 3-OH groups form the wider opened aperture of these truncated cone-type structures.<sup>39,44,45</sup> A similar trend is observed for **1** as evidenced by tilt angles larger than  $90^\circ$  (cf. Table 1). However, the strait-jacket of the 3<sup>I</sup>,2<sup>II</sup>-anhydro linkage in **2** and **3** leads to a considerable contraction along this torus rim: the unmodified glucose residues (rings III–VI) are aligned almost perpendicular to the macroring, whereas the rings I and II, as well as the center dioxane unit, display severe misalignments with pronouncedly decreased and inverted inclinations. The effects of very low tilt angles on the backbone structures of **1–3** become particularly evident from the solid-surface models given in Fig. 1: of all structures, both conformers **2a** and **2b** exhibit the most asymmetrically distorted over-all shapes.

The relative stabilities of the conformers **2a** and **2b** and their stereoisomer **3** are expressed in the MD-derived averages of the total energies of the simulation system, a cautious analysis made possibly by identical simulation parameters (i.e. equal temperature, pressure, box size, number of water molecules, constant set of force-field parameters, long simulation periods), despite the lack of direct conformational transitions in either unconstrained (free) or constrained (chemical or structural perturbation) form. From the plot of the total energies ( $E_{\text{kin}} + E_{\text{pot}}$ ) of the MD systems given in Fig. 2, **3** turns out as the energetically most favorable structure, whereas **2a** and **2b** appear to be—within the limits of error—about 28 and 64 kJ/mol higher in average total energy. As deduced above, the main reasons for these relative stabilities seem to originate from strain within the cis–trans (**3**) versus cis–cis (**2a**, **2b**) type linkages in the tricyclic system and their alignments in the macrocycle.

Obviously, **3** is the thermodynamically most favored product emerging from intramolecular ring opening of the epoxide in **1**. An

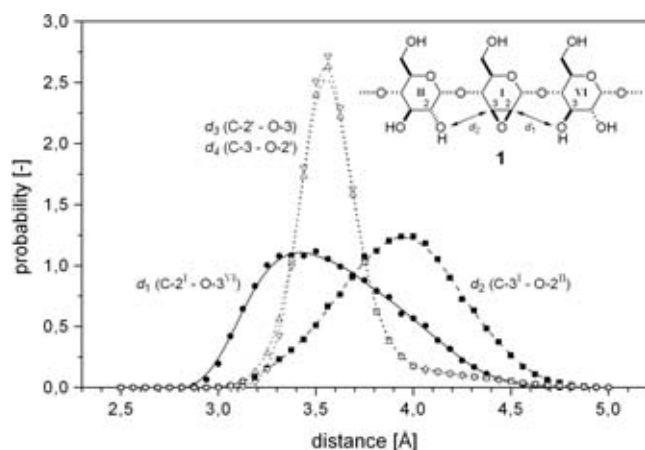


Fig. 3. Probability distributions of intramolecular distances between epoxide ring carbon atoms C-2<sup>I</sup> and C-3<sup>I</sup> and neighboring hydroxyl oxygen atoms O-3<sup>VI</sup> and O-2<sup>II</sup> as obtained from MD simulations of **1** in water. The distribution of  $d_1$  (C-2<sup>I</sup>...O-3<sup>VI</sup>, solid line and circles) is significantly shifted towards lower distances as compared to  $d_2$  (C-3<sup>I</sup>...O-2<sup>II</sup>, dashed line and squares), apparently favoring intramolecular attack of the 3<sup>VI</sup>-OH group (**1** → **3**) over the 2<sup>II</sup>-OH hydroxyl (**1** → **2**) onto the epoxide. For comparison, the distributions  $d_3$  and  $d_4$  of the C-2'...O-3 and C-3'...O-2' interresidue distances averaged over all neighboring unmodified glucose portions were included (triangles and dotted lines).

indication that **3** is also the kinetically preferred product of this reaction can be deduced from the comparison of intramolecular distances between the epoxide ring carbon atoms and neighboring hydroxyl oxygens suitable for attack: the probability distributions plotted in Fig. 3 display significantly shorter distances between the epoxide carbon C-2<sup>I</sup> and O-3<sup>VI</sup> ( $\langle d_1 \rangle = 3.59(34)$  Å) as compared to C-3<sup>I</sup> and O-2<sup>II</sup> ( $\langle d_2 \rangle = 3.93(32)$  Å), favoring the reaction **1** → **3** rather than **1** → **2**. That this effect is indeed caused by the <sup>o</sup>H<sub>5</sub> ring conformation of the 2,3-anhydro-*manno*-epoxide unit within the macrocycle is displayed by the rather equal and uniform distances C-2'...O-3 and C-3'...O-2' between all unmodified glucose units ( $\langle d_3 \rangle \approx \langle d_4 \rangle \approx 3.62$  Å).

**Crystallographic analysis.**—Precipitation of **3** from aqueous *n*-propanol yielded crystals suitable for X-ray analysis, and thus allows comparison of its solid-state structure with the MD-derived conformation in solution. The low-temperature ( $T = 173$  K) structure analysis revealed a composition of bis-(3<sup>I</sup>,2<sup>II</sup>-anhydro)- $\alpha$ -cyclodextrin (**3**)·3 *n*-PrOH·9 H<sub>2</sub>O of the block-shaped, monoclinic crystals with space group  $P2_1$  (cf. Fig. 4).

The CD hosts are stacked in parallel columns in an alternating head-to-head and tail-to-tail fashion. The *n*-propanol guest molecules are all located within the almost linear, nano-tube like channels formed by the columnar CD arrangement, whereas the water molecules are located without exception on interstitial positions outside of the macrocycles. As evidenced by their rather large displacement ellipsoids (Fig. 4, top left), the guest molecules retain some considerable degree of disorder even at low temperatures. As is typically observed for glucopyranose residues, all 6-CH<sub>2</sub>OH groups on the CD hosts are twofold disordered over *gauche-gauche* (*gg*) and *gauche-trans* (*gt*) orientations, the former being favored over the latter by a ratio of 7.67:4.33 (calculated from the occupancy factors of all 12 O-6 positions included in the asymmetric unit).

The crystal architecture displays an intensive three-dimensional hydrogen bonding network, in which all hydroxyl groups and water molecules are involved; a schematic drawing is given in Fig. 5 and some distances are listed in Table 2. From the different types of hydrogen bonds observed—i.e. CD...CD intramolecular (O-3'...O-2) and intermolecular H-bonds, CD...water, water...water, CD...*n*-propanol and *n*-propanol...*n*-propanol—it is obvious that the guest molecules are not hydrogen bonded to any of the water molecules, but are shielded by their macrocyclic hosts from the water positions in the crystal environment. Of the three *n*-propanol contained in the asymmetric unit of the lattice, one is twofold H-bonded to O-2 and O-3' of the anhydro-glucopyranose portion of one molecule **3** (hydrogen bonds labeled 14 and 15 in Fig. 5 and Table 2). The remaining two *n*-propanol face each other in a head-to-head like arrangement interacting through their hydroxyl groups (H-bond no. 16); a detailed plot of this configuration is provided in Fig. 5 by the slices through the corresponding molecular surfaces. Obviously, the tube-like cavity of a dimeric unit of **3** in the crystal lattice is perfectly able to accommodate the three guest molecules *n*-PrOH with their arrangement being determined through the necessity to satisfy their hydrogen bonding requirements.

As the most characteristic feature of **3**, its ribbon model displays the significant contraction along the front aperture of the torus carrying the 2- and 3-OH groups. The unusual conicity of this CD derivative expresses itself in rather low tilt angles  $\tau$  for the 3<sup>I</sup>,2<sup>II</sup>-anhydro-ring system ( $\tau \approx 60^\circ$ , cf. Table 3), in contrast to unmodified CDs where the 6-CH<sub>2</sub>OH side invariably represents the narrower opening ( $\tau > 100^\circ$ )<sup>39</sup> of these truncated cone structures. As was already deduced for the MD derived geometry of **3**, the pyranose and diox-

ane rings adopt standard chair conformations within their rather rigid link-ups (cf. Cremer–Pople parameters<sup>37,38</sup> listed in Table 3). Indeed, both independently derived structures of **3** for the crystal and solution state feature identical over-all shapes, their backbones (heavy atoms including all substituents except the O-6 atoms) being superimposable with average deviations in their atomic positions of less than 0.1 Å. Obviously, the crystal conformation of **3** undergoes no significant changes upon dissolution in water.

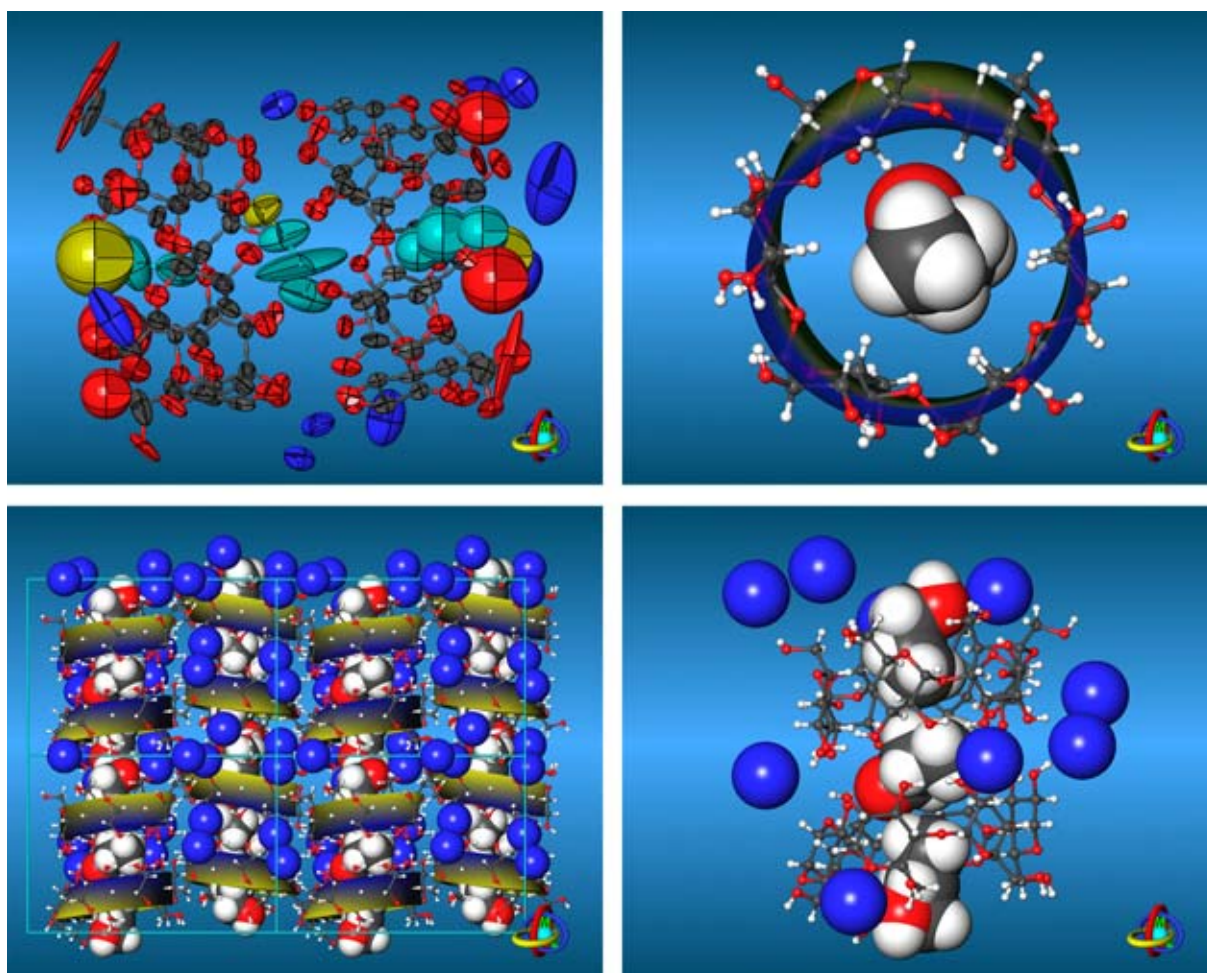


Fig. 4. Solid-state structure of 3<sup>I</sup>,2<sup>II</sup>-anhydro- $\alpha$ -cyclodextrin (**3**). Top left: Molecular geometry and 50% thermal ellipsoids of the asymmetric unit ( $[3]_2 \cdot 3 n\text{-PrOH} \cdot 9 \text{H}_2\text{O}$ ); for clarity, the water oxygen atoms are colored dark blue and the *n*-propanol guests are displayed in yellow (oxygens) and cyan (carbon atoms). Top right: Single complex extracted from the asymmetric unit, the semi-transparent ribbon-model shows the distorted conicity of the host molecule (blue, ring side carrying the 2- and 3-OH groups; yellow, 6-CH<sub>2</sub>OH) with the *n*-propanol guest (CPK model) centered along its central axis (view perpendicular to the ring plane of **3**). Bottom left: Crystal lattice (1·2·2 unit cells, view down the *a*-axis) made up of columnar head-to-head and tail-to-tail stacked anhydro-CDs (ribbon models) including almost linear and parallel assemblies of *n*-propanol guest molecules (CPK models); the guest–host arrangement being surrounded by water molecules (blue spheres) in the crystal. Bottom right: Section extracted from the lattice, displaying in detail the alignment of three guest molecules in a dimeric unit of **3**. For all ball-and-stick type models of **3** only the preferably occupied configurations of all disordered 6-CH<sub>2</sub>OH groups were retained for the graphics.

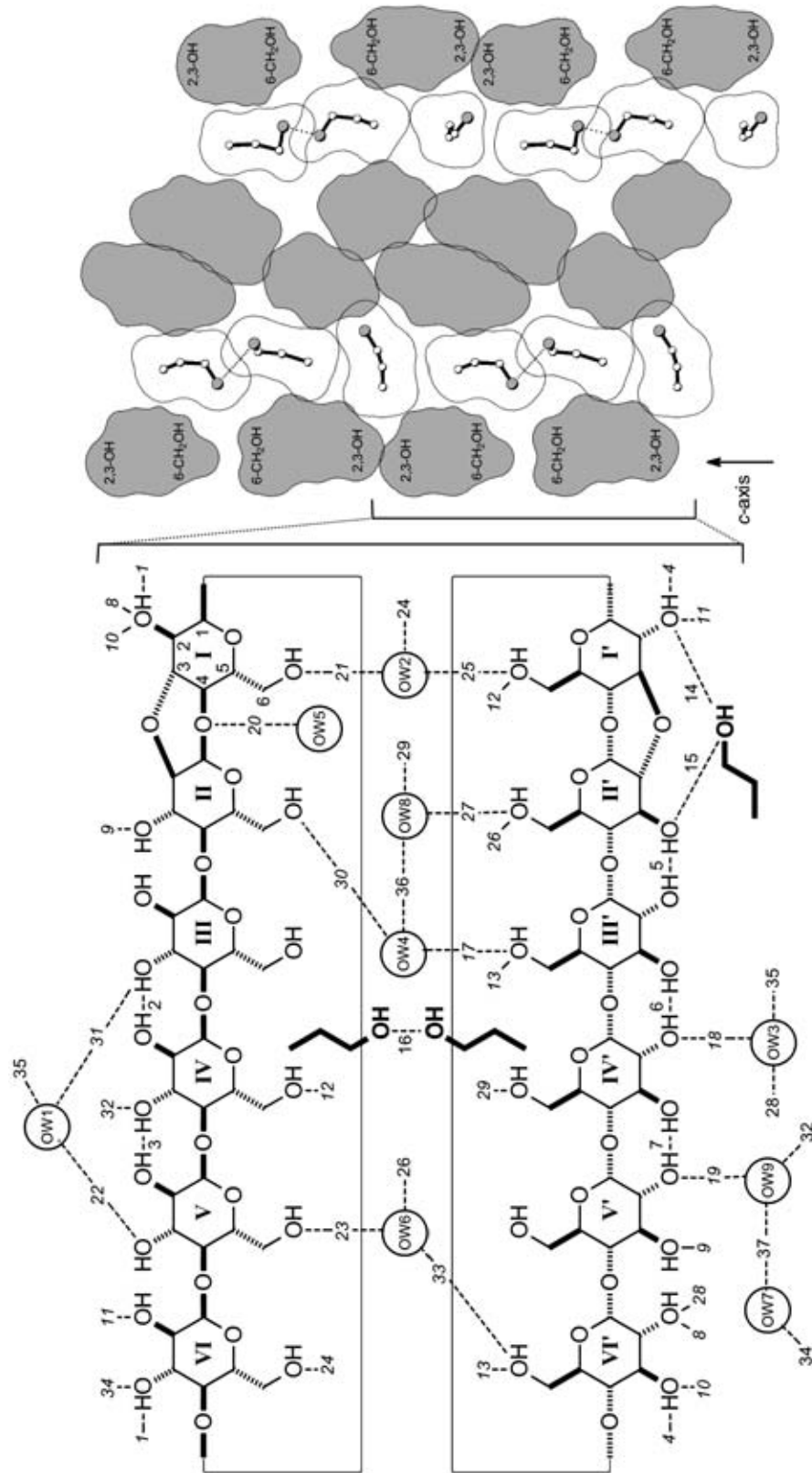


Fig. 5. Scheme of intra- and intermolecular hydrogen bonds in the solid-state structure of the bis-(3',2'1'-anhydro)- $\alpha$ -CD-3- $\eta$ -propanol nonahydrate inclusion complex (left). The individual glucose units within the asymmetric unit are labeled I–VI and I'–VI', the water molecules OW1–OW9, the numbers in italics correspond to the indices given in Table 3. On the right, a larger segment of the crystal (four asymmetric units) displays the nano-tube like environment of stacked CD hosts into which the  $\eta$ -propanol guest molecules are embedded (water molecules omitted for clarity). The surface slices are given for the individual molecules, ball-and-stick type models without hydrogens are shown for  $\eta$ -propanol only, the CD surfaces are indicated by shading; dotted lines indicate hydrogen bonds between the guest molecules.

Table 2

Hydrogen bonds in the solid-state structure of bis-3·3 *n*-PrOH·9 H<sub>2</sub>O, listed for acceptor...donor distances < 3.2 Å; the water molecules are labeled OW1–OW9, the glucose labeling I–VI, I'–VI', and the indices given in the first column correspond to Fig. 5

		Distance	Symmetry			Distance	Symmetry
<i>CD–CD intramolecular:</i>				<i>CD–water:</i>			
1	O(3 <sup>VI</sup> )...O(2 <sup>I</sup> )	2.753	a	17	O(6 <sup>III</sup> )...O(W4)	2.826	a
2	O(2 <sup>IV</sup> )...O(3 <sup>III</sup> )	2.988	a	18	O(2 <sup>IV</sup> )...O(W3)	2.721	a
3	O(2 <sup>V</sup> )...O(3 <sup>IV</sup> )	2.905	a	19	O(2 <sup>V</sup> )...O(W9)	2.700	a
4	O(3 <sup>VI</sup> )...O(2 <sup>I</sup> )	2.789	a	20	O(4 <sup>I</sup> )...O(W5)	3.013	b
5	O(3 <sup>II</sup> )...O(2 <sup>III</sup> )	2.865	a	21	O(6 <sup>I</sup> )...O(W2)	2.626	b
6	O(3 <sup>III</sup> )...O(2 <sup>IV</sup> )	2.776	a	22	O(3 <sup>V</sup> )...O(W1)	2.847	b
7	O(3 <sup>IV</sup> )...O(2 <sup>V</sup> )	2.815	a	23	O(6 <sup>V</sup> )...O(W6)	2.993	b
<i>CD–CD intermolecular:</i>							
8	O(2 <sup>I</sup> )...O(2 <sup>VI</sup> )	2.946	b	24	O(6 <sup>VI</sup> )...O(W2)	2.709	b
9	O(3 <sup>II</sup> )...O(3 <sup>V</sup> )	2.842	b	25	O(6 <sup>I</sup> )...O(W2)	2.222	b
10	O(2 <sup>I</sup> )...O(3 <sup>VI</sup> )	2.855	b	26	O(6 <sup>II</sup> )...O(W6)	2.903	b
11	O(2 <sup>I</sup> )...O(2 <sup>VI</sup> )	2.858	c	27	O(6 <sup>II</sup> )...O(W8)	2.811	b
12	O(6 <sup>I</sup> )...O(6 <sup>IV</sup> )	2.619	d	28	O(2 <sup>VI</sup> )...O(W3)	2.817	d
13	O(6 <sup>III</sup> )...O(6 <sup>VI</sup> )	2.498	e	29	O(6 <sup>IV</sup> )...O(W8)	2.515	f
<i>CD–propanol:</i>							
14	O(2 <sup>I</sup> )...O(1P)	2.787	a	30	O(6 <sup>II</sup> )...O(W4)	2.926	g
15	O(3 <sup>II</sup> )...O(1P)	2.766	a	31	O(3 <sup>III</sup> )...O(W1)	2.879	g
<i>propanol–propanol:</i>							
16	O(2P)...O(3P)	3.156	b	32	O(3 <sup>IV</sup> )...O(W9)	2.827	h
				33	O(6 <sup>VI</sup> )...O(W6)	2.800	i
				34	O(3 <sup>VI</sup> )...O(W7)	2.816	j
				<i>water–water:</i>			
				35	O(W1)...O(W3)	2.754	k
				36	O(W4)...O(W8)	2.082	b
				37	O(W7)...O(W9)	2.726	

Symmetry operations: (a)  $x, y, z$ . (b)  $x, y, z-1$ . (c)  $x, y, z+1$ . (d)  $x-1, y, z$ . (e)  $x+1, y, z$ . (f)  $-x, y+1/2, -z-1$ . (g)  $-x, y+1/2, -z-2$ . (h)  $-x, y-1/2, -z-2$ . (i)  $-x-1, y+1/2, -z-1$ . (j)  $-x-1, y-1/2, -z-2$ . (k)  $-x, y-1/2, -z-1$ .

Table 3

Selected geometry parameters (Cremer–Pople ring puckering parameters  $Q/\theta/\phi$ ,<sup>37,38</sup> and pyranose tilt angles  $\tau$ <sup>39</sup>) computed for the solid-state geometry of bis-3·3 *n*-PrOH·9 H<sub>2</sub>O; values are listed for both 3<sup>I</sup>, 2<sup>II</sup>-anhydro- $\alpha$ -CD molecules separately (unit 1 and 2), except for the combined averages for all eight unmodified glucose residues; see also Table 1 and the comments given there

Compound	Ring	Configuration	$Q$ (Å)		$\theta$ (°)		$\phi$ (°)		Conformation	Tilt $\tau$ (°)	
			Unit 1	Unit 2	Unit 1	Unit 2	Unit 1	Unit 2		Unit 1	Unit 2
3	I	gluco	0.563	0.587	1.9	3.8	189.8	274.4	<sup>4</sup> C <sub>1</sub>	64.8	69.0
			0.568	0.551	170.4	173.5	243.4	259.0	<sup>0</sup> 3C <sub>O4'</sub>	67.8	69.9
	II	gluco	0.535	0.544	16.5	12.2	297.8	294.5	<sup>4</sup> C <sub>1</sub>	53.9	52.4
			0.557(11)		6.2(1.3)		62(18)		<sup>4</sup> C <sub>1</sub>	97.6(6.2)	

<sup>a</sup> Combined averages for all unmodified glucopyranose rings in both molecules of **3** with standard deviations in parentheses.

### 3. Conclusions

Although intramolecular opening of epoxide **1** by the 3-OH of a neighboring glucose unit occurs in an unexpected diequatorial fashion to afford **3** in high yield, MD calculations reveal **3** to be the favored product when comparing the average total energies of the

stereoisomers **2a**, **2b**, and **3** in simulated water boxes. Provided that atomic distances are a decisive factor for the regioselectivity of epoxide opening, **3** also turns out to be the kinetically preferred product. The over-all molecular shape of this rigid CD derivative, as evident from its solid-state structure, not only undergoes little changes upon dissolution in

water retaining its unusual conicity caused by the contracted tricyclic pyran–dioxane–pyran ring system, but also provides a picture of an inclusion complex of **3** with *n*-propanol.

#### 4. Experimental

**Molecular dynamics simulations.**—The starting geometries of **1**, **2a**, **2b**, and **3** were generated by editing the solid-state geometry of  $\alpha$ -CD<sup>46</sup> and subsequent single-point energy minimization. All MD simulations starting from these structures were carried out using CHARMM<sup>31,32</sup> with a force-field particularly adapted for the treatment of carbohydrates<sup>33,34</sup> and explicit incorporation of water as the solvent. Each compound was centered in a periodic box (truncated octahedron) filled with pre-equilibrated TIP3-type water, yielding—after removal of the solvent molecules that overlap with the solute—simulation systems including 609 water molecules, respectively. After full-lattice energy minimizations, all boxes were slowly heated from 0 to 300 K within a 15 ps MD time frame, and subsequently equilibrated for an additional 85 ps; the final MD data were sampled using simulations of 1 ns in each case, molecular configurations were saved every 50 fs for analysis purposes. All MD runs were carried for constant pressure ( $P_{\text{ref}} = 1$  atm, isothermal compressibility  $4.63 \times 10^{-5}$  atm<sup>-1</sup>, pressure coupling constant  $\tau_p = 5$  ps) and constant temperature ( $T_{\text{ref}} = 300$  K, temperature coupling constant  $\tau_T = 5$  ps, allowed temperature deviation  $\Delta T = \pm 10$  K) conditions (*NPT* ensemble) using the following simulation

parameters: timestep  $\Delta t = 1$  fs (leap-frog integrator, all X–H bond lengths were constrained using the SHAKE protocol<sup>47</sup>), dielectric constant  $\epsilon = 1.0$ , cut-off distance for long-range interactions 12 Å, cut-off radius for images in atom lists 13 Å; for some specific parameters recalculated from the MD trajectories see Table 4.

For each MD time series, the mean solute geometry was obtained by 3D fitting of all configurations (heavy atoms only, excluding CH<sub>2</sub>OH-oxygen atoms); the best-fit models from this procedure were selected as representative molecular geometries in aqueous solution (Fig. 1, center and bottom row). The corresponding atomic anisotropic thermal displacement ellipsoids (cf. Fig. 1, top row) were obtained from diagonalization of the displacement tensor calculated from all atomic displacement vectors (for each atom, the eigenvectors and the root of the eigenvalues of this tensor yield the principal axis of the thermal ellipsoid and the root-mean-square atomic displacements along these directions).<sup>48</sup>

**Crystal structure of bis-(3<sup>I</sup>,2<sup>II</sup>-anhydro)- $\alpha$ -cyclodextrin·3 *n*-PrOH·9 H<sub>2</sub>O.**—A mixture of 60 mg of **3**, 100  $\mu$ L of water and 100  $\mu$ L of *n*-propanol was heated up to 90 °C to give a clear solution and then filtered through a membrane filter PTFE (pore size, 0.5  $\mu$ m; TOSOH). The filtrate was sealed and allowed to stand at rt for 1 week to yield colorless, block-shaped crystals with parameters as follows:  $M_r = 1126.04$  g/mol, monoclinic, space group  $P2_1$ ,  $a = 14.257(1)$ ,  $b = 22.623(2)$ ,  $c = 16.644(1)$  Å,  $\beta = 104.82(1)^\circ$ ,  $V = 5189.7(7)$  Å<sup>3</sup>,  $Z = 4$ ,  $\rho = 1.414$  g/cm<sup>3</sup>,  $\mu(\text{Mo K}\alpha) = 0.126$

Table 4

Selected MD simulation parameters recalculated from the time series (all MD systems include 609 H<sub>2</sub>O molecules,  $M_{\text{tot}} = 11926.42$  g/mol) with standard deviations in parentheses

Compound	$T$ [K]	$E_{\text{tot}}$ (kJ/mol)	$E_{\text{kin}}$ (kJ/mol)	$E_{\text{pot}}$ (kJ/mol)	$E_{\text{rel}}$ (kJ/mol) <sup>a</sup>	Box size (Å)	Volume (Å <sup>3</sup> ) <sup>b</sup>	Density $\sigma$ (g/cm <sup>3</sup> )
<b>1</b>	295.2(5.3)	−20,281(41)	4863(88)	−25,143(98)		33.47(6)	18,740(135)	1.057(8)
<b>2a</b>	295.3(5.3)	−21,237(14)	4864(88)	−26,101(107)	27.9	33.46(9)	18,726(142)	1.057(8)
<b>2b</b>	295.2(5.3)	−21,200(35)	4863(88)	−26,063(100)	64.0	33.47(6)	18,747(141)	1.056(8)
<b>3</b>	295.3(5.3)	−21,264(34)	4864(87)	−26,129(96)	0.0	33.47(9)	18,747(129)	1.056(7)

<sup>a</sup> Relative total energies for the 3<sup>I</sup>,2<sup>II</sup>-anhydro- $\alpha$ -cyclodextrins **2a**, **2b**, and **3** only.

<sup>b</sup> Volume = (box size)<sup>3</sup>/2.0 for the truncated octahedron.

mm<sup>-1</sup>, crystal dimensions 0.5 × 0.4 × 0.15 mm, *T* = 173(2) K. Of 29,184 reflections collected on a Siemens CCD three-circle diffractometer using graphite-monochromated Mo K<sub>α</sub> ( $\lambda = 0.71073$  Å) radiation, 19,278 are independent ( $R_{\text{int}} = 0.0585$ );  $\theta$  range of data collection 1.27–28.01°, completeness to  $\theta = 28.01^\circ$  82.4%, limiting indices *h*: -16 → 15, *k*: -28 → 29, and *l*: -16 → 21. The structure was solved by shake and bake methods<sup>49</sup> and successive Fourier synthesis. Refinement (on  $F^2$ ) was performed by full-matrix least-squares method (19,278 reflections, 18 restraints, 1403 independent parameters).<sup>50</sup>  $R(F) = 0.1017$  for reflections with  $I > 2\sigma(I)$ ,  $wR(F^2) = 0.2193$  for 19,278 reflections ( $w = 1/[\sigma^2(F_o^2) + (0.1337P)^2 + 4.1868P]$ ); where  $P = (F_o^2 + 2F_c^2)/3$ ;  $R(F) = 0.2205$  and  $wR(F^2) = 0.2966$  for all reflections. The final goodness-of-fit on  $F^2$  equals 1.005, the largest difference peak and hole of electron density are +0.503 and -0.296 e Å<sup>3</sup>, respectively. All bond length and angles fall within normal ranges for carbohydrate structures.

All 6-CH<sub>2</sub>OH groups on both cyclodextrin units are twofold disordered over the gauche-gauche (*gg*, torsion angle  $\omega$  O<sub>5</sub>-C<sub>5</sub>-C<sub>6</sub>-O<sub>6</sub> approx. -60°) and the gauche-trans (*gt*,  $\omega \approx +60^\circ$ ) orientation, with the former being favored over the latter by a ratio of 7.67:4.33 based on relative occupancy factors. All non-hydrogen atoms (except of one *n*-propanol molecule and eight of the 12 O-6 position with lower occupancy) were refined anisotropically, hydrogen atoms were positioned geometrically and considered in calculated positions with the 1.2 $U_{\text{eq}}$  value of the corresponding bound atom. The ribbon models of **3** (Fig. 4) were computed by connecting the centers and normal vectors of the least-squares best-fit mean planes of all pyranose rings (without substituents) via cubic splines.<sup>48</sup>

## 5. Supplementary material

Crystallographic data (excluding structure factors) for the structure in this paper have been deposited with the Cambridge Crystallographic Data Centre as supplementary publication no. CCDC-168467. Copies of the data

can be obtained, free of charge, on application to The Director, CCDC, 12 Union Road, Cambridge CB2 1EZ, UK, (fax: +44-1223-336033 or e-mail: deposit@ccdc.cam.ac.uk or www: <http://www.ccdc.cam.ac.uk>).

## Acknowledgements

The authors are grateful to Professor F.W. Lichtenthaler (S.I.) for prolific discussions and carefully editing the manuscript, and Professor H.J. Lindner (M.B.) for lucid suggestions.

## References

1. Immel, S.; Lichtenthaler, F. W.; Lindner, H. J.; Nakagawa, T. *Tetrahedron: Asymmetry* **2001**, *12*, in press.
2. Fujita, K.; Nagamura, S.; Imoto, T. *Tetrahedron Lett.* **1984**, *25*, 5673–5676.
3. Ikeda, H.; Nagano, Y.; Du, Y.; Ikeda, T.; Toda, F. *Tetrahedron Lett.* **1990**, *31*, 5045–5048.
4. Coleman, A. W.; Zhang, P.; Ling, C. C.; Mahuteau, J.; Parrot-Lopez, H.; Miocque, M. *Supramol. Chem.* **1992**, *1*, 11–14.
5. Zhang, P.; Coleman, A. W. *Supramol. Chem.* **1993**, *2*, 255–263.
6. Immel, S.; Fujita, K.; Lindner, H. J.; Nogami, Y.; Lichtenthaler, F. W. *Chem. Eur. J.* **2000**, *6*, 2327–2333.
7. Immel, S.; Lichtenthaler, F. W.; Lindner, H. J.; Fujita, K.; Fukudome, M.; Nogami, Y. *Tetrahedron: Asymmetry* **2000**, *11*, 27–36.
8. Khan, A. R.; Barton, L.; D'Souza, V. T. *J. Chem. Soc., Chem. Commun.* **1992**, 1112–1114.
9. Khan, A. R.; Barton, L.; D'Souza, V. T. *J. Org. Chem.* **1996**, *61*, 8301–8303.
10. Isac-Garcia, J.; Lopez-Paz, M.; Santoyo-Gonzalez, F. *Carbohydr. Lett.* **1998**, *3*, 109–116.
11. Khan, A. R.; Forgo, P.; Stine, K. J.; D'Souza, V. T. *Chem. Rev.* **1998**, *98*, 1977–1996.
12. Gattuso, G.; Nepogodiev, S. A.; Stoddart, J. F. *Chem. Rev.* **1998**, *98*, 1919–1958.
13. Kelly, D. R.; Mish'al, A. K. *Tetrahedron: Asymmetry* **1999**, *10*, 3627–3648.
14. Fujita, K.; Ohta, K.; Ikegami, Y.; Shimada, H.; Tahara, T.; Nogami, Y.; Koga, T.; Saito, K.; Nakajima, T. *Tetrahedron Lett.* **1994**, *35*, 9577–9580.
15. Harata, K.; Nagano, Y.; Ikeda, H.; Ikeda, T.; Ueno, A.; Toda, F. *J. Chem. Soc., Chem. Commun.* **1996**, 2347–2348.
16. Fujita, K.; Chen, W.-H.; Yuan, D.-Q.; Nogami, Y.; Koga, T.; Fujioka, T.; Mihashi, K.; Immel, S.; Lichtenthaler, F. W. *Tetrahedron: Asymmetry* **1999**, *10*, 1689–1696.
17. Ohta, K.; Fujita, K.; Shimada, H.; Ikegami, Y.; Nogami, Y.; Koga, T. *Chem. Pharm. Bull.* **1997**, *45*, 631–635.
18. Fujita, K.; Shimada, H.; Ohta, K.; Nogami, Y.; Nasu, K.; Koga, T. *Angew. Chem., Int. Ed. Engl.* **1995**, *34*, 1621–1622.
19. Nogami, Y.; Fujita, K.; Ohta, K.; Nasu, K.; Shimada, H.; Shinohara, C.; Koga, T. *J. Inclusion Phenom. Mol. Recognit. Chem.* **1996**, *25*, 57–60.

20. Nogami, Y.; Nasu, K.; Koga, T.; Ohta, K.; Fujita, K.; Immel, S.; Lindner, H. J.; Schmitt, G. E.; Lichtenthaler, F. W. *Angew. Chem., Int. Ed. Engl.* **1997**, *36*, 1899–1902.
21. Fujita, K.; Ohta, K.; Nogami, Y.; Nasu, K.; Shiratani, T.; Sudo, M.; Koga, T. In *Proceedings of the 9th International Symposium on Cyclodextrins, Santiago de Compostela, Spain, May 31–June 3*; Torres Labandeira, J. J.; Vila-Jato, J. L., Eds.; Kluwer Academic: Dordrecht/Boston, 1999; pp. 113–115.
22. Immel, S.; Fujita, K.; Lichtenthaler, F. W. *Chem. Eur. J.* **1999**, *5*, 3185–3192.
23. Yan, J.; Watanabe, R.; Yamaguchi, M.; Yuan, D.-Q.; Fujita, K. *Tetrahedron Lett.* **1999**, *40*, 1513–1514.
24. Fujita, K.; Tahara, T.; Sasaki, H.; Egashira, Y.; Shingu, T.; Imoto, T.; Koga, T. *Chem. Lett.* **1989**, 917–920.
25. Immel, S. In *Proceedings of the 10th International Symposium on Cyclodextrins, May 21–24*; Szejtli, J., Ed.; MIA Digital Publishers: Ann Arbor, MI, 2000; pp. 274–281.
26. Koshland, Jr., D. E. *Angew. Chem., Int. Ed. Engl.* **1994**, *33*, 2475–2478.
27. Fujita, K.; Okabe, Y.; Ohta, K.; Yamamura, H.; Tahara, T.; Nogami, Y.; Koga, T. *Tetrahedron Lett.* **1996**, *37*, 1825–1828.
28. Lichtenthaler, F. W. *Angew. Chem., Int. Ed. Engl.* **1994**, *33*, 2364–2374.
29. Lichtenthaler, F. W.; Mondel, S. *Carbohydr. Res.* **1997**, *303*, 293–302.
30. Cuny, E.; Lichtenthaler, W.; Lindner, H. J. *Acta Crystallogr., Sect. C* **1994**, *50*, 1599–1601.
31. Brooks, B. R.; Bruccoleri, R. E.; Olafson, B. D.; States, D. J.; Swaminathan, S.; Karplus, M. *J. Comput. Chem.* **1983**, *4*, 187–217.
32. Nilsson, L.; Karplus, M. *J. Comput. Chem.* **1986**, *7*, 591–616.
33. Reiling, S.; Schlenkrich, M.; Brickmann, J. *J. Comput. Chem.* **1996**, *17*, 450–468.
34. Reiling, S.; Brickmann, J. *Macromol. Theory Simul.* **1995**, *4*, 725–743.
35. Connolly, M. L. *J. Appl. Crystallogr.* **1983**, *16*, 548–558.
36. Connolly, M. L. *Science* **1983**, *221*, 709–713.
37. Cremer, D.; Pople, J. A. *J. Am. Chem. Soc.* **1975**, *97*, 1354–1358.
38. Jeffrey, G. A.; Yates, J. H. *Carbohydr. Res.* **1979**, *74*, 319–322.
39. Lichtenthaler, F. W.; Immel, S. *Liebigs Ann.* **1996**, 27–37.
40. Wu, X.; Kong, F.; Lu, D.; Li, G. *Carbohydr. Res.* **1992**, *235*, 163–178.
41. Allen, F. H.; Ballard, S.; Brice, M. D.; Cartwright, B. A.; Doubleday, A.; Higgs, H.; Hummelink, T.; Hummelink-Peters, B. G.; Kennard, O.; Motherwell, W. D. S.; Rodgers, J. R.; Watson, D. G. *Acta Crystallogr., Sect. B* **1979**, *35*, 2331–2339.
42. Allen, F. H.; Kennard, O.; Taylor, R. *Acc. Chem. Res.* **1983**, *16*, 146–153.
43. Pozsgay, V.; Dubois, E. P.; Lotter, H.; Neszmelyi, A. *Carbohydr. Res.* **1997**, *303*, 165–173.
44. Lipkowitz, K. B.; Green, K.; Yang, J. A. *Chirality* **1992**, *4*, 205–215.
45. Saenger, W.; Jacob, J.; Gessler, K.; Steiner, T.; Hoffmann, D.; Sanbe, H.; Koizumi, K.; Smith, S. M.; Takaha, T. *Chem. Rev.* **1998**, *98*, 1787–1802.
46. Chacko, K. K.; Saenger, W. *J. Am. Chem. Soc.* **1981**, *103*, 1708–1715.
47. Van Gunsteren, W. F.; Berendsen, H. J. C. *Mol. Phys.* **1977**, *34*, 1311–1327.
48. Immel, S. *MOLARCH<sup>+</sup>: Molecular Architecture Modeling Program V6.15*; Technical University of Darmstadt: Germany, 2001.
49. Sheldrick, G. M. *SHELXD-97: Program for Crystal Structure Solution of Macromolecules*; University of Göttingen: Germany, 2000.
50. Sheldrick, G. M. *SHELXL-97: Program for Crystal Structure Refinement*; University of Göttingen: Germany, 1997.



## The First Successful Crystallographic Characterization of a Cyclodextrin Dimer: Efficient Synthesis and Molecular Geometry of a Doubly Sulfur-Bridged $\beta$ -Cyclodextrin\*\*

De-Qi Yuan,<sup>[b]</sup> Stefan Immel,<sup>\*[a]</sup> Katzutaka Koga,<sup>[b]</sup> Masatoshi Yamaguchi,<sup>[c]</sup> and Kahee Fujita<sup>[b]</sup>

**Abstract:**  $\beta$ -Cyclodextrin is transannularly disulfonylated at the 6<sup>A</sup>- and 6<sup>B</sup>-positions, and then converted to the corresponding 6<sup>A</sup>,6<sup>B</sup>-diiodide and 6<sup>A</sup>,6<sup>B</sup>-dithiol. Cross-coupling of the latter two species yields a single head-to-head-coupled  $\beta$ -cyclodextrin dimer **5** with two sulfur linkers at adjacent 6-methylene carbons. NMR and X-ray analysis

revealed the *trans*-type (“aversive”) linkage of both  $\beta$ -cyclodextrin units. In the solid-state structure of **5**·5MeOH·23H<sub>2</sub>O, the undistorted cyclodextrin

macrocycles feature almost parallel ring planes pointing away from each other, leaving **5** with a “handcuff-like” appearance of approximate C<sub>2</sub> symmetry. This work represents the first successful crystallographic study on a cyclodextrin dimer.

**Keywords:** cross-coupling · cyclodextrins · molecular structure · sulfide-bridges · X-ray diffraction

### Introduction

Exciting achievements have been witnessed with cyclodextrins (CDs) as artificial hosts in many of the most actively pursued research fields, such as drug delivery systems, molecular sensing technologies, biomimetic recognition, and catalysis.<sup>[1]</sup> However, the recognition ability of native CDs is greatly confined by their C<sub>n</sub> symmetry and limitations in cavity size, shape, flexibility, and hydrophobicity. Bridging two or more CD units together provides a promising way to alter both the binding ability and guest selectivity. In the pioneering works, Tabushi synthesized a doubly bridged  $\beta$ -CD dimer with two ethylenediamine spacers,<sup>[2]</sup> and Fujita found that the two CD moieties of disulfide-bridged  $\beta$ -CD could cooperate in the binding of ethyl orange, yielding an association constant about

220 times that of  $\beta$ -CD.<sup>[3]</sup> Breslow et al. demonstrated that the same CD dimer selectively bound appropriate “ditopic guests” almost as strongly as antigen–antibody binding.<sup>[4]</sup> Large varieties of CD dimers have been synthesized in which two CD units are linked on either their primary or secondary face by single or double linkers ranging from single atoms to oligopeptide segments.<sup>[5]</sup> Heterodimers,<sup>[6]</sup> -trimers,<sup>[7]</sup> and -tetramers<sup>[8]</sup> have also been reported. The *cis* forms of doubly bridged CD dimers were found to bind appropriate guests with very high affinities and shape selectivities.<sup>[9]</sup> Nolte et al. demonstrated that, depending on the nature of linkers, CD dimers can bind tetrakis(sulfophenyl)porphyrin to form 1:1 *syn*-, *syn/anti*-, and 2:2 (crossed double-zigzag-type) complexes.<sup>[10]</sup> CD dimers were found to have sequence-selective binding ability toward peptides and to disrupt protein aggregation.<sup>[11]</sup> Catalytic functionalities within the linker or on the rims of a dimer may result in strong catalysis. For example, the La<sup>III</sup> complex of a bipyridyl-bridged  $\beta$ -CD dimer has been used to significantly enhance the hydrolysis of phosphodiester.<sup>[12]</sup> Thiazolio-appended CD dimers were used to promote benzoin condensation,<sup>[13]</sup> Se–Se-bridged CD dimers were used to effect glutathione peroxidase-like activity,<sup>[14]</sup> CD-sandwiched metalloporphyrin has been used to catalyze the epoxidation of alkene,<sup>[15]</sup> metalloporphyrin-based CD tetramers have been used to demonstrate site-specific oxidation of steroids,<sup>[16]</sup> and  $\beta$ -carotene<sup>[17]</sup> and, quite recently, EDTA–Ce<sup>IV</sup>-bridged CD dimers have been used to amplify luminol chemiluminescence,<sup>[18]</sup> among many others.

Undoubtedly, three-dimensional structural information on the CD oligomers is very important for understanding the

[a] Dr. S. Immel  
Clemens Schöpf-Institut für Organische Chemie und Biochemie  
Technische Universität Darmstadt  
Petersenstrasse 22, 64287 Darmstadt (Germany)  
Fax: (+49) 6151-166674  
E-mail: lemmit@sugar.oc.chemie.tu-darmstadt.de

[b] Prof. Dr. De-Q. Yuan, Prof. Dr. K. Koga, Prof. Dr. K. Fujita  
Faculty of Pharmaceutical Sciences, Nagasaki University  
Bunkyo-machi, Nagasaki 852-8521 (Japan)

[c] Dr. M. Yamaguchi  
Faculty of Pharmaceutical Sciences, Fukuoka University  
Nanakuma, Jonan-ku, Fukuoka 814-0180 (Japan)

[\*\*] Molecular Modeling of Saccharides, Part 31; for Part 30 see: S. Immel, K. Fujita, M. Fukudome, M. Bolte, *Carbohydr. Res.* **2001**, *336*, 297–308.

## FULL PAPER

S. Immel et al.

process of molecular recognition by CD dimers.<sup>[19]</sup> Unfortunately, we know surprisingly little about the spatial structures of CD oligomers in spite of the many efforts directed to their synthesis and properties. We do not even have enough knowledge to make a convincing judgment on the most fundamental aspects of the large host molecules: do the two or more CD cavities distort or not upon being bridged? How are they spatially arranged? In the following we report a highly efficient synthesis of a new  $\beta$ -CD dimer with two very short sulfur linkers and its unequivocal structural characterization through NMR analysis. Single-crystal X-ray-diffraction analysis was employed for the first time to obtain structural information on a CD dimer and it successfully afforded a clear image of the solid-state structure of the doubly sulfur-bridged  $\beta$ -CD dimer.

## Results and Discussion

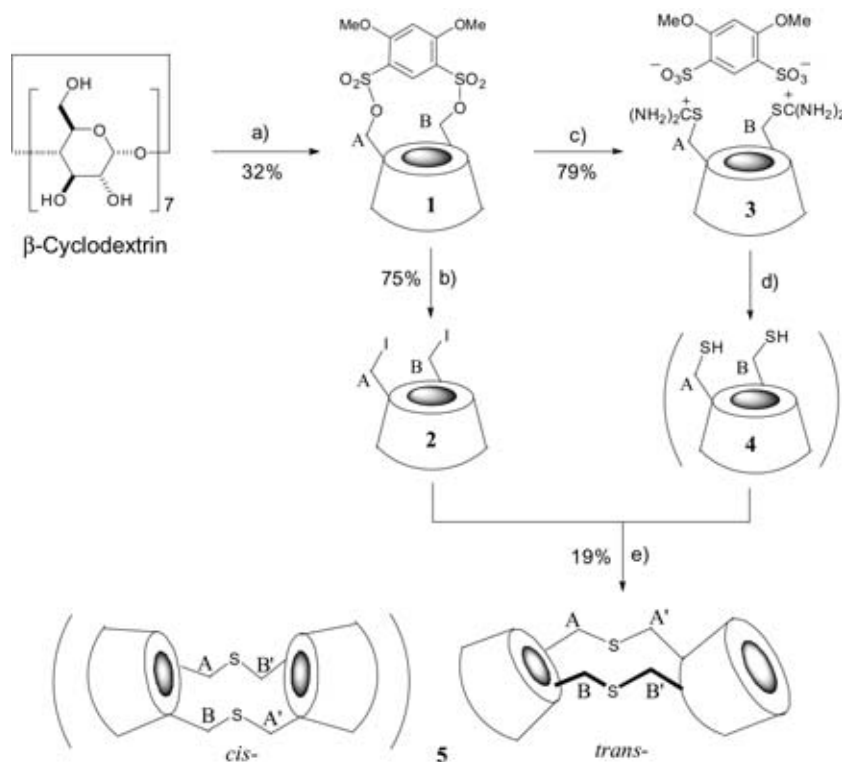
The synthetic approach to the doubly bridged CD dimer is depicted in Scheme 1.  $\beta$ -CD was selectively activated by employing the “looper’s walk” method.<sup>[20]</sup> Treatment of  $\beta$ -CD with 4,6-dimethoxy-1,3-benzenedisulfonyl chloride in dry pyridine afforded the 6<sup>A</sup>,6<sup>B</sup>-capped CD **1**,<sup>[21]</sup> whose yield is clearly dependent on the molar ratio of capping reagent to CD. Utilization of the capping reagent in 50% excess ensured a good yield of the capped product **1**, usually ranging from 30 to 40%. Compound **1** was converted to the corresponding 6<sup>A</sup>,6<sup>B</sup>-diiodide **2** by stirring a mixture of **1** and KI in DMF at 80 °C. Treatment of **1** with thiourea in DMF gave the

thiuronium salt **3** in 79% yield. This was treated with 0.25 N aqueous NaOH, and the generated 6<sup>A</sup>,6<sup>B</sup>-dithiol **4** was collected by precipitation with acetone. The crude 6<sup>A</sup>,6<sup>B</sup>-dithiol **4** was used in the following reaction without further purification. Reaction of the dithiol **4** and diiodide **2** was carried out in DMF in the presence of Cs<sub>2</sub>CO<sub>3</sub> at room temperature and under an argon atmosphere. Reversed-phase chromatography of the reaction mixture afforded the doubly bridged  $\beta$ -CD dimer **5** in 19% yield. The FAB-MS spectrum showed the molecular peak [*M*<sup>+</sup>] at *m/z* = 2266.1, consistent with the expected structure of a doubly bridged  $\beta$ -CD dimer with two sulfur linkers (calcd C<sub>84</sub>H<sub>136</sub>O<sub>66</sub>S<sub>2</sub><sup>+</sup>: 2266.2).

In principal, two isomeric head-to-head  $\beta$ -CD dimers may be formed in the course of the cross-coupling reaction, with either a *cis*-type linkage across the glucose 6<sup>A</sup>,6<sup>B</sup>- and 6<sup>B</sup>,6<sup>A</sup>-positions, or alternatively a *trans* connection of the 6<sup>A</sup>,6<sup>A</sup> and 6<sup>B</sup>,6<sup>B</sup> type. Both isomers retain C<sub>2</sub> symmetry, yet differ substantially in their molecular shapes: the *cis* isomer is expected to adopt a compact, occlusive geometry (“clamshell”),<sup>[9]</sup> whereas the *trans* compound should be characterized by an extended, aversive appearance (“loveseat”).<sup>[9]</sup> However, NMR spectra of the isolated product indicate the presence of only a single isomer, the alternative form was not recognized from the fractions of column chromatography.

Both the <sup>1</sup>H and <sup>13</sup>C NMR spectra of **5** (Figure 1) maintain the basic pattern of  $\beta$ -CD, the weaker signals shifted out from the normal ones are related to the modified sugar residues. Partial assignment of the spectra based on 2D COSY experiment reveals only two sorts of functional glucosides; this confirms the C<sub>2</sub> symmetry of the dimer. Both of them demonstrated significant upfield shifts for their methylene geminal protons (up to the range of 2.75–3.25 ppm), a moderate upfield shift for H-4 and small to moderate downfield shifts for H-5, but trivial shifts for H-1, H-2 and H-3. The <sup>13</sup>C NMR spectrum demonstrated remarkable upfield shifts for C-6, small upfield shifts for C-5, and downfield shifts for C-4 of the modified sugar units. This chemical shift pattern is in good agreement with the replacement of the primary hydroxyl groups by alkyl thiols. Apart from the modified units, no other glucosides showed meaningful shifts. These observations suggest that no apparent distortion should have occurred in the hydrophobic cavities of the doubly bridged CD dimer.

The assignment of the bridging mode (*cis*- or *trans*- with respect to the ring containing both linkers) of the dimer is attempted by using NMR tech-



Scheme 1. Synthesis of the doubly bridged  $\beta$ -CD dimer **5**. a) 1.5 equiv 4,6-dimethoxy-1,3-benzenedisulfonyl chloride, dry pyridine, 40 °C, 2.5 h. b) KI, DMF, 80 °C, 4.5 h. c) Thiourea, DMF, 90 °C, 20 h. d) 0.25 N aqueous NaOH, 90 °C, 10 min; NaBH<sub>4</sub>, RT, 10 min. e) Cs<sub>2</sub>CO<sub>3</sub>, DMF, Ar gas, RT, 66 h.

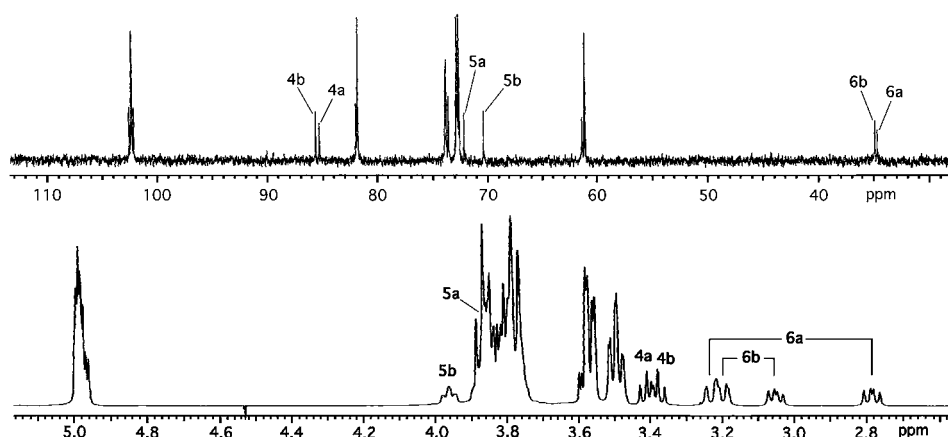


Figure 1.  $^1\text{H}$  and  $^{13}\text{C}$  NMR spectra of  $\beta$ -CD dimer **5** ( $\text{D}_2\text{O}$ ,  $\text{CH}_3\text{CN}$  int.).

niques. In the *cis* structure, each sulfur atom bridges the “A” glucoside of one CD moiety and “B” glucoside of another, that is, the two sorts of modified sugar residues are correlated by one sulfur atom. This correlation is expected to be probed by the HMBC (heteronuclear multiple bond correlation) method.<sup>[22]</sup> In the *trans* isomer, each sulfur connects one pair of equivalent sugar residues, thus no HMBC signals are expected to appear between the two sorts of modified sugar residues. As shown in Figure 2, no cross-signals were observed between the two sorts of modified methylene groups; this suggests a *trans* structure for dimer **5**. This assignment is confirmed by the result of single-crystal X-ray diffraction.

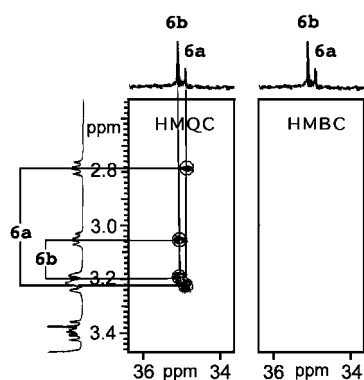


Figure 2. HMQC and HMBC spectra of **5** (only the modified methylene part is shown for clarity). No HMBC cross signals appeared between 6a and 6b; this suggests a *trans*-structure for **5**.

**Solid-state structure analysis of 5:** Single crystals of **5** were obtained after chromatographic purification as described above. Low-temperature X-ray analysis revealed a crystal composition of  $\mathbf{5} \cdot 5\text{MeOH} \cdot 23\text{H}_2\text{O}$ , the molecular and crystal structures are displayed in Figure 3, unequivocally establishing the *trans*-type linkage of the  $\beta$ -CD moieties and the approximate  $C_2$  symmetry of **5**. The  $\beta$ -CD dimers are packed in a herringbone-like fashion forming individual cavities that are blocked by adjacent CD rings and thus do not form tube-like channels. The  $\beta$ -CD cavities are partially filled with four and five water molecules of crystallization, the other water molecules and methanol fill interstitial positions between

the macrocycles. All hydroxyl groups and oxygen atoms participate in the formation of a three-dimensional hydrogen-bonding network in the crystal lattice.

For the dimeric  $\beta$ -CD unit a few relevant geometry descriptors are listed in Table 1, a comprehensive list of atomic coordinates and all bond length and angles—all of which are within standard ranges for organic compounds—may be obtained from the data deposited with the Cambridge Crystallographic Data Centre (see Experimental Section). The molecular geometry of **5** is characterized by an almost coplanar alignment of the  $\text{C6}^{\text{A}}\text{-S-C6}^{\text{A}}$  and  $\text{C6}^{\text{B}}\text{-S-C6}^{\text{B}}$  fragments within the sulfur linkages, with the shape of an elongated planar hexagon. Within this linkage, the  $\text{O6-C5-C6-S}$  dihedral angles invariably adopt (*-*)-*gauche* arrangements, yet the calculated values for the  $\text{C5-C6-S-C6}'$  torsion angles differ significantly at both positions (approx.  $75^\circ$  and  $-130^\circ$ , cf. Table 1).

Table 1. Selected geometry parameters for the dimeric  $\beta$ -CD unit as calculated from the solid-structure of  $\mathbf{5} \cdot 5\text{MeOH} \cdot 23\text{H}_2\text{O}$ .

Linkage	A – A'	B – B'	
torsion angles [°]			
O5-C5-C6-S	–45.7	–68.9	
C5-C6-S-C6'	–128.1	75.5	
C6-S-C6'-C5'	–133.6	76.1	
S-C6'-C5'-O5'	–44.5	–67.2	
CD unit	I	II	
tilt angle <sup>[a]</sup>	$\tau$ [°]	$103 \pm 8$	$104 \pm 9$
ring diameter <sup>[b]</sup>	$r$ [Å]	$9.86 \pm 0.26$	$9.85 \pm 0.47$
ring puckering <sup>[c]</sup>	$d$ [Å]	$0.12 \pm 0.06$	$0.06 \pm 0.03$
inclination <sup>[d]</sup>	[°]	2.9	2.9

[a] Angle between the least-squares best-fit mean plane of the macrocycle (defined by all intersaccharidic O4 atoms) and the mean plane of the pyranose rings (atoms O5 and C1–C5); values of  $\tau > 90^\circ$  indicate outward tilting of the C2 and C3 side of the glucoses; parameter averaged over all glucose residues. [b] Average  $\text{O4-O4}''$  separations within the CD macrocycles. [c] Average deviation of all O4-atoms of the CD macrocycles from planarity. [d] Angle between the least-squares best-fit mean ring planes (all O4 atoms) of both linked  $\beta$ -CD units.

Both linked  $\beta$ -CD-rings feature almost parallel mean ring planes with a relative inclination of only  $2.9^\circ$ ; the centers of the two cavities being  $13.6 \text{ \AA}$  apart. The geometries of the  $\beta$ -CD units are within the usual ranges observed for these compounds and their complexes<sup>[24, 25]</sup> (tilt angles  $\tau$ <sup>[25]</sup> of the glucose residues in relation to the macroring of approx.  $105^\circ$ , ring diameters of about  $9.9 \text{ \AA}$ ). As evidenced by their Cremer–Pople parameters<sup>[26]</sup>  $Q$ ,  $\theta$ , and  $\phi$ , all glucose units adopt standard  $^4\text{C}_1$  chair conformations ( $Q \approx 0.563 \pm 0.018 \text{ \AA}$ ,  $\theta \approx 4 \pm 2^\circ$ ,  $\phi$  is not significant). Out of the total of ten  $6\text{-CH}_2\text{OH}$  groups six adopt *gauche-trans* (*gt*) arrangements with  $\text{O5-C5-C6-O6}$ -torsion angles of  $\omega \approx +60^\circ$ , the remaining four are in *gauche-gauche* (*gg*) orientations ( $\omega \approx -60^\circ$ ) and

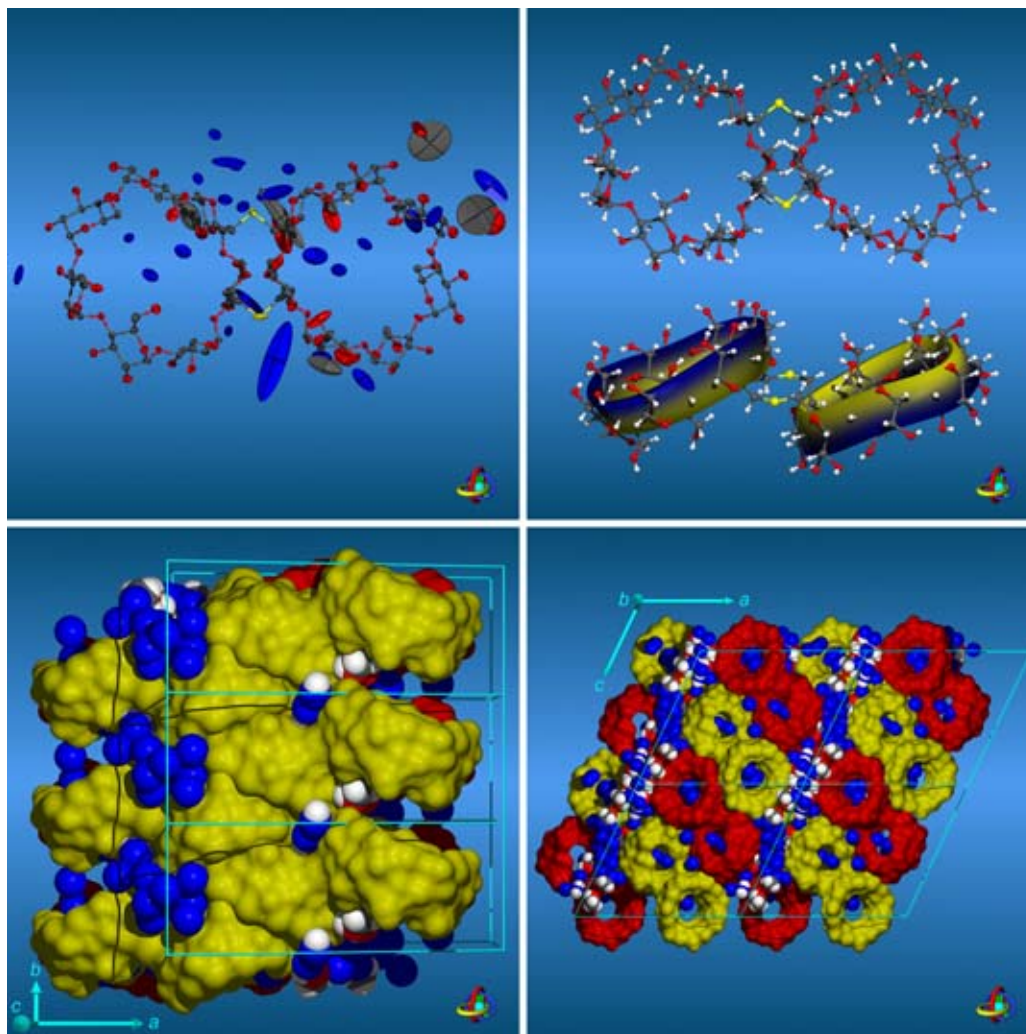


Figure 3. Solid-state structure of  $5 \cdot 5\text{MeOH} \cdot 23\text{H}_2\text{O}$ . Top left: Molecular geometry and anisotropic 50% probability ellipsoids for the non-hydrogen atoms of the asymmetric unit; for clarity the water oxygen atoms are colored blue. Top right: Front- and side-view ball-and-stick-type models displaying the sulfur linker between the two  $\beta$ -CD units. The ribbon model (the black edge of which corresponds to the side of the CDs carrying the secondary 2- and 3-OH groups, while the yellow rim corresponds to the primary 6- $\text{CH}_2\text{OH}$  groups) clearly shows the *trans*-relationship between both CD rings. Bottom left: As represented by their yellow contact-surfaces,<sup>[23]</sup> the  $\beta$ -CD-dimers are stacked in the crystal lattice in a herringbone-like fashion ( $1 \cdot 3 \cdot 1$  unit cells, viewed down the *c*-axis). Bottom right: The stacks of CDs are arranged in layers as indicated by alternating red and yellow surfaces ( $2 \cdot 1 \cdot 2$  unit cells, view down the *b*-axis); each  $\beta$ -CD cavity is occupied by four or five water molecules, the rest of the waters of crystallization and the methanol molecules occupy interstitial positions between the macrocycles; water molecules (blue spheres) and methanol are represented as CPK-type solid spheres.

no disorder was observed. The linked CD macrocycles feature almost identical over-all shapes, their backbones being superimposable with an average deviation of only 0.22 Å in their atomic positions (non-hydrogen atoms except for all O6 atoms).

## Conclusion

A short and efficient synthesis of a new  $\beta$ -CD dimer has been presented, in which two  $\beta$ -CD units are connected in a head-to-head fashion with a very short sulfur linker. Of the two isomers expected to emerge from the cross-coupling reaction, only the *trans*-type compound was isolated while the *cis*-type compound was not detected. X-ray analysis unequivocally established the *trans*-type linkage of the CD moieties of **5** in a zigzag shape. The molecular geometry of **5** is characterized by

an almost parallel arrangement of the mean ring planes of the two undistorted CD rings fused together through an elongated planar hexagon consisting of the  $\text{C6}^{\text{A}}\text{-S-C6}^{\text{A}}$  and  $\text{C6}^{\text{B}}\text{-S-C6}^{\text{B}}$  fragments within the sulfur linkages. The *trans* dimer opens up the possibility of specifically forming inclusion complexes with potential guest molecules of 1:2 stoichiometry. Moreover, the rather rigid linkage and the “handcuff-like” shape of the dimeric host molecule with two separated cavities may allow included guest molecules and their long-range interactions at well-defined distances to be studied.

## Experimental Section

**General:**  $\beta$ -CD was obtained from the Japan Maize Products Co. Ltd. and used without further purification. 4,6-Dimethoxy-1,3-benzenedisulfonyl chloride was synthesized by chlorosulfonation of 1,3-dimethoxybenzene.<sup>[27]</sup>

Pyridine and DMF were dried over 4 Å molecular sieves. Other solvents and chemicals were of reagent grade and used as received from commercial sources. Reversed-phase column chromatography was performed on a Merck prepacked Lobar column (LiChroprep® RP-18, Size B or C). NMR spectra were recorded on a Varian Unity plus 500 spectrometer, and D<sub>2</sub>O was used as solvent. Chemical shifts were referenced to acetonitrile (internal standard,  $\delta_{\text{H}} = 1.98$  ppm,  $\delta_{\text{C}} = 1.70$  ppm). FAB-MS spectra were recorded on a JEOL JMS-HX110 spectrometer.

**6<sup>A</sup>,6<sup>B</sup>-(4,6-dimethoxy-1,3-benzenedisulfonyl)- $\beta$ -cyclodextrin (1):** 4,6-Dimethoxy-1,3-benzenedisulfonyl chloride (2.50 g, 9.23 mmol) was added to a solution of  $\beta$ -CD (6.33 g, 5.58 mmol) in dry pyridine (500 mL). The mixture was stirred at 40 °C for 2.5 h. After the reaction had been quenched by adding water (5 mL), the solvent was removed in vacuo. The residue was taken into 10% aqueous MeOH solution (1 L) and filtered, and the filtrate was then subjected to reversed-phase Lobar column chromatography with gradient elution from 10–40% aqueous methanol (1 L for each). The 20 mL fractions containing the capped CD were combined and evaporated. Lyophilization of the residue afforded the desired product **1** (2.52 g, 32%).

**6<sup>A</sup>,6<sup>A'</sup>:6<sup>B</sup>,6<sup>B'</sup>-bis(thia)-bis(6<sup>A</sup>,6<sup>B</sup>-dideoxy- $\beta$ -cyclodextrin) (5):** KI (3.90 g, 23.5 mmol) was added to a solution of the capped CD **1** (3.19 g, 2.29 mmol) in dry DMF, and the resultant mixture was stirred at 80 °C for 4.5 h. After removal of the solvent in vacuo, the residue was taken into 35% aqueous MeOH solution and filtered. Chromatography of the filtrate on a reversed-phase Lobar column with gradient elution from 10–40% aqueous methanol (1 L for each) gave 6<sup>A</sup>,6<sup>B</sup>-diiodo- $\beta$ -CD **2** (2.31 g, 75%).

Alternatively, the capped CD **1** (0.5 g, 0.36 mmol) was treated with thiourea (0.55 g, 7.2 mmol) in DMF at 90 °C for 20 h. The product was precipitated with acetone (0.2 L) and purified by Lobar column chromatography. Eluting the column with a gradient from 100% H<sub>2</sub>O–10% aqueous MeOH (1 L for each) yielded the 6<sup>A</sup>,6<sup>B</sup>-dithiuronium salt **3** (0.44 g, 79%). This (0.15 g, 0.10 mmol) was dissolved in aqueous NaOH solution (0.25 N, 2.5 mL) and stirred at 90 °C for 10 min. The solution was cooled down to RT, and NaBH<sub>4</sub> (25 mg, 0.66 mmol) was added. Ten minutes later, the reaction solution was acidified to pH 3 with 1 N HCl while being cooled with ice-water bath, then acetone (300 mL) was added to precipitate the dithiol **4**. The crude dithiol **4** was dried in vacuo, taken into DMF (6 mL), and filtered. Diiodide **2** (0.15 g, 0.11 mmol) and cesium carbonate (0.13 g, 0.4 mmol) were added to the filtrate. The mixture was degassed, stirred at RT for 66 h under argon, neutralized with 1 N HCl followed by addition of acetone (300 mL) to precipitate the CD species. Chromatography of the precipitate on a reversed-phase Lobar column (gradient elution from 100% H<sub>2</sub>O to 40% aqueous MeOH, 1 L for each) gave the pure CD dimer **5** (41 mg, 19% based on engaged dithiuronium salt **3** or 16% based on the capped CD **1**). FAB-MS:  $m/z$ : 2266.1 [ $M^+$ ] (calcd 2266.2 for C<sub>84</sub>H<sub>136</sub>O<sub>66</sub>S<sub>2</sub><sup>+</sup>). <sup>1</sup>H and <sup>13</sup>C NMR are given in Figure 1. Cooling the NMR sample solution (30 mg in 0.6 mL D<sub>2</sub>O, CH<sub>3</sub>CN as internal standard) to 5 °C yielded single crystals suitable for X-ray diffraction.

**Solid-state structure of 5·5MeOH·23H<sub>2</sub>O:** A suitable single crystal of **5** with dimensions 0.52 × 0.24 × 0.16 mm was sealed in a tube and subjected to X-ray analysis on a Siemens CCD three-circle diffractometer with graphite-monochromated radiation MoK $\alpha$  ( $\lambda = 0.71073$  Å) at low temperature  $T = 100(2)$  K. The electron density of the solvent in the crystal lattice was approximated through molecules of water and methanol. Analysis of the structure and the hydrogen-bonding network in the crystal lattice yielded 23 additional water molecules and five molecules of methanol (presumably from chromatographic purification) per dimeric  $\beta$ -CD unit. Structure parameters were determined as follows:  $M_r = 2840.61$  g mol<sup>-1</sup> (C<sub>84</sub>H<sub>136</sub>O<sub>66</sub>S<sub>2</sub>·5CH<sub>3</sub>OH·23H<sub>2</sub>O), monoclinic, space group C2,  $a = 35.557(2)$ ,  $b = 12.3387(5)$ ,  $c = 31.543(2)$  Å,  $\beta = 115.272(4)$ ,  $V = 12514.3(12)$  Å<sup>3</sup>,  $Z = 4$ ,  $\rho = 1.508$  g cm<sup>-3</sup>,  $\mu(\text{MoK}\alpha) = 0.167$  mm<sup>-1</sup>,  $F(000) = 5888$ ,  $\theta$  range 0.71–25.31°, with limiting indices  $-42 \leq h \leq 42$ ,  $-14 \leq k \leq 14$ , and  $-37 \leq l \leq 37$ . Of the 72505 reflections collected 22474 were independent ( $R_{\text{int}} = 0.0740$ ). The structure was solved by direct methods (SHELXS-97)<sup>[28]</sup> and successive Fourier synthesis. Refinement (on  $F^2$ ) was performed by the full-matrix least-squares method with SHELXL-97.<sup>[28]</sup>  $R(F) = 0.0823$  for 18524 reflections with  $I > 2\sigma(I)$ ,  $\omega R(F^2) = 0.2382$  for all 22474 reflections ( $\omega = 1/[\sigma^2(F_o^2) + (0.1670P)^2 + 23.4030P]$ ); in which  $P = (F_o^2 + 2F_c^2)/3$ . All non-hydrogen atoms (except for one methanol oxygen atom) were refined anisotropically (reflections 22474/parameters 1663/

restraints 6). Hydrogen atoms were considered in calculated positions with the 1.2  $U_{\text{eq}}$  value of the corresponding bound atom.

CCDC-190090 contains the supplementary crystallographic data for this paper. These data can be obtained free of charge via www.ccdc.cam.ac.uk/conts/retrieving.html (or from the Cambridge Crystallographic Data Centre, 12 Union Road, Cambridge CB2 1EZ, UK; fax: (+44) 1223-336033; or deposit@ccdc.cam.ac.uk).

Molecular graphics were generated by using the MolArch<sup>+</sup> program.<sup>[30]</sup>

## Acknowledgement

The authors are grateful to Prof. F. W. Lichtenthaler and Prof. H. J. Lindner for lucid discussions and to Sabine Foro for collecting the crystallographic data.

- [1] A special issue on cyclodextrins: *Chem. Rev.* **1998**, 98(5).
- [2] I. Tabushi, Y. Kuroda, K. Shimokawa, *J. Am. Chem. Soc.* **1979**, 101, 1614–1615.
- [3] a) K. Fujita, S. Ejima, T. Imoto, *J. Chem. Soc. Chem. Commun.* **1984**, 1277–1278; b) *Chem. Lett.* **1985**, 11–14.
- [4] R. Breslow, N. Greenspoon, T. Guo, R. Zarzycki, *J. Am. Chem. Soc.* **1989**, 111, 8296–8297.
- [5] a) D.-Q. Yuan, Y. Okabe, K. Fujita, *Chin. Chem. Lett.* **1997**, 8, 475–476; b) Y. Ishimaru, T. Masuda, T. Iida, *Tetrahedron Lett.* **1997**, 38, 3743–3744; c) B. Brady, R. Darcy, *Carbohydr. Res.* **1998**, 309, 237–241; d) F. Charbonnier, A. Marsura, I. Pintér, *Tetrahedron Lett.* **1999**, 40, 6581–6583; e) J. Yan, R. Watanabe, M. Yamaguchi, D.-Q. Yuan, K. Fujita, *Tetrahedron Lett.* **1999**, 40, 1513–1514; f) J. Yan, R. Breslow, *Tetrahedron Lett.* **2000**, 41, 2059–2062; g) S.-H. Chiu, D. C. Myles, R. L. Garrell, J. F. Stoddart, *J. Org. Chem.* **2000**, 65, 2792–2796; h) M. R. de Jong, J. F. J. Engbersen, J. Huskens, D. N. Reinhoudt, *Chem. Eur. J.* **2000**, 6, 4034–4040; i) K. J. C. van Bommel, M. R. de Jong, G. A. Metselaar, W. Verboom, J. Huskens, R. Hulst, H. Kooijman, A. L. Spek, D. N. Reinhoudt, *Chem. Eur. J.* **2001**, 7, 3603–3615; j) Y. Liu, Y. Chen, L. Li, G. Huang, C.-C. You, H.-Y. Zhang, T. Wada, Y. Inoue, *J. Org. Chem.* **2001**, 66, 7209–7215; k) Y. Liu, B. Li, C.-C. You, T. Wada, Y. Inoue, *J. Org. Chem.* **2001**, 66, 225–232.
- [6] a) Y. Wang, A. Ueno, F. Toda, *Chem. Lett.* **1994**, 167; b) F. Venema, C. M. Baselier, M. C. Feiters, R. J. M. Nolte, *Tetrahedron Lett.* **1994**, 35, 8661–8664; c) Y. Okabe, M. Yamamura, K. Obe, K. Ohta, M. Kawai, K. Fujita, *J. Chem. Soc. Chem. Commun.* **1995**, 581–582; d) D.-Q. Yuan, K. Fujita, H. Mizushima, M. Yamaguchi, *J. Chem. Soc. Perkin Trans. 1* **1997**, 3135–3136.
- [7] a) M. Luo, W. Chen, D.-Q. Yuan, R. Xie, *Synth. Commun.* **1998**, 28, 3845–3848; b) D. K. Leung, J. H. Atkins, R. Breslow, *Tetrahedron Lett.* **2001**, 42, 6255–6258; c) K. Sasaki, M. Nagasaka, Y. Kuroda, *Chem. Commun.* **2001**.
- [8] a) T. Jiang, M. Li, D. S. Lawrence, *J. Org. Chem.* **1995**, 60, 7293–7297; b) R. Breslow, X. Zhang, R. Xu, M. Maletic, R. Merger, *J. Am. Chem. Soc.* **1996**, 118, 11678–11679.
- [9] R. Breslow, S. Sung, *J. Am. Chem. Soc.* **1990**, 112, 9659–9660.
- [10] a) F. Venema, A. E. Rowan, R. J. M. Nolte, *J. Am. Chem. Soc.* **1996**, 118, 257–258; b) F. Venema, P. Berthault, R. J. M. Nolte, *Chem. Eur. J.* **1998**, 4, 2237–2250.
- [11] a) R. Breslow, B. Zhang, *J. Am. Chem. Soc.* **1992**, 114, 5882–5883; b) R. Breslow, B. Zhang, *J. Am. Chem. Soc.* **1994**, 116, 7893–7894; c) B. Zhang, R. Breslow, *J. Am. Chem. Soc.* **1997**, 119, 1676–1681.
- [12] a) R. Breslow, Z. Yang, R. Ching, G. Trojandt, F. Odobel, *J. Am. Chem. Soc.* **1998**, 120, 3536–3537; b) D. K. Leung, Z. Yang, R. Breslow, *Proc. Natl. Acad. Sci. USA* **2000**, 97, 5050–5053.
- [13] H. Ikeda, Y. Horimoto, M. Nakata, A. Ueno, *Tetrahedron Lett.* **2000**, 41, 6483–6487.
- [14] J. Liu, G. Luo, X. Ren, Y. Mu, Y. Bai, J. Shen, *Biochim. Biophys. Acta* **2000**, 1481, 222–228.
- [15] a) Y. Kuroda, T. Hiroshige, T. Sera, Y. Shiroiwa, H. Tanaka, H. Ogoshi, *J. Am. Chem. Soc.* **1989**, 111, 1921; b) Y. Kuroda, M. Ito, T. Sera, H. Ogoshi, *J. Am. Chem. Soc.* **1993**, 115, 7003–7004.

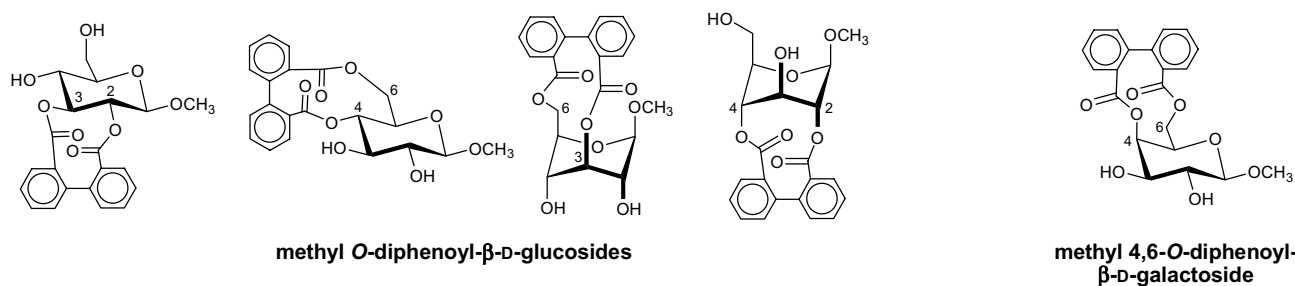
- [16] a) R. Breslow, Y. Huang, J. Yang, *Proc. Natl. Acad. Sci. USA* **1997**, *94*, 11156–11158; b) J. Yang, R. Breslow, *Angew. Chem.* **2000**, *112*, 2804–2806; *Angew. Chem. Int. Ed.* **2000**, *39*, 2692–2694.
- [17] a) R. R. French, P. Holzer, M. G. Leuenberger, W.-D. Woggon, *Angew. Chem.* **2000**, *112*, 1321–1323; *Angew. Chem. Int. Ed.* **2000**, *39*, 1267–1269; b) R. R. French, W.-D. Woggon, J. Wirz, *Helv. Chim. Acta* **1998**, *81*, 1521–1527.
- [18] D.-Q. Yuan, J.-Z. Lu, M. Atsumi, A. Izuka, M. Kai, K. Fujita, *Chem. Commun.* **2002**, 730–731.
- [19] R. Breslow, S. Halfon, B. Zhang, *Tetrahedron* **1995**, *51*, 377–388.
- [20] a) I. Tabushi, K. Shimokawa, N. Shimizu, H. Shirakata, K. Fujita, *J. Am. Chem. Soc.* **1976**, *98*, 7855–7856; b) I. Tabushi, Y. Kuroda, K. Yokota, L. C. Yuan, *J. Am. Chem. Soc.* **1981**, *103*, 711–712; c) I. Tabushi, K. Yamamura, T. Nabeshima, *J. Am. Chem. Soc.* **1984**, *106*, 5267–5270.
- [21] R. Breslow, J. W. Canary, M. Verney, S. T. Waddell, D. Yang, *J. Am. Chem. Soc.* **1990**, *112*, 5212–5219.
- [22] *Two-Dimensional NMR Spectroscopy* (Eds.: W. R. Croasmun, R. M. K. Carlson), VCH, Weinheim, **1994**.
- [23] a) M. L. Connolly, *J. Appl. Crystallogr.* **1983**, *16*, 548–558; b) M. L. Connolly, *Science* **1983**, *221*, 709–713.
- [24] K. B. Lipkowitz, K. Green, J. A. Yang, *Chirality* **1992**, *4*, 205–215.
- [25] F. W. Lichtenthaler, S. Immel, *Liebigs Ann.* **1996**, 27–37.
- [26] a) D. Cremer, J. A. Pople, *J. Am. Chem. Soc.* **1975**, *97*, 1354–1358; b) G. A. Jeffrey, J. H. Yates, *Carbohydr. Res.* **1979**, *74*, 319–322.
- [27] M. Sekine, J. Matsuzaki, T. Hata, *Tetrahedron* **1985**, *41*, 5279–5288.
- [28] Sheldrick, G. M. *SHELXS-97 and SHELXL-97 Programs for Crystal Structure Solution and Refinement*, University of Göttingen, Germany, **1997**.
- [29] a) F. H. Allen, S. Bellard, M. D. Brice, B. A. Cartwright, A. Doubleday, H. Higgs, T. Hummelink, B. G. Hummelink-Peters, O. Kennard, W. D. S. Motherwell, J. R. Rodgers, D. G. Watson, *Acta Crystallogr. Sect. B* **1979**, *35*, 2331–2339; b) F. H. Allen, O. Kennard, R. Taylor, *Acc. Chem. Res.* **1983**, *16*, 146–153.
- [30] S. Immel, *MolArch<sup>+</sup>, MOLEcular ARCHitecture Modeling Program V7.05*, Technical University of Darmstadt, **2002**.

Received: August 2, 2002

Revised: March 8, 2003 [F4310]

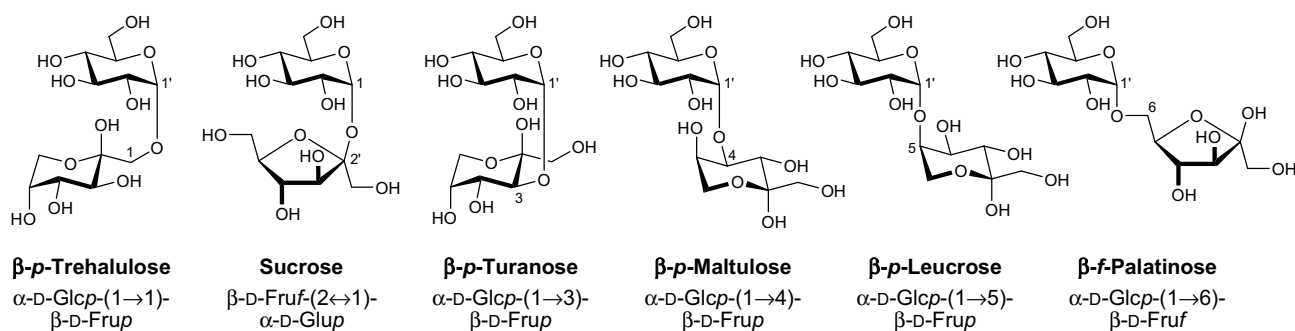
## Chapter 8

### Molecular Modelling of Saccharides



Atropdiastereoisomers of Ellagitannin Model Compounds: Configuration, Conformation, and Relative Stability of D-Glucose Diphenoyl Derivatives

S. Immel, K. Khanbabaee,  
*Tetrahedron: Asymmetry* **2000**, *11*, 2495-2507.



Metabolism of Sucrose and Its Five Linkage-isomeric  $\alpha$ -D-Glucosyl-D-fructoses by *Klebsiella pneumoniae*

J. Thompson, S. A. Robrish, S. Immel, F. W. Lichtenthaler, B. G. Hall, and A. Pikis,  
*J. Biol. Chem.* **2001**, *276*, 37415-37425.

Metabolism of Sucrose and Its Five  $\alpha$ -D-Glucosyl-D-fructose Isomers by *Fusobacterium mortiferum*

A. Pikis, S. Immel, S. A. Robrish, and J. Thompson,  
*Microbiology* **2002**, *148*, 843-852.







Pergamon

Tetrahedron: *Asymmetry* 11 (2000) 2495–2507

---

---

**TETRAHEDRON:**  
**ASYMMETRY**

---

---

# Atropdiastereoisomers of ellagitannin model compounds: configuration, conformation, and relative stability of D-glucose diphenoyl derivatives<sup>1</sup>

Stefan Immel<sup>a,\*</sup> and Karamali Khanbabaee<sup>b</sup><sup>a</sup>*Institut für Organische Chemie, Technische Universität Darmstadt, Petersenstraße 22, D-64287 Darmstadt, Germany*<sup>b</sup>*Fachbereich Chemie und Chemietechnik der Universität-GH Paderborn, Warburgerstraße 100,  
D-33098 Paderborn, Germany*

Received 18 April 2000; accepted 9 May 2000

---

## Abstract

Conformational analysis reveals a remarkable rigidity of 2,3-, 4,6-, 3,6-, and 2,4-*O*-(*S*)- and (*R*)-diphenoyl (DP) bridged methyl β-D-glucosides, which were used as model compounds to evaluate the atropisomeric features of the natural ellagitannins, which possess at least one hexahydroxydiphenoyl (HHDP) moiety. The 2,3- and 4,6-*O*-(*S*)-DP bridged glucosides with <sup>4</sup>C<sub>1</sub> pyranose geometries are thermodynamically more stable than their (*R*)-DP counterparts, whilst in the 3,6- and 2,4-*O*-linked series with <sup>1</sup>C<sub>4</sub> glucopyranose geometries the (*R*)-DP configuration is preferred. The chiral scaffold of glucose exerts a strong atropdiastereoselective effect onto the diphenoyl units, which is mediated through 10- to 12-membered rings via ester linkages. The calculated results not only explain the observed (*S*)-diastereoselectivity of di-esterification reactions of suitably protected racemic hexaoxydiphenic acids with 4,6-unsubstituted D-glucopyranose derivatives, but also correlate the observed configuration of axially chiral HHDP-moieties of natural ellagitannins with conformational parameters. © 2000 Elsevier Science Ltd. All rights reserved.

---

## 1. Introduction

Ellagitannins constitute members of a large class of polyphenolic natural products that can be obtained by extraction from higher plants.<sup>2</sup> These extracts are widely used in folk medicine, leather and wine industry, and the tannin-components exhibit a broad range of biological activities.<sup>2</sup> The common structural element of the ellagitannins is a hexahydroxydiphenoyl (HHDP) unit located at the 2,3-, 4,6-, 1,6-, 3,6-, and/or 2,4-positions of the D-glucopyranose core.

The axially chiral HHDP-units of the 2,3- and 4,6-*O*-HHDP ellagitannins exhibit almost invariably the (*S*)-configuration with only very few exceptions (Cercidin A and B,<sup>3</sup> Cuspinin,<sup>3</sup> and Platycaryanin D<sup>4</sup>) amongst more than 500 structurally characterized compounds (Fig. 1).<sup>2,5</sup>

---

\* Corresponding author. E-mail: lemmit@sugar.oc.chemie.tu-darmstadt.de

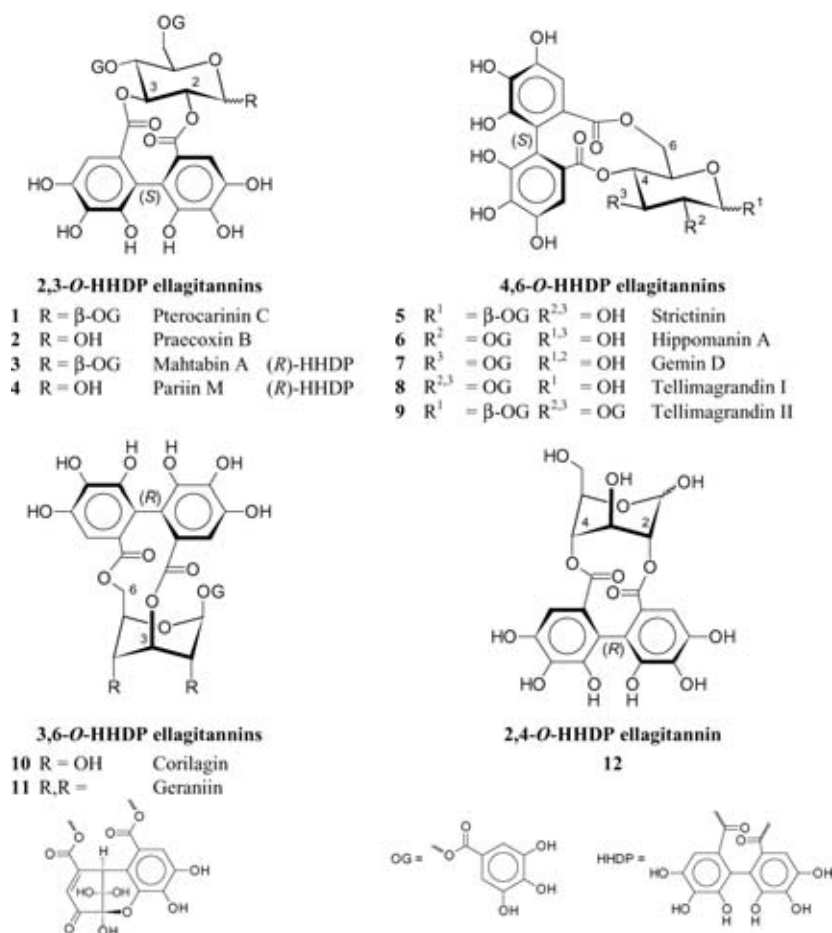


Figure 1. Chemical formulas of 2,3-, 4,6-, 3,6-, and 2,4-*O*-hexahydroxydiphenyl (HHDP) glucosides (ellagitannins) with axial chirality of the HHDP moieties

Recently, it was shown that the postulated structures for the unusual ellagitannins Cercidin A and B,<sup>3</sup> each possessing a 2,3-(*R*)-HHDP unit, are incorrect and must be revised.<sup>6</sup>

Prominent examples for the 2,3-*O*-(*S*)-HHDP ellagitannins are Pterocarinin C **1** and Praecoxin B **2**,<sup>7</sup> their non-natural, unusual (*R*)-HHDP counterparts Mahtabin A **3** and Pariin M **4** have become accessible in enantiomerically pure form through ring forming di-esterification of the *o*-nitrobenzyl 4,6-*O*-benzylidene- $\beta$ -D-glucoside with racemic hexabenzoyloxydiphenic acid.<sup>6</sup> Total syntheses of the natural 4,6-*O*-(*S*)-HHDP ellagitannins **5–7**<sup>8,9</sup> were achieved through unexpectedly highly atropdiastereoselective di-esterification reactions of racemic hexabenzoyloxydiphenic acid with different 4,6-unsubstituted D-glucopyranose derivatives, exclusively leading to the corresponding 4,6-*O*-(*S*)-HHDP diastereomers. In contrast, in the same reactions the (*R*)-component of the racemic hexabenzoyloxydiphenic acid gave rise to the formation of oligomers through the possible intermolecular competition pathway only.<sup>8–10</sup> On the other hand, the naturally occurring ellagitannins in which the HHDP-units are attached to the 3,6- (Corilagin **10**<sup>11</sup> and Geraniin **11**<sup>12,13</sup>) or 2,4-positions<sup>14</sup> **12** of glucopyranose exhibit (*R*)-HHDP configuration,<sup>2</sup> although the latter invariably undergo further biochemical transformations under physiological conditions.<sup>2</sup>

The highly atropdiastereoselective formation of the ellagitannins from their biochemical gallo-tannin precursors has been explained through conformational preferences of the galloyl residues, and strain in the transition states of the oxidative coupling reactions between galloyl esters.<sup>2,12,15–17</sup> However, despite the wide-spread occurrence of polyphenolic compounds of tannin class natural products, very little structural data on gallotannins or ellagitannins at atomic resolution is available through crystal structure analysis; the only examples available from the Cambridge Crystallographic Database<sup>18</sup> are Geraniin **11**<sup>19</sup> and methyl 4,6-*O*-benzylidene-2,3-*O*-(*S*)-hexamethoxydiphenoyl- $\alpha$ -D-glucopyranoside **13**.<sup>20</sup>

As chemical syntheses of the ellagitannins proceed either via oxidative coupling of galloyl residues in galloylated glucose substrates, or alternatively through di-esterification of methyl- or benzyloxy-protected enantiopure or racemic hexahydroxydiphenic acid with appropriately substituted D-glucosides,<sup>2</sup> stereocontrol of these reactions is of fundamental importance. Therefore, we have undertaken a molecular modeling study of some ellagitannin model compounds with the aim of obtaining structural models on an atomic level, and to explain the relative stabilities of the various (*R* and *S*)-HHDP diastereomers under equilibrium conditions.

## 2. Results and discussion

We chose the compounds **14–21** (Fig. 2) as a starting point for our study on the different types of ellagitannins. The hydroxyl groups of the HHDP- and galloyl-residues were omitted in order to reduce the number of local minima on the energy potentials surfaces of the ellagitannins originating from different OH-rotamers ( $\rightarrow$  diphenoyl and benzoyl-substituents). This simplification also avoids conformational artifacts stabilized by strong intramolecular hydrogen bonds, as the geometry analyses were carried out for the isolated molecules only without the explicit incorporation of a solvent; for the same reason, the methyl  $\beta$ -D-glucosides were considered only. Starting geometries were generated for all types of 2,3-, 4,6-, 3,6-, and 2,4-type linkages, and both (*S*)- and (*R*)-diphenoyl (DP) atropdiastereoisomers, respectively. In the first class of compounds, the 4- and 6-OH groups of glucose were ‘blocked’ by benzoyl groups as mimics for the galloyl residues (vide supra).

In each case, the conformational space was explored by a mixed molecular dynamics (MD) and molecular mechanics (MM) approach, applying a full energy optimization to 5000 structures extracted along a 500 ps MD trajectory (for details, see Experimental). As was established through monitoring a number of molecular parameters along the MD runs, this methodology did not only produce glucose conformations other than  ${}^4C_1$  or  ${}^1C_4$ , but it also generated a large number of conformers of the diphenoyl ring system. The atropstereochemical configuration of all diphenoyl units was retained during all MD simulations, and no (*S*) $\leftrightarrow$ (*R*) transitions were recorded. The fully relaxed, global energy-minimum structures obtained were used in this report, and for each model compound some characteristic geometry parameters (cf. Fig. 2) are listed in Table 1.

### 2.1. 2,3-*O*-Diphenoyl glucosides **14** and **15**

The global energy-minimum structures of **14** and **15** are shown in Fig. 3, with **14** being about 7.4 kJ/mol more stable than **15** (cf. Table 1). The glucopyranose units adopt standard  ${}^4C_1$  ring geometries as evidenced by their Cremer-Pople ring puckering parameters<sup>21</sup> (cf. Table 1), and the

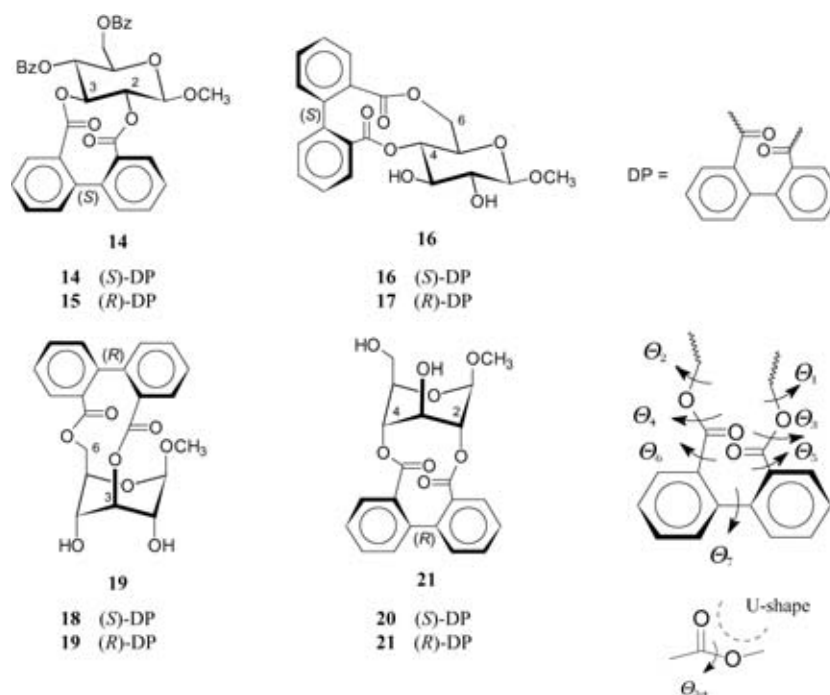


Figure 2. Methyl 2,3-, 4,6-, 3,6-, and 2,4-*O*-(*R,S*)-diphenoyl- $\beta$ -D-glucosides **14–21** used as model structures for evaluating the conformational properties of ellagitannins (DP = diphenoyl). On the right, some ring torsion angles  $\theta_1$ – $\theta_7$  used in the geometry analysis are given.  $\theta_1$  and  $\theta_2$  define the mode of attachment of the diphenoyl-unit to the glucopyranose ring. The preferred U-shape of both ester groups is characterized by  $\theta_3$  and  $\theta_4$  with ideal values of approximately  $0^\circ$ ;  $\theta_5$  and  $\theta_6$  denote the inclination of the carbonyl groups towards the phenyl rings (ideal values  $0^\circ$  and  $\pm 180^\circ$  for conjugated  $\pi$ -systems). The atropisomeric diphenoyl units display torsion angles  $\theta_7$  of opposite sign (*R*: negative, *S*: positive values);  $\theta_7$  is approximately equivalent to the tilt angle between the phenyl rings

conformational preferences of the 10-membered diphenoyl ring system are largely determined by its rather rigid *trans*-type linkage to the pyranose scaffold. The two ester groups display a highly characteristic tendency to maintain an U-shape (Fig. 2), although the torsion angles  $\theta_3$  and  $\theta_4$  indicate about a  $30^\circ$  deviation from the ideal geometry for **14** (Table 1). In **15**, the glucose 2-OCO-ester group is forced by the (*R*)-DP residue into a strained *trans*-type conformation with  $\theta_3 \approx 140^\circ$ . In both compounds **14** and **15**, the carbonyl groups are inclined by about  $40$ – $50^\circ$  ( $\theta_5$  and  $\theta_6$ ) relative towards the planes of phenyl ring  $\pi$ -systems. The phenyl rings of the DP-units are tilted towards each other by about  $50$ – $60^\circ$  (torsion angle  $\theta_7$  in Table 1, positive values of  $\theta_7$  indicating (*S*)-DP units and negative (*R*)-DP configurations). Most notably, the ester groups tend to adopt an antiparallel arrangement of their C=O dipoles (angles  $\varphi$  of  $150$ – $165^\circ$ ), whereas the tilt angles  $\tau$  indicate an almost parallel (stacked) alignment of the planes formed by the C-COO-atoms of each ester fragment. These geometry parameters clearly reveal the torsion angle  $\theta_3$  as the main reason for the lower stability of **15** as compared to **14**.

This notion is further substantiated through color-coded projection of the force-field derived split-terms of strain energy originating from angle- and torsion-bending onto the ball-and-stick models of **14** and **15**. In Fig. 4, blue colors correspond to relaxed molecular fragments, whereas yellow to red colors indicate strain on distinct residues. In both cases, the type of ring-anellation

Table 1

Relative energies and selected geometry parameters calculated for the global energy-minimum structures of the ellagitannin model compounds **14–21**. For each type of 2,3-, 4,6-, 3,6-, and 2,4-*O*-diphenoyl bridged glucopyranose derivative, the (*S*)- and (*R*)-atropdiastereomers are listed; the *galacto*-configured compounds **23** and **24** lack naturally occurring counterparts amongst the ellagitannins, but were included for comparison (cf. text)

compound		<b>14</b>	<b>15</b>	<b>16</b>	<b>17</b>	<b>18</b>	<b>19</b>	<b>20</b>	<b>21</b>	<b>23</b>	<b>24</b>
$\Delta H_{\text{calc}}$ [kJ/mol]	linkage type	2,3-( <i>S</i> )	2,3-( <i>R</i> )	4,6-( <i>S</i> )	4,6-( <i>R</i> )	3,6-( <i>S</i> )	3,6-( <i>R</i> )	2,4-( <i>S</i> )	2,4-( <i>R</i> )	4,6-( <i>S</i> ) <sup>d1</sup>	4,6-( <i>R</i> ) <sup>d1</sup>
	absolute	-	-	-	-	-	-	-	-	-	-
	relative	1245.	1238.	1158.	1153.	1145.	1172.	1125.	1130.	1150.	1159.
		4	0	7	2	3	4	3	9	9	5
		0.0	7.4	0.0	5.5	27.1	0.0	5.6	0.0	8.6	0.0
pyranose Cremer-Pople parameters <sup>21)</sup>	conformation	<sup>4</sup> C <sub>1</sub>	<sup>4</sup> C <sub>1</sub>	<sup>4</sup> C <sub>1</sub>	<sup>4</sup> C <sub>1</sub>	<sup>1</sup> C <sub>4</sub>	<sup>1</sup> C <sub>4</sub>	<sup>1</sup> C <sub>4</sub>	<sup>1</sup> C <sub>4</sub>	<sup>4</sup> C <sub>1</sub>	<sup>4</sup> C <sub>1</sub>
	$Q$ [Å]	0.545	0.615	0.556	0.557	0.490	0.528	0.543	0.543	0.577	0.545
	$\theta$ [°]	11.6	8.4	11.5	7.3	176.2	172.6	173.6	172.6	3.8	5.4
	$\phi$ [°]	37.8	243.8	341.2	285.1	208.0	31.2	43.3	317.8	288.1	21.9
torsion angles <sup>1b)</sup> [°]	$\theta_1$ (C <sub>pyr</sub> <sup>+</sup> -C <sub>pyr</sub> <sup>-</sup> -O-C)	-81.6	-84.3	-130.9	-162.8	73.2	75.2	-64.1	-68.9	164.5	128.8
	$\theta_2$ (C <sub>pyr</sub> <sup>-</sup> -C <sub>pyr</sub> <sup>+</sup> -O-C)	-82.1	48.2	-111.8	91.5	118.3	125.2	58.1	63.7	116.8	115.3
	$\theta_3$ (C <sub>pyr</sub> <sup>+</sup> -O-C=O)	-32.7	136.9	-28.9	-116.0	53.9	0.1	-20.5	-166.0	130.5	26.4
	$\theta_4$ (C <sub>pyr</sub> <sup>-</sup> -O-C=O)	-33.0	34.1	-30.5	18.8	28.6	40.5	-176.1	23.5	177.1	29.5
	$\theta_5$ (O=C-C <sub>dp</sub> -C <sub>dp</sub> )	42.4	-44.6	49.2	-107.0	138.3	-43.5	63.5	-61.1	124.6	-47.6
	$\theta_6$ (O=C-C <sub>dp</sub> <sup>+</sup> -C <sub>dp</sub> <sup>-</sup> )	42.9	-50.9	36.9	-38.3	141.7	-33.6	49.9	-60.6	78.4	-38.9
	$\theta_7$ (C <sub>dp</sub> <sup>-</sup> -C <sub>dp</sub> <sup>+</sup> -C <sub>dp</sub> <sup>-</sup> -C <sub>dp</sub> <sup>+</sup> )	48.9	-61.9	56.2	-74.6	90.8	-58.3	63.9	-70.1	114.6	-54.5
	$\omega$ (O <sub>S</sub> -C <sub>S</sub> -C <sub>S</sub> -O <sub>N</sub> )	43.7 <sup>k1</sup>	71.0 <sup>l1</sup>	-80.9	-170.7	-99.0	175.3	173.0 <sup>k1</sup>	167.6 <sup>l1</sup>	168.8	-173.9
angle [°]	$\varphi$ (C=O / C=O) <sup>d1</sup>	165.9	153.3	150.6	120.7	167.1	154.1	138.9	138.2	130.4	151.4
tilt angle [°]	$\tau$ (COO / COO) <sup>e1</sup>	175.6	176.2	168.5	132.4	88.0	160.6	162.8	167.3	134.4	168.9

a) D-*galacto*-configuration. — b) C<sub>pyr</sub><sup>+</sup> and C<sub>pyr</sub><sup>-</sup> denote the pyranose positions linked to the diphenoyl moiety, i.e. C<sub>pyr</sub><sup>+</sup> / C<sub>pyr</sub><sup>-</sup> = C<sub>2</sub> / C<sub>3</sub> for **14** and **15**; C<sub>4</sub> / C<sub>6</sub> for **16**, **17**, **23**, and **24**; C<sub>3</sub> / C<sub>5</sub> for **18** and **19**; C<sub>1</sub> / C<sub>4</sub> for **20** and **21**; C<sub>dp</sub><sup>+</sup> and C<sub>dp</sub><sup>-</sup> refer to the diphenoyl unit. — c) torsion angle  $\omega$  not part of the diphenoyl ring system in **14**, **15**, **20** and **21**. — d) angle between the bond vectors of the ester carbonyl groups. — e) tilt angle between the two planes defined by the ester groups (atoms C-COO).

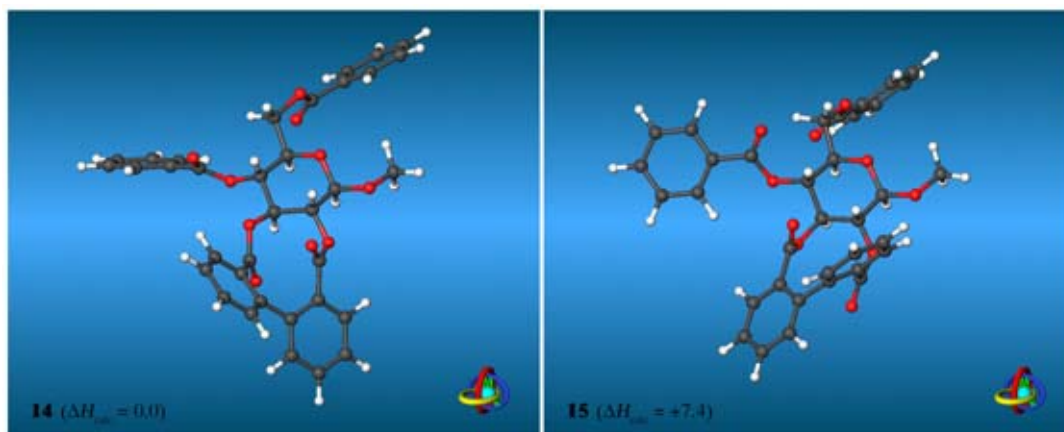


Figure 3. Ball-and-stick models of the global energy-minimum structures of the 2,3-*O*-(*S*)-DP **14** and (*R*)-DP **15** glucosides; calculated relative energies are given in kJ/mol

exerts strain on the position C-4 of the glucopyranose. In addition, **15** clearly displays through red colors internal strain centered around the 2-OCO ester. The rather rigid glucose unit serves as chiral strait-jacket, to which only a (*S*)-DP unit can be attached in a ‘relaxed’ conformation to the 2-*O*- and 3-*O*-groups, the atropstereochemical induction being mediated through the stiff ester groups in the attached ring.

2500

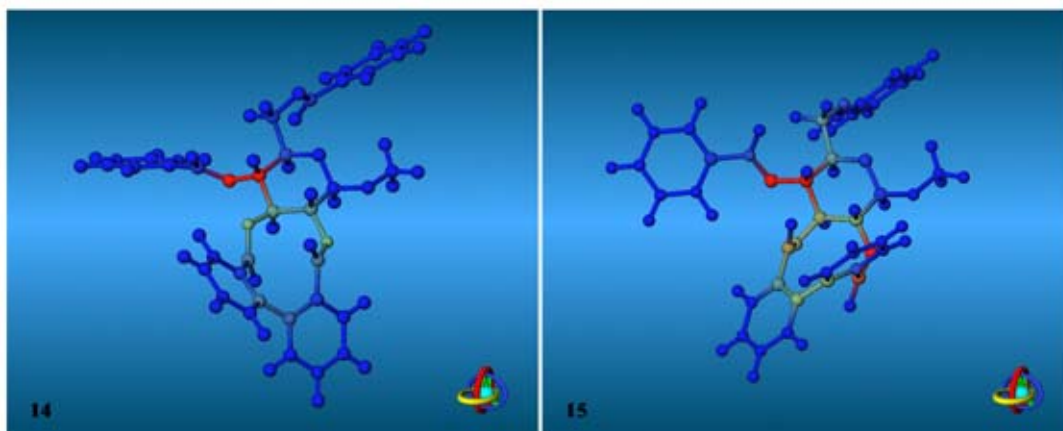
*S. Immel, K. Khanbabaee / Tetrahedron: Asymmetry 11 (2000) 2495–2507*

Figure 4. Color-coded projection of the force-field derived sum of split terms of angle- and torsion-bending strain energy onto ball-and-stick models of 2,3-*O*-(*S*)-DP **14** (left) and (*R*)-DP **15** (right) glucosides; blue colors indicate relaxed molecular parts, and yellow/green to red colors designate strained fragments (strain energies 0–5 kJ/mol); the mode of viewing corresponds to Fig. 3. The rigidity of both the pyranose and DP-ring systems, as well as the stiffness of the ester groups lead to a high energy conformation of the glucose 2-*O*-ester linkage in **15**

Some indications on the relevance of the computer-generated geometries are derived from comparison of **14** with the conformation of methyl 4,6-*O*-benzylidene-2,3-*O*-(*S*)-hexamethoxydiphenoyl- $\alpha$ -D-glucopyranoside **13** obtained from crystal structure analysis.<sup>20</sup> Superimposition of the common molecular fragments of **14** and **13** (Fig. 5) displays a high degree of correlation between the theoretically predicted and experimentally observed structures: in particular the ring linkage, the alignment of the ester groups, as well as the relative tilt of the phenyl rings are predicted accurately.

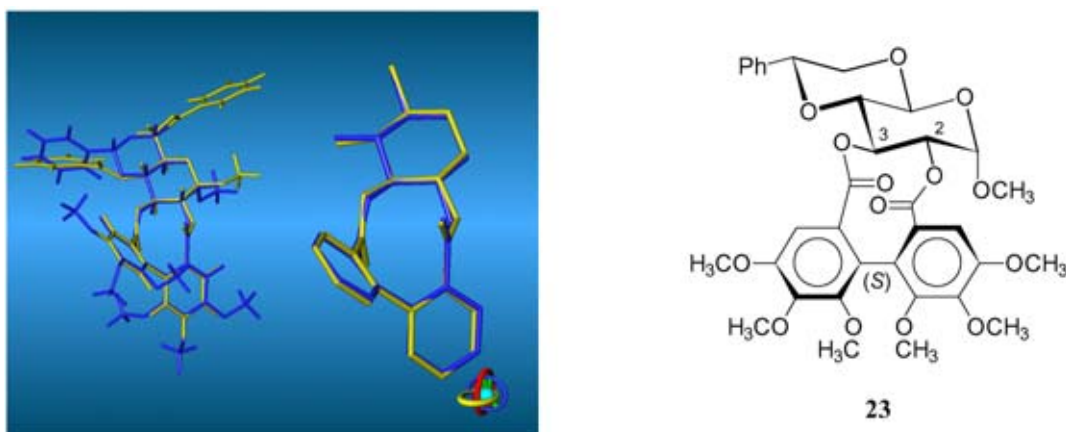


Figure 5. Superimposition of the computer-generated geometry of **14** (yellow model) with the solid-state conformation of methyl 4,6-*O*-benzylidene-2,3-*O*-(*S*)-hexamethoxydiphenoyl- $\alpha$ -D-glucopyranoside<sup>20</sup> (**13**, blue model). On the left, both structures are displayed entirely, whereas on the right only the common molecular fragments used for 3D-fitting are shown in enlarged form; the best-fit yielded a root mean square (RMS) deviation of  $\sigma = 0.08$  Å for these atomic positions

2.2. 4,6-*O*-Diphenoyl glucosides **16** and **17**

In the 4,6-*O*-DP bridged glucosides **16** and **17** (Fig. 6), the same basic conformational effects as in the 2,3-*O*-DP series (**14** and **15**) are operative: the rather stiff U-shape of both ester groups, the preferred antiparallel C=O-dipole–dipole alignment, the conjugation of carbonyl and phenyl ring  $\pi$ -systems, as well as the tilt between the phenyl rings. In addition, the glucose 6-CH<sub>2</sub>O-group is less flexible than it appears: of the three principal staggered conformations of the 6-C–O-linkage, the *trans-gauche* (*tg*)<sup>22</sup> form is commonly the least preferred one, as it is destabilized by 1,3-diaxial like repulsions between O-4 and O-6 (Scheme 1).<sup>22,23</sup> Although the *gauche-gauche* (*gg*) and *gauche-trans* (*gt*) forms<sup>22</sup> are usually equivalent in energy in non-cyclic glucose derivatives,<sup>23</sup> the latter becomes inaccessible in the 11-membered ring systems of the 4,6-*O*-DP glucosides **16** and **17** for sterical reasons. The *gg*-form<sup>22</sup> is realized in **16** ( $\omega \approx -80^\circ$ , cf. Table 1), still allowing almost relaxed U-shaped ester linkages ( $\theta_3$  and  $\theta_4 \approx -30^\circ$ ). As discussed above, a value of  $\theta_3 \approx -116^\circ$  indicates a highly bent 6-OCO-ester linkage in **17**, and its strain is only partly relaxed through sacrificing the 6-O *gg*-form to a less preferred *tg*-geometry ( $\omega \approx -170^\circ$  in **17**). However, superimposition of multiple low-energy conformers for both **16** and **17** (Fig. 7) indicates a lower flexibility of **16** as all ring fragments reside in a ‘relaxed’ state, whereas the strain in **17** (vide supra) allows for multiple conformations of the 6-C-OCO-fragments with different orientations of the ester carbonyl group. The data listed in Table 1 also indicates a less favorable alignment of the ester groups in **17** as compared to **16** (angles of  $\varphi \approx 120^\circ$  vs.  $150^\circ$  and tilts  $\tau \approx 130^\circ$  vs.  $170^\circ$  in **17** and **16**).

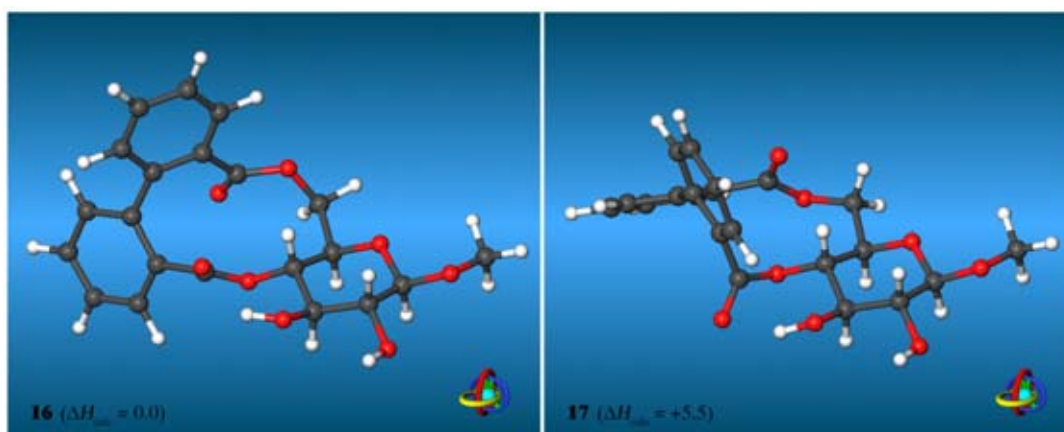
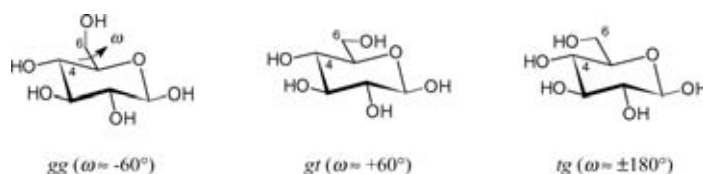


Figure 6. Ball-and-stick models of the global energy-minimum structures of the 4,6-*O*-(*S*)-DP **16** and (*R*)-DP **17** glucosides; relative energies are given in kJ/mol



Scheme 1.

2502

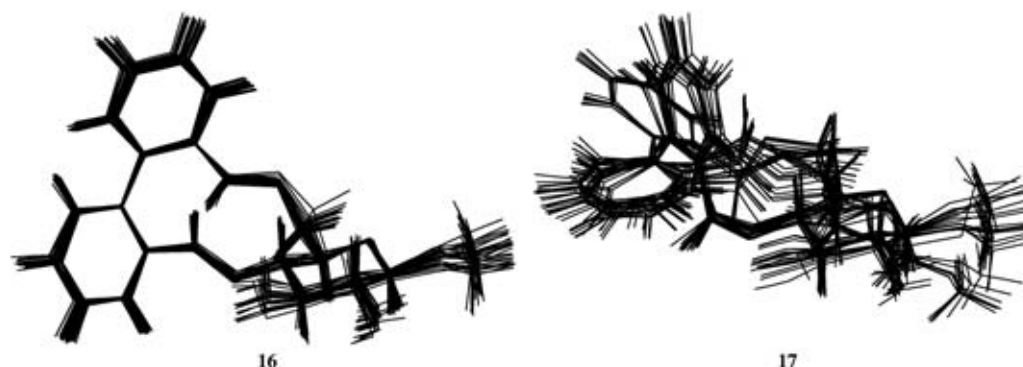
*S. Immel, K. Khanbabaee / Tetrahedron: Asymmetry 11 (2000) 2495–2507*

Figure 7. Superimposition of the 25 most stable geometries found within an energy range of approx. 0–10 kJ/mol above the global energy-minima for the atropdiastereomeric 4,6-*O*-DP glucoside model compounds **16** and **17**, respectively; the viewpoint relative to the glucopyranose ring is identical in both cases. The more stable (*S*)-DP compound **16** is remarkably rigid with rather stiff ring conformations. (*R*)-**17** displays some flexibility, and particularly the 6-CH<sub>2</sub>-OCO ester carbonyl group adopts different orientations with almost equal energies (cf. text)

In Fig. 8, the calculated geometry of **16** is compared with the corresponding (*S*)-binaphthalene conformation in the crystal structure of racemic **22**:<sup>24</sup> although the 11-membered ring in the latter compound includes a *C**sp*<sup>2</sup> carbonyl bridge head versus a 5-*C**sp*<sup>3</sup> carbon in *D*-glucose, the 3D-fit displays very similar ring conformations in both compounds. In total, the geometry parameters obtained are consistent with preferred 4,6-*O*-(*S*)-DP *D*-glucose type linkages over (*R*)-DP geometries, and thus agree well with the absence of natural ellagitannins of the latter type.

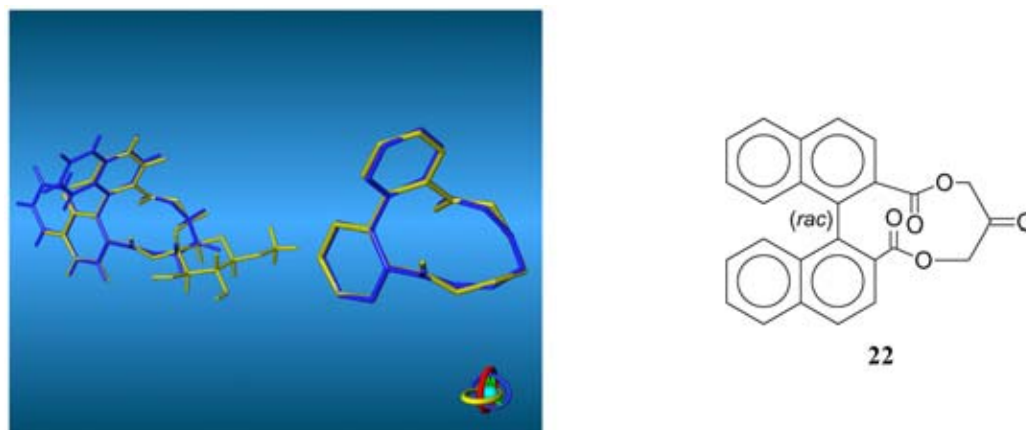


Figure 8. Superimposition of the 3D-structures of methyl 4,6-*O*-(*S*)-diphenyl- $\beta$ -*D*-glucoside (**16**) with the corresponding (*S*)-binaphthalene geometry extracted from the solid-state structure of racemic **22**:<sup>24</sup> the mode of viewing corresponds to Fig. 5. Despite the chemical differences of both compounds, the 11-membered rings display similar conformations with RMS deviations in the atomic positions of  $\sigma \approx 0.1$  Å only

It is noteworthy, that the atropstereochemical induction on the DP-units strongly depends on the type of linkage and the configuration of the carbohydrate template: comparison of the 4,6-*O*-(*S*)-DP and 4,6-*O*-(*R*)-DP *D*-galactopyranosides **23** and **24**<sup>25</sup> with their *D*-glucose analogs **16** and **17** reveals opposite effects on the chirality of the DP-residues. The (*R*)-configuration of **24** is



about 8.6 kJ/mol more stable than the corresponding (*S*)-geometry (cf. Table 1 and Fig. 9). Due to the axial configuration at C-4 in *D*-galactose, the conformational preference of the 6-CH<sub>2</sub>O-group is shifted from the *gg*- to the *tg*-form.<sup>22</sup>

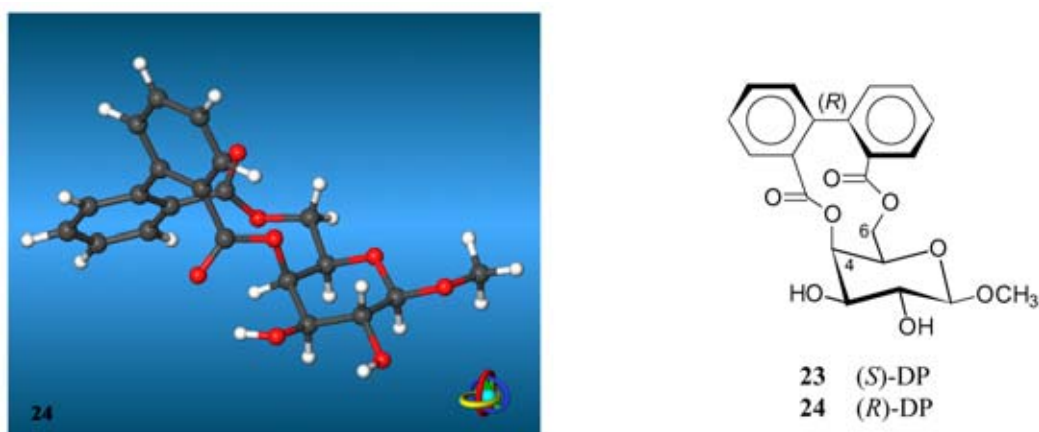


Figure 9. Global energy-minimum structure of 4,6-*O*-(*R*)-DP galactopyranoside **24** (left)

### 2.3. 3,6- and 2,4-*O*-Diphenoyl glucosides **18–21**

In both series of 3,6-*O*-DP (**18**, **19**) and 2,4-*O*-DP (**20**, **21**) bridged methyl β-*D*-glucosides, the glucose units are forced into <sup>1</sup>C<sub>4</sub> chair geometries to affect ring closure (cf. Cremer–Pople ring puckering parameters<sup>21</sup> in Table 1); a behavior that is well-documented in the chemistry of 3,6-anhydro glucose derivatives.<sup>26</sup> Thus, the linkage positions as well as all other ring substituents adopt axial orientations on the pyranose ring, and in both 3,6-*O*-DP and 2,4-*O*-DP glucosides the (*R*)-DP configuration **19** and **21** is energetically preferred over the (*S*)-DP analogs **18** and **20** (cf. Table 1, and Figs. 10 and 11).

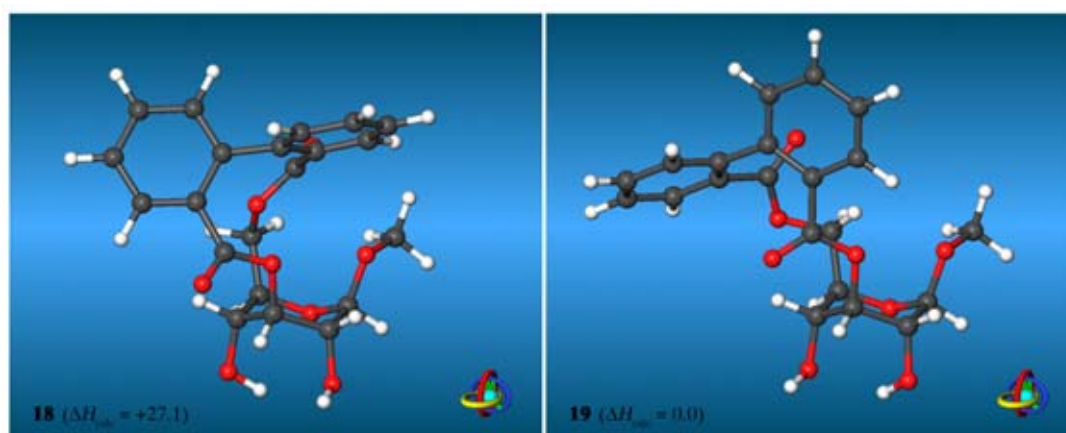


Figure 10. Global energy-minimum structures of the 3,6-*O*-(*S*)-DP **18** and (*R*)-DP **19** glucosides; relative energies are given in kJ/mol

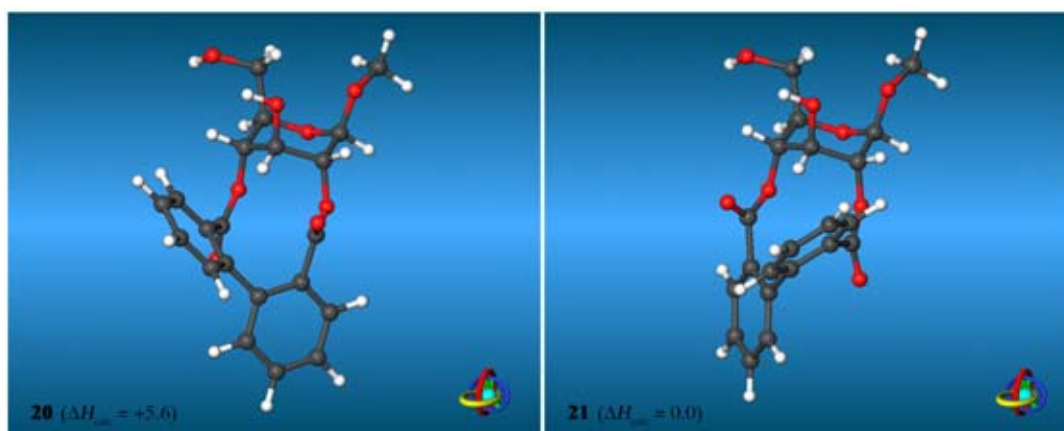


Figure 11. Global energy-minimum structures of the 2,4-*O*-(*S*)-DP **20** and (*R*)-DP **21** glucosides

As discussed above, it is the high tendency of the ester groups to maintain their characteristic U-shape, that transmits the chiral information of the carbohydrate backbone into the DP-residue, and thus induces their atropstereochemical configuration. Comparison of the calculated structure of **19** with the solid-state conformation of the natural ellagitannin Geraniin **11**<sup>19</sup> (Fig. 12) reveals very similar over all-shapes for both 3,6-*O*-(*R*)-DP ring systems, although the puckering of the pyranose ring is calculated to be smaller than found in the crystal structure of **11**.<sup>19</sup> However, the ring flattening effect observed in **19** is counterbalanced in **11** through an additional rigid linkage between the axial 2- and 4-OH groups of the D-glucoside core.

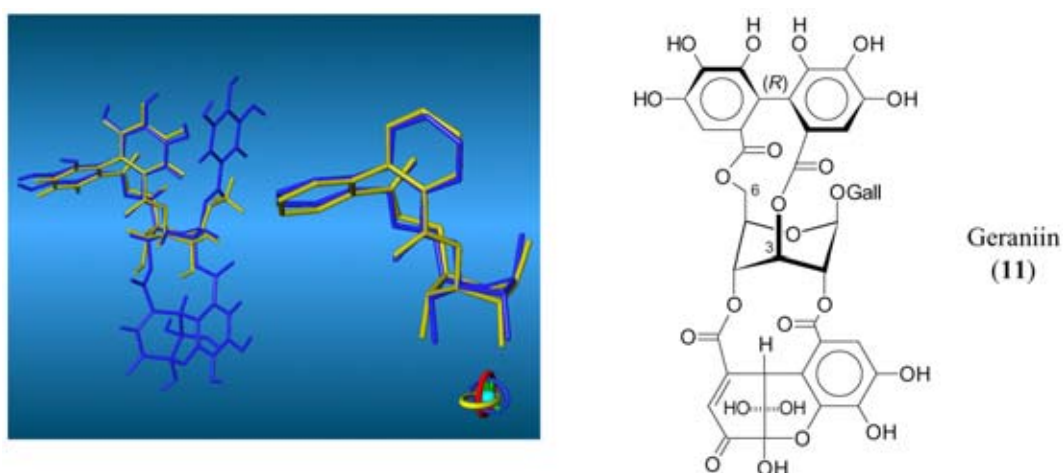


Figure 12. Superimposition of the energy-minimum structure **19** (yellow model) with the solid-state geometry of Geraniin **11**<sup>19</sup> (blue colors); the mode of viewing is analog to Figs. 5 and 8 (RMS deviation of  $\sigma=0.11$  Å for all equivalent atomic positions)

It is noteworthy, that in neither the 2,4-*O*-(*S*)- or (*R*)-DP glucosides **20** and **21** both ester groups are capable to maintain their typical U-shape simultaneously. The internal strain inherent to these compounds may be considered one reason why their ellagitannin analogs are not stable under physiological conditions and undergo very characteristic transformations into ring systems as realized in **11**<sup>2</sup> (Figs. 1 and 12; in the solid-state geometry of **11** the ester U-shape is realized in both the 2-OCO and 4-OCO linkages). However, the structure of Geraniin **11**, and the stereochemical course of this process indicates, that 2,4-*O*-(*R*)-HHDP units are the precursors rather than (*S*)-HHDP diastereomers.<sup>2</sup> The observation that these (*R*)-HHDP intermediates have to play an important role along the biochemical pathways of some ellagitannins correlates well with the observed stability of 2,4-*O*-(*R*)-DP glucosides over the corresponding (*S*)-DP geometries.

### 3. Conclusion

Without exception, the calculated relative thermodynamic stabilities of the atropdiastereomeric methyl 2,3-, 4,6-, 3,6-, and 2,4-*O*-DP- $\beta$ -D-glucosides **14–21** correlate with the configuration of the corresponding naturally occurring HHDP-bridged ellagitannins,<sup>2</sup> i.e. the 2,3- and 4,6-*O*-(*S*)-DP, as well as the 3,6- and 2,4-*O*-(*R*)-DP glucosides are more stable than their diastereomers. The molecular modeling data and the calculated energy differences are consistent with limited flexibility of bis-equatorial linked DP-residues in 2,3- and 4,6-positions of D-glucose (<sup>4</sup>C<sub>1</sub> pyranose conformation), the 10-membered ring in the 2,3-*O*-DP glucosides being less flexible than the 11-membered 4,6-*O*-DP macrocycle with one additional CH<sub>2</sub>-group. Even more rigid are the bis-axial linked 3,6-*O*- and 2,4-*O*-DP glucosides with <sup>1</sup>C<sub>4</sub> glucose *anti*-chair geometries, the latter bearing even so much internal strain that they immediately undergo ensuing biochemical transformations under physiological conditions (*vide supra*).<sup>2</sup> Comparison of the calculated structures with the few solid-state structures available for **11**, **13**, and **22** attests to the consistency of the methodology applied. The strait-jacket of the carbohydrate scaffold exerts a strong chiral induction onto the attached diphenoyl-residues in all types of linkages discussed within this study, the major effect in chirality transduction emerging from the tendency of the ester groups to maintain their characteristic U-shape. Indeed, preliminary results indicate that the atropchiral induction is significantly weakened or even inverted<sup>27</sup> when replacing the -COO-ester groups with -CH<sub>2</sub>-O-type linkages. As detailed for the non-natural methyl 4,6-*O*-DP galactosides **23** and **24**, the configuration of the DP-units is highly sensitive towards changes in the linkage type and/or geometry.

On the basis of the molecular geometries discussed here, not only molecular models for the various ellagitannins can be derived, but also the configuration of the HHDP-units found in the class of ellagitannins can be rationalized. Although biosynthesis of the ellagitannins proceeds via HHDP ring formation through oxidative coupling of galloyl residues, and thus the strain inherent to the transition states of ring closure is the decisive kinetic factor for the atropdiastereoselective formation of (*S*)- or (*R*)-HHDP ellagitannins, the transitions states may somewhat 'resemble' the final ellagitannin products. For this reason, the obvious build-up of torsional strain in one of the corresponding diastereomers each is apt to explain the very uniform patterns of HHDP-configurations found in the natural ellagitannins.

Oxidation of the ellagitannins at C-1 ( $\rightarrow$  gluconolactons) and subsequent strain-induced pyranose ring opening<sup>10</sup> leads to open-chain tannins such as the Lagerstannin A, B, and C.<sup>28</sup> We hope to report on their geometries and conformational preferences in the near future.

## 4. Experimental

### 4.1. Crystal structures, fitting, and molecular graphics

The solid-state structures of Geraniin **11**,<sup>19</sup> **13**,<sup>20</sup> and **22**<sup>24</sup> were extracted from the Cambridge Crystallographic Database.<sup>18</sup> Hydrogen atoms not included in the structure determinations or disordered positions were positioned geometrically. 3D-fitting of molecular geometries was carried out by rigid-body translation and rotation, considering all equivalent non-hydrogen atoms with equal weights. All molecular graphics were generated using the MolArch<sup>+</sup> program.<sup>29</sup>

### 4.2. Molecular dynamics (MD) and molecular mechanics (MM)

All MD and MM calculations were carried out using the PIMM91 force-field<sup>30</sup> without the explicit incorporation of solvent molecules. All starting geometries of compounds **14–21** were generated using the MolArch<sup>+</sup> program,<sup>29</sup> different starting geometries for **16** and **17** were used to ensure the self-consistency of the search procedure for the global energy-minimum structures. For each compound, 500 ps MD trajectories were generated (time step  $\Delta t = 0.5$  fs,  $T = 300$  K), and molecular configurations were saved every 200 steps. Monitoring the glucopyranose geometries, as well as torsion angles along the DP-ring systems was used to ensure comprehensive coverage of the conformational space by the MD runs. For each compound **14–21**, a total of 5000 MD snapshot conformations were subjected to full MM energy minimization, and the global energy-minimum conformations found in each case were used in this report, and all geometry parameters (cf. Fig. 2) listed in Table 1 were calculated from this data set.<sup>29</sup> It is noteworthy, that the global energy-minimum structures were found multiple times in all cases, and that most of the low energy conformers within a range of 0–5 kJ/mol cluster into the same conformational family as the most stable geometry (for example, see Fig. 7).

## References

1. Part 28 of the series Molecular Modelling of Saccharides. For Part 27, see: Immel, S.; Nakagawa, T.; Lindner, H.-J.; Lichtenthaler, F. W. *Chem. Eur. J.* **2000**, *6*, in press.
2. For a review, see: Quideau, S.; Feldmann, K. S. *Chem. Rev.* **1996**, *96*, 475–503.
3. Nonaka, G.-I.; Ishimatsu, M.; Ageta, M.; Nishioka, I. *Chem. Pharm. Bull.* **1989**, *37*, 50–53.
4. Tanaka, T.; Kirahara, S.; Nonaka, G.-I.; Nishioka, I. *Chem. Pharm. Bull.* **1993**, *41*, 1708–1716.
5. Feldmann, K. S.; Smith, R. S. *J. Org. Chem.* **1996**, *61*, 2606–2612.
6. Khanbabaee, K.; Lötzerich, K. *J. Org. Chem.* **1998**, *63*, 8723–8728.
7. Khanbabaee, K.; Lötzerich, K. *Liebigs Ann./Recueil* **1997**, 1571–1575.
8. Khanbabaee, K.; Lötzerich, K.; Borges, M.; Großer, M. *J. Prakt. Chem.* **1999**, *341*, 159–166.
9. Khanbabaee, K.; Schulz, C.; Lötzerich, K. *Tetrahedron Lett.* **1997**, *38*, 1367–1368.
10. Khanbabaee, K.; Lötzerich, K. *Eur. J. Org. Chem.* **1999**, 3079–3083.
11. (a) Schmidt, O. T.; Schmidt, D. M.; Herok, J. *Liebigs Ann. Chem.* **1954**, *587*, 67–74. (b) Schmidt, O. T.; Blinn, F.; Lademann, R. *Liebigs Ann. Chem.* **1952**, *576*, 75–84. (c) Schmidt, O. T.; Schmidt, D. M. *Liebigs Ann. Chem.* **1952**, *578*, 31–33.
12. Haddock, E. A.; Gupta, R. K.; Haslam, E. *J. Chem. Soc., Perkin Trans. 1* **1982**, 2535–2545.
13. Okuda, T.; Yoshida, T.; Hatano, T. *J. Chem. Soc., Perkin Trans. 1* **1982**, 9–14.
14. Tanaka, T.; Nonaka, G.-I.; Nishioka, I.; Miyahara, K.; Kawasaki, T. *J. Chem. Soc., Perkin Trans. 1* **1986**, 369–376.
15. Gupta, R. K.; Al-Shafi, S. M. K.; Layden, K.; Haslam, E. *J. Chem. Soc., Perkin Trans. 1* **1982**, 2525–2534.

16. Haslam, E. *Prog. Chem. Org. Nat. Prod.* **1982**, *41*, 1–46.
17. The proposed models for the transition states of the galloyl coupling reaction of 4,6-di-*O*-galloyl glucose ( $\rightarrow$ 4,6-*O*-HHDP ellagitannins) correlate the preferred formation of (*S*)-HHDP entities with conformational strain energy in the intermediates leading to the (*R*)-HHDP ellagitannins.<sup>2</sup> However, for both transition states, the *tg*-forms<sup>22</sup> of the glucose 6-CH<sub>2</sub>O-galloyl residues were assumed. Although these rotamers frequently emerge from force-field calculations as the most stable ones, the *tg*-form is in fact the least populated state for D-glucose and its derivatives,<sup>22,23</sup> and does not play any significant role in glucose chemistry. The postulated transition states for the formation of 2,3-*O*-HHDP ellagitannins are almost equal in energy with very similar interatomic distances between the decisive galloyl carbon atoms, and strain is built up only in the final products.<sup>2</sup> To the best of our knowledge, no models for the formation of 3,6-*O*- or 2,4-*O*-HHDP ellagitannins have been put forth on an atomic level. The Monte-Carlo (MC) simulations described in Ref. 2 also did not allow to carry out a comprehensive geometry analysis of the complex fused ring systems of the ellagitannins.
18. Allen, F. H.; Kennard, O. *Chem. Des. Automat. News* **1993**, *8*, 1, 31–37; Cambridge Crystallographic Data File (Oct. 1999), Version 5.18. Refcodes: SAQZUF<sup>19</sup> and TASQOT.<sup>20</sup>
19. Luger, P.; Weber, M.; Kashino, S.; Amakura, Y.; Yoshida, T.; Okuda, T.; Beurskens, G.; Dauter, Z. *Acta Crystallogr., Sect. B* **1998**, *54*, 687–694.
20. Itoh, T.; Chika, J.; Shirakami, S.; Ito, H.; Yoshida, T.; Kubo, Y.; Uenishi, J. *J. Org. Chem.* **1996**, *61*, 3700–3705; erroneously the mirror image geometry of **13** is filed in the CCDF.
21. (a) Cremer, D. A.; Pople, J. A. *J. Am. Chem. Soc.* **1975**, *97*, 1354–1358. (b) Jeffrey, G. A.; Taylor, R. *Carbohydr. Res.* **1980**, *81*, 182–183.
22. In carbohydrate nomenclature, the three staggered conformations of the glucopyranose 6-CH<sub>2</sub>OH groups are denoted *gauche-gauche* (*gg*), *gauche-trans* (*gt*), and *trans-gauche* (*tg*). The first letter refers to the position of O-6 relative to O-5, the second relative to C-4; the torsion angle  $\omega$  is defined through the atoms O<sub>5</sub>–C<sub>5</sub>–C<sub>6</sub>–O<sub>6</sub>. For glucose, the *gg*- and *gt*-rotamers are equally preferred over *tg*, which is destabilized by 1,3-diaxial like interactions between O-6 and O-4.<sup>23</sup> For the C-4 epimer galactose, the conformers are populated in the order *gt*  $\approx$  *tg*  $>$  *gg* (Scheme 1).
23. (a) Jeffrey, G. A.; Saenger, W. *Hydrogen Bonding in Biological Structures*; Springer-Verlag: Berlin/New York, 1991. (b) Kroon-Batenburg, L. M. J.; Kroon, J. *Biopolymers* **1990**, *29*, 1243–1248. (c) Bock, K.; Duus, J. Ø. *J. Carbohydr. Chem.* **1994**, *13*, 513–543.
24. Yang, D.; Yip, Y.-C.; Tang, M.-W.; Wong, M.-K.; Zheng, J.-H.; Cheung, K.-K. *J. Am. Chem. Soc.* **1996**, *118*, 491–492.
25. To the best of our knowledge, D-galactose or D-mannose derived ellagitannins are not known to occur in nature; but we envisage their chemical synthesis as an interesting target.
26. The six examples of 3,6-anhydro glycosides contained in the CCDF<sup>18</sup> invariably display almost undistorted <sup>1</sup>C<sub>4</sub> *anti*-chair geometries of their pyranose portions.
27. Preliminary results indicate that for the 2,2'-bismethylenbiphenyl analogs of methyl 4,6-*O*-diphenoyl- $\beta$ -D-glucoside (-COO-linkages $\rightarrow$ -CH<sub>2</sub>O-) the (*R*)-atropisomers are preferred over the (*S*)-forms.
28. Tanaka, T.; Tong, H.-H.; Xu, Y.-M.; Ishimaru, K.; Nonaka, G.-I.; Nishioka, I. *Chem. Pharm. Bull.* **1992**, *40*, 2975–2980.
29. Immel, S. *MolArch<sup>+</sup>: Molecular Architecture Modeling Program*; Darmstadt University of Technology, 2000.
30. Lindner, H. J.; Kroeker, M. *PIMM91-Closed Shell PI-SCF-LCAO-MO-Molecular Mechanics Program*; Darmstadt University of Technology, 1997. Smith, A. E.; Lindner, H. J. *J. Comput.-Aided Mol. Des.* **1991**, *5*, 235–262.



## Metabolism of Sucrose and Its Five Linkage-isomeric $\alpha$ -D-Glucosyl-D-fructoses by *Klebsiella pneumoniae*

PARTICIPATION AND PROPERTIES OF SUCROSE-6-PHOSPHATE HYDROLASE AND PHOSPHO- $\alpha$ -GLUCOSIDASE\*

Received for publication, July 11, 2001, and in revised form, July 24, 2001  
Published, JBC Papers in Press, July 25, 2001, DOI 10.1074/jbc.M106504200

John Thompson<sup>‡§</sup>, Stanley A. Robrish<sup>‡</sup>, Stefan Immel<sup>¶</sup>, Frieder W. Lichtenthaler<sup>¶</sup>, Barry G. Hall<sup>||</sup>, and Andreas Pikiš<sup>\*\*‡‡</sup>

From the <sup>‡</sup>Microbial Biochemistry and Genetics Unit, Oral Infection and Immunity Branch, NIDCR, National Institutes of Health, Bethesda, Maryland 20892, the <sup>¶</sup>Institut für Organische Chemie, Technische Universität Darmstadt, D-64287 Darmstadt, Germany, the <sup>||</sup>Biology Department, University of Rochester, Rochester, New York 14627-0211, the <sup>\*\*</sup>Vaccine and Therapeutic Development Section, Oral and Infection and Immunity Branch, NIDCR, National Institutes of Health, Bethesda, Maryland 20892, and the <sup>‡‡</sup>Department of Infectious Diseases, Children's National Medical Center, Washington, D. C. 20010-2970

*Klebsiella pneumoniae* is presently unique among bacterial species in its ability to metabolize not only sucrose but also its five linkage-isomeric  $\alpha$ -D-glucosyl-D-fructoses: trehalulose, turanose, maltulose, leucrose, and palatinose. Growth on the isomeric compounds induced a protein of molecular mass  $\sim 50$  kDa that was not present in sucrose-grown cells and which we have identified as an NAD<sup>+</sup> and metal ion-dependent 6-phospho- $\alpha$ -glucosidase (AglB). The *aglB* gene has been cloned and sequenced, and AglB ( $M_r = 49,256$ ) has been purified from a high expression system using the chromogenic *p*-nitrophenyl  $\alpha$ -glucopyranoside 6-phosphate as substrate. Phospho- $\alpha$ -glucosidase catalyzed the hydrolysis of a wide variety of 6-phospho- $\alpha$ -glucosides including maltose-6'-phosphate, maltitol-6-phosphate, isomaltose-6'-phosphate, and all five 6'-phosphorylated isomers of sucrose ( $K_m \sim 1$ –5 mM) yet did not hydrolyze sucrose-6-phosphate. By contrast, purified sucrose-6-phosphate hydrolase ( $M_r \sim 53,000$ ) hydrolyzed only sucrose-6-phosphate ( $K_m \sim 80 \mu\text{M}$ ). Differences in molecular shape and lipophilicity potential between sucrose and its isomers may be important determinants for substrate discrimination by the two phosphoglucosyl hydrolases. Phospho- $\alpha$ -glucosidase and sucrose-6-phosphate hydrolase exhibit no significant homology, and by sequence-based alignment, the two enzymes are assigned to Families 4 and 32, respectively, of the glycosyl hydrolase superfamily. The phospho- $\alpha$ -glucosidase gene (*aglB*) lies adjacent to a second gene (*agIA*), which encodes an EII(CB) component of the phosphoenolpyruvate-dependent sugar:phosphotransferase system. We suggest that the products of the two genes facilitate the phosphorylative translocation and subsequent hydrolysis of the five  $\alpha$ -D-glucosyl-D-fructoses by *K. pneumoniae*.

ent sugar:phosphotransferase system (PEP:PTS)<sup>1</sup> by Roseman and colleagues (1) is a landmark in our understanding of carbohydrate dissimilation by microorganisms. Since the initial description of this multi-component system in *Escherichia coli*, the PEP:PTS has been established as the primary route for the transport and concomitant phosphorylation of a wide variety of sugars by bacteria from both Gram-negative (2, 3) and Gram-positive genera (4, 5). In many species, including *Bacillus subtilis*, *Lactococcus lactis*, *Streptococcus mutans*, *Escherichia coli*, and *Klebsiella pneumoniae* (6, 7), sucrose is accumulated via the PTS simultaneously with phosphorylation at C-6 of the glucopyranosyl moiety of the disaccharide. Intracellularly, sucrose-6-phosphate (sucrose-6-P) is hydrolyzed by sucrose-6-phosphate hydrolase (8, 9) to glucose-6-phosphate and fructose, which are then fermented via the glycolytic pathway to yield primarily lactic acid.

The structures of sucrose, its five isomeric  $\alpha$ -D-glucosyl-D-fructoses (trivially designated trehalulose, turanose, maltulose, leucrose, and palatinose), and some related  $\alpha$ -linked disaccharides are depicted in Fig. 1. In contrast to the many reports of sucrose fermentation, there are few references to the utilization of the isomeric glucosyl-fructoses by microorganisms (12). This fact is of particular relevance to oral biology in light of the associative role(s) of sucrose and streptococcal species in the etiology of dental caries (13, 14). Sucrose is the precursor for glucan synthesis that facilitates attachment of *S. mutans* to the tooth surface; subsequent fermentation of the disaccharide to lactic acid initiates the demineralization of tooth enamel. In this context, isomers of sucrose attract attention as potential substitutes for dietary sucrose (15–17) because they are about half as sweet as sucrose, are not metabolized (noncariogenic), and, in the case of palatinose and leucrose, are produced on an industrial scale (18, 19). From the limited information available, one might reasonably conclude that the isomers cannot be translocated by the membrane-localized transporter EII(CB) of the sucrose-PTS or that intracellular sucrose-6-P hydrolase is unable to hydrolyze the phos-

The discovery in 1964 of the phosphoenolpyruvate-depend-

\* The costs of publication of this article were defrayed in part by the payment of page charges. This article must therefore be hereby marked "advertisement" in accordance with 18 U.S.C. Section 1734 solely to indicate this fact.

The nucleotide sequence(s) reported in this paper has been submitted to the GenBank™/EBI Data Bank with accession number(s) AF337811.

§ To whom correspondence and reprint requests should be addressed: NIDCR, National Institutes of Health, Bldg. 30, Rm. 528, Convent Dr. MSC-4350, Bethesda, MD 20892. Tel.: 301-496-4083; Fax: 301-402-0396; E-mail: jthompson@dir.nidcr.nih.gov.

<sup>1</sup> The abbreviations used are: PEP:PTS, phosphoenolpyruvate-dependent sugar:phosphotransferase system; pNP $\alpha$ Glc, *p*-nitrophenyl  $\alpha$ -D-glucopyranoside; pNP $\alpha$ Glc6P, *p*-nitrophenyl  $\alpha$ -D-glucopyranoside 6-phosphate; MES, 2(*N*-morpholino)ethanesulfonic acid; PAGE, polyacrylamide gel electrophoresis; PCR, polymerase chain reaction; IPTG, isopropyl- $\beta$ -D-thiogalactopyranoside; MD, molecular dynamics; MLP, molecular lipophilicity pattern.

phorylated PTS products.

Our interest in these issues stemmed from a survey of disaccharide utilization by *K. pneumoniae* that revealed excellent (and unexpected) growth of this organism on all five isomers of sucrose (12). Furthermore, although organisms grown previously on a particular isomer readily metabolized sucrose and all other isomers, cells of *K. pneumoniae* grown previously on sucrose fermented only sucrose (12). Comparative analyses of proteins in various cell extracts (by two-dimensional PAGE) revealed high level expression of a specific polypeptide (molecular mass ~ 50 kDa) during growth on the isomers, but this protein was not induced by growth of the organism on sucrose. These observations provided the first indication that for *K. pneumoniae*, the initial steps in metabolism of sucrose, and those of its analogs, might be separable and distinct. In the present study we have identified two adjacent genes (*aglA* and *aglB*) in *K. pneumoniae* that encode a membrane-localized transport protein of the PTS (EIICB, or *AglA*) and a nucleotide (NAD<sup>+</sup>) plus metal-dependent phospho- $\alpha$ -glucosidase (*AglB*), respectively. Together, these proteins facilitate the phosphorylative translocation and subsequent hydrolysis of the five  $\alpha$ -linked isomers of sucrose.

To facilitate the comparison of the properties of sucrose-6-P hydrolase with those of *AglB*, the genes encoding the two proteins (*scrB* (7) and *aglB*, respectively) have been cloned, and both enzymes have been purified from high expression systems. Recently, we prepared trehalulose-6'-P, turanose-6'-P, maltulose-6'-P, leucrose-6'-P, and palatinose-6'-P in substrate quantity (12), and the availability of these novel compounds permitted the determination of the substrate specificities of highly purified *AglB* and sucrose-6-P hydrolase. Remarkably, sucrose-6-P hydrolase, which by sequence-based alignment is assigned to Family 32 of glycosyl hydrolases, hydrolyzed only sucrose-6-P. In contrast *AglB*, which belongs to Family 4, catalyzed the cleavage of the five isomeric 6'-phosphoglucosyl-fructoses. In this paper, a comparative assessment of conformational, overall shape and polarity features of sucrose-6-P and its isomeric disaccharide-6'-phosphates is given, providing insight into the molecular basis for substrate discrimination by the two phosphoglucosyl hydrolases.

#### EXPERIMENTAL PROCEDURES

**Materials**—Carbohydrates were obtained from the following sources: trehalulose from Südzucker, Mannheim/Ochsenfurt, Germany; maltulose and isomaltose from TCI America; leucrose from Fluka; and palatinose from Wako Chemicals. Sucrose, turanose, and other high purity sugars were purchased from Pfanstiehl Laboratories. Maltitol, NADP<sup>+</sup>, trehalose-6-P, *p*-nitrophenyl  $\alpha$ -D-glucopyranoside (pNP $\alpha$ Glc), and PEP were obtained from Sigma. Phosphorylated derivatives trehalulose-6'-P, sucrose-6-P; turanose-6'-P, maltulose-6'-P, leucrose-6'-P; palatinose-6'-P, maltose-6'-P, isomaltose-6'-P, and maltitol-6-P were prepared in this laboratory by PEP:PTS activity in permeabilized (palatinose-grown) cells of *K. pneumoniae* (12). The chromogenic substrate pNP $\alpha$ Glc6P was prepared by selective phosphorylation of pNP $\alpha$ Glc with phosphorus oxychloride in trimethyl phosphate containing small proportions of water (20). Glucose-6-phosphate dehydrogenase/hexokinase (EC 1.1.1.49; EC 2.7.1.1), and phosphoglucose isomerase (EC 5.3.1.9) were from Roche Molecular Biochemicals. Ultrogel AcA-44 and TrisAcryl M-DEAE were from Sepharac.

**Growth of *K. pneumoniae* ATCC 23357**—The organism was grown at 37 °C in 1-liter bottles, each containing 800 ml of the medium defined by Sapico *et al.* (21) supplemented with 0.4% (w/v) of the appropriate sugar. After growth to stationary phase, the cells were harvested by centrifugation (13,000  $\times$  g for 10 min at 5 °C) and washed twice in 25 mM Tris-HCl buffer (pH 7.5) containing 1 mM MgCl<sub>2</sub>. The yield was ~2 g wet weight of cells/liter.

**Electrophoresis Procedures**—SDS-PAGE was carried out in the Novex XCell Mini-Cell system (Invitrogen). Novex NuPage (4–12%) Bis-Tris gels and MES-SDS running buffer (pH 7.3) were used together with Novex Mark 12<sup>TM</sup> protein standards, and proteins were stained with Coomassie Brilliant Blue R-250. For Western blots, proteins were

transferred to nitrocellulose membranes using NuPage transfer buffer and SeeBlue<sup>TM</sup> prestained standards. The Amersham Pharmacia Biotech Multiphor flat-bed electrophoresis unit, precast Ampholine PAG plates (pH range, 3.5–9.5) and broad range standards were used for electrofocusing experiments.

**Analytical Methods**—During purification, the activity of *AglB* in column fractions was detected by hydrolysis of the chromogenic substrate, pNP $\alpha$ Glc6P. The specific activity of the enzyme was determined in a discontinuous assay that contained in 2-ml: 0.1 M Tris-HCl buffer (pH 7.5), 1 mM MnCl<sub>2</sub>, 0.5 mM NAD<sup>+</sup>, and 1 mM pNP $\alpha$ Glc6P. After the addition of the enzyme preparation, samples of 0.25 ml were removed at 20-s intervals (over a 2-min period) and immediately injected into 0.75 ml of 0.5 M Na<sub>2</sub>CO<sub>3</sub>. The A<sub>400 nm</sub> of the yellow solution was measured, and rates of pNP formation were calculated by assuming a molar extinction for the *p*-nitrophenoxide anion  $\epsilon$  = 18,300 M<sup>-1</sup> cm<sup>-1</sup>. One unit of *AglB* activity is the amount of enzyme that catalyzes the formation of 1  $\mu$ mol of pNP min<sup>-1</sup>. Two-dimensional polyacrylamide gel electrophoresis (PAGE) and protein microsequencing were carried out by Kendrick Laboratories, Inc. and by the Protein Chemistry Core Facility, Columbia University, NY, respectively. The mass of *AglB* was determined by electrospray in an HP1100 mass spectrometer, and the sequence of N-terminal amino acids was determined with an ABI 477A protein sequencer (Applied Biosystems Inc.) with an on-line ABI 120A phenylthiohydantoin analyzer. Protein concentrations were determined by the BCA protein assay kit (Pierce). The procedure for immunodetection of *AglB* with polyclonal antibody to MalH from *F. mortiferum* has been described previously (20).

**Cloning and Characterization of a Region Encoding the *aglA* and *aglB* Genes of *K. pneumoniae* ATCC 23357**—Initially, using the unfinished genome sequence of *K. pneumoniae* (Washington University Genome Sequencing Center, St. Louis, MO) and our own sequence data later, five primer sets were designed to amplify, clone, and characterize the DNA fragment encoding genes *aglA* and *aglB* of *K. pneumoniae* ATCC 23357. The five primer sets were constructed as follows: KP1F-KP1R, 5'-GCCAGT<sup>TTTTT</sup>TCTCTCTGGTAGC-3' and 5'-GCATAT-TACGAAAGACGGYCCAGC-3'; KP2F-KP2R, 5'-CCCTACGAGTTGT-TACATGAGGATTTTC-3' and 5'-CCCCAATGACCACAAACG-3'; KP3F-KP3R, 5'-GGCTGGACCGTCTTTCGTAATATG-3' and 5'-TTCG-AGTTACCGTGCAGGGCAAAG-3'; KP4F-KP4R, 5'-CGCTTGGGTGT-GGGTTACAC-3' and 5'-GCCGTGGTTTACCTCGTGC-3'; KP5F-KP5R, 5'-CCCTGATCCTGCGTCTGAACC-3' and 5'-GTTAGCCAGC-GAA AAGCGG-3'.

The components of the amplification mixtures (100  $\mu$ l) were: 5 units of *Pfu* DNA polymerase (Stratagene, La Jolla, CA), 1 $\times$  buffer provided by the manufacturer, 20 mM each of the four dNTPs, 100 ng of DNA, and 250 ng of each primer. Amplifications were carried out in a thermal cycler (PerkinElmer 9600, PerkinElmer Life Sciences). After an initial 2-min denaturation at 95 °C, the mixtures were subjected to 30 cycles of amplification. Each cycle consisted of 1 min denaturation at 95 °C, 1 min annealing at 58 °C, and extension at 72 °C for 2 min/kilobase of insert. These were followed by a 10-min runoff at 72 °C. The PCR products were purified (QIAquick PCR purification kit, Qiagen) and ligated into pCR-Blunt vector (Invitrogen, Carlsbad, CA). After transformation into *E. coli* TOP 10 competent cells, colonies were selected on LB agar plates containing 50  $\mu$ g/ml kanamycin.

**Cloning of the *K. pneumoniae* ATCC 23357 *aglB* Gene in *E. coli***—For amplification of the gene *aglB*, two primers were synthesized from the nucleotide sequence shown in Fig. 4: forward primer KPBF, 5'-CCCAC-CATGGGAGGCAGTATCATG-3' (the *aglB* sequence, base pairs 2001–2015, is in bold face, and the *NcoI* site is underlined); reverse primer KPBR, 5'-CCCAGAATTC<sup>TTAATGCAGCTCAGG</sup>-3' (the sequence complementary to the downstream region of *aglB*, base pairs 3321–3335, is in bold face, and the *EcoRI* site is underlined). PCR amplification was performed using high fidelity *Pfu* DNA polymerase. The amplified 1.3-kilobase DNA fragment was digested with restriction endonucleases (*NcoI* and *EcoRI*), electrophoresed through 1% agarose gel, and purified (QIAquick gel extraction kit). The fragment was ligated into the similarly digested (*NcoI-EcoRI*) high expression vector pSE380 (Invitrogen) to form pAP-16. (In this construct, the *aglB* gene is under control of the powerful *trc* hybrid promoter, which is also regulated by the *lacO* operator and the product of the *lacI<sup>q</sup>* gene. Because the plasmid also carries *lacI*, expression of *aglB* is strongly repressed in the absence but is fully induced in the presence of isopropyl- $\beta$ -D-thiogalactopyranoside (IPTG)). Plasmid pAP-16 was transformed into competent cells of *E. coli* TOP 10 (Invitrogen), and transformants were selected on LB agar containing 150  $\mu$ g/ml ampicillin.

**DNA Sequence Analysis**—DNA fragments cloned in pCR-Blunt vector were sequenced by the dideoxynucleotide chain termination method



## Phosphoglucosyl Hydrolases from *K. pneumoniae*

37417

using the Sequenase 7-deaza-dGTP sequencing kit (U. S. Biochemicals, Cleveland, OH), and [ $\alpha$ - $^{35}$ S]deoxyadenosine triphosphate was used for labeling. For all clones, both strands of DNA inserts were sequenced. The MacVector sequence analysis package (Version 7.0, Genetics Computer Group, Madison, WI) was used to compile, edit, and analyze the results.

**Growth of Cells and Preparation of Extract Containing AglB**—*E. coli* TOP 10 (pAP-16) was grown at 37 °C in LB medium containing ampicillin (150  $\mu$ g/ml) to a density  $A_{600\text{ nm}} \sim 0.4$  units. IPTG (0.5 mM) was then added to the culture, and growth was continued for 3 h. The culture was harvested by centrifugation (13,000  $\times g$  for 10 min at 5 °C), and the cells ( $\sim 2.1$  g wet weight/liter) were washed by resuspension and centrifugation from 25 mM Tris-HCl buffer (pH 7.5) containing 1 mM MnCl<sub>2</sub> and 0.1 mM NAD<sup>+</sup> (designated TMN buffer). Washed cells ( $\sim 38$  g) were resuspended in 80 ml of TMN buffer, and the organisms were disrupted (at 0 °C) by 2  $\times$  1.5-min periods of sonic oscillation in a Branson instrument (model 350) operating at  $\sim 75\%$  of maximum power. The extract was clarified by centrifugation (180,000  $\times g$  for 2 h at 5 °C), and the high-speed supernatant was transferred to sacs and dialyzed overnight against 4 liters of TMN buffer.

### Purification of AglB

The enzyme was purified by low pressure chromatography, and all procedures were performed in a cold room.

**Step 1: TrisAcryl M-DEAE (Anion Exchange) Chromatography**—Dialyzed high-speed supernatant ( $\sim 85$  ml) was transferred at a flow rate of 0.8 ml/min to a column of TrisAcryl M-DEAE (2.6  $\times$  14 cm) previously equilibrated with TMN buffer. Nonadsorbed material was removed by washing with TMN buffer, and AglB was eluted with 800 ml of a linear, increasing concentration gradient of NaCl (0–0.3 M) in TMN buffer. Fractions (8 ml) were collected, and AglB activity was revealed by the intense yellow color formed upon addition of fraction samples (4  $\mu$ l) to microtiter wells containing 100  $\mu$ l of pNP $\alpha$ Glc6P assay solution. Fractions with the highest activity (22–26) were pooled and concentrated to 19 ml by pressure filtration (Amicon PM-10 membrane, 40 psi). Ammonium sulfate crystals (1.9 g) were added slowly with stirring to a concentration of 0.75 M.

**Step 2: Phenyl-Sepharose CL-4B (Hydrophobic) Chromatography**—The  $\sim 20$  ml solution from step 1 was transferred (flow rate 0.5 ml/min) to a column of phenyl-Sepharose CL-4B (2.6  $\times$  14 cm) equilibrated with TMN buffer containing 0.75 M (NH<sub>4</sub>)<sub>2</sub>SO<sub>4</sub>. Nonadsorbed protein(s) were eluted, and then 500 ml of a decreasing, linear gradient of (NH<sub>4</sub>)<sub>2</sub>SO<sub>4</sub> (0.3–0 M) in TMN buffer was passed through the column. Fractions of 5 ml were collected, and AglB was recovered primarily in fractions 45–60. These fractions were pooled and concentrated by Amicon filtration to  $\sim 9$  ml.

**Step 3: Ultrogel AcA-44 (Molecular Sieve) Chromatography**—Approximately 3 ml of preparation from step 2 was applied at a flow rate of 0.15 ml/min to a column of Ultrogel AcA-44 (1.6  $\times$  94 cm) previously equilibrated with TMN buffer containing 0.1 M NaCl. Fractions of 2.1 ml were collected, and those containing maximum AglB activity (50–53) were pooled. (This procedure was repeated with the remaining 2  $\times$   $\sim 3$ -ml portions of concentrate from phenyl-Sepharose chromatography). AcA-44 chromatography yielded a total of  $\sim 24$  ml of highly purified AglB (3 mg/ml; specific activity 4.15 units/mg).

**Kinetic Analysis and Substrate Specificity of AglB**—A continuous spectrophotometric assay was used for substrate specificity studies and determination of kinetic parameters for AglB. This indirect glucose-6-P dehydrogenase/NADP<sup>+</sup>-coupled assay monitors formation of glucose-6-P during the AglB-catalyzed hydrolysis of substrates. The standard 1-ml assay contained: 0.1 M HEPES buffer (pH 7.5), 1 mM MgCl<sub>2</sub>, 1 mM MnCl<sub>2</sub>, 1 mM NAD<sup>+</sup>, 1 mM NADP<sup>+</sup>, 1 mM substrate (6'-P isomer of sucrose, or phospho- $\alpha$ -glucoside), and 2 units of glucose-6-P dehydrogenase/hexokinase. Reactions were initiated by addition of 15  $\mu$ l (45  $\mu$ g) of AglB preparation, and the increase in  $A_{340\text{ nm}}$  was recorded in a Beckman DU 640 spectrophotometer. Initial rates were determined using the kinetics program of the instrument, and a molar extinction coefficient  $\epsilon = 6,220\text{ M}^{-1}\text{ cm}^{-1}$  was assumed for calculation of NADPH formed (equivalent to glucose-6-P liberated). In kinetic analyses the concentration range of substrate was usually 0.2–4 mM, and kinetic parameters were determined from Hofstee plots with an Enzyme Kinetics program (dogStar software, Version 1.0c). The products of turanose-6'-P hydrolysis (glucose-6-P and fructose) were determined by inclusion of 5 mM ATP and 2 units of phosphoglucose isomerase in the assay.

### Cloning of the Sucrose-6-P Hydrolase Gene (*scrB*) from *K. pneumoniae*

The *scrB* gene was amplified from *K. pneumoniae* genomic DNA using the low-error-rate FailSafe™ polymerase (Epicentre). In the forward primer (5'-GGCCATGGCGCTCTCTGACGCTGAA-3'), base pairs 3119–3137 of the *K. pneumoniae scrYAB* operon (GenBank™ accession number X57401) are bolded, and the *Nco*I site is underlined. In the reverse primer (5'-GGGGGTTCGACTACGCGTTGGTTTTCATCA-3'), base pairs 4587–4606 of *scrYAB* are bolded, and the *Sal*I site is underlined. The amplicon was digested with *Nco*I and *Sal*I and ligated into similarly digested pProEX Hta (Life Technologies, Inc.), and the recombinant plasmid(s) was transformed into *E. coli* K12 strain DH5 $\alpha$ E (Life Technologies, Inc.). Ampicillin-resistant transformants were selected, and the *scrB* genes of four plasmids containing inserts of approximately the correct size were sequenced. All shared the following differences from the published (7) *scrB* coding sequence: 991C $\rightarrow$ T, 1006G $\rightarrow$ T, 1249C $\rightarrow$ T, 1270C $\rightarrow$ T, 1549C $\rightarrow$ T, 1552A $\rightarrow$ G, 1675G $\rightarrow$ A, 1699T $\rightarrow$ C, 1738G $\rightarrow$ A (numbering as in pScrBLong). All of these differences are silent, and one plasmid was chosen and designated pScrBLong.

### Growth of *E. coli* DH5 $\alpha$ E (pScrBLong) and Expression of Sucrose-6-P Hydrolase

The organism was grown in LB medium containing 200  $\mu$ g/ml ampicillin. At  $A_{600\text{ nm}} = 0.5$ , IPTG was added (1 mM) and growth was continued for  $\sim 4$  h. Cells were harvested and washed with 25 mM HEPES buffer (pH 7.5) as described earlier. The yield was  $\sim 2.9$  g wet weight of cells/liter.

### Purification of Sucrose-6-P Hydrolase

Briefly, the purification of sucrose-6-P hydrolase was as follows. A high-speed supernatant was prepared, after resuspension and sonication, of 10 g of *E. coli* DH5 $\alpha$ E (pScrBLong) resuspended with 20 ml of 25 mM HEPES buffer (pH 7.5). The dialyzed preparation was applied to a column of TrisAcryl M-DEAE, and after washing with the same buffer, sucrose-6-P hydrolase was eluted with an increasing gradient of NaCl (0–0.5 M). Fractions with sucrose-6-P hydrolase activity were pooled, concentrated to 8 ml, and then mixed gently with 30 ml of 0.1 M MES buffer (pH 5). Precipitated material was removed by centrifugation, and the clarified solution was applied to a column of phosphocellulose P-11 (Whatman) previously equilibrated with 0.1 M MES buffer (pH 5). Nonadsorbed proteins were removed, and sucrose-6-P hydrolase was eluted with the same buffer containing an increasing concentration of potassium phosphate buffer (0–0.1 M, pH 7). Active fractions (eluted at  $\sim 50$  mM P<sub>i</sub>) were pooled and concentrated. sucrose-6-P hydrolase was purified to homogeneity by passage of this solution through an AcA-44 gel filtration column previously equilibrated with 50 mM HEPES buffer, pH 7.5, containing 0.1 M NaCl. Concentration of active fractions yielded about 22 mg of sucrose-6-P hydrolase of specific activity 12.5 units/mg (with 10 mM sucrose as substrate in the assay; see below).

### Sucrose-6-P Hydrolase Assay

Sucrose-6-P is the natural substrate for sucrose-6-P hydrolase, but the enzyme also hydrolyzes sucrose when the disaccharide is present at high concentration. Because of the limited availability of sucrose-6-P, the parent sugar was used as substrate during purification of sucrose-6-P hydrolase, and the glucose-6-P dehydrogenase/hexokinase-NADP<sup>+</sup>-coupled assay measured glucose formed by sucrose hydrolysis. The 1-ml assay contained: 0.1 M HEPES buffer (pH 7.5), 1 mM MgCl<sub>2</sub>, 1 mM NADP<sup>+</sup>, 1 mM ATP, 10 mM sucrose, 2 units of glucose-6-P dehydrogenase/hexokinase, and enzyme solution. One unit of sucrose-6-P hydrolase activity is the amount of enzyme that catalyzes the formation of 1  $\mu$ mol of glucose/min.

### Computational Methods

A conformational analysis of all disaccharides and their 6'-phosphates was carried out using a molecular dynamics (MD) simulations, *i.e.* CHARMM (22, 23), with a force field particularly adapted for the treatment of carbohydrates (24, 25), with the explicit incorporation of water as the solvent. The starting structures used were derived either from the corresponding x-ray-based solid-state geometries of sucrose (26, 27),  $\beta$ -*p*-turanose (28),  $\beta$ -*p*-leucrose (29),  $\beta$ -*f*-palatinose (30),  $\alpha$ ,  $\alpha$ -trehalose (31),  $\beta$ -*p*-maltose (32, 33), and maltitol (34, 35) or from compounds of similar backbone structure found in the Cambridge Crystallographic Database ([www.ccdc.com.ac.uk](http://www.ccdc.com.ac.uk)) (36, 37). Any water molecules present in the crystal structures were removed. For compounds

37418

Phosphoglucosyl Hydrolases from *K. pneumoniae*

that equilibrate between different anomeric or ring (pyranoid or furanoid) forms, only the most predominant tautomer was considered, *i.e.* the 6'-phosphates of  $\beta$ -*p*-trehalulose,  $\beta$ -*p*-turanose,  $\beta$ -*p*-maltulose,  $\beta$ -*p*-leucrose,  $\beta$ -*f*-palatinose,  $\beta$ -*p*-maltose, and  $\beta$ -*p*-isomaltose. Each compound was centered in a periodic box (truncated octahedron, box size  $\sim 33.5$  Å) filled with pre-equilibrated TIP3 (transferable intermolecular potential-3) water molecules, yielding (after removal of the solvent molecules that overlap with the solute) simulation systems including 643 (disaccharides) or 641 (disaccharide phosphates) water molecules, respectively. In the latter series, two  $\text{NH}_4^+$  counterions were added at random positions within 6 Å around the glucose-6- $\text{CH}_2\text{OPO}_3^{2-}$  groups. After full lattice energy minimization, all boxes were slowly heated from 0 to 300 K within 15 ps of MD simulation and were subsequently equilibrated for an additional 85 ps; the final MD data were sampled using simulations of 1 ns in each case; molecular configurations were saved every 100 fs for analysis purposes. All MD runs were carried for constant pressure ( $P_{\text{ref}} = 1$  atm, isothermal compressibility  $4.63 \cdot 10^{-5}$  atm $^{-1}$ , pressure coupling constant  $\tau_p = 5$  ps) and constant temperature ( $T_{\text{ref}} = 300$  K, temperature coupling constant  $\tau_T = 5$  ps, allowed temperature deviation  $\Delta T = \pm 10$  K) conditions (NPT ensemble (constant number of molecules, constant pressure, and constant temperature)) using the following simulation parameters: time step  $\Delta t = 1$  fs (leapfrog integrator, all X-H bond lengths were constrained using the SHAKE protocol), dielectric constant  $\epsilon = 1.0$ , cut-off distance for long range interactions 12 Å, cut-off for images in atom lists 13 Å. The following averages were recalculated from the final MD runs (standard deviations are in parentheses): disaccharides: temperature  $\langle T \rangle = 296(5)$  K, box size 33.66(8) Å, volume  $\langle V \rangle = 19060(145)$  Å $^3$ , density  $\langle \rho \rangle = 1.039(8)$  g cm $^{-3}$ ; disaccharide 6'-phosphates: temperature  $\langle T \rangle = 296(5)$  K, box size 33.59(5) Å, volume  $\langle V \rangle = 18950(130)$  Å $^3$ , density  $\langle \rho \rangle = 1.049(8)$  g cm $^{-3}$ . For each MD time series a mean solute geometry was obtained by three-dimensional fitting of all configurations (heavy atoms only, excluding  $\text{CH}_2\text{OH}$  oxygen atoms); the best-fit models from this procedure were selected as representative molecular geometries in aqueous solution (Fig. 9, 10). For a comparison, the conformation of all glucosyl-6'- $\text{CH}_2\text{OH}$  groups were set to *gauche-trans* (*gt*, torsion angle  $\text{O}5'-\text{C}5'-\text{C}6'-\text{O}6'$   $\omega = +60^\circ$ ). Solvent-accessible surfaces (38) and color-coded molecular lipophilicity patterns (MLPs) (39, 40) were generated using the MOLCAD modeling program (41, 42).<sup>2</sup>

## RESULTS

**Growth of *K. pneumoniae* on Sucrose and Its Isomers**—Recently (12) we reported the growth of *K. pneumoniae* on sucrose and its five isomeric  $\alpha$ -D-glucosyl-D-fructoses (see Fig. 1 for structures). Additionally, we showed that organisms grown previously on a particular isomer readily fermented sucrose as well as each of the  $\alpha$ -D-glucosyl-D-fructoses, whereas sucrose-grown cells, surprisingly, metabolized only sucrose (12). Examination of the protein composition of the various cell extracts by two-dimensional PAGE revealed high level expression of one specific polypeptide (molecular mass  $\sim 50$  kDa) during growth on either of the five sucrose isomers (*e.g.* palatinose and maltulose, Fig. 2) and in fact on related disaccharides such as maltose, isomaltose, maltitol (for formulae, see Fig. 1), and even methyl- $\alpha$ -D-glucopyranoside (data not shown). Significantly, the  $\sim 50$ -kDa protein was not detectable in an extract prepared from sucrose-grown cells (Fig. 2).

**Identity of the Protein Induced during Growth on Sucrose-Isomeric Glucosyl-fructoses**—Proteins from a duplicate two-dimensional PAGE gel of maltulose-grown cell extract were transferred by Western blot to a polyvinylidene difluoride membrane. Microsequence analysis provided the following sequence for the first 25 residues from the N terminus of the highly expressed  $\sim 50$ -kDa protein: MKKFSVVIAGGGSTFTP-GIVLMLLA. A BLAST (43) search of the nonredundant protein data bases with this sequence as probe revealed 91 and 82% identity, respectively, with the N termini of an unusual 6-phospho- $\alpha$ -glucosidase (EC 3.2.1.122), previously purified from *Fusobacterium mortiferum* (MalH (44)) and *B. subtilis* (GlvA (45)).

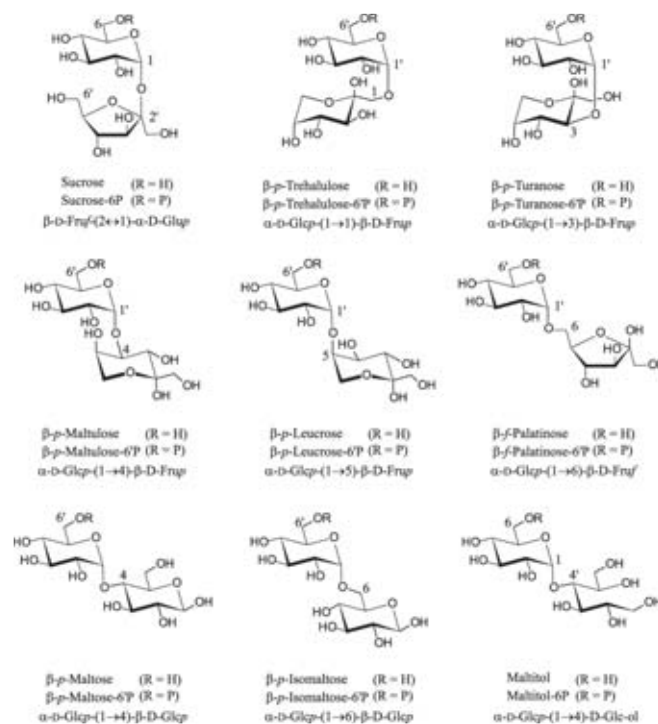


FIG. 1. Chemical formulae and established abbreviations (10) of sucrose, its five linkage isomeric glucosyl-fructoses, and of some related disaccharides ( $R = \text{H}$ ) and their respective mono-phosphates ( $R = \text{PO}_3^{2-}$ ), invariably carrying their phosphate ester groups attached to the glucosyl-C-6. For the reducing disaccharides, only the tautomeric form predominating in solution (10, 11) is depicted. The nonreducing sucrose-6-P is the singular substrate for the sucrose-6-P hydrolase, whereas all others are hydrolyzed by the 6-phospho- $\alpha$ -glucosidase described herein.

Phospho- $\alpha$ -glucosidase activity is readily detected by the intensely yellow *p*-nitrophenolate (pNP) anion released upon hydrolysis of pNP $\alpha$ Glc6P. This chromogenic substrate was rapidly hydrolyzed by extracts of cells grown on the glucosyl-fructoses and other  $\alpha$ -glucosides, but essentially no activity was detectable in the extract from sucrose-grown cells (Table I). Western blots performed with antibody raised against phospho- $\alpha$ -glucosidase from *F. mortiferum* (20) revealed a striking correlation between the amount of induced immunoreactive protein of  $\sim 50$  kDa (Fig. 3) and the hydrolytic activities of the various extracts (Table I). The protein induced during growth on the five  $\alpha$ -D-glucosyl-D-fructoses was thus identified as phospho- $\alpha$ -glucosidase.

**Cloning and Sequence Analysis of the *Agl* Region of *K. pneumoniae***—Although suggestive, the available data (Figs. 2 and 3 and Table I) did not establish a functional role for phospho- $\alpha$ -glucosidase in dissimilation of the five  $\alpha$ -D-glucosyl-D-fructoses by *K. pneumoniae*. Recently, we demonstrated the PEP-dependent phosphorylation of the five sucrose isomers via the PTS activity of palatinose-grown cells of *K. pneumoniae*, and trehalulose-6'-P, turanose-6'-P, maltulose-6'-P, leucrose-6'-P, and palatinose-6'-P were prepared in 20–50-mg amounts (12). To determine whether these derivatives were hydrolyzed by AglB, it was first necessary to purify this enzyme. To this end, *aglB*, the gene encoding the phospho- $\alpha$ -glucosidase, and an adjacent upstream gene, *aglA*, were cloned and sequenced. Fig. 4 shows the  $\sim 3.5$ -kilobase pair nucleotide sequence containing the two genes (*aglA* and *aglB*) of the alpha-glucoside utilization region of the *K. pneumoniae* genome. The *aglA* gene comprises a coding sequence of 1,619 nucleotides commencing with an ATG codon at position 394 and terminating with a TGA (stop) codon at position 2014. This open reading frame encodes a

<sup>2</sup> The major part of the MOLCAD program is included in the SYBYL package of TRIPOS Associates, St. Louis, MO.

Phosphoglucosyl Hydrolases from *K. pneumoniae*

37419

FIG. 2. Analysis by two-dimensional PAGE of proteins in extracts prepared from cells of *K. pneumoniae* grown on various disaccharides. The white circles indicate the induced ~50-kDa phospho- $\alpha$ -glucosidase (AglB) in organisms grown previously on either maltulose, palatinose, or maltulose. This protein was not detectable (white arrow) in the extract prepared from sucrose-grown cells of *K. pneumoniae*. Approximately 50  $\mu$ g of protein was applied per gel, and polypeptides were visualized by silver staining. Prior to electrophoresis, tropomyosin (1  $\mu$ g) was added to each sample as an IEF internal standard. This protein (black arrowhead) migrates as a doublet with the lower polypeptide spot ~33 kDa and pI = 5.2.

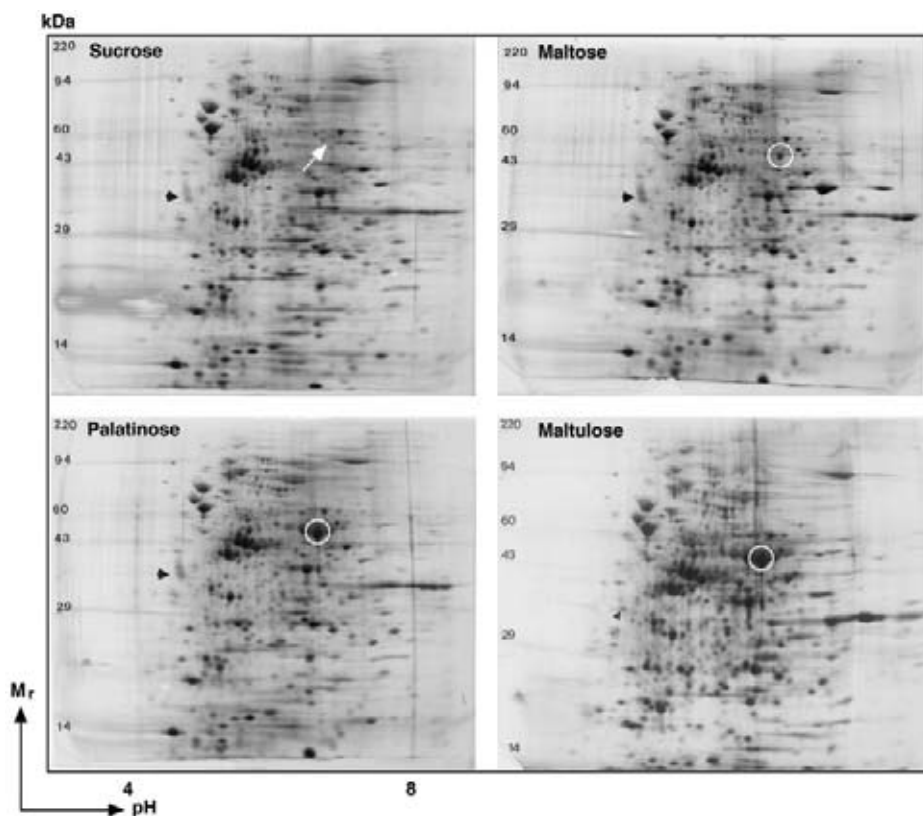


TABLE I  
Hydrolysis of *p*-nitrophenyl  $\alpha$ -D-glucopyranoside 6-phosphate by extracts prepared from cells of *K. pneumoniae* grown on different sugars

Growth sugar	Rate of pNP $\alpha$ Glc6P hydrolysis <sup>a</sup>
<b>Maltulose</b> ( $\alpha$ ,1-4) <sup>b</sup>	0.256 (100) <sup>c</sup>
<b>Palatinose</b> ( $\alpha$ ,1-6)	0.214 (84)
<b>Leucrose</b> ( $\alpha$ ,1-5)	0.202 (79)
<b>Trehalulose</b> ( $\alpha$ ,1-1)	0.160 (63)
Methyl- $\alpha$ -D-glucoside	0.119 (46)
<b>Turanose</b> ( $\alpha$ ,1-3)	0.096 (38)
Maltitol	0.073 (29)
Maltose	0.031 (12)
Sucrose	0.002 (<1)
Cellobiose	0.002 (<1)
Galactose	ND <sup>d</sup>
Trehalose	ND
Glucose	ND

<sup>a</sup>  $\mu$ mol pNP $\alpha$ Glc6P hydrolyzed min<sup>-1</sup> mg protein<sup>-1</sup>.

<sup>b</sup> Compounds in boldface are sucrose isomers.

<sup>c</sup> Values in parentheses = rate as % activity in maltulose extract.

<sup>d</sup> ND, no detectable activity.

polypeptide of 540 residues (calculated  $M_r$  = 58,373) that contains fused C and B domains characteristic of a membrane-localized EII(CB) transport protein of the PTS (46). The *aglA* gene is preceded by a potential ribosome-binding site (GAGGA) centered ~11 nucleotides from the start codon. The *aglA* stop codon overlaps the Met start codon of *aglB*. The latter gene extends from nucleotide 2013 and terminates with a TAA codon at position 3333. Translation of *aglB* predicts a polypeptide of 440 amino acids (calculated  $M_r$  = 49,256), in which residues 138–169 display the signature pattern of Family 4 glycosyl hydrolases (47, 48):<sup>3</sup> PX(S/A)(W/T)(L/I/V/M/F)<sup>2</sup>(Q/N)X<sup>2</sup>NPX<sup>4</sup>(T/A)X<sup>9,10</sup>(K/R)X(L/I/V)(G/N)XC. From the alignment shown in Fig. 5, it is clear that AglB exhibits homology with phospho- $\alpha$ -glucosidases from other species including MalH from *F. mor-*

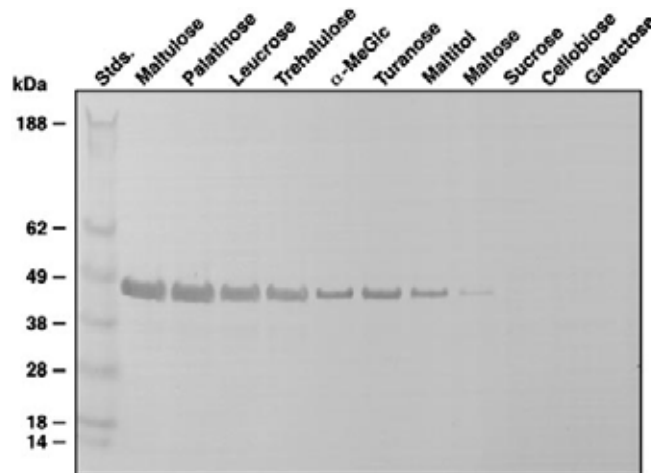


FIG. 3. Western blot showing the sugar-specific induction and cross-reactivity of the ~50-kDa protein (AglB) with antibody raised against purified MalH (phospho- $\alpha$ -glucosidase) from *F. mortiferum* (20). Extracts were prepared from cells of *K. pneumoniae* grown on the indicated sugars, and approximately 15  $\mu$ g of cell extract was applied per lane. Note the absence of immunoreactive protein in sucrose-grown cells. Stds., standards.

*tiferum* (75% identity), GlvA from *B. subtilis* (72%), and truncated GlvG from *E. coli* (77%), respectively.

**Purification of Phospho- $\alpha$ -glucosidase (AglB) from *E. coli* TOP(pAP-16)**—Cells of *E. coli* TOP(pAP-16) produced high levels of an IPTG-inducible protein with an estimated  $M_r$  ~ 50 kDa as expected for the full-length polypeptide encoded by *aglB* (Fig. 6A, lane 1). This protein cross-reacted with phospho- $\alpha$ -glucosidase antibody (Fig. 6B, lane 1), and the cell extract catalyzed the immediate hydrolysis of pNP $\alpha$ Glc6P. AglB was purified by conventional low-pressure chromatography, and to stabilize the enzyme, 0.1 mM NAD<sup>+</sup> and 1 mM Mn<sup>2+</sup> ion were included in all buffers. Throughout the four-stage procedure,

<sup>3</sup> On line at [www.expasy.ch/cgi-bin/lists?glycosid.txt](http://www.expasy.ch/cgi-bin/lists?glycosid.txt).

37420

Phosphoglucosyl Hydrolases from *K. pneumoniae*

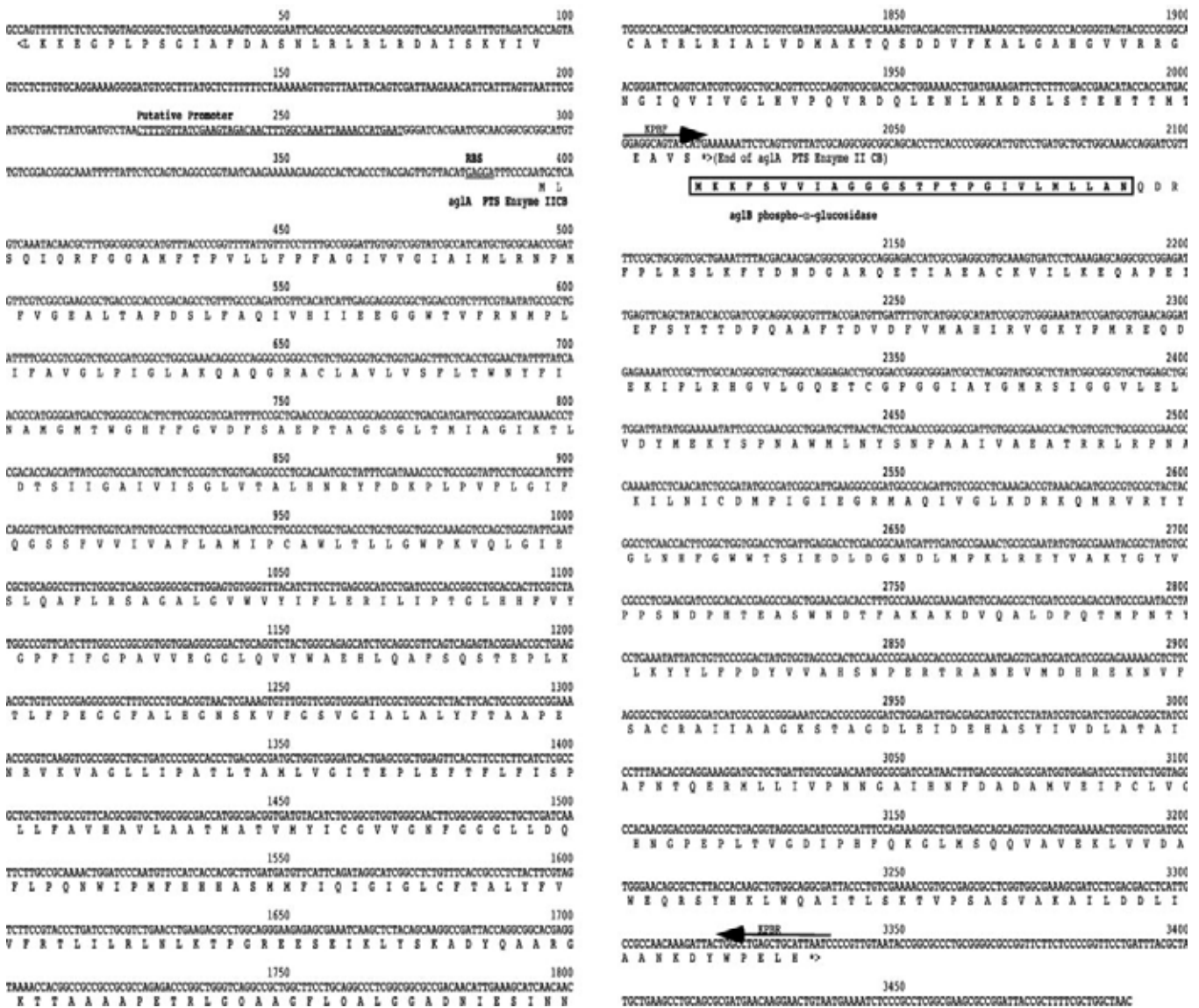


FIG. 4. Nucleotide sequence of the Agl region of *K. pneumoniae*. This ~3.5-kilobase DNA fragment contains genes *aglA* and *aglB* that encode an EIICB transport protein of the PEP:PTS and an NAD<sup>+</sup> plus metal-dependent 6-phospho- $\alpha$ -glucosidase, respectively. A potential ribosomal binding site (RBS) preceding *aglA* is underlined. The deduced amino acid sequences are shown below the nucleotide sequence in single-letter code. The N-terminal amino acid sequence of AglB obtained by Edman degradation is boxed. The positions of primers KPBF and KPBR used for PCR amplification of *aglB* are indicated by arrows above the nucleotide sequence.

the purification of AglB was monitored by enzymatic assay (Table II), SDS-PAGE (Fig. 6A), and immunoblot methods (Fig. 6B). Approximately 70 mg of electrophoretically pure enzyme was obtained from ~38 g wet weight of cells. Although purified in reasonably active form, AglB was progressively inactivated throughout the purification, and the specific activity of the final preparation (4.2 units/mg) was only ~3-fold higher than that of the original dialyzed cell extract (1.2 units/mg).

**Properties of AglB**—The molecular weight of AglB determined by electrospray/MS ( $M_r$  49,254) was within two units of the theoretical weight average  $M_r$  of 49,256 deduced from the amino acid sequence encoded by *aglB*. However, in the final stage of purification, AglB emerged from the AcA-44 gel filtration column in a volume suggestive of a protein of molecular mass ~100 kDa. Cross-linking studies also revealed the formation of a similarly sized product after incubation of the enzyme with various homo-bifunctional imidoesters (Fig. 6C, lanes 2–4). It appears likely that in solution AglB exists as a catalytically active homodimer. Analytical electrofocusing revealed two species (Fig. 6D, lane 2) having estimated pI values

of 5.4 and 5.6 that agreed fairly well with the theoretical pI (5.69) deduced from the amino acid composition of AglB. The homogeneity of the purified enzyme was confirmed by the unambiguous determination of the first 26 residues from the N terminus, MKKFSVVIAGGGSTFTPGIVLMLLAN. This sequence was precisely that deduced by translation of *aglB* and, importantly, was in perfect agreement with that of the polypeptide induced during growth of *K. pneumoniae* on the sucrose-isomeric glucosyl-fructoses (Fig. 2).

**Cofactor, Metal Ion Requirements, and Substrate Specificity of AglB**—Phospho- $\alpha$ -glucosidases MalH and GlvA from *F. mortiferum* (20, 44) and *B. subtilis* (45), respectively, exhibit requirements for nucleotide (NAD<sup>+</sup>) and divalent metal ion (Mn<sup>2+</sup>, Co<sup>2+</sup>, or Ni<sup>2+</sup>) for activity. AglB exhibited similar requirements and, in the absence of these cofactors, was unable to hydrolyze pNP $\alpha$ Glc6P (Table III). Inclusion of NAD<sup>+</sup> in the assay elicited substrate cleavage, but enzyme activity increased 3–6-fold upon further addition of Mn<sup>2+</sup>, Co<sup>2+</sup>, or Ni<sup>2+</sup>. Other divalent metal ions tested, including Mg<sup>2+</sup>, Ca<sup>2+</sup>, and Zn<sup>2+</sup>, were either without effect or were inhibitory. The activity

Phosphoglucosyl Hydrolases from *K. pneumoniae*

37421

AglB Klepn	--MKKFSVVTAGGGSTTPGIVMLLANQDRFPFLRSIKFYDNDGARQFTIARACKVILKE	58
MalH Fusmr	--MKQFSILTAGGGSTTPGIVMLLANQDRFPFLRSIKFYDNDGARQFTIARACKVILKE	58
GlvA Bacsu	MKKKFSFVIAGGGSTTPGIVMLLANQDRFPFLRSIKFYDNDGARQFTIARACKVILKE	60
GlvG Eco	--MKKFSVVTAGGGSTTPGIVMLLANQDRFPFLRSIKFYDNDGARQFTIARACKVILKE	58
	* * * * *	
AglB Klepn	QAPETIEFSYTTDPAQAFITDVFVMAHIRVQKYPMRQDEKIPLRHGVGCGEPCGPGGIAY	118
MalH Fusmr	KAPQIKFSYSENPEARTDIDFVMAHIRVQKYPMRQDEKIPLRHGVGCGEPCGPGGIAY	118
GlvA Bacsu	KAPDIEFAFTDPEEARTDIDFVMAHIRVQKYPMRQDEKIPLRHGVGCGEPCGPGGIAY	120
GlvG Eco	KADIAFSYTTDPEEAFSDVDFVMAHIRVQKYPMRQDEKIPLRHGVGCGEPCGPGGIAY	118
	* * * * *	
AglB Klepn	GMRISGCVLELDVMEKYSNPAWMLNYSNPAATVAEATRRLRPNKILNICDMPGIEGR	178
MalH Fusmr	GMRISGCVLELDVMEKYSNPAWMLNYSNPAATVAEATRRLRPNKILNICDMPGIEGR	178
GlvA Bacsu	GMRISGCVLELDVMEKYSNPAWMLNYSNPAATVAEATRRLRPNKILNICDMPGIEGR	180
GlvG Eco	GMRISGCVLELDVMEKYSNPAWMLNYSNPAATVAEATRRLRPNKILNICDMPGIEGR	180
	* * * * *	
AglB Klepn	MAQIVGLQDRKQMRVRYGLNHFQWTSIEDLDGNDLMPKLEHYVAKYGYVPPSND-PHT	237
MalH Fusmr	MAEILGLSRRKMDIMYGLNHFQWTSVDRQDNDLMPKLEHYVAKYGYVPPSND-PHT	238
GlvA Bacsu	MAQIVGLQDRKQMRVRYGLNHFQWTSIQDQEGNDLMPKLEHYVAKYGYVPPSND-PHT	239
GlvG Eco	MAQIVGLQDRKQMRVRYGLNHFQWTSIQDQEGNDLMPKLEHYVAKYGYVPPSND-PHT	212
	* * * * *	
AglB Klepn	EASWNTFAKAKVQALDPTMPTNTLYKYLFPDYVVAHNSPNERTRANEVMDHREKNVFS	297
MalH Fusmr	EASWNTFAKAKVQALDPTMPTNTLYKYLFPDYVVAHNSPNERTRANEVMDHREKNVFS	298
GlvA Bacsu	EASWNTFAKAKVQALDPTMPTNTLYKYLFPDYVVAHNSPNERTRANEVMDHREKNVFS	299
	* * * * *	
AglB Klepn	ACRAIIAAGKSTAGDLEIDHASYIVDLATAIAFNQERMLLVNNGAIIHNFDAWAVE	357
MalH Fusmr	ECEKVKVNGSSESCALHIDHASYIVDLATAIAFNQERMLLVNNGAIIHNFDAWAVE	358
GlvA Bacsu	QCDDITRQSSSENSEIKIDHASYIVDLATAIAFNQERMLLVNNGAIIHNFDAWAVE	359
	* * * * *	
AglB Klepn	IPCLVGHNGPEPLTVGDIHPQKGLMSQQVAVEKLVVDVAEQRSYHKLQWAILTSKTVPS	417
MalH Fusmr	IPCLVGSNGPEPLTVGRIIPQKGLMEQQVTVEKLVVEAWIEGYSYQLWQAITMSKTVPS	418
GlvA Bacsu	VPCIVGSGPEPLTVGTITPQKGLMEQQVSVKLVVEAWIEGYSYQLWQAITMSKTVPS	419
	* * * * *	
AglB Klepn	ASVAKAIIIDDLIAANKDYWPELH----- 440	
MalH Fusmr	AKVAKDIIIDDLIRANKDYWPELIR----- 441	
GlvA Bacsu	ARVARLIIIDDLVANKDYWPELDQSPTRIS 449	
	* * * * *	

FIG. 5. Comparative alignment of the sequence of AglB from *K. pneumoniae* with 6-phospho- $\alpha$ -glucosidase(s) from *F. moritiferum* 25557 (MalH (Fusmr), Swiss Protein Database accession no. O06901); *B. subtilis* 168 (GlvA (Bacsu), SwissProt identifier P54716) and *E. coli* K-12 MG1655 (GlvG, truncated (Eco) Ref. 49, Swiss Protein Database accession no. P31450). The bold underline at the N terminus indicates a probable NAD<sup>+</sup>-binding domain, and the DND motif is highlighted. Catalytically important glutamyl residues are boxed, and conserved residues are indicated by asterisks. Residues representing the signature motif for Family 4 glucosyl hydrolases (Swiss Protein Databank; Prosite name, PS01324 (48)) are indicated by the shaded underline.

of AglB was optimal at ~36 °C in either 0.1 M Tris-HCl or HEPES buffers (pH 7.5) containing 0.1 mM NAD<sup>+</sup> and 1 mM Mn<sup>2+</sup> ion. In the presence of requisite cofactors, AglB hydrolyzed all 6-phospho- $\alpha$ -D-glucosides tested including all phosphorylated isomers of sucrose. The kinetic parameters for each substrate are presented in Table IV. There was no detectable cleavage of the corresponding nonphosphorylated compounds. Importantly, sucrose-6-P itself was not hydrolyzed by AglB nor was it an inhibitor of enzyme activity. Studies with turanose-6'-P (Table V) established that, as for the chromogenic analog (pNP $\alpha$ Glc6P), the same cofactors were required for the hydrolysis of this PTS product. Throughout the time course of the experiment, the 1:1 stoichiometry between [glucose-6-P:fructose] confirmed these two metabolites as the only reaction products from AglB-catalyzed hydrolysis of turanose-6'-P.

**Purification and Substrate Specificity of Sucrose-6-P Hydrolase**—AglB readily hydrolyzed the five 6-phosphoglucosyl-fructoses, whereas sucrose-6-P, remarkably, was not a substrate for this enzyme. It was of interest, to determine whether sucrose-6-P hydrolase would exhibit the converse specificity with respect to potential substrates. sucrose-6-P hydrolase was purified from *E. coli* DH5 $\alpha$ E (pScrB Long) as described under "Experimental Procedures." The four-stage procedure (Fig. 7) provided 20–30 mg of electrophoretically pure sucrose-6-P hydrolase with an estimated molecular mass of ~53 kDa by SDS-PAGE (Fig. 7, lane 4), which was in agreement with the molecular weight of 52,708 deduced by translation of the *scrB* gene (ref. 7 and Swiss Protein Database accession no. P27217). The mass of sucrose-6-P hydrolase determined experimentally by electrospray mass spectrometry ( $M_r$ , 52,581) was about 127 mass units lower than the calculated mass<sub>av</sub>. Except for the absence of methionine at the N terminus, microsequence analysis confirmed exactly the predicted sequence of the first 28

residues of the polypeptide SLPSRLPAILQAVMQGQPQAL-ADSHYPQ. Sucrose-6-P hydrolase catalyzed the hydrolysis of sucrose and sucrose-6-P at comparable rates ( $V_{\max}^{\text{sucrose}} = 31.2 \pm 1.1$ ;  $V_{\max}^{\text{sucrose-6-P}} = 40.4 \pm 2.3$   $\mu\text{mol hydrolyzed min}^{-1} \text{mg}^{-1}$ ). However, the affinity of the enzyme for the phosphorylated disaccharide ( $K_m^{\text{sucrose-6-P}} = 85.3 \pm 15.1$   $\mu\text{M}$ ) was >200-fold greater than for sucrose ( $K_m^{\text{sucrose}} = 20.3 \pm 1.9$  mM). There was no detectable hydrolysis (at 1 mM) of any of the phosphorylated isomers of sucrose, and sucrose-6-P hydrolase failed to hydrolyze other phospho- $\alpha$ -glucosides including maltose-6'-P and trehalose-6-P.

**Conformational Analysis of Sucrose-6-P and Disaccharide-6'-phosphates**—Insight into the remarkable discrimination of sucrose-6-P hydrolase and phospho- $\alpha$ -glucosidase for their substrates was provided by conformational analysis of these phosphorylated compounds using molecular dynamics simulations. Sucrose and sucrose-6-P differ from other disaccharides not only by the fact that they are nonreducing (the two sugar units are linked through their anomeric centers) but by the predetermined orientation of the glucose and fructose portions toward each other. In the solid state, the two sugars are conformationally fixed by two intramolecular hydrogen bonds (Fig. 8 and Refs. 26, 27, 50, 51). On dissolution of the disaccharide in water, these bonds are replaced by an H<sub>2</sub>O molecule bridging glucosyl-O-2 and fructosyl-O-1 through hydrogen bonding (Fig. 8, center, and Ref. 52), to yield an overall conformation close to that in the crystalline state. The molecular geometry of sucrose-6-P in water, which emerges from a nanosecond molecular dynamics simulation in a truncated octahedron box containing 641 water molecules, again is very similar to that of sucrose in the crystal and in aqueous solution (Fig. 8, right), so that a water bridge of the Glc-2-O $\cdots$ H<sub>2</sub>O $\cdots$ O-1-Fru is likewise to be inferred. A comparison of the molecular geometry of sucrose-6-P in water with the geometries of the nine disaccharide-6'-phosphates reveals their distinctly different molecular shapes. Unlike sucrose-6-P, which by virtue of the intramolecular water bridge between glucose and fructose assumes a remarkably compact conformation in solution, the nine disaccharide-6'-phosphates lack any interaction of this type and hence invariably adopt a more extended, longish molecular geometry. These differences in molecular shape are emphasized by juxtaposition of the solvent-accessible surface of sucrose-6-P (Fig. 9, top) with those of the nine disaccharide-6'-phosphates shown superimposed in Fig. 9 (bottom).

## DISCUSSION

**Transport and Hydrolysis of Sucrose and Its Isomers by *K. pneumoniae***—Circumstantial evidence indicated that the transport and dissimilation of the five O- $\alpha$ -linked isomers of sucrose by *K. pneumoniae* occurred by a route different from the PTS-sucrose-6-P hydrolase route used for sucrose itself (12). For example, sucrose-grown cells failed to metabolize any of the isomers, and the PEP:PTS activity of cells grown on a particular isomer (e.g. palatinose) catalyzed the phosphorylation of all other isomers. Importantly, growth of *K. pneumoniae* on the five  $\alpha$ -D-glucosyl-D-fructoses induced a high level expression of a polypeptide (molecular mass ~ 50 kDa) that was not present in organisms grown on sucrose. In this study, the gene (*aglB*) that encodes the induced protein has been cloned and sequenced, and the protein itself (AglB) has been identified as an NAD<sup>+</sup> and metal-dependent phospho- $\alpha$ -glucosidase. The gene *aglB* lies adjacent to a second gene, *aglA*, which encodes an EII(CB) component of the PEP:PTS (46). It is our contention that together, AglA and AglB facilitate the phosphorylation and subsequent cleavage of phosphorylated isomers of sucrose (and related  $\alpha$ -glucosides) by *K. pneumoniae*.

**Properties of sucrose-6-P hydrolase and Phospho- $\alpha$ -glucosi-**

37422

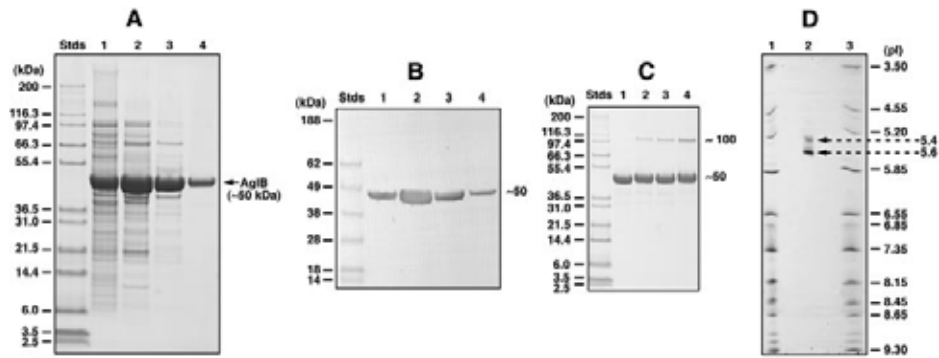
Phosphoglucosyl Hydrolases from *K. pneumoniae*

FIG. 6. Determination of the  $M_r$ , pI, and structural composition of AglB by analytical PAGE. A, purification and  $M_r$  estimate of AglB. Samples from each stage of purification were denatured, resolved by SDS-PAGE, and stained with Coomassie Brilliant Blue R-250. Lane 1, high-speed supernatant; lane 2, TrisAcryl M-DEAE; lane 3, phenyl-Sepharose Cl-4B; and lane 4, Ultrogel AcA-44. B, Western blot of a duplicate gel of panel A showing cross-reaction of AglB with MalH antibody. Stds, standards. C, cross-linking of AglB subunits to the dimeric state by treatment with: lane 1, no agent; lane 2, dimethyladipimidate; lane 3, dimethylpimelimidate; and lane 4, dimethylsuberimidate. D, determination of the pI of AglB by analytical electrofocusing (lane 2).

TABLE II  
Summary of the purification of AglB (phospho- $\alpha$ -glucosidase) from *E. coli* TOP 10 (pAP-16)

Purification step	Total protein	Total activity	Specific activity	Purification	Yield
	mg	units <sup>a</sup>	units/mg	-fold	%
Dialyzed high-speed supernatant	2304	2815	1.22	1	100
TrisAcryl M-DEAE	618	1743	2.82	2.3	62
Phenyl-Sepharose CL-4B	174	715	4.12	3.4	25
AcA-44	72	299	4.15	3.4	11

<sup>a</sup> Units expressed as  $\mu\text{mol}$  of pNP $\alpha$ Glc6P hydrolyzed  $\text{min}^{-1}$ .

TABLE III  
NAD<sup>+</sup> and metal ion requirements for activity of AglB (phospho- $\alpha$ -glucosidase)

The purified enzyme had been dialyzed against 25 mM Tris-HCl buffer (pH 7.5).

Addition to assay <sup>a</sup>	Specific activity <sup>b</sup>
No additions	ND <sup>c</sup>
+ NAD <sup>+</sup>	0.35
+ Mg <sup>2+</sup>	0.01
+ NAD <sup>+</sup> + Mg <sup>2+</sup>	0.32
+ Ni <sup>2+</sup>	0.11
+ NAD <sup>+</sup> + Ni <sup>2+</sup>	0.59
+ Co <sup>2+</sup>	0.26
+ NAD <sup>+</sup> + Co <sup>2+</sup>	1.01
+ Mn <sup>2+</sup>	0.25
+ NAD <sup>+</sup> + Mn <sup>2+</sup>	1.35

<sup>a</sup> The 2-ml assay solution contained 50 mM Tris-HCl buffer (pH 7.5). When required, appropriate divalent metal ion (1 mM) and NAD<sup>+</sup> (0.5 mM) were included. Phospho- $\alpha$ -glucosidase (60  $\mu\text{g}$ ) was added, and after 2 min of preincubation at 25 °C, pNP $\alpha$ Glc6P was added to a final concentration of 1 mM. Hydrolysis of substrate (*i.e.* formation of pNP) was followed as described under "Experimental Procedures."

<sup>b</sup> Expressed as  $\mu\text{mol}$  of pNP $\alpha$ Glc6P hydrolyzed  $\text{min}^{-1}$  mg enzyme<sup>-1</sup>.

<sup>c</sup> ND, no detectable activity.

dase (AglB)—In some of their properties, sucrose-6-P hydrolase and AglB show similarity. For example they are of comparable (monomer) size, they are exacting for the glucose-6-P moiety of their substrates, and both exhibit poor or no affinity for non-phosphorylated disaccharides. However, in their amino acid sequences, cofactor requirements, and assignments to different families of the glycosyl hydrolase superfamily, sucrose-6-P hydrolase and AglB are quite different. The amino acid sequence of sucrose-6-P hydrolase (deduced from the *scrB* gene (7)) has essentially no homology with that of AglB, and by the amino acid-based sequence classification of Henrissat (47), AglB and sucrose-6-P hydrolase are assigned to Families 4 and 32, respectively, of the glycosyl hydrolase superfamily (48).<sup>3</sup> Sucrose-6-P hydrolase has no cofactor requirements, whereas AglB is dependent upon both NAD<sup>+</sup> and divalent metal ion (Mn<sup>2+</sup>, Ni<sup>2+</sup>, or Co<sup>2+</sup>) for catalytic activity (Table III). Indeed, these

TABLE IV  
Substrate specificity and kinetic parameters of purified AglB (phospho- $\alpha$ -glucosidase) from *Klebsiella pneumoniae*

Compounds in bold face are sucrose isomers.

Phospho- $\alpha$ -glucoside	$K_m$	$V_{\text{max}}$
	mM	$\mu\text{mol mg}^{-1} \text{min}^{-1}$
<b>Trehalose-6'-P</b> ( $\alpha$ ,1-1)	1.23 $\pm$ 0.10	0.89 $\pm$ 0.03
<b>Turanose-6'-P</b> ( $\alpha$ ,1-3)	1.68 $\pm$ 0.26	2.41 $\pm$ 0.19
<b>Maltulose-6'-P</b> ( $\alpha$ ,1-4)	1.20 $\pm$ 0.12	1.15 $\pm$ 0.05
<b>Leucrose-6'-P</b> ( $\alpha$ ,1-5)	5.63 $\pm$ 1.24	0.85 $\pm$ 0.13
<b>Palatinose-6'-P</b> ( $\alpha$ ,1-6)	2.42 $\pm$ 0.39	0.90 $\pm$ 0.08
Maltose-6'-P	3.08 $\pm$ 0.49	1.31 $\pm$ 0.13
Isomaltose-6'-P	4.48 $\pm$ 1.00	1.55 $\pm$ 0.23
Maltitol-6-P	0.82 $\pm$ 0.23	1.87 $\pm$ 0.21
Trehalose-6-P	1.16 $\pm$ 0.30	0.31 $\pm$ 0.03
pNP $\alpha$ Glc6P	0.05 $\pm$ 0.01	2.42 $\pm$ 0.25

TABLE V  
Product stoichiometry and requirement(s) for NAD<sup>+</sup> and Mn<sup>2+</sup> ion for hydrolysis of turanose-6'-P by AglB (phospho- $\alpha$ -glucosidase)

The 1-ml reaction mixture contained 1  $\mu\text{mol}$  of turanose-6'-P. For composition of the reaction, details of sampling, and enzymatic analyses, see "Experimental Procedures."

Reaction time	NAD <sup>+</sup> and Mn <sup>2+</sup> present <sup>a</sup>		NAD <sup>+</sup> and Mn <sup>2+</sup> omitted	
	Glucose-6-P	Fructose	Glucose-6-P	Fructose
min				
0	ND <sup>b</sup>	ND	ND	ND
2	0.32 <sup>c</sup>	0.32	0.03	0.03
5	0.57	0.53	0.05	0.05
10	0.87	0.85	0.07	0.07
15	0.95	0.91	0.10	0.08
20	1.00	0.94	0.11	0.10

<sup>a</sup> NAD<sup>+</sup> and Mn<sup>2+</sup> were both present at a concentration of 1 mM.

<sup>b</sup> ND, not detectable.

<sup>c</sup> Numerical values indicate  $\mu\text{mol}$  of glucose-6-P and fructose formed.

cofactor requirements for AglB were predicted by virtue of the extraordinarily high sequence identity between the putative polypeptide encoded by *aglB* and those of the Family 4 phospho- $\alpha$ -glucosidases shown in the multiple alignment in Fig. 5. The role(s) for NAD<sup>+</sup> and metal ion have not been established,

Phosphoglucosyl Hydrolases from *K. pneumoniae*

37423

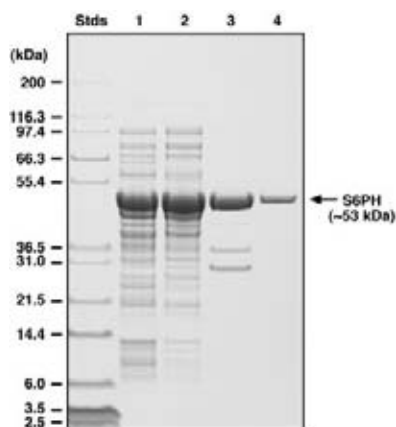


FIG. 7. SDS-PAGE of samples from each stage of purification of sucrose-6-P hydrolase from *E. coli* DH5 $\alpha$ E (pScrBLong). Lane 1, high-speed supernatant; lane 2, TrisAcryl M-DEAE; lane 3, phosphocellulose P-11; and lane 4, Ultrogel AcA-44 gel filtration chromatography. *Stds*, standards.

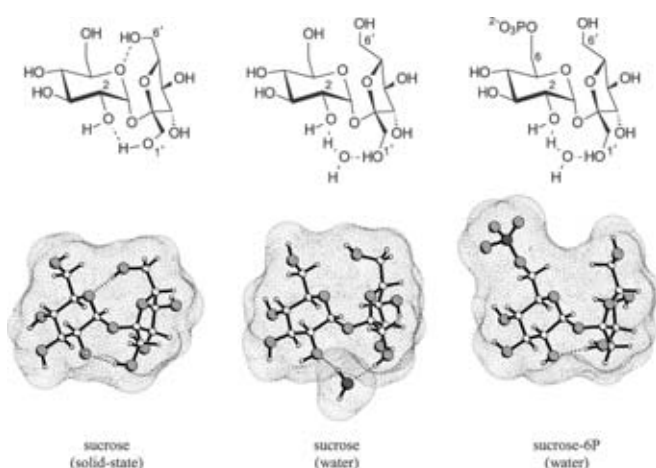


FIG. 8. Preferred molecular geometries of sucrose in the solid state (*left*) characterized by two intramolecular hydrogen bonds (26, 27, 50, 51) and in water (*center*), shown here with the water molecule bridging glucosyl-O-2 and fructosyl-O-1 through hydrogen bonding (52). The conformation of sucrose-6-phosphate emerging from a 1000-ps MD simulation in a box containing 641 water molecules (*right*) is so similar to that of sucrose in water that a Glc-2-O $\cdots$ H $_2$ O $\cdots$ O-1-Fru water bridge is likewise inferred. The dotted contours refer to the solvent-accessible surface into which ball-and-stick models have been inserted; for easier comparison, the glucosyl moiety is kept in the same orientation.

and it is presently unclear whether these cofactors play catalytic and/or structural roles in AgIB and related enzymes of Family 4 (44, 45, 53, 54). Results obtained from site-directed mutagenesis of the phospho- $\alpha$ -glucosidase (GlvA) in *B. subtilis* (45) suggest that residues close to the N terminus comprise the NAD $^+$ -binding domain (*see*, Fig. 5). Glycosyltransferases comprise a superfamily of Mn $^{2+}$ -dependent enzymes (55) that use UDP-glucose, UDP-galactose, and related compounds as substrates for modification (via glycosylation) of a wide variety of biological molecules in both prokaryotes and eukaryotes. Most, if not all, members of this large family contain a conserved motif D(X)D that participates in the substrate recognition/catalytic process by interaction of the aspartyl residues with the ribose moiety of the nucleotide or via coordination with Mn $^{2+}$  ion (56). Interestingly, this motif is also present in AgIB and in other phospho- $\alpha$ -glucosidases, and the conserved DND residues lie adjacent to the putative NAD $^+$ -binding domain of these enzymes (Fig. 5). Furthermore, site-directed substitution at the first aspartic residue of this motif (D41G and D41E) in GlvA results in loss of hydrolytic activity (45). These findings

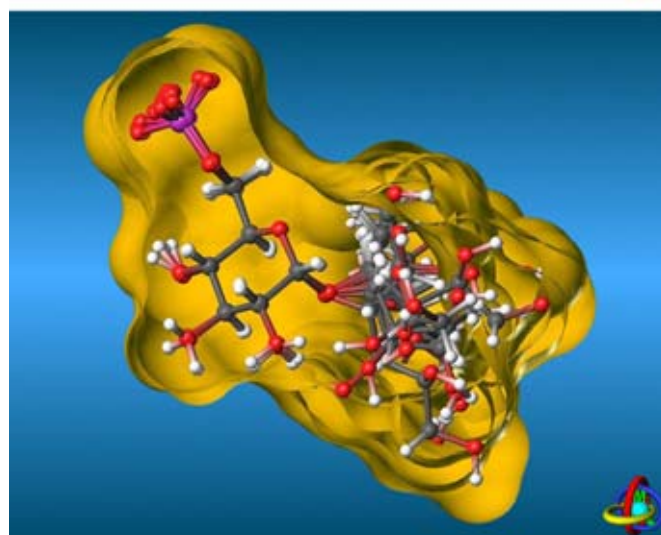
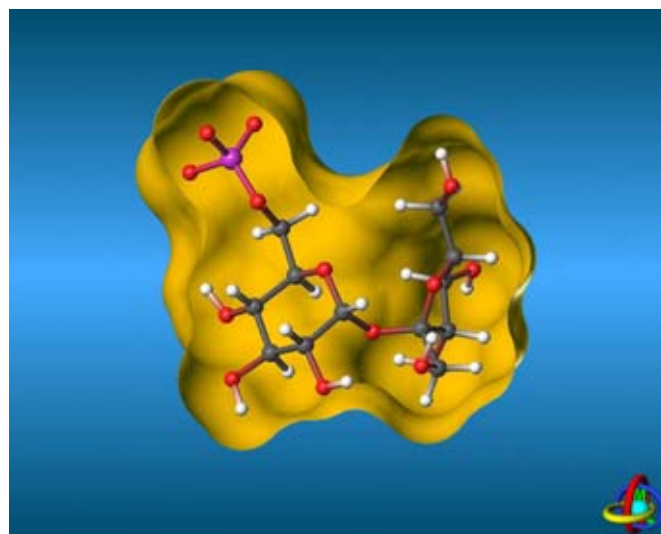


FIG. 9. Solvent-accessible surface of sucrose-6-P in front-opened form with ball-and-stick model insert (*top*) as set against those of the nine other disaccharide-6'-phosphates (*bottom*) superimposed on each other with the  $\alpha$ -D-glucose-6-P portion (*left half*) kept in the same orientation. The slender form of the fructose moiety of sucrose-6-P (*top, right half*) renders the shape of the molecule different; notably it is more compact than that of the other disaccharide-6-phosphates.

plus the fact that the D(X)D motif is conserved in other members of Family 4 (see Fig. 4 in Ref. 45) may indicate a role for the two acidic residues in Me $^{2+}$  ion-binding in AgIB and related glycosyl hydrolases.

**Substrate Discrimination by Sucrose-6-P Hydrolase and 6-Phospho- $\alpha$ -glucosidase**—Sucrose-6-P and its five phosphorylated linkage isomers have recently been prepared and characterized by  $^1$ H and  $^{13}$ C NMR spectroscopy (12). The availability of these derivatives in substrate amount permitted specificity and kinetic analyses to be carried out with highly purified sucrose-6-P hydrolase and AgIB. These studies establish unequivocally that sucrose-6-P hydrolase hydrolyzes only sucrose-6-P to form glucose-6-P and fructose. The specificity of sucrose-6-P hydrolase for its single substrate (sucrose 6-phosphate) is noteworthy because it suggests that their reciprocal molecular recognition (as a prerequisite to fission of the intersaccharidic linkage to glucose-6-P and fructose) is unique, not even tolerating minor changes in the linkup of the two sugars, as for example those realized in the five isomeric glucosyl-fructoses. In contrast, the 6-phospho- $\alpha$ -glucosidase (AgIB), which is in-

37424

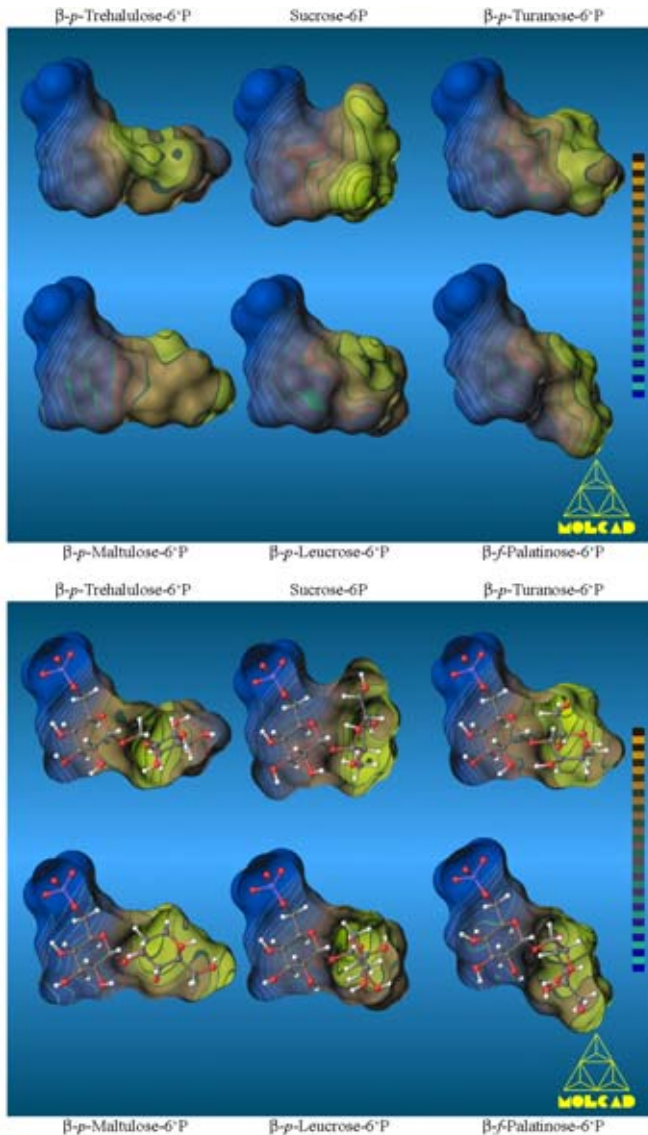
Phosphoglucosyl Hydrolases from *K. pneumoniae*

FIG. 10. Molecular lipophilicity patterns (MLPs) of sucrose-6-P (top center entry) and its five isomeric 6'-phosphoglucosyl-fructoses in fully closed and front-side-opened form with ball-and-stick model inserts. The relative hydrophobicity portraits were mapped in color-coded form onto their individual contact (solvent-accessible) surfaces with the colors ranging from dark blue (most hydrophilic areas) to yellow-brown (hydrophobic domains).

duced by growth of *K. pneumoniae* on the five glucosyl-fructoses, appears to be less specific and is tolerant of a considerable variation in both the structure and size of the *O*-linked aglycone. Indeed, the  $\text{NAD}^+$  and metal ion-dependent phospho- $\alpha$ -glucosidase hydrolyzed not only the 6'-phosphoglucosyl-fructoses but also the phosphorylated derivatives of related  $\alpha$ -linked disaccharides such as maltose-6'-P, isomaltose-6'-P, and maltitol-6-P. Remarkably, AglB was unable to hydrolyze sucrose-6-P. Explanations for enzyme specificity and substrate discrimination must reside in the molecular geometries and polarities of the individual disaccharide phosphates and/or in the three-dimensional structures of the two enzymes. Presently, only a structural model based on threading methods has been proposed for those enzymes (including sucrose-6-P hydrolase) that by sequence-based alignment are assigned to Family 32 of glycosyl hydrolases (57). Moreover, only a preliminary x-ray analysis has been reported for one enzyme member (GlvA from *B. subtilis*, (58)) of Family 4, to which AglB is assigned. Thus, we were led to probe the substrates with respect to structure,

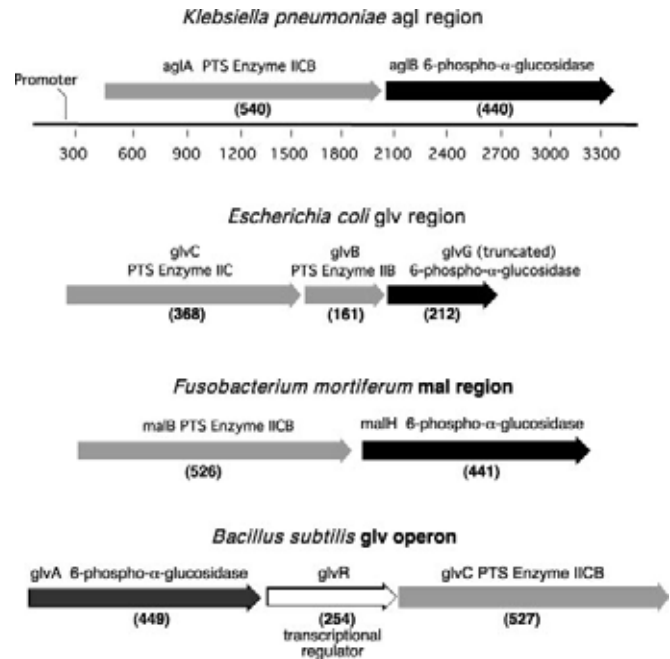


FIG. 11. Comparison of the Agl region of *K. pneumoniae* (this paper; GenBank™ accession no. AF337811) with homologous regions of *E. coli* (Glv region (49)), *F. mortiferum* (Mal region; GenBank™ accession no. U81185 (44)), and *B. subtilis* (Glv operon; GenBank™ accession no. D50543 (60)). Genetic elements are drawn to scale. Functionally equivalent genes are shown by the same types of arrows, and the numbers in parentheses indicate the number of residues encoded by the gene.

molecular shape, and polarity for clues to understanding the specificity of the two phosphoglucosyl hydrolases. From the markedly different molecular geometries of the phosphorylated disaccharides in solution (Figs. 8–10), one might reasonably assume that shape recognition (by the respective binding domains) may be an important determinant of enzyme specificity. Another and conceivably more significant contribution to substrate discrimination may originate from differences in the distribution of hydrophobic and hydrophilic regions over the contact surfaces of the disaccharide phosphates. In eliciting the sweetness response, for example, sucrose is believed to dock onto the taste bud receptor protein via its hydrophobic region (59), which, on the basis of the calculated MLP profiles, encompasses the entire outer surface side of the fructose moiety (51, 59). The same docking procedure is expected for sucrose-6-phosphate at the active site of sucrose-6-P hydrolase, inasmuch as the MLP profile of sucrose and its 6-phosphate (Fig. 10, top center) are essentially the same, i.e. a pronounced hydrophilic 6-phosphoglucosyl part (blue areas) facing a distinctly hydrophobic (yellow) fructose portion. Fig. 10 shows the MLPs of sucrose-6-P and its five isomeric 6'-phosphoglucosyl-fructoses in the fully closed (upper portion) and in the front-side-opened form with ball-and-stick model inserts (lower portion). The MLP patterns of the five 6'-phosphoglucosyl-fructoses, albeit having essentially identical hydrophilic (blue) glucose-6-P halves, clearly differ from sucrose-6-P with respect to the shape, intensity, and distribution of their hydrophobic (yellow) surface domains (Fig. 10). These may perhaps be the major factors that prevent docking of the isomeric phosphates at the sucrose-6-P binding site of sucrose-6-P hydrolase and, conversely, that preclude binding of sucrose-6-P to the active site of phospho- $\alpha$ -glucosidase.

**Conclusion**—This study and our earlier paper (12) are the first reports of bacterial growth on the five isomers of sucrose. However, genetic units similar to the Agl region of *K. pneu-*



Phosphoglucosyl Hydrolases from *K. pneumoniae*

37425

*moniae* are present in the genomes of *B. subtilis*, *F. mortiferum*, and *E. coli* (Fig. 11). The phospho- $\alpha$ -glucosidase(s) of these species are clearly homologous (Fig. 5), and the PTS transporter (AglA) has extensive homology with GlvC of *B. subtilis*, MalB of *F. mortiferum*, and Glv(CB) of *E. coli*. The gene organization is similar in the three Gram-negative species, but for *B. subtilis* (Gram-positive) the gene order is reversed and a gene *glvR*, which encodes a regulatory protein, separates the phospho- $\alpha$ -glucosidase and PTS genes (60, 61). Our recent finding that *F. mortiferum* can also grow on the sucrose isomers<sup>4</sup> suggests that genes homologous to *aglA* and *aglB* may be prerequisites for bacterial growth on these compounds. Parenthetically, it may be noted that neither of these genes has been found during sequencing of the *S. mutans* genome, and these deficiencies may explain the inability of this organism to metabolize the sucrose isomers.

**Acknowledgments**—We express our thanks to Drs. Jack London and Edith C. Wolff for their encouragement, advice, and constructive criticisms. We also thank Drs. Nga Nguyen and Lewis Pannell for provision of microsequence and mass spectrometry data.

## REFERENCES

- Kundig, W., Ghosh, S., and Roseman, S. (1964) *Proc. Natl. Acad. Sci. U. S. A.* **52**, 1067–1074
- Meadow, N. D., Fox, D. K., and Roseman, S. (1990) *Annu. Rev. Biochem.* **59**, 497–542
- Postma, P. W., Lengeler, J. W., and Jacobson, G. R. (1993) *Microbiol. Rev.* **57**, 543–594
- Reizer, J., Saier, M. H., Jr., Deutscher, J., Grenier, F., Thompson, J., and Hengstenberg, W. (1988) *Crit. Rev. Microbiol.* **15**, 297–338
- Thompson, J. (1987) in *Sugar Transport and Metabolism in Gram-positive Bacteria* (Reizer, J., and Peterkofsky, A., eds) pp. 13–38, Ellis Horwood, Chichester, UK
- Sprenger, G. A., and Lengeler, J. W. (1988) *J. Gen. Microbiol.* **134**, 1635–1644
- Titgemeyer, F., Jahreis, K., Ebner, R., and Lengeler, J. W. (1996) *Mol. Gen. Genet.* **250**, 197–206
- Kunst, F., Pascal, M., Lepesant, J.-A., Walle, J., and Dedonder, R. (1974) *Eur. J. Biochem.* **42**, 611–620
- Thompson, J., Nguyen, N. Y., Sackett, D. L., and Donkersloot, J. A. (1991) *J. Biol. Chem.* **266**, 14573–14579
- IUPAC (1996) *IUPAC Recommendations for Nomenclature of Carbohydrates*, Academic Press, San Diego
- Lichtenthaler, F. W., and Rönninger, R. (1990) *J. Chem. Soc. Perkin Trans. 2*, 1489–1497
- Thompson, J., Robrish, S. A., Pikis, A., Brust, A., and Lichtenthaler, F. W. (2001) *Carbohydr. Res.* **331**, 149–161
- Loesche, W. J. (1986) *Microbiol. Rev.* **50**, 353–380
- Newbrun, E. (1989) in *Cariology* (Newbrun, E., ed) 3rd Ed., Quintessence Publications Inc., Chicago
- Takazoe, I., Frostell, G., Ohta, K., Topitsoglou, V., and Sasaki, N. (1985) *Swed. Dent. J.* **91**, 81–87
- Ooshima, T., Izumitani, A., Takei, T., Fujiwara, T., and Sobue, S. (1990) *Caries Res.* **24**, 48–51
- Moynihan, P. J. (1998) *J. Dentistry* **26**, 209–218
- Schiweck, H., Munir, M., Rapp, K. M., Schneider, B., and Vogel, M. (1990) *Zuckerindustrie (Berlin)* **115**, 555–565
- Schwengers, D. (1991) in *Carbohydrates As Organic Raw Materials* (Lichtenthaler, F. W., ed) pp. 183–195, VCH Publishers, New York
- Thompson, J., Gentry-Weeks, C. R., Nguyen, N. Y., Folk, J. E., and Robrish, S. A. (1995) *J. Bacteriol.* **177**, 2505–2512
- Sapico, V., Hanson, T. E., Walter, R. W., and Anderson, R. L. (1968) *J. Bacteriol.* **96**, 51–54
- Brooks, B. R., Brucoleri, R. E., Olafson, B. D., States, D. J., Swaminathan, S., and Karplus, M. (1983) *J. Comput. Chem.* **4**, 187–217
- Nilsson, L., and Karplus, M. (1986) *J. Comput. Chem.* **7**, 591–616
- Reiling, S., Schlenkrich, M., and Brickmann, J. (1996) *J. Comput. Chem.* **17**, 450–468
- Reiling, S., and Brickmann, J. (1995) *Macromol. Theory Simul.* **4**, 725–743
- Brown, G. M., and Levy, H. A. (1973) *Acta Crystallogr. Sect. B Struct. Sci.* **29**, 790–797
- Hanson, J. C., Sieker, L. C., and Jensen, L. H. (1973) *Acta Crystallogr. Sect. B Struct. Sci.* **29**, 797–808
- Kanters, J. A., Gaykema, W. P. J., and Roelofsen, G. (1978) *Acta Crystallogr. Sect. B Struct. Sci.* **34**, 1873–1881
- Thiem, J., Kleeberg, M., and Klaska, K.-H. (1989) *Carbohydr. Res.* **189**, 65–77
- Dreissig, V. W., and Luger, P. (1973) *Acta Crystallogr. Sect. B Struct. Sci.* **29**, 514–521
- Jeffrey, G. A., and Nanni, R. (1985) *Carbohydr. Res.* **137**, 21–30
- Quigley, G. J., Sarko, A., and Marchessault, R. H. (1970) *J. Am. Chem. Soc.* **92**, 5834–5839
- Gress, M. E., and Jeffrey, G. A. (1977) *Acta Crystallogr. Sect. B Struct. Sci.* **33**, 2490–2495
- Ohno, S., Hirao, M., and Kido, M. (1982) *Carbohydr. Res.* **108**, 163–171
- Schouten, A., Kanters, J. A., Kroon, J., Looten, P., Dufloot, P., and Mathlouthi, M. (1999) *Carbohydr. Res.* **322**, 298–302
- Cambridge Crystallographic Data Center (2001) *Cambridge Structural Database*, Version 5.21, Cambridge Crystallographic Data Center, Cambridge, UK
- Allen, F. H., Bellard, S. A., Brice, M. D., Cartwright, B. A., Doubleday, A., Higgs, H., Hummelink, T., Hummelink-Peters, B. G., Kennard, O., Motherwell, W. D. S., Rodgers, J. R., and Watson, D. G. (1979) *Acta Crystallogr. Sect. B Struct. Sci.* **35**, 2331–2339
- Connolly, M. L. (1983) *Science* **221**, 709–713
- Heiden, W., Moeckel, G., and Brickmann, J. (1993) *J. Comput. Aided Mol. Des.* **7**, 503–514
- Teschner, M., Henn, C., Vollhardt, H., Reiling, S., and Brickmann, J. (1994) *J. Mol. Graph.* **12**, 98–105
- Brickmann, J. (1996) *MOLCAD-Molecular Computer Aided Design*, Darmstadt University of Technology, Germany
- Waldherr-Teschner, M., Goetze, T., Heiden, W., Knoblauch, M., Vollhardt, H., and Brickmann, J. (1992) in *Advances in Scientific Visualization* (Post, F. H., and Hin, A. J. S., eds) pp. 58–67, Springer, Heidelberg, Germany
- Altschul, S. F., Madden, T. L., Schäffer, A. A., Zhang, J., Zhang, Z., Miller, W., and Lipman, D. J. (1997) *Nucleic Acids Res.* **25**, 3389–3402
- Bouma, C. L., Reizer, J., Reizer, A., Robrish, S. A., and Thompson, J. (1997) *J. Bacteriol.* **179**, 4129–4137
- Thompson, J., Pikis, A., Ruvinov, S. B., Henrissat, B., Yamamoto, H., and Sekiguchi, J. (1998) *J. Biol. Chem.* **273**, 27347–27356
- Lengeler, J. W., Jahreis, K., and Wehmeier, U. F. (1994) *Biochim. Biophys. Acta* **1188**, 1–28
- Henrissat, B. (1991) *Biochem. J.* **280**, 309–316
- Swiss Institute of Bioinformatics (2000) *SWISS-PROT, Protein Sequence Data Bank*, Release 39.0, SIB, Geneva
- Reizer, J., Michotey, V., Reizer, A., and Saier, M. H., Jr. (1994) *Protein Sci.* **3**, 440–450
- Lichtenthaler, F. W., Immel, S., and Kreis, U. (1991) *Starch/Stärke* **43**, 121–132
- Lichtenthaler, F. W., and Immel, S. (1995) *Int. Sugar J.* **97**, 12–22
- Immel, S., and Lichtenthaler, F. W. (1995) *Liebigs Ann.* 1925–1937
- Thompson, J., Ruvinov, S. B., Freedberg, D. I., and Hall, B. G. (1999) *J. Bacteriol.* **181**, 7339–7345
- Raasch, C., Streit, W., Schanzer, J., Bibel, M., Gosslar, U., and Liebl, W. (2000) *Extremophiles* **4**, 189–200
- Campbell, J. A., Davies, G. J., Bulone, V., and Henrissat, B. (1997) *Biochem. J.* **326**, 929–939
- Pedersen, L. C., Tsuchida, K., Kitagawa, H., Sugahara, K., Darden, T. A., and Negishi, M. (2000) *J. Biol. Chem.* **275**, 34580–34585
- Pons, T., Olmea, O., Chinae, G., Beldarrain, A., Márquez, G., Acosta, N., Rodríguez, L., and Valencia, A. (1998) *Proteins* **33**, 383–395
- Varrot, A., Yamamoto, H., Sekiguchi, J., Thompson, J., and Davies, G. J. (1999) *Acta Crystallogr. Sect. D Biol. Crystallogr.* **55**, 1212–1214
- Lichtenthaler, F. W., and Immel, S. (1993) in *Correlations of Hydrophobicity Potential Profiles of Sucrose, Sucralose and Fructose with AH-B-X Assignment in Sweet Taste Chemoreception* (Mathlouthi, M., Kanters, J. A., and Birch, G. G., eds) pp. 21–53, Elsevier Science, New York
- Yamamoto, H., Uchiyama, S., Fajar, A. N., Ogasawara, N., and Sekiguchi, J. (1996) *Microbiology-UK* **142**, 1417–1421
- Yamamoto, H., Serizawa, M., Thompson, J., and Sekiguchi, J. (2001) *J. Bacteriol.* **183**, 5110–5121

<sup>4</sup> A. Pikis, S. Immel, S. A. Robrish, and J. Thompson, unpublished data.



## Metabolism of sucrose and its five isomers by *Fusobacterium mortiferum*

Andreas Pikis,<sup>1,2</sup> Stefan Immel,<sup>3</sup> Stanley A. Robrish<sup>1</sup> and John Thompson<sup>1</sup>

Author for correspondence: John Thompson. Tel: +1 301 496 4083. Fax: +1 301 402 0396.  
e-mail: jthompson@dir.nidcr.nih.gov

<sup>1</sup> Microbial Biochemistry and Genetics Unit, Oral Infection and Immunity Branch, National Institute of Dental and Craniofacial Research, National Institutes of Health, Bethesda, MD 20892-4350, USA

<sup>2</sup> Department of Infectious Diseases, Children's National Medical Center, Washington DC 20010-2970, USA

<sup>3</sup> Institut für Organische Chemie, Technische Universität Darmstadt, D-64287 Darmstadt, Germany

***Fusobacterium mortiferum* utilizes sucrose [glucose-fructose in  $\alpha(1\rightarrow2)$  linkage] and its five isomeric  $\alpha$ -D-glucosyl-D-fructoses as energy sources for growth. Sucrose-grown cells are induced for both sucrose-6-phosphate hydrolase (S6PH) and fructokinase (FK), but the two enzymes are not expressed above constitutive levels during growth on the isomeric compounds. Extracts of cells grown previously on the sucrose isomers trehalulose  $\alpha(1\rightarrow1)$ , turanose  $\alpha(1\rightarrow3)$ , maltulose  $\alpha(1\rightarrow4)$ , leucrose  $\alpha(1\rightarrow5)$  and palatinose  $\alpha(1\rightarrow6)$  contained high levels of an NAD<sup>+</sup> plus metal-dependent phospho- $\alpha$ -glucosidase (MalH). The latter enzyme was not induced during growth on sucrose. MalH catalysed the hydrolysis of the 6'-phosphorylated derivatives of the five isomers to yield glucose 6-phosphate and fructose, but sucrose 6-phosphate itself was not a substrate. Unexpectedly, MalH hydrolysed both  $\alpha$ - and  $\beta$ -linked stereomers of the chromogenic analogue *p*-nitrophenyl glucoside 6-phosphate. The gene *malH* is adjacent to *malB* and *malR*, which encode an EII(CB) component of the phosphoenolpyruvate-dependent sugar:phosphotransferase system and a putative regulatory protein, respectively. The authors suggest that for *F. mortiferum*, the products of *malB* and *malH* catalyse the phosphorylative translocation and intracellular hydrolysis of the five isomers of sucrose and of related  $\alpha$ -linked glucosides. Genes homologous to *malB* and *malH* are present in both *Klebsiella pneumoniae* and the enterohaemorrhagic strain *Escherichia coli* O157:H7. Both these organisms grew well on sucrose, but only *K. pneumoniae* exhibited growth on the isomeric compounds.**

**Keywords:** phospho- $\alpha$ -glucosidase, sucrose isomers, sucrose-6-phosphate hydrolase, *Klebsiella pneumoniae*, *Escherichia coli* O157:H7

### INTRODUCTION

Many bacterial species, including *Klebsiella pneumoniae* (Sprenger & Lengeler, 1988; Tittgemeyer *et al.*, 1996), *Bacillus subtilis* (Fouet *et al.*, 1987), *Lactococcus lactis* (Thompson & Chassy, 1981; Thompson *et al.*, 1991; Rauch & deVos, 1992), *Fusobacterium mortiferum* (Thompson *et al.*, 1992), *Escherichia coli* (Schmid *et al.*, 1988) and *Clostridium beijerinckii* (Tangney *et al.*, 1998; Reid *et al.*, 1999) translocate sucrose simultaneously

with phosphorylation at C-6 of the glucosyl moiety via the phosphoenolpyruvate-dependent sucrose:phosphotransferase system (PEP:PTS) (Meadow *et al.*, 1990; Postma *et al.*, 1993). Sucrose 6-phosphate is hydrolysed intracellularly by sucrose-6-phosphate hydrolase (S6PH) to yield glucose 6-phosphate and fructose, which are further metabolized via the glycolytic pathway. The multi-component sucrose-PEP:PTS and S6PH are also expressed by oral streptococci, including *Streptococcus mutans* (St Martin & Wittenberger, 1979; Slee & Tanzer, 1979) and *Streptococcus sobrinus* (Chen & LeBlanc, 1992) and dietary sucrose is fermented primarily to lactic acid. By its demineralizing action upon tooth enamel, this organic acid initiates or contributes to the aetiology of dental caries (Loesche, 1986; Van Houte, 1994).

The linkage between the two component sugars of sucrose, i.e. D-glucose and D-fructose, can be modified to

**Abbreviations:** FK, fructokinase; G6P, glucose 6-phosphate; G6PDH, glucose-6-phosphate dehydrogenase; HK, hexokinase; 4-MU- $\alpha$ -G6P, 4-methylumbelliferyl  $\alpha$ -D-glucopyranoside-6-phosphate; PEP:PTS, phosphoenolpyruvate-dependent sucrose:phosphotransferase system; pNP- $\alpha$ -G6P, *p*-nitrophenyl  $\alpha$ -D-glucopyranoside 6-phosphate; pNP- $\beta$ -G6P, *p*-nitrophenyl  $\beta$ -D-glucopyranoside 6-phosphate; S6PH, sucrose-6-phosphate hydrolase.

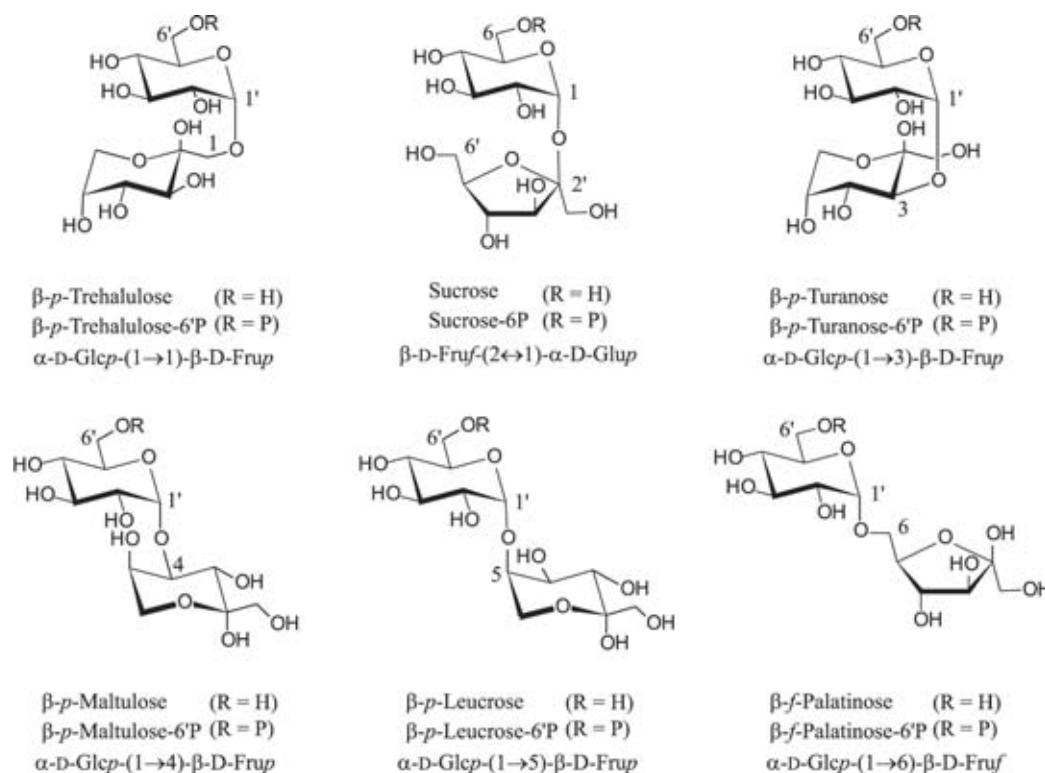


**Fig. 1.** Molecular formulae of sucrose and its five isomeric  $\alpha$ -D-glucosyl-D-fructoses, in both free and phosphorylated forms.

yield five isomeric compounds (Fig. 1) that trivially are designated trehalulose, turanose, maltulose, leucrose and palatinose (Lichtenthaler & Rönninger, 1990; Lichtenthaler *et al.*, 1991; Immel & Lichtenthaler, 1995). Until recently (Thompson *et al.*, 2001a), there were no reports of the bacterial utilization of the five sucrose isomers. Indeed, the inability of mutans streptococci to metabolize these comparatively sweet disaccharides suggests their use as non-cariogenic substitutes for dietary sucrose (Ooshima *et al.*, 1983, 1991; Ziesenitz *et al.*, 1989; Minami *et al.*, 1990; Peltroche-Llacsahuanga *et al.*, 2001). In light of these reports, we were surprised to discover that *K. pneumoniae* readily utilized all five  $\alpha$ -D-glucosyl-D-fructoses as energy sources for growth (Thompson *et al.*, 2001a, b), and that the enzymes encoded by the sucrose (*scr*) operon (Titgemeyer *et al.*, 1996) did not participate in dissimilation of these compounds. Remarkably, the sucrose isomers and structurally related  $\alpha$ -glucosides (including maltose, isomaltose, maltitol and methyl  $\alpha$ -D-glucoside) are first translocated by an  $\alpha$ -glucoside-specific EII(CB) transport protein, and the accumulated 6-phospho- $\alpha$ -D-glucosides are hydrolysed by a metal-requiring, NAD<sup>+</sup>-dependent phosphoglucosyl hydrolase belonging to family 4 of the glycosylhydrolase superfamily (Henrissat, 1991). In *K. pneumoniae*, the genes for the EII(CB) transport protein (*aglA*) and the phospho- $\alpha$ -glucosidase (*aglB*) lie adjacent, and are chromosomally encoded (Thompson *et al.*, 2001b).

Fusobacteria are Gram-negative anaerobic rods that are usually described as weakly or asaccharolytic, and most species, including *Fusobacterium nucleatum*, use amino acids as fermentable energy sources (Robrish *et al.*, 1987; Robrish & Thompson, 1990). The products of metabolism (acetic, butyric and propionic acids) may penetrate periodontal tissue, thereby contributing to the aetiology of gingivitis and periodontal disease. In contrast to other species, *F. mortiferum* ferments an extraordinarily wide variety of carbohydrates (Robrish *et al.*, 1991). Previously, in studies of maltose metabolism in *F. mortiferum*, we cloned and expressed a gene (*malH*) whose deduced sequence exhibits ~75% residue identity with the phospho- $\alpha$ -glucosidase of *K. pneumoniae* (Thompson *et al.*, 1995; Bouma *et al.*, 1997). In the present report, we show that the gene adjacent to *malH* (designated *malB*) also encodes a putative EII(CB) protein that is ~60% identical with AglA of *K. pneumoniae*. Coincident with our studies, publication of the complete genome sequence of enterohaemorrhagic *E. coli* O157:H7 (Perna *et al.*, 2001) also revealed two adjacent genes with extensive homology to those found in *K. pneumoniae*. It was of interest, therefore, to determine whether possession of these genetic elements would also permit growth of *F. mortiferum* and *E. coli* O157:H7 on the five isomers of sucrose. Our findings are summarized in this communication. Additionally, we describe the purification, and some unexpected properties, of the phospho- $\alpha$ -

glucosidase (MalH) that catalyses the hydrolysis of phosphorylated sucrose isomers in *F. mortiferum*.

## METHODS

**Materials and reagents.** Sucrose isomers were obtained from the following sources: trehalulose, Südzucker, Mannheim/Ochsenfurt; turanose, Pfanstiehl Laboratories; maltulose, TCI America; leucrose, Fluka; palatinose, Wako Chemicals. Other sugars and glucosides were purchased from Sigma and Pfanstiehl Laboratories. Phosphorylated derivatives were biosynthesized via the PEP:PTS of permeabilized (palatinose-grown) cells of *K. pneumoniae* and were purified by Ba<sup>2+</sup>/ethanol precipitation, ion-exchange and paper chromatography (Thompson *et al.*, 2001a). The chromogenic and fluorogenic substrates *p*-nitrophenyl  $\alpha$ -D-glucopyranoside 6-phosphate (pNP- $\alpha$ -G6P), *p*-nitrophenyl  $\beta$ -D-glucopyranoside 6-phosphate (pNP- $\beta$ -G6P) and 4-methylumbelliferyl  $\alpha$ -D-glucopyranoside-6-phosphate (4-MU- $\alpha$ -G6P) were prepared by selective phosphorylation (at C6-OH) of the parent glucosides with phosphorus oxychloride in trimethyl phosphate containing small proportions of water (Thompson *et al.*, 1995). Glucose-6-phosphate dehydrogenase (G6PDH, EC 1.1.1.49) and hexokinase (HK, EC 2.7.1.1) were purchased from Boehringer Mannheim, and Ultrogel AcA-44 and Tris-Acryl M-DEAE from Sigma.

**Bacterial strains and culture media.** *K. pneumoniae* ATCC 23357, *E. coli* O157:H7 (EDL 933) and *F. mortiferum* ATCC 25557 were obtained from the American Type Culture Collection. *K. pneumoniae* and *E. coli* O157:H7 were grown in a medium of the following composition (per litre): Na<sub>2</sub>HPO<sub>4</sub>, 7.1 g; KH<sub>2</sub>PO<sub>4</sub>, 1.5 g; (NH<sub>4</sub>)<sub>2</sub>SO<sub>4</sub>, 3 g; MgSO<sub>4</sub>·7H<sub>2</sub>O, 0.1 g; FeSO<sub>4</sub>·7H<sub>2</sub>O, 5 mg. Filter-sterilized sugars were added to autoclaved media (pH 7.4) to a final concentration of 4 g per litre. Cells of *K. pneumoniae* were grown in standing cultures, but *E. coli* O157:H7 was grown with vigorous aeration on a rotary shaker (~250 r.p.m.). *E. coli* PEP43(pCB4.11) was grown with aeration in Luria-Bertani (LB) medium supplemented with 50 µg kanamycin ml<sup>-1</sup>. *F. mortiferum* was grown anaerobically (GasPak, BBL) in a medium comprising (per litre): Tryptone (Difco), 17 g; Protease Peptone (Difco), 3 g; Na<sub>2</sub>HPO<sub>4</sub>, 2.5 g; NaCl, 5 g; final pH 7.3.

**DNA sequence analysis.** Automated DNA sequencing incorporating Big Dye terminators was used to sequence *malB*, and an adjacent upstream gene (*malR*), directly from genomic DNA of *F. mortiferum*. From data previously reported by Bouma *et al.* (1997), a reverse primer 1R1 (5'-AACTCTCTCTAACTTGTTGGTACTGAAAGTC-3') was designed to obtain initial sequence information. Subsequent data were obtained by the primer synthesis and the chromosomal 'walking' technique. PCR primers were designed for sequencing of the second strand, and for amplification (from genomic DNA) of the fragment encoding the two genes by use of *Taq* DNA polymerase. The amplicon was cloned into the TOPO TA cloning vector (Invitrogen). All sequencing was performed by BioServe Biotechnologies (Laurel, MD, USA), and the MacVector 7.0 sequence analysis package (Genetics Computer Group, Madison, WI, USA) was used to assemble and analyse the data.

**Metabolism of sugars by washed cells of *F. mortiferum*.** To maintain anaerobic conditions, centrifuge tubes were flushed with a gas mixture (5% CO<sub>2</sub>, 5% H<sub>2</sub>, 90% N<sub>2</sub>, by vol.) prior to harvesting of the sucrose-grown cells (5000 g for 10 min at 5 °C). The supernatant fluid was discarded, and the cell pellet

was resuspended as quickly as possible in 30 ml anaerobically prepared wash solution [50 mM potassium phosphate buffer (pH 7) containing 1 mM MgCl<sub>2</sub>]. After centrifugation, the washed cells were resuspended in 5 ml wash buffer, and the mixture was maintained at 0 °C under anaerobic conditions until required. For studies of disaccharide utilization, the washed cells (equivalent to 30 mg total cell protein) were added to 10 ml of wash buffer containing the desired sugar (sucrose or isomer) at a final concentration of 10 mM. The cell suspensions were incubated at 37 °C in 100 ml serum bottles filled with anaerobic gas and, at intervals, 1 ml samples were withdrawn by insertion of a gas-flushed tuberculin syringe through the butyl rubber cap. The cells were removed by filtration through Millex-GS filter units (0.22 µm pore size; Millipore) and filtrates were collected. Samples were heated in 1 M HCl for 1 h at 100 °C, cooled, and neutralized with 1 M KOH. Glucose (equivalent to disaccharide remaining) was determined by the ATP-G6PDH/HK-NADP<sup>+</sup> coupled enzyme assay.

**Preparation and analysis of *F. mortiferum* extracts.** Cells of *F. mortiferum* grown on the different sugars were harvested from 400 ml anaerobic culture. The cell pellets (~1–2 g wet weight) were resuspended with 3 vols 25 mM Tris/HCl buffer (pH 7.5) containing 0.1 mM NAD<sup>+</sup> and 1 mM MnCl<sub>2</sub> (designated TNM buffer). The cells were disrupted by sonication at 0 °C (6 × 15 s bursts in a Branson instrument, model 185), and centrifuged at 14000 r.p.m. for 20 min at 5 °C in an Eppendorf bench-top instrument. The clarified supernatants were assayed for S6PH, FK and phospho- $\alpha$ -glucosidase activities.

**Enzyme assays.** The activities of S6PH, FK and phospho- $\alpha$ -glucosidase (with disaccharide phosphate substrates) were determined from the formation of glucose, fructose 6-phosphate and G6P, respectively, in the appropriate reaction mixture. Production of the three metabolites was coupled to the enzymic reduction of NADP<sup>+</sup> (measured as A<sub>340</sub>), and rates were determined in a Beckman DU 640 recording spectrophotometer. In all calculations, a molar absorption coefficient ( $\epsilon$ ) of 6220 M<sup>-1</sup> cm<sup>-1</sup> was assumed for NADPH.

**S6PH.** This enzyme catalyses the hydrolysis of both sucrose 6-phosphate (to G6P and fructose) and sucrose (to glucose and fructose), albeit with significantly different  $K_m$  for the two compounds (0.1 mM and ~100 mM, respectively; see Thompson *et al.*, 1992). Because of the limited supply of sucrose 6-phosphate, sucrose was used as substrate for the spectrophotometric assay of S6PH in cell extracts. The standard 1 ml assay contained: 0.1 M potassium phosphate buffer (pH 7.2); 50 mM sucrose; 5 mM ATP; 10 mM MgCl<sub>2</sub>; 1 mM NADP<sup>+</sup>, ~3 U each of G6PDH/HK, and cell extract.

**FK.** Activity was determined in a similar mixture to that used for S6PH, containing 10 mM fructose as substrate, 3 U G6PDH and 5 U phosphoglucose isomerase.

**Phospho- $\alpha$ -glucosidase (MalH).** Activity was determined by two methods in which either chromogenic analogues or phosphorylated disaccharides served as substrates. Cofactors NAD<sup>+</sup> and Mn<sup>2+</sup> were included in both reaction mixtures. Throughout the purification of MalH, enzyme activity was determined in a discontinuous assay with pNP- $\alpha$ -G6P and pNP- $\beta$ -G6P as substrates. The 2 ml reaction mixture (at 37 °C) contained: 50 mM Tris/HCl buffer (pH 7.5); 0.5 mM NAD<sup>+</sup>; 1 mM MnCl<sub>2</sub>; and 0.5 mM of the chromogenic substrate. After enzyme addition, samples (0.25 ml) were removed at intervals throughout a 3 min period of incubation, and were immediately added to 0.75 ml 0.5 M Na<sub>2</sub>CO<sub>3</sub> solution containing 0.1 M EDTA to stop the reaction. The A<sub>400</sub> was

A. Píkis and others

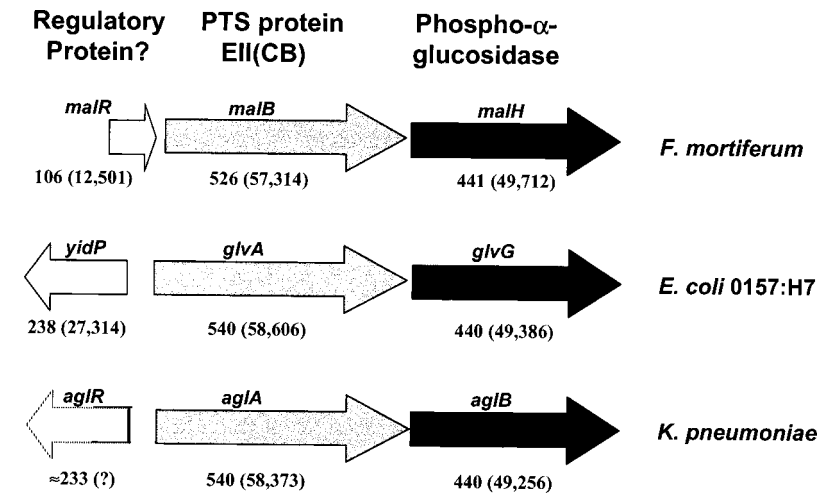


**Fig. 2.** Structural organization of the putative  $\alpha$ -glucoside operons of: *F. mortiferum* (GenBank accession number U81185); *E. coli* O157:H7 (*yidP*, GenBank AAG58886; *glvA*, GenBank AAG58885; *glvG*, GenBank AAG58884) and *K. pneumoniae* (GenBank AF337811). The numbers below the arrows are predicted amino acid residues, with calculated molecular masses (Da) of the encoded polypeptides in parentheses. Dotted lines indicate incomplete sequence for *aglR* of *K. pneumoniae*.

measured, and the amount of pNP formed (substrate hydrolysed) was calculated from the molar absorption coefficient of the yellow *p*-nitrophenolate anion,  $\epsilon = 18300 \text{ M}^{-1} \text{ cm}^{-1}$ . A continuous NADP<sup>+</sup>-coupled assay was used to measure G6P formed by MalH-catalysed hydrolysis of phosphorylated disaccharides. The assay mixture contained in 1 ml: 0.1 M HEPES buffer (pH 7.5); 1 mM MgCl<sub>2</sub>; 1 mM MnCl<sub>2</sub>; 1 mM NAD<sup>+</sup>; 1 mM NADP<sup>+</sup>; 2 mM disaccharide phosphate, 3 U G6PDH and purified MalH (35  $\mu\text{g}$  protein).

**Purification of MalH from *E. coli* PEP43(pCB4.11).** A 2.2 kb *Sau*3AI chromosomal DNA fragment of *F. mortiferum* that includes the *malH* gene and its promoter has previously been cloned and the enzyme has been expressed from plasmid pCB4.11 (Bouma *et al.*, 1997). This plasmid was transferred by electroporation to *E. coli* PEP43  $\Delta cel \Delta (bgl-pho) leu metA$  or *B. his rpsL lacZ $\Delta$ 4680 *lacY*<sup>+</sup> *arbT*<sup>+</sup> Tn10:::*bglA* dTn10<sub>cam</sub>::*ebgA*5100 *ebgR*<sup>+</sup> L532 (B. G. Hall, Biology Department, University of Rochester, NY, USA, laboratory collection). *E. coli* PEP43 expresses no phospho- $\beta$ -glucosidases because the *cel* and *bglGFB* operons have been deleted, *bglA* is disrupted by Tn10 and the *asc* operon is cryptic.*

Cells of *E. coli* PEP43(pCB4.11) (~ 25 g wet weight) were resuspended with 40 ml TNM buffer, and the organisms were disrupted by 2  $\times$  1.5 min sonication with a Branson model 350 instrument. The preparation was clarified by ultracentrifugation (180000 *g* for 2 h at 5  $^{\circ}\text{C}$ ), and the supernatant fluid was dialysed against 4 litres of TNM buffer. The dialysed material was transferred (~ 0.6 ml min<sup>-1</sup>) to a column of TrisAcryl M-DEAE (2.6  $\times$  10 cm) that had been equilibrated with TNM buffer. The column was washed to elute non-adsorbed material, and then MalH activity was eluted with 500 ml of a linear, increasing concentration gradient of NaCl (0–150 mM) in TNM buffer. Fractions of 5 ml were collected, and those containing highest MalH activity (54–65 inclusive) were pooled and concentrated in an Amicon pressure cell to ~ 3 ml. The concentrated sample was transferred (0.15 ml min<sup>-1</sup>) to an Ultrogel AcA-44 gel filtration column (1.6  $\times$  94 cm; linear fractionation range, 10–130 kDa) previously equilibrated with TNM buffer containing 0.1 M NaCl. Fractions of 2 ml were collected, and tetrameric MalH (~ 200 kDa) was eluted at the void volume of the column. Fractions that contained a single protein by SDS-PAGE (47–50, inclusive) were pooled, and concentrated to yield ~ 5 mg

purified MalH [specific activity 2.9  $\mu\text{mol}$  pNP- $\alpha$ -G6P hydrolysed min<sup>-1</sup> (mg protein)<sup>-1</sup>].

**Analytical methods.** Protein concentrations were determined by the BCA protein assay (Pierce). The Novex X-Cell system was used for both native (nonreducing) and SDS-PAGE. For SDS-PAGE experiments, precast NuPage (4–12%) Bistris gels and MES-SDS running buffer (pH 7.3) were used with Novex Mark 12 protein size standards. Proteins were stained with Coomassie brilliant blue R-250. Electrophoresis of cell extracts under nonreducing conditions was carried out at 10  $^{\circ}\text{C}$  in Tris/glycine (4–20%) precast gels from Novex, with Tris/glycine (pH 8.3) supplemented with 1 mM MnCl<sub>2</sub> and 0.1 mM NAD<sup>+</sup> as the running buffer. For detection of phospho- $\alpha$ -glucosidase activity, the gel was immersed in 30 ml of a solution that contained 25 mM Tris/HCl buffer (pH 7.5); 1 mM MnCl<sub>2</sub>; 0.1 mM NAD<sup>+</sup> and 0.1 mM 4MU- $\alpha$ -G6P. After ~ 5 min incubation, the gel was photographed under long-wave UV light with Ektopan Kodak film (2 min exposure with a green filter). For Western blot analysis, proteins in the cell extracts together with pre-stained markers (SeeBlue from Novex), were first separated by SDS-PAGE and then transferred to a nitrocellulose membrane. Immunodetection of phospho- $\alpha$ -glucosidase was performed with polyclonal antibody to MalH from *F. mortiferum* as described previously (Thompson *et al.*, 1995). Molecular dynamics simulations and procedures for the determination of solvent-accessible surfaces have been described previously (Immel & Lichtenthaler, 1995; Thompson *et al.*, 2001b).

## RESULTS

### Gene organization in *F. mortiferum*, *K. pneumoniae* and *E. coli* O157:H7

The genes that constitute the putative  $\alpha$ -glucoside operons, and their organization in the three bacterial species, are shown in Fig. 2. In *K. pneumoniae*, adjacent chromosomal genes *aglA* and *aglB* encode, respectively, an EII(CB) transport protein and phospho- $\alpha$ -glucosidase. These proteins promote the phosphorylative translocation and hydrolysis of sucrose isomers by this organism (Thompson *et al.*, 2001a, b). The partial

**Table 1.** Enzyme activities in extracts prepared from cells of *F. mortiferum* grown previously on various carbohydrates

Growth sugar	Enzyme specific activity†		
	Phospho- $\alpha$ -glucosidase‡	FK§	S6PH
Trehalulose*	11.6	2.6	2.2
Sucrose	ND	26.3	63.4
Turanose*	3.5	0.7	1.9
Maltulose*	3.4	1.6	1.6
Leucrose*	12.7	2.4	6.5
Palatinose*	3.2	1.2	4.0
Glucose	ND	2.1	ND
Fructose	ND	1.0	3.6
Maltose	8.5	3.1	2.8
Methyl $\alpha$ -D-glucoside	23.9	ND	2.8

\* Sucrose isomers.

† The same cell extracts were used for the assay of the three enzyme activities; values are means of two separate assays. ND, No detectable activity.

‡ nmol pNP- $\alpha$ -G6P hydrolysed min<sup>-1</sup> (mg protein)<sup>-1</sup>.

§ nmol fructose phosphorylated min<sup>-1</sup> (mg protein)<sup>-1</sup>.

|| nmol sucrose hydrolysed min<sup>-1</sup> (mg protein)<sup>-1</sup>.

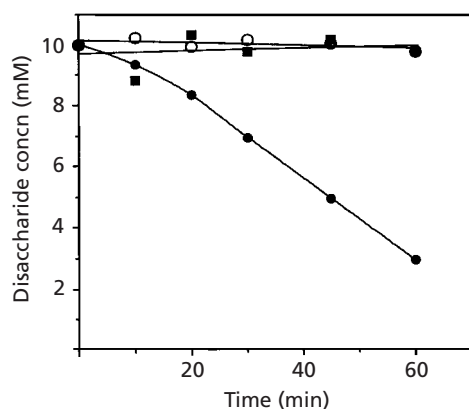


**Fig. 3.** Studies of the metabolism of sucrose and two of its isomers by sucrose-grown cells of *F. mortiferum*. Washed cells were resuspended, under anaerobic conditions, in buffered solution containing the disaccharides at an initial concentration of 10 mM. Samples were removed at intervals and residual disaccharide was determined by the enzymic assay of glucose produced by acid hydrolysis. ●, Sucrose; ○, turanose; ■, palatinose.

sequence of the regulatory gene, *aglR*, was compiled from our own work, together with data obtained from the Washington University (St Louis) sequencing project of the *K. pneumoniae* genome (<http://genome.wustl.edu>). The recently published genome sequence of enterohaemorrhagic *E. coli* O157:H7 (Perna *et al.*, 2001) revealed the same organization of the three genes (designated *yidP*, *glvA* and *glvG*) as described for *K. pneumoniae*. The amino acid sequence deduced from

**Table 2.** Expression of S6PH and FK during growth of *K. pneumoniae* on different sugars

Growth sugar	Enzyme specific activity	
	FK†	S6PH‡
Trehalulose*	69	289
Sucrose	103	247
Turanose*	64	342
Maltulose*	54	170
Leucrose*	51	184
Palatinose*	87	289
Maltose	15	29
Trehalose	3	ND
Melibiose	9	18
Cellobiose	2	6
Maltitol	1	3
Glucose	ND	2
Methyl $\alpha$ -D-glucoside	1	ND
Galactose	8	6

ND, No detectable activity.

\* Sucrose isomers.

† nmol fructose phosphorylated min<sup>-1</sup> (mg protein)<sup>-1</sup>.

‡ nmol sucrose hydrolysed min<sup>-1</sup> (mg protein)<sup>-1</sup>.

*yidP* of *E. coli* O157:H7 predicts a polypeptide of 238 residues that exhibits 91% overall identity with the 233 residues deduced by translation of the incomplete gene *aglR* of *K. pneumoniae*. At their N-termini, the products of *aglR* and *yidP* contain a helix–turn–helix (HTH)

A. Pikiš and others

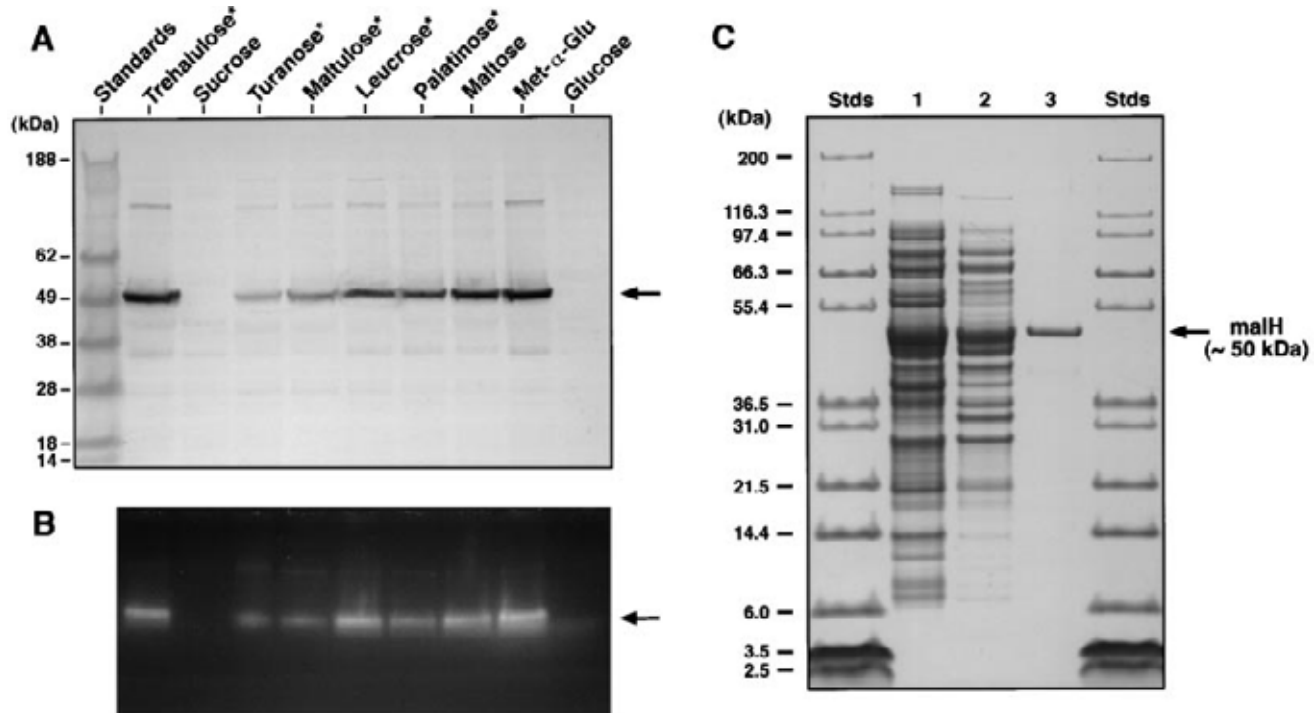


**Fig. 4.** Demonstration by PAGE of the expression, *in situ* activity, and purification of phospho- $\alpha$ -glucosidase (MalH) from *F. mortiferum*. (A) Immunodetection of MalH expression during growth of *F. mortiferum* on different sugars, by Western blotting using polyclonal antibody to MalH. Note the absence of immunoreactive polypeptide ( $\sim 50$  kDa, arrow) in the extract from sucrose-grown cells. (B) Zymogram demonstration of MalH activity in cell extracts by hydrolysis (arrow) of the fluorogenic substrate 4MU $\alpha$ G6P. Again, note the absence of fluorescence in the lane containing the extract from sucrose-grown cells. (C) Purification and determination of the molecular mass of MalH. Samples from each of the three stages of purification were denatured, and polypeptides were resolved by SDS-PAGE: lane 1, dialysed high-speed supernatant; lane 2, TrisAcryl M-DEAE; lane 3, purified MalH (molecular mass  $\sim 50$  kDa) obtained by AcA-44 gel filtration chromatography. The asterisks in panel A indicate sucrose isomers.

motif that assigns the two proteins to the GntR family of transcriptional regulators. The complete sequence of the phospho- $\alpha$ -glucosidase gene (*malH*) of *F. mortiferum*, together with a partial sequence for the gene (*malB*), were described in an earlier report (Bouma *et al.*, 1997). The entire sequences for *malB*, and the upstream gene (*malR*), have now been obtained by chromosome 'walking' (GenBank accession no. U81185). Translation of *malR* predicts a 106-residue polypeptide that shows extensive homology with the 13 members of the UPF0087 family of regulatory proteins.

#### Sequence alignment of phospho- $\alpha$ -glucosidase and EII(CB) proteins

Alignment of the amino acid sequences predicted for the phospho- $\alpha$ -glucosidase(s) and EIIs reveals a high degree of similarity among these proteins (data not shown). MalH from *F. mortiferum* exhibits  $\sim 75\%$  residue identity with the phosphoglucosyl hydrolase(s) from *E. coli* O157:H7 and *K. pneumoniae*. The EII(CB) transport protein of *F. mortiferum* (MalB) shows  $\sim 60\%$  amino acid identity throughout its length with GlvA and AglA in *E. coli* O157:H7 and *K. pneumoniae*, respectively. For the two enteric species, phospho- $\alpha$ -gluc-

osidase and EII(CB) proteins exhibit overall identities of 89% and 81%, respectively. By sequence-based alignment (Henrissat, 1991) and signature pattern (P-X-[SA]-X-[LIVMFY](2)-[QN]-X(2)-N-P-X(4)-[TA]-X(9,10)-[KRD]-X-[LIV]-[GN]-X-C), the three phospho- $\alpha$ -glucosidases can be assigned to family 4 of glycosylhydrolases (see <http://www.expasy.ch/cgi-bin/lists?glycosid.txt> and <http://afmb.cnrs-mrs.fr/~cazy/CAZY/index.html>). By their composition and modular structure, proteins MalB, GlvA and AglA, can be assigned to the EII<sup>Glc/Ser</sup> family of PTS transporters (Lengeler *et al.*, 1994; Lanz & Erni, 1998).

#### Growth studies with *F. mortiferum*, *K. pneumoniae* and *E. coli* O157:H7

Growth studies were performed to determine if possession of the putative operons would permit growth of the three organisms on sucrose isomers and other  $\alpha$ -glucosides. Both *K. pneumoniae* and *F. mortiferum* showed excellent growth on all sugars tested, including glucose, fructose, methyl  $\alpha$ -glucoside, maltose, maltitol, sucrose and all five  $\alpha$ -D-glucosyl-D-fructoses. *E. coli* O157:H7 grew well on glucose, fructose, maltose and



sucrose, but the pathogen was unable to grow on methyl  $\alpha$ -glucoside, maltitol or any of the sucrose isomers.

### Enzyme expression during growth of *F. mortiferum* on sucrose and its isomers

S6PH and ATP-dependent fructokinase (FK) are induced by growth of *F. mortiferum* on sucrose (Robrish *et al.*, 1991; Thompson *et al.*, 1992). Because sucrose and its isomers comprise the same hexose moieties, it was of interest to determine whether sucrose-grown cells of *F. mortiferum* would also metabolize the isomeric compounds. As expected, sucrose-grown cells readily fermented sucrose, but there was no detectable metabolism of the five isomers, including palatinose and turanose (Fig. 3). Furthermore, whereas sucrose-grown cells of *F. mortiferum* contained high levels of S6PH and FK activity (Table 1), after growth on the isomers, the activities of the two enzymes were not significantly greater than the constitutive levels found in glucose- or fructose-grown cells. These findings contrast markedly with the high levels of S6PH and FK that are expressed during growth of *K. pneumoniae* on the isomeric compounds (Table 2).

### Phospho- $\alpha$ -glucosidase (MalH) is expressed during growth of *F. mortiferum* on sucrose isomers

From the results of fermentation studies and enzymic analyses (Fig. 3 and Table 1, respectively), it was evident that that dissimilation of the sucrose isomers by *F. mortiferum* was via a route that was separate from that encoded by the *scr* regulon. Because previous studies with *K. pneumoniae* (Thompson *et al.*, 2001a) showed that growth on the sucrose isomers induced high-level expression of phospho- $\alpha$ -glucosidase (AglB), the various cell extracts of *F. mortiferum* were accordingly assayed for phospho- $\alpha$ -glucosidase (MalH) activity (Table 1). Extracts prepared from organisms grown previously on the sucrose isomers and other  $\alpha$ -glucosides (e.g. maltose and methyl  $\alpha$ -glucoside) readily hydrolysed pNP- $\alpha$ -G6P (Table 1). However, there was no detectable hydrolysis of the chromogenic analogue by similarly prepared extracts from organisms grown on glucose, fructose or sucrose. The results of a Western blot (Fig. 4A), performed with polyclonal antibody to MalH, confirmed expression of the phospho- $\alpha$ -glucosidase (molecular mass  $\sim$  50 kDa) during growth on sucrose isomers and other  $\alpha$ -glucosides. Significantly, the immunoreactive protein (MalH) was not detectable in either sucrose- or glucose-grown cell extracts. The data presented in Fig. 4(B) established the co-identity of the immunoreactive polypeptide and the enzymically active protein. In this experiment, samples of the various cell extracts of *F. mortiferum* were electrophoresed under non-denaturing conditions, prior to *in situ* staining for phospho- $\alpha$ -glucosidase activity using the fluorogenic substrate 4-MU- $\alpha$ -G6P. The zymogram (Fig. 4B) yielded three significant results: (i) the intensely fluorescent aglycone (4-methylumbelliferone) was generated only

**Table 3.** Cofactor requirements for the hydrolysis of chromogenic substrates pNP- $\alpha$ -G6P and pNP- $\beta$ -G6P by purified MalH from *F. mortiferum*

Assay composition and procedures are described in Methods. NAD<sup>+</sup>, metal ions and chromogenic substrates were present at 1 mM final concentration. Hydrolysis rates, expressed as  $\mu$ mol pNP formed min<sup>-1</sup> (mg protein)<sup>-1</sup>, are the means of two determinations. ND, No detectable activity.

Additions to assay	Activity with chromogenic analogue:	
	pNP- $\alpha$ -G6P	pNP- $\beta$ -G6P
None	ND	ND
NAD <sup>+</sup>	0.11	0.08
Mn <sup>2+</sup>	1.61	1.19
NAD <sup>+</sup> + Mn <sup>2+</sup>	2.91	1.56
NAD <sup>+</sup> + Mg <sup>2+</sup>	0.39	0.16
NAD <sup>+</sup> + Ni <sup>2+</sup>	0.51	0.54
NAD <sup>+</sup> + Co <sup>2+</sup>	1.47	2.28

by those extracts that contained the immunoreactive protein (MalH); (ii) formation of a single zone of fluorescence (at the same migration distance in the gel) provided evidence for only one species of phospho- $\alpha$ -glucosidase in the extracts, and (iii) absence of fluorescence in lane 2 was consistent with the inability of *F. mortiferum* to express MalH during growth on sucrose.

### Purification, cofactor requirements, and substrate specificity of MalH

The data presented thus far (although suggestive), did not establish a functional role for MalH in dissimilation of the  $\alpha$ -D-glucosyl-D-fructoses by *F. mortiferum*. Clearly, it was necessary to purify MalH, and demonstrate hydrolysis of either free or phosphorylated derivatives of the isomers by the enzyme. To this end a plasmid (pCB4.11) containing the cloned *malH* gene under its own promoter (Bouma *et al.*, 1997) was transformed into *E. coli* strain PEP43. Importantly, the latter strain is deficient in all phospho- $\beta$ -glucosidase activities, and an extract of these cells is unable to hydrolyse the chromogenic substrate pNP- $\beta$ -G6P. Unexpectedly, after expression of MalH in *E. coli* PEP43(pCB4.11), the resultant cell extract caused the hydrolysis of both pNP- $\alpha$ - and pNP- $\beta$ -G6P. Hydrolysis of both compounds was observed throughout purification of MalH (Fig. 4C), and the same cofactors (divalent metal ion and NAD<sup>+</sup>) were required for cleavage of both chromogenic substrates by electrophoretically pure enzyme (Table 3). We conclude that a single protein (MalH) is responsible for the hydrolysis of the two stereomers, pNP- $\alpha$ -G6P and pNP- $\beta$ -G6P. Studies of substrate specificity revealed that neither purified MalH, nor extracts prepared from cells of *F. mortiferum* grown previously on the isomers, were

**Table 4.** Hydrolysis of phosphorylated sucrose isomers by MalH from *F. mortiferum*

Assay procedures are described in Methods. Phosphorylated compounds were present at a concentration of 2 mM. Enzyme activity is expressed as  $\mu\text{mol G6P formed min}^{-1} (\text{mg protein})^{-1}$ ; values are means of two determinations. ND, No detectable hydrolysis.

Disaccharide phosphate in assay	Specific activity
Trehalulose-6'P*	0.15
Sucrose-6P	ND
Turanose-6'P*	0.68
Maltulose-6'P*	0.40
Leucrose-6'P*	0.08
Palatinose-6'P*	0.11
Maltose-6'P	0.15
Cellobiose-6'P†	ND
Gentiobiose-6'P‡	ND

\* Sucrose isomers.

† Cellobiose: 4-O- $\beta$ -D-glucopyranosyl-D-glucopyranose.

‡ Gentiobiose: 6-O- $\beta$ -D-glucopyranosyl-D-glucopyranose.

able to hydrolyse the free (non-phosphorylated) forms of the isomeric compounds (data not shown). However, the 6'-O-phosphorylated derivatives of the five  $\alpha$ -D-glucosyl-fructoses were hydrolysed by MalH (Table 4), albeit at a rate considerably slower than that determined for the  $\alpha$ -linked chromogenic substrate, pNP- $\alpha$ -G6P. Significantly, sucrose 6-phosphate itself was not a substrate for MalH, and the enzyme also failed to hydrolyse  $\beta$ -O-linked phosphorylated disaccharides such as cellobiose 6'-phosphate and gentiobiose 6'-phosphate (Table 4).

## DISCUSSION

Here we report the metabolism of sucrose isomers by *F. mortiferum*, and provide insight into the enzymic and genetic basis for growth on these isomers. Presently, *F. mortiferum* and *K. pneumoniae* are the only organisms known to ferment the five  $\alpha$ -D-glucosyl-D-fructoses. Earlier we showed that MalH from *F. mortiferum* hydrolysed maltose 6'-phosphate (Thompson *et al.*, 1995), and now we provide evidence for the cleavage of the phosphorylated isomers of sucrose by this enzyme. The phospho- $\alpha$ -glucosidase gene (*malH*) is adjacent to the gene *malB*, whose now completed sequence predicts a polypeptide that in size, domain structure, and conserved motifs (GITE and CATRLR) is characteristic of an EII(CB) transporter of the PEP:PTS. Genes *malB* and *malH* are homologous to *aglA* and *aglB*, respectively, of *K. pneumoniae*. We suggest that the polypeptides encoded by these genetic elements are required for growth of *F. mortiferum* and *K. pneumoniae* on the isomers of sucrose and related  $\alpha$ -glucosides, including maltose. A common feature of these genetic units is the absence of a gene encoding a third (and usually sugar-specific) protein (EIIA) that is required for operation of

all PTS systems. Interestingly, both sucrose:PTS and trehalose:PTS operons in *Bacillus subtilis* also lack the expected EIIA genes and, for these systems, it is believed that EIIA<sup>Glc</sup> can serve as substitute (Sutrina *et al.*, 1990; Dahl, 1997). A similar cross-complementation may also occur between the EIIA<sup>Glc</sup> and EII(CB) proteins of *F. mortiferum* and *K. pneumoniae* to yield a functional  $\alpha$ -glucoside:PTS in these species.

Proteins encoded by the *scr* operons of *K. pneumoniae* and *F. mortiferum* are expressed during growth of both organisms on sucrose (Sprenger & Lengeler, 1988; Thompson *et al.*, 1992). Hydrolysis of sucrose 6-phosphate by S6PH yields G6P and fructose, and for *K. pneumoniae*, fructose is believed to be the inducer of the *scr* operon (Jahreis & Lengeler, 1993). Hydrolysis of the phosphorylated isomers by AgIB of *K. pneumoniae* also yields G6P and fructose, and formation of the latter ketohexose is consistent with the high levels of S6PH and FK present in cells grown on the isomers (Table 2). Surprisingly, similar studies with *F. mortiferum* showed that, for this organism, growth on the isomeric compounds did not induce significant expression of either S6PH or FK (Table 1). These findings explain why these cells were unable to metabolize sucrose, and additionally, the data point to sucrose 6-phosphate (rather than fructose) as the likely inducer of the *scr* operon in *F. mortiferum*.

## Substrate specificity and hydrolysis of chromogenic substrates by MalH

MalH is an oligomeric protein comprising four identical subunits (molecular mass  $\sim 50$  kDa) that, by sequence-based alignment, is assigned to family 4 of the glycosylhydrolase superfamily. As reported for other members of this unusual family, MalH is inherently unstable and Mn<sup>2+</sup> and NAD<sup>+</sup> are prerequisite cofactors for activity (Nagao *et al.*, 1988; Thompson *et al.*, 1998, 1999; Raasch *et al.*, 2000). Whether the nucleotide and metal ion fulfil catalytic or structural functions has not been ascertained for any member of family 4. Phosphorylation at O-6 of the glucosyl moiety of the isomers is necessary for substrate cleavage, and MalH is unable to hydrolyse the corresponding non-phosphorylated compounds. MalH is also exacting with respect to the  $\alpha$ -O linkage of its PTS-derived substrates (see below) and, because there is no detectable hydrolysis of  $\beta$ -O-linked stereoisomers such as cellobiose 6'-phosphate and gentiobiose 6'-phosphate (Table 4), the enzyme may reasonably be classified as a phospho- $\alpha$ -glucosidase. In this context, it is not clear why MalH should hydrolyse both pNP- $\alpha$ -G6P and pNP- $\beta$ -G6P with comparable efficiency (Table 3). Co-purification of MalH with a phospho- $\beta$ -glucosidase resident in the host (*E. coli* PEP43) can be discounted because of gene inactivation or crypticity, and analysis of the final preparation by SDS-PAGE provided evidence for only a single polypeptide. That the same cofactors should also be required for catalysis is further evidence that the same enzyme hydrolyses both  $\alpha$ - and  $\beta$ -forms of the chromogenic compound(s).

Unlike the phosphorylated sucrose isomers (where G6P is linked to a fructose moiety), the essential G6P moiety of the chromogenic substrates is attached to *p*-nitrophenol. Perhaps the aromatic aglycone exerts an effect (electron-withdrawing?) upon the *O*-linkage such that  $\alpha/\beta$  conformation is no longer a determinant of substrate specificity. It is of comparative interest to note that cellobiose-6-phosphate hydrolase (CelF) from *E. coli* is also a member of glycosylhydrolase family 4 (Thompson *et al.*, 1999). In contrast to MalH, this NAD<sup>+</sup>- and metal-dependent phospho- $\beta$ -glucosidase hydrolyses only pNP- $\beta$ -G6P.

### Molecular basis for substrate recognition by MalH

Sucrose 6-phosphate and its phosphorylated isomers are not commercially available, but all of these derivatives were recently prepared in our laboratory (Thompson *et al.*, 2001a). Studies of substrate specificity showed that whereas MalH hydrolysed all of the phosphorylated isomers, the enzyme failed to hydrolyse sucrose 6-phosphate itself. Insight into the molecular basis for this remarkable discrimination among potential substrates was gained by molecular dynamics simulations, which revealed the probable solution-state geometries of the various disaccharide phosphates (Thompson *et al.*, 2001b). Molecular dynamics simulations and determination of solvent-accessible surfaces indicate pronounced conformational differences between sucrose 6-phosphate and its five isomeric 6'-phosphates. By virtue of an interresidue water bridge between Glc-2-O $\cdots$ H<sub>2</sub>O $\cdots$ O-1-Fru, both sucrose and sucrose 6-phosphate assume a compact, globular shape in solution (Immel & Lichtenthaler, 1995; Thompson *et al.*, 2001b). This water bridge is not present in the 6'-phosphoglucosyl-fructoses and, in consequence, the phosphorylated isomers adopt a more linear (extended) molecular geometry. The specificity of MalH for the isomeric phosphates presumably reflects recognition by the enzyme's binding domain of both the shape and the molecular lipophilicity potential of the contact surfaces of these particular molecules (Thompson *et al.*, 2001b).

### Conclusions

Both *F. mortiferum* and *K. pneumoniae* readily metabolize the five isomers of sucrose. In contrast, *E. coli* O157:H7 (which grows well on sucrose) failed to grow on any of the isomeric compounds. These results were surprising, because this enterohaemorrhagic strain has three genes (*yidP*, *glvA* and *glvG*) whose organization and deduced amino acid sequences are virtually identical to those of *aglR*, *aglA* and *aglB*, respectively, in *K. pneumoniae*. Although contrary to expectation, the results obtained for *E. coli* O157:H7 were nevertheless important. First, the data established for *E. coli* O157:H7 (as for the other species), that the sucrose-PTS/S6PH pathway is neither induced by, nor does it provide a route for dissimilation of, sucrose isomers. Secondly, the data indicate that possession of genes encoding  $\alpha$ -glucoside-specific EII(CB) and phospho- $\alpha$ -

glucosidase (while necessary), may not be entirely sufficient for dissimilation of  $\alpha$ -D-glucosyl-D-fructoses by micro-organisms.

### ACKNOWLEDGEMENTS

We thank Carolyn L. Bouma for construction and provision of pCB4.11. We would like to thank Jack London and Edith C. Wolff for their review and constructive criticisms of this article. We express appreciation to Professor Frieder W. Lichtenthaler for his encouragement and interest in our investigation.

### REFERENCES

- Bouma, C. L., Reizer, J., Reizer, A., Robrish, S. A. & Thompson, J. (1997). 6-Phospho- $\alpha$ -D-glucosidase from *Fusobacterium mortiferum*: cloning, expression, and assignment to family 4 of the glycosylhydrolases. *J Bacteriol* **179**, 4129–4137.
- Chen, Y.-Y. M. & LeBlanc, D. J. (1992). Genetic analysis of *scrA* and *scrB* from *Streptococcus sobrinus* 6715. *Infect Immun* **60**, 3739–3746.
- Dahl, M. K. (1997). Enzyme II<sup>Glc</sup> contributes to trehalose metabolism in *Bacillus subtilis*. *FEMS Microbiol Lett* **148**, 233–238.
- Fouet, A., Arnaud, M., Klier, A. & Rapoport, G. (1987). *Bacillus subtilis* sucrose-specific enzyme II of the phosphotransferase system: expression in *Escherichia coli* and homology to enzymes II from enteric bacteria. *Proc Natl Acad Sci USA* **84**, 8773–8777.
- Henrissat, B. (1991). A classification of glycosyl hydrolases based on amino acid sequence similarities. *Biochem J* **280**, 309–316.
- Immel, S. & Lichtenthaler, F. W. (1995). Molecular modeling of saccharides. 7. The conformation of sucrose in water: a molecular dynamics approach. *Liebigs Ann Chem* 1925–1937.
- Jahreis, K. & Lengeler, J. W. (1993). Molecular analysis of two ScrR repressors and of a ScrR-FruR hybrid repressor for sucrose and D-fructose specific regulons from enteric bacteria. *Mol Microbiol* **9**, 195–209.
- Lanz, R. & Erni, B. (1998). The glucose transporter of the *Escherichia coli* phosphotransferase system. Mutant analysis of the invariant arginines, histidines, and domain linker. *J Biol Chem* **273**, 12239–12243.
- Lengeler, J. W., Jahreis, K. & Wehmeier, U. F. (1994). Enzymes II of the phosphoenolpyruvate-dependent phosphotransferase systems: their structure and function in carbohydrate transport. *Biochim Biophys Acta* **1188**, 1–28.
- Lichtenthaler, F. W. & Rönninger, S. (1990).  $\alpha$ -D-Glucopyranosyl-D-fructoses: distribution of furanoid and pyranoid tautomers in water, dimethyl sulphoxide, and pyridine. Studies on ketoses. Part 4. *J Chem Soc Perkin Trans 2*, 1489–1497.
- Lichtenthaler, F. W., Immel, S. & Kreis, U. (1991). Evolution of the structural representation of sucrose. *Starch/Stärke* **43**, 121–132.
- Loesche, W. J. (1986). Role of *Streptococcus mutans* in human dental decay. *Microbiol Rev* **50**, 353–380.
- Meadow, N. D., Fox, D. K. & Roseman, S. (1990). The bacterial phosphoenolpyruvate:glycose phosphotransferase system. *Annu Rev Biochem* **59**, 497–542.
- Minami, T., Fujiwara, T., Ooshima, T., Nakajima, Y. & Hamada, S. (1990). Interaction of structural isomers of sucrose in the reaction between sucrose and glucosyltransferases from mutans streptococci. *Oral Microbiol Immunol* **5**, 189–194.
- Nagao, Y., Nakada, T., Imoto, M., Shimamoto, T., Sakai, S., Tsuda, M. & Tsuchiya, T. (1988). Purification and analysis of the structure

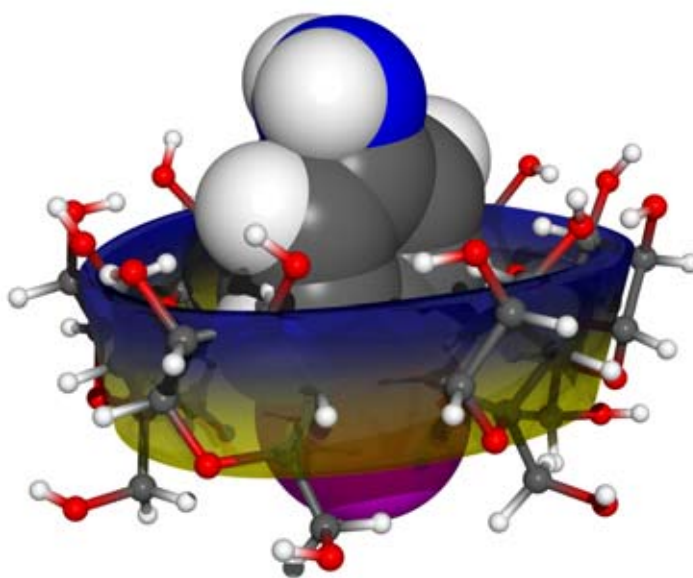
## A. Pikis and others

- of  $\alpha$ -galactosidase from *Escherichia coli*. *Biochem Biophys Res Commun* **151**, 236–241.
- Ooshima, T., Izumitani, A., Sobue, S., Okahashi, N. & Hamada, S. (1983). Non-cariogenicity of the disaccharide palatinose in experimental dental caries of rats. *Infect Immun* **39**, 43–49.
- Ooshima, T., Izumitani, A., Minami, T., Fujiwara, T., Nakajima, Y. & Hamada, S. (1991). Trehalulose does not induce dental caries in rats infected with mutans streptococci. *Caries Res* **25**, 277–282.
- Peltroche-Llacsahuanga, H., Hauk, C. J., Kock, R., Lampert, F., Lütticken, R. & Haase, G. (2001). Assessment of acid production by various human oral micro-organisms when palatinose or leucrose is utilized. *J Dent Res* **80**, 378–384.
- Perna, N. T., Plunkett, G., III, Burland, V. & 25 other authors (2001). Genome sequence of enterohaemorrhagic *Escherichia coli* O157:H7. *Nature* **409**, 529–533.
- Postma, P. W., Lengeler, J. W. & Jacobson, G. R. (1993). Phosphoenolpyruvate:carbohydrate phosphotransferase systems of bacteria. *Microbiol Rev* **57**, 543–594.
- Raasch, C., Streit, W., Schanzer, J., Bibel, M., Gosslar, U. & Liebl, W. (2000). *Thermotoga maritima* AglA, an extremely thermostable NAD<sup>+</sup>-, Mn<sup>2+</sup>-, and thiol-dependent  $\alpha$ -glucosidase. *Extremophiles* **4**, 189–200.
- Rauch, P. J. G. & deVos, W. M. (1992). Transcriptional regulation of the Tn5276-located *Lactococcus lactis* sucrose operon and characterization of the *sacA* gene encoding sucrose-6-phosphate hydrolase. *Gene* **121**, 55–61.
- Reid, S. J., Rafudeen, M. S. & Leat, N. G. (1999). The genes controlling sucrose utilization in *Clostridium beijerinckii* NCIMB 8052 constitute an operon. *Microbiology* **145**, 1461–1472.
- Robrish, S. A. & Thompson, J. (1990). Regulation of fructose metabolism and polymer synthesis by *Fusobacterium nucleatum* ATCC 10953. *J Bacteriol* **172**, 5714–5723.
- Robrish, S. A., Oliver, C. & Thompson, J. (1987). Amino acid-dependent transport of sugars by *Fusobacterium nucleatum* ATCC 10953. *J Bacteriol* **169**, 3891–3897.
- Robrish, S. A., Oliver, C. & Thompson, J. (1991). Sugar metabolism by fusobacteria: regulation of transport, phosphorylation, and polymer formation by *Fusobacterium mortiferum* ATCC 25557. *Infect Immun* **59**, 4547–4554.
- Schmid, K., Ebner, R., Altenbuchner, J., Schmitt, R. & Lengeler, J. (1988). Plasmid-mediated sucrose metabolism in *Escherichia coli* K12: mapping of the *scr* genes of pUR400. *Mol Microbiol* **2**, 1–8.
- Slee, A. M. & Tanzer, J. M. (1979). Phosphoenolpyruvate-dependent sucrose phosphotransferase activity in *Streptococcus mutans* NCTC 10449. *Infect Immun* **24**, 821–828.
- Sprenger, G. A. & Lengeler, J. W. (1988). Analysis of sucrose catabolism in *Klebsiella pneumoniae* and in Scr<sup>+</sup> derivatives of *Escherichia coli* K12. *J Gen Microbiol* **134**, 1635–1644.
- St Martin, E. J. & Wittenberger, C. L. (1979). Characterization of a phosphoenolpyruvate-dependent sucrose phosphotransferase system in *Streptococcus mutans*. *Infect Immun* **24**, 865–868.
- Sutrina, S. L., Reddy, P., Saier, M. H., Jr & Reizer, J. (1990). The glucose permease of *Bacillus subtilis* is a single polypeptide chain that functions to energize the sucrose permease. *J Biol Chem* **265**, 18581–18589.
- Tangney, M., Rouse, C., Yazdani, M. & Mitchell, W. J. (1998). Sucrose transport and metabolism in *Clostridium beijerinckii* NCIMB 8052. *J Appl Microbiol* **84**, 914–919.
- Thompson, J. & Chassy, B. M. (1981). Uptake and metabolism of sucrose by *Streptococcus lactis*. *J Bacteriol* **147**, 543–551.
- Thompson, J., Nguyen, N. Y., Sackett, D. L. & Donkersloot, J. A. (1991). Transposon-encoded sucrose metabolism in *Lactococcus lactis*. Purification of sucrose-6-phosphate hydrolase and genetic linkage to N<sup>5</sup>-(L-1-carboxyethyl)-L-ornithine synthase in strain K1. *J Biol Chem* **266**, 14573–14579.
- Thompson, J., Nguyen, N. Y. & Robrish, S. A. (1992). Sucrose fermentation by *Fusobacterium mortiferum* ATCC 25557: transport, catabolism, and products. *J Bacteriol* **174**, 3227–3235.
- Thompson, J., Gentry-Weeks, C. R., Nguyen, N. Y., Folk, J. E. & Robrish, S. A. (1995). Purification from *Fusobacterium mortiferum* of a 6-phosphoryl-O- $\alpha$ -D-glucopyranosyl:6-phosphoglucohydrolase that hydrolyzes maltose 6-phosphate and related phospho- $\alpha$ -D-glucosides. *J Bacteriol* **177**, 2505–2512.
- Thompson, J., Pikis, A., Ruvinov, S. B., Henrissat, B., Yamamoto, H. & Sekiguchi, J. (1998). The gene *glvA* of *Bacillus subtilis* 168 encodes a metal-requiring, NAD(H)-dependent 6-phospho- $\alpha$ -glucosidase. Assignment to family 4 of the glycosylhydrolase superfamily. *J Biol Chem* **273**, 27347–27356.
- Thompson, J., Ruvinov, S. B., Freedberg, D. I. & Hall, B. G. (1999). Cellobiose-6-phosphate hydrolase (Celf) of *Escherichia coli*: characterization and assignment to the unusual family 4 of glycosylhydrolases. *J Bacteriol* **181**, 7339–7345.
- Thompson, J., Robrish, S. A., Pikis, A., Brust, A. & Lichtenthaler, F. W. (2001a). Phosphorylation and metabolism of sucrose and its five linkage-isomeric  $\alpha$ -D-glucosyl-D-fructoses by *Klebsiella pneumoniae*. *Carbohydr Res* **331**, 149–161.
- Thompson, J., Robrish, S. A., Immel, S., Lichtenthaler, F. W., Hall, B. G. & Pikis, A. (2001b). Metabolism of sucrose and its five linkage-isomeric  $\alpha$ -D-glucosyl-D-fructoses by *Klebsiella pneumoniae*: participation and properties of sucrose-6-phosphate hydrolase and phospho- $\alpha$ -glucosidase. *J Biol Chem* **276**, 37415–37425.
- Titgemeyer, F., Jahreis, K., Ebner, R. & Lengeler, J. W. (1996). Molecular analysis of the *scrA* and *scrB* genes from *Klebsiella pneumoniae* and plasmid pUR400, which encode the sucrose transport protein enzyme II<sup>Ser</sup> of the phosphotransferase system and a sucrose-6-phosphate invertase. *Mol Gen Genet* **250**, 197–206.
- Van Houte, J. (1994). Role of microorganisms in caries etiology. *J Dent Res* **73**, 672–681.
- Ziesnitz, S. C., Siebert, G. & Imfeld, T. (1989). Cariological assessment of leucrose [D-glucopyranosyl- $\alpha$ (1-5)-D-fructopyranose] as a sugar substitute. *Caries Res* **23**, 351–357.

Received 3 September 2001; revised 5 November 2001; accepted 8 November 2001.

## Chapter 9

### Molecular Graphics



*MolArch*<sup>+</sup> - Molecular Architecture Modelling Program  
S. Immel,  
<http://caramel.oc.chemie.tu-darmstadt.de/immel/>.



## ***MolArch*<sup>+</sup> - Molecular Architecture Modelling Program**

S. Immel, <http://caramel.oc.chemie.tu-darmstadt.de/immel/>.

Many of the experimental and molecular modelling studies described in the preceding Chapters of this work required highly specific, computer-assisted tools for processing and visualizing molecular data. For this purpose, the preliminary *Molecular Architecture Modelling Program MolArch*<sup>+</sup><sup>[1]</sup> has been developed for analyzing geometries of molecular structures and generating high-quality color graphics and animations. Main emphasis has been put on the possibility to automatically process large numbers of structure files and molecular configurations without the need to manually intervene at each step. The basic idea was to provide tools for the efficient and fast visualization, particularly including the animation of molecular ensembles from pre-computed data for the purpose of scientific and educational presentations.

Besides basic graphical representations, *MolArch*<sup>+</sup> was designed to visualize at low-cost advanced objects such as atomic ellipsoids, non-protein ribbon models, molecular surfaces, and 3D-grid based properties with modes that are not available with other programs, or which have only become available latter with expensive commercial applications. In an effort to not copy computational procedures such as molecular mechanics (MM) and molecular dynamics (MD), *MolArch*<sup>+</sup> provides interfaces or shared file formats for data exchange with numerous applications used for molecular modelling (structure generation and optimization) and crystallography. Although numerous programs for the computation of molecular properties are available for *UNIX* and *LINUX* operating systems, there is still a need for visualization software on these computers. Of particular importance was the use of highest-quality color graphics provided by external ray-tracing programs without restrictions on the resolution of the final graphics. All display parameters and settings used by *MolArch*<sup>+</sup> had to be user-definable in order to provide a highly versatile visualization tool.

This Chapter briefly describes the options offered by *MolArch*<sup>+</sup> software package (current version *v7.50 24.Nov.2003*), and provides some examples of various types of molecular graphics that can be generated.<sup>[1]</sup>

### **Technical Notes**

The *MolArch*<sup>+</sup> program is written almost completely in *FORTRAN* with some minor parts in *C*, containing about 125,000 lines of source code. The program was designed for *LINUX* computer systems and was tested on *RedHat* and *SuSe* distributions of this operating system (releases 7.x or latter), but may also be used with other *LINUX* distributions; it has also been exported to *SGI (IRIX)* and *IBM (AIX)* machines. *MolArch*<sup>+</sup> only features a very simple graphics display based on the

VOGLE (“*Very Ordinary Graphics Library*”) interface without graphical menus, but a powerful command line. All commands and options may be entered in abbreviated form via this command line, or may be specified directly on the controlling shell console. The advantages of this design are full batch processing capabilities and the possibility to automatically carry out recurring tasks on large ensembles of molecular structure files.

## Supported File Types and External Modules

Molecular structures, and related objects may be imported or exported by MolArch<sup>+</sup> through a large variety of different file formats. The following list provides an overview on the most important file types supported (file name extensions in parenthesis):

- *Protein Data Bank*<sup>[2]</sup> (PDB) files as the most commonly used file type for molecular structures.
- Files used by the force-field programs *PIMM*<sup>[3]</sup> (EIN, OPT), *MacroModel*<sup>[4]</sup> (OUT, MAC), *CHARMm*<sup>[5]</sup> (RST, DCD), and *HyperChem*<sup>[6]</sup> (HIN).
- *Crystallographic Information Files*<sup>[7]</sup> (CIF) and *ShellX*<sup>[8]</sup> (INS) data files of solid-state structures of organic and inorganic compounds.
- Crystal structure data files exported from the data base maintained by the *Cambridge Crystallographic Data Centre*<sup>[9]</sup> (CCDF, FDAT file type); file type used by the crystallographic programs *Conquest*<sup>[10]</sup> and *Mercury*.<sup>[11]</sup>
- *Spartan*<sup>[12]</sup> and *Gaussian*<sup>[13]</sup> output files (including atomic charges); for *Gaussian* 3D-grid and density properties (electron densities, molecular orbitals, potential data, etc.) can be imported from the cube grid files (CUB).
- Various MolArch<sup>+</sup> specific file formats for molecular structures, surfaces, related objects, and script (batch) processing files.

MolArch<sup>+</sup> also includes interfaces to the following external programs and modules:

- Interface to the force-field program *PIMM*<sup>[3]</sup> for the energy optimization of geometries of organic structures.
- *MolCont*<sup>+[14]</sup> program for 2D- and 3D-contouring for orthogonal and polar coordinate data sets.
- *MolSurf*<sup>+[15]</sup> script for the generation of Hirshfeld- (crystal packing)<sup>[16]</sup> and Connolly-type (contact and solvent-accessible)<sup>[17]</sup> molecular surfaces and surface mapped properties; molecular surfaces can be triangulated by modified procedures based on algorithms described by Brickmann et al.<sup>[18]</sup>
- *MolGrid*<sup>+[19]</sup> program for the generation adiabatic energy potential surfaces by the method of “prudent ascent”<sup>[20]</sup> using the force-field program *PIMM*.
- *MolSymm*<sup>+[21]</sup> program and external module<sup>[22]</sup> for the analysis of molecular symmetry, symmetry elements, and point groups.
- *XFarbe*<sup>[23]</sup> program for the visualization of 2D-data sets; external module for finding maxima, minima, and saddle points on energy potential surfaces; external modules used by MolArch<sup>+</sup> for generating molecular geometries along reaction coordinates.
- *GnuPlot*<sup>[24]</sup> program for scientific plotting of data sets.

The programs *MolCont*<sup>+</sup> and *MolSymm*<sup>+</sup> are directly interfaced to MolArch<sup>+</sup>; the other programs mentioned may be used separately to process data.



## Geometry Analysis Options

The *MolArch*<sup>+</sup> program may be used for the analysis of a wide range of geometry parameters of molecular structures which are listed below:

- Standard interatomic distances and bond lengths, angles, torsion angles, as well as virtual angles and torsions between vectors.
- Puckering amplitudes of rings relative to least-squares (LSQ) best-fit mean ring planes and out-of-plane deviations.
- Tilt angles<sup>[25]</sup> between rings and LSQ-planes; flip angles<sup>[26]</sup> for out-of-plane deviations.
- Cremer-Pople parameters<sup>[27]</sup> for five-<sup>[28]</sup> and six-membered<sup>[29]</sup> rings (including the automatic detection of cyclopentane, cyclohexane, furanoid, and pyranoid ring conformations).
- $J^3_{\text{H-C-C-H}}$ <sup>[30]</sup> and  $J^3_{\text{C-O-C-H}}$ <sup>[31]</sup> NMR coupling constants.
- Automatic detection of Cahn-Ingold-Prelog (*R/S*) stereo descriptors for tetrahedral centers, bond-orders (single, double, triple, and quadruple bonds), aromaticity (for rings), and of hydrogen-bonds and their geometry parameters (including symmetry descriptors for crystal structures).
- Molecular shape parameters such as mean-radius of rings, radius of gyration, circularity and asphericity<sup>[16]</sup> (for both molecular structures and surfaces).
- Molecular connectivity indices<sup>[32]</sup> ( $\chi$ ) of various order.
- Least-squares 3D-fitting<sup>[33]</sup> and superimposition of series of molecules or molecular fragments (sub-structures) with different weighting schemes.

Most geometry parameters can be manipulated and reset to user defined values (distances, angles, torsions, tilt and flip angles, puckering, etc.) in the structure editing section of *MolArch*<sup>+</sup>; atom types and names can be changed. All methods related to molecular geometries (analysis and manipulation) can be applied to single molecules or series of molecular configurations with the option of automated averaging of data sets. Most notably, *MolArch*<sup>+</sup> offers the possibility to simultaneously manipulate or analyze and average geometry parameters of similar or identical (symmetry related) molecular fragments in automated procedures.

## Visualization and Molecular Graphics

All molecular graphics contained within this work have been generated using *MolArch*<sup>+</sup>. Although *MolArch*<sup>+</sup> features a simple graphics display only, the program is fully interfaced to produce highest-quality color models with the *POVRAY* (“*Persistence of Vision*”)<sup>[34]</sup> ray-tracing program or any *VRML* (“*Virtual Reality Modelling Language*” for 3D molecular models)<sup>[35]</sup> viewing program. The latter option is of particular use in the process of presenting 3D-structures on the internet with the possibility of rotating and modifying these options on the client side. A large number of different viewing modes is available, and almost all display parameters may be modified via user specific settings. Figure 1 provides a overview on the various modes of visualization that are available with *MolArch*<sup>+</sup>; many more examples can be found in the original publications in the preceding Chapters of this work.

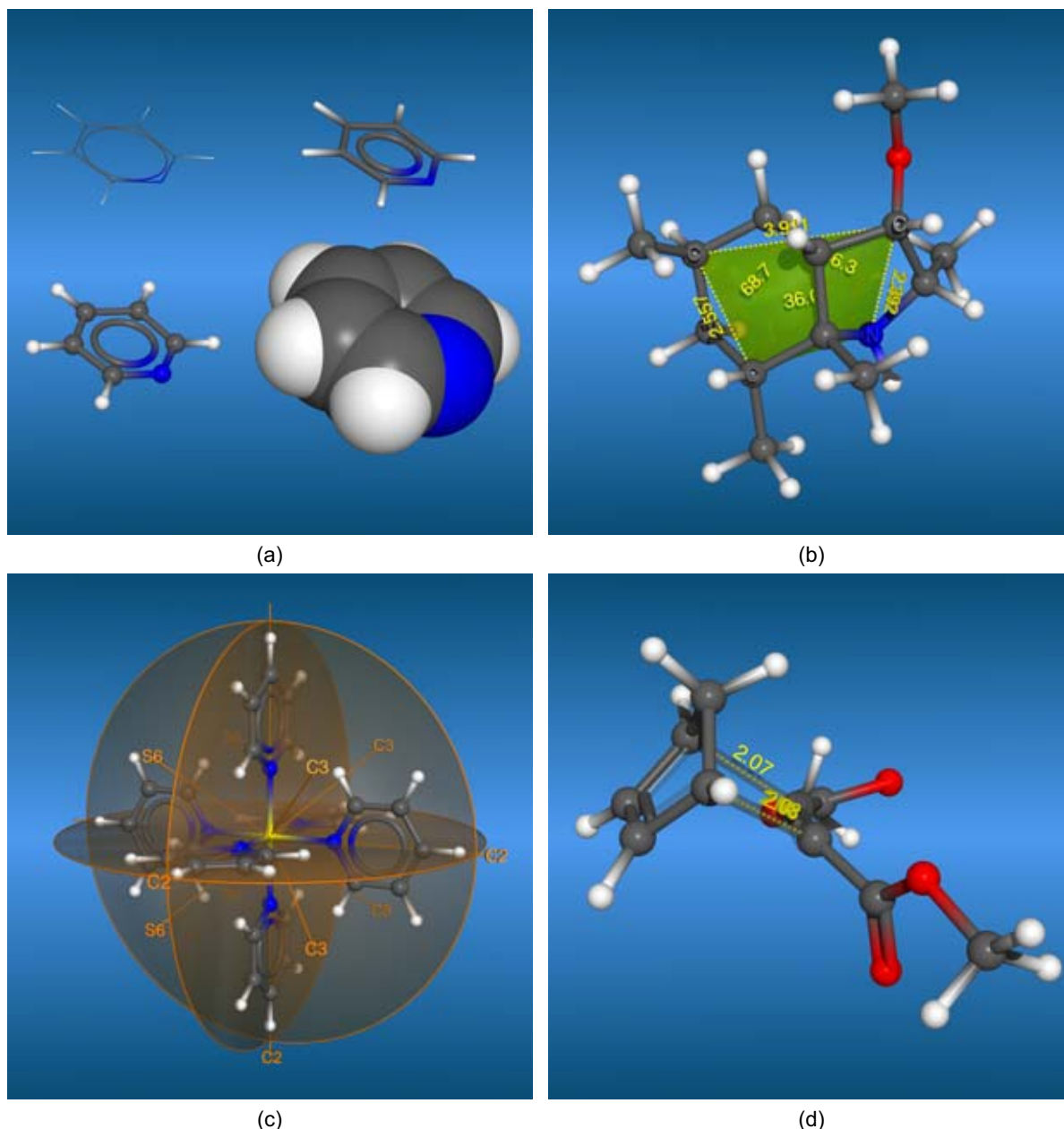
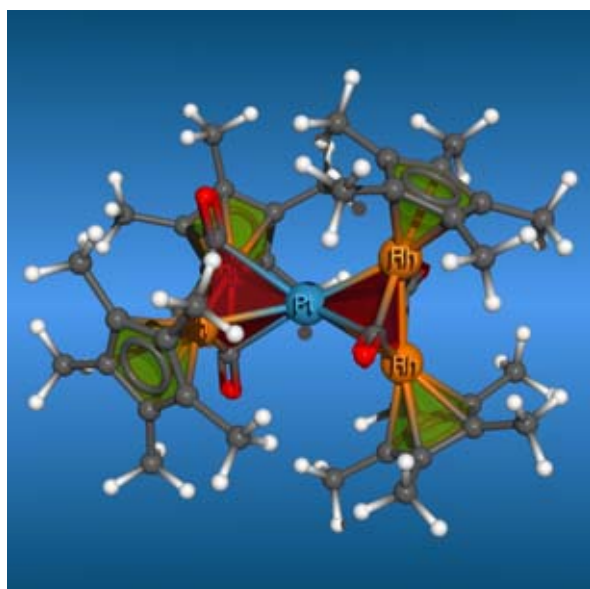
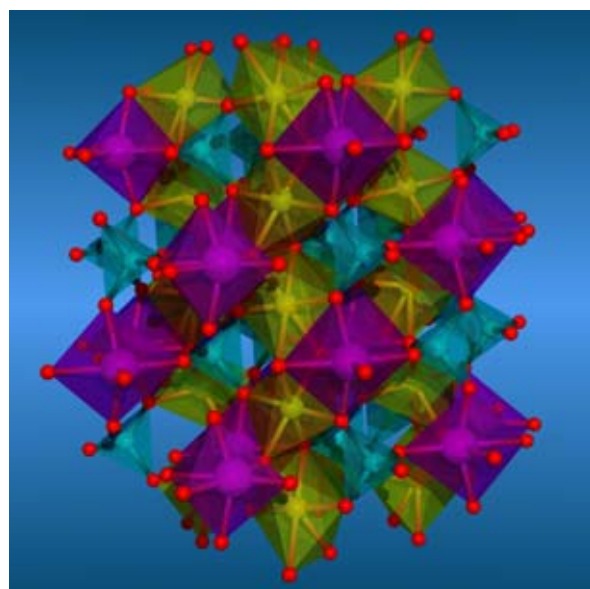


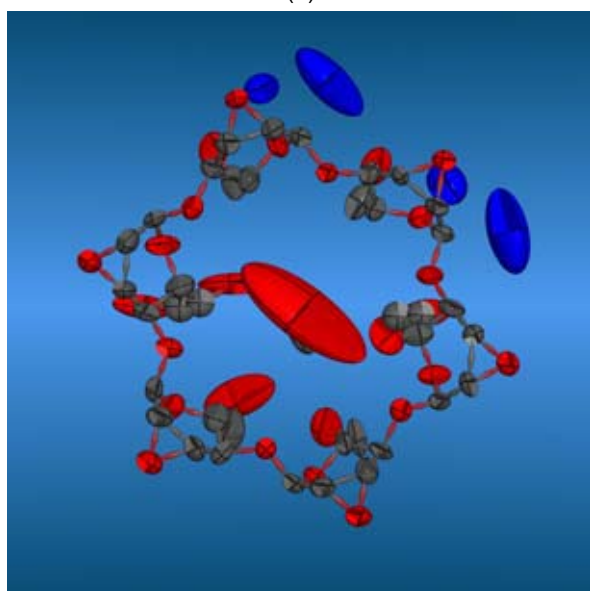
Figure 1 (continued on the next pages). Various examples for original molecular graphics generated using MolArch<sup>+</sup>; all models were finally rendered using the POV-Ray ray-tracing program. – (a) Basic modes for the representation of structures (wire, capped-stick, ball-and-stick, and CPK-type models of pyridine); – (b) Labeling of selected geometry parameters in molecular structures (distances, angles, and virtual torsion angles of a  $\beta$ -turn mimeticum); – (c) Symmetry elements (center of inversion  $i$ , mirror planes,  $C_n$  rotary and  $S_n$  rotary reflection axes) for molecular geometries ( $[\text{Fe}(\text{Pyr})_6]^{2+}$ , point group  $T_h$ ); – (d) Transition state modelling with semi-transparent bonds (Diels-Alder reaction of cyclopentadiene with acetylene dicarboxylic acid dimethyl ester); – (e) Molecular geometry and coordination polyhedra of organometallic structures (trigonal-bipyramids and pentagonal-pyramids in the structure of  $\text{PtRh}_4(\text{CO})_4(\text{Cp}^*)_4$ ); – (f) Inorganic solid-state structures and coordination polyhedra (tetrahedrons and octahedrons for  $\text{CuInOPO}_4$ ); – (g) Anisotropic thermal ellipsoids of crystal structures (X-ray structure of per-2,3-anhydro- $\alpha$ -cyclomannin methanol hydrate); – (h) Crystal structures including transparent Hirshfeld surfaces visualizing the mode of molecular packing (two unit cells for the low-temperature solid-state structure of acetylene); – (i) Molecular surfaces with color-coded mapped properties (molecular electrostatic potential of benzene); – (j) Clipped surfaces (benzene, surface clipped at iso-contour values of the electrostatic potential); – (k) Solid iso-electron-density models of molecular orbitals (HOMO of salicylic acid computed using *Gaussian*); – (l) Transparent models of molecular orbitals (LUMO of salicylic acid, the transparency was adjusted according to the computed electron density); – (m+n) Ribbon models (structure of T3R3 human insulin and bacterial ribonuclease P RNA with solid-ring representation of the base pairs); – (o) Visualization of 3D-grid based densities and properties of molecules using transparent iso-density contours (molecular dynamics derived relative water densities around  $\alpha$ -cyclodextrin providing a view on the hydration shell of this compound in aqueous solution); – (p) Display of grid properties and potentials with excluded volumes defined by molecular surfaces (electrostatic potential of salicylic acid); – For additional examples see all Figures in the preceding Chapters of this work or the MolArch<sup>+</sup> website.<sup>[1]</sup>



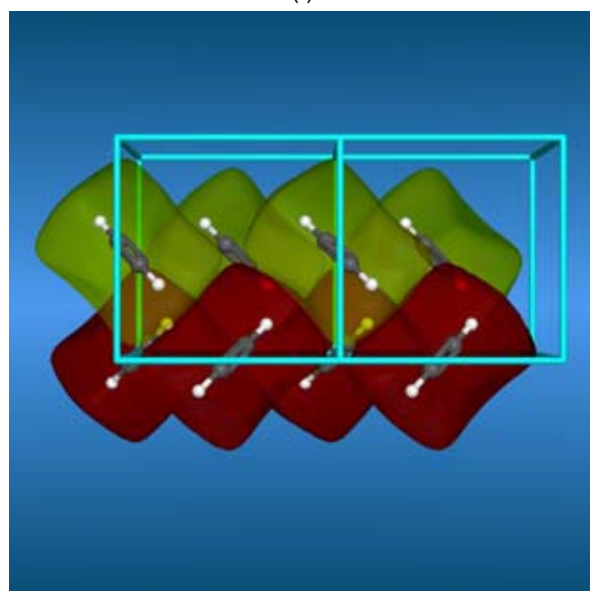
(e)



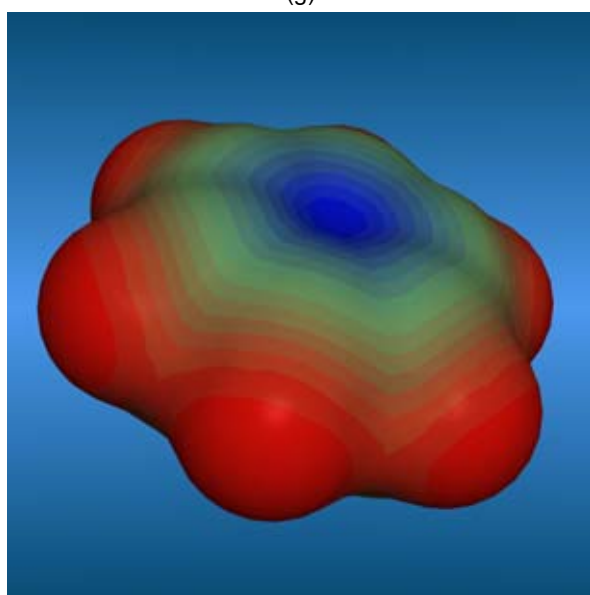
(f)



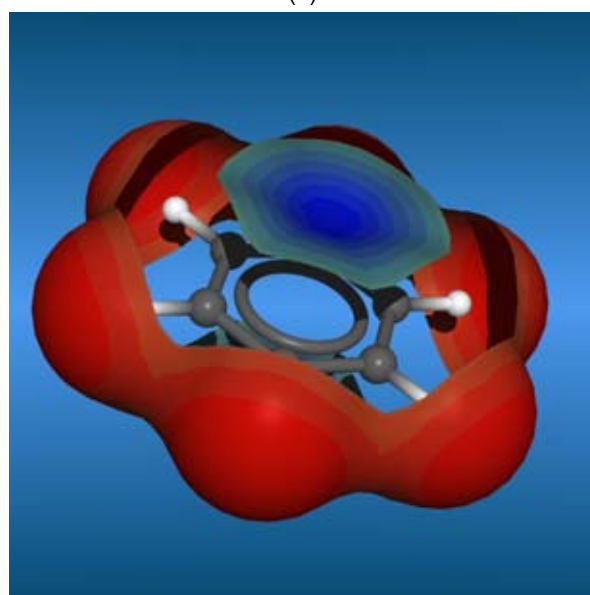
(g)



(h)



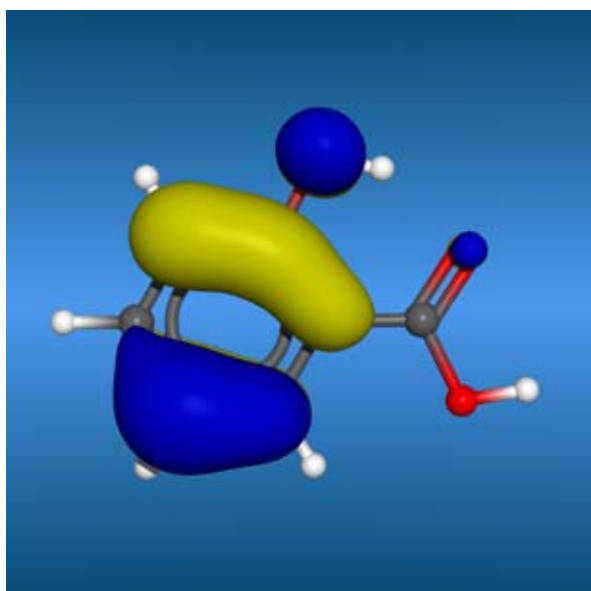
(i)



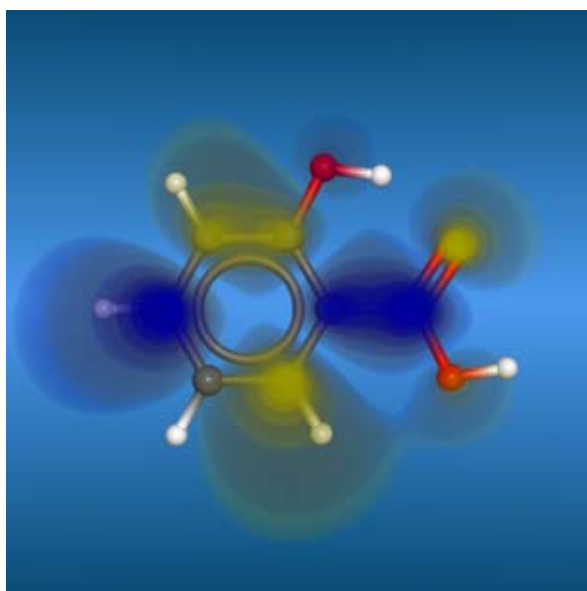
(j)

Figure 1 (continued from previous page).

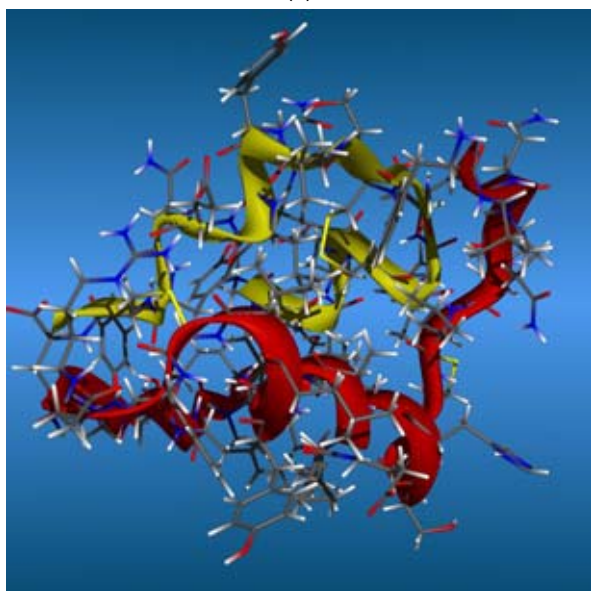
(continued on next page)



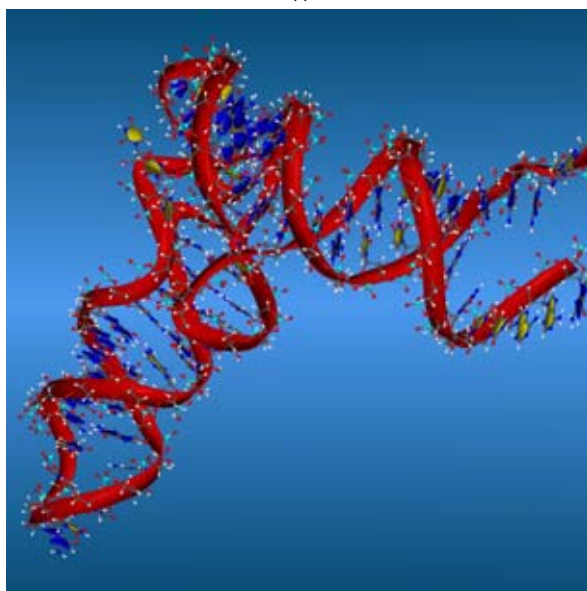
(k)



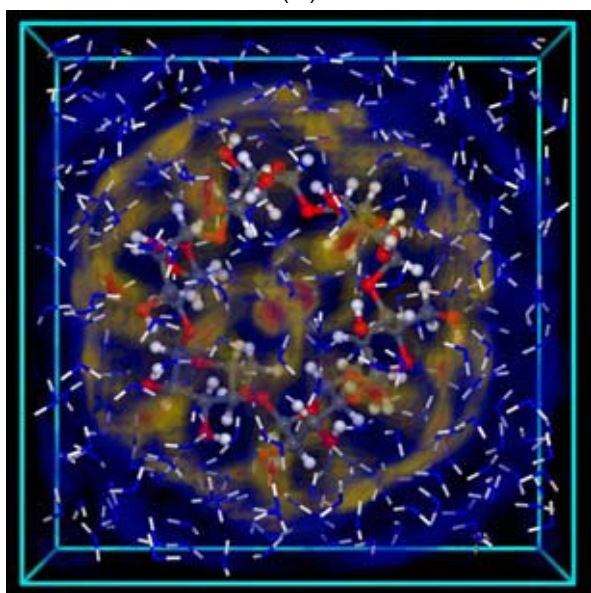
(l)



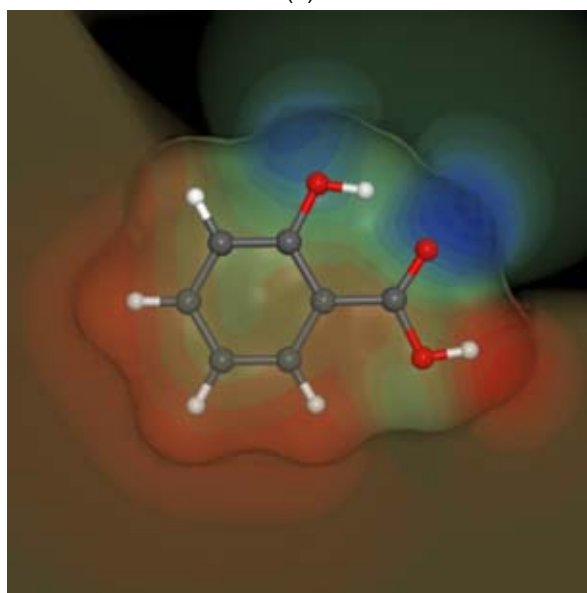
(m)



(n)



(o)



(p)

Figure 1 (continued from previous page).

Among the possibilities offered by *MolArch*<sup>+</sup> are the following modes of visualization:

- Organic and inorganic molecular structures with different modes of display (wire-, capped-, ball-and-stick-, and CPK-type molecular models), including the visualization of bond orders (single to quadruple bonds) and aromaticity (ring type visualization instead of successions of double bonds; Fig. 1a).
- Selected bond distances, angles, torsions, planes, and other geometry descriptors (Fig. 1b).
- Symmetry elements of molecules (center of inversion *i*, mirror planes  $\sigma$ ,  $C_n$  rotary and  $S_n$  rotary reflection axes; Fig. 1c).
- Transition state geometries with transparent bonds (Fig. 1d).
- Coordination polyhedra including tetrahedrons, octahedrons, cubes, dodecahedrons, icosahedrons, truncated icosahedrons, prisms, pyramids (square, pentagonal, and hexagonal), and trigonal bi-pyramids (Fig. 1e-f).
- Atom types (labels) and names, as well as atom mapped (color-coded) properties.
- *ORTEP*<sup>[36]</sup> style thermal isotropic and anisotropic ellipsoids (Fig. 1g).
- Crystal structures including unit cells (Fig. 1h).
- Molecular surfaces (Connolly-, solvent-accessible-, and Hirshfeld-type surfaces) in dotted and solid form with various modes of color-coded display of surface related (mapped) properties, surfaces can be colored, sliced, and clipped independently, including the possibility to display transparent or opaque surface models (Fig. 1h-j).
- Molecular and atomic (schematic) orbitals (*Molden*<sup>[37]</sup> style display; Fig. 1k-l).
- Ribbon models of arbitrary (including non-protein) structures (Fig. 1m-n).
- 3D-grid and density data (Fig. 1o-p).

Options are included to generate series of molecular images for large sets of molecular configurations along reaction coordinates or molecular dynamics simulations, offering the possibility to generate animations on chemical reactions, molecular dynamics, and molecular recognition processes.

The command line interface and the batch-processing capabilities make *MolArch*<sup>+</sup> a highly versatile tool for the visualization, animation, and automated geometry analysis of a wide range of molecular scenarios. The *MolArch*<sup>+</sup> website includes additional archives of molecular graphics generated in the course of the studies described in this work. In addition, a variety of educational courses with *MolArch*<sup>+</sup> generated graphics and animations on this site are aimed at basic and advanced students of organic chemistry. Examples include the structure, symmetry, and chirality of organic molecules; animations on various basic reaction mechanisms of organic chemistry are provided (Cope and Claisen-rearrangement and degenerate versions thereof, Diels-Alder reactions, sigmatropic ring-opening and ring-closure mechanisms,  $S_N1$  and  $S_N2$  reaction, bromination of alkenes, and various conformational rearrangements; see also Fig. 2).

In total, *MolArch*<sup>+</sup> is a highly useful program for the analysis and visualization of molecular structures for scientific and educational purposes.<sup>[1]</sup>

Dr. Stefan Inzelt

Technische Universität Darmstadt

Label News: MolArch+ available for Download now

Publications | Graphics | Structures | Courses | Research | Curriculum Vitae | Miscellaneous

### Crown Acetals

Comparison of the cyclodextrin derived crown acetals with 30-crown-12, 35-crown-14, and 40-crown-16 skeletal backbones (all X-ray crystal structures)

**Crown Acetals**  $\text{cyclo}[-\text{CH}(\text{CH}_2\text{OAc})-\text{CH}(\text{CH}_2\text{OAc})-\text{O}-\text{CH}(\text{CH}_2\text{OAc})-\text{O}-]_n$  with  $n = 5-9$

#### 30-Crown-12 Hexaacetal

Grid of molecular models for 30-crown-12 hexaacetal structures, including 3D ball-and-stick models and 2D surface models.

#### 35-Crown-14 Heptaacetal

Grid of molecular models for 35-crown-14 heptaacetal structures, including 3D ball-and-stick models and 2D surface models.

Dr. Stefan Inzelt

Technische Universität Darmstadt

Label News: MolArch+ available for Download now

Publications | Graphics | Structures | Courses | Research | Curriculum Vitae | Miscellaneous

### MOLEcular ARCHitecture - MolArch+ Movies

This page gives an overview on different types of molecular animations that were generated using the MolArch+ program.

- Racemization of [8]helicene

#### Racemization of [8]helicene

Helicenes are benzologues of phenanthrene. With four or more rings (tetrahelicene, or [4]helicene) the compounds exist in two helical, enantiomeric forms, with  $C_2$  symmetry. Racemization experiments, carried out in the seventies, gave surprising results: not only did racemization occur at lower temperatures than expected from hardware models, the barriers even showed a tendency to level off for a higher number of rings. Calculations confirmed that for [4] to [8]helicene the racemization occurs via a  $C_2$  symmetric transition state (TS). For [8]helicene shown in the animations on the left, the energy barrier to racemization was measured as well as calculated calculated to amount to about 175 kJ/mol. Data and transition state structures were taken from <http://www.cmbi.kun.nl/~boekendrostr/video.html>.

For details see also R. H. Janke, G. Hauke, E.-U. Wüthwein, and J. H. Borkert, *J. Amer. Chem. Soc.* **1996**, *118*, 6031; and S. Gimme and S. D. Peyerimhoff, *Chem. Phys.* **1996**, *204*, 411.

Ball-and-Stick Models

CPK Models

Ribbon Models

Surface Models

© Copyright Dr. S. Inzelt  
Last updated: May 20, 2003

Figure 2. Examples for MolArch<sup>+</sup> generated graphics on the MolArch<sup>+</sup> website.<sup>[1]</sup> The top entry presents supporting graphics and information on current research projects (molecular geometries of cyclodextrin-derived crown acetals, for details see Chapter 6 of this work); on the bottom a webpage providing additional information on lectures for students is shown (MolArch<sup>+</sup> animations for the mechanism of the racemization of [8]helicene).

## References

- [1] S. Immel, *MolArch<sup>+</sup> - MOlecular ARCHitecture Modeling Program v7.50*, Technical University of Darmstadt, Germany, **2003**; additional *MolArch<sup>+</sup>* generated graphics can be found on the web site at <http://caramel.oc.chemie.tu-darmstadt.de/immel/>.
- [2] H. M. Berman, J. Westbrook, Z. Feng, G. Gilliland, T. N. Bhat, H. Weissig, I. N. Shindyalov, and P. E. Bourne, *Nucl. Acids. Res.* **2000**, *28*, 235-242; *PDB - Protein Data Bank*, Research Collaboratory for Structural Bioinformatics (RCSB); <http://www.rcsb.org/pdb/>.
- [3] A. E. Smith and H. J. Lindner, *Journal of Computer-Aided Molecular Design* **1991**, *5*, 235-262; H. J. Lindner, M. Kroeker, *PIMM - Closed Shell PI-SCF-LCAO-MO Molecular Mechanics Program*, Technical University of Darmstadt, Germany, **1995**; [http://www.oc.chemie.tu-darmstadt.de/alte\\_hp/lin/](http://www.oc.chemie.tu-darmstadt.de/alte_hp/lin/).
- [4] F. Mohamadi, N. G. J. Richards, W. C. Guida, R. Liskamp, M. Lipton, C. Caufield, G. Chang, T. Hendrickson, and W. C. Still, *Journal of Computational Chemistry* **1990**, *11*, 440-467; *MacroModel - Molecular Modelling Program*, Schrödinger, Inc., Portland, OR, USA; <http://www.schrodinger.com/Products/macromodel.html>.
- [5] B. R. Brooks, R. E. Bruccoleri, B. D. Olafson, D. J. States, S. Swaminathan, and M. Karplus, *J. Comput. Chem.* **1983**, *4*, 187-217; A. D. Mackerell, Jr., D. Bashford, R. L. Bellott, R. L. Dunbrack, Jr., J. D. Evanseck, M. J. Field, S. Fischer, J. Gao, H. Guo, S. Ha, D. Joseph-McCarthy, L. Kuchnir, K. Kuczera, F. T. K. Lau, C. Mattos, S. Michnick, T. Ngo, D. T. Nguyen, B. Prodhom, W. E. Reiher, III, B. Roux, M. Schlenkrich, J. C. Smith, R. Stote, J. Straub, M. Watanabe, J. Wiorkiewicz-Kuczera, D. Yin, and M. Karplus, *J. Phys. Chem. B* **1998**, *102*, 3586-3616; *CHARMM - Chemistry at HARvard Macromolecular Mechanics*, Accelrys Inc., Burlington, MA, USA, **2001-2003**; <http://www.accelrys.com/insight/charmm.html>.
- [6] *HyperChem - Molecular Modelling Program*, Hypercube, Inc., Gainesville, FL, USA; <http://www.hyper.com/>.
- [7] *CIF - Crystallographic Information File*, International Union of Crystallography (IUCr); <http://www.iucr.org/iucr-top/cif/>.
- [8] G. M. Sheldrick, *SHELX - Crystal Structure Determination from Single-crystal Diffraction Data*, University of Göttingen, Germany; <http://shelx.uni-ac.gwdg.de/>.
- [9] F. H. Allen, J. E. Davies, J. J. Galloy, O. Johnson, O. Kennard, C. F. Macrae, E. M. Mitchell, G. F. Mitchell, J. M. Smith, and D. G. Watson, *J. Chem. Inf. Comput. Sci.* **1991**, *31*, 187-204.
- [10] *ConQuest - Program for Searching and Retrieving Information from the Cambridge Structural Database (CSD)*, Cambridge Crystallographic Data Centre (CCDC), Cambridge, UK; <http://www.ccdc.cam.ac.uk/>.
- [11] *Mercury - Crystal Structure Visualisation and Exploration*, Cambridge Crystallographic Data Centre (CCDC), Cambridge, UK; <http://www.ccdc.cam.ac.uk/>.
- [12] *Spartan - Molecular Mechanics and Quantum Chemical Calculations*, Wavefunction, Inc., Irvine, CA, USA; <http://www.wavefun.com/>.
- [13] M. J. Frisch, G. W. Trucks, H. B. Schlegel, G. E. Scuseria, M. A. Robb, J. R. Cheeseman, V. G. Zakrzewski, J. A. Montgomery, R. E. Stratmann, J. C. Burant, S. Dapprich, J. M. Millam, A. D. Daniels, K. N. Kudin, M. C. Strain, O. Farkas, J. Tomasi, V. Barone, M. Cossi, R. Cammi, B. Mennucci, C. Pomelli, C. Adamo, S. Clifford, J. Ochterski, G. A. Petersson, P. Y. Ayala, Q. Cui, K. Morokuma, D. K. Malick, A. D. Rabuck, K. Raghavachari, J. B. Foresman, J. Cioslowski, J. V. Ortiz, B. B. Stefanov, G. Liu, A. Liashenko, P. Piskorz, I. Komaromi, R. Gomperts, R. L. Martin, D. J. Fox, T. Keith, M. A. Al-Laham, C. Y. Peng, A. Nanayakkara, C. Gonzalez, M. Challacombe, P. M. W. Gill, B. Johnson, W. Chen, M. W. Wong, J. L. Andres, C. Gonzalez, M. Head-Gordon, E. S. Replogle, J. A. Pople, *Gaussian - Electronic Structure Program*, Gaussian, Inc., Pittsburgh, PA, USA; <http://www.gaussian.com/>.
- [14] S. Immel, *MolCont<sup>+</sup> - 2D- and 3D-Contouring Program for Orthogonal and Polar Coordinate Data Sets v7.35*, Technical University of Darmstadt, Germany, **2003**; *MolCont<sup>+</sup>* is part of the *MolArch<sup>+</sup>* program package.
- [15] S. Immel, *MolSurf<sup>+</sup> - Program for the Generation of Triangulated Molecular Surfaces v7.35*, Technical University of Darmstadt, Germany, **2003**; *MolSurf<sup>+</sup>* is part of the *MolArch<sup>+</sup>* program package.

- [16] J. J. McKinnon, A. S. Mitchell, and M. A. Spackman, *Chem. Eur. J.* **1998**, *4*, 2136-2141.
- [17] B. Lee and F. M. Richards, *J. Mol. Biol.* **1971**, *55*, 379-400; F. M. Richards, *Ann. Rev. Biophys. Bioeng.* **1977**, *6*, 151-176; M. L. Connolly, *J. Appl. Crystallogr.* **1983**, *16*, 548-558; M. L. Connolly, *Science* **1983**, *221*, 709-713.
- [18] W. Heiden, M. Schlenkrich, and J. Brickmann, *J. Comp.-Aided Mol. Design* **1990**, *4*, 255-269; W. Heiden, T. Goetze, and J. Brickmann, *J. Comput. Chem.* **1993**, *14*, 246-250.
- [19] S. Immel, *MolGrid<sup>+</sup> - Program for the Generation of Adiabatic Energy Potential Surfaces v7.35*, Technical University of Darmstadt, Germany, **2003**; *MolGrid<sup>+</sup>* is part of the *MolArch<sup>+</sup>* program package.
- [20] R. W. W. Hooft, J. A. Kanters, and J. Kroon, *J. Comput. Chem.* **1991**, *12*, 943-947.
- [21] S. Immel, *MolSymm<sup>+</sup> - Program for the Analysis of Molecular Symmetry and Point Groups v7.35*, Technical University of Darmstadt, Germany, **2003**; *MolSymm<sup>+</sup>* is part of the *MolArch<sup>+</sup>* program package.
- [22] S. Pachkovsky, *symmetry.c - Brute Force Symmetry Analyzer*, **1996**;  
<http://bioinformatics.org/cgi-bin/cvsweb.cgi/ghemical/small-utilities/>.
- [23] A. Preusser, *XFarbe - Filled Contours with Bicubics - Visualization of 2D-Arrays and Finding Maxima, Minima, and Saddle Points*, Fritz-Haber-Institut of the Max-Planck Gesellschaft, Berlin, Germany; <http://www.fhi-berlin.mpg.de/~grz/pub/xfarbe.html>.
- [24] *GnuPlot - Scientific Plotting*; <http://www.gnuplot.info/>.
- [25] F. W. Lichtenthaler and S. Immel, *Liebigs Ann.* **1996**, 27-37.
- [26] S. Immel, G. E. Schmitt, and F. W. Lichtenthaler, *Carbohydr. Res.* **1998**, *313*, 91-105.
- [27] D. Cremer and J. A. Pople, *J. Am. Chem. Soc.* **1975**, *97*, 1354-1358.
- [28] G. A. Jeffrey and R. Taylor, *J. Comput. Chem.* **1980**, *1*, 99-109.
- [29] G. A. Jeffrey and J. H. Yates, *Carbohydr. Res.* **1979**, *74*, 319-322.
- [30] C. A. G. Haasnoot, F. A. A. M. D. Leeuw, and C. Altona, *Tetrahedron* **1980**, *36*, 2783-2792.
- [31] I. Tvaroska, *Carbohydr. Res.* **1989**, *189*, 359-362.
- [32] L. H. Hall and L. B. Kier, *Topol. Indices Relat. Descriptors QSAR QSPR* **1999**, 307-360; L. H. Hall and L. B. Kier, *J. Mol. Graphics & Modelling* **2001**, *20*, 4-18; L. B. Kier and L. H. Hall, *J. Mol. Graphics & Modelling* **2001**, *20*, 76-83.
- [33] D. J. Heisterberg, *QTRFIT - Rigid Body Rotation and Fitting Program*, The Ohio Supercomputer Center, Columbus, Ohio, USA, **1991**;  
<http://www.ccl.net/cca/software/SOURCES/FORTRAN/fitest/fitest.shtml>.
- [34] *POV-Ray - Persistence of Vision Raytracer v3.5*, Persistence of Vision Development Team;  
<http://www.povray.org/>.
- [35] H. Vollhardt, C. Henn, M. Teschner, and J. Brickmann, *J. Mol. Graphics* **1995**, *13*, 368-372.
- [36] M. N. Burnett, C. K. Johnson, *ORTEP-III - Oak Ridge Thermal Ellipsoid Plot Program for Crystal Structure Illustrations*, Oak Ridge National Laboratory, Oak Ridge, TN, USA;  
<http://www.ornl.gov/ortep/>.
- [37] G. Schaftenaar and J. H. Noordik, *J. Comput.-Aided Mol. Des.* **2000**, *14*, 123-134; G. Schaftenaar, *MOLDEN - A Pre- and Post-processing Program of Molecular and Electronic Structure*, Centre for Molecular and Biomolecular Informatics, University of Nijmegen, Nijmegen, Netherlands; <http://www.cmbi.kun.nl/~schaf/molden/molden.html>.



## Conclusion



## Concluding Remarks

Within this work, new approaches towards the introduction of flexibility into macrocycles starting from cyclodextrins have been demonstrated: the synthesis and structural evaluation of non-glucose cyclooligosaccharides such as the cycloaltrins, mono-*altro*-cyclodextrins, cyclofructins, cyclogalactofuranosides, and notably the crown acetals. The properties of these compounds have been evaluated in detail and the effects of the increased flexibility on the formation of inclusion complexes have been studied. Multiple examples of macrocycles displaying the phenomenon of pseudorotation were evaluated, clearly demonstrating that lowering the symmetry results in favorable conformations of molecular hosts, that are accessible for inclusion complexation. In contrast to the rather rigid cyclodextrins and their static *lock-and-key*-type host-guest chemistry, the flexible hosts have unequivocally been shown to display a vivid, dynamic *induced-fit*-type formation of inclusion complexes.

The studies on flexible host-guest systems are complemented by approaches towards artificially rigidified hosts such as the intra- and intermolecularly bridged cyclodextrins.

Additional molecular modelling studies were directed towards the evaluation of the chemical and biological properties of some saccharides, amply demonstrating reasons for the atropiastereoselectivity found in ellagitannins, as well as providing explanations for the enzyme substrate specificity observed in bacterial strains of *Klebsiella pneumoniae* and *Fusobacterium mortiferum*.

The experimental studies were supported by multiple molecular modelling investigations, which required the development of tools for the automated analysis and visualization of the data. With *MolArch*<sup>+</sup>, a software solution has been created that not only supplements many existing tools used in computational chemistry, but also provides access to graphics in unsurpassed quality and resolution. In this work, the usefulness of high-quality visualizations have been demonstrated for scientific and educational purposes.

The combination of experimental and computational studies presented in this work provides a series of principally new insights in the wide field of carbohydrate chemistry.



## **Appendix**

List of Publications

Poster Presentations and Conference Contributions

Oral Presentations

Curriculum Vitae



## List of Publications

### 2003

- [37] The First Successful Crystallographic Characterization of a Cyclodextrin Dimer: Efficient Synthesis and Molecular Geometry of a Doubly Sulfur-bridged  $\beta$ -Cyclodextrin. D.-Q. Yuan, **S. Immel**, K. Koga, M. Yamaguchi, and K. Fujita, *Chem. Eur. J.* **2003**, *9*, 3501-3506.

### 2002

- [36] Metabolism of Sucrose and Its Five  $\alpha$ -D-Glucosyl-D-fructose Isomers by *Fusobacterium mortiferum*. A. Pikis, **S. Immel**, S. A. Robrish, and J. Thompson, *Microbiology* **2002**, *148*, 843-852.

### 2001

- [35] Two Stereoisomeric 3<sup>I</sup>,2<sup>II</sup>-Anhydro- $\alpha$ -cyclodextrins: A Molecular Dynamics and Crystallographic Study. **S. Immel**, K. Fujita, M. Fukudome, and M. Bolte, *Carbohydr. Res.* **2001**, *336*, 297-308.
- [34] Hydroxymethyl-substituted Crown Acetals with 35-C-14 and 40-C-16 Skeletal Backbones: Synthesis and Molecular Geometries. **S. Immel**, F. W. Lichtenthaler, H. J. Lindner, and T. Nakagawa, *Tetrahedron: Asymmetry* **2001**, *12*, 2767-2774.
- [33] Metabolism of Sucrose and Its Five Linkage-isomeric  $\alpha$ -D-Glucosyl-D-fructoses by *Klebsiella pneumoniae*. J. Thompson, S. A. Robrish, **S. Immel**, F. W. Lichtenthaler, B. G. Hall, and A. Pikis, *J. Biol. Chem.* **2001**, *276*, 37415-37425.

### 2000

- [32] Atropdiastereoisomers of Ellagitannin Model Compounds: Configuration, Conformation, and Relative Stability of D-Glucose Diphenoyl Derivatives. **S. Immel**, K. Khanbabaee, *Tetrahedron: Asymmetry* **2000**, *11*, 2495-2507.
- [31] Synthesis and Molecular Geometry of an Achiral 30-Crown-12 Polyacetal from  $\alpha$ -Cyclodextrin. **S. Immel**, T. Nakagawa, H. J. Lindner, and F. W. Lichtenthaler, *Chem. Eur. J.* **2000**, *6*, 3366-3371.
- [30] The 2,3-Anhydro- $\alpha$ -cyclomannin - 1-Propanol Hexahydrate: Topography, Lipophilicity Pattern, and Solid-State Architecture. **S. Immel**, F. W. Lichtenthaler, H. J. Lindner, K. Fujita, M. Fukudome, and Y. Nogami, *Tetrahedron: Asymmetry* **2000**, *11*, 27-36.
- [29] Structure and Lipophilicity Profile of 2,3-Anhydro- $\alpha$ -cyclomannin and its Ethanol Inclusion Complex. **S. Immel**, K. Fujita, H. J. Lindner, Y. Nogami, and F. W. Lichtenthaler, *Chem. Eur. J.* **2000**, *6*, 2327-2333.
- [28] The Hydrophobic Topographies of Amylose and its Blue Iodine Complex. **S. Immel** and F. W. Lichtenthaler, *Starch/Stärke* **2000**, *52*, 1-8.
- [27] Topography of the 1:1  $\alpha$ -Cyclodextrin - Nitromethane Inclusion Complex. T. Nakagawa, **S. Immel**, H. J. Lindner, and F. W. Lichtenthaler, *Carbohydr. Res.* **2000**, *324*, 141-146.
- [26] Flexible Non-glucose Cyclooligosaccharides. **S. Immel**, *Proc. 10<sup>th</sup> Int. Symp. Cyclodextrins* (Ed.: J. Szejtli), Mia Digital Publ., Ann Arbor, Michigan, **2000**, pp. 24-31.
- [25] Large-ring Crown Acetals from Cyclodextrins. T. Nakagawa, **S. Immel**, H. J. Lindner, and F. W. Lichtenthaler, *Proc. 10<sup>th</sup> Int. Symp. Cyclodextrins* (Ed.: J. Szejtli), Mia Digital Publ., Ann Arbor, Michigan, **2000**, pp. 18-23.

### 1999

- [24] Conformations and Lipophilicity Profiles of some Cyclic  $\beta$ (1 $\rightarrow$ 3)- and  $\beta$ (1 $\rightarrow$ 6)-linked Oligogalactofuranosides. H. Gohlke, **S. Immel**, and F. W. Lichtenthaler, *Carbohydr. Res.* **1999**, *321*, 96-104.
- [23] Solution Geometries and Lipophilicity Patterns of  $\alpha$ -Cycloaltrin. **S. Immel**, K. Fujita, and F. W. Lichtenthaler, *Chem. Eur. J.* **1999**, *5*, 3185-3192.

- [22] Guest-induced Conformational Change in a Flexible Host: Mono-*altro*- $\beta$ -Cyclodextrin.  
K. Fujita, W.-H. Chen, D.-Q. Yuan, Y. Nogami, T. Koga, T. Fujioka, K. Mihashi, **S. Immel**, and F. W. Lichtenthaler, *Tetrahedron: Asymmetry* **1999**, *10*, 1689-1696.
- [21]  $\alpha$ -Cycloaltrin: Conformation and Properties in the Solid-State and Aqueous Solution.  
**S. Immel**, G. E. Schmitt, and F. W. Lichtenthaler, *Proceedings of the 9<sup>th</sup> Internat. Symp. on Cyclodextrins* (Eds.: J. J. Torres-Labandeira and J. L. Vila Jato), Kluwer Acad. Publ., Dordrecht, NL, **1999**, 41-48.
- [20] Molecular Geometries of Furanoid  $\beta(1\rightarrow3)$ - and  $\beta(1\rightarrow6)$ -linked Cyclogalactins.  
H. Gohlke, **S. Immel**, F. W. Lichtenthaler, and G. E. Schmitt, *Proceedings of the 9<sup>th</sup> Internat. Symp. on Cyclodextrins* (Eds.: J. J. Torres-Labandeira and J. L. Vila Jato), Kluwer Acad. Publ., Dordrecht, NL, **1999**, 63-68.
- [19] The Molecular Geometries of Cyclofructins.  
**S. Immel**, G. E. Schmitt, and F. W. Lichtenthaler, *Proceedings of the 9<sup>th</sup> Internat. Symp. on Cyclodextrins* (Eds.: J. J. Torres-Labandeira and J. L. Vila Jato), Kluwer Acad. Publ., Dordrecht, NL, **1999**, 57-62.
- 1998**
- [18] Cyclofructins with Six to Ten  $\beta(1\rightarrow2)$ -linked Fructofuranose Units: Geometries, Electrostatic Profiles, Lipophilicity Patterns, and Potential for Inclusion Complexation.  
**S. Immel**, G. E. Schmitt, and F. W. Lichtenthaler, *Carbohydr. Res.* **1998**, *313*, 91-105.
- 1997**
- [17] Synthesis, Structure, and Conformational Features of  $\alpha$ -Cycloaltrin: a Cyclooligosaccharide with alternating  ${}^4C_1$  and  ${}^1C_4$  Pyranose Chairs.  
Y. Nogami, K. Nasu, T. Koga, K. Ohta, K. Fujita, **S. Immel**, H. J. Lindner, G. E. Schmitt, and F. W. Lichtenthaler, *Angew. Chem.* **1997**, *109*, 1987-1991; *Angew. Chem. Int. Ed. Engl.* **1997**, *35*, 1899-1902.
- 1996**
- [16] The Lipophilicity Patterns of Cyclodextrins and of Non-glucose Cyclooligosaccharides.  
F. W. Lichtenthaler and **S. Immel**, *J. Inclusion Phenom. Mol. Recognit. Chem.* **1996**, *25*, 3-16.  
F. W. Lichtenthaler and **S. Immel**, *Proceedings of the 8<sup>th</sup> Internat. Symp. on Cyclodextrins* (Eds.: J. Szejtli and L. Szenté), Kluwer Acad. Publ., Dordrecht, NL, **1996**, pp. 3-16.
- [15] Permethylated  $\alpha$ - and  $\beta$ -CD: Cyclodextrins with Inverse Hydrophobicity.  
**S. Immel** and F. W. Lichtenthaler, *Starch/Stärke* **1996**, *48*, 225-232.
- [14] Sucrose as a Renewable Organic Raw Material: New Selective Entry Reactions via Computer Simulation of its Solution Conformations and its Hydroxyl Group Reactivities.  
F. W. Lichtenthaler, P. Pokinskyj, and **S. Immel**, *Zuckerindustrie (Berlin)* **1996**, *12*, 170-190.
- [13] Towards Understanding the Formation and Stability of Cyclodextrin Inclusion Complexes: The Lipophilicity Patterns of some Typical Examples.  
F. W. Lichtenthaler and **S. Immel**, *Starch/Stärke* **1996**, *48*, 145-154.
- [12] Molecular Electrostatic and Lipophilic Potential Profiles of  $\alpha$ -Cyclofructin: Computation, Visualization, and Conclusions.  
**S. Immel** and F. W. Lichtenthaler, *Liebigs Ann. Chem.* **1996**, 39-44.
- [11] On the Hydrophobic Characteristics of Cyclodextrins: Computer-Aided Visualization of Molecular Lipophilicity Patterns.  
F. W. Lichtenthaler and **S. Immel**, *Liebigs Ann. Chem.* **1996**, 27-37.
- 1995**
- [10] Selective 2-O-Benzoylation of Sucrose: A Facile Entry to its 2-Deoxy- and 2-Keto-Derivatives and to Sucrosamine.  
F. W. Lichtenthaler, **S. Immel**, and P. Pokinskyj, *Liebigs Ann. Chem.* **1995**, 1938-1947.
- [9] The Conformation of Sucrose in Water: a Molecular Dynamics Approach.  
**S. Immel** and F. W. Lichtenthaler, *Liebigs Ann. Chem.* **1995**, 1925-1937.
- [8] Small Ring Cyclodextrins: their Geometries and Hydrophobic Topographies.  
**S. Immel**, J. Brickmann, and F. W. Lichtenthaler, *Liebigs Ann. Chem.* **1995**, 929-942.
- [7] Computer Simulation of Chemical and Biological Properties of Sucrose, the Cyclodextrins, and Amylose.  
F. W. Lichtenthaler and **S. Immel**, *Int. Sugar J.* **1995**, *97*, 12-22.



**1994**

- [6] Cyclodextrins, Cyclomannins, and Cyclogalactins with five and six (1→4)-linked Sugar Units: a Comparative Assessment of their Conformations and Hydrophobicity Potential Profiles.  
F. W. Lichtenthaler and **S. Immel**, *Tetrahedron: Asymmetry* **1994**, 5, 2045-2060.
- [5] A Practical Synthesis of  $\beta$ -D-Xyl-(1→2)- $\beta$ -D-Man-(1→4)- $\beta$ -D-Glc-OMe, a Trisaccharide Component of the Glycosphingolipid of *Hyriopsis schlegelii*.  
F. W. Lichtenthaler, T. Schneider-Adams, and **S. Immel**, *J. Org. Chem.* **1994**, 59, 6735-6738.

**1993**

- [4] Solid-State Conformations of 2,6-cis- and 2,6-trans-substituted Dihydropyran-3-ones.  
F. W. Lichtenthaler, S. Rönninger, H. J. Lindner, **S. Immel**, and E. Cuny, *Carbohydr. Res.* **1993**, 249, 305-326.
- [3] Sucrose, Sucralose, and Fructose: Correlations Between Hydrophobicity Potential Profiles and AH-B-X Assignments.  
F. W. Lichtenthaler and **S. Immel**, in: *Sweet Taste Chemoreception* (Eds.: M. Mathlouthi, J. A. Kanters, and G. G. Birch), Elsevier Appl. Science, London/New York, **1993**, pp. 21-53.

**1992**

- [2] Some Disaccharide-derived Building Blocks of Potential Industrial Utility.  
F. W. Lichtenthaler, **S. Immel**, D. Martin, and V. Müller, *Starch/Stärke* **1992**, 44, 445-456.

**1991**

- [1] Evolution of the Structural Representation of Sucrose.  
F. W. Lichtenthaler, **S. Immel**, and U. Kreis, in: *Carbohydrates as Organic Raw Materials* (F. W. Lichtenthaler, Ed.), VCH, Weinheim/New York, **1991**, pp. 1-32.  
Übersetzung ins Japanische: *Shokuhin Kogyo* ("The Food Industry") **1992**, 35, 65-85.



## Poster Presentations and Conference Contributions

### 1999

- [13] Large Ring Crown Acetals from Cyclodextrins.

T. Nakagawa, S. Immel, H. J. Lindner, and F. W. Lichtenthaler, *XVII<sup>th</sup> Japanese Cyclodextrin Symposium*, Osaka, Japan, October 13-14, **1999**.

### 1998

- [12]  $\alpha$ -Cyclodextrin: Hydration Properties and Hydrogen Bonding.

S. Immel and G. E. Schmitt, *XIX<sup>th</sup> International Carbohydrate Symposium*, San Diego, California, August 9-14, **1998**, Abstract AO008.

- [11]  $\alpha$ -Cycloaltrin: Molecular Shape and Hydration Properties.

S. Immel, G. E. Schmitt, and F. W. Lichtenthaler, *XIX<sup>th</sup> International Carbohydrate Symposium*, San Diego, California, August 9-14, **1998**, Abstract AP124.

- [10]  $\beta(1\rightarrow3)$ - and  $\beta(1\rightarrow6)$ -Linked Cyclogalactofuranosides: Conformations and Molecular Shapes.

H. Gohlke, S. Immel, F. W. Lichtenthaler, and G. E. Schmitt, *9<sup>th</sup> International Symposium on Cyclodextrins*, Santiago de Compostela, Spain, May 31 - June 3, **1998**, Abstract 2-P-4.

- [9] Cyclofructins: Conformations, Molecular Electrostatic and Lipophilicity Patterns, and Inclusion Complexes.

S. Immel, G. E. Schmitt, and F. W. Lichtenthaler, *9<sup>th</sup> International Symposium on Cyclodextrins*, Santiago de Compostela, Spain, May 31 - June 3, **1998**, Abstract 2-P-3.

- [8]  $\alpha$ -Cycloaltrin: Conformation and Properties in Aqueous Solution.

S. Immel, G. E. Schmitt, and F. W. Lichtenthaler, *9<sup>th</sup> International Symposium on Cyclodextrins*, Santiago de Compostela, Spain, May 31 - June 3, **1998**, Abstract 2-O-5.

### 1997

- [7] Structure and Conformational Features of  $\alpha$ -Cycloaltrin: a Cyclooligosaccharide with alternating  ${}^4C_1$  and  ${}^1C_4$  Pyranose Chairs.

S. Immel, G. E. Schmitt, and F. W. Lichtenthaler, *9<sup>th</sup> European Carbohydrate Symposium (EUROCARB IX)*, Utrecht, Netherlands, July 6-11, **1997**, Abstract C5.

### 1996

- [6] Cyclofructins: Geometries, Electrostatic and Lipophilicity Patterns, and Inclusion Complexes.

S. Immel, G. E. Schmitt, and F. W. Lichtenthaler, *10<sup>th</sup> Molecular Modeling Workshop*, Darmstadt, May 14-15, **1996**.

S. Immel, G. E. Schmitt, and F. W. Lichtenthaler, *IV<sup>th</sup> Intl. Satellite Meeting on Conformational Studies of Carbohydrates*, La Thuile (Aosta), Italy, July 17-20, **1996**.

S. Immel, G. E. Schmitt, and F. W. Lichtenthaler, *XVIII<sup>th</sup> International Carbohydrate Symposium*, Milano, Italy, July 21-26, **1996**, Abstract AO027.

### 1995

- [5] A New Look at the Hydrophobic Characteristics of Cyclodextrins, Cyclomannins, Cyclogalactins, Cyclofructins, and of Starch.

S. Immel and F. W. Lichtenthaler, *8<sup>th</sup> European Carbohydrate Symposium (EUROCARB VIII)*, Seville, Spain, July 2-7, **1995**, Abstract B38.

### 1992

- [4] Sucrose, Fructose, and some Non-Carbohydrate Sweeteners: Correlations Between Hydrophobicity Potential Profiles and AH-B-X Assignments.

S. Immel and F. W. Lichtenthaler, *Symposium on Conformational Studies of Oligosaccharides, Polysaccharides and Glycoconjugates*, Le Croisic, June 29 - July 2, **1992**, Abstract VI-2.

S. Immel and F. W. Lichtenthaler, *XVI<sup>th</sup> International Carbohydrate Symposium*, Paris, July 5-10, **1992**, Abstract C163.

### 1991

- [3] Structural Representation of Sucrose: From Tollens' 1883 Formula to Graphic Displays of its Hydrophobicity Potential Profile.

U. Kreis, S. Immel, and F. W. Lichtenthaler, *6<sup>th</sup> European Carbohydrate Symposium (EUROCARB VI)*, Edinburgh, September **1991**.

- [2] The Electrostatic and Hydrophobicity Potential Profiles of Sucrose and Related Disaccharides.  
U. Kreis, **S. Immel**, and F. W. Lichtenthaler, *201<sup>st</sup> ACS Meeting*, New York, August **1991**, Abstract CARB 3.
- [1] Die Hydrophobieverteilerung bei Saccharose, und ihre Auswirkung auf derzeitige Struktur-Süßkraft Konzepte.  
**S. Immel**, U. Kreis, and F. W. Lichtenthaler, *5<sup>th</sup> Molecular Modeling Workshop*, Darmstadt, May **1991**.

## Oral Presentations

### 2003

- [16] Flexible und rigide Cyclodextrinderivate: Synthese, Struktur und Eigenschaften.  
**S. Immel**, *Chemiedozententagung*, Technische Universität Chemnitz, Chemnitz, Germany, March 16-19, **2003**, Abstract A20.

### 2001

- [15] Von Cyclodextrinderivaten bis hin zur Stärke: Molecular Modelling der Eigenschaften und Geometrien.  
**S. Immel**, Kolloquium für Anorganische und Organische Chemie, Universität Wuppertal, Prof. Dr. H.-J. Altenbach, Nov. 22, **2001**.

### 2000

- [14] From Rigid Cyclodextrins to Flexible Non-glucose Cyclooligosaccharides.  
**S. Immel**, *10<sup>th</sup> International Symposium on Cyclodextrins*, Ann Arbor, Michigan USA, May 21-24, **2000**.
- [13] The Topographies of Starch and Cyclodextrins: Analogies and Differences.  
**S. Immel**, *51. Stärke Tagung*, Detmold, April 12-14, **2000**.

### 1999

- [12] From Cyclodextrins to Starch: Structures and Hydrophobic Characteristics.  
**S. Immel**, Workshop on the "Chemistry of Cyclodextrins" held by Prof. Dr. G. Wenz, Universität Karlsruhe, May 6, **1999**.

### 1998

- [11] - The Hydrophobic Properties of Cyclodextrins and some Non-glucose Cyclooligosaccharides,  
[5] and Their Properties in Aqueous Solution.  
**S. Immel**, hosted by:
- Prof. Dr. Kahee Fujita, Faculty of Pharmaceutical Sciences, Nagasaki University, Nagasaki, Japan, November 4, **1998**.
  - Prof. Dr. Yasuyoshi Nogami, Department of Pharmaceutical Sciences, Kyushu University, Fukuoka, Japan, November 5, **1998**.
  - Prof. Dr. Naoki Kashimura and Prof. Dr. Shinichi Kitamura, *3<sup>rd</sup> Domestic Meeting on "Bioactive Carbohydrates"*, Department of Biological Resource Chemistry, Kyoto Prefectural University, Kyoto, Japan, November 7, **1998**, Abstract 3-10.
  - Prof. Dr. Akihiko Ueno, Department of Chemistry, Faculty of Bioscience and Biotechnology, Tokyo Institute of Technology, Yokohama, Japan, November 10, **1998**.
  - Prof. Dr. Ken-ichi Sato, Department of Applied Chemistry, Kanagawa University, Yokohama, Japan, November 11, **1998**.
  - Prof. Dr. Seiichiro Ogawa, Department of Applied Chemistry, Faculty of Science and Technology, Keio University, Yokohama, Japan, November 13, **1998**.
  - Prof. Dr. Haruhisa Ueda, Department of Physical Chemistry, Faculty of Pharmaceutical Sciences, Hoshi University, Tokyo, Japan, November 14, **1998**.

- [4]  $\alpha$ -Cyclodextrin: Hydration Properties and Hydrogen Bonding.  
**S. Immel** and G. E. Schmitt, *XIX<sup>th</sup> International Carbohydrate Symposium*, San Diego, California, August 9-14, **1998**, Abstract AO008.

- [3]  $\alpha$ -Cycloaltrin: Conformation and Properties in Aqueous Solution.  
**S. Immel**, G. E. Schmitt, and F. W. Lichtenthaler, *9<sup>th</sup> International Symposium on Cyclodextrins*, Santiago de Compostela, Spain, May 31-June 3, **1998**, Abstract 2-O-5.

### 1994

- [2] Towards Understanding Sweetness: Structure-Activity Relationships on the Basis of Hydrophobicity Potential Profiles.  
**S. Immel** and F. W. Lichtenthaler, *207<sup>th</sup> ACS Meeting*, San Diego, March 13-18, **1994**, Abstract CARB 11.

### 1993

- [1] Towards Understanding Sweetness: Structure-Activity Relationships on the Basis of Hydrophobicity Potential Profiles.  
**S. Immel** and F. W. Lichtenthaler, *7<sup>th</sup> European Carbohydrate Symposium (EUROCARB VII)*, Cracow, August 22-27, **1993**, Abstract C026.



## Curriculum Vitae

### Persönliche Daten

Name: Dr. Stefan Immel  
 Privatanschrift: Bismarckstraße 43d, D-64293 Darmstadt  
 Tel.: (+49) 6151 29 36 71  
 Geburtsdatum: 11. 11. 1965  
 Geburtsort: Darmstadt  
 Staatsangehörigkeit: Deutsch  
 Familienstand: ledig, keine Kinder

### Schul- und Universitätsausbildung

- 08.1997 - 11.2003 Arbeiten an der Technischen Universität Darmstadt mit dem Ziel der Habilitation und dem Schwerpunkt *"Synthese, Struktur und Eigenschaften von Cyclodextrinen und Cyclodextrinderivaten"*.
11. - 12.1998 Forschungsaufenthalt bei Prof. Dr. K. Fujita, Nagasaki Universität, Japan.
- 06.1996 - 07.1997 Postdoktorand bei K. B. Sharpless, The Scripps Research Institute, San Diego, Kalifornien, über:  
*"Computersimulations on the Mechanism of Osmium-Catalyzed Reactions"*.
- 01.1995 - 05.1996 Forschungsarbeiten mit F. W. Lichtenthaler:  
*"Molecular Dynamics Simulations of Saccharides"*.
- 01.1995 Promotion an der Technischen Universität Darmstadt zum Dr.-Ing. *"mit Auszeichnung"*.
- 08.1990 - 12.1994 Dissertation unter Anleitung von F. W. Lichtenthaler über:  
*"Computersimulations of Chemical and Biological Properties of Saccharides: Sucrose, Fructose, Cyclodextrins, and Starch"*.
06. - 08.1991 Gastaufenthalt an der ETH Zürich bei W. F. van Gunsteren; Arbeiten über:  
*"Molecular Dynamics of Sucrose in Aqueous Solution"*.
- 07.1990 Hauptdiplom Chemie, Technische Universität Darmstadt (*"mit Auszeichnung"*)  
 Diplom Arbeit unter Anleitung von F. W. Lichtenthaler über die  
*"Stereoselektivität von Dialdehyd-Nitromethan-Cyclisierungen"*.
- 06.1987 Vordiplom Chemie, Technische Universität Darmstadt (*"mit Auszeichnung"*).
- 10.1984 Beginn des Studiums der Chemie an der Technischen Universität Darmstadt.
- 06.1984 Abitur am Lichtenberg Gymnasium in Darmstadt.

### Mitgliedschaften in wissenschaftlichen Gesellschaften

- Seit 1996 American Chemical Society  
 Seit 1990 Gesellschaft Deutscher Chemiker

### Mitgliedschaften in Editorial Boards

- Seit 2000 Editorial Board von *Carbohydrate Research*

### Wissenschaftliche Auszeichnungen und Stipendien

- 1996 - 1997** Postdoktoranden-Stipendium der Deutschen Forschungsgemeinschaft (DFG).
- 1991 - 1992** Doktoranden-Stipendium des Fonds der Chemischen Industrie.
- 02.1988** Preisträger der Dr. Anton-Keller-Stiftung der Technischen Universität Darmstadt, Auszeichnung für herausragende Leistungen im Vordiplom.

### Forschungsschwerpunkte

- Synthese, Struktur, und Eigenschaften flexibler und rigider Cyclooligosaccharide: Molekulare Erkennung nach dem "*Induced-Fit*" und "*Schlüssel-Schloss*" Prinzip.
- Von Cyclodextrinen abgeleitete Kronen-Acetale: Neue Kationen-Fänger?
- Molekülmodellierung chemischer und biologischer Eigenschaften von Kohlenhydraten.
- Konformation von Kohlenhydraten im Kristall und in Lösung.
- Anwendung von Kraftfeld-gestützten Rechenverfahren zur Charakterisierung von Kohlenhydraten, insbesondere hydrophober Oberflächenregionen.
- Wechselwirkung von Kohlenhydraten mit Lösungsmitteln (Wasser) und deren Hydratationseigenschaften.
- Struktur-Süßkraft Beziehungen von Zuckern und künstlichen Süßstoffen.

### Lehrtätigkeiten und Vorlesungen

- Vorlesung „Metallorganische Chemie“ für Chemiker im Hauptstudium.
- Vorlesung „Grundlagen und Reaktionsmechanismen in der Organischen Chemie“ für Chemiker und Biologen im Grundstudium.
- Begleitende Seminare und Übungen zur Vorlesung „Organische Experimentalvorlesung“ für Chemiker im Grundstudium.
- Blockseminar „Physikalische Methoden in der Organischen Chemie“ (IR, UV, NMR Spektroskopie und MS Spektrometrie) für Chemiker im Fortgeschrittenen Praktikum.
- Vortragsübungen für Chemiker und Biologen im Rahmen der Fortgeschrittenen Praktika.